YEAR END TECHNICAL REPORT

May 18, 2011 to May 17, 2012

Remediation and Treatment Technology Development and Support

Submitted on June 22, 2012

Principal Investigators:

Leonel E. Lagos, Ph.D., PMP®
David Roelant, Ph.D.

Florida International University Collaborators:

Dave Roelant, PhD
Georgio Tachiev, PhD, PE, Project Manager
Siamak Malek-Mohammadi, PhD
Angelique Lawrence, MS, GISP
Mandar Zope, MS
Lilian Marrero, DOE Fellow
Heidi Henderson, DOE Fellow
Amy Cook, MS
Yong Cai, PhD
Guangliang Liu, PhD
Yanbin Li, PhD

Prepared for:

U.S. Department of Energy
Office of Environmental Management
Under Grant No. DE- EM0000598

FIU Applied Research Center
FLORIDA INTERNATIONAL UNIVERSITY

Addendum:

This document represents one (1) of five (5) reports that comprise the Year End Reports for the period of May 18, 2011 to May 17, 2012 prepared by the Applied Research Center at Florida International University for the U.S. Department of Energy Office of Environmental Management under Cooperative Agreement No. DE-EM0000598.

The complete set of FIU's Year End Reports for this reporting period includes the following documents:

1. Chemical Process Alternatives for Radioactive Waste
   Document number: FIU-ARC-2012-800000393-04b-211
2. Rapid Deployment of Engineered Solutions for Environmental Problems at Hanford
   Document number: FIU-ARC-2012-800000438-04b-208
3. Remediation and Treatment Technology Development and Support
   Document number: FIU-ARC-2012-800000439-04b-210
4. Waste and D&D Engineering and Technology Development
   Document number: FIU-ARC-2012-800000440-04b-212
5. DOE-FIU Science & Technology Workforce Development Initiative
   Document number: FIU-ARC-2012-800000394-04b-059

Each document has been submitted to OSTI separately under the respective project title and document number as shown above.

TABLE OF CONTENTS

LIST OF FIGURES

LIST OF TABLES

PROJECT OVERVIEW

Approximately 75 to 150 metric tons of elemental mercury (used in a lithium-isotope separation process for production of nuclear fusion weapons), were released into East Fork Poplar Creek (EFPC) watershed from the Y-12 National Security Complex (Y-12 NSC) in eastern Tennessee, USA. Under typical environmental conditions, elemental mercury is oxidized to mercuric ion which has a greater solubility and mobility in groundwater and surface water. The increased mobility of the mercuric ion results in elevated concentrations of total mercury in soil, surface water and groundwater. The mercuric ion has high affinity to many organic ligands and in the water column the majority of the mercuric ions are bound to suspended and colloidal particles. Storm events increase the turbulence and velocity of river flow and may result in additional mobilization and transport of mercury downstream in the EFPC.

In order to analyze the mercury cycle in the environment and to provide forecasting capabilities for the fate and transport of contamination within the watershed, an integrated surface and subsurface flow and transport model for the Y-12 NSC was developed. The model couples the hydrology of the watershed with mercury transport and provides a tool for analysis of changes of mercury load as function of changes in hydrology, including remediation scenarios which modify the hydrological cycle. The model couples the overland and subsurface flow module with the river flow and transport module. The model includes the main components of the hydrological cycle: groundwater flow (3D saturated and unsaturated), 2D overland flow, 1D flow in rivers, precipitation, and evapotranspiration. Furthermore, the model includes 57 outfalls along Upper East Fork Poplar Creek (UEFPC) which have been listed in the National Pollutant Discharge Elimination System (NPDES) permit from 2005. A sedimentation module was included to simulate the interactions between sediment particles, water and mercury species within the EFPC.

The numerical model was calibrated for the period of 1996-2009 using recorded stream flow and mercury concentrations measured in groundwater, surface water and soil. The model was subsequently applied to evaluate the effect of hydrology on mercury concentrations within the creek and the floodplain. For each simulation, flow duration curves and mercury load duration curves were compared at Station 17 for the computed and recorded data. The effect on the watershed was determined by comparing the percent change of mercury loads downstream of Station 17 and along EFPC. The results of numerical simulations showed that exchange of mercury species between sediment, pore water, aqueous media and suspended solids significantly affects the mercury load detected along each station of the creek.

A series of laboratory studies were conducted to analyze the effect of various environmental factors (pH, pE) on methylation and demethylation processes in the water column. Experimental work was used to obtain critical mercury exchange parameters between pore water, colloidal and suspended particles, and streambed sediment, which were applied in the numerical model to study the effect of sediment transport on mercury mobilization.

For years 2010-2011, the model, which was developed for the Y-12 NSC, was extended to include the EFPC watershed and the creek between Y-12 NSC and Station EFK 6.4. The research focused on conducting additional simulations using the EFPC watershed model which extend the studies for Y-12 NSC. In addition, flow and transport studies were conducted for the Bear Creek watershed (a sub-watershed of the larger EFPC watershed). A geodatabase was

developed as a strategy for supporting hydrological model data input by creating a centralized data storage system to store model parameters. The database extends the capabilities of the GIS data and allows for automating time consuming GIS processing for water resources applications.

For FY2012 (May 2012-May 2013), FIU is proposing a scope which will rely on previously developed models of EFPC to provide simulation of fate and transport of contaminants within the EFPC watershed. The stochastic analysis of hydrological and transport data will be extended for the entire watershed. A detailed mass balance will be developed for the site for contaminants of concern, including inorganic (Hg) and organic contaminants. The work will provide insight on the contribution of each outfall to the load at Station 17. The laboratory work will include additional studies to determine experimental parameters related to cinnabar dissolution and contribution for mercury distribution between various phases (aqueous and soil) for different environmental factors including pH, dissolved oxygen, dissolved organic matter, organic and inorganic content of soils and pore water, on mercury fate and transport within the creek and for overland flow. The work will provide a better understanding of the mercury dynamics within the Oak Ridge Reservation watersheds (EFPC, Y-12 NSC, Bear Creek, White Oak Creek) for variable environmental conditions and for specified remediation alternatives. Student support will also be provided for numerical modeling of subsurface flow and transport at Moab site.

TECHNICAL PROGRESS SUMMARY FOR FY11

During FY2008-2011, FIU developed integrated flow and transport models of East Fork Poplar Creak (EFPC), Upper EFPC and White Oak Creek (WOC) watersheds and conducted numerical modeling and reviews of monitoring data available from OREIS and related to mercury (Hg) contamination and remediation within these watersheds. In addition, experimental studies provided experimental kinetic and equilibrium data about important parameters related to Hg transport, speciation and methylation/demethylation kinetics within the watershed. The following outlines the project-wide and individual task accomplishments for FY2011.

- A **Draft Project Technical Task Plan** was submitted on 08/12/2011 (see APPENDIX I).
- **PowerPoint presentations** were delivered to DOE personnel and site contractors during an ORR site visit in November 2011 (see APPENDIX II) and to ORNL personnel (Dr. Eric Pierce and Dr. Liyuan Liang) during a visit to the Applied Research Center in February 2012 (see APPENDIX III). The presentations covered the following:
    - Introduction to the FIU Water Resources and Environment Research Group
    - A summary of FIU's work to date
    - Hydrologic modeling of surface, groundwater and river sedimentation including WOC, EFPC, Y12-NSC and Building 81-12
    - Fate and transport of contaminants
    - Support for remediation activities
    - Benchmarking, sensitivity and uncertainty analysis
    - Experimental mercury speciation studies
    - Results
    - Path forward
- **Project factsheets** of each task were prepared which summarized the research conducted under each individual subtask (see APPENDIX IV). Several were distributed during the Waste Management 2012 Symposium.
- **Nine publications and presentations** were submitted to journals and conference proceedings based on the research performed on this project (see APPENDIX V), including the following:
    - A peer reviewed article entitled, "Simulation of Flow and Mercury Transport in Upper East Fork Poplar Creek, Oak Ridge, Tennessee," was published in the Spring 2012 edition of the Remediation Journal.
    - Best Professional Poster for Waste Management 2011 Symposium was awarded to "Simulation of Flow and Mercury Transport in Upper East Fork Poplar Creek, Oak Ridge, TN." A related paper was also submitted to the conference. This research was associated with development of the integrated surface and groundwater model for flow and mercury transport at EFPC. The model is being developed and used to predict transport patterns of mercury and evaluate risks during deactivation and decommissioning of mercury contaminated facilities at the Y-12 National Security Complex in Oak Ridge, TN.

- A first place in track 7 "Remediation" was awarded to "Groundwater Transport of Organic Compounds in Old Salvage Yard, Oak Ridge, TN," at the Waste Management Symposium 2012. A related paper was also submitted to the conference.
- A poster was also submitted by DOE Fellow, Lilian Marrero, entitled, "Improvements in the Suspended Sediment Interactions Module of an Integrated Flow and Mercury Transport Model for East Fork Poplar Creek Watershed, Oak Ridge, TN (12588)."
- A journal article entitled, "Migration of Plume of Organic Compounds in a Highly Fractured Subsurface Domain," was submitted to the Ground Water Journal and is currently under review.
- A review paper entitled, "Progress in the Study of Mercury Methylation and Demethylation in Aquatic Environments," was accepted for publication in Fall 2012 in the Chinese Science Bulletin.
- A paper entitled, "Estimation of the Major Source and Sink of Methylmercury in the Florida Everglades," was published in the Environmental Science and Technology Journal online on April 26, 2012 (DOI: 10.1021/es204410x).
- A paper entitled, "Degradation of Methylmercury and its Effects on Mercury Distribution and Cycling in the Florida Everglades" was published in the Environmental Science and Technology Journal in November 2010.
- A paper entitled, "Spatial Variability in Mercury Cycling and Relevant Biogeochemical Controls in the Florida Everglades" was published in the Environmental Science and Technology Journal in May 2009.

TASK 1: EFPC MODEL UPDATE, CALIBRATION & UNCERTAINTY ANALYSIS

Subtask 1: Extension of the water quality and sedimentation module

- The sedimentation module which was developed for the UEFPC (the section of EFPC upstream of Station 17) was extended to include the entire EFPC down to EFK 6.4 and Bear Creek. The sedimentation module provides the coupling between the flow and transport within the creek and the overland flow used to analyze the significance of floodplain contamination downstream EFPC. Fifty-two (52) outfalls were added to the EFPC model. Van Genuchten parameters for the unsaturated flow in the aquifer were also updated. The model was reconfigured following the incorporation of the sedimentation module and outfalls. A series of numerical simulations have been performed using a range of Manning's number values, threshold run-off water depths, and drainage coefficients to calibrate the flow for the period of 2000 – 2008.
- MATLAB scripts have been prepared for the statistical analysis of observed and computed data. Laboratory and field data on surface water level and discharge, groundwater level, and mercury contamination in soil, groundwater and surface water were obtained from OREIS database. Data were organized and incorporated into the numerical model for calibration and verification purposes.
- A progress report was drafted and submitted 11/17/2011, outlining the incorporation of the sedimentation module, assignment of specific parameters, description of the methodology for the download, organization and analysis of field and laboratory data from OREIS database, and incorporation into the numerical model. This report has since been updated and re-submitted as a final report (see APPENDIX T1-001).

Subtask 2: EFPC model uncertainty and sensitivity analysis

- The probabilistic distribution of critical subsurface parameters, such as hydraulic conductivity, porosity, pore size distribution, and storage coefficients were defined specifically for the karst areas. MATLAB's statistical toolbox and scripting tools were used to develop a series of functions for a random generation of distributed hydrologic parameters based on a selected probability density function and statistical parameters. Randomly generated grids were created using the MATLAB toolbox for the uncertainty analysis. Numerical simulations were conducted for each randomly generated input grid. The output was used to generate daily timeseries for selected hydrological, fate and transport parameters, including groundwater flow velocity at selected points, potential head at selected points, rate of mercury absorption at various locations, concentrations of total mercury at the key stations (EFK 6, EFK 14, EFK 18), total mercury load at the key stations, flux exchange between subsurface and surface. The simulations were used to determine the model uncertainty in terms of stochastic variations of input parameters. Graphical plots of the variation of the output parameters were then used to present the results of the sensitivity analysis, identifying significant parameters and a range of certainty for the model.

TASK 2: TMDL ANALYSIS FOR THE ENTIRE EFPC

Total maximum daily loads (TMDL) analysis for the entire East Fork Poplar Creek (EFPC) was the objective for this project task.

Subtask 1: Update the database

- Field and laboratory data pertaining to water quantity (surface and groundwater levels, and water flow) and water quality (i.e. temporal and spatial distribution of pollutant sources in soil, water, and sediments, bioassessment) were extracted from the OREIS database. Excel spreadsheets were developed and the data categorized based on media type (i.e., soil, surface water, sediment, and groundwater). Previously submitted reports were then updated with the newly extracted data for 2010 and 2011 (Appendix C of Mercury Remediation Strategy (MRS), submitted to DOE). The data was analyzed to identify any data gaps and additional data needs and monitoring recommendations. Spatial analysis was performed to identify spatial variations of mercury in EFPC water, in shallow and deep soil layers, and in stream bank and streambed sediments. Temporal analysis was performed to evaluate the timing of impairment and potential source loading or other conditions contributing to impairment. Specifically, the effect of rainfall and runoff flow was investigated on the concentration of mercury in the creek. The effect of rainfall/runoff and high flow conditions were investigated on the sediment transport, and thereby, mercury transport in the creek.

Subtask 2: Review and analysis of NPDES and TMDL requirements (literature review)

- A comprehensive review was conducted on NPDES and TMDL requirements for EFPC established by EPA and Tennessee Department of Environment and Conservation (TDEC). A report was developed which includes water quality criteria and TMDL target, water quality assessment and deviation from the TMDL target, water quality data analysis, and source identification.
- Water quality data analysis has been completed including temporal and spatial variations of data points, seasonal analysis of data points, and removal of data outliers and anomalies using methods suggested by the EPA.

Subtask 3: NPDES and TMDL analysis of UEFPC

- Target mercury concentration for the EFPC was determined based on TDEC regulations for surface waters. The target concentration was determined to be 51 ppt for recreational use. Based on this target concentration, a "Loading Capacity" duration curve was developed.
- The flow and concentration timeseries associated with NPDES outfalls were revisited. Load and flow duration curves were developed for the outfalls and compared with simulation results. Flow duration curves were developed for two key stations along EFPC (EFK 23.4 and EFK 6.3). Flow duration intervals and zones were determined to study the effect of flow conditions on the distribution of impairments. Impairments observed in the low flow zones (dry seasons) were indicated as the influence of point sources (outfalls),

while sediments (non-point sources) were determined to be effective during high flow conditions (wet seasons).

- Load duration curves were developed for key stations. A series of numerical simulations were performed to determine the percentages of the load associated with outfalls, sediments, and overland flow (load allocation analysis). Based on the numerical simulation results, waste load allocations (WLAs) were developed for continuous point source discharges using the duration curves. In the case of sediments, specific simulations were performed only with contaminant sources inside the sediments to determine the contribution of sediments to the total load observed in the creek. Load duration curves and load percentiles were developed for each source (i.e., outfalls, sediments and overland wash-off).
- A technical report entitled, "Simulation of TMDL for the Entire EFPC," which includes information on NPDES and TMDL target definition, as well as development of flow and load duration curves and load allocation analysis, was compiled and submitted in February 2012. This report has since been updated and re-submitted as a final report (see APPENDIX T2-001).

TASK 3: PARAMETERIZATION OF MAJOR TRANSPORT PROCESSES OF MERCURY SPECIES

Subtask 1: Photomethylation of Hg^{2+} in Natural Water:

- The double isotope addition technique ($^{199}Hg^{2+}$ and $Me^{201}Hg$) was applied to measure the photomethylation of Hg^{2+} in water. A new model was developed to calculate the methylation rate constant of the spiked Hg^{2+} in water. This model corrected for the defect of previous models, in which the degradation of ambient MeHg and the newly produced MeHg was not taken into account. Methylation of Hg^{2+} was observed in natural water, with a rate of 1.14±0.02 ($\times 10^{-4}$ d^{-1}). This process is mediated by sunlight. However, its rate was much slower than that of MeHg photodemethylation (k_d=0.26±0.04 d^{-1}), indicating that methylation in water plays a minor role in the cycling of MeHg. In addition, the contributions of the photodemethylation of ambient and newly produced $Me^{199}Hg$ were proven not to be negligible for the variation of $Me^{199}Hg$.

Subtask 2: Estimation of the Bioavailability of Hg^{2+} and Methylmercury for Methylation and Demethylation in Natural Sediment

- The difference between the ambient and newly input Hg species in methylation/demethylation efficiency was often neglected in the previous models which may have caused a significant error. Here, we developed a method to calculate the bioavailability of Hg^{2+} and methylmercury for methylation and demethylation in natural sediment using double stable isotope ($^{199}Hg^{2+}$ and $Me^{201}Hg$) addition experiments. The percentage of bioavailable Hg^{2+} and MeHg for methylation/demethylation (α_x and β_x) was estimated to be 0.02-0.06 and 0.71-0.93, separately in studied sediments, indicating that there is a significant difference between the ambient and newly input Hg species in methylation/demethylation efficiency. The difference in methylation/demethylation efficiency of the ambient and newly input Hg species must be taken into account when

net MeHg production (or degradation) rates are estimated. If α and β were not considered, the estimated net production (or degradation) rate of MeHg in sediment could be overestimated by a factor of 20.

Subtask 3: Effect of Thiol-Containing Compounds on Cinnabar Dissolution

- Thiol-containing compounds could significantly promote the dissolution of cinnabar. In the absence of thiol-containing compounds, Hg^{2+} concentration in water was at the level of ~1-2 μg/L. The addition of 10μmol/L L-cysteine increased it to more than 100 μg/L. Glutathione could also increase the dissolution of cinnabar. However, its effect was much smaller compared to cysteine, suggesting that the effect of thiol varies in different thiol species. In addition, oxygen plays a significant role in the dissolution of cinnabar. The concentration of Hg^{2+} in the aqueous phase was in the order of saturated oxygen > air > anaerobic. A model based on chemical thermodynamics was developed to calculate the dissolution of cinnabar under different conditions and elucidate the relative importance of pH, O_2 and thiol-containing compounds in cinnabar dissolution. By taking into consideration the adsorption of released Hg^{2+} on cinnabar, the proposed model could well predict the dissolution of cinnabar with or without cysteine. Both model and experimental results suggest that oxidization of S (-II) may be the driving force for cinnabar dissolution in aquatic environments. Complexation of cysteine with Hg^{2+} also plays an important role in this process by inhibiting the absorption of released Hg^{2+} on the cinnabar surface.

Dr. Yong Cai visited ORR to present his research and to coordinate plans for the next year. A detailed Technical Task Plan (TTP) for FY 2011-2012 was then prepared for the project and submitted to DOE for review. A technical report entitled, "Parameterization of Major Transport Processes of Mercury Species," was also submitted (see APPENDIX T3-001).

TASK 4: GEODATABASE DEVELOPMENT FOR HYDROLOGICAL MODELING SUPPORT

- A geodatabase was created for the EFPC model including feature datasets and raster catalogs which contain model configuration and output data. The database is based on the ArcHydro and ArcGIS Basemap data models and has been customized according to model input data specifications to facilitate import/export of model data.
- A progress report entitled, "GIS & Hydrological Modeling Data Server Management," was created to provide configuration methods and parameters.
- The ORR Geodatabase was then populated with relevant model data. The import/export of spatial data into the geodatabase and execution of geoprocessing tasks as necessary for model simulations is an ongoing process.
- Data stored in the ORR Geodatabase were used for visualization, map production and analysis through the ArcGIS ArcMap interface, often utilizing the MIKE 11 GIS extension tool for timeseries file management and integration of MIKE 11 model files. Graphical plots were also generated using the observed and computed model data for reporting purposes.

- A technical report entitled, "Geodatabase Development for Hydrological Modeling Support," was submitted to DOE in March 2012. This report has since been updated and re-submitted as a final report (see APPENDIX T4-001).

TASK 5: STUDENT SUPPORT FOR MODELING OF GROUNDWATER FLOW AND TRANSPORT AT MOAB SITE

- Obtained and organized the hydrological data for the analysis and modeling and completed hydrologic budget calculations to be used for developing constraints for the surface and groundwater model.
- Completed analysis of groundwater quality data adjacent to the Colorado River for calculating the flux of contamination into the river and will use results to generate water quality contour maps to assess the pattern of contaminant transport.
- Conducted simulations with the existing hydrological model (developed by a DOE consultant). Compared results obtained from carrying out simulations using the existing model with the results presented by the subcontractor of the DOE Moab Site.
- Reconfigured the existing Moab model with more current spatial and timeseries data and currently conducting numerical simulations to simulate fate and transport of contaminants including uranium and ammonia in the subsurface domain at the Moab site in Utah.
- Extracted pumping test data and regular monitoring data from literature, which will be used in the model to show the natural seasonal variations and responses to other stresses.
- Completed DOE Fellow (Mr. Alex Henao) internship during the summer of 2011 and submitted a report entitled, "Preliminary Studies of Nitrogen Concentration in Wells 0437, 0438, and 0439 at the Moab Site," in November 2011 (see APPENDIX T5-001).
- Participated in a 2-day modeling webinar, "Using Groundwater Vistas," conducted by the DOE subcontractor that developed the existing groundwater model. This model is to be used for some of the planned FIU modeling work.
- Ran simulations with the Moab air dispersion model for the new location of the landsharks and created a report which included the new results.
- Finalized the Moab model and its configuration according to Advanced Simulation Capabilities for Environmental Management (ASCEM) specifications.
- Calibrated the model with water level measurements collected from several monitoring wells. Variable hydraulic conductivity values were used for the top 3 layers and uniform conductivity values for the rest.
- Pumping test data and several years of regular monitoring data which shows the natural seasonal variations and responses to other stresses was used for transient calibration of the model. The model was also used for well field optimization to predict capture zones and mass removal.

- Simulations were conducted to identify the discharge zone for the legacy plume in the brine zone and to identify areas of uncertainty.
- A technical report entitled, "Student support for modeling of groundwater flow and transport at Moab, UT site," was submitted to DOE in February 2012. This report has since been updated and re-submitted as a final report (see APPENDIX T5-002).

TASK 1: EFPC MODEL UPDATE, CALIBRATION AND UNCERTAINTY ANALYSIS

INTRODUCTION

The main objectives of this task were to extend the existing EFPC model by adding sedimentation and reactive transport modules, and to use the model to perform numerical simulations, that are relevant for the NPDES and TMDL regulations. The simulations provide a better understanding of the flow and transport within the watershed on a regional scale. Simulations were conducted using historic observations of rainfall, evapotranspiration, and contaminant distribution within the watershed to determine transport patterns within the domain. During FY11, the focus was on extending the sedimentation module to include the entire EFPC and Bear Creek. This research has also provided stochastic modeling of the system and has included an analysis of the spatial and temporal patterns as a result of the stochastic variations of selected properties of the sub domain.

RESULTS AND DISCUSSION

While keeping all other parameters constant, one parameter at a time was varied within the verified range and the computed TSS and mercury concentration timeseries at the selected key stations (EFK 18, EFK 14, and EFK 6) compared with historically recorded timeseries. Figure 1 below depicts this concept. The value for the parameter was selected based on a least mean square error analysis on the computed and recorded timeseries. This process was then repeated for the rest of the parameters and the best combination of values for the significant parameters that provide the least mean square error between the computed and observed timeseries selected.

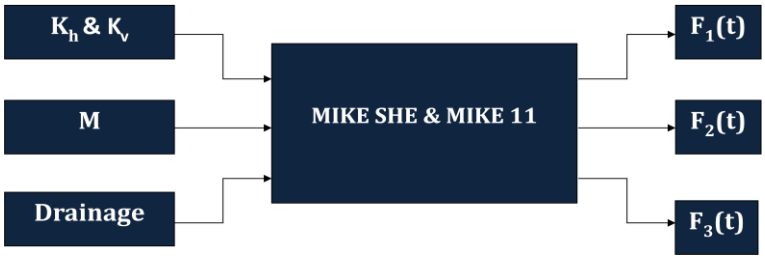

Figure 1. Simulation conceptual diagram.

A variety of simulations have been executed with the purpose of calibrating the recently modified model for Manning's number. Simulations were executed for 1 year (2000 – 2001) and pertain only to the water movement within the system. Point sources from the Y-12 Model were added to the boundary file with their respective time series for flow and mercury transport. The hydraulic conductivity settings remain spatially uniform. Manning's number is the only variable. The variability in time of discharge (m^3/s) for simulations EFPC001 (Manning's at 100% of original), and EFPC004 (at 25%) shown in comparison to observed data from Station 17 was analyzed. The general base flow is observed in all; the extent of the peaks appears to be slightly accentuated by a decrease in Manning's number.

CONCLUSIONS

Extension of the Water Quality and Sedimentation Module

The sedimentation module which was developed for the UEFPC (the section of EFPC upstream of Station 17) was extended to include the entire EFPC down to EFK 6 and Bear Creek. The sedimentation module provides the coupling between the flow and transport within the creek and the overland flow and was used to analyze the significance of floodplain contamination downstream EFPC. Fifty-two outfalls were added to the EFPC model. Van Genuchten parameters for the unsaturated flow in the aquifer were updated. The model was reconfigured following the incorporation of the sedimentation module and outfalls. A series of numerical simulations have been performed using a range of Manning's number values, threshold run-off water depths, and drainage coefficients to calibrate the flow for the period of 2000 – 2008.

MATLAB scripts were prepared for the statistical analysis of observed and computed data. Laboratory and field data on surface water level and discharge, groundwater level, and mercury contamination in soil, groundwater and surface water were obtained from OREIS database. Observed and computed data were organized and incorporated into the numerical model for calibration and verification purposes.

EFPC Model Uncertainty and Sensitivity Analysis

The probabilistic distribution of critical subsurface parameters, such as hydraulic conductivity, porosity, pore size distribution, and storage coefficients were defined specifically for the karst areas. MATLAB's statistical toolbox and scripting tools were used to develop a series of functions for a random generation of distributed hydrologic parameters based on a selected probability density function and statistical parameters. Randomly generated grids were created using the MATLAB toolbox for the uncertainty analysis. Numerical simulations were then conducted for each randomly generated input grid. The output was used to generate daily timeseries for selected hydrological, fate and transport parameters, including groundwater flow velocity at selected points, potential head at selected points, rate of mercury absorption at various locations, concentrations of total mercury at the key stations (EFK 6, EFK 14, EFK 18), total mercury load at the key stations, and flux exchange between subsurface and surface. The simulations were used to determine the model uncertainty in terms of stochastic variations of input parameters. Graphical plots of the variation of the output parameters were then used to present the results of the sensitivity analysis, identifying significant parameters and a range of

certainty for the model. The simulations showed that the model had greatest sensitivities for hydraulic conductivities of the layer closest to the surface and each of the multiple distribution coefficients implemented to reflect mercury exchange between different model subdomains.

FUTURE WORK

FIU will use the numerical model of EFPC to determine the impact of hydrologic cycle, the transport overland and in surface water and rivers, sediment transport and reactions, and mercury exchange with sediments. The major objective of this task is to provide analysis of the coupling between hydrology and mercury transport within the context of decreasing the risk of D&D and remediation activities. The major deliverable of this task will be numerical and stochastic analysis of observed and computed time series for flow and contaminant concentration for NPDES-regulated outfalls within the watershed. Model simulations will be used to account for a range of hydrological impacts related to remediation alternatives plans, including:

Subtask 1.1: Statistical analysis of observed data and development of timeseries, probability exceedance curves, and probability distribution models of flow, concentration and load data that integrates already downloaded data, and new data that will be obtained from DOE contactors with the support of ORNL personnel. The data will include groundwater well monitoring, concentrations in groundwater wells, outfall flow, and concentration and load data. The task will also provide a refinement of the existing EFPC model by inclusion of historical outfall flow data for the area extending from WEMA to Station 17 to determine the effects of precipitation and stormwater drainage on the flux of mercury into EFPC. The deliverable of this subtask will include timeseries, probability exceedance curves, load exceedance curves, probability distribution models for each monitoring point and a report. The subtask will provide support for the team developing the mercury conceptual model and will provide considerably better estimates for the stochastic nature of mercury fluxes within the EFPC domain.

Subtask 1.2: Reduction of model parameter uncertainty (i.e., uncertainty analysis) for existing EFPC model via a series of probability distributions derived from running multiple simulations for selected specified parameters. In the previous scope the major variables were the hydraulic conductivities of each of the five geological layers. The current scope will focus on analysis of the upper layer and the leakage factor between the creek and subsurface media, and on the exchange of flow and mercury between the creek and the river. Uncertainty analysis will be provided for the parameters governing the distribution of mercury species within pore water, sorbed mercury within pores, sorbed mercury on suspended particles and "free" mercury (dissolved and chelated mercury species). The major variable that will be analyzed will be total mercury considering that all regulatory documents are expressed as total mercury. The work in this subtask will help to improve the confidence in the predictive capability of the watershed-scale model. The deliverables from this task will include analysis of the uncertainties associated with the parameters governing exchange of mercury within each of the subdomains (mercury migration in the vadose zone during flooding, pore space in the sediments, sorption on sediments, sorption on particles, and aqueous species). All research will be collected, analyzed and documented in a technical report sent to DOE.

Subtask 1.3: Re-creation of the existing ORNL stormwater management system layout via a numerical surface water one dimensional model (SWMM or similar) to provide a better understanding of the flow patterns on-site, including flow rates as a function of rainfall intensity and the fraction of drainage volumes and rates reaching each outfall. The objective is to create a detailed surface water flow and contaminant transport model for the ORNL area using XPSWMM, incorporating flow data and other significant drainage system parameters, initially starting with a smaller model for the ORNL area. This would be a benchmark study to be extended to the Y-12 NSC (once reviewed and accepted by ORNL and the site). The deliverable of this subtask will be a calibrated and validated drainage model that will provide detailed analysis of how much water reaches each outfall and the source of the water based on drainage areas. By providing better understanding of the drainage system, the site will be provided with a tool that can be used to investigate the best remediation scenarios for setting up remediation priorities, e.g., helping identify the greatest contributors to mercury loads.

Subtask 1.4: Simulations of surface water flow and contaminant transport utilizing collected piezometric data for EFPC. This will facilitate calibration and validation of the existing EFPC model developed by FIU and will provide data for comparison with new measurements to be taken by ORNL in their effort to refine the existing conceptual model for EFPC. This task will be executed in collaboration with ORNL. Additionally, modifications of the flow hydrology along EFPC, including reduction of the flow augmentation, addition of a down-gradient diversion ditch, alternatives which result in reduced mercury fluxes in major outflows and simulation of flow and transport of other contaminants whose partitioning coefficients vary several orders of magnitude (including uranium and other contaminants of interest) will be investigated within this subtask.

REFERENCES

1. R. R. Turner and G. R. Southworth, "Mercury contaminated industrial and mining sites in North America: an overview with selected case studies," Springer-Verlag, pp. 89 -112, 1999.
2. Tennessee Department of Environment and Conservation, "2008 303 (d) List," Division of Water Pollution Control Planning and Standards Section, 2008.
3. F. X. Han, Y. Su, D. L. Monts, C. A. Waggoner, and M. J. Plodinec, "Binding, distribution, and plant uptake of mercury in a soil from Oak Ridge, Tennessee, USA.," Science of The Total Environment, vol. 368, no. 2-3, pp. 753-768, September 2006.
4. S. Malek-Mohammadi, G. Tachiev, E. Cabrejo, and A. Lawrence, "Simulation of Flow and Mercury Transport in Upper East Fork Poplar Creek, Oak Ridge, Tennesse," Remediation, pp. 119-131, 2012.
5. E. Cabrejo, "Mercury Interaction with Suspended Solids at the Upper East Fork Poplar Creek, Oak Ridge, Tennessee.," Florida International University, Environmental Engineering Department, Miami, Master Thesis 2010.
6. U.S. Department of the Interior. U.S. geological Survey (USGS), Mercury in the Environment, 2000, fact sheet 146-00.
7. U.S. Department of Energy (US DOE), "Record of Decision for Phase I Interim Source Control Actions in Upper East Fork Popler Cereek Characterization Area, Oak Ridge,

Tennessee," U.S. Department of Energy, Office of Environmental Management, DOE/OR/01-1951&D3.n Oak Ridge, TN, 2002.
8. U.S. Department of Energy (US DOE), "Record Decision for Phase II Interim Source Control Actions in Upper East Fork Poplar Creek Characterization Area, Oak Ridge, Tennessee," U.S. Department of Energy, Office of Environmental Management, Oak Ridge, Tennessee, DOE/OR/01-2229%D3.n Oak Ridge, 2006.
9. H. R. Sorensen, T. V. Jacobsen, J. T. Kjelds, J. Yan, and E. Hopkins, "Application of MIKE SHE and MIKE 11 for Integrated Hydrological Modeling in South Florida," South Florida Water Management District (SFWMD) & Danish Hydraulic Institute (DHI), 2012.
10. Danish Hydraulic Institute. (2012, May) MIKE by DHI. [Online]. http://www.mikebydhi.com/~/media/Microsite_MIKEbyDHI/Publications/SuccessStories/MIKE%20by%20DHI%20Success%20Story-MSHE-BrowardCounty.ashx
11. North Carolina Department of Environment and Natural Resources, "Total Maximum Daily Load for Mercury in the Cashie River, North Carolina, Public Review," North Carolina Department of Environment and Natural Resources, 2004.
12. N. Gandhi et al., "Development of mercury speciation, fate, and biotic uptake (BIOTRANSPEC)," Environmental Toxicology and Chemisty, vol. 26, pp. 2260-2273, 2007.
13. Danish Hydraulic Institute (DHI), MIKE 11 Short Descriptions, 2008.
14. Danish Hydraulic Institute (DHI), MIKE SHE Reference Manual, 2008.
15. Danish Hydraulic Institute, ECOLAB Reference Manual, 2008.
16. S. Long, "An Integrated Flow and Transport Model to Study the Impact of Mercury Remediation Strategies for East Fork Poplar Creek Watershed, Oak Ridge, Tennessee," Florida International University, Environmental Engineering Department, Miami, Master Thesis 2009.
17. Oak Ridge national Laboratory (ORNL), "Conceptual Model of Primary Mercury Sources, Transport Pathways, and Flux at the Y-12 Complex and Upper East Fork Poplar Creek," Oak Ridge, Tennessee, ORNL/TM-2011/75, 2011.
18. R. R. Truner, C. R. Olsen, and W. J. Jr. Wilcox, "Environmental Fate of Hg and 137 Cs Discharged from Oak Ridge Facilities," in CONF-8406143-2, 1985.
19. U.S. Department of Energy (US DOE), "2009 Remediation Effectiveness Report for the U.S. Department of Energy Oak Ridge Reservation, Oak Ridge, Tennessee," U.S. Department of Energy Office of Environmental Management, Oak ridge, Tennessee, 2009.
20. G. R. Southworth et al., "Controlling Mercury Release from Source Zones to Surface Water: Initital Results of Pilot Tests at the Y-12 National Security Complex," 2009.
21. G. R. Southworth, M. Greely, M. Peterson, K. Lowe, and R. Kettelle, "Sources of Mercury to East Fork Poplar Creek Downstream from the Y-12 National Security Complex: Inventories and Export Rates.," Oak Ridge National Laboratory, Oak Ridge, 2010.

TASK 2: SIMULATION OF TMDL FOR THE ENTIRE EFPC

INTRODUCTION

Section 303(d) of the 1972 Clean Water Act (CWA) [1, 3] requires each state to list those waters within its boundaries for which technology-based effluent limitations are not stringent enough to protect any water quality standard applicable to such waters. Listed waters are prioritized with respect to designated use classifications and the severity of the pollution. In accordance with this prioritization, states are required to develop Total Maximum Daily Loads (TMDLs) for those waterbodies that are not attaining water quality standards. State water quality standards consist of designated uses for individual waterbodies and appropriate numeric and narrative water quality criteria protective of the designated uses. The TMDL process establishes the maximum allowable loadings of pollutants for a waterbody that will allow the waterbody to maintain water quality standards. The TMDL may then be used to develop controls for reducing pollution from both point and non-point sources in order to restore and maintain the quality of water resources [2]. Application of TMDLs has been broadened significantly in the last decade to include many watershed-scale efforts.

The East Fork Poplar Creek (EFPC), bordering the Y-12 National Security Complex (Y-12 NSC) and located inside of the Oak Ridge Reservation (ORR), has recently been identified on the Final 2008 303(d) List by the Tennessee Department of Environment and Conservation (TDEC) [13] as an impaired waterbody not supporting designated uses due to contamination by mercury, PCBs, nitrates, and phosphates. Contamination by E. Coli has yet not been investigated. EFPC lies entirely inside the state of Tennessee, shared by Roane and Anderson counties. The waterbody is of moderate priority for the development of a TMDL for mercury.

To support the TMDL development for the EFPC, a need for an integrated, receiving water, hydrodynamic and water quality modeling system was identified. Models are frequently used to support development of TMDLs—to estimate source loading and evaluate loading capacities that will meet water quality standards. The modeling demonstrates the allocation of point and non-point source loads that would result in meeting the water quality standards. This requires that point and non-point sources be evaluated as separate sources so that they can be simulated under various loading scenarios.

The detailed report found in APPENDIX T2-001 documents the application of a hydrology and transport model developed to support the TMDL analysis of mercury for the EFPC watershed. The integrated surface/subsurface model was built using the numerical package, MIKE (MIKE-11 coupled with MIKE-SHE and ECOLAB), developed by the Danish Hydraulic Institute (DHI). The MIKE package has been identified by EPA as an effective model to support TMDL analysis. The report also presents details of TMDL development for the entire East Fork Poplar Creek (EFPC). The main pollutant sources in the creek were identified as stormwater and industrial wastewater outfalls (point sources) and contaminated streambed sediments, floodplain and streambank soils (non-point sources). The numerical model was used to develop flow and load duration curves at several stations along the creek.

RESULTS AND DISCUSSION

This work is based on the primary hypothesis that the concentration of total mercury in the hydrologic subdomains (surface, subsurface, streams and sediments) and the transport of mercury species are the governing factors for the levels of mercury in fish from East Fork Popular Creek (EFPC). The numerical model described in this report covers sections of the Upper East Fork Poplar Creek (UEFPC) and Upper Bear Creek (UBC) watersheds and provides a tool for analyzing the coupling between watershed hydrology and transport of total mercury. An average mercury concentration was computed from summing the total contribution of mercury mass from each outfall and dividing by the total flow volume. Comparison of the concentrations measured at Station 17 and those calculated from the average mercury concentration from all outfalls shows that measured mercury peaks are considerably higher than the averages computed from all outfalls. This indicates that sediment transport in surface water is important to consider for modeling. The exchange of mercury between sediments and stream flow was accounted for by implementing a sedimentation module. The model was calibrated using observed data of flow, stage, and mercury concentrations in soil, surface water, groundwater and sediments at Station 17. The modeling work focused on analyzing the results for the period 1/1/2000-12/31/2008 for which the flow augmentation strategy of adding an average of 2.4 million gallons per day (MGD) was already in place.

To analyze the impact of hydrological events on mercury transport, the computed load duration curves at Station 17 were compared with the historical load duration curves to determine the percent change of mercury discharges downstream of Station 17. The percent change was computed based on the ratio between the mean values of the computed load duration curves versus the mean values of observed load duration curves. Simulations were conducted for selected events. For each simulation alternative, multiple tests were conducted to determine the uncertainties (defined as one standard deviation) of the computed load for selected parameters for which the model had high sensitivity (defined as rate of change of the modeling output to rate of change of parameter input).

The most significant factor which determined the efficiency of source elimination (soil excavation) is the soil/water partitioning coefficient, which describes the linear equilibrium between aqueous and soil concentration. The magnitude of the partitioning soil/water coefficient has significant impact on remedial actions related to soil excavation on surface water since it is correlated to the retardation factor and more specifically, the velocity of the plume. Due to its high affinity to forming complexes with solid species, mercury has a large retardation factor, the significance of which is that source removal in the vicinity of the stream will have greatest effect where there is exchange between the river and subsurface domain. Contaminant reduction at the small sources of highest contamination can therefore be an effective short-term remediation strategy for immediate reduction of downstream contamination. The majority of mercury in soil is present as HgS(s) which is a mineral of low solubility. HgS(s) can become mobilized by complexing with organic ligands naturally occurring in soil and migrate to surface waters. Therefore, closing off the outfalls (by plugging and abandonment) eliminates this pathway to UEFPC. Migration of HgS complexes in groundwater occurs to a lesser degree in low permeability soils with high organic content and high distribution coefficients. Therefore, removing the outfalls is effective in hydrologic isolation of mercury sources in soil and

groundwater above the shale. Simulations for reducing the flow augmentation showed that concentrations of total mercury increased less than 30% as there was less dilution. Elimination of augmented surface water flow reduced infiltration of contaminated surface water and no longer recharged the groundwater system along the creek. The total flow of water needing potential treatment in the watershed is reduced by 0.48 MGD.

Three major sources of mercury to EFPC include: (i) water-borne mercury from stormwater and industrial wastewater outfalls; (ii) land surface and shallow groundwater; and (iii) streambed sediment and streambank. Considering the transport pathways to EFPC including outfalls, groundwater flow and surface sheet flow, a conceptual model has been developed for the mercury transport in EFPC watershed as shown in **Figure 2.**

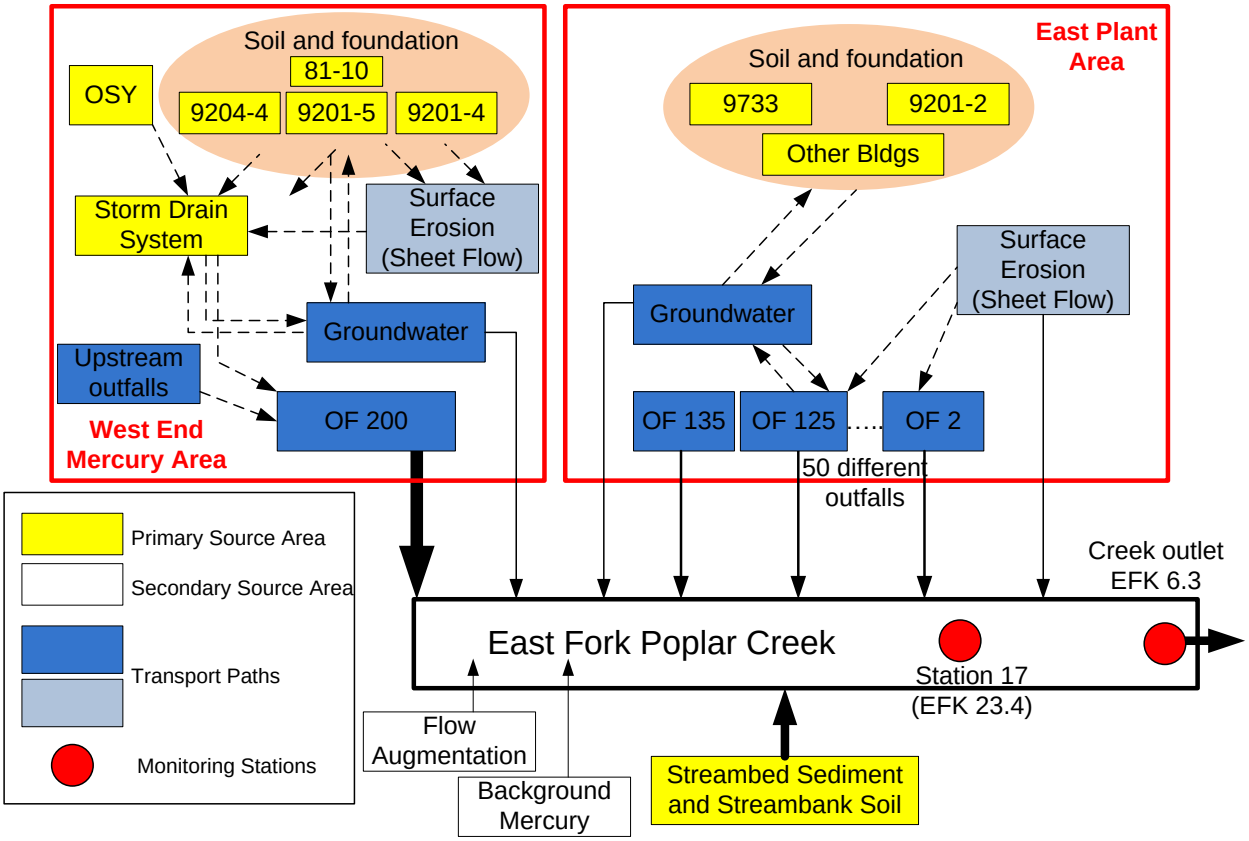

Figure 2. Conceptual model of EFPC.

SEDIMENT TRANSPORT CALIBRATION

The numerical model was calibrated for the sediment transport using an extensive collection of historical records of total suspended solids (TSS) in the creek water recorded at key stations along EFPC. For calibration purposes, four parameters were considered in the ECOLAB module that directly affect the concentration of TSS in the water column; critical current velocity (Vc),

settling velocity (Vs), resuspension rate (RR), and particle production rate (PPR). Simulations were performed for a range of these parameters and sensitivity and uncertainty analyses conducted for each parameter from which the best values were selected. The sensitivity analysis on these parameters is shown in **Figure 3**.

In **Figure 4**, the recorded TSS load is compared with the numerical simulation results at Station 17 (EFK 23.4). The TSS load is calculated by multiplying the concentration of TSS by the discharge at a particular time.

MERCURY TRANSPORT CALIBRATION

The most important parameters in calibration of mercury transport were the carbon partitioning and diffusive transport coefficients, as well as the effective parameters on sediment transport which provided earlier. The computed mercury concentration at Station 17 (EFK 23.4) is compared with the recorded timeseries in **Figure 5**.

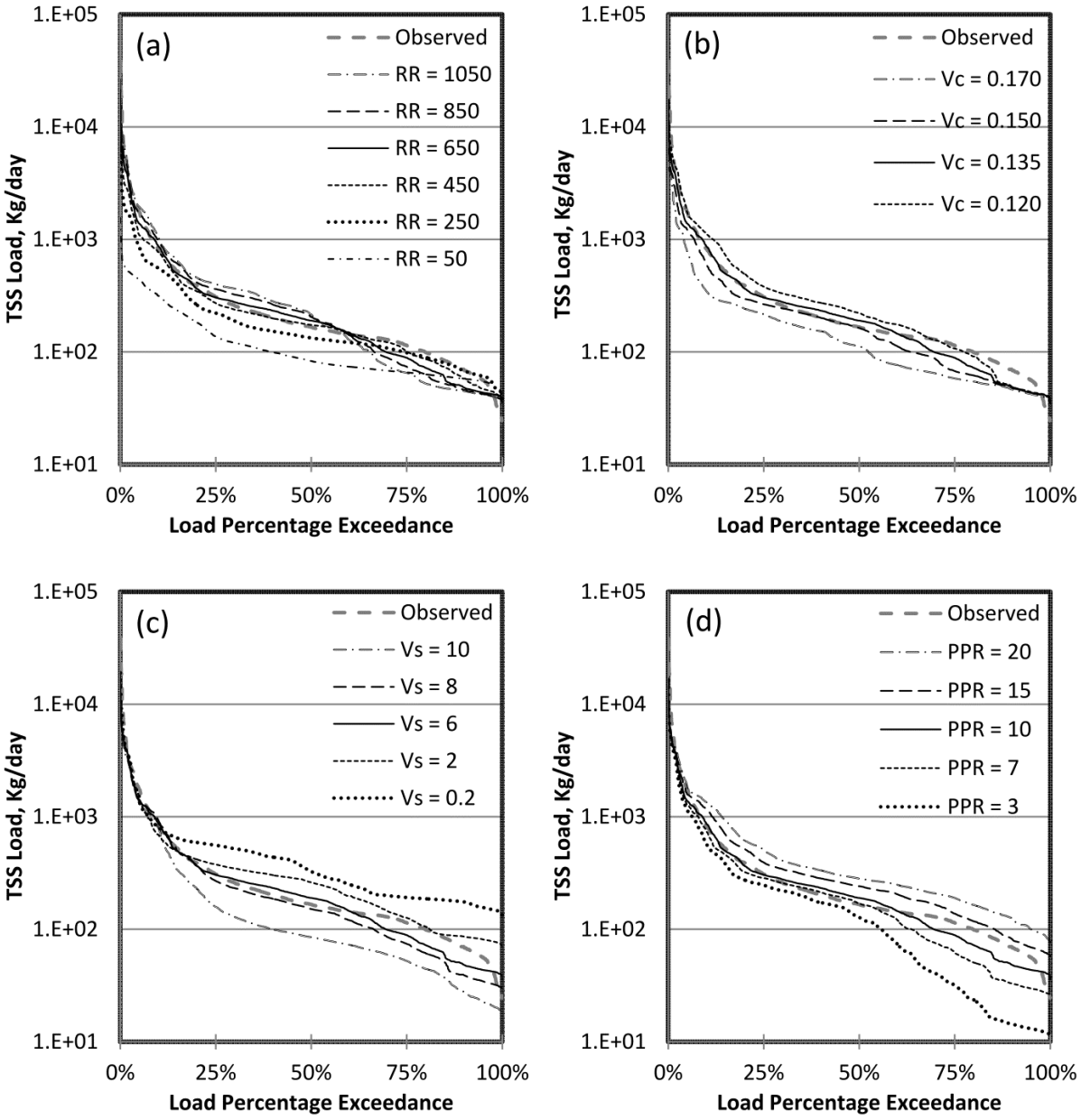

Figure 3. Sensitivity analysis on TSS load for effective parameters: (a) resuspension rate, g/m2/day, (b) critical current velocity, m/s, (c) settling velocity, m/day, (d) particle production rate, g/m2/day.

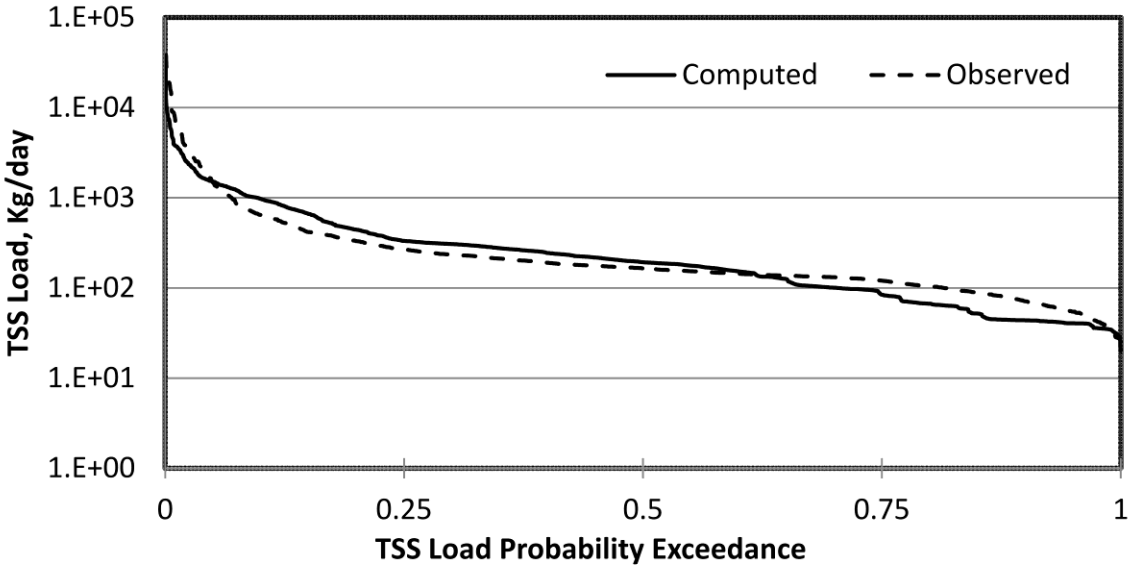

Figure 4. computed and recorded TSS load at Station 17 (EFK 23.4).

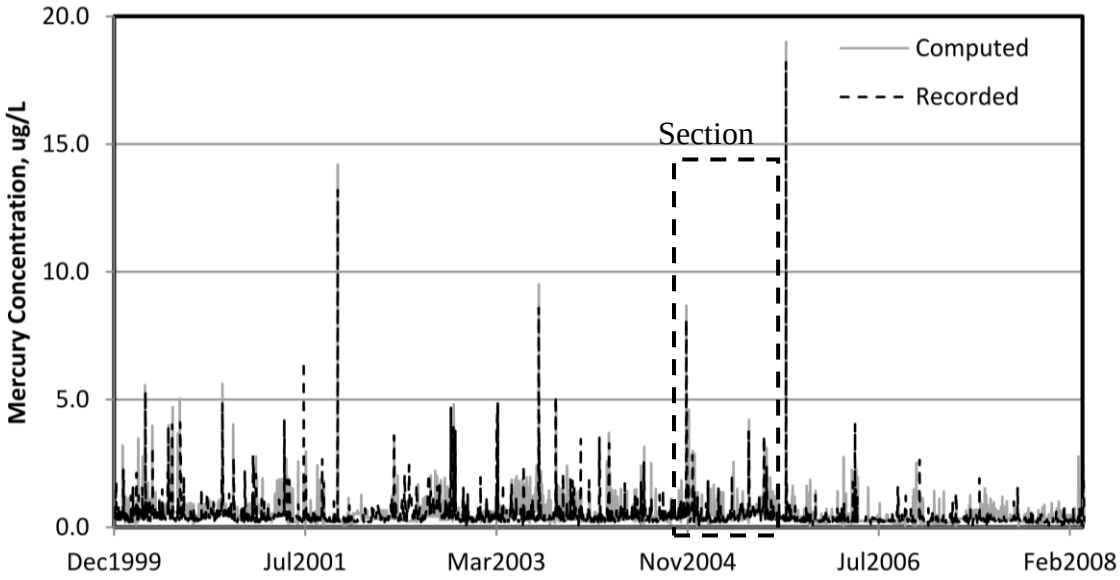

Figure 5. Comparison of computed and observed mercury concentration at Station 17 (EFK 23.4).

A section of **Figure 5** is shown in greater detail in **Figure 6**. The figure shows a close match between observed and computed mercury concentration at Station 17 (EFK 23.4).

Based on the numerical results, it is clear that most of the mercury in the creek is in a form that is sorbed to the suspended particles. As shown in **Figure 7**, more than 75% of the total mercury is adsorbed and only 25% is in the form of dissolved mercury. This was confirmed by field investigations performed by ORNL in the latter 2000's. This highlights the significance of suspended particles in affecting the total mercury concentration in the creek.

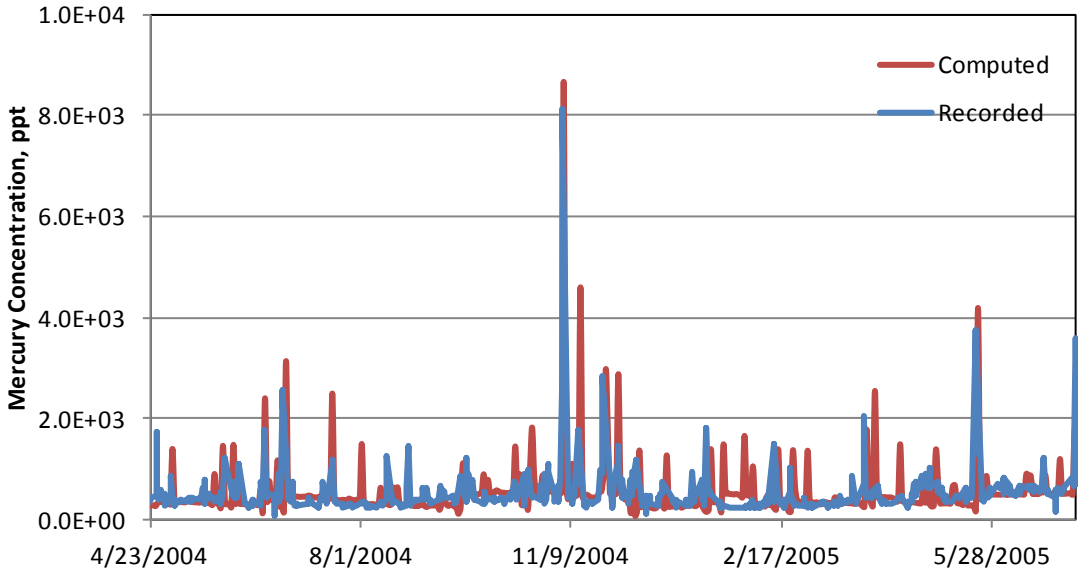

Figure 6. Timeseries of computed and observed mercury concentration (section A shown in Figure 5).

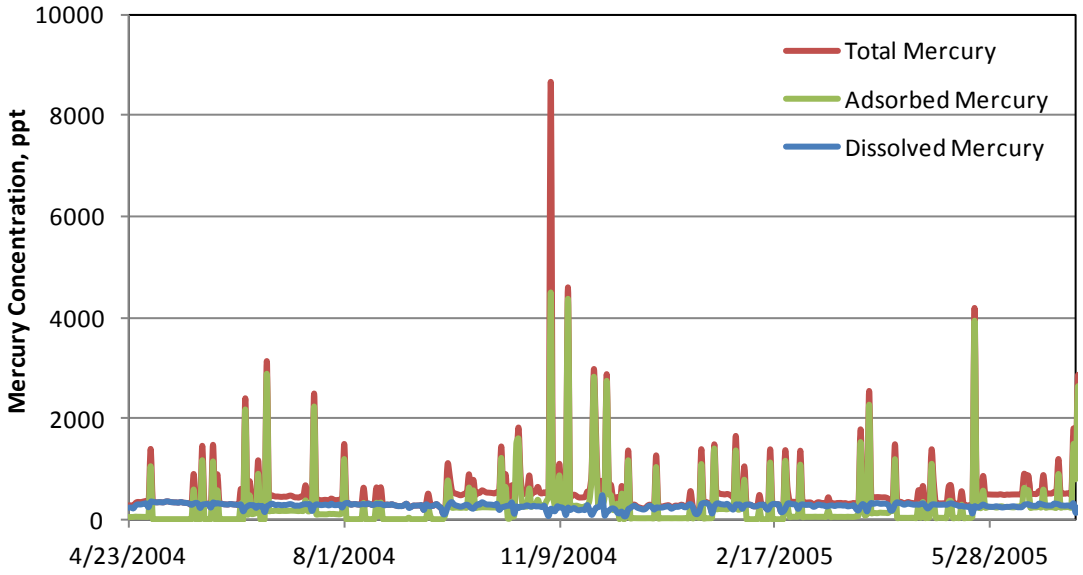

Figure 7. Comparison between numerical results for the adsorbed and dissolved mercury timeseries in the creek at Station 17 (EFK 23.4).

There is limited water quality data available at Station EFK 6.3 in EFPC. The computed timeseries is compared with the few data points available for mercury concentration at EFK 6.3 in **Figure 8**.

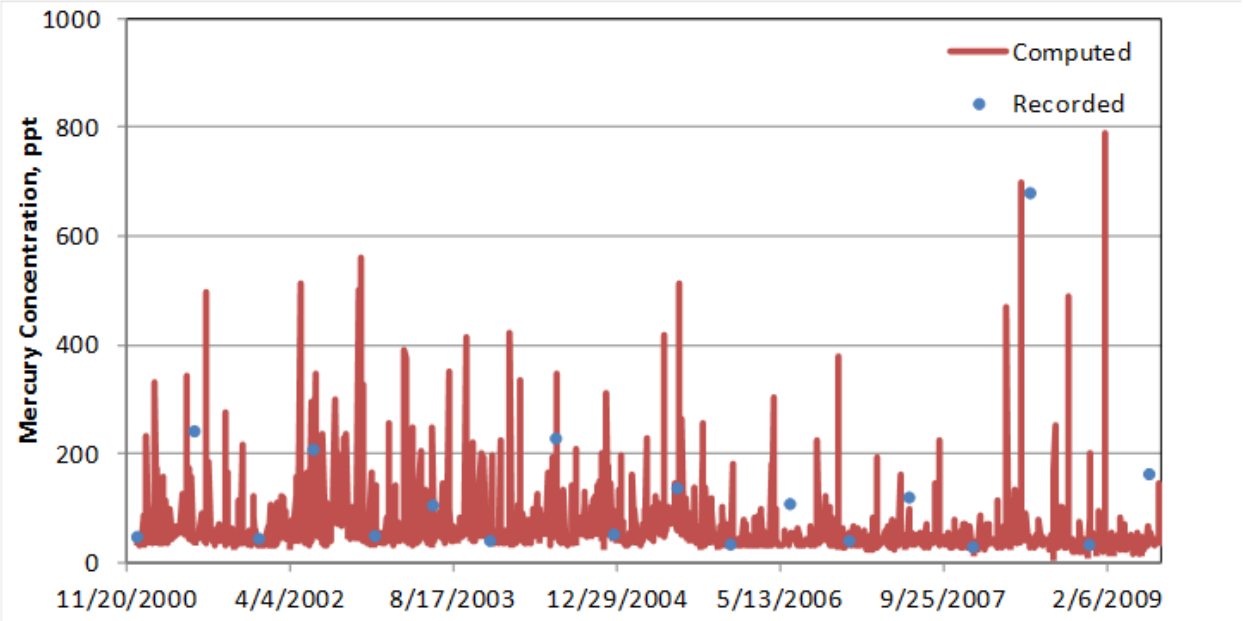

Figure 8. Timeseries of computed and observed mercury concentration at EFK 6.3.

In order to assess the significance of sediment transport on the fate and transport of mercury within UEFPC, numerical simulations were performed for two different cases; with and without consideration of sediment-mercury interactions. Computed mercury load duration curves at Sta. 17 for the period 2000-2009 were compared with corresponding historical records for both scenarios (**Figure 9**).

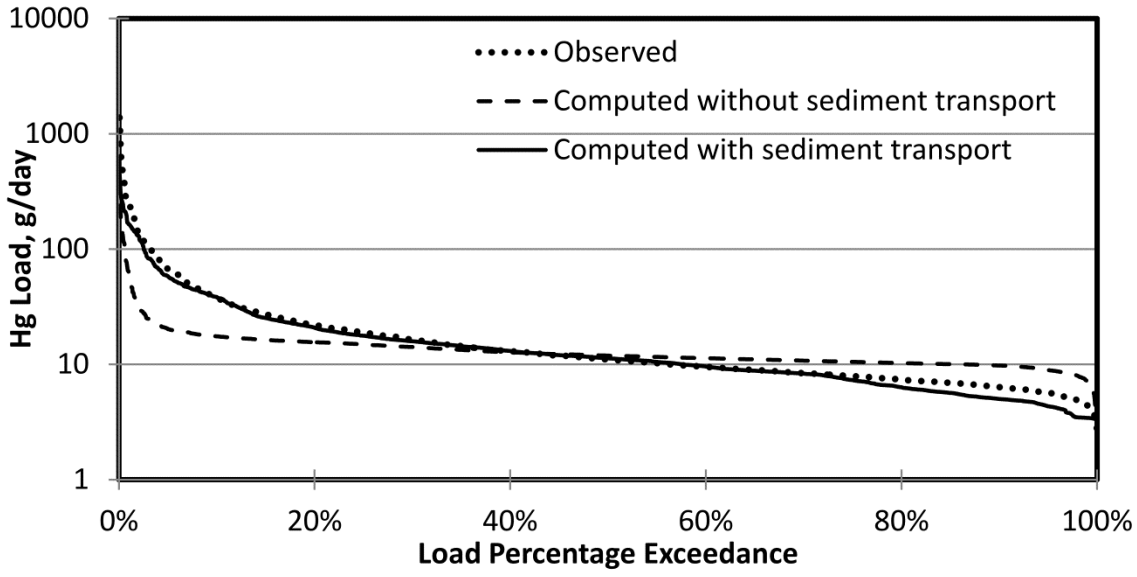

Figure 9. Mercury load duration curves at Station 17 (EFK 23.4).

As shown in **Figure 9**, sediment-mercury interactions significantly affect the concentration of mercury recorded at Station 17 (EFK 23.4). Higher velocity during the wet seasons increases the shear stress on highly contaminated streambed sediments, and therefore, through a process often called "colloidal transport", resuspends more mercury-laden fine particulates.

WATER QUALITY ASSESSMENT OF EFPC

Mercury concentration data for the stations along EFPC were extracted from the OREIS database. After an initial study of the data, stations with less than 3 data points and stations with data for a very short period of time (less than a few months) were removed from the database, resulting in14 stations along EFPC being selected for use in verification of the numerical simulations and performing TMDL analysis. The 14 stations are shown in **Figure 10.**

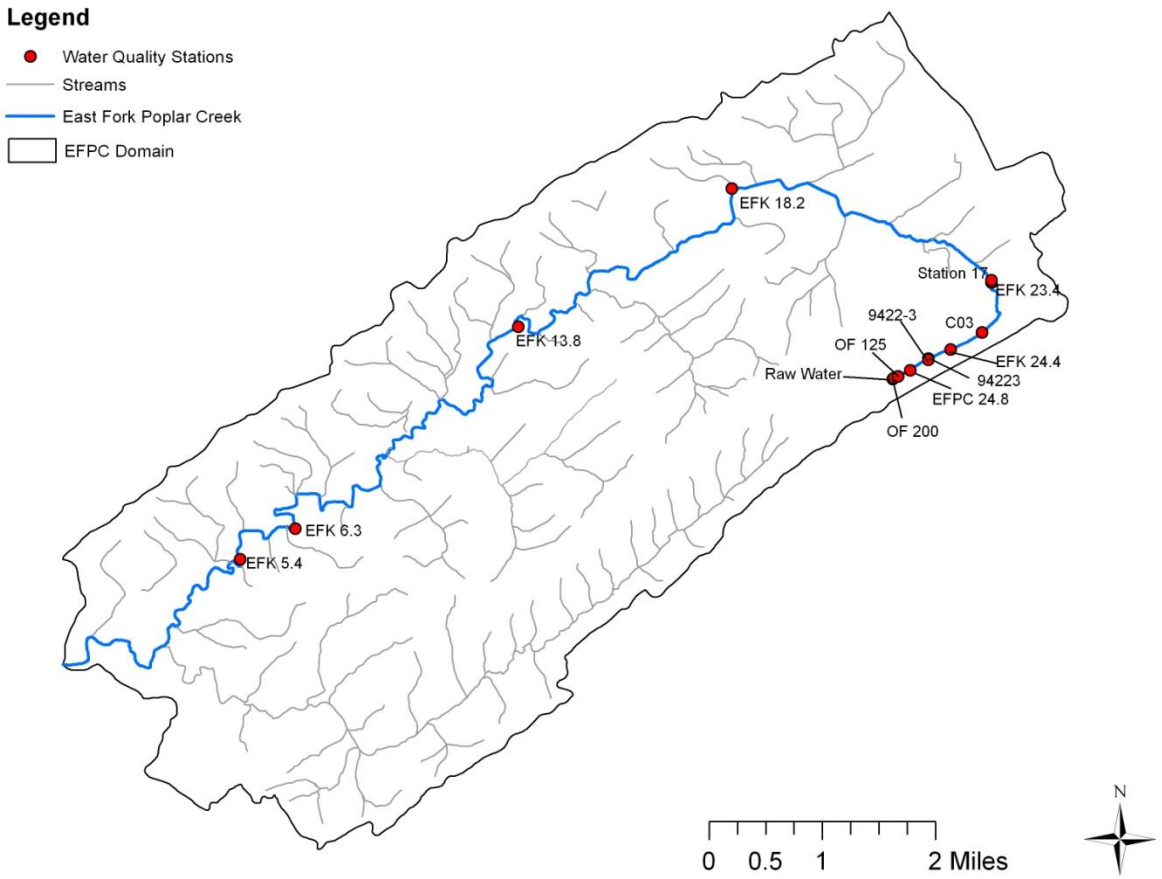

Figure 10. Water quality monitoring stations along EFPC.

The Raw Water station shown in **Figure 10** at the outset of the creek is uncontaminated management water which was purchased by the Y-12 NSC facility from the city of Oak Ridge in 1997 to maintain a daily average flow of 7 MGD at Station 17 in accordance with the 1996 NPDES permit (TN0002968). The augmented water is pumped from the Melton Hill Lake on the Clinch River and discharged to the creek adjacent to Outfall 200 (OF200) at a constant rate of 4.5 MGD.

Examination of the water quality data shows exceedances of the 50 ppt maximum mercury concentration standard at all of the monitoring stations along EFPC. Characteristics of water quality data following the data analysis are summarized in **Table 1**.

Table 1. Summary of Water Quality Monitoring Data

Station	Data Pts.	Date Range	Min., ppt	Mean, ppt	Max., ppt	Exceed WQ Max. Target Pts. (50 ppt)
OF125	347	12/00 – 12/10	200.6	704.8	27,777	347
94223	1353	01/92 – 08/10	200.5	1009.6	15,000	4308
EFK 24.4	20	05/96 – 12/10	235.6	456.5	1927.2	12
EFK 23.4	4308	01/92 – 12/10	200.7	741.6	11,000	347
EFK 18.2	12	11/96 – 12/10	206.0	294.1	430.4	1353
EFK 13.8	10	11/96 – 12/10	213.8	323.3	458.4	20
EFK 6.3	9	12/00 – 12/10	201.4	442.6	1346.2	4308

Annual average concentrations of total mercury at different stations are summarized in **Table 2**. Values show a continuous decrease in concentration following the remedial actions that started since the mid 1990's; however, there is an increase after 2002 in OF125, EFK 24.4, EFK 23.4, and 92334. This might be the consequence of augmenting the flow at OF200 which resulted in resuspension of highly contaminated bed sediment to the creek water as reported in field investigations. The average total concentration of mercury at all stations downstream of OF200 however, is still above the State of Tennessee water quality standard of 51 ppt. Variations of total mercury concentration at different stations along the creek from 1992 to 2010 are compared in **Figure 11.**

Table 2. Concentrations of Total Mercury at Different Stations along EFPC in ppt

YEAR	OF 125	94223	EFK 24.4	EFK 23.4	EFK 18.2	EFK 13.8	EFK 6.3
1992		1159.87		1498.59			
1993		1075.86		1205.39			
1994		1166.38		1231.82			
1995		1134.52		1292.94			
1996		977.46		768.31	206.00		
1997		648.46		740.56			
1998		637.78		1072.99			
1999		525.00		647.54			
2000		500.00	316.00	543.13			
2001		339.64	341.90	474.75	370.95	392.09	465.67
2002	508.20	574.77	423.40	615.55	282.90	346.20	400.30

2003	1787.15	974.15	1168.35	521.73	209.90		
2004	886.78	572.43	382.40	529.73	430.40	450.40	443.00
2005	688.10	591.10	461.95	526.38	415.00	389.95	251.50
2006	313.16	1165.50	348.93	347.30	280.70	225.25	201.40
2007	285.43	1165.50	312.90	324.98	279.00	230.30	223.50
2008	343.92	1070.00	259.05	383.47	339.05	458.40	1346.20
2009	618.59	552.50	484.93	374.47	236.73	280.00	315.05
2010	395.18	1010.00	365.00	541.03	230.70	234.80	336.70

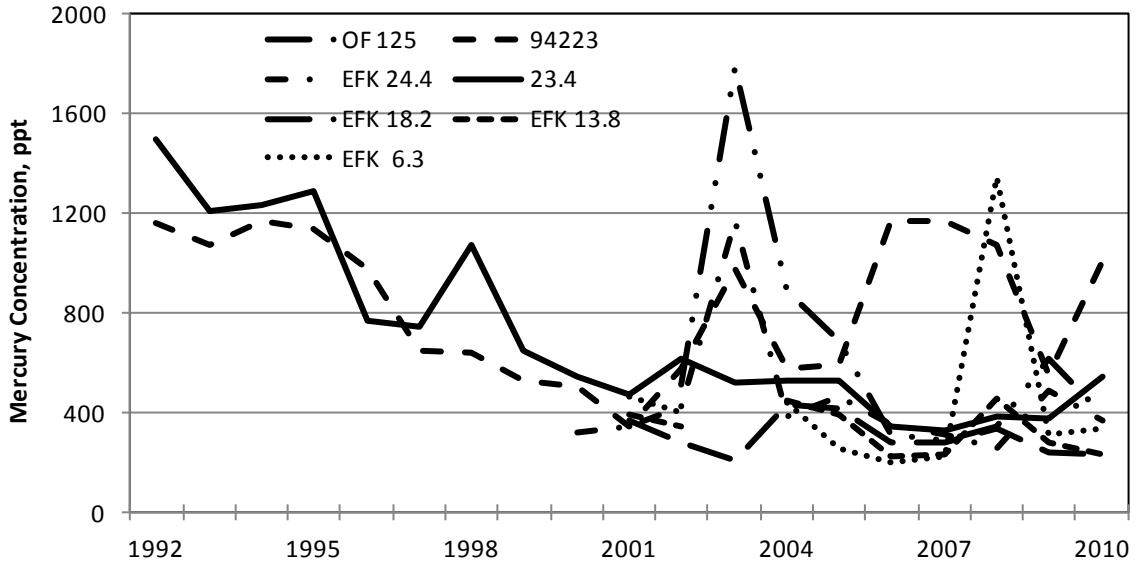

Figure 11. Variation of average mercury concentration at the stations along EFPC.

Total Maximum Daily Load (TMDL) is a regulatory term defined in section 303 (d) of the 1972 U.S. Clean Water Act (CWA) as the maximum amount of a pollutant that a body of water can receive while still meeting water quality standards. Alternatively, a TMDL is defined as the allocation of a particular pollutant as acceptable to receiving waters. This includes both point and non-point pollutant sources within a watershed. The TMDL concept has long been used by the United States Environmental Protection Agency (EPA) and state environmental agencies (such as the Tennessee Department of Environment and Conservation [TDEC] in the case of Oak Ridge watersheds) in implementing the CWA by establishing maximum pollution limits for industrial wastewater dischargers. EPA published regulations in 1992 establishing TMDL procedures.

A TMDL is the sum of all point source loads (Waste Load Allocations, WLAs), non-point source loads and natural background (Load Allocations, LAs), with a margin of safety (MOS) that takes into account any uncertainty about the relationship between pollutant loads and receiving water quality, and can be generically described as:

$$TMDL = \Sigma WLA + \Sigma LA + MOS \quad (1)$$

The objective of a TMDL analysis for EFPC is to allocate loads among pollutant sources that are contributing to the watershed impairment, and thereby, to implement appropriate control measures to achieve water quality standards. This document describes TMDL, Waste Load Allocation (WLA), and Load Allocation (LA) development for EFPC which has been identified as impaired due to mercury on the Final 2006 303(d) List. In this document, TMDLs are expressed as the percentage reduction required to maintain the desired mercury concentration target levels in fish tissue. WLAs and LAs are also expressed as required percentage reductions in mercury loading.

The TMDL for EFPC was developed based on the analysis of water quality data. Concentration of mercury in the water of EFPC from 1992 was examined, but load reductions were estimated based on more recent data (1992 to the present). The percentage load reduction required to decrease the mercury concentration in water from the "mean + 95% confidence interval" to the desired target level was calculated at each sampling location. Load reductions ranged from 84.6% to 95.1%. The highest percentage load reduction (at location 92334) was selected as the TMDL for the entire waterbody. A summary of monitoring data of mercury concentration in water from 1992 to 2010 is presented in **Table 3**.

Table 3. Analysis of Mercury Concentration in Creek Water (2000 - Present)

	OF125 ppt	C11 ppt	92334 ppt	EFK 23.4 ppt	EFK 24.4 ppt	EFK 18.2 ppt	EFK 13.8 ppt	EFK 6.3 ppt
Number of samples	347	108	1353	4308	20	12	10	9
Minimum	200.6	210.0	200.5	200.7	235.6	206	213.8	201.4
Mean	704.85	389.02	1009.58	741.64	456.52	294.15	323.26	442.59
Standard Deviation	1861.16	413.86	693.53	780.56	356.82	77.72	95.42	351.60
95% CI	195.82	78.05	36.95	23.31	156.38	43.98	59.14	229.71
Mean + 95% CI	900.68	467.07	1046.53	764.95	612.89	338.13	382.41	672.30
90% CI	164.34	65.50	31.01	19.56	131.24	36.90	49.63	192.78
Mean + 90% CI	869.20	454.52	1040.59	761.20	587.75	331.06	372.90	635.37
Target	51	51	51	51	51	51	51	51
%Reduction from 90%	94.1%	88.8%	95.1%	93.3%	91.3%	84.6%	86.3%	92.0%
%Reduction from 95%	94.3%	89.1%	95.1%	93.3%	91.7%	84.9%	86.7%	92.4%

Note: The % Reduction from 95% is calculated as follows: % Reduction = [(Mean + 95% CI) - Target] / (Mean + 95% CI).
The % Reduction from 90% is calculated in a similar manner.

MARGIN OF SAFETY

There are two methods for incorporating MOS in TMDL analysis: a) implicitly incorporate the MOS using conservative model assumptions; or b) explicitly specify a portion of the TMDL as the MOS and use the remainder for allocations. For development of the mercury TMDL in EFPC, an implicit MOS was utilized for determination of WLAs and LAs. The conservative assumption is that the TMDL was selected based on the percentage load reduction from the worst-case stretch of EFPC (Station 92334). This approach assumes that the mercury concentration is the same along EFPC and equals the highest concentration recorded at OF125.

DETERMINATION OF TMDL, WLAS AND LAS

Mercury load reductions were calculated for impaired segments of EFPC based on an analysis of mercury concentration in water. WLAs and LAs were determined based on currently available information. WLAs for existing STPs are equal to their existing NPDES permit limits. No additional load reduction is required at this time. Based on currently available data, treated wastewater and groundwater from the Y-12 facility are the only known point sources for mercury in the EFPC watershed. Therefore, a WLA equal to the TMDL should be assigned to the Y-12 facility. Due to lack of adequate data regarding non-point sources, a LA equal to the TMDL has also been assigned. TMDL, WLAs, and LAs are summarized in the table below.

Table 4. TMDL, WLAs, and LAs for EFPC in the Lower Clinch River Watershed

Waterbody ID	Impacted Waterbody	Miles Impaired	TMDL % Reduction	WLAs % Reduction	Las % Reduction
TN06010207026 – 1000	EFPC (from Clinch River embayment to Gum Hollow Rd.)	9.7	95.10%	95.10%	95.10%
TN06010207026 – 2000	EFPC (from Gum Hollow Rd. to headwaters)	11.3	95.10%	95.10%	95.10%

FLOW DURATION CURVES

As a first step in developing load duration curves, flow duration curves weregenerated. Flow duration analysis provides the cumulative frequency of historic flow data over a specified period for a particular location. A flow duration curve relates flow values to the percent of time those values have been equaled or exceeded. This includes the following steps.

EXTRACTING THE HISTORICAL FLOW DATA

Flow data for riverine systems in the United States is available from a number of sources including the United States Geological Survey (USGS), Water Management Districts (WMDs), and county, city or privately operated gauges. EFPC flow data was mainly obtained from the OREIS database (USGS gauges) provided by Bechtel Jacobs for key stations. The key stations along the creek include Station 17 (EFK 23.4), EFK 18.2, EFK 13.8, and EFK 6.3.

Flow data will be estimated for the other key stations for which there is no flow data availabl. There are two different ways of performing this estimation, (i) using flow data of a similar representative creek, or (ii) using rainfall/runoff models to estimate the flow.

FLOW DATA ANALYSIS

Before using flow data obtained from the OREIS database for the load duration analysis, a preliminary data analysis was conducted. This started with simple graphical plots of flow data to evaluate the completeness and consistency of the data visually. Statistical characteristics of flow data at OF125, EFK 24.4, EFK 23.4, EFK 18.2, EFK 13.8, and EFK 6.3 are summarized in **Table 5** for the period of 1995 to 2010. **Figure 12** shows a comparison of the flow data at Station 17 (EFK 23.4) with the flow data recorded at the other outfalls being studied along with the flow augmentation. This approach ensured that the data follows the normal hydrological pattern (for a specific period of time, adding the upstream flow from upstream sources should result in the total flow in the downstream station). Rainfall does not significantly contribute to the total flow in EFPC, so there was no need to compare the flow at Station 17 with the rainfall patterns. Recorded flow data summarized in **Figure 12** shows a consistent trend between the flow sources and the total discharge in EFPC from 1995 to 2010. There was enough flow data at Station 17 (EFK 23.4) for statistical comparison with computed timeseries data; however, there was insufficient recorded data available for the other stations downstream of Station 17 (i.e. EFK 18.2, EFK 13.8, and EFK 6.3). Since there is no outfall beyond Station 17 towards the end of the creek at EFK 6.3, the daily contribution to total flow in the creek was assumed to be from overland flow, groundwater exchange and municipal water outlets to the creek. Therefore, typical statistical or linear interpolation/extrapolation techniques can be used to estimate the flow timeseries at the downstream stations, such as (i) precipitation-runoff relationships; (ii) ratio of drainage area method; (iii) correlation of records from similar gauging stations; (iv) comparison with similar flow duration curves; or (v) some other hydrological synthesis method such as the Markov process or autoregressive models, or moving average models.

Table 5. Statistical Characteristics of Flow Data from 1995 to 2010, in m3/s

	EFK 24.4	EFK 23.4	EFK 18.2	EFK 13.8	EFK 6.3
No. of Data	17	3961	17	18	17
Min	0.14	0.03	0.37	0.41	0.60
Max	0.44	3.81	0.81	1.15	2.07
Mean	0.34	0.34	0.53	0.61	1.08
Median	0.34	0.32	0.49	0.51	0.82
Range	0.30	3.78	0.44	0.74	1.47
Interquartile Range	0.07	0.07	0.13	0.28	0.67
Variance	0.00	0.04	0.02	0.04	0.23
Standard Deviation	0.07	0.21	0.13	0.21	0.48
Coefficient of Variation	0.20	0.60	0.25	0.35	0.44

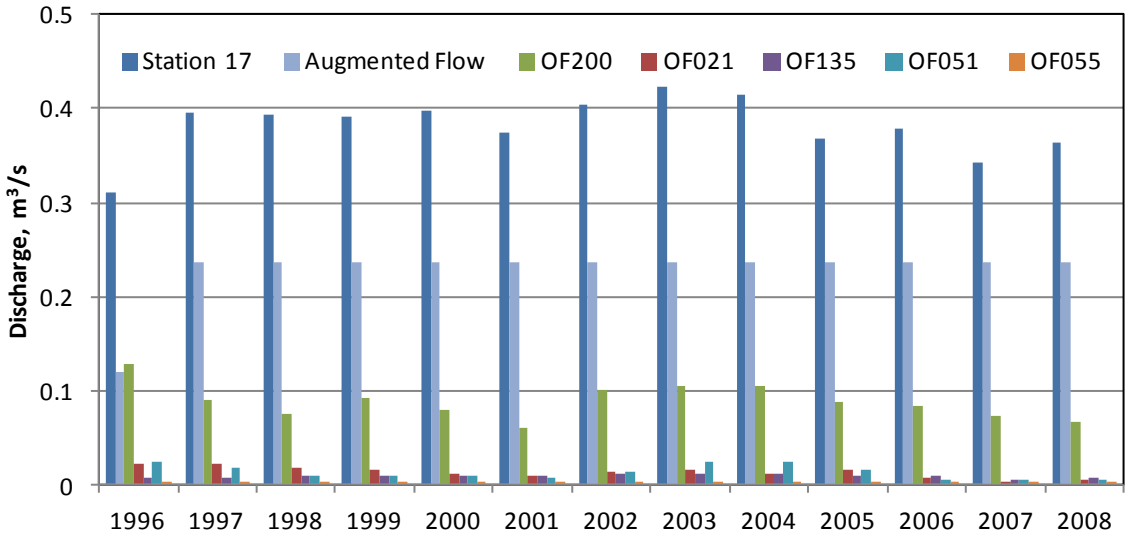

Figure 12. Flow contribution chart for EFPC.

As shown in **Figure 12**, a major portion of the flow in EFPC originates from the outfall discharges. **Figure 12** compares the contribution of major outfalls and augmented flow to the total discharge recorded at Station 17 (EFK 23.4).

The result of the numerical simulation for the total flow at Station 17 solely as a result of flow from the outfalls and flow augmentation is shown in **Figure 13**a; and the total flow at Station 17 considering the contribution from precipitation (overland runoff) and groundwater exchange is shown in **Figure 13**b. The contribution of overland flow and groundwater is calculated as the difference between the results shown on **Figure 13**. The numerical results show that the contribution from the groundwater and overland flow to the total flow recorded at Station 17 (EFK 23.4) is only 11%. Stormwater and wastewater outfalls and flow augmentation produce the largest contributions at 37% and 57%, respectively.

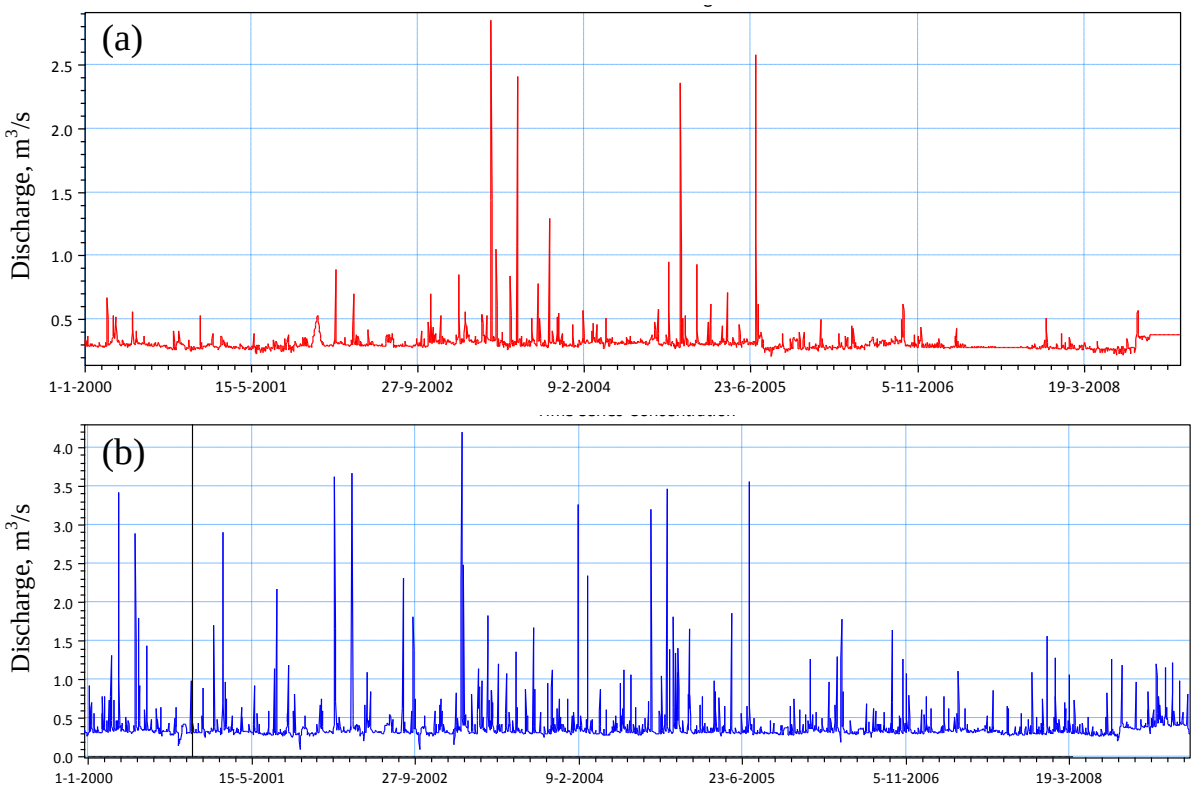

Figure 13. (a) Recorded discharge timeseries from all outfalls with flow augmentation excluding groundwater exchange; (b) Recorded discharge timeseries at Station 17.

GENERATING THE FLOW DURATION CURVES

A flow duration curve for EFPC was constructed from daily flow measurements taken at Station 17 (EFK 23.4) from 1/1/1995 through 12/26/2010. This 15-year period contained a range of hydrologic conditions that included both low and high stream flows. The flow duration curve is shown in **Figure 14** and represents the cumulative distribution of daily discharges arranged to show the percentage of time specific flows were exceeded during the period of record.

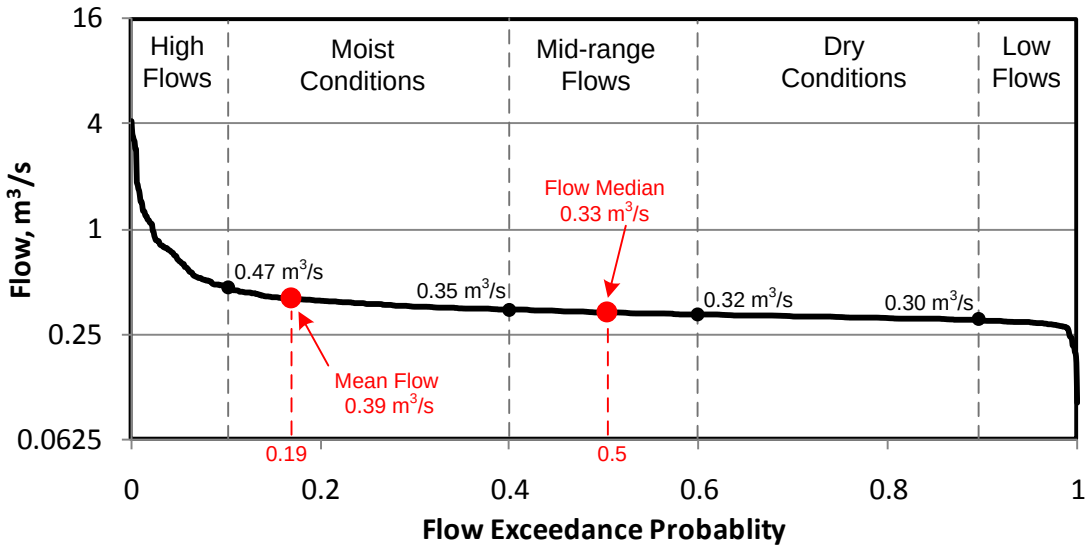

Figure 14. Flow duration curve for Station 17.

In order to provide insight regarding the conditions and patterns associated with creek impairment, flow duration curves are divided into five zones: high flows (0-10%), moist conditions (10-40%), mid-range flows (40-60%), dry conditions (60-90%), and low flows (90-100%), as shown in Figure 14 for the flow duration curve of Station 17. This approach places the midpoints of the moist, mid-range, and dry zones at the 25th, 50th, and 75th percentiles respectively (i.e., the quartiles).

The computed flow duration curve is compared with the observed flow duration curve at Station 17 (EFK 23.4) in **Figure 15**. The computed and observed mean values are exactly the same up to the second decimal place as shown in **Figure 15**. The flow duration curves and the mean flow values for groundwater/overland flow, outfalls/augmentation, and total flow at Station 17 (EFK 23.4), are compared in **Figure 16.**

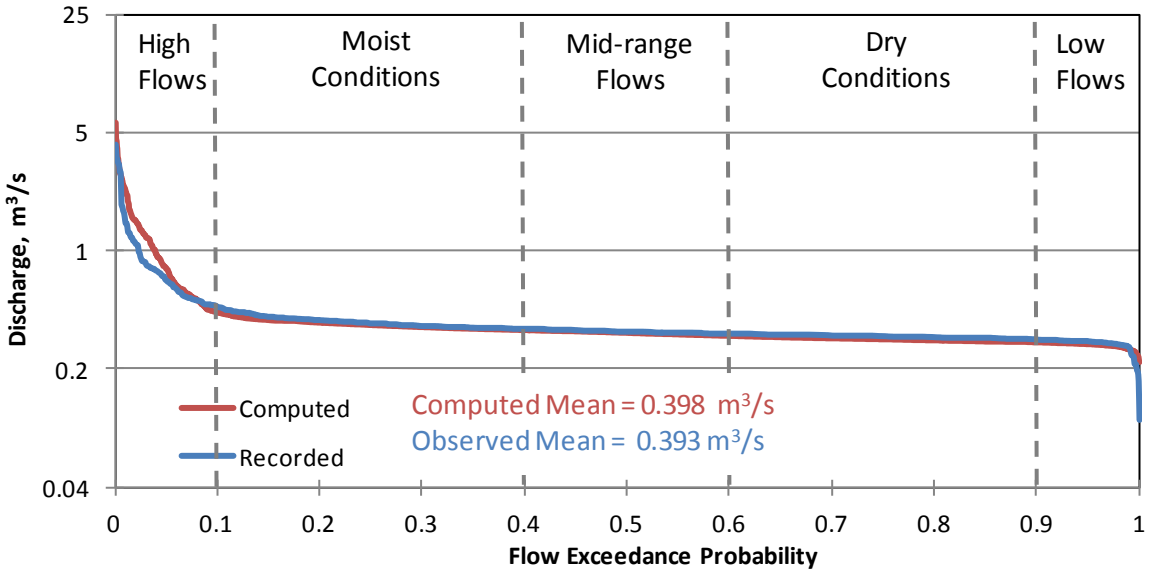

Figure 15. Computed and observed flow duration curves at Station 17 (EFK 23.4).

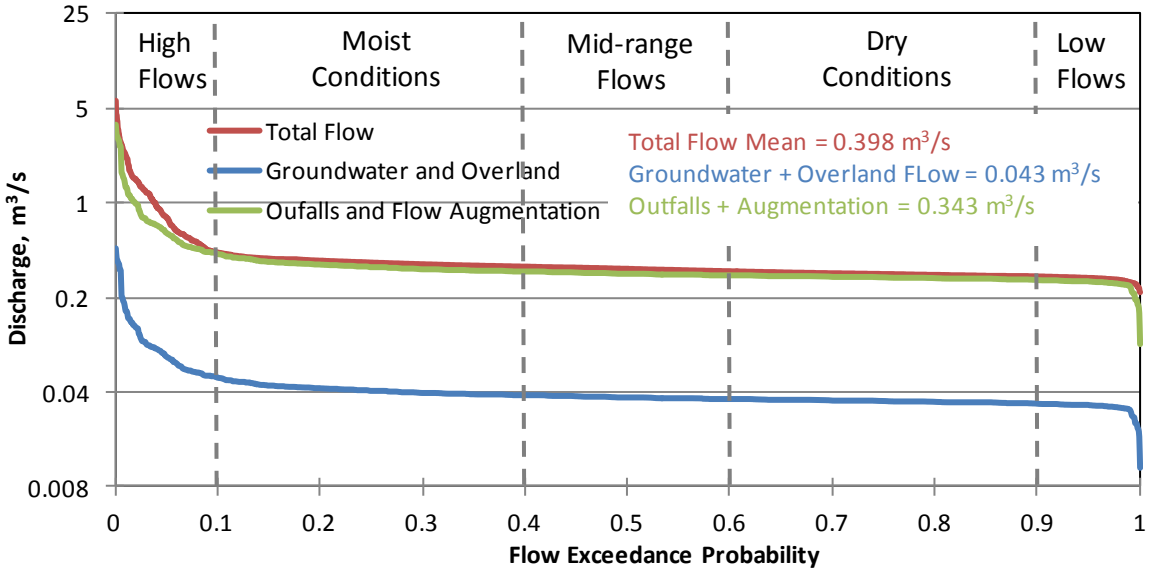

Figure 16. Computed load duration curves for overland flow/groundwater, outfalls/flow augmentation, and total flow at Station 17 (EFK 23.4).

LOAD DURATION CURVES

Instantaneous load values are calculated by multiplying the computed concentration of the contaminant of concern (e.g. mercury) at that particular station (e.g. Station 17) with the

corresponding value of the computed flow on the flow duration curve. In other words, concentration of the contaminant of concern, taken with some measure or estimate of flow at the time of sampling, can be used to compute an instantaneous load. Using the relative percentage exceedance from the flow duration curve that corresponds to the stream discharge at the time the water quality sample was taken, the computed load can be plotted in what is called a load duration curve. The x-axis still represents flow duration intervals while the y-axis represents the load values. The mercury load duration curve for the EFPC was developed from the flow duration curve and available water quality monitoring data.

A load duration curve is a cumulative frequency graph that illustrates existing water quality conditions (as represented by loads calculated from monitoring data), how these conditions compare to desired targets, and the portion of the waterbody flow regime represented by these existing loads. The load duration curve was developed using the following procedure:

Step1 – Target Load Duration Curve

This is done in order to specify criteria for the TMDL analyses to evaluate attainment of water quality standards in the waterbody of interest. In general, the target for the TMDL analyses is the numeric water quality criterion for the pollutant of concern for a specified waterbody. In the case of EFPC, the target concentration is defined in the previous section of this report and is based on the detailed description of water uses and regulations established by EPA and TDEC. The numeric water quality targets are translated into TMDLs through the loading capacity. EPA's current regulation defines loading capacity as "the greatest amount of loading that a waterbody can receive without violating water quality standards". The loading capacity provides a reference, which helps guide pollutant reduction efforts needed to bring a waterbody into compliance with standards. The maximum allowable concentration of mercury in EFPC at Station 17 (EFK 23.4) is defined by EPA and TDEC as 51 ppt. There is also the ROD target of 200 ppt for Station 17 (EFK 23.4) proposed by DOE. A target load duration curve was generated for EFPC by applying the mercury target concentration of 51 ppt to each of the ranked flows used to generate the flow duration curve and plotting the results.

The maximum mercury load target corresponding to each ranked daily mean flow is [(51 ppb) x (Q) x (UCF)], where Q is daily mean flow and UCF is the required unit conversion factor. The same calculation was performed for the ROD target concentration of 200 ppt. The target TMDL for mercury at Station 17 based on these numerical target values was calculated and depicted in **Figure 17**.

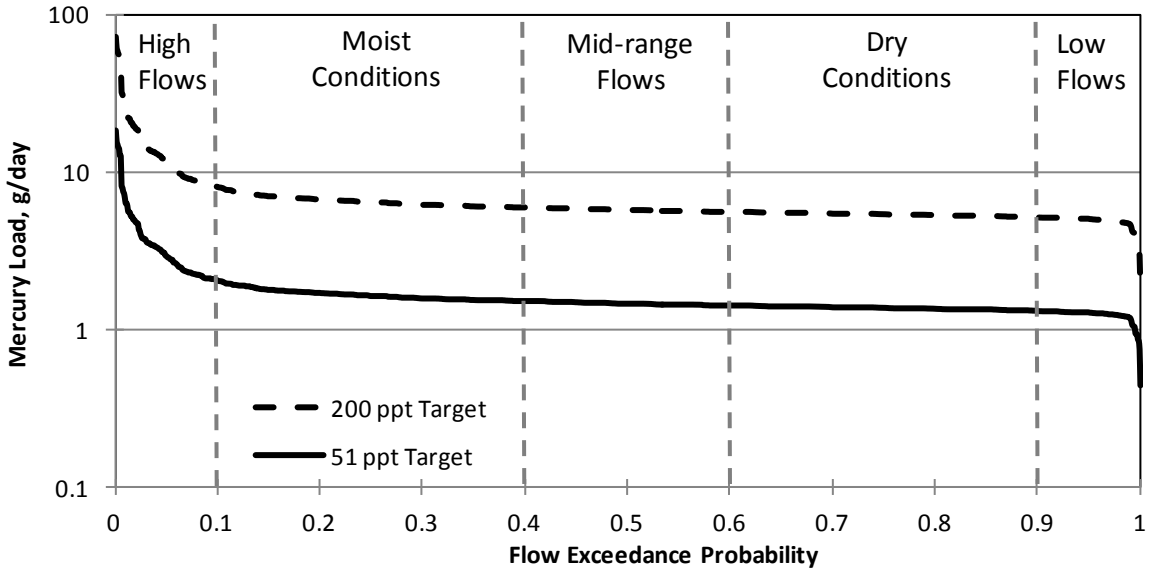

Figure 17. Target TMDL for Station 17.

Step 2 – Calculating Daily Loads

Daily loads were calculated for each of the water quality samples collected at Station 17 (EFK 23.4) by multiplying the sample concentration by the daily flow for the sampling date and the required unit conversion factor.

Step 3 – Calculating Percent of Days the Flow was Exceeded (PDFE)

Using the flow duration curve developed in Section 0, the PDFE was determined for each sampling event. Each sample load was then plotted on the load duration curve developed in Step 1 according to the PDFE. The resulting mercury load duration curve is shown in **Figure 18** for the observed data at Station 17. In this figure the continuous black line is the 51 ppt water quality target established by EPA and TDEC; the dashed black line is the 200 ppt limit from the measurement technique EPA-245.1 used before 2001 and the ROD water quality target defined for Station 17 (EFK 23.4); and the dashed red line is the 90^{th} percentile for the mercury load under each flow regime. The 90^{th} percentile by definition is the Hg load value for which 90 percent of the values are lower or equal to that value for that particular flow regime.

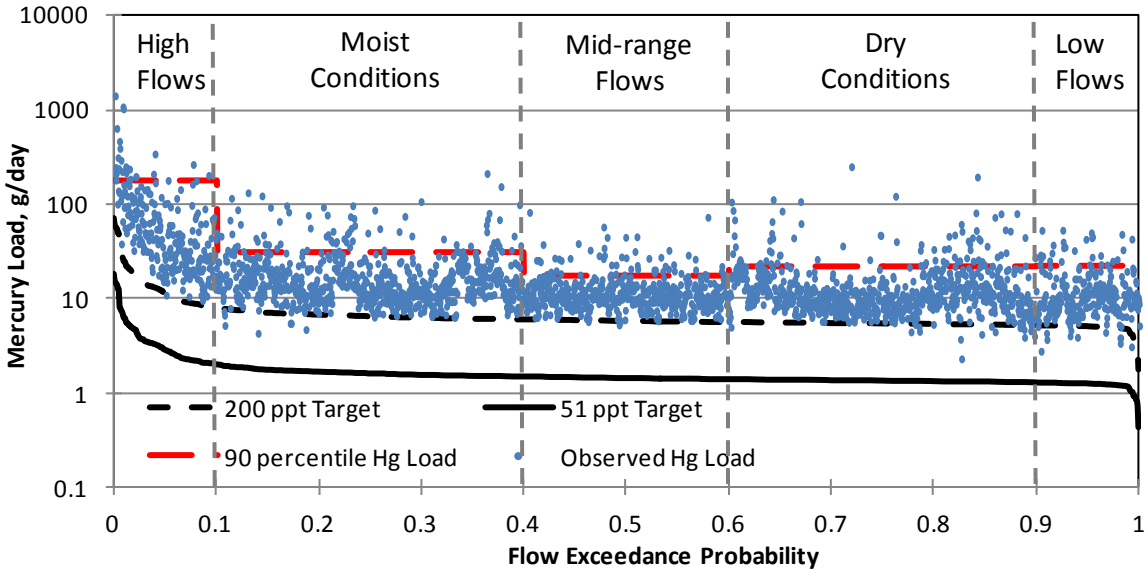

Figure 18. Mercury load duration curve for EFPC at Station 17 (EFK 23.4).

The 90th percentile was determined for flow conditions duringtwo different time periods, 1992 – 2000 and 2001 – 2010, which are compared with the 200 ppt and 51 ppt target load duration curves in **Figure 19**.

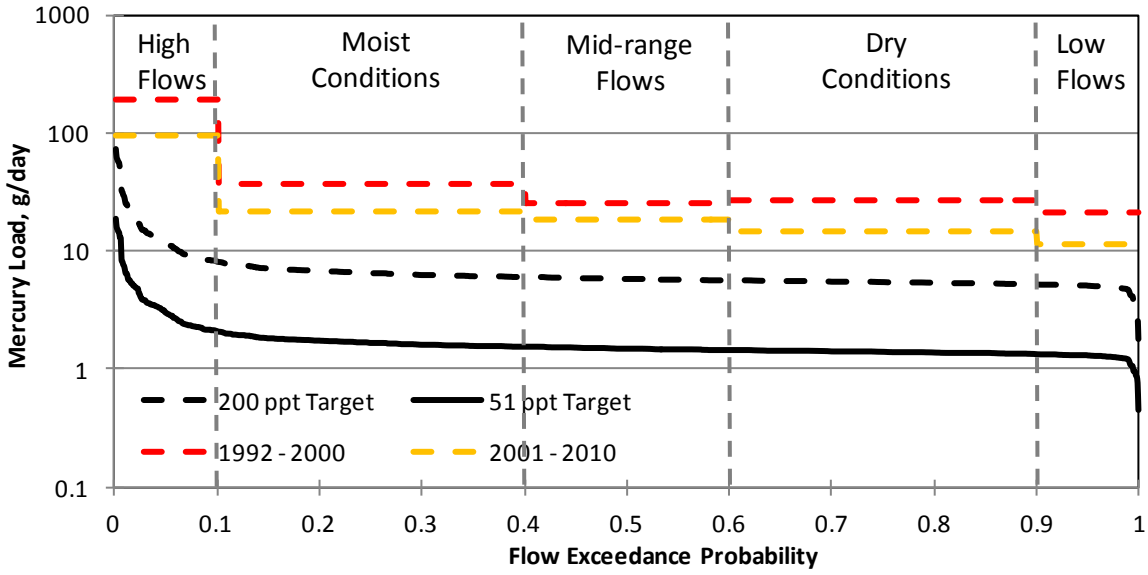

Figure 19. Comparison of mercury loading levels for EFPC at Station 17 (EFK 23.4) - (1992 – 2000) vs (2001 – 2010).

The mercury loads were calculated at Station 17 (EFK 23.4) utilizing the recorded timeseries for flow and mercury concentrations at the outfalls.. **Figure 20** shows the flow and load duration curves at Station 17 (EFK 23.4) solely derived from the outfalls and flow augmentation.

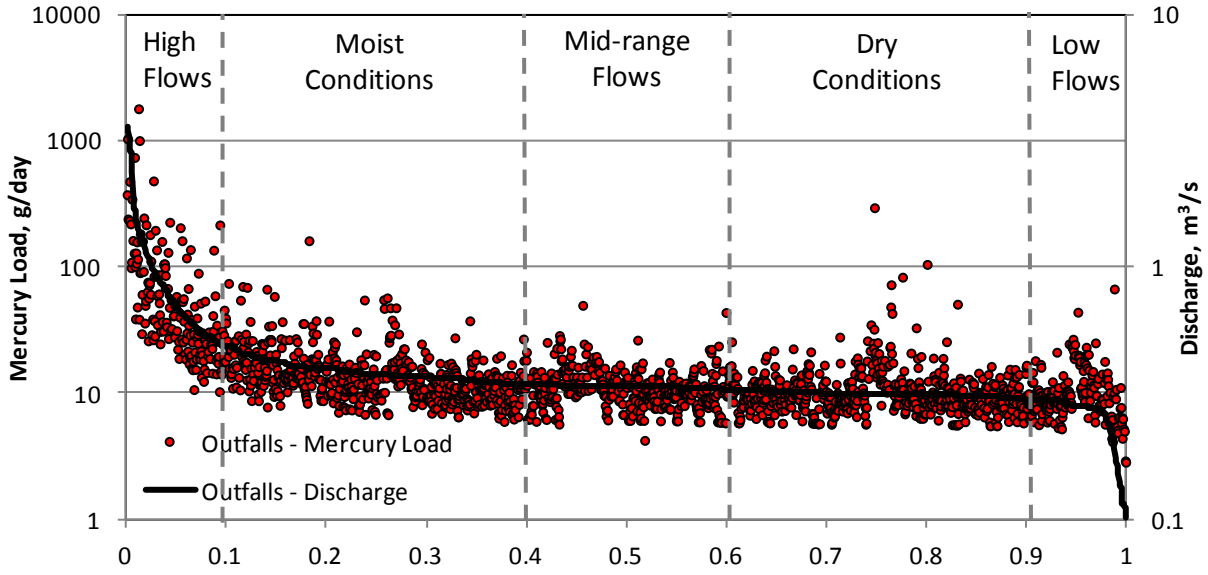

Figure 20. Flow and load duration curves resulting from the sum of all outfalls (excluding groundwater, sediment and overland contribution).

In order to identify the contribution from sediments, groundwater, and overland flow to the total mercury at Station 17 (EFK 23.4), the mercury loads calculated in the previous step were subtracted from the total mercury load recorded at Station 17 (EFK 23.4). The results are compared in **Figure 21** in terms of percentiles for each of the flow regimes. Statistical characteristics of this contribution to the total mercury load at Station 17 are summarized in **Table 6.**

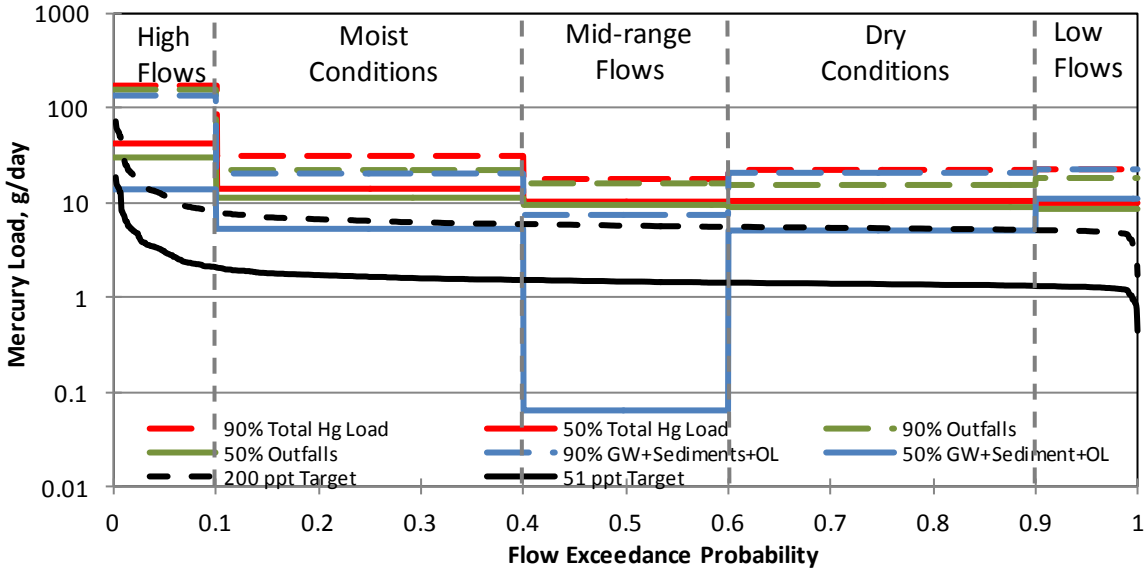

Figure 21. Contribution of outfalls, groundwater, sediments and overland flow to the total mercury load at Station 17 (EFK 23.4).

Table 6. Contribution of Mercury Sources to the Total Mercury Load Recorded at Station 17 (EFK 23.4), g/day

Flow Condition	GW + OL + Sediments			Outfalls			Total mercury		
	Mean	Median	90%	Mean	Median	90%	Mean	Median	90%
High Flows	51.1	13.6	136.2	73.8	29.8	160.1	81.7	41.7	174.3
Moist Conditions	9.8	5.2	20.7	12.5	11.3	21.8	18.9	14.1	31.2
Mid-range Flows	2.2	0.06	7.6	9.1	9.5	15.7	12.1	10.3	17.7
Dry Conditions	8.6	5.0	21.0	10.0	9.0	15.0	14.4	10.5	22.1
Low Flows	14.6	10.8	22.8	9.7	8.7	17.9	12.6	10.0	22.5

Step 4 – Mercury Water Quality Duration Curve

Based on the PDFE determined in Step 3, recorded mercury concentration values were plotted and compared to the water quality criterion of 51 ppt. The resulting mercury water quality duration curve is shown in **Figure 22** for the period 1992 – 2010. **Figure 23** compares the 90th percentile of Hg concentration with the target values for the two separate periods, 1992 – 2000 and 2001 – 2010.

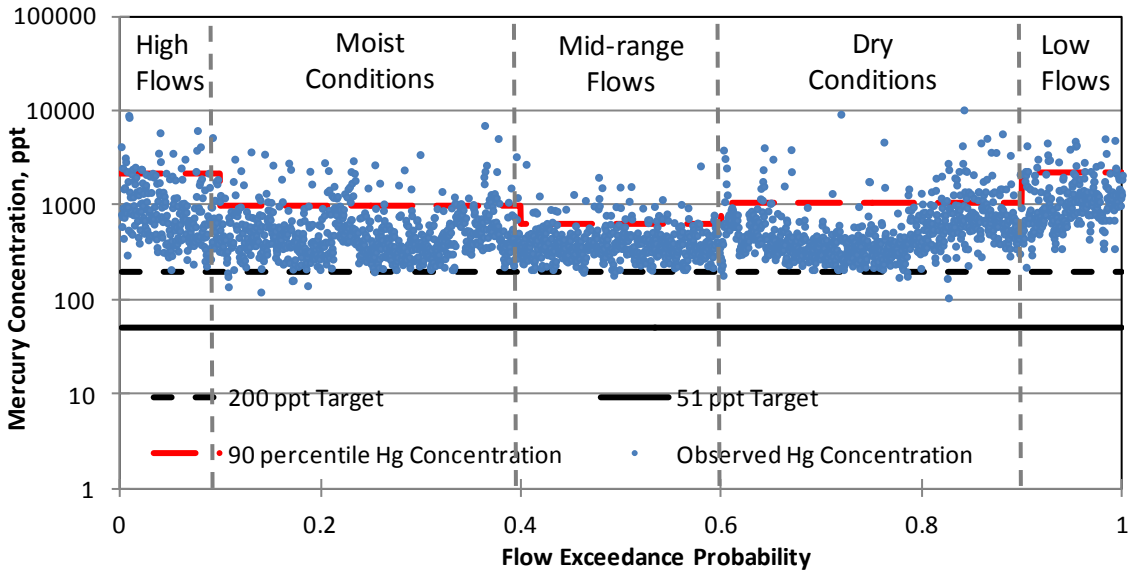

Figure 22. Mercury water quality duration curve for EFPC at Station 17 (EFK 23.4).

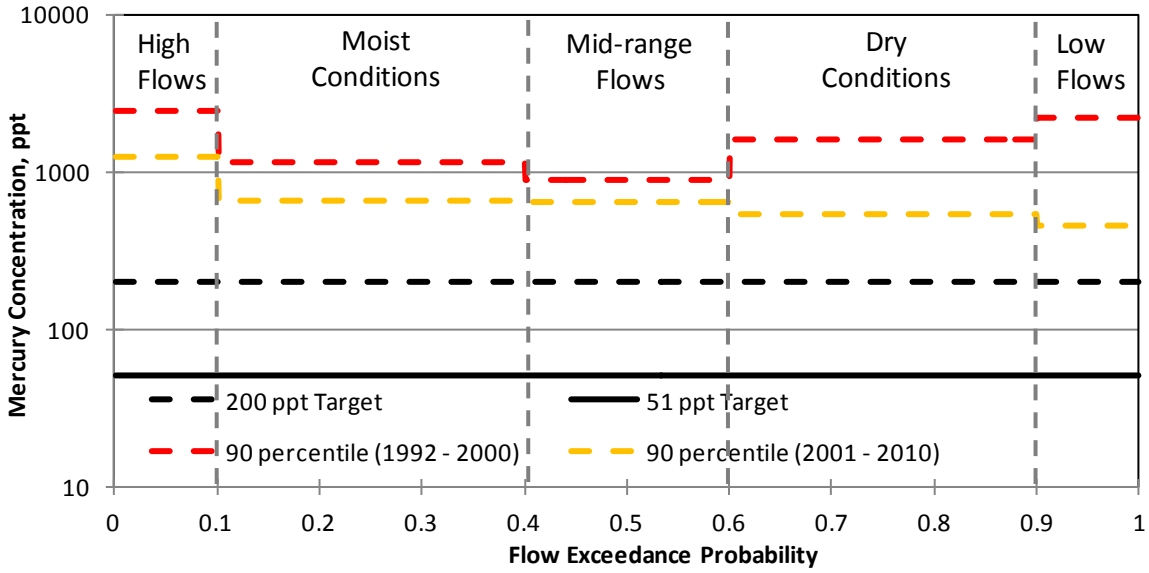

Figure 23. Comparison of mercury concentration recordings for EFPC at Station 17 (EFK 23.4) - (1992 – 2000) vs (2001 – 2010).

Step 6 – Water Quality Statistical Characteristics

Statistical analysis of recorded mercury values at Station 17 was conducted for two different periods, 1992 – 2000 and 2001 – 2010, and listed in **Table 7**. The reduction required to decrease the water column concentration from the "mean + 95% confidence interval" to the desired target level was calculated to be 89.5%.

Table 7. Analysis of Water Column Monitoring Data at Station 17 (EFK 23.4)

	1992 - 2000		2001 - 2010	
	Mercury Concentration, ppt	Mercury load, g/day	Mercury concentration, ppt	Mercury load, g/day
Number of samples	1511	1511	1143	1143
Minimum	210	3.3	105.5	2.3
Mean	868.3	26.1	460.9	16.2
Standard Deviation	816.1	58.0	499.4	36.2
95% CI	41.1	2.9	28.9	2.1
Mean + 95% CI	909.4	29.0	489.9	18.3
90% CI	34.5	2.5	24.3	1.8
Mean + 90% CI	902.8	28.6	485.2	18.0
WQ Target	51		51	
%Reduction from 90%	94.4%		89.5%	
%Reduction	94.4%		89.5%	

from 95%		
ROD Target	200	200
%Reduction from 90%	77.8%	58.8%
%Reduction from 95%	78.0%	59.2%

Recorded and computed TSS and mercury load duration curves are compared for different flow conditions in **Figure 24**. Resuspension of mercury-laden fine particulates during high flow conditions (i.e., the wet seasons) plays a significant role in the enhancement of local concentration of mercury along the creek. Furthermore, the streambed pore water within the reach contains very high concentrations of dissolved mercury, often exceeding 20 µg/L (approximately 30 to 50 times the concentration in overlying surface water); thus, a higher flow in the river not only resuspends the mercury-laden particulates, but also recirculates the highly contaminated water trapped in sediment pores back into the water column of the creek. Therefore, dissolved mercury in sediment pore water contributes to the high mercury concentration in the creek water column through diffusive transport and porewater recirculation or advection. Close conformity between computed and recorded mercury and TSS loads at Station 17 (EFK 23.4) is clearly depicted in **Figure 24**. For the purpose of better visualization, a comparison has been made between percentiles of the computed and observed mercury loads.

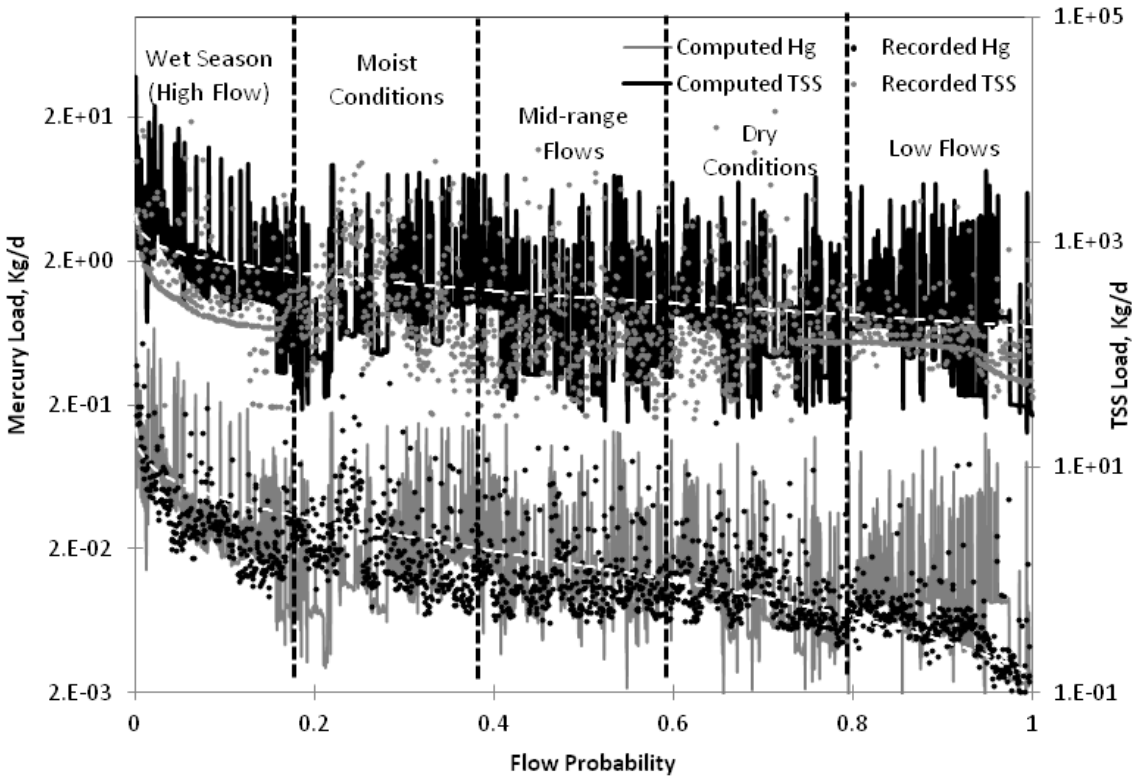

Figure 24. Load duration curves at Station 17 based on flow probability. White dashed lines are linear-moving average trendlines.

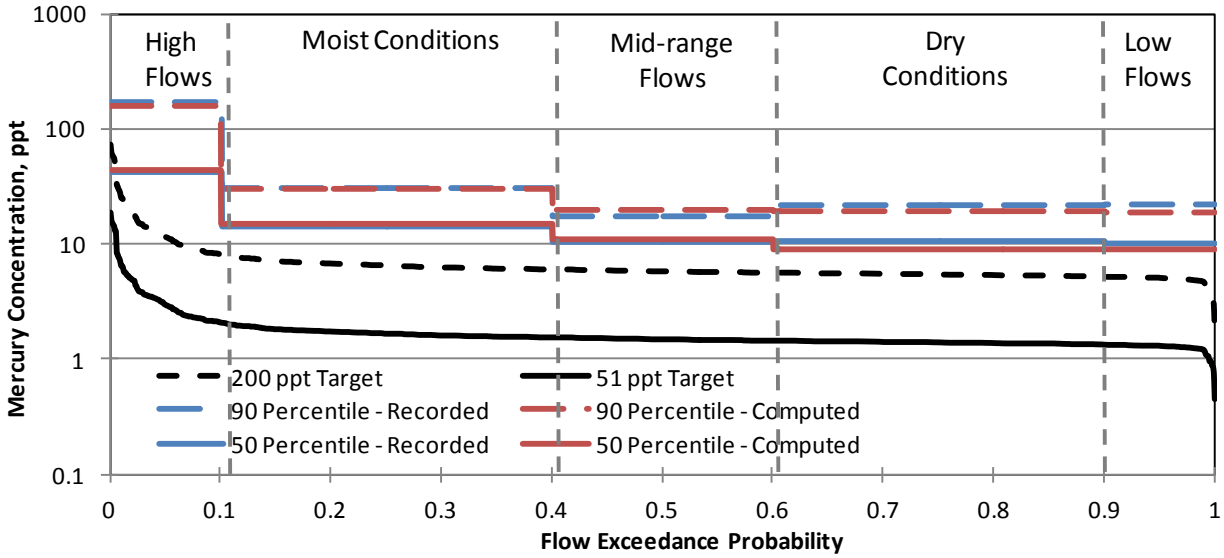

Figure 25. Comparison of computed and observed mercury loads at Station 17 (EFK 23.4) in terms of percentiles for different flow conditions.

Conclusions

In order to analyze the mercury cycle in the environment and provide forecasting capabilities for the flow and transport of mercury within the EFPC, an integrated surface and subsurface flow and transport model was developed using the hydrodynamic and transport numerical package MIKE, developed by the DHI. The model was calibrated for the flow and transport using historical field records obtained from the OREIS database.

Computed model outputs show close correlation with the water discharge, mercury concentration, and TSS field data recorded at different stations along the creek, which implies a high level of accuracy and reliability of the model. TSS and mercury concentration time-series data were compared at the integration point of the creek, Sta. 17. Due to the high dependency of suspended solids and mercury concentration on the level of discharge in the creek, results and discussions are mostly presented based on load duration curves for both suspended solids and total mercury.

The significance of sediment-mercury interactions on the fate and transport of mercury along the creek was investigated, performing simulations for two different cases: with and without consideration of sediment-mercury interactions. As reported in recent field surveys, stream sediments highly affect the concentration of mercury in the creek. Diffusive transfer through sediment pore water and colloidal transport were identified as two main mechanisms responsible for at least 90 percent of the mercury in the creek water. However, resuspension of mercury-laden fine particulates plays the most important role in the unexpectedly high concentration of mercury (peaks in mercury concentration time series) reported at different locations along the UEFPC. Simulations show that at least 65 percent of the total mercury concentration in the water is in a form that is adsorbed to suspended particles, which is consistent with the field surveys at the site. High flow conditions in the river following heavy rainfalls increase the velocity in the river and intensify the resuspension of mercury particulates, thereby increasing the concentration of mercury in the creek, as clearly indicated by numerical simulation results. Sensitivity analysis performed on parameters affecting TSS in the water column revealed the high dependence of TSS to critical current velocity. Four parameters have been considered in the model that directly affects the concentration of TSS in the water column: critical current velocity (Vc), settling velocity (Vs), resuspension rate (RR), and particle production rate (PPR). The sensitivity of the TSS load at Sta. 17 to each of these parameters was examined by performing simulations for a range of values.

The results from this work show that a well calibrated computer model can provide a information that is critical for a TMDL study and particularly for determining remediation objectives and how to accomplish TMDL targets.

The results presented in this study can be considerably improved by incorporating additional boundary and calibrating data: timeseries of flow and mercury concentration measurement across the entire domain, including creeks, soil and subsurface data.

FUTURE WORK

This subtask will provide numerical analysis of contaminant flow and transport within the EFPC watershed and will determine the impact of model parameters on NPDES and TMDL regulations. During FY2012 the objective of this task is to determine the effect of the hydrological events (including changes in hydrology caused by D&D activities on the site) on contaminant loading (changes in external and internal loading in time and space), and how imminent ecosystem restoration may affect existing contaminant pools. Work proposed for FY12 includes the following subtasks.

Subtask 2.1: Modeling of previously proposed actions to facilitate IFDP and meet load discharge standards at Station 17. Modeling will be performed with an already calibrated and verified model using the commercial flow and transport software MIKESHE/MIKE 11. The model was developed as part of the scope in FY2011. The emphasis will be on stochastic analysis of the load reduction effects resulting from remedial actions. The task will provide a series of simulations to analyze each action. In addition, major parameters will be varied (such as hydraulic conductivity of the upper layer, rainfall intensities, evapotranspiration values, parameters of the vadose zone) to characterize the impact of each action on the loads at Station 17 and the associated uncertainties. The deliverable of this subtask will include development of probability exceedance curves for each scenario; this data will provide additional insight of the effect for the entire range of hydrologic regimes (very wet to very dry conditions). The task will study the modifications of the hydrology which limit the amount of overland flow over site surfaces, and limit the infiltration of rainwater through areas with underlying mercury contamination.

Subtask 2.2: Analysis of the risks associated with the inorganic contaminants including uranium and mercury (the list of contaminants can be easily expanded using the same flow model and by applying the correct thermodynamic and reactive properties). The task will additionally provide analysis of the geochemical and engineering properties of various mixtures of structural (flowable) fill for Oak Ridge Reservation EM Scope Projects and in support of the IFDP D&D activities. The aim is to determine the efficacy of plugging and abandoning storm drains that contain mercury sediments at the Y-12 Complex and creating a structural fill in basement air spaces for supporting heavy demolition equipment. In addition, the testing of fill should allow a determination of whether liquid elemental mercury and high concentrations of mercury in soil beneath the facilities can be hydraulically isolated and geochemically sequestered. The analysis will be performed with collaboration from ORNL and the site and will provide understanding of the potential point and distributed sources of inorganic and organic contaminants that are coupled with hydrological events and D&D activities.

REFERENCES

1. U.S. Clean Water Act 1972 Section 303 (d), 33 U.S. Code Section 1313 (d).
2. U.S. EPA, 1991. “Guidance for Water Quality-Based Decisions: The TMDL Process.” Doc. No. EPA 440/4-91-001. April 1991.
3. U.S. EPA, 1992. “Water Quality Planning and Management.” Code of Federal Regulations, 40 CFR 130.7.

4. U.S. EPA, 2007. “An Approach for Using Load Duration Curves in the Development of TMDLs.”, EPA 841-B-07-006.
5. U.S. EPA, 2009. “Handbook for Developing Watershed TMDLs”.
6. TDEC 2006. State of Tennessee NPDES Permit No. TN0002968, “Authorization to discharge under the National Pollutant Discharge Elimination System (NPDES),” Issued March 13, 2006; effective May 1, 2006.
7. Southworth, G.R., et al. Controlling Mercury Release from Source Zones to Surface Water: Initial Results of Pilot Tests at the Y-12 National Security Complex. Oak Ridge, TN: ORNL, 2009.
8. Southworth, George, Max Greeley, Mark Peterson, Kenneth Lowe, and Richard Kettelle. Sources of Mercury to East Fork Poplar Creek Downstream from the Y-12 National Security Complex: Inventories and Export Rates. Oak Ridge: Oak Ridge National Laboratory, 2010.
9. TDEC, Tennessee Department of Environment and Conservation, Division of Water Pollution Control. "Proposed Total Maximum Daily Load (TMDL) for Mercury in East Fork Poplar Creek, Lower Clinch River Watershed, Preliminary Second Draft. Anderson and Roane Counties." Oak Ridge, TN, 2008.
10. Moran, Barry. "Modeling of the Hydrologic Transport of mercury in the Upper East Fork Poplar Creek." Knoxville (Ternnessee), December 1996.
11. TMDL Protocol, Florida Department of Environmental Protection, June 2006, Version 6.0.
12. D.R. Maidment, Handbook of Hydrology, , McGraw-Hill, 1993.
13. TDEC. 2006. Final 2006 303(d) List. State of Tennessee, Department of Environment and Conservation, Division of Water Pollution Control, October 2006.
14. U.S. EPA. 1997. Ecoregions of Tennessee. U.S. Environmental Protection Agency, National Health and Environmental Effects Research Laboratory, Corvallis, Oregon. EPA/600/R-97/022.
15. ATSDR (Agency for Toxic Substances and Disease Registry), Federal Facilities Assessment Branch and Division of Health Assessment and Consultation. 2006. Public Health Assessment: Evaluation of Potential Exposures to Contaminated Off-Site Groundwater from the Oak Ridge Reservation (USDOE) Oak Ridge, Tennessee.
16. Hatcher, R. D., Lemiszki, P. J., Dreier, R. B., Ketelle, R. H., Lee, R. R., Leitzke, D. A., McMaster, W. M., Foreman, J. L., and S. Y. Lee. 1992. Status Report on the Geology of the Oak Ridge Reservation, ORNL/TM-12074. Prepared for the Office of Environmental Restoration and Waste Management.
17. TDEC, 2007, Rules of Tennessee Department of Environment and Conservation, Division of Water Pollution Control, Chapter 1200-4-4, Use Classification for Surface Waters.
18. U.S. DOE, 2008, Recommendations to Address Technical Uncertainties in the Mitigation and Remediation of Mercury Contamination at the Y-12 Plant, Oak Ridge, Tennessee, WSRC-STI-2008-00212.
19. TDEC, 2008, Rules of Tennessee Department of Environment and Conservation, Division of Water Pollution Control, Chapter 1200-4-3, General Water Quality Criteria.
20. U.S. EPA, 2006, Data Quality Assessment: Statistical Methods for Practitioners, EPA QA/G-9S.
21. U.S. EPA, 2006. Data Quality Assessment: A Reviewer’s Guide, EPA QA/G-9R.

22. U.S. EPA, 2006. Draft Guidance for Implementing the January 2007 Methylmercury Water Quality Criterion. U.S. Environmental Protection Agency, Office of Science and Technology, Washington, DC. EPA-823504-001, August 2006.
23. Van Winkle, W., et al. 1982, Mercury Contamination in East Fork Poplar Creek and Bear Creek, Publication 2051, October 7. 1982.
24. U.S. DOE. 1998. Report on the Remedial Investigation of the Upper East Fork Poplar Creek Characterization Area at the Oak Ridge Y-12 Plant, Oak Ridge, Tennessee. DOE/OR/01-1641V1&D2, August 1998.
25. U.S. DOE. 2006, 2006 Remedial Effectiveness Report/CERCLA Five-Year Review for the US Department of Energy, Oak Ridge Reservation, Oak Ridge, TN. DOE/OR/01-2290&D1. U.S. Department of Energy. March 2006.
26. U.S. DOE. 2002. Phase I Interim Source Control Actions in the Upper East Fork Poplar Creek Characterization Area, Oak Ridge, TN - Record of Decision (ROD) dated May 2002.
27. U.S. DOE. 1996. Wastewater Control Report for the Oak Ridge Y-12 Plant. Y/TS-1466/R1.
28. U.S. DOE. 1997. Final Report for the Central-Mercury Treatment System in Building 9623 at the Oak Ridge Y-12 Plant, Oak Ridge, Tennessee, Y/ER-282.
29. ORNL. 2009. Controlling Mercury Release from Source Zones to Surface Water: Initial Results of Pilot Tests at the Y -12 National Security Complex, ORNL/TM-2009/035.
30. BJC (Bechtel Jacobs Co. LLC). 1998. Mercury Abatement Report for the U.S. DOE Oak Ridge Y-12 Plant for Fiscal Year 1998. BJC/OR-183.
31. BJC. 1999. Mercury Abatement Report for the U.S. Department of Energy Oak Ridge Y-12 Plant for Fiscal Year 1999, Oak Ridge, Tennessee. BJC/OR-422.
32. U.S. DOE. 1995. Record of Decision for Lower East Fork Poplar Creek, Oak Ridge, Tennessee. DOE/OR/02-1370&D2.
33. U.S. DOE. 1996. Explanation of Significant Differences for the Lower East Fork Poplar Creek Record of Decision, Oak Ridge, Tennessee. DOE/OR/02-1443&D2.
34. Southworth, G., Greeley, M., Peterson, M., Lowe, K., & Kettelle, R. 2010. Sources of Mercury to East Fork Poplar Creek Downstream from the Y-12 National Security Complex: Inventories and Export Rates. Oak Ridge: Oak Ridge National Laboratory.
35. Turner, R. R. and G. R. Southworth. 1999. Mercury-Contaminated Industrial and Mining Sites in North America: an Overview with Selected Case Studies. In Mercury Contaminated Sites, R. Ebinghaus, R. R. Turner, L. D. de Lacerda, O. Vasiliev, and W. Salomons (Eds.) Springer-Verlag, Berlin, FRG.
36. Rhoades, E. L., M. A. O'Neal, and J. E. Pizzuto. 2009. Quantifying bank erosion on the South River from 1937 to 2005, and its importance in assessing mercury contamination. Applied Geology 29:125 – 134.
37. U.S. DOE. 2005. The Oak Ridge Annual Site Environmental Report. U.S. DOE. March 2005.
38. U.S. EPA 2005. TMDL Model Evaluation and Research Needs, November 2005. EPA/600/R-05/149.
39. U.S. DOE 1998. Report on the Remedial Investigation of the Upper East Fork Poplar Creek Characterization Area at the Oak Ridge Y-12 Plant, Oak Ridge, Tennessee, DOE/OR/01-1641/V1-V4&D2.

40. Tachiev, G., Garcia R. Modeling of the White Oak Creek and East Fork Poplar Creek Watersheds. Applied Research Center Florida International University, 2009.
41. Martin Marietta Inc. 1995. Decision Document for Performing a Long-Term Pumping Test at the S-3 Site, Oak Ridge Y-12 Plant, Oak Ridge, Tennessee, submitted to DOE.

TASK 3: PARAMETERIZATION OF MAJOR TRANSPORT PROCESSES OF MERCURY SPECIES

INTRODUCTION

The overall objective of this task is to provide laboratory measurements for critical mercury (Hg) transport, transformation, and exchange processes (i.e., methylation/demethylation, and dissolution) to be used in the numerical model. The laboratory experimental work will provide insight on parameters relevant to the Oak Ridge Reservation (ORR) and which are required in the numerical model, such as dissolution rate of mercury and the proportion of mercury species available for methylation/demethylation in sediments. In addition, experimental work will be conducted to analyze the effect of significant environmental factors (pH, Eh, sunlight) on the major transport and transformation processes of Hg.

Under this task the stability, bioavailability, and mobility of the aged mercury species in soils and sediments will be systematically investigated. The proportion of Hg species available for methylation and demethylation in sediments will be estimated by using isotope addition techniques. In addition, the dissolution of cinnabar and Hg beads, which have often been observed at this site and are thought to be recalcitrant mercury species, will be investigated by using both experimental and theoretical calculation methods. Three factors, oxidation-reduction, pH, and complexation with organic ligands (e.g., low molecular weight thiols such as cysteine and glutathione and large molecular NOM), will be particularly investigated for their role in mobilizing the aged mercury species. These studies will provide a better understanding of the bioavailability and dissolution of aged Hg species in soils and sediments. In FY11, we studied 1) photomethylation of Hg^{2+} in natural water, 2) bioavailability of Hg^{2+} and methylmercury for methylation and demethylation in sediment, and 3) enhancement of cinnabar dissolution by thiol-containing compounds.

RESULTS AND DISCUSSION

Photomethylation of Hg^{2+} in Natural Water

The double isotope addition technique ($Me^{201}Hg$ and $^{199}Hg^{2+}$) was adopted to study the methylation of Hg^{2+} in water. A new model was developed to calculate the methylation rate constant of the spiked $^{199}Hg^{2+}$ (k_m) in water (Eq. (2)). In this model, contributions of both $^{199}Hg^{2+}$ methylation and $Me^{199}Hg$ demethylation are taken into account in the function. The $[Me^{199}Hg]_t$ /$[Me^{202}Hg]_t$ ratio ($R_{202}^{199}(t)$), was employed to calculate the k_m in water. The rate constant of MeHg degradation, k_d, was included in this equation to represent the photodegradation of $Me^{199}Hg$. k_d was obtained by linear regression of $\ln([Me^{201}Hg])_t$ against t (Eq. (1)) [24, 34].

$$\ln([Me^{201}Hg]_t) = \ln([Me^{201}Hg]_0) - k_d t \quad (1)$$

$$R_{202}^{199}(t) = \frac{[Me^{199}Hg]_t}{[Me^{202}Hg]_t} = \frac{k_m[^{199}Hg^{2+}]_0 - (k_m[^{199}Hg^{2+}]_0 - k_d[Me^{199}Hg]_0)e^{-k_d t}}{k_m[^{202}Hg^{2+}]_0 - (k_m[^{202}Hg^{2+}]_0 - k_d[Me^{202}Hg]_0)e^{-k_d t}} \quad (2)$$

$(k_d > 0)$

$$R_{202}^{199}(t) = \frac{[Me^{199}Hg]_t}{[Me^{202}Hg]_t} = \frac{k_m[^{199}Hg^{2+}]_0 t + [Me^{199}Hg]_0}{k_m[^{202}Hg^{2+}]_0 t + [Me^{202}Hg]_0}$$

$(k_d = 0)$

where $[Me^{m}Hg]_0$ (m=199, 201 or 202) is the concentration of m isotope MeHg at 0 day (ng L^{-1}); $[Me^{m}Hg]_t$ is the concentration of m isotope MeHg at t time (ng L^{-1}); $[^{199}Hg^{2+}]_0$ and $[^{202}Hg^{2+}]_0$ are the concentrations of $^{199}Hg^{2+}$ and $^{202}Hg^{2+}$ at 0 day (ng L^{-1}).

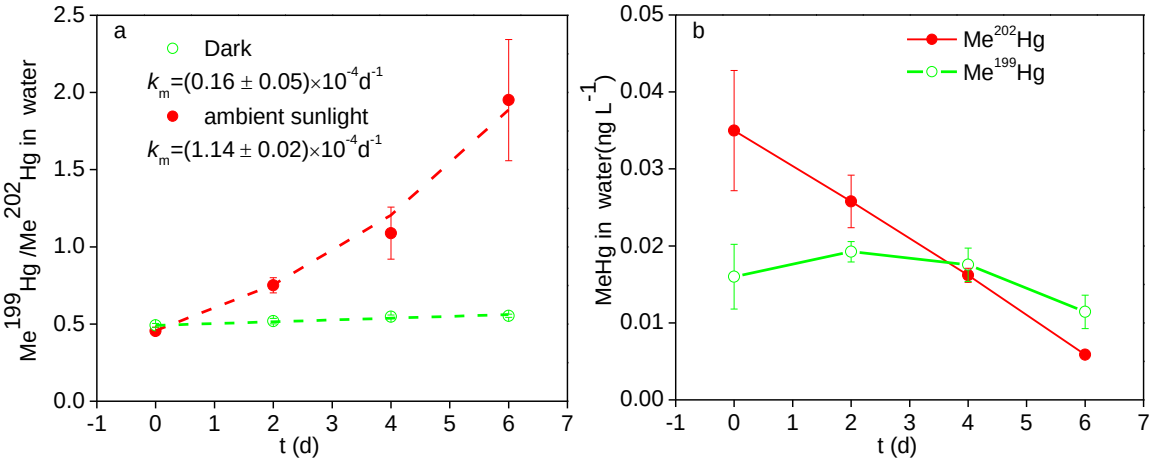

Figure 26. Variation of $Me^{199}Hg/Me^{202}Hg$ ratio (a) and concentrations of $Me^{199}Hg$ and $Me^{202}Hg$ (b) during the incubation of natural water. $Me^{199}Hg/Me^{202}Hg$ ratio was used to calculate the methylation rate constant of spiked $^{199}Hg^{2+}$ (Eq. (2)). Points in plot 2a represent the measured values, while the dashed line shows the simulated results.

Figure 26a shows the methylation of spiked $^{199}Hg^{2+}$ in surface water. The 199/202 ratio of MeHg increased gradually from 0.5 to approximately 2 after 6 days of exposure to sunlight, while negligible change occurred in the dark. To further validate the effect of sunlight on methylation, k_m values at trials with and without sunlight were calculated according to Eq. (2). The $^{199}Hg^{2+}$ in water had a k_m of 1.14±0.02 (×10^{-4} d^{-1}) under ambient sunlight, while it was 0.16±0.05 (×10^{-4} d^{-1}) in the dark. These results suggest that methylation, which is dependent upon sunlight, occurs in natural water. However, its rate was much slower than that of MeHg photodemethylation (k_d =

0.26±0.04 d^{-1}), indicating that methylation in water plays a minor role in the cycling of MeHg. The changes in $Me^{202}Hg$ concentration were taken into account in order to correct for the effect of MeHg demethylation during the incubation. No significant increase in $Me^{199}Hg$ concentration was observed, but a substantial decrease in $Me^{202}Hg$ did occur (Fig. 1b), due to the faster rate of photodemethylation compared to methylation. This indicates that contributions of the photodemethylation of ambient and newly produced $Me^{199}Hg$ were not negligible for the variation of $Me^{199}Hg$. These results suggest that photodegradation of ambient and newly produced $Me^{199}Hg$ should be considered when determining k_m in water, especially for systems with $k_m << k_d$.

Estimation of the Bioavailability of Hg^{2+} and Methylmercury for Methylation and Demethylation in Natural Sediment

The difference between the ambient and newly input Hg species in methylation/demethylation efficiency was often neglected in the previous models[28] which may cause a significant error. Here, a model was developed to calculate the bioavailability of Hg^{2+} and methylmercury for methylation and demethylation in natural sediment using double stable isotope ($^{199}Hg^{2+}$ and $Me^{201}Hg$) addition experiments. The specific methylation and demethylation rate constants of newly spiked $^{199}Hg^{2+}$ and $Me^{201}Hg$ (k_m and k_d) and measured net ambient MeHg production (or degradation) rate (R) were calculated from the increased amount of $Me^{199}Hg$ derived from the spiked $^{199}Hg^{2+}$ ($\Delta[Me^{199}Hg]_{SP}$), the decreased amount of spiked $Me^{201}Hg$ ($\Delta[Me^{201}Hg]_{SP}$), and the net change in the amount of ambient $Me^{202}Hg$ ($\Delta[Me^{202}Hg]_N$), respectively (Eq. (3-5)). In many previous studies[32], the changes in concentrations of measured $Me^{199}Hg$ and $Me^{201}Hg$ were used to substitute for $\Delta[Me^{199}Hg]_{SP}$ and $\Delta[Me^{201}Hg]_{SP}$ to simplify the calculation. However, this simplification could cause a significant error if the methylation or demethylation of ambient mercury is not negligible.

In this study, this defect was overcome by directly calculating the values of $\Delta[Me^{199}Hg]_{SP}$, $\Delta[Me^{201}Hg]_{SP}$, and $\Delta[Me^{202}Hg]_N$ to determine the k_m, k_d and R. They were calculated using equations similar to previously proposed functions for detecting transformations of Hg species.[35] Then, α (ratio of methylation rate constant of ambient to newly spiked Hg) and β (ratio of demethylation rate constant of ambient to newly spiked MeHg) were calculated by fitting the data of measured net MeHg production (or degradation) rate against the potential methylation rate ($k_m[Hg^{2+}]$) and potential demethylation rate ($k_d[MeHg]$) (Eq. (6)). This method was applied to estimate the values of α and β in two types of sediment (Figure 2). α and β in these two sediments were estimated to be 0.06 and 0.93, and 0.02 and 0.71, respectively, indicating that there is a significant difference between the ambient and newly input Hg species in methylation/demethylation efficiency. If α and β were not considered, the estimated net production (or degradation) rate of MeHg in sediment 1 could be overestimated by a factor of 20. The average of the estimated net production (or degradation) rate of MeHg in sediment 2 would increase from -70 to 600 ng m^{-2} d^{-1}. In that case, the net per day increase in MeHg concentration in soil would account for 400% of ambient MeHg concentration. This fails to account for the

mass balance of ambient MeHg. This ratio is decreased to 20% if the estimated α and β are included in the calculation. These results indicate that the difference in methylation/demethylation efficiency of the ambient and newly input Hg species must be taken into account when net MeHg production (or degradation) rates are estimated.

$$k_{\mathrm{m}} = \frac{\Delta[\mathrm{Me}^{199}\mathrm{Hg}]_{\mathrm{SP}}}{[^{199}\mathrm{Hg}^{2+}]_{\mathrm{SP}} \times \mathrm{t}} \quad (3)$$

$$k_{\mathrm{d}} = \frac{\ln \dfrac{[\mathrm{Me}^{201}\mathrm{Hg}]_{\mathrm{SP}}}{[\mathrm{Me}^{201}\mathrm{Hg}]_{\mathrm{SP}} - \Delta[\mathrm{Me}^{201}\mathrm{Hg}]_{\mathrm{SP}}}}{\mathrm{t}} \quad (4)$$

$$R = \frac{\Delta[\mathrm{Me}^{202}\mathrm{Hg}]_{\mathrm{N}}}{P_{202} \times \mathrm{t}} \quad (5)$$

$$R_{\mathrm{x}} = k_{\mathrm{m}}(\mathrm{X}) \times \alpha_{\mathrm{x}} \times [\mathrm{Hg}^{2+}]_{\mathrm{x}} - k_{\mathrm{d}}(\mathrm{X}) \times \beta_{\mathrm{x}} \times [\mathrm{MeHg}]_{\mathrm{X}} \quad (6)$$

where k_{m} is the specific methylation rate constant of spiked $^{199}Hg^{2+}$ (d^{-1}); k_{d} is the specific demethylation rate constant of spiked $Me^{201}Hg$ (d^{-1}); R is the measured production ($R > 0$) or degradation ($R < 0$) rate of ambient MeHg (ng g^{-1} d^{-1}); t is the incubation time (d); $[^{199}Hg^{2+}]_{sp}$ and $[Me^{201}Hg]_{sp}$ are the concentrations of spiked $^{199}Hg^{2+}$ and $Me^{201}Hg$ (ng g^{-1}), respectively; P_{202} is the natural abundance of ^{202}Hg in ambient mercury (29.86%); X represents a specific compartment (soil (X = S), floc (X = F), periphyton (X = P), or water (X = W)); $\bar{R}_{\mathrm{x}}$ is the average net production or degradation rate of ambient MeHg (ng g^{-1} d^{-1}); α_{x} is the ratio of methylation rate constant of ambient to newly spiked Hg for X compartment and β_{x} is the ratio of demethylation rate constant of ambient to newly spiked MeHg; $[\mathrm{Hg}^{2+}]_{\mathrm{x}}$ and $[\mathrm{MeHg}]_{\mathrm{x}}$ are the concentrations of Hg^{2+} and MeHg in X compartment (ng g^{-1} or ng L^{-1}).

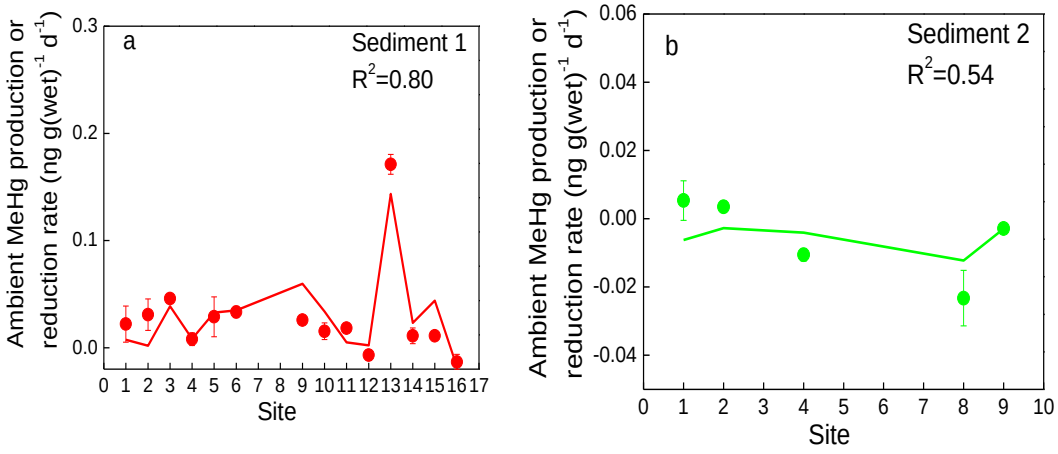

Figure 27. Simulation (line) and measured results (scatter) of net MeHg change rate in sediment 1 (with a relatively lower water content) and sediment 2 (flocculent, with a relatively higher water content).

Enhancement of Cinnabar Dissolution by Thiol-Containing Compounds

Effect of Thiol-Containing Compounds on Cinnabar Dissolution

Effects of thiol-containing compounds on cinnabar dissolution were shown in Figure 3. In the absence of thiol-containing compounds, Hg^{2+} concentration in water was at the level of ~1-2 μg/L (see Fig.3). The addition of 10μmol/L L-cysteine increased it to more than 100 μg/L, indicating the dramatic increase of cinnabar dissolution by cysteine. Glutathione could also increase the dissolution of cinnabar. However, its effect was much smaller compared to cysteine, suggesting that the effect of thiol varies in different species.

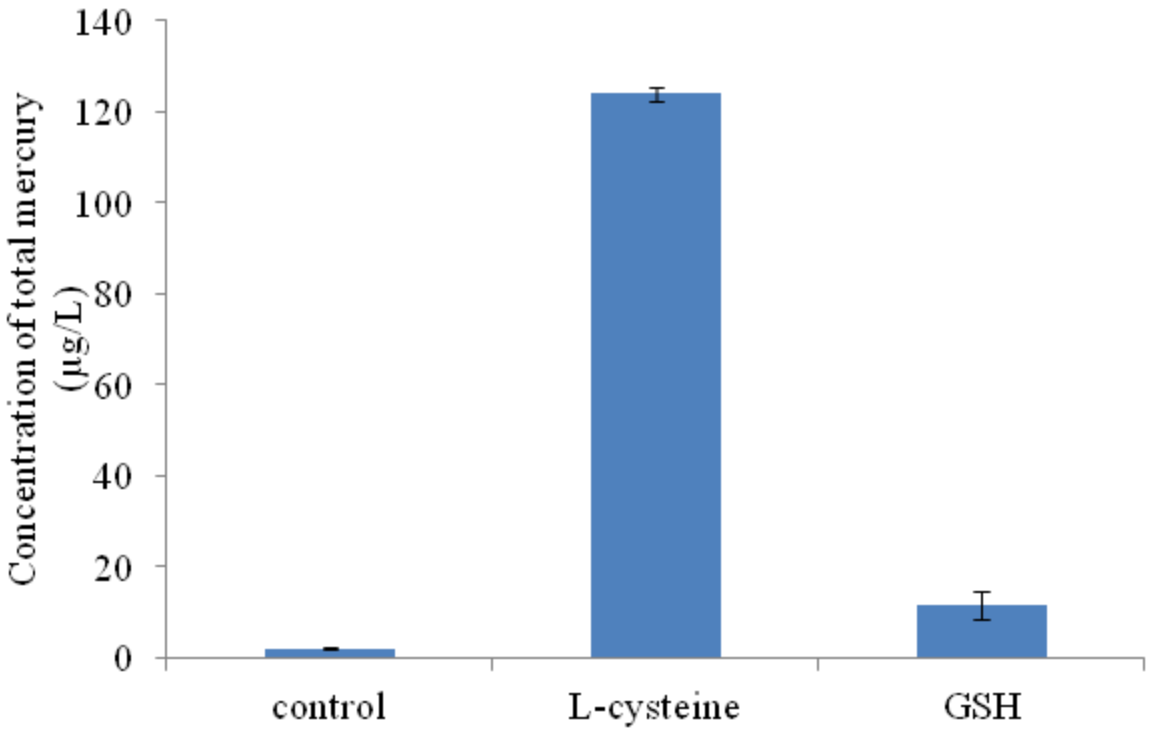

Figure 28. Effects of thiol-containing group on the dissolution of cinnabar under oxic conditions.

Effect of Dissolved Oxygen on Cysteine-Promoted Dissolution of Cinnabar

Figure 4 shows the effect of dissolved oxygen on the cysteine-promoted dissolution of cinnabar. The concentration of Hg^{2+} in aqueous phase was in the order of saturated oxygen> air> anaerobic. Under oxic conditions, Hg^{2+} in water could be as high as 120 μg Hg/L, while this value decreased to about 30 μg Hg/L under anaerobic conditions. These results indicate that oxygen plays a significant role in the dissolution of cinnabar.

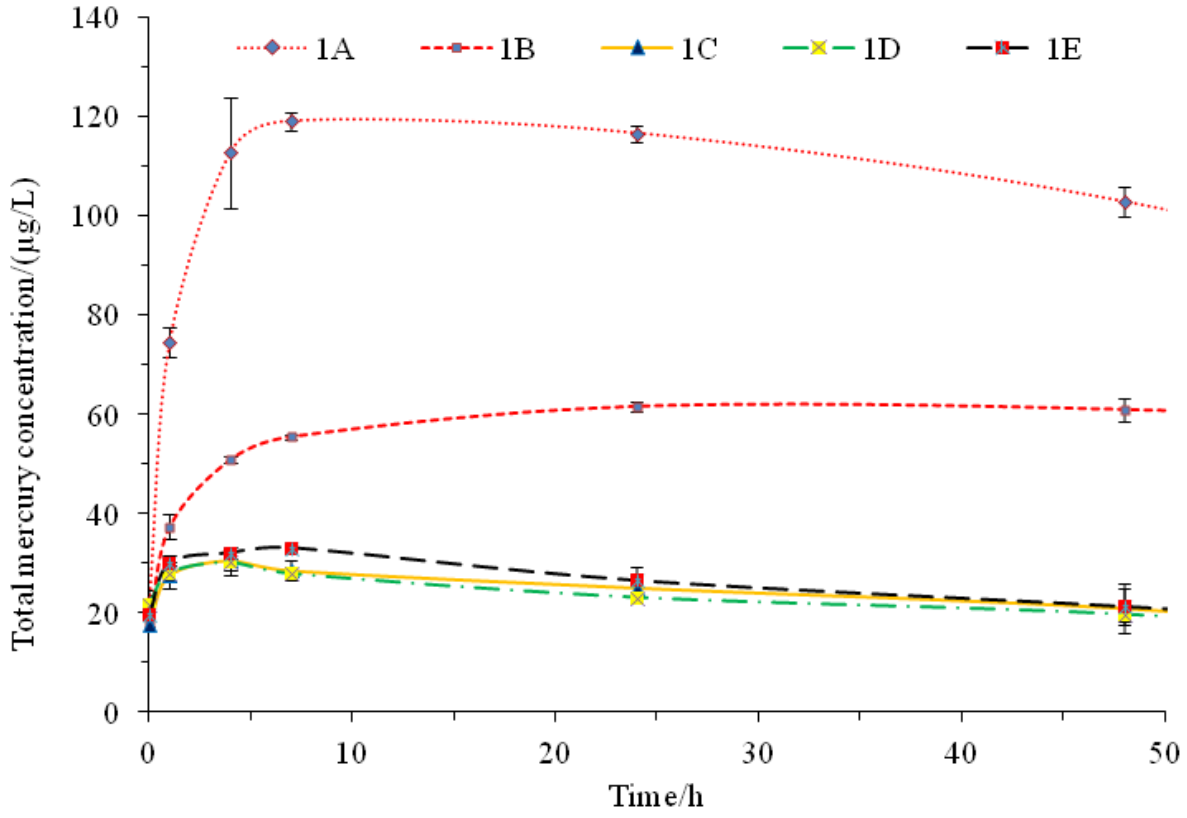

Figure 29. Effects of dissolved oxygen on thiol-promoted dissolution of cinnabar. 1A, in the presence of saturated oxygen; 1B, in the presence of air; 1C, 1D, 1E, under anaerobic conditions.

Modeling Dissolution of Cinnabar in an Aquatic Environment

A model based on chemical thermodynamics was developed to calculate the dissolution of cinnabar under different conditions and elucidate the relative importance of pH, O_2 and cysteine in cinnabar dissolution. Results of the model indicate that dissolved oxygen has the largest enhancing effect on cinnabar dissolution, while pH and cysteine concentrations have no significant promotion on this process. According to the prediction from chemical thermodynamics principles, the solubility of cinnabar in anaerobic environment of pH 8.0 are $8.0\times10^{-14\ \sim\ -2}$ μg/L, this value increased to ~100 μg/L in the presence of dissolved saturated oxygen. In addition, there is no significant difference in the solubility of cinnabar with or without cysteine under oxic conditions. The experimental results suggested that the concentration of Hg^{2+} in water was close to the predicted value in the presence of cysteine. However, it was much lower than the predicted value in the absence of cysteine. Further adsorption experiments showed that a large proportion of added Hg^{2+} could be adsorbed on the surface of cinnabar. By taking consideration of the adsorption of released Hg^{2+} on cinnabar, the proposed model could well predict the dissolution of cinnabar with or without cysteine. These results indicate that oxidization of S (-II) may be the driving force for cinnabar dissolution in aquatic environments. Complexation of cysteine compounds with Hg^{2+} also plays an important role in this process by inhibiting the absorption of released Hg^{2+} on the cinnabar surface.

CONCLUSIONS

Photomethylation of Hg^{2+} in Natural Water

The double isotope addition technique ($^{199}Hg^{2+}$ and $Me^{201}Hg$) was applied to measure the photomethylation of Hg^{2+} in water. A new model was developed to calculate the methylation rate constant of the spiked Hg^{2+} in water. This model corrected for the defect of previous models, in which the degradation of ambient MeHg and the newly produced MeHg was not taken into account. Methylation of Hg^{2+} was observed in natural water, with a rate of 1.14±0.02 ($\times 10^{-4}$ d^{-1}). This process is mediated by sunlight. However, its rate was much slower than that of MeHg photodemethylation (k_d=0.26±0.04 d^{-1}), indicating that methylation in water plays a minor role in the cycling of MeHg. In addition, the contributions of the photodemethylation of ambient and newly produced $Me^{199}Hg$ were proven not to be negligible for the variation of $Me^{199}Hg$.

Estimation of the Bioavailability of Hg^{2+} and Methylmercury for Methylation and Demethylation in Natural Sediment

The difference between the ambient and newly input Hg species in methylation/demethylation efficiency was often neglected in the previous models which may cause a significant error. Here, we developed a method to calculate the bioavailability of Hg^{2+} and methylmercury for methylation and demethylation in natural sediment using double stable isotope ($^{199}Hg^{2+}$ and $Me^{201}Hg$) addition experiments. The percentage of bioavailable Hg^{2+} and MeHg for methylation/demethylation (α_x and β_x) was estimated to be 0.02-0.06 and 0.71-0.93, separately in studied sediments, indicating that there is a significant difference between the ambient and newly input Hg species in methylation/demethylation efficiency. The difference in methylation/demethylation efficiency of the ambient and newly input Hg species must be taken into account when net MeHg production (or degradation) rates are estimated. If α and β were not considered, the estimated net production (or degradation) rate of MeHg in sediment could be overestimated by a factor of 20.

Effect of Thiol-Containing Compounds on Cinnabar Dissolution

Thiol-containing compounds could significantly promote the dissolution of cinnabar. In the absence of thiol-containing compounds, Hg^{2+} concentration in water was at the level of ~1-2 μg/L. The addition of 10μmol/L L-cysteine increased it to more than 100 μg/L. Glutathione could also increase the dissolution of cinnabar. However, its effect was much smaller compared to cysteine, suggesting that the effect of thiol varies in different thiol species. In addition, oxygen plays a significant role in the dissolution of cinnabar. The concentration of Hg^{2+} in the aqueous phase was in the order of saturated oxygen > air > anaerobic. A model based on chemical thermodynamics was developed to calculate the dissolution of cinnabar under different conditions and elucidate the relative importance of pH, O_2 and thiol-containing compounds in cinnabar dissolution. By taking into consideration the adsorption of released Hg^{2+} on cinnabar, the proposed model could well predict the dissolution of cinnabar with or without cysteine. Both model and experimental results suggest that oxidization of S (-II) may be the driving force for cinnabar dissolution in aquatic environments. Complexation of cysteine with Hg^{2+} also plays an

important role in this process by inhibiting the absorption of released Hg^{2+} on the cinnabar surface.

FUTURE WORK

Experimental activity conducted during FY2011 has revealed that 1) the percentage of Hg species available for methylation or demethylation is a critical parameter for evaluating the production and reduction of MeHg in aquatic ecosystems, and 2) dissolution of cinnabar can significantly increase Hg concentrations in water and that thiols can promote this process. The proposed FY2012 scope for this task will focus on further understanding of these two important processes in modeling the cycling of Hg in aquatic ecosystems. Experiments will be conducted to determine 1) effects of various environmental factors (pH, Eh, mineral oxides, water content, NOM (natural organic matter)) on the percentage of legacy Hg species available for methylation and demethylation in sediment, and 2) effects of DOM (dissolved organic matter) and other complexing reagents (e.g., Cl^-) on the dissolution of cinnabar, and through which process these factors affect the dissolution of cinnabar.

In order to estimate the difference between legacy and newly input Hg species in methylation and demethylation, the stable isotope addition method will be employed in these incubation experiments. The formation of $Me^{199}HgCl$, the decrease in $Me^{201}HgCl$, and the change in the amount of $Me^{202}HgCl$ will be measured simultaneously by GC-ICP-MS, and the ratios of methylation/demethylation rate constant of legacy to newly input Hg will be calculated. Experiments will be conducted on sediment samples with various levels of pH, Eh, mineral oxides, water content, and NOM to determine the effects of these factors on this parameter.

In addition, experiments will be carried out to investigate the effects of DOM and Cl^- on the dissolution of cinnabar. Natural DOM (>3000 Da) will be isolated from natural waters by using cross-flow ultra-filtration technique. Various concentrations of DOM and Cl^- will be added to the cinnabar suspension. The mixtures will be shaken under different redox conditions (purging with N_2 or O_2) and various pH levels. The concentrations of Hg^{2+} in aqueous phase will be determined by CV-AFS. In FY2011, a mechanism was proposed (including chemical thermodynamics and adsorption/desorption of released Hg^{2+} on cinnabar) for the cinnabar dissolution and a model was established to predict the dissolution of cinnabar under different conditions of pH and O_2.This model will be improved by incorporating the binding of Hg2+ with DOM and Cl^- and effects of DOM and Cl^- on the adsorption/desorption of Hg^{2+} on cinnabar. These improvements will make the model better represent the natural environment. Two important parameters for this model, the binding constants of Hg^{2+} and DOM and adsorption/desorption constants of Hg^{2+} in the presence of DOM and Cl^-, will be experimentally measured. The proposed mechanism of cinnabar dissolution in the presence of DOM and Cl^- will be validated by simulating the observed experimental results with the improved model. The model will also be used to determine through which process DOM and Cl^- affect the dissolution of cinnabar.

Subtask 3.1: Effects of various environmental factors on the percentage of legacy Hg species available for methylation and demethylation in sediment

The double stable isotope addition method will be employed in incubation experiments to measure the ratios of methylation/demethylation rate constant of legacy to newly input Hg. Effects of a number of biogeochemical factors, including pH, Eh, mineral oxides, water content, and NOM, on this ratio will be determined.

Subtask 3.2: Effects of DOM and Cl^- on the dissolution of cinnabar

Natural DOM (>3000 Da) will be isolated from natural waters by using cross-flow ultra-filtration technique. Effects of DOM and Cl^- on cinnabar dissolution will be investigated under different redox conditions (purging with N_2 or O_2) and various pH levels.

Subtask 3.3: Modeling the dissolution of cinnabar in the presence of DOM and Cl^-

Based on the chemical thermodynamics and adsorption/desorption of released Hg^{2+} on cinnabar, a model will be developed to predict the dissolution of cinnabar in the presence of DOM and Cl^- under different conditions of pH and dissolved O_2. Two important parameters for this model, the binding constants of Hg^{2+} and DOM and adsorption/desorption constants of Hg^{2+} in the presence of DOM and Cl^-, will be experimentally measured. The model will be validated through simulating the observed experimental results. The model will be used to determine through which process DOM and Cl^- affect the dissolution of cinnabar.

REFERENCES

1. Liu, G. L.; Cabrera, J.; Allen, M.; Cai, Y. Mercury characterization in a soil sample collected nearby the DOE Oak Ridge Reservation utilizing sequential extraction and thermal desorption method. Science of the Total Environment 2006, 369 (1-3), 384-392.
2. Mikac, N.; Foucher, D.; Niessen, S.; Fischer, J. C. Extractability of HgS (cinnabar and metacinnabar) by hydrochloric acid. Analytical and Bioanalytical Chemistry 2002, 374 (6), 1028-1033.
3. Mikac, N.; Foucher, D.; Niessen, S.; Lojen, S.; Fischer, J. C. Influence of chloride and sediment matrix on the extractability of HgS (cinnabar and metacinnabar) by nitric acid. Analytical and Bioanalytical Chemistry 2003, 377 (7-8), 1196-1201.
4. Paquette, K.; Helz, G. SOLUBILITY OF CINNABAR (RED HGS) AND IMPLICATIONS FOR MERCURY SPECIATION IN SULFIDIC WATERS. Water Air and Soil Pollution 1995, 80 (1-4), 1053-1056.
5. Paquette, K. E.; Helz, G. R. Inorganic speciation of mercury in sulfidic waters: The importance of zero-valent sulfur. Environmental Science & Technology 1997, 31 (7), 2148-2153.
6. Ravichandran, M.; Aiken, G. R.; Reddy, M. M.; Ryan, J. N. Enhanced dissolution of cinnabar (mercuric sulfide) by dissolved organic matter isolated from the Florida Everglades. Environmental Science & Technology 1998, 32 (21), 3305-3311.

7. Waples, J. S.; Nagy, K. L.; Aiken, G. R.; Ryan, J. N. Dissolution of cinnabar (HgS) in the presence of natural organic matter. Geochimica Et Cosmochimica Acta 2005, 69 (6), 1575-1588.
8. Burkstaller, J. E.; McCarty, P. L.; Parks, G. A. Oxidation of cinnabar by iron(III) in acid mine waters. Environmental Science & Technology 1975, 9 (7), 676-678.
9. Holley, E. A.; McQuillan, A. J.; Craw, D.; Kim, J. P.; Sander, S. G. Mercury mobilization by oxidative dissolution of cinnabar (alpha-HgS) and metacinnabar (beta-HgS). Chemical Geology 2007, 240 (3-4), 313-325.
10. Barnett, M. O.; Turner, R. R.; Singer, P. C. Oxidative dissolution of metacinnabar (beta-HgS) by dissolved oxygen. Applied Geochemistry 2001, 16 (13), 1499-1512.
11. Ngu-Schwemlein, M.; Merle, J. K.; Healy, P.; Schwemlein, S.; Rhodes, S. Thermodynamics of the complexation of Hg(II) by cysteinyl peptide ligands using isothermal titration calorimetry. Thermochimica Acta 2009, 496 (1-2), 129-135.
12. Ravichandran, M. Interactions between mercury and dissolved organic matter - a review. Chemosphere 2004, 55 (3), 319-331.
13. Mah, V.; Jalilehvand, F. Mercury(II) complex formation with glutathione in alkaline aqueous solution. Journal of Biological Inorganic Chemistry 2008, 13 (4), 541-553.
14. Aiken, G.; Waples, J.; Nagy, K. L.; Ryan, J.; Ravichandran, M. Dissolution of cinnabar by dissolved organic matter. Abstracts of Papers of the American Chemical Society 2001, 222, U425-U425.
15. Ravichandran, M.; Aiken, G. R.; Reddy, M. M.; Ryan, J. N. Enhanced dissolution of cinnabar (mercuric sulfide) by aquatic humic substances. Abstracts of Papers of the American Chemical Society 1998, 216, U785-U785.
16. Nagy, K. L.; Kerr, M. Enhanced dissolution of cinnabar by dissolved organic matter in anoxic solutions. Geochimica Et Cosmochimica Acta 2010, 74 (12), A744-A744.
17. 1Compeau, G. C.; Bartha, R. Sulfate-reducing bacteria: principal methylators of mercury in anoxic estuarine sediment. Appl. Environ. Microbiol. 1985, 50 (2), 498-502.
18. Kerin, E. J.; Gilmour, C. C.; Roden, E.; Suzuki, M. T.; Coates, J. D.; Mason, R. P. Mercury methylation by dissimilatory iron-reducing bacteria. Appl. Environ. Microbiol. 2006, 72 (12), 7919-7921.
19. Gilmour, C. C.; Henry, E. A. Mercury Methylation by Sulfate-Reducing Bacteria - Biogeochemical and Pure Culture Studies, In American Chemical Society; San Francisco, USA, 1992.
20. Gray, J. E.; Hines, M. E. Biogeochemical mercury methylation influenced by reservoir eutrophication, Salmon Falls Creek Reservoir, Idaho, USA. Chem. Geol. 2009, 258 (3-4), 157-167.
21. Mitchell, C. P. J.; Gilmour, C. C. Methylmercury production in a Chesapeake Bay salt marsh. J. Geophys. Res. (G Biogeosci.) 2008, 113, G00C04.
22. Tsui, M. T. K.; Finlay, J. C.; Nater, E. A. Effects of Stream Water Chemistry and Tree Species on Release and Methylation of Mercury during Litter Decomposition. Environ. Sci. Technol. 2008, 42 (23), 8692-8697.
23. Zizek, S.; Guevara, S. R.; Horvat, M. Validation of methodology for determination of the mercury methylation potential in sediments using radiotracers. Anal. Bioanal. Chem. 2008, 390 (8), 2115-2122.
24. Hammerschmidt, C. R.; Fitzgerald, W. F. Photodecomposition of methylmercury in an arctic Alaskan lake. Environ. Sci. Technol. 2006, 40 (4), 1212-1216.

25. Li, Y. B.; Mao, Y. X.; Liu, G. L.; Tachiev, G.; Roelant, D.; Feng, X. B.; Cai, Y. Degradation of Methylmercury and Its Effects on Mercury Distribution and Cycling in the Florida Everglades. Environ. Sci. Technol. 2010, 44 (17), 6661-6666.
26. Lehnherr, I.; St Louis, V. L.; Hintelmann, H.; Kirk, J. L. Methylation of inorganic mercury in polar marine waters. Nat. Geosci. 2011, 4 (5), 298-302.
27. Siciliano, S. D.; O'Driscoll, N. J.; Tordon, R.; Hill, J.; Beauchamp, S.; Lean, D. R. S. Abiotic Production of Methylmercury by Solar Radiation. Environ. Sci. Technol. 2005, 39 (4), 1071-1077.
28. Gilmour, C. C.; Riedel, G. S.; Ederington, M. C.; Bell, J. T.; Benoit, J. M.; Gill, G. A.; Stordal, M. C. Methylmercury concentrations and production rates across a trophic gradient in the northern Everglades. Biogeochemistry 1998, 40, 327-345.
29. Gray, J. E.; Hines, M. E.; Biester, H. Mercury methylation influenced by areas of past mercury mining in the Terlingua district, Southwest Texas, USA. Appl. Geochem. 2006, 21 (11), 1940-1954.
30. Gray, J. E.; Hines, M. E.; Higueras, P. L.; Adatto, I.; Lasorsa, B. K. Mercury speciation and microbial transformations in mine wastes, stream sediments, and surface waters at the Almaden Mining District, Spain. Environ. Sci. Technol. 2004, 38 (16), 4285-4292.
31. Hintelmann, H.; Keppel-Jones, K.; Evans, R. D. Constants of mercury methylation and demethylation rates in sediments and comparison of tracer and ambient mercury availability. Environ. Toxicol. Chem. 2000, 19 (9), 2204-2211.
32. Drott, A.; Lambertsson, L.; Bjorn, E.; Skyllberg, U. Do potential methylation rates reflect accumulated methyl mercury in contaminated sediments? Environ. Sci. Technol. 2008, 42 (1), 153-158.
33. Eckley, C. S.; Hintelmann, H. Determination of mercury methylation potentials in the water column of lakes across Canada. Sci. Total Environ. 2006, 368 (1), 111-125.
34. Lehnherr, I.; St. Louis, V. L. Importance of Ultraviolet Radiation in the Photodemethylation of Methylmercury in Freshwater Ecosystems. Environ. Sci. Technol. 2009, 43 (15), 5692-5698.
35. Hintelmann, H.; Evans, R. D. Application of stable isotopes in environmental tracer studies - Measurement of monomethylmercury (CH3Hg+) by isotope dilution ICP-MS and detection of species transformation. Fresenius J. Anal. Chem. 1997, 358 (3), 378-385.

TASK 4: GEODATABASE DEVELOPMENT FOR HYDROLOGICAL MODELING SUPPORT

INTRODUCTION

During 2007-2011, FIU has developed and used three integrated watershed models for Y-12 NSC, White Oak Creek (WOC), and EFPC. These models include overland, stream and groundwater flows in the variable and fully saturated zones, and implement the complex biological and chemical dynamics of mercury species to simulate the broader range of mercury distribution throughout the delineated WOC and EFPC watersheds. More than a hundred simulations were completed to calibrate the models, to derive model uncertainties and to provide analysis of remediation scenarios. The simulations resulted in hundreds of gigabytes of simulation data. The main objective of this task was to therefore create a geodatabase to support hydrological model development and simulation of contaminant fate and transport at Oak Ridge Reservation (ORR), TN and to make the data accessible to project team members for editing and data management, storage and backup purposes. The geodatabase serves as a centralized data management system which facilitates storage, editing, and versioning of model parameters. Model input parameters include standard Geographic Information Systems (GIS) data derived from readily available sources including the Oak Ridge Environmental Information System (OREIS), USGS, NRCS STATSGO or SSURGO soil database, and the U.S. EPA MRLC or NALC land cover database.

A working prototype was developed by FIU ARC during FY 2010. The ORR Geodatabase is a multiuser relational database management system (RDBMS) built upon a Microsoft SQL Server platform developed using Environmental Systems Research Institute (ESRI) ArcSDE technology. The geodatabase structure facilitates concurrent multi-user editing and management of spatial data within the ArcGIS framework and is comprised of a series of tables which contain feature, raster and attribute data, as well as metadata. Since the ORR database, as previously mentioned, is primarily based on the ArcHydro data model, it possesses a spatial relational database management (RDMS) schema and relationship structure specific to hydrologic systems where spatial relationships between hydrological parameters and geographical features can be defined.

The multiuser functionality of this system is its most significant feature as it facilitates simultaneous editing of the geographic data utilized and generated during hydrological model development and model simulation. A mechanism referred to as "versioning" records all the database changes as rows in tables, so that GIS transactions can be stored in the database and the metadata for each “version” can be used to isolate multiple edit sessions, share replicas, synchronize contents across multiple databases, perform automatic archiving, and support historical queries.

Tools to support the import, export or conversion of various file formats also exist, which is especially important for interoperability between the ArcGIS and MIKE modeling software. MIKE 11 GIS [9] for example, which is a pre- and post-processing module for MIKE 11 that is included as an extension to the ESRI ArcMap 10.0 version, was used to assist in the import,

processing and export of network, cross-section and boundary files used within the MIKE 11 models. MIKE 11 GIS can also be used for comprehensive timeseries data management to present timeseries results and maps from MIKE 11 simulations, and includes non-point and point pollutant load estimation tools for MIKE 11 water quality simulations. These types of tools are useful in this case as the GIS and MIKE SHE/11 model are, as Gogu et al., 2001 [5] describe, "loosely coupled" at this stage of development, where the software packages remain independent systems and data is transferred as predefined input/output model files, the advantage of this being that it facilitates potential future changes in the software in an independent manner.

As FIU ARC continues to conduct model simulations to support the D&D remediation activity at ORR, there will be an ongoing need for the update of the geodatabase and the utilization of the integrated GIS-hydrological modeling system developed. To support model development, the following tasks were completed during FY 2011:

1. Compilation of MIKE-SHE/MIKE-11 model configuration files and conversion when necessary to GIS format to facilitate easy integration into the system being developed.
2. Import of simulation input and output files for the Y-12 NSC, WOC and EFPC models into the geodatabase, utilizing the in-built ArcGIS versioning utility when necessary during simultaneous multi-user editing of data files and geoprocessing tasks.

RESULTS AND DISCUSSION

Once the ORR geodatabase was created, observed hydrogeological data was imported into existing feature and raster datasets which were defined according to their use (e.g. for hydrological modeling and analysis, mapping or 3D display) and the model compartment where the file was to be utilized (e.g. land cover/land use, transportation, topologies, networks, contaminant concentrations, etc.). Metadata which specifies whether the data is an original downloaded file, a file modified for model development or a file generated from running model simulations was also defined at this point.

The Arc Hydro data model is designed to support hydrologic simulation models within the ArcGIS environment, such as MIKE SHE/11, which requires and generates spatial and temporal data, most significantly data such as channel cross sections, stream geometric networks and nodes, monitoring points, watersheds and subwatersheds, and other hydrographic and drainage files. The ArcHydro geodatabase structure incorporates these hydrologic elements and their topographic relationships used in the hydrologic simulations, and is therefore suitable for integration with the MIKE SHE/11 models developed by ARC-FIU for the ORR which share the same watershed structure and stream network, for example the models developed for the Old Salvage Yard (OSY) at Y-12 NSC and Upper East Fork Poplar Creek (UEFPC) which share data common data files related to the entire EFPC watershed. The geodatabase structure of this model uses tables which each have a field in common with a unique identification number that is used to establish relationships between the various hydrologic files. This structure enables linkage with scalable hydrologic modeling tools and applications to model hydrologic systems. The Arc Hydro data model also facilitates the import of timeseries data into ArcGIS object classes which are tables within the geodatabase that store temporal data that is often related to the hydrologic spatial features.

MIKE SHE/11 requires several model-specific input parameters. Many of these file types, can be imported into a geodatabase through the ArcGIS GUI via MIKE 11 GIS and are stored as both feature and object classes, or as raster grid files. Object classes represent some of the timeseries (dfs0) data used for model simulations. MIKE 11 GIS is a pre- and post-processing ArcGIS extension tool for MIKE 11 files, which essentially serves as a geodata model that generates a geodatabase within the ArcMap interface to store MIKE 11 spatial and timeseries (i.e., geographic, numeric and text) input data and simulation results. This dynamic geodatabase serves as a temporary repository of MIKE 11 files in this case, and GIS and hydrologic model integration is achieved via the import and export of data between the ArcGIS system and the MIKE SHE/11 hydrological model. Data is ultimately stored in the static ORR Geodatabase which serves as what is described by Olivera et al., 2006 [10] as a "hub data model", which is a non-model-specific repository of information from various sources that the models developed for the different areas of Oak Ridge Reservation may have in common.

It is significant to note that ArcObjects which is a part of the ArcGIS system is based on Microsoft's Component Object Model (COM) which is an interface-based programming model that can be used to extend the functionalities of existing ArcGIS applications. COM defines a protocol that enables functionality of Windows-based applications within ArcGIS, so that modules or components of various software products can be dynamically interchanged [12]. MIKE 11 GIS takes advantage of the ArcGIS GUI and uses ArcObjects for programming that conforms to the COM design standard.

Since the MIKE 11 GIS geodatabase is model-specific, the ORR Geodatabase was designed as a non-model-specific repository for data from various sources used for model development and also for transfer of simulation data from the MIKE 11 GIS geodatabase. Future plans which are not within the work scope for FY 2011, include the development of a protocol to automate the process of data transfer between the dynamic MIKE 11 GIS geodatabase and the static hub ORR Geodatabase. According to Olivera et al., 2006 [10], this concept was derived from Olivera et al., 2003 which describes the use of an ArcHydro geodatabase as a data “hub”, which is the same manner in which the ORR Geodatabase is used.

Several model-specific output files including computed flow data at each node (head pressures in the saturated zone for each timestep), computed flow data in the rivers for each time step, computed concentrations in the overland, unsaturated, saturated zones and river (daily timeseries) and sedimentation information (total suspended particles, mercury concentrations, sediments) are created after model simulation, many of which are raster (dfs2) grid files. These files can be loaded into the database in several ways including: (1) the ArcGIS/geoprocessing graphical user interface (GUI), (2) the SDERASTER command line loader, (3) the ArcObjects COM API customized application, or (4) using geoprocessing functions such as scripting.

Raster files generated by model simulations can also be kept in the default system folders created by the MIKE SHE/11 model, and instead system tables within the ORR Geodatabase used to store the metadata related to these files with hyperlinks that serve as pointers to the locations of the actual data files.

In many instances, file modification is necessary either for use at smaller scales or to modify appended timeseries or attribute data to run comparative simulations. This was done using ArcGIS geoprocessing tools to generate compatible MIKE SHE/11 model input data. A process referred to as versioning is also supported within the ArcGIS system, which facilitates concurrent editing by authorized users and tracks the edits made to a specific dataset. Versioning is especially beneficial for management of the hydrological modeling workflow within a geodatabase environment, where different stages of the modeling process can be represented by different file versions. This facilitates simulation of what-if scenarios without affecting original datasets and provides a framework for security management and quality assurance in data editing. Once a user has completed editing, changes made in a new version may be merged into a previous version. This process of version reconciliation facilitates effective conflict resolution between the version being edited and any of its ancestor versions, which is especially important when edits are being made to the data by various editors.

CONCLUSIONS

The ORR geodatabase was developed by FIU-ARC researchers during FY 2010 for storage and management of spatial and temporal data used in the development of hydrological models of the EFPC and WOC watersheds. It is based primarily on the ArcHydro data model which has a structure that can support hydrologic model simulations through incorporation of traditional spatial and temporal hydrogeologic parameters within the ArcGIS system. This geodatabase serves as a central data "hub" or repository of information from various sources required for model configuration and simulation of surface and subsurface flow and contaminant transport. The ArcGIS interface also enables storage, processing and visualization of model results. MIKE 11 GIS was used as an extension tool embedded within the ArcMap interface to assist in the interchange of files between the MIKE SHE/11 model and the ArcGIS system. A dynamic geodatabase is generated upon the use of MIKE 11 GIS which is used to temporarily import and process model-specific data files. Processed data is then either exported for use in model simulations or transferred to the ORR Geodatabase for storage, backup and retrieval when necessary.

A "GIS & Hydrological Modeling Data Server Management" document was created as an internal reference document which provides system configuration details and credentials to be used for accessing the database. As FIU-ARC continues to conduct model simulations to support the D&D remediation activity at ORR, there will be an ongoing need for update of the geodatabase and the utilization of the integrated GIS-hydrological modeling system developed. As such, there is a continuous import/export of spatial data into the geodatabase and execution of geoprocessing tasks as necessary for model simulations. The update of metadata is also a continuous work in progress as a data quality assurance measure.

FUTURE WORK

The work proposed for FY12 will serve to extend the geodatabase capabilities by creating a GIS-based model using ArcGIS Model Builder as well as Python scripting that will automate the process of data transfer between the dynamic MIKE 11 GIS geodatabase and the static hub ORR Geodatabase, querying the existing ORR Geodatabase based on specific environmental

parameters, performing analyses based on specified algorithms and generating maps with the spatial distribution of computed and observed data. This can then be further extended to facilitate online querying of the database using downloadable freeware and generation of maps, graphs and reports, to more easily share the data with other project stakeholders such as DOE personnel and ORR site contractors.

REFERENCES

1. Castle, E. (2003). Geodatabases in Design: A Floodpain Analysis of Little Kitten Creek. Thesis. Brigham Young University.
2. ESRI. (n.d.). ArcGIS Server .NET Help - Setting up a direct connection to SQL Server. Retrieved 2010, from ArcGIS Resource Center: http://goo.gl/N4jpq.
3. ESRI. (n.d.). ArcGIS Server 10 Server Requirements. Retrieved 2010, from ArcGIS Resource Center: http://goo.gl/hNMP5.
4. ESRI. (n.d.). Server 10 .NET Install Guide - Installing ArcGIS Server for the Microsoft .NET Framework overview. Retrieved 2010, from ArcGIS Resource Center: http://goo.gl/4Xy7W.
5. Gogu, R. (2001). GIS-based hydrogeological databases and groundwater modelling. Hydrogeology Journal, 9:555–569. DOI 10.1007/s10040-001-0167-3.
6. Law, D. (2010). Versioning 101: Essential information about ArcSDE geodatabases. ArcUser Online (Winter), 42-48.
7. Maidment, D. R. (2002). Arc Hydro: GIS for Water Resources. ESRI Press.
8. Miessau, R. R. (2007). Using ArcGIS to Support a Regional Hydrologic Model - Paper 2191. ESRI User Conference Proceedings. San Diego, CA: ESRI.
9. MIKE by DHI. (2011). MIKE 11 GIS User's Guide.
10. Olivera, F. V. (2006). ArcGIS-SWAT: A Geodata Model and GIS Interface for SWAT. Journal of the American Water Resources Association.
11. ESRI. (2005). Raster Data in ArcSDE 9.1. An ESRI White Paper. Retrieved 2010, from ArcGIS Resource Center: http://goo.gl/sRvOy.
12. ESRI. (n.d.). Programming against ArcObjects. Introduction to COM. Retrieved 2010, from ArcGIS Resource Center: http://goo.gl/qZjQR.

TASK 5: STUDENT SUPPORT FOR MODELING OF GROUNDWATER FLOW AND TRANSPORT AT MOAB SITE

INTRODUCTION

FIU, in collaboration with the DOE's Moab site, is using an existing groundwater numerical model to evaluate the tailings pore-water seepage in order to assist in effective dewatering of the tailings pile and to optimize the groundwater extraction well field as part of the DOE Uranium Mill Tailings Remedial Action (UMTRA) for the Moab site. The work was carried out with support from student interns who assisted in the collection of groundwater samples and site data and applied the existing groundwater and transport model (SEAWAT available from the public domain) to analyze the groundwater flow and transport data of the Moab site. The objective of this model is to analyze the nitrogen and uranium cycle in the environment and provide forecasting capabilities for the fate and transport of contamination within the Moab site and to provide information which can be used to determine the efficiency of remedial actions in reducing the concentration and load of contaminants and to assist DOE in deciding the effectiveness of remedial actions. Modeling is to be performed with MODFLOW, SEAWAT and FEFLOW as a benchmark. The main objective is to determine the effect of discharge of a legacy ammonia plume from the brine zone after the extraction wells and injection system have been shut off. The model will be used to predict capture zones for different operating scenarios, mass removal; and time to complete remediation.

EXECUTIVE SUMMARY

An estimated 16 million tons of uranium mill tailings have been left behind following the cessation of processing operations at the Moab Uranium Mill Tailings Remedial Action (UMTRA) Project site in 1984. These tailings were accumulated in an unlined impoundment, a portion of which is in the 100-year floodplain of the Colorado River. In 2001, ownership of the Moab site was transferred to DOE along with the responsibility for its remediation in accordance with Title I of the Uranium Mill Tailings Radiation Control Act (UMTRCA). Results of investigations indicate that site-related contaminants have leached from the tailings pile into the shallow groundwater and some of the more mobile constituents have migrated downgradient and are discharging to the Colorado River adjacent to the site. The most pervasive and highest concentration constituents are ammonia and uranium. In order to address concerns regarding elevated ammonia levels in groundwater discharging to the Colorado River from the Moab site, DOE implemented an interim action system consisting of a series of extraction wells which have removed more than 168 million gallons of groundwater and prevented more than 687,000 lbs of ammonia and about 3,150 lbs of uranium from reaching the river. In support of this effort and to better understand the subsurface hydrology, a finite difference transient groundwater flow and transport model was developed by one of DOE's contractors. FIU is applying this groundwater numerical model to evaluate the tailings pore-water seepage in order to assist in effective dewatering of the tailings pile and to optimize the groundwater extraction well field as part of the DOE UMTRA for the Moab site. In order to reduce contaminant mass in the groundwater system and to be protective of potential endangered fish habitat in backwater areas of the river, the model will be used to simulate remedial actions proposed by DOE including pumping

contaminated groundwater from the shallow plume to an evaporation pond on top of the tailings pile, and injecting the diverted Colorado River water into the alluvial aquifer. Numerical simulation of the proposed remedial actions will aid in prediction of the time to reach cleanup levels and assist DOE in optimization of the operation of groundwater extraction well fields, infiltration of treated water, and injection of clean fresh water for the DOE UMTRA site in Moab, Utah.

SIMULATIONS AND RESULTS

FIU has applied the groundwater numerical model to evaluate the tailings pore-water seepage in order to assist in effective dewatering of the tailings pile and to optimize the groundwater extraction well field as part of the DOE UMTRA for the Moab site. Preliminary simulation results show a good match of observed and computed monthly data [**Figure 30**].

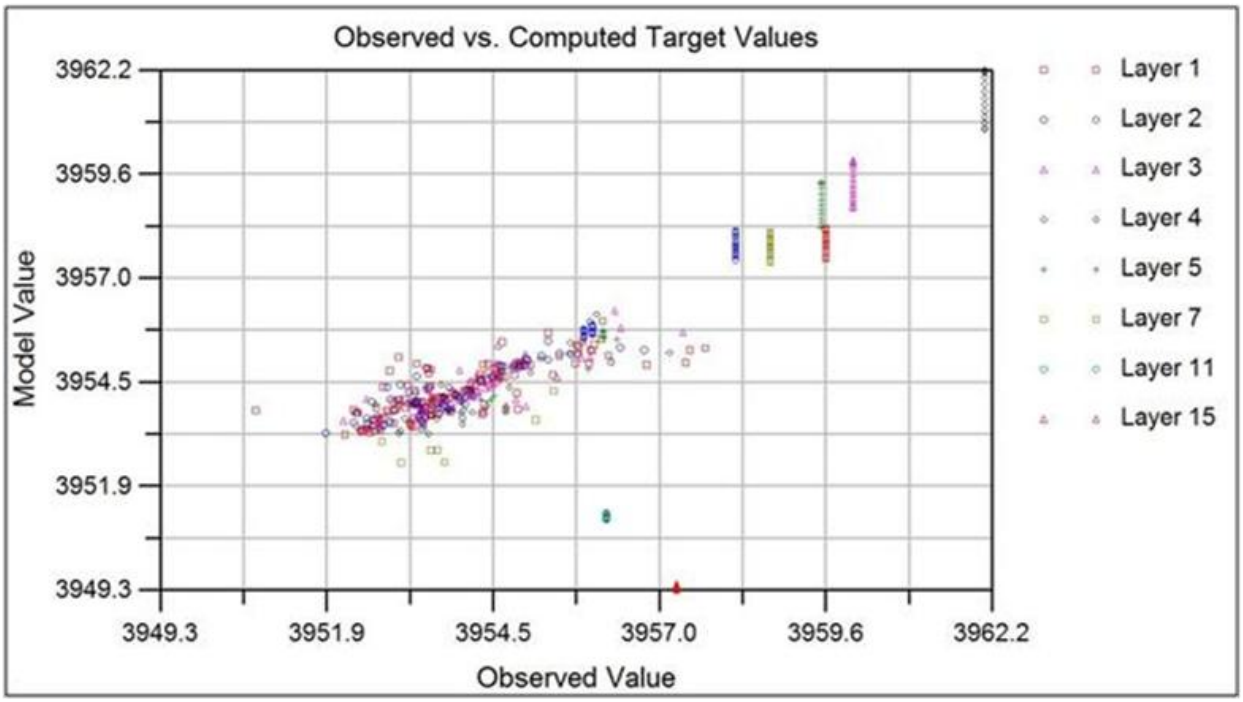

Figure 30. Calibration plot of observed vs. computed heads.

The calibrated model predicts a median monthly groundwater mass balance of 275 gallons per minute. With the exception of April through June, groundwater discharges to the Colorado River from the Moab Site. For April through June, the river recharges the aquifer at between 340 to 1,449 gallons per minute. Simulations results show that ambient recharge (precipitation) occurs in January, February, November and December at rates ranging from 46 to 195 gallons per minute. Tailings pile recharge is constant monthly at 9 gallons per minute. Recharge associated with Moab Wash and the surrounding bedrock is also constant monthly at 39 gallons per minute.

Discharge to the Colorado River is predicted to range between 159 to 495 gallons per minute. Evapotranspiration (ET), which is active May through September and again in November ranges from 22 to 840 gallons per minute.

The model predicts that approximately 60% of the water entering the groundwater flow system from Moab Wash and bedrock occurs in the upper three model layers. This result is in agreement with the conceptual model that hypothesizes that recharge and salinity are correlated, the fresher the groundwater the higher the recharge rate.

Examination of the simulated water table shows that January through March groundwater discharges to the Colorado River. The model-predicted April through June water tables shows Colorado River water recharging the aquifer. In July and August simulation results show the effects of ET. September through December the simulated water table once again shows groundwater discharge to the Colorado River.

The model reasonably reproduces the general trends present in site well hydrographs [**Figure 32**, **Figure 33** and **Figure 34**]. Differences in measured and modeled hydrographs are likely a function of assigned Colorado River stage. In summary, the model reasonably matches conceptual mass balance information and replicates expected temporal groundwater flow patterns.

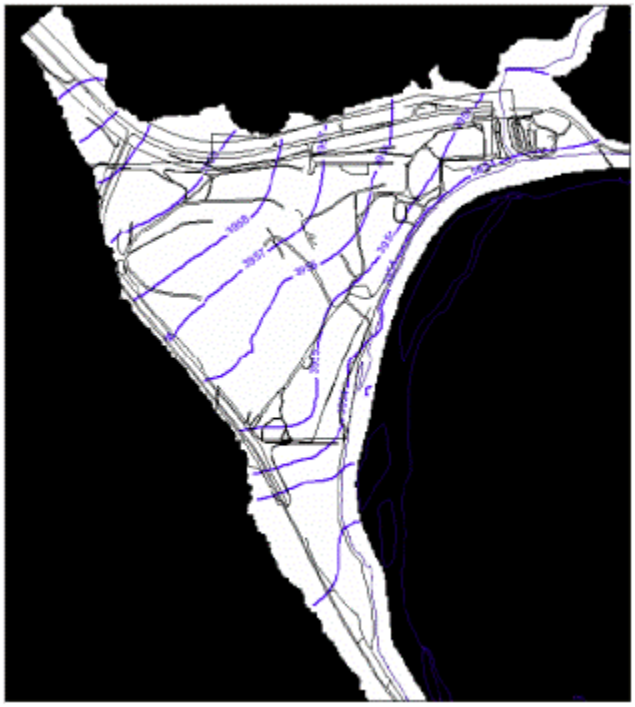

January Water table

February Water table

March Water table

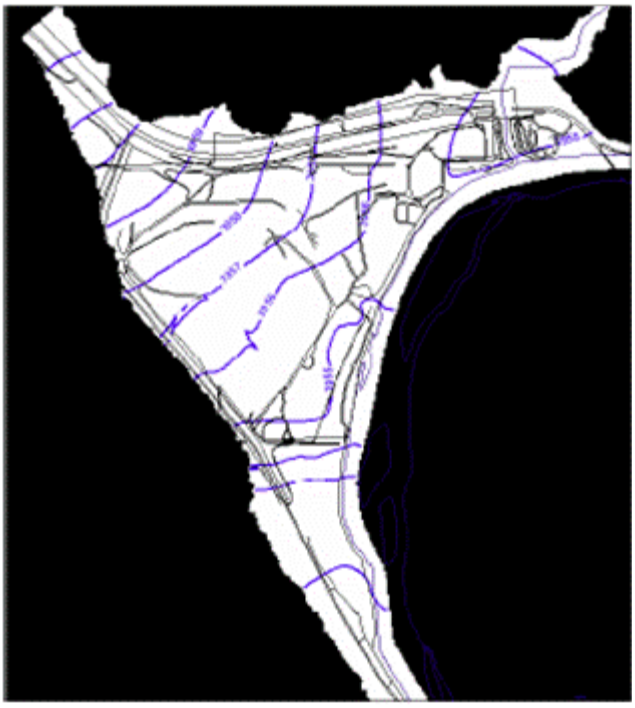

April Water table

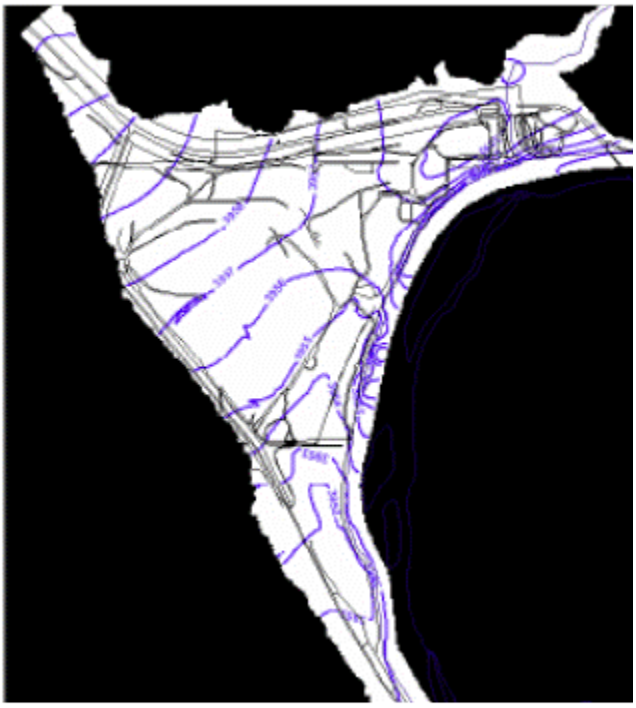

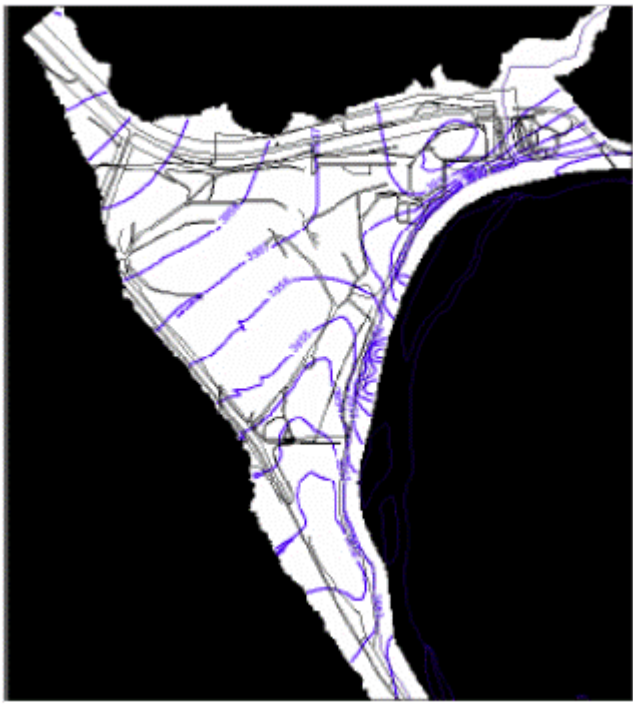

May Water table

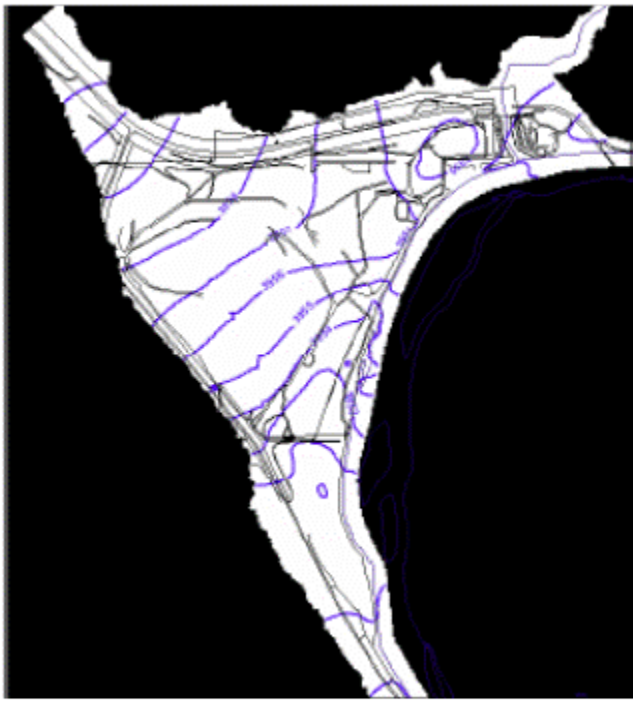

June Water table

July Water table

August Water table

September Water table

October Water table

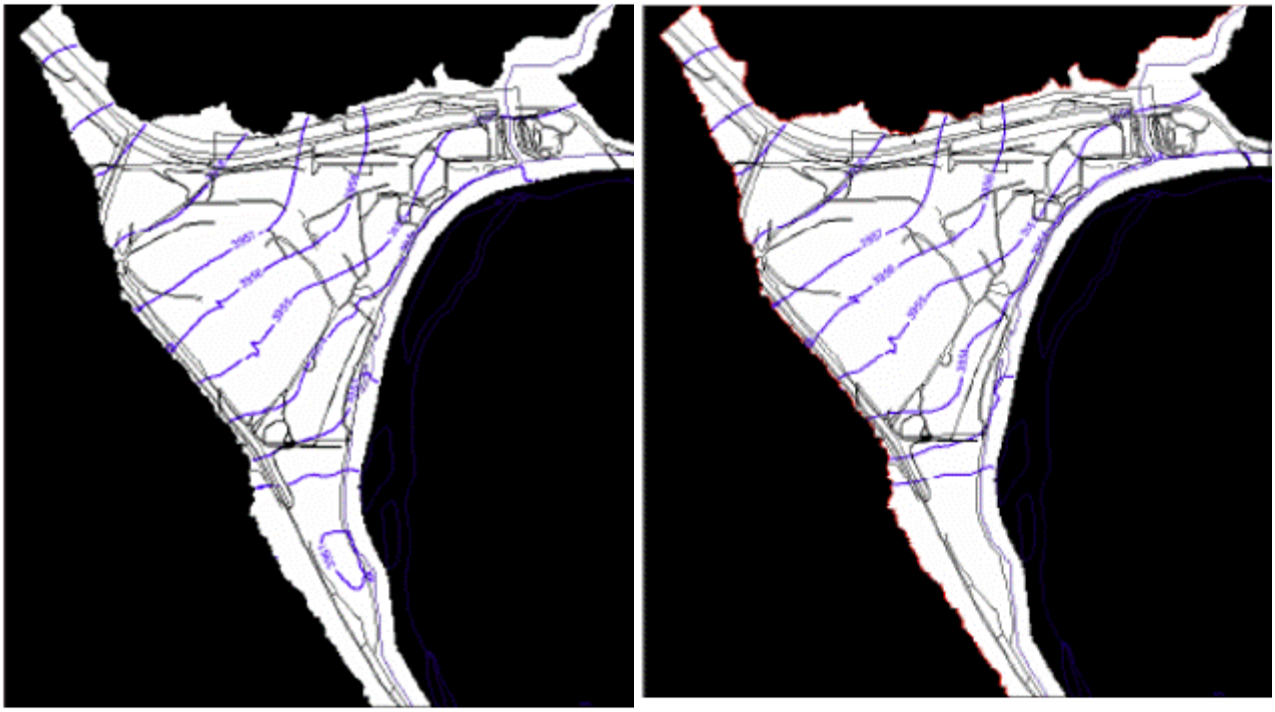

November Water table

December Water table

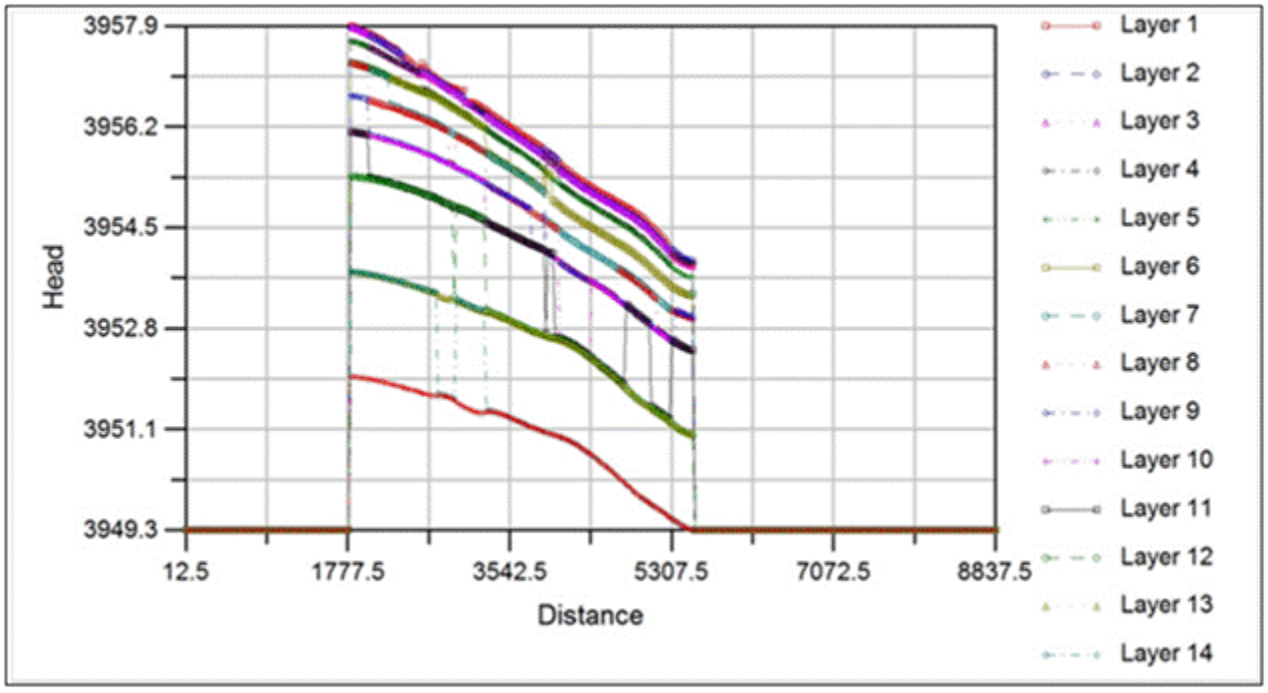

Figure 31. Sectional profile of heads for all layers.

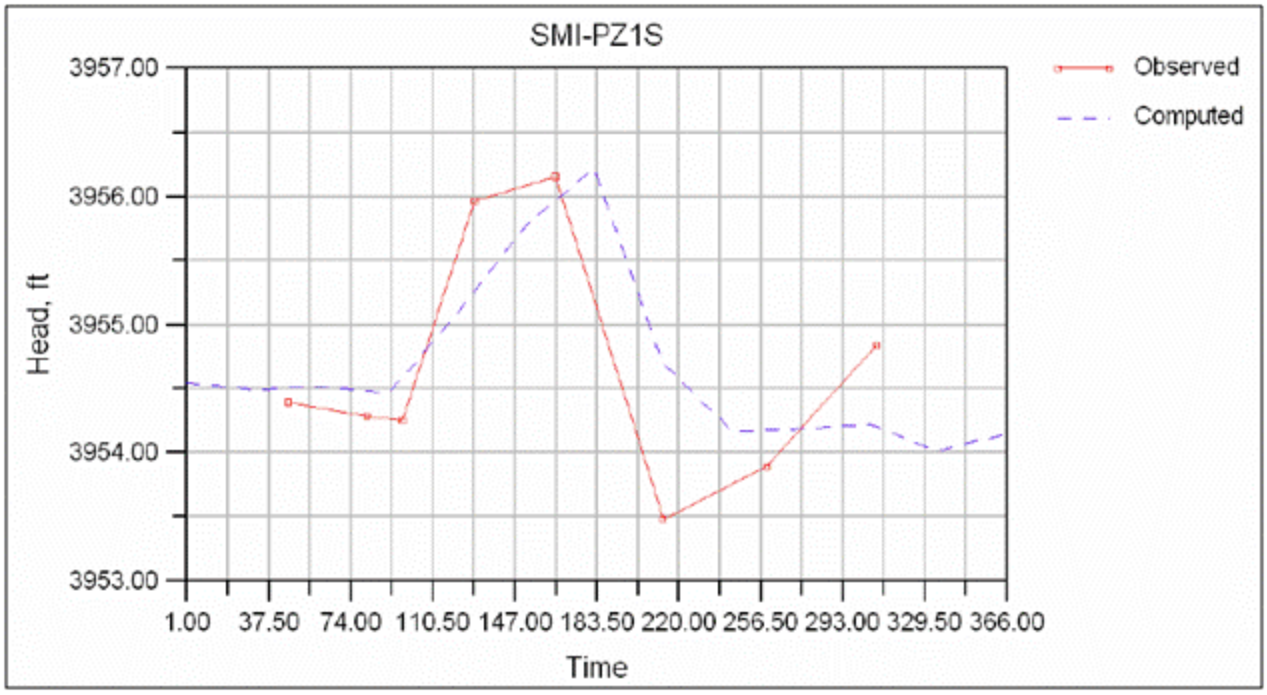

Figure 32. Layer 1 hydrograph at SMI-PZ1S.

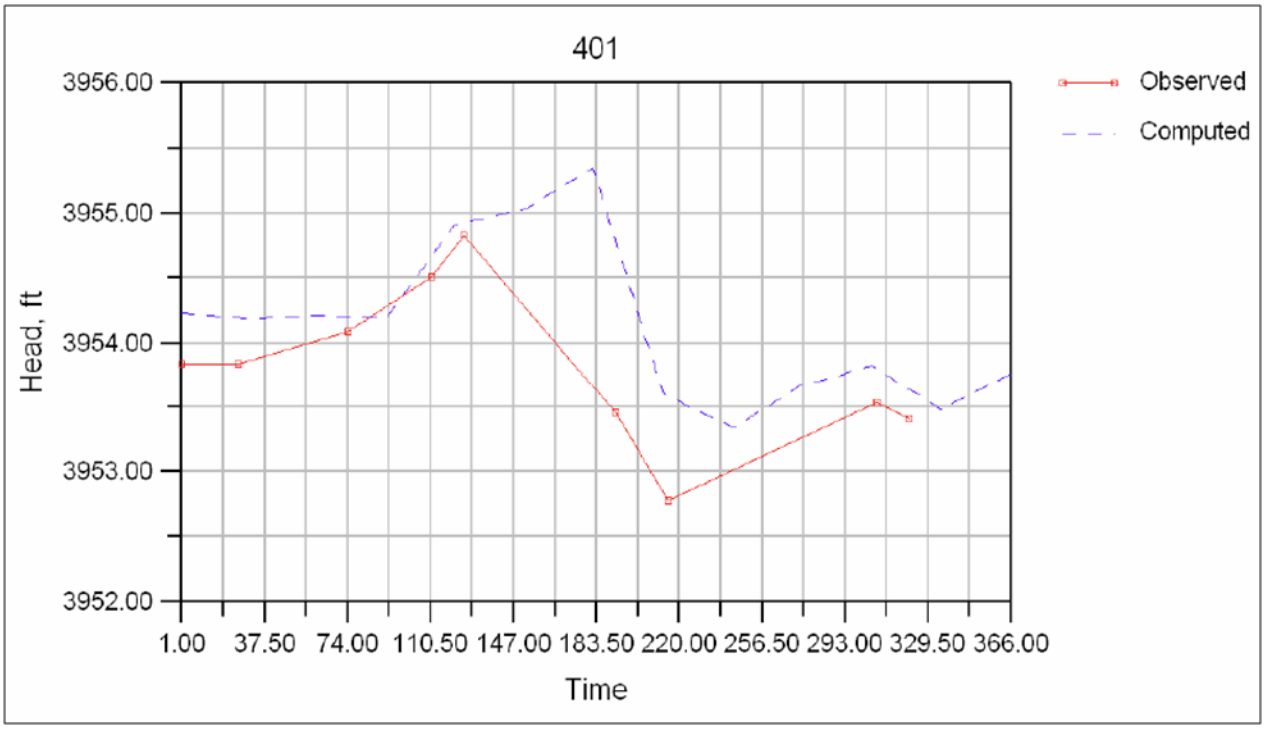

Figure 33. Layer 1 hydrograph at well no. 401.

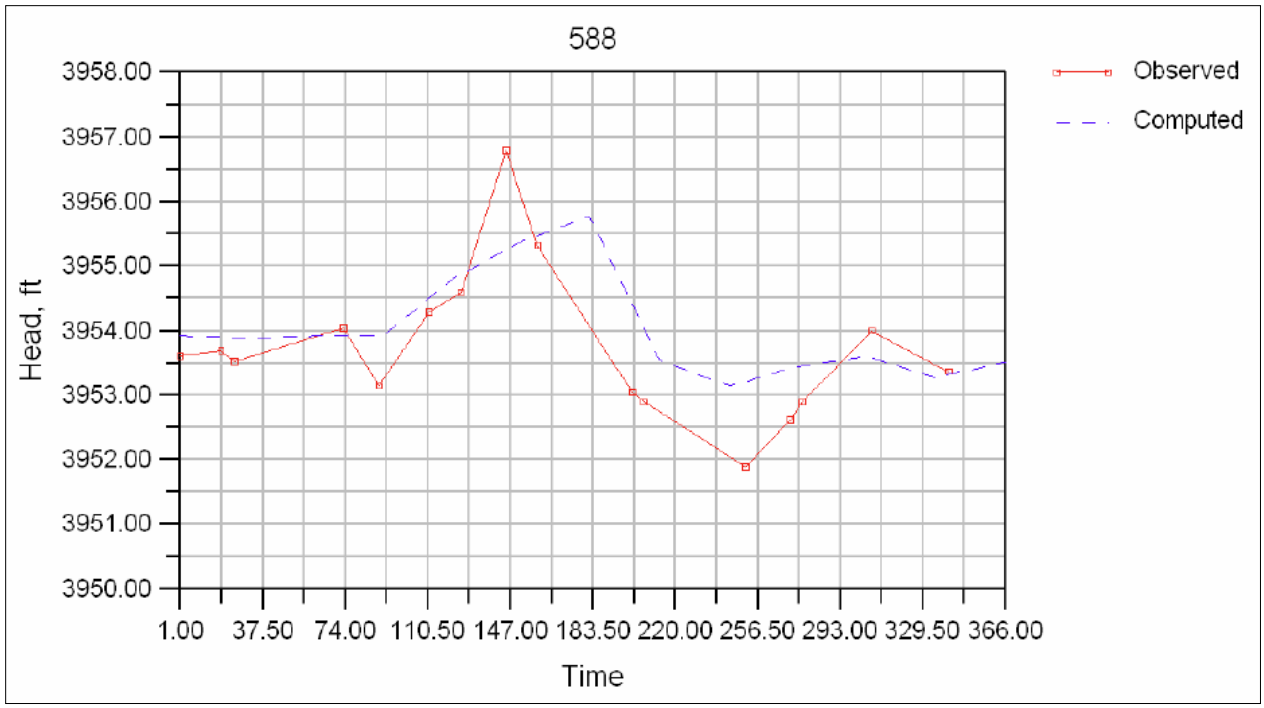

Figure 34. Layer 2 hydrograph at well no. 588.

SIMULATION FOR COMPARING HEADS AT 10 DIFFERENT LOCATIONS

The Following graphs show relationship of stage data obtained from the simulation results for ten points close to the Colorado river [**Figure 35**].

Figure 35. Points selected for showing relationship of stage data.

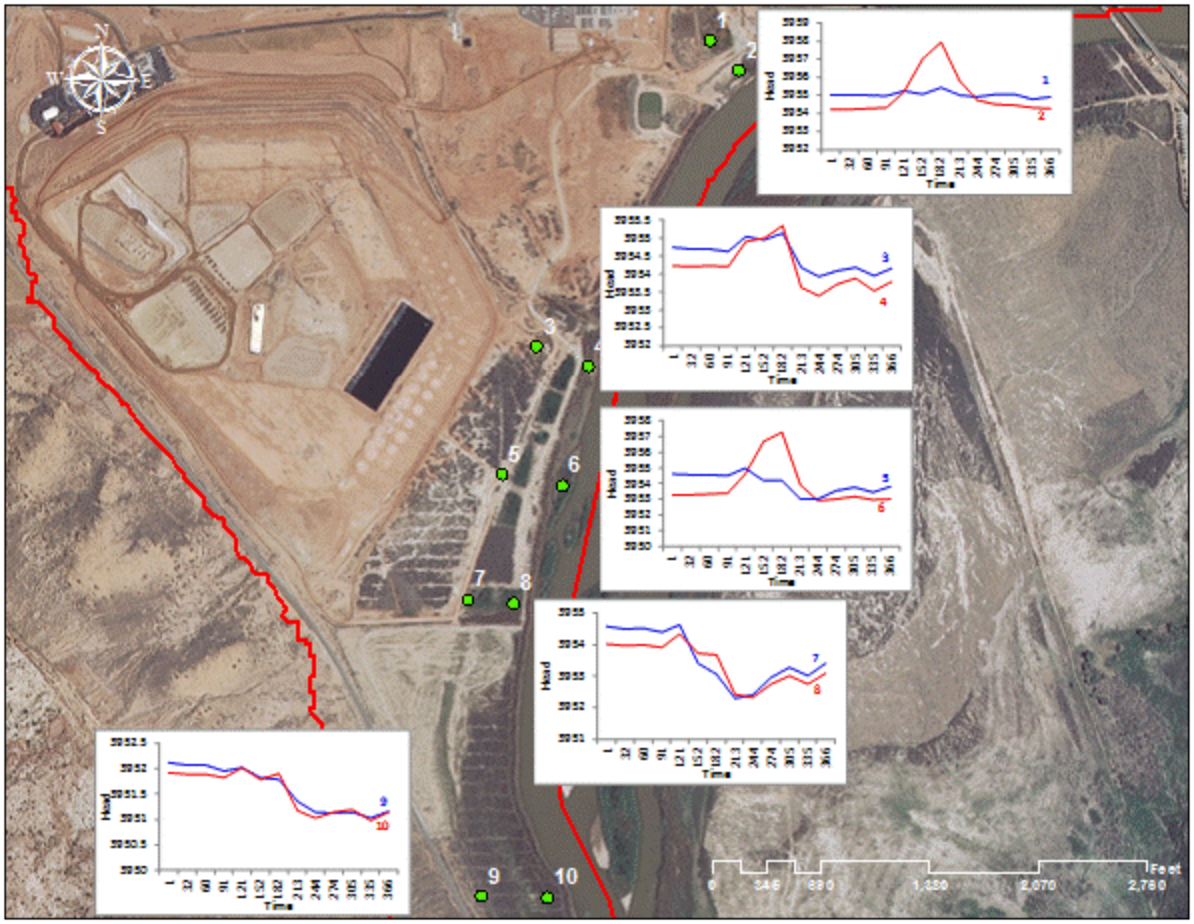

Figure 36. Comparison of stage data at different locations close to Colorado river.

SIMULATION FOR PUMPING AND INJECTION SYSTEMS

Simulations were carried out for scenarios involving various increases in groundwater-pumping/injection rates and were analyzed with the calibrated groundwater-flow model to assess possible changes in the flow system. Pumping rates were increased by 25%, 50%, 100% and 200%. For comparison, simulation results were extracted for a small area close to the Colorado river, tailings and the well fields [**Figure 37**]. Following simulation were carried out:

- No Pumping and Injection
- Actual scenario for pumping and injection
- 0.25 x pumping and injection
- 0.5 x pumping and injection
- 2 x pumping and injection
- 3 x pumping and injection

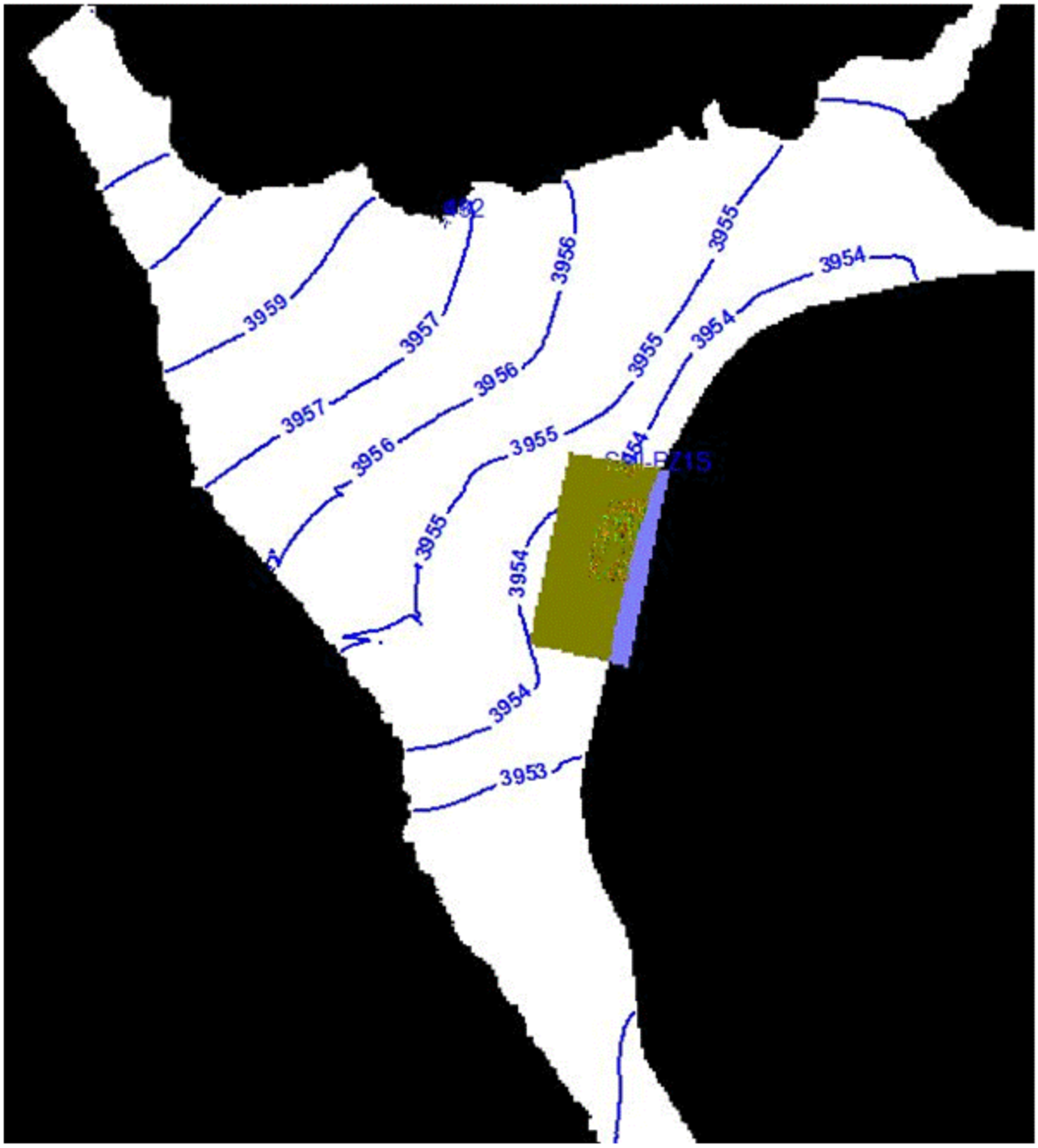

Figure 37. Polygon which was used for extracting results for mass balances.

Figure 37 shows the polygon which was used for extracting results for carrying out the mass balances.

COMPARISON OF INFLOWS AND OUTFLOWS FROM WELLS

Mass balances analysis was done for the hypothetical scenarios to assess the groundwater flow in and out of the selected polygon area shown in **Figure 37.** Results in **Figure 38**show an increase in

flux by approximately 25% after each simulation where the pumping and injection rates were increased [**Table 8**].

Table 8. Inflows and Outflows from Wells

Scenario	Inflows (gpm)	Outflows(gpm)
No Pumping	0	0.00
Actual scenario	21.4	118.11
0.25 X actual	26.75	147.64
0.5 X actual	32.1	177.16
2 X actual	42.8	224.28
3 X actual	64.2	270.70

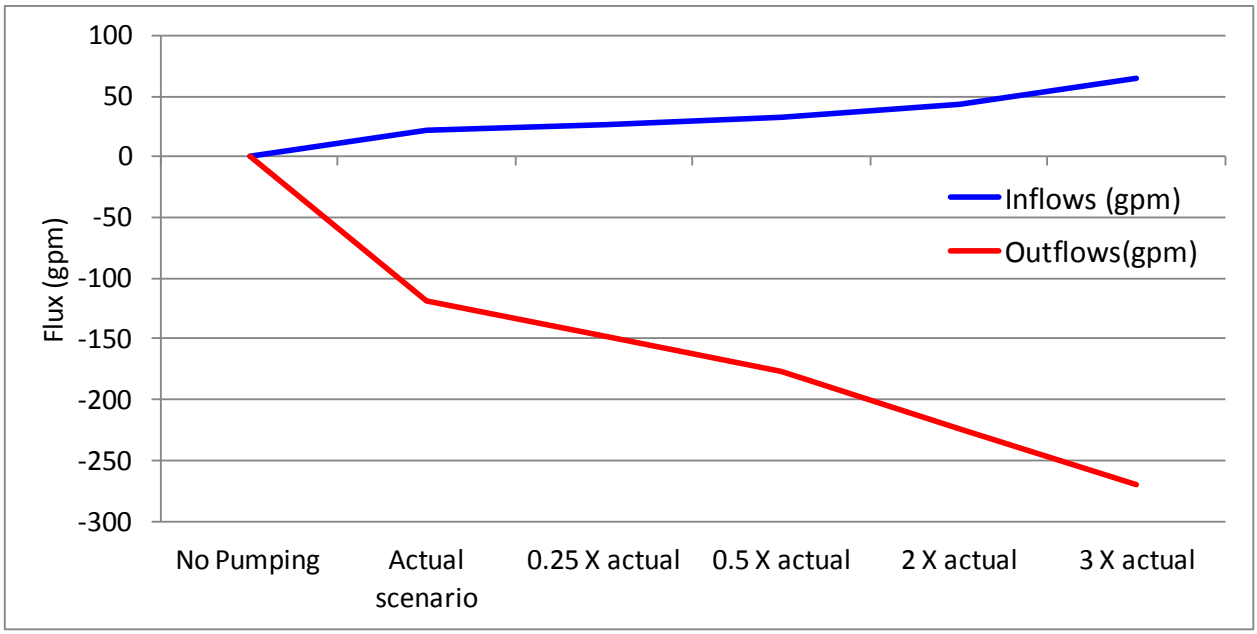

Figure 38. Inflows and outflows from the wells [for selected polygon].

COMPARISON OF INFLOWS AND OUTFLOWS TO RIVER

Mass balances analysis was done for the hypothetical scenarios to assess the inflows and outflows to the Colorado river for the selected polygon area shown in **Figure 37.** Results in **Figure 39** show an increase in flux by approximately 30% after each simulation where the pumping and injection rates were increased [

Table 9].

Table 9. Inflows and Outflows from River

Scenario	Inflows (gpm)	Outflows(gpm)
No Pumping	0.00	50.69
Actual scenario	15.12	5.41
0.25 X actual	28.02	3.56
0.5 X actual	41.31	2.50
2 X actual	60.51	1.18
3 X actual	71.31	0.71

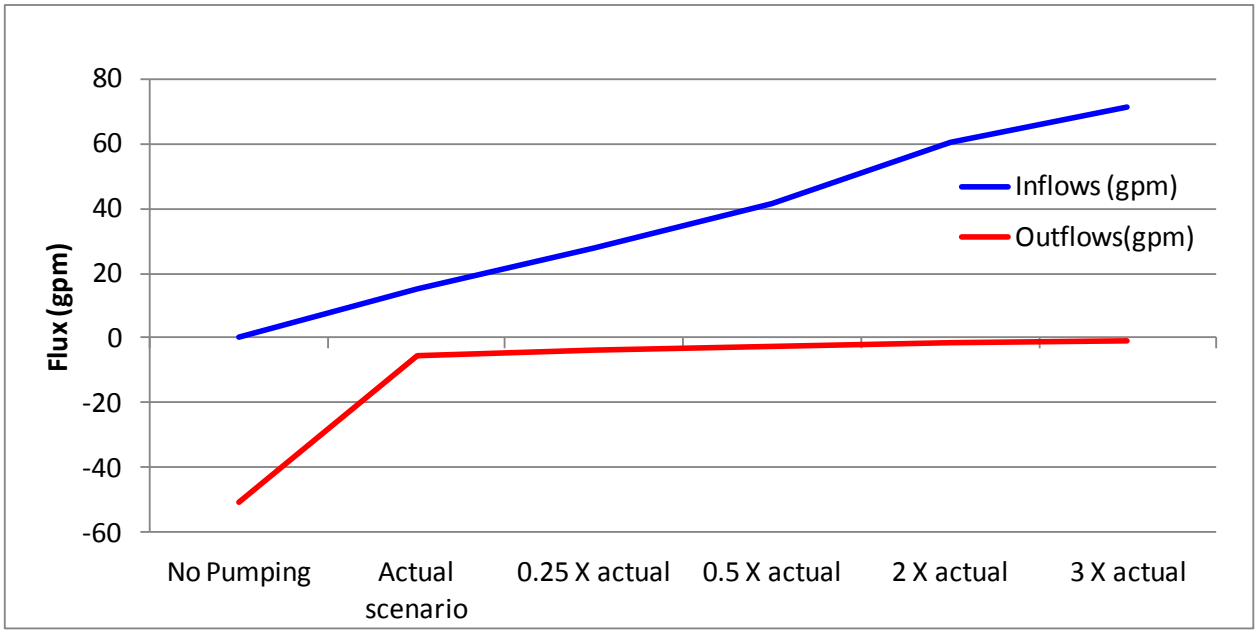

Figure 39. Inflows and outflows from river [for selected polygon].

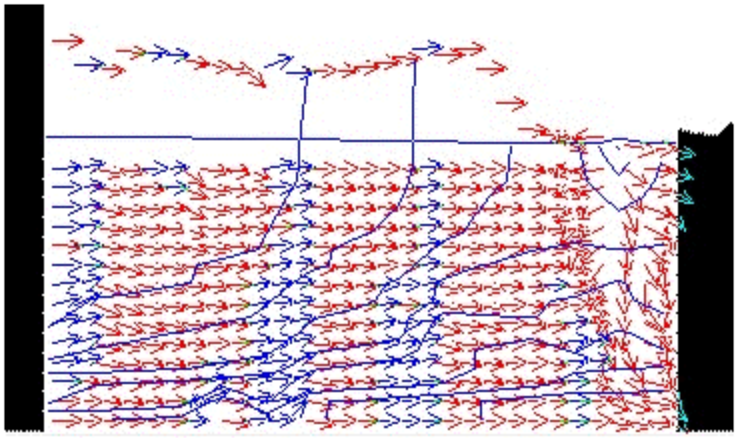

Figure 40. Cross sectional view showing the groundwater flow pattern.

Figure 40 shows the groundwater flow pattern at the Moab site and it follows the conceptual model for the general effects of freshwater injection.

CONCLUSIONS

Preliminary simulation results show a good match of observed and computed monthly data. The calibrated model predicts a median monthly groundwater mass balance of 275 gallons per minute. Tailings pile recharge is constant monthly at 9 gallons per minute. Recharge associated with Moab Wash and the surrounding bedrock is also constant monthly at 39 gallons per minute. Discharge to the Colorado River is predicted to range between 159 to 495 gallons per minute. Evapotranspiration (ET), which is active May through September and again in November ranges from 22 to 840 gallons per minute.

The model predicts that approximately 60% of the water entering the groundwater flow system from Moab Wash and bedrock occurs in the upper three model layers. This result is in agreement with the conceptual model that hypothesizes that recharge and salinity are correlated, the fresher the groundwater the higher the recharge rate.

The model reasonably reproduces the general trends present in site well hydrographs [**Figure 32**, **Figure 33** and **Figure 34**]. Differences in measured and modeled hydrographs are likely a function of assigned Colorado River stage. Simulations with increased pumping and injection rates show an increase in inflows and outflows by approximately 25%. In summary, the model reasonably matches conceptual mass balance information and replicates expected temporal groundwater flow patterns.

FUTURE WORK

During FY12, students will be involved in the DOE-FIU Science and Technology Workforce Development Program, and will work with the transport model to perform numerical simulations of remedial scenarios proposed by DOE including pumping of contaminated groundwater from the shallow plume to an evaporation pond on top of the tailings pile, and injecting the diverted Colorado River water into the alluvial aquifer in order to predict the outcome of each remedial action and to investigate the effectiveness of each scenario. Numerical simulation of remedial actions assists DOE in deciding their effectiveness. Modeling is to be performed with MODFLOW, SEAWAT and FEFLOW as a benchmark. The following is a list of the proposed tasks to support this initiative:

1. Predictive simulations will be carried out with maximum and minimum values of flow parameters such as the hydraulic conductivity fluxes from Glen Canyon and Moab Fault, evapotranspiration and recharge.
2. Simulations to analyze the effects of pumping at well field Configuration 5 on ammonia and uranium concentrations in the upper saline zone and infiltration of freshwater in Configuration 1 to 4 will be conducted. Upgradient infiltration locations will be optimized relative to the tailings and extraction wells to maximize the number of pore volumes for flushing and reduce remediation time.
3. Simulations to identify the discharge zone for the legacy plume in the brine zone and to identify areas of uncertainty will be conducted. The effect of discharge of a legacy plume in the brine zone after the extraction wells have been shut off will be modeled.

The proposed scope for FY12 includes the following subtasks:

Subtask 5.1: Update existing Moab model by implementing geostatistically interpolated ammonia and uranium plumes and current well operation data into the model for evaluating effects of pumping on contaminant concentrations and determining potential surface water concentrations in riparian habitat areas under a range of operating conditions. The subtask will develop plumes of aqueous species of concern (nitrate, uranimum) with the width of the tailings that would be conservative. The model will be updated by implementing a diversion ditch into the flow model (as drain cells) and by setting the head levels will be set in each drain cell at the elevations of the drains

Subtask 5.2: Conduct simulations with the SEAWAT model to analyze the nitrogen and uranium cycle in the environment and provide forecasting capabilities for the fate and transport of contamination within the Moab site. Analyze the model output and determine the efficiency of remedial actions in reducing the concentration and load of contaminants. A list of the simulations that have been discussed with the site include:

- Simulate ammonia transport applying as initial condition the ammonia plume (for couple of cycles) and determine yearly rise and fall in the river and see if the ammonia concentrations moving up into the saline zone into the brine zone due to the fluctuations of concentrations in the river

- Determine the spatial extent of the discharge zone for the ammonia legacy plume in the brine zone and its effect on natural flushing. The objective will be to determine the effect of discharge of a legacy ammonia plume from the brine zone after the extraction wells and injection system have been shut off.
- Implement a configuration that includes infiltration and provide information about the reoccurrence of the concentrations within the recharge assuming the existence of a freshwater lens. Determine the effect of mixing water from the river and the diversion ditch
- Determine the effectiveness of running both systems at the same time and derive the benefits from running the extraction wells.

Subtask 5.3: Simulate proposed remedial actions including pumping of contaminated groundwater from the shallow plume to an evaporation pond on top of the tailings pile, and injecting the diverted Colorado River water into the alluvial aquifer in order to predict the outcome of each remedial action and to investigate the effectiveness of each scenario. Determine the effects of the brine zone beneath the site on an overlying saline zone. After implementing plumes into the model as initial conditions, conduct additional simulations to optimize mass removal and capture from the existing system. Optimize the mass removal without additional bleeding of ammonia from the deep zone into the shallow zone and assuming that injection systems operates at the same time

Subtask 5.4: Determine the effects of the brine zone beneath the site on an overlying saline zone. A student will be involved in the student internship program and will work with the transport model to perform numerical simulations of remedial scenarios proposed by DOE.

REFERENCES

1. DOE (U.S. Department of Energy), 2003b. Site Observational Work Plan for the Moab, Utah, Site, GJO-2003-424-TAC, prepared by the U.S. Department of Energy, Grand Junction, Colorado.
2. Kenney, T., 2005, Initial-phase investigation of multi-dimensional streamflow simulations in the Colorado River, Moab Valley, Grand County, Utah, 2004: U.S. Geological Survey Scientific Investigations Report 2005-5022, 69 p.
3. Morris, D.A., and A.I. Johnson, 1967. Summary of hydrologic and physical properties or rock and soil materials as analyzed by the Hydrologic Laboratory of the U.S. Geological Survey 1948-1960, U.S. Geological Survey Water Supply Paper 1839-D, 42 pp.
4. Zheng, C., and G.D. Bennett, 1995. Applied Contaminant Transport Modeling Theory and Practice, Van Nostrand Reinhold, New York.
5. DOE (U.S. Department of Energy), 2009. Moab UMTRA Project Well Field Optimization Plan, DOE–EM/GJTAC1791, prepared by the U.S. Department of Energy, Grand Junction, Colorado.
6. Peterson D, Kautsky M, Karp K, Wright T, Metzler D (2004) Modeling of density-dependent groundwater flow and transport at the uranium mill tailings site near Moab, Utah. Tailings and Mine Waste ‘04, A.A. Balkema.
7. Kenney, T.A., 2005, Initial-Phase Investigation of Multi-Dimensional Streamflow Simulations in the Colorado River, Moab Valley, Grand County, Utah, 2004: U.S. Geological Survey Scientific Investigations Report 2005-5022, 69 p.

APPENDICES

Appendices I –V are provided separately and can be found at:
ftp://www.hcet.fiu.edu/pub/FIU_Year_End_Reports_2011/Project 3 Appendices

APPENDIX I: FY11 PROJECT TECHNICAL PLAN (EXTERNAL FTP SITE)

APPENDIX II: PROJECT OVERVIEW PRESENTATION I (EXTERNAL FTP SITE)

APPENDIX III: PROJECT OVERVIEW PRESENTATION II (EXTERNAL FTP SITE)

APPENDIX IV: PROJECT FACTSHEETS (EXTERNAL FTP SITE)

APPENDIX V: PUBLICATIONS (EXTERNAL FTP SITE)

APPENDIX T1-001: TASK 1 FINAL REPORT

APPENDIX T1-001

TASK 1: INTEGRATED SURFACE AND SUBSURFACE MERCURY TRANSPORT MODEL OF EAST FORK POPLAR CREEK, OAK RIDGE, TENNESSEE

OF

REMEDIATION AND TREATMENT TECHNOLOGY DEVELOPMENT AND SUPPORT

Prepared for:
U.S. Department of Energy
Oak Ridge Operations Office
Oak Ridge Reservation

FINAL REPORT, VERSION 1, 06/17/12

Prepared by:
Lilian Marrero, EI, DOE Fellow
Angelique Lawrence, MS, GISP
Georgio Tachiev, PhD, PE

Principal Investigator: David Roelant, PhD
david.roelant@fiu.edu
phone: 305-348-6625
fax: 305-348-1852

Applied Research Center
Florida International University
10555 W. Flagler Street, EC 2100
Miami, Florida 33174

DISCLAIMER

ACRONYMS

DHI	Danish Hydraulic Institute
EFPC	East Fork Poplar Creek
EPA	Environmental Protection Agency
FDC	Flow Duration Curve
FDI	Flow Duration Interval
foc	Fraction Organic Carbon
LDC	Load Duration Curve
MHL	Melton Hill Lake
NPDES	National Pollution Discharge Elimination System
OREIS	Oak Ridge Environmental Information System
ORNL	Oak Ridge National Laboratory
ORR	Oak Ridge Reservation
TMDL	Total Maximum Daily Load
TSS	Total Suspended Solids
USGS	United States Geologic Survey
WCS	Watershed Characterization System
WEMA	West End Mercury Area
UEFPC	Upper East Fork Poplar Creek
USLE	Universal Soil Loss Equation

VARIABLES

difv	Diffusion coefficient in water
dz	Thickness of the actual layer in computational grid
dzds	Thickness of diffusion layer in sediment
dzwf	Average thickness water film that metals have to diffuse through
$f_{biot.difw}$	Factor for diffusion due to bioturbation
K_d	Partitioning coefficient for mercury between particulate matter and water
K_{ds}	Partitioning coefficient for mercury between sediment and pore water
k_s	Desorption rate in sediment
k_a	Adsorption rate [d-1]
k_w	Desorption rate [d-1]
por_s	Porosity of sediment
S_{HM}	Dissolved Mercury Concentration in Water
S_{HMS}	Dissolved mercury concentration in sediment pore water
X_{HM}	Adsorbed mercury concentration in water
X_{HMS}	Adsorbed mercury concentration in sediment
X_{SED}	Mass of sediment
Vs	Settling velocity [m/d]
Vc	Critical current velocity for initiation of the movement [m/s]
RR	Resuspension rate [g/m2.d]
PPR	Particle production rate [g/m2.d]

TABLE OF CONTENTS

FIGURES

TABLES

EXECUTIVE SUMMARY

An integrated flow and transport model has been developed in past years using the MIKE software packages created by the Danish Hydraulic Institute (DHI) in an effort to forecast mercury transport and contamination within the watershed at East Fork poplar Creek (EFPC), Oak Ridge, Tennessee. The water quality model (MIKE SHE and MIKE 11) analyzes the impact of hydrological events on mercury contamination in the Upper EFPC (UEFPC). In FY10 a sediment transport module was created for the site. This document details the extensions and modifications made to the sedimentation module to include the entire EFPC and Bear Creek. The sedimentation module will provide the coupling between the flow and transport within the creek and the overland flow which will be used to analyze the significance of floodplain contamination downstream EFPC. The research also emphasizes the stochastic modeling of the system and includes an analysis of the spatial and temporal patterns as a result of the stochastic variations of selected properties of the sub domain.

At this point simulation results reveal rainfall as a facilitating agent in the exchange of mercury and its movement through hydrologic zones. The attenuation of mercury concentrations downstream of EFPC is consistent with previous studies.

1 INTRODUCTION

The United States Department of Energy (DOE) decontamination and decommissioning activities of industrial, radiological and nuclear facilities seek to restore environmental conditions of contaminated sites to accepted levels designated by local, state and federal regulations. The East Fork Poplar Creek (EFPC) Watershed is located in the state of Tennessee and represents one of the contaminated sites. EFPC has been severely impacted by the release of more than 100 metric tons of elemental mercury as a byproduct of nuclear processing activities employed in the lithium-isotope separation process used in the production of nuclear fusion weapons during the 1950's [1]. Studies have identified over 77,000 kg of mercury present in the upper 10 feet of soils along a 15-mile long stretch of EFPC [3]. Mercury is present in the sediment, surface water, groundwater, and infrastructure in the National Security Complex (Y-12) area and in the upper reaches of EFPC [Figure 1] [3]. The state of Tennessee continues to list portions of the EFPC as not supporting their designated use classifications such as aquatic life, irrigation, livestock watering, wildlife, and recreation due to mercury contamination [2].

Figure 1 Evidence of mercury.

Mercury releases into the creek ceased in 1963; nonetheless, the pollution continues to spread. Although remediation strategies have been implemented since the problem's

inception, the issue of mercury contamination continues to prevail. The elemental mercury dissolves and under certain environmental conditions oxidizes to mercuric ion with a considerably greater solubility, resulting in increased mobility of mercury. Higher than expected concentrations of mercury and suspended solids have been recorded as a byproduct of higher volumes and higher stream velocities during and post flood events. Mercury is released from bed sediments as bed layer particles are resuspended. Mercury exchange occurs between the water column and sediment as well as between the dissolved and adsorbed phases of mercury via adsorption-desorption processes [4]. The mercury within the system is continuously recycled by the surrounding environment, making the successful implementation of remediation strategies difficult to execute.

1.1.Significance of Study

Mercury present in surface water is converted to various forms. Mercury particles may settle with sediments, may be consequently diffused into the water column, resuspended, or hidden within sediments until a hydrological event disturbs the particles and reignites the complex cycle through which it is recycled [5]. Methyl mercury is the most toxic form of mercury because it can accumulate at a faster rate within organisms in comparison to the rate at which it can be eliminated; as takes longer for organisms to remove it from their systems [6]. Effects are dependent upon the chemical form and type of exposure. Mercury contamination in the environment represents a health concern for wildlife, as well as humans [6]. Studies have shown a correlation between total mercury concentration within the creek and methyl mercury concentrations and long term bioaccumulation and biomagnifications. Understanding the processes by which mercury is transported and recycled within the EFPC environment is an essential step towards complying with applicable and relevant or appropriate requirements (ARARs) in the DOE's Record of Decision (ROD) Phase I and Phase II [7][8].

1.2.Research Objectives

The purpose of this research was to correlate the hydrology of the EFPC and Bear Creek with the long term distribution of mercury within the overland, subsurface, river, and vadose

zone sub-domains. Previous modeling efforts which originally included only the upper portions of EFPC, were extended to include the entire EFPC, down to station EFK 6.4 and Bear Creek. Modeling software MIKE SHE, MIKE 11, and ECO Lab were combined in a comprehensive package to model the flow, transport, and mercury exchange within sediment layers. The research includes an analysis of spatial and temporal patterns as a result of variations of selected properties of the sub-domain and also emphasizes the stochastic modeling of the system. The impact of sedimentation within the mercury recycling process was assessed through a series of simulations. This component was analyzed in greater detail within this study through the incorporation of a sedimentation layer module (ECO Lab) by addressing the dissolved mercury in the water, the adsorbed mercury concentration on suspended matter, the dissolved mercury in sediment pore water, and the adsorbed mercury in the sediment.

1.3.Research Questions and Hypothesis

Question #1: Will the extended EFPC model provide a practical solution in assessing the impact of various remediation scenarios?

The extended model will address the most significant parameters and processes of flow and mercury transport for the study site by incorporating a flow, advection, dispersion, water quality and sedimentation (ECO Lab) module. It will serve as a useful remediation tool since the site will be characterized within the model using relevant historical records for precipitation, groundwater levels, river discharges obtained from OREIS and ORNL databases and incorporated into the model in the form of boundary or calibration conditions.

Question #2: Does the sediment layer representation through the ECO Lab implementation improve the modeling capabilities for the project site?

The incorporation of the ECO Lab module is expected to better characterize the mercury processes in the EFPC environment as proposed by earlier studies, mercury species are known to diffuse from contaminated sediment pore water to creek water in the form of diffusive transport.

1.4.Site Description

East Fork Poplar Creek (EFPC) is located within the Oak Ridge Reservation (ORR) in the state of Tennessee, in the counties of Roane and Anderson [Figure 2]. The reservation encompasses an area of about 14,260 ha, and has three major US Department of Energy facilities: the Y-12 National Security Complex, the East Tennessee Technology Park (ETTP) or K-25 complex, and the Oak Ridge National Laboratory.

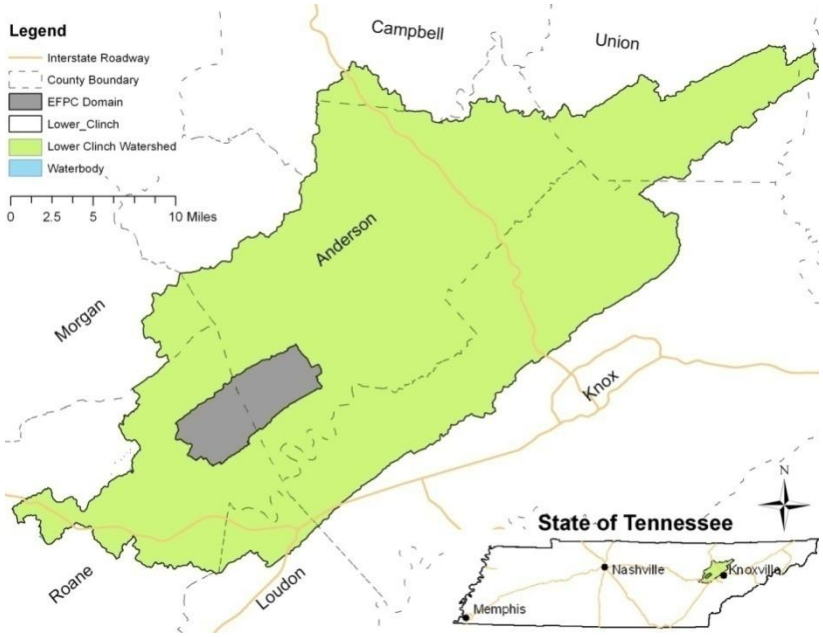

Figure 2 EFPC regional settings.

The EFPC watershed located in the eastern part of Tennessee at about 270 to 280 meters above mean sea level is a sub-watershed of the larger Poplar Creek watershed; one of four sub-watersheds of the Lower Clinch River watershed (Hydrologic Unit Code (HUC) 06010207). The EFPC watershed domain covers approximately 29.7 square miles. An estimated 88 square miles of streams and tributary branches have been identified within the domain. Bear Creek and EFPC are two small rivers with a length of more than 12,500 kilometers in length. Gum Hallow Branch, Mill Branch, Pinhook Branch, and other tributaries are also identified in Figure 3 below. As can be observed from Figure 3, EFPC is recharged by Bear Creek, Gum Hollow Branch, Mill Branch, and Pin Hook Branch in addition to 30 unnamed tributaries.

These are all included in the model. EFPC runs primarily in a northeast to northwest (NE – SW) direction and is about 24.5 kilometers long. The creek bottom begins at a depth of about 287 meters above the mean sea level and ends at about 226 m near the river's hydrologic boundary, for a general slope of about 0.23% or 0.13 degrees. Stream valley width along EFPC ranges from 60 to 300 meters. Additional information regarding the remaining tributaries and streams is detailed in Long, 2009.

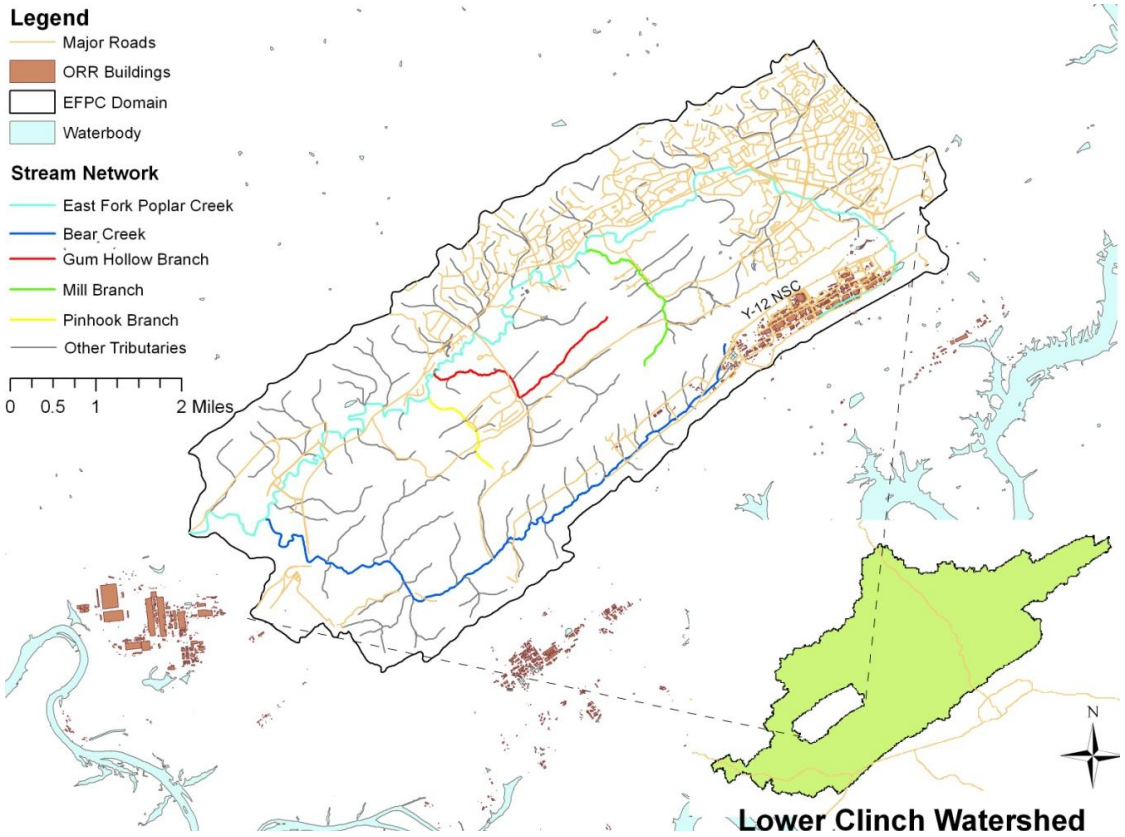

Figure 3 EFPC stream network.

Watershed health in the state of Tennessee is assessed in a 5 year cycle. The first year consists of planning meetings and the development of a monitoring plan. Water quality data is collected in year 2 through 3, followed by the water quality assessment in year 4. A watershed plan and drafts of the NPDES permits are published in year 5. Streams and lakes in violation of one or more water quality standards within the state of Tennessee are described in the 303 (d). Portions of this list are summarized in Table 1 below for streams near the Oak Ridge

Reservation. Those streams with pollutants originating from a DOE site are highlighted in bold text.

Table 1 Contaminated Streams within EFPC Watershed in Violation of Water Quality Standards

WATERBODY ID	IMPACTED WATERBODY	COUNTY	MILES/ACRES IMPAIRED
TN06010207 026 – 0600	**BEAR CREEK**	**Roane**	**10.87**
TN06010207 026 – 1000	**EFPC**	**Roane**	**9.7**
TN06010207 026 – 2000	**EFPC**	**Anderson Roane**	**11.3**
TN08010208 009 - 1000	POPLAR CREEK	Haywood Fayette	23.6
TN08010208 011 - 2000	BEAR CREEK	Fayette	7.9
TN08010209 021 – 0110	BEAR CREEK	Shelby Tipton	14.5
TN05130104 050 - 0100	EAST BRANCH BEAR CREEK	Scott	5.7
TN05130104 050 - 1000	BEAR CREEK	Scott	2.6
TN06010102 003 – 0500	BEAR CREEK	Sullivan	4.6
TN08010204 004 - 0100	BETHEL BRANCH	Dyer Gibson	30.4
TN06010207 001 - 0100	**POPLAR CREEK EMBAYMENT, WATTS BAR RESERVOIR**	**Roane**	**141 ac**

Total Maximum Daily Load (TMDL) studies, identify the sources of pollutant in a stream, quantify the amount, and recommend appropriate actions to be taken in order for the steam to no longer be polluted. These studies are required for the above mentioned streams. Contaminated streams relevant to the present study include 9.7 impaired miles of EFPC within Roane County, 11.3 miles within Anderson and Roane. Approximately 141 acres of the Poplar Creek Embayment, Watts Bar Reservoir, within Roane County is also contaminated. These streams have been classified by the EPA as category 5. Since they have been heavily impacted

by releases at DOE's Oak Ridge facilities (K-25, Y-12 and ORNL), one or more of its uses are not being met and a TMDL study is therefore required. According to the EPA TMDL priorities list, mercury TMDLs for these streams are of low priority due to the lack of available tools that may be able to generate them. Therefore, further analysis and modeling of the area is necessary so that TMDLs may be developed in the future.

The US EPA National Health and Environmental Effects Research Laboratory identified the Ridge and Valley Level III eco-region, along with two Level IV eco-regions within the watershed domain. These regions include the Southern Limestone/Dolomite Valleys and Low Rolling Hills as well as Southern Dissected Ridges and Knobs. As described by the US EPA, the Southern Limestone/Dolomite Valleys and Low Rolling Hills consist of a heterogeneous region composed predominantly of limestone and cherty dolomite. Landforms are mostly low rolling ridges and valleys, and the solids vary in their productivity. Land cover includes intensive agriculture, urban and industrial, or areas of thick forest. White oak forests, bottomland oak forests, and sycamore-ash-elm riparian forests are the common forest types, and grassland barrens intermixed with cedar-pine glades also occur here. On the other hand, the Southern Dissected Ridges and Knobs contain more crenulated, broken, or hummocky ridges, compared to smoother, more sharply pointed sandstone ridges. Although shale is common, there is a mixture and interblending of geologic materials. The ridges on the east side of Tennessee's Ridge and Valley tend to be associated with the Ordovician-age Sevier shale, Athens shale, and Holston and Lenoir limestone. These can include calcareous shale, limestone, siltstone, sandstone, and conglomerate. In the central and western part of the ecoregion, the shale ridges are associated with the Cambrian-age Rome Formation: shale and siltstone with beds of sandstone. Chestnut oak forests and pine forests are typical for the higher elevations of the ridges, with areas of white oak, mixed mesophytic forest, and tulip poplar on the lower slopes, knobs, and draws.

Geological formations beneath ORR include primary group formations recognized as: the Knox (OCk), Rome (Cr), Chickamauga (Och), and Conasuaga (Cc), Sequatchie Formation (Os), Fort Payne Chert (Mfp), Rockwood Formation (Sr), Copper Ridge Dolomite (Ccr), Maynardville

Limestone (Cmn). The Knox aquifer and the Chickamauga Group are the dominant hydrologic units in which flow is controlled by solution conduits, leaky confining units in which flow is dominated by fractures and relatively low hydraulic conductivity.

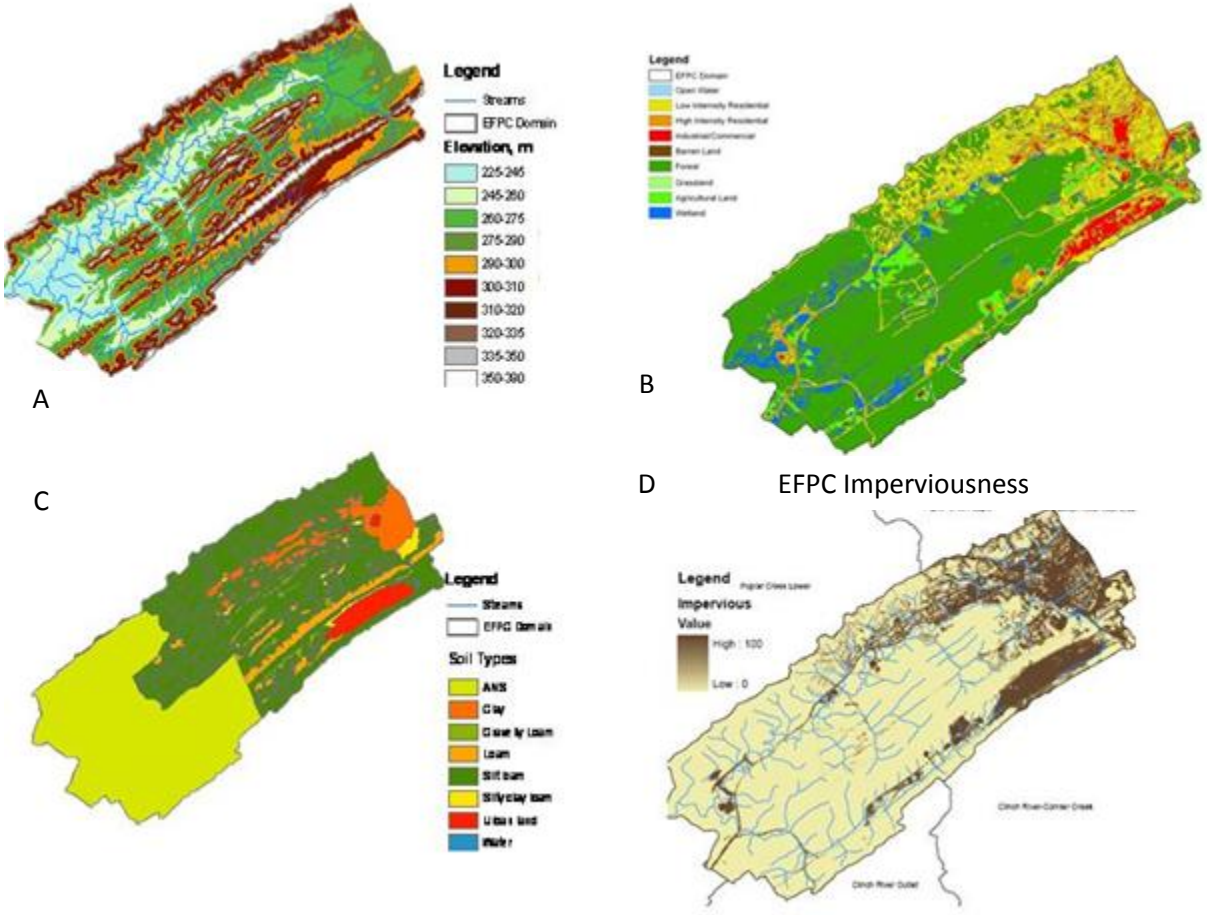

Figure 4 (A) Topography, (B) Land Use, (C) Soil Type, and (D) Imperviousness Distribution, for EFPC.

A total of 14 classifications are added to the model in accordance with the land cover characteristics of the domain: (1) deciduous forest, (2) open water, (3) pasture hay, (4) high intensity developed, (5) open space developed, (6) medium intensity developed, (7) low intensity developed, (8) woody wetlands, (9) barren land, rock, sand and clay, (10) herbaceous grassland, (11) evergreen forest, (12) scrub shrub, (13) mixed forest, and (14) cultivated crops. Based on Multi-Resolution Land Characteristic (MRLC), 2001, the watershed is over 62% forest land followed by urban (33.2%).

About 87% of the forested areas are considered deciduous forests (typical hardwoods such as oaks, maples, hickories, etc.), 33% of the watershed is used for agricultural purposes, and 9.3% of the total watershed area has an imperviousness of 50% or greater. These areas of high imperviousness may tend to transport contaminants more rapidly due to the increased rate of overland flow and infrastructure facilitation. Additional information regarding the domain area's surface elevation (topography), land use, soil type, and imperviousness is available in the form of GIS files and was previously incorporated into the existing model for the project site.

2 NUMERICAL MODEL DEVELOPMENT

Models are generally categorized as stochastic or deterministic, and further classified as conceptual or empirical depending on their ability to obey the physical laws. Stochastic models are dependent upon random variables dominated by a probability distribution function. In deterministic models all the input parameters are known within a specific certainty range. Modeling tools have been used extensively to simulate system dynamics. For instance, MIKE SHE/MIKE 11 modeling systems have been applied by the South Florida Water Management District (SFWMD) in an integrated approach that successfully simulates wetland dynamics as part of the Everglades Nutrient Removal (ENR) project [9]. The models have also been applied in Broward County to develop an Integrated Water Resources Master Management Plan (IWRMMP) [10].

Other studies have employed computer models to emphasize the significance of sediments and suspended matter in contaminant transport. A study performed by the North Carolina Department of Natural Resources revealed that 75% of the total mercury load present in the Cashie River Watershed resulted from eroded sediments [11]. A study on the "Development of a Mercury Speciation, Fate and Biotic Uptake (BIOTRANSPEC) Model" applied to the Lohatan Reservoir in Nevada, showed that 90% of the mercury released into the system was maintained within the sediments and constituted a continuous source of pollution [12]. Similarly, Cabrejo, 2010 analyzed how mercury within the sediment serves as a continuous source of pollution within portions of the Y-12 National Security Complex, a sub-domain of the EFPC Watershed [5]. A study simulating flow and mercury transport in upper portions of EFPC also confirmed that for the sub-domain, a large portion of the mercury in the river is present as mercury bound to sediment particles [4]. These studies summarize the importance of the adsorption-desorption process in mercury contaminated environments, especially when the contaminant has an affinity to sorb to soils in the sediment bed layer.

2.1 Model Theory

An integrated flow and transport model that was previously implemented using MIKE software packages created by the Danish Hydraulic Institute (DHI) for the project site developed, is herein used to analyze and forecast mercury transport and contamination within the East Fork Poplar Creek watershed in Oak Ridge, Tennessee. The model strengths described by the EPA include:

- Interfacing with GIS with respect to model input and presentation of model output.
- Easy connectivity to other MIKE models including MIKE SHE, ECO Lab, and MIKE 21.
- The advantage of a modular structure which enables each module to be operated separately and automatically transfer data between modules, as well as couple physical processes such as river morphology, sediment re-suspension and water quality.

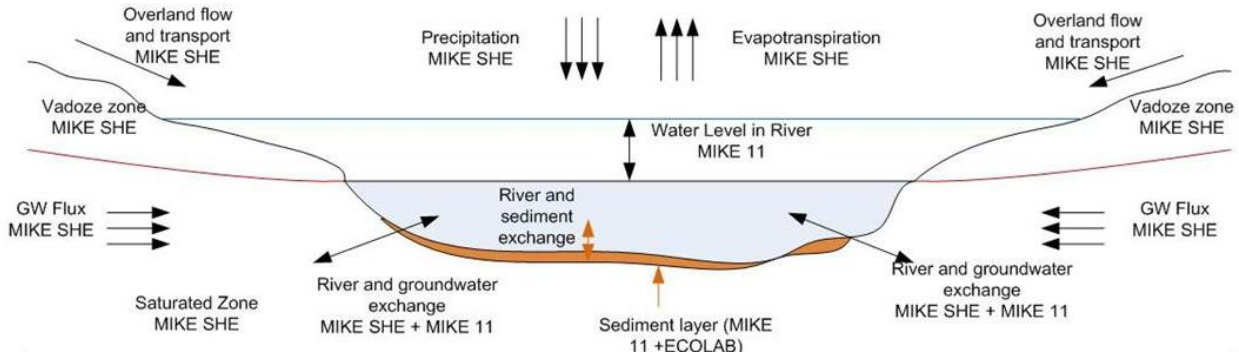

Figure 5 Flow and transport model component.

The model includes the main components of the hydrological cycle and contaminant transport; groundwater flow and transport (3D saturated and unsaturated), overland flow, flow in rivers, precipitation, and evapotranspiration. The model enables full, dynamic coupling of surface and subsurface flow processes, which allows calculations of water and contaminant exchange between the land, rivers, and the groundwater. By providing detailed spatial information and characteristics including hydrological and transport properties in the four sub-domains, Saturated Zone (SZ), Unsaturated Zone (UZ), Overland Flow (OL), and Transport in

Streams (OC), the model provides accurate water and contaminant mass balance for the domain. MIKE SHE and MIKE 11 are used to simulate and assess the impact of hydrological events on mercury contamination. The processes simulated by each module (MIKE 11, MIKE SHE, and ECO Lab) in the EFPC model are described below.

This project seeks to extend the existing model to include the entire EFPC watershed as well as couple MIKE SHE and MIKE 11 with the sedimentation module ECO Lab. The sedimentation module will provide the coupling between the flow and transport within the creek and the overland flow which will be used to analyze the significance of floodplain contamination downstream EFPC.

2.2 MIKE 11 and MIKE SHE

MIKE 11 is a one-dimensional river flow and transport model that requires logitudinal profiles, cross sections, Manning's numbers, and other hydrodynamic parameters [13]. It uses the dynamic Saint Venant equations to determine river flow and water levels. The complete nonlinear equations of open channel flow (Saint Venant) can be solved numerically between all grid points at specified time intervals for given boundary conditions. In addition to this fully dynamic description, other descriptions are also available to choose from including high-order, fully dynamic, diffusive wave, kinematic wave, quasi-steady state, and kinematic routing (Muskingum, Muskingum-Cunge).

MIKE SHE is a fully integrated model for the 3D simulation and linkage of hydrologic systems including overland, subsurface, and river flows. It has been successfully applied at multiple scales, using spatially distributed and continuous climate data to simulate a broad range of integrated hydrologic, hydraulic, and transport problems. MIKE SHE represents the two-dimensional overland, one-dimensional unsaturated zone, three-dimensional saturated and vadose zone flow and transport components [14]. The hydrologic processes are described based on physical laws such as the conservation of mass, energy and momentum. MIKE SHE couples several partial differential equations that describe flow in the saturated and unsaturated zones with the overland and river flow. Different numerical solution schemes are

then used to solve the different partial differential equations for each process. A solution to the system of equations associated with each process is found iteratively by use of different numerical solvers.

The model enables MIKE SHE and MIKE 11 Hydrodynamic (HD) modules to interact through branches or stream reaches defined within the domain. This coupling allows for one-dimensional simulation of river flows and water levels through the fully dynamic Saint Venant equations. Hydraulic control structures, area-inundation modeling, dynamic overland flooding flow in relation to the MIKE 11 river network, and the dynamic coupling of surface and sub-surface flow is simulated. Floodplain flooding is simulated by first establishing the floodplain through the MIKE SHE topography and then activating the direct overbank spilling option in MIKE 11 while simultaneously restricting cross sections to the main channel. The cross sections defined in MIKE 11 are used to calculate the river water levels and volumes. Consistency with topographical elevations is of extreme importance since the bank elevation is the primary reference for cell flooding. River and groundwater exchange is modeled by defining the river in contact with the aquifer. In this case, the water exchange between MIKE 11 and MIKE SHE is performed through a river-link cross section. The river cross sections link as shown in Figure 6 below is a function of Conductance (C), the grid node, and river link as depicted by the subsequent equation:

$$C = (K\,(da)(dx))/ds$$

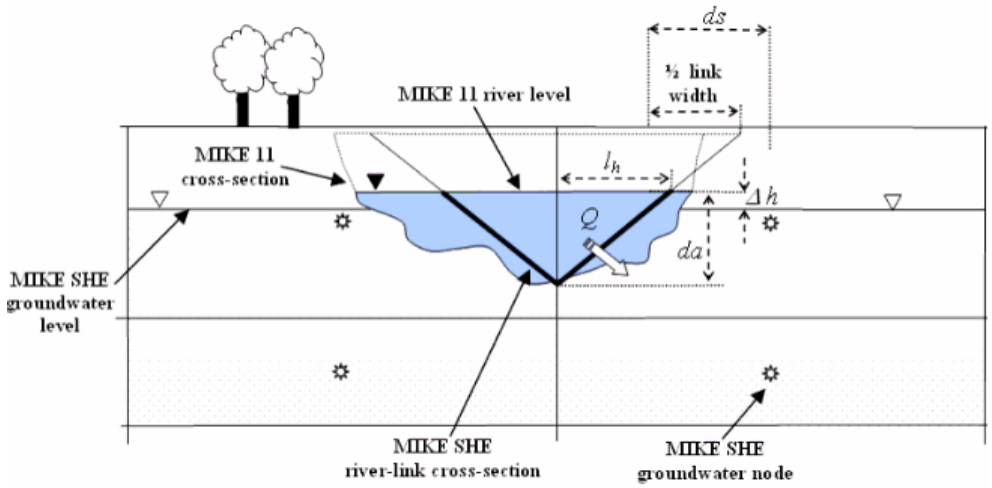

Figure 6 River link cross-section (DHI, 2008).

The variables K, da, dx, and ds represent the horizontal hydraulic conductivity for a specific grid cell, the vertical surface available for flow, grid size in saturated zone, and the average flow length within a range of 0.5 to 0.25 that of the cell width.

2.3 ECO Lab

ECO Lab is an equation solver for the sedimentation and exchange of mercury within sediments, suspended particles, pore water and dissolved mercury species [15]. An ECO Lab template can be developed by the user to model the ecological processes as required by any specific project; however, some templates have already been developed by DHI in the areas of water quality (17 templates), heavy metal transport (1 template), eutrophication (3 templates), and xenobiotics (1 template). For the modeling of mercury fate and transport in EFPC, the heavy metal transport template of ECO Lab is used coupled with both MIKE 11 and MIKE SHE to simulate the interaction of mercury species with the sediment particles and water molecules in the creek. The heavy metal template describes the adsorption/desorption of mercury to suspended matter, the sedimentation of sorbed mercury to the streambed, as well as resuspension of the settled mercury. It also includes exchange of mercury between particulates of the bed sediment and the interstitial waters of the bed. The diffusive exchange of dissolved mercury in the water and in the interstitial waters is also described.

Mercury transport processes in ECO Lab are defined by specifying the following:

- Dissolved mercury in the water (S_{HM}),
- Adsorbed mercury concentration on suspended matter (X_{HM})
- Dissolved mercury in the sediment pore water (S_{HMS})
- Adsorbed mercury in the sediment (X_{HMS}).

S_{HM} is the byproduct of mercury exchange between suspended solids and the water column. This exchange is mainly driven by the organic carbon partitioning coefficient (K_d); indicating the contaminant's affinity towards the soil phase. Dissolved mercury is computed using the following set of interconnected equations:

$$(dS_{HM})/dt = -adss + dess + difv$$

$$adss = k_w K_d S_{HM} TSS$$

$$dess = k_w X_{HM}$$

$$difv = (f_{biot(difw)})\ (S_{HMS}/((pors)(dzds)) - S_{HM}\ ))/(dzwf + dzds)dz$$

The equations above clearly represent the relation between adsorption (adss), desorption (dess), and diffusive transfer (difv). The variables k_w, K_d, TSS, $f_{biot(difw)}$, $pors$, $dzwf$ and dz are equivalent to the desorption rate (d^{-1}), partitioning coefficient for mercury (m^3 H_2O/gDW), total suspended solids concentration (g DW/m^3 bulk), factor for diffusion due to bioturbation (dimensionless), thickness of diffusion layer in sediment (m), and thickness of the computational grid layer (m) respectively.

X_{HM}, the adsorbed mercury concentration on suspended matter within the water column, results from mercury being absorbed by both the suspended solids and particles resuspended by the river bed layer, and eliminating the mercury desorbed from suspended solids into water column, and also those adsorbed by settling particles.

$$(dX_{HM})/dt = adss - dess - sev + resv$$

$$sev = (v_s X_{HM})/dz$$

$$resv = (RR\, X_{HMS}/X_{SED})/dz$$

Sev and resv represent the sedimentation and resuspension of particles. V_s defines the settling velocity (m/d) of suspended solids. RR denotes the resuspension rate (gDW/m^2/d). X_{SED} is the sediment mass gDW/m^2). These equations assume that the current speed is greater than the critical speed responsible for initiating movement.

S_{HMS} is calculated based on the equations below:

$$(dS_{HM})/dt = -adss + dess - difv$$
$$adss = k_s K_{ds} S_{HMS}\ X_{SED}/(dzs.por_s)$$
$$dess = k_s X_{HMS}$$

The desorption rate in sediment (d-1), metal partitioning coefficient between particulates and water (m^3 H_2O/gDW), sediment porosity (m^3 H_2O/ m^3 bulk), is given by k_s, K_{ds}, and $.por_s$. The above variables in the above equations have been defined earlier in this section.

X_{HMS} is calculated using the following:

$$(dX_{HMS})/dt = adss - dess - sev + resv$$
$$adss = k_s K_{ds} S_{HMS}\ X_{SED}/(dzs.por_s)$$
$$sev = v_s X_{HM}$$
$$resv = RR\, X_{HMS}/X_{SED}$$

In the model sediment porosity $(.por_s)$ has a constant value of 0.4 as assumed by Cabrejo, 2010.

2.4 Methodology

The following approach was taken in order to apply a hydrology and transport model developed in support of the DOE's remediation strategies for the EFPC watershed. These techniques expand upon previous modeling efforts including the diffusive transport between

the water column and sediment pore water, and the adsorption-desorption processes between dissolved mercury and suspended matter in the water column as part of the total mercury concentration. The integrated surface/subsurface model was built using the numerical package, MIKE (MIKE 11 coupled with MIKE SHE and ECO Lab), developed by the Danish Hydraulic Institute (DHI). The sedimentation module, which originally included UEFPC was extended to include the entire EFPC, down to EFK 6.4 and Bear Creek. The sedimentation and water quality module was extended to the entire EFPC watershed in the following phases:

1) The water quality and sedimentation module (ECO Lab) was extended for Bear Creek and for the remaining section of EFPC (downstream of Station 17) to include EFK 6.
2) Water quality, transport-related, and sediment-related parameters, such as carbon partitioning coefficient, adsorption rates of mercury species to sediment particles and water molecules, resuspension rate of sediments, settling velocity of suspended particles, and critical current velocity for sediment resuspension was estimated from literature, such as DOE reports of field surveys, laboratory experiments reported by FIU or other research institutes, and referenced publications.
3) Simulations were executed for a range of significant input parameters to correlate stochastic hydrologic events with mercury distribution patterns.
4) The extended EFPC model was calibrated using observed total suspended solids and total mercury concentration timeseries (including dissolved and adsorbed mercury concentrations) recorded at the key stations, EFK 18, EFK 14, EFK 6, downstream of Station 17 (EFK 23). The calibration procedures consisted of:
    a. Identifying the significant input parameters in the water quality module. This step was carried out for the UEFPC model and the significant parameters were identified. There are two major sets of input parameters associated with the water quality modeling: (1) transport-related parameters including carbon partitioning coefficient and adsorption coefficients; and (2) sediment-related parameters including resuspension rate of sediment particles, particle production rate along the creek, settling velocity of suspended particles, and critical current velocity for the suspension of sediment particles.

5) Model simulations using observed total suspended solids and total mercury concentration timeseries. The simulations will be analyzed using a range of correlations, including:
   a. Time series plots of observed and simulated values for fluxes or state variables (e.g., stage, sediment concentration, and biomass concentration);
   b. Observed versus simulated scatter plots, with a best-fit linear regression line displayed, for fluxes or state variables; and
   c. Cumulative frequency distributions of observed and simulated fluxes or state variables (e.g., flow duration curves).

3 EXISTING EFPC MODEL

3.1 Topography

Surface elevations were originally embedded in the model in the form of a dfs2 extension file as shown in the model topography snapshot below [Figure 7]. These surface elevations are measured in meters.

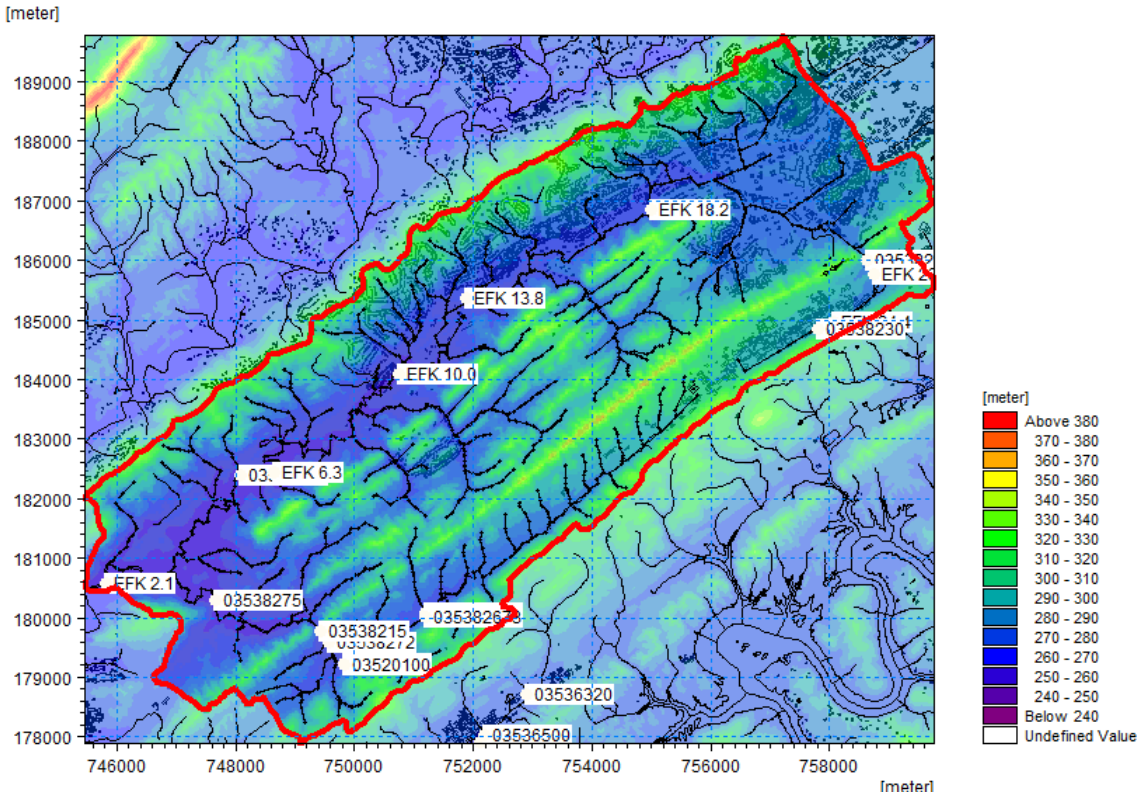

Figure 7 Model topography.

3.2 Climate

The precipitation component of the model determines surface water flows and defines the basics for the groundwater table. The precipitation timeseries is presented in the form of mm/day from 01/01/2000 through 12/31/2000. Data may be updated to include a larger time span.

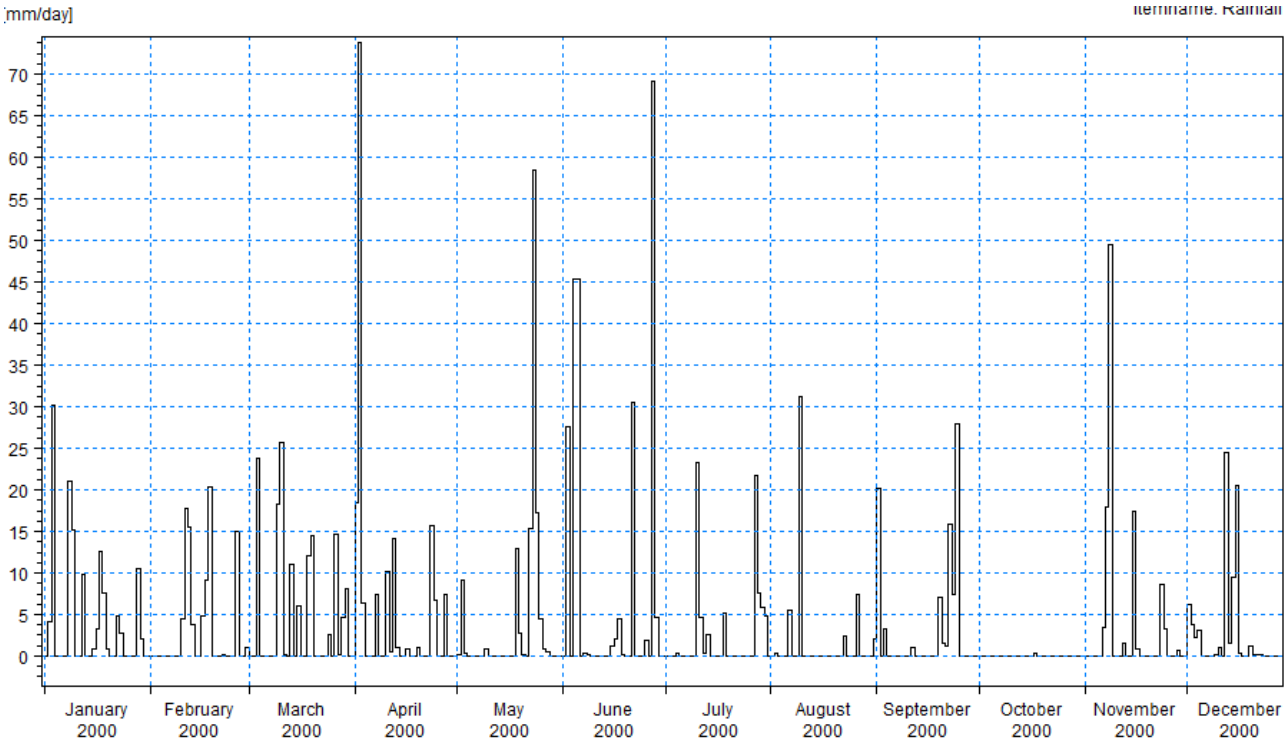

Figure 8 Model rainfall data.

3.3 Evapotranspiration

The evapotranspiration (ET) component of the model is dependent upon meteorological and vegetative data as it must predict evapotranspiration due to rainfall interception by canopy, canopy drainage to soil surface, evaporation from plant and soil surface, and water uptake by roots. A spatially uniform constant value of 2.01168 mm/day is observed based on records for the state of Tennessee. The model adjusts ET based on the leaf area index and root depth specified under land use.

3.4 Land Use

The land use consists of vegetation maps with assigned Leaf Area Index (LAI) constants and Root Depth (RD) values obtained from USGS. LAI and RD spatially adjust the reference ET stated previously. Table 2 below depicts the gridded codes and their classifications along with assigned LAI, RD and Manning's M (1/n).

Table 2 Land Use Classifications

GRIDCODE	CLASS	LAI	RD (mm)	M
11	Open water	0	0	50
21	Developed, Open Space	3	2000	50
22	Developed, Low Intensity	2.5	2000	20
23	Developed, Medium Intensity	2	2000	10
24	Developed, High Intensity	1.5	2000	7
31	Barren Land, Rock, Sand, Clay	1.31	4000	11
41	Deciduous Forest	5.5	2000	10
42	Evergreen Forest	5.5	1800	9
43	Mixed Forest	5.5	2400	10
52	Shrub, Scrub	2.08	2500	20
71	Grassland, Herbaceous	1.71	1500	29
81	Pasture, Hay	1.71	1500	30
82	Cultivated Crops	3.62	1500	27
90	Woody Wetlands	6.34	2000	10
95	Emergent Herbaceous Wetlands	6.34	2400	22

3.5 Saturated Zone

A horizontal hydraulic conductivity, vertical hydraulic conductivity, specific yield, and specific storage of 1.0 e^{-04} m/s, 1.0 e^{-05} m/s, 0.2 and 3.0 $x10^{-5}$ respectively were originally set. The drainage level was assumed -1.0 m relative to the ground, and the drainage time constant has been preset to $1.0x10^{-6}$ sec^{-1} based on calibration and uncertainty analysis performed by other modelers (Long, 2009).

3.6 Unsaturated zone

The unsaturated zone makes use of the Van Genuchten algorithm for the soil water content and hydraulic conductivity of the soil based on defined parameters. The total saturated water content, capillary head, and the alpha-empirical constant, and M-empirical constant must be specified in order for the algorithm to compute the soil water content. Hydraulic conductivity is expressed as a ratio between the hydraulic conductivity for given water content and the saturated hydraulic conductivity.

3.7 Overland Flow

Drainage is routed downhill based on adjacent drain levels. If drain flow is produced it is routed to the recipient point using a linear reservoir routing technique based on a pre-processor generated reference system that utilizes the slope of the drains calculated from the drainage levels in each cell.

3.8 Boundary Conditions

Open boundary conditions for free upstream and downstream ends within the model domain. Boundary conditions were in place for inflow specified with a time-varying or constant flow hydrograph condition (for the HD model) at times with a solute component (for the AD model). Tables detailing the Q-h relation are specified when the relationship between the discharge and the water level (HD model) is known. The solute component is added for the AD module. Table 3 below (Long, 2011) summarizes the original boundary conditions settings for select rivers. Boundary conditions for branches were also defined assuming a zero constant inflow.

Table 3 Original Boundary Conditions for the Rivers (Long, 2011)

RIVER	BOUNDARY DESCRIPTION	BOUNDARY TYPE	CHAINAGE
East Fork Poplar Creek	Open	Q-h	25485.2
East Fork Poplar Creek	Open	Point Source	3120.175
East Fork Poplar Creek	Open	Inflow	0
Bear Creek Inflow	Open	Inflow	0
Mill Branch	Open	Inflow	0
Gum Hollow Branch	Open	Inflow	0
Pinhook Branch	Open	Inflow	0

3.9 River Network and Cross Sections

The river and stream network is shown in Figure 9 below for the study domain. It consists of 112 branches/MIKE SHE links and 1086 nodes. Cross-sections are set to allow for

overbank spilling. The left and right bank elevations and bed layer are consistent with topography files. Resistance (Manning's M) values range between 10 and 20 throughout the domain.

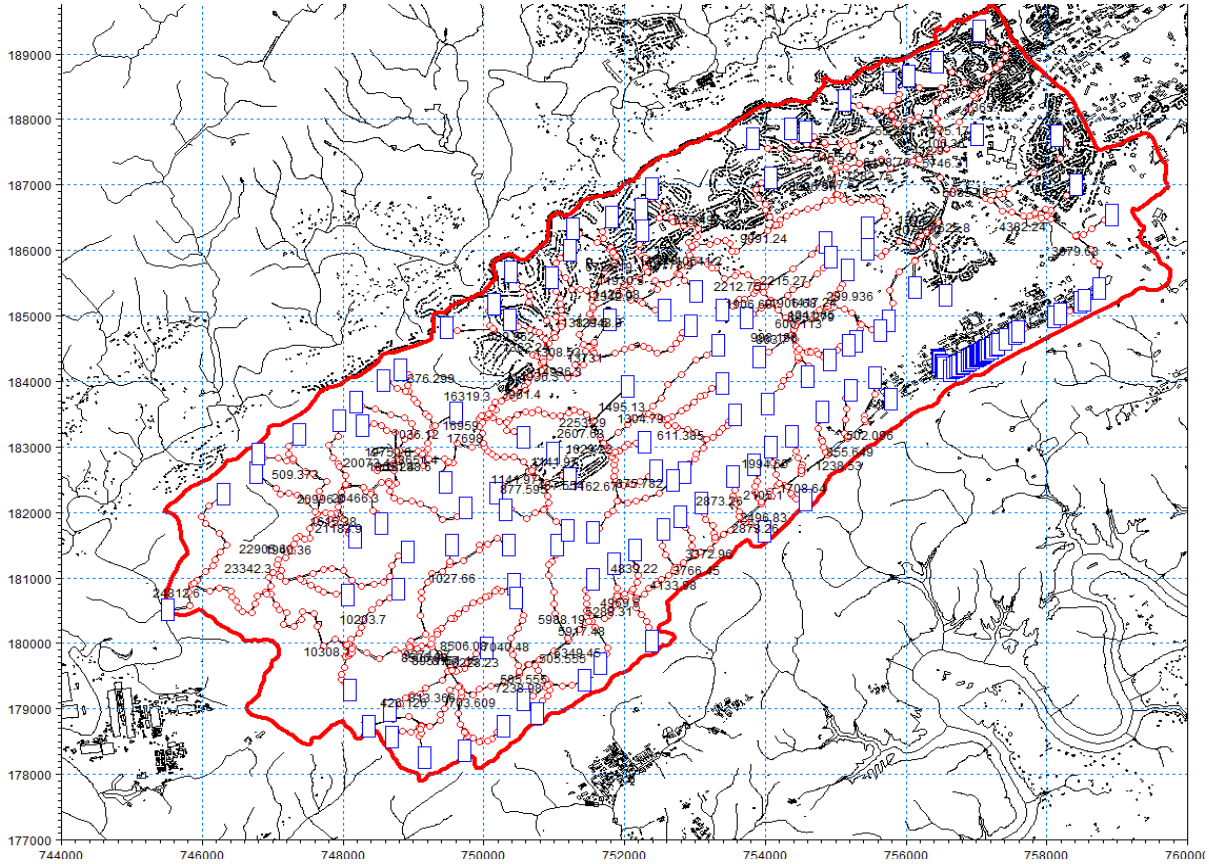

Figure 9 River network showing nodes and cross-sections.

4 EFPC MODEL EXTENSION

The original EFPC model originally developed by Long was modified to include the following changes:

1. Boundary conditions were created based on a merger between the previously existing EFPC model boundary file and the Y-12 model boundary file, links to mercury & flow time series were also established.
2. Vegetation data input format has been changed from shape to gridded codes; increasing the model's preprocessing speed.
3. Van Genuchten's soil parameters have been updated according to site-specific literature.
4. ECO Lab template has been incorporated and activated.
5. Additional observations stations have been included (EFK 23.4, 18.2, 13.8, and sta. 3538250).
6. Cross sections have been modified to reduce numerical instabilities.

4.1 Data Extraction and Processing

The Oak Ridge Environmental Information System (OREIS) is a centralized, standardized, quality-assured, and configuration-controlled environmental data management system belonging to the US Department of Energy (US DOE). The environmental data retrieved from the OREIS database for the purposes of this research include known quality measurement and spatial data from groundwater, surface water, sediment, and soil. The spatial data was extracted by utilizing the OREIS Spatial Query Tool; the interface is shown in Figure 10 below.

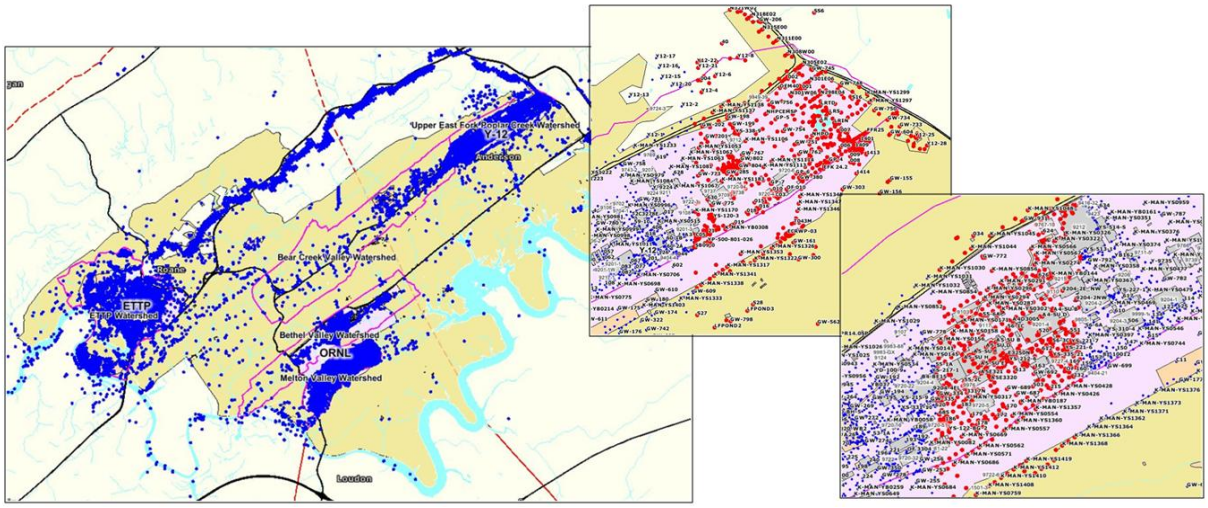

Figure 10 OERIS spatial query overview (left), and sample segments extracted.

The study domain was divided into 16 sub segments in an effort to minimize the time and computer resources spent in the data extraction process. The data was initially extracted in the form of text files. It was archived into Excel spreadsheets, converted into appropriate units, converted to timeseries, and ultimately added to the model as additional observation stations. Stations 2236AQ06, 3538250, 3215AQ05, 3904AQ04, EFK 13.8, 5313AQ03, EFK 18.2, 6262AQ02, and 6361AQ01 shown in Figure 11 below were initially identified as potential observation stations to be added to the model. PCM 5.5-1, PCM 5.5-2, PCM 5.5-3, PCM 5.5-4, PCM 5.5-5, PCM 6.0, PCM 6.5, PCM 7.0, LASD01, and CCSD01 were removed as these represented invalid results. Ultimately, 3538250, EFK 13.8, and EFK 18.2 were the only discharge (flow rate measurement) stations with sufficient data to be included in the model.

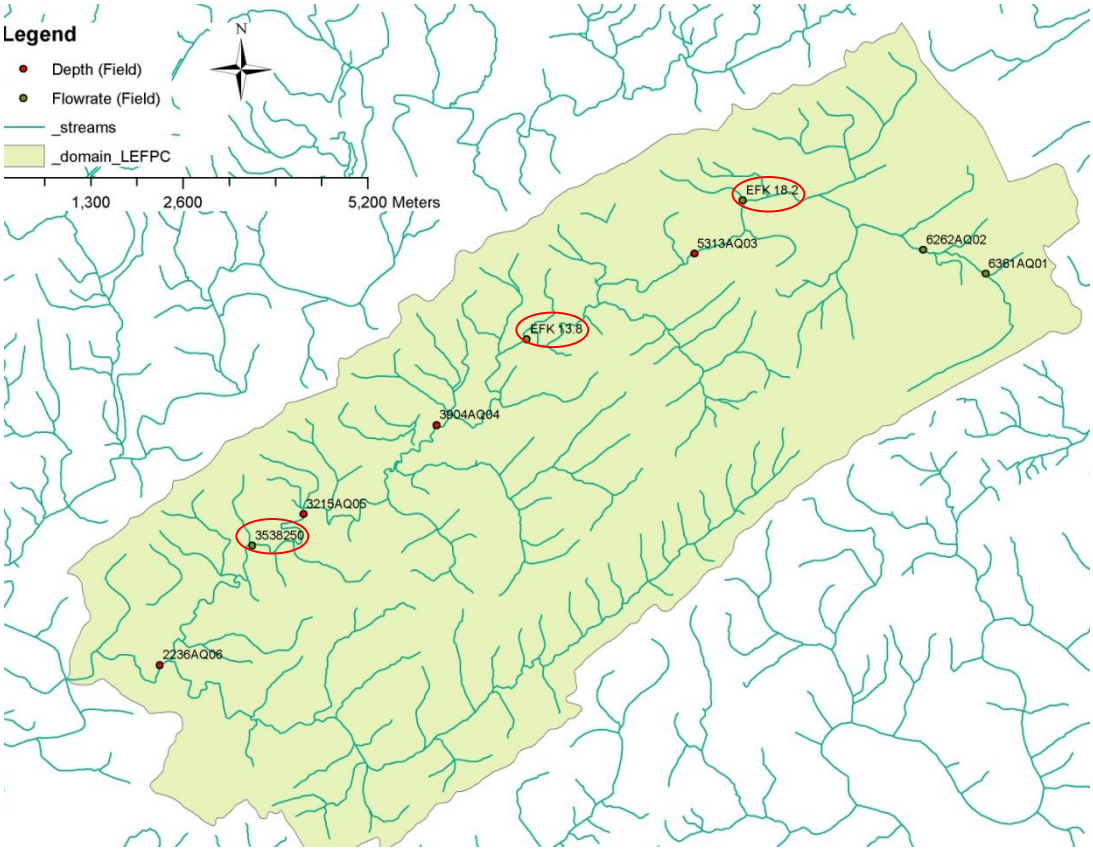

Figure 11 Processed stations and new model observation stations.

Sample discharge plots are shown in Figure 12, Figure 13 and Figure 14 for one of the stations. Flow rate data extracted for station 3538250 is shown first for a twenty year span. A few outliers are present characterized by extremely high flow rate values falling outside the successive pattern of high and low flow rates. These variations are potentially driven by hydrological events. A more detailed plot of station 3538250 is shown subsequently where flow rate varies between 0.5 to 5.0 m^3/s. An average flow rate value of 1.469 m^3/s is observed along with a base flow of 0.5 m^3/s. Rainfall and discharge data were also plotted for the same time period in order to identify any correlation between the two.

The mercury and methyl mercury observation stations identified have not been analyzed or incorporated into the model as this preliminary phase is focused on flow. The water quality will be addressed at a later time.

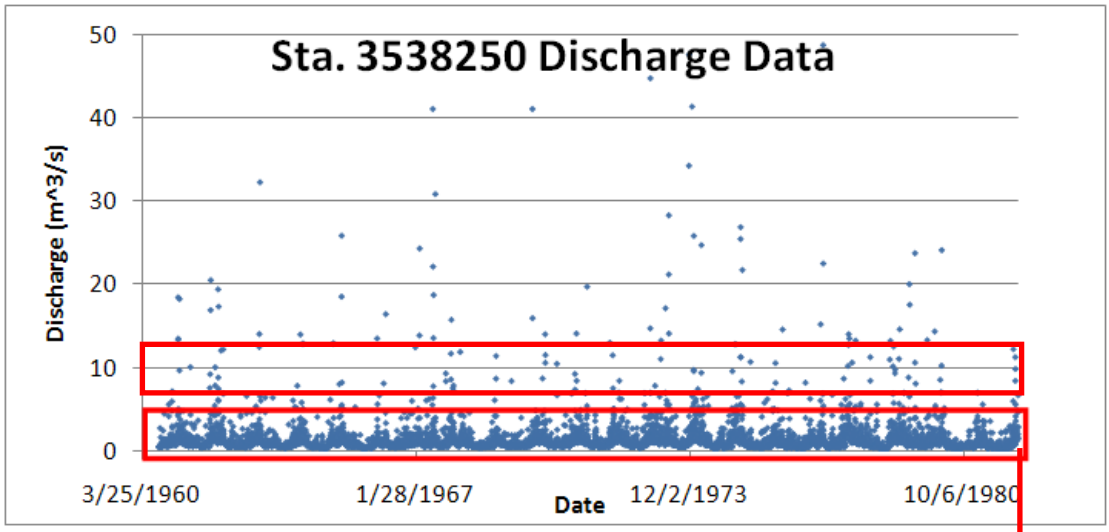

Figure 12 Flow rate data extracted for Sta. 3538250.

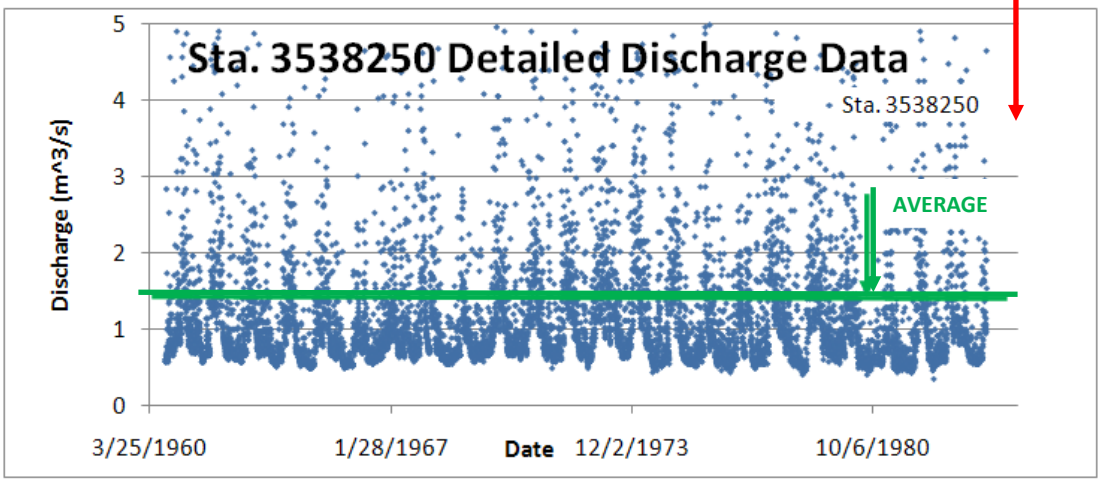

Figure 13 Detailed graph for flow rate (Sta. 3538250) showing seasonal fluctuations.

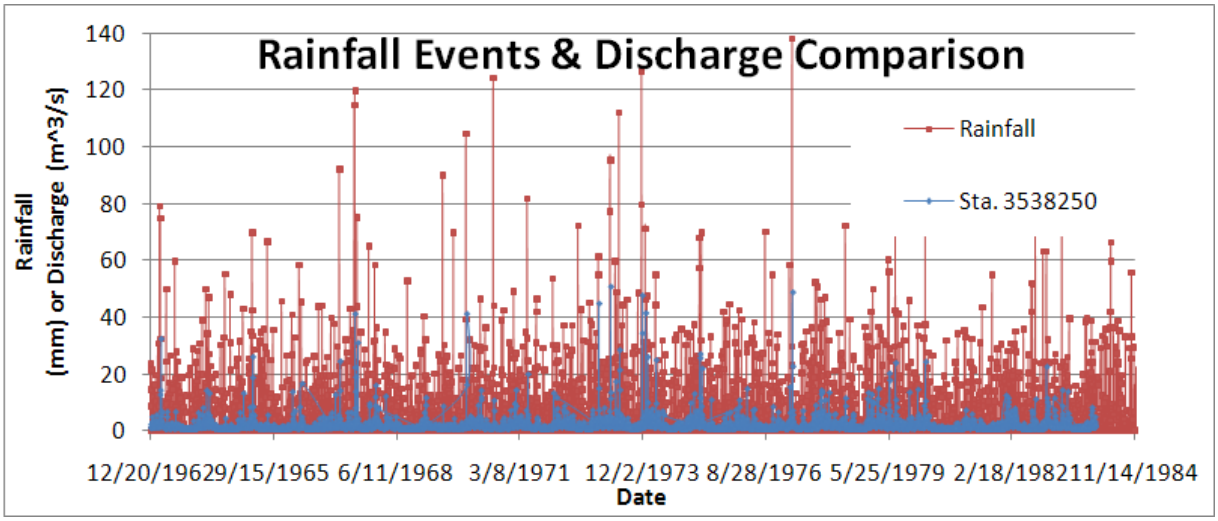

Figure 14 Comparison of hydrological events to flow rate data.

4.2 Boundary Conditions

The EFPC model was modified by adding Outfalls (point sources) to the boundary file in both the Hydrodynamic (HD) and Advection (AD) module. The newly developed boundary conditions file for the modules consists of a merger between the previously existing EFPC Model Boundary file and the Y12 Model boundary file. The new boundary condition files consist of a total of 157 branches. Forty-two point sources are included within these. These point sources listed in Appendix A: Boundary Conditions include discharge and mercury timeseries for the hydrodynamic and advection modules.

4.3 Van Genuchten Parameters

Van Genuchten's hydraulic conductivity and moisture content parameters have been updated for the upper and lower layers of the aquifer as shown in Figure 15 and Table 4 below.

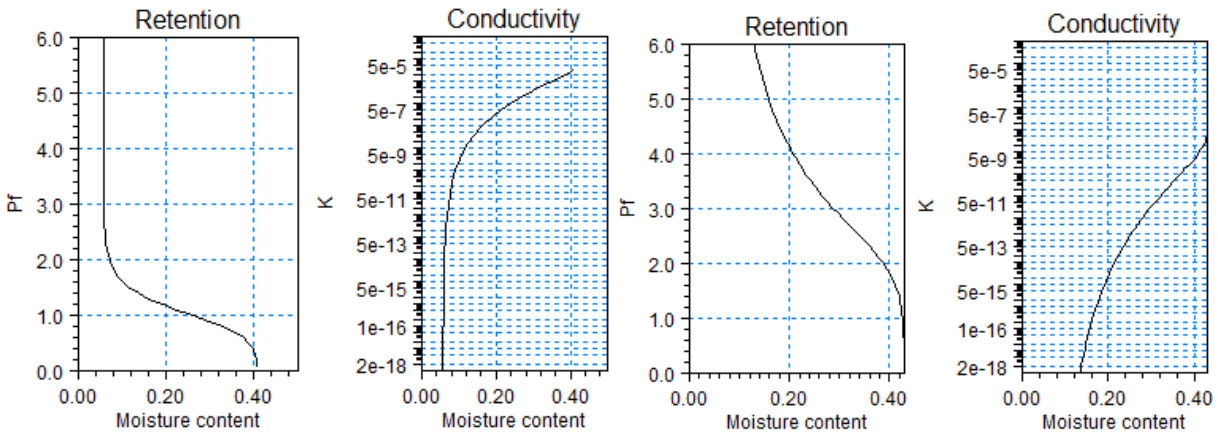

Figure 15 Retention and hydraulic conductivity curves for the upper and lower aquifer layers.

Table 4 Parameters of the Retention and Hydraulic Conductivity Curves

Retention Curve Parameters									
Upper Layer					**Lower Layer**				
θ_s	**θ_r**	**α**	**n**	**m**	**θ_s**	**θ_r**	**α**	**n**	**m**
0.41	0.057	0.124	2.28	0.5614	0.43	0.089	0.01	1.23	0.1869
Hydraulic Conductivity Curve Parameters									
Upper Layer					**Lower Layer**				
K_s	**α**	**n**	**Shape factor**	**m**	**K_s**	**α**	**n**	**Shape factor**	**m**
4.05e-5	0.124	2.28	0.5	0.5614	1.95e-7	0.01	1.23	0.5	0.1869

4.4 Drainage

A special saturated zone drainage boundary condition has been set within MIKE SHE to define the natural and artificial drainage systems within the domain. The saturated zone drainage is applied to the layer of the saturated zone model containing the drain levels. A drain level and leakage factor (time constant) was spatially defined for each cell. Drainage within the saturated zone was initially set to be routed downhill based on adjacent drain levels. This option has been modified to better represent the domain area by establishing a series of distributed drainage options. Different drainage options were implemented for different areas

of the model by specifying an integer code for each respective area. Essentially each cell in the distributed option consist of a value of 1 in which the drainage reference system is calculated based on the drain levels or code 2 in which it is calculated based on the drain codes.

Drain codes within the system were set to 0 or 1. Drain flow is neither produced nor received for cells with a value of 0. Cells with a positive drain code value drain to the nearest river, boundary, or local depression in said order if the cell contains the same drain code value. This last option was established for areas within the domain with a higher building density as drainage in these areas is dominated by drainage structures and routing channels. Drainage in natural areas was set to be dependent on the slope of the drain levels.

Simulations results for which the drainage option was incorporated coincide with the overall baseline of flow. Additional calibration is necessary to obtain the peaks. A gridded code option for the drainage will be developed and implemented to compare its effects with the distributed drainage option.

4.5 Cross Sections

The model cross sections within the domain are shown in Figure 16 below. All these cross sections were checked for consistency in the left and right bank elevations, and bed layer elevation with the topography elevations. Overbank spilling was allowed in all cross sections. In addition, the cross sections were all deepened by 1 meter to allow for greater stability in computations.

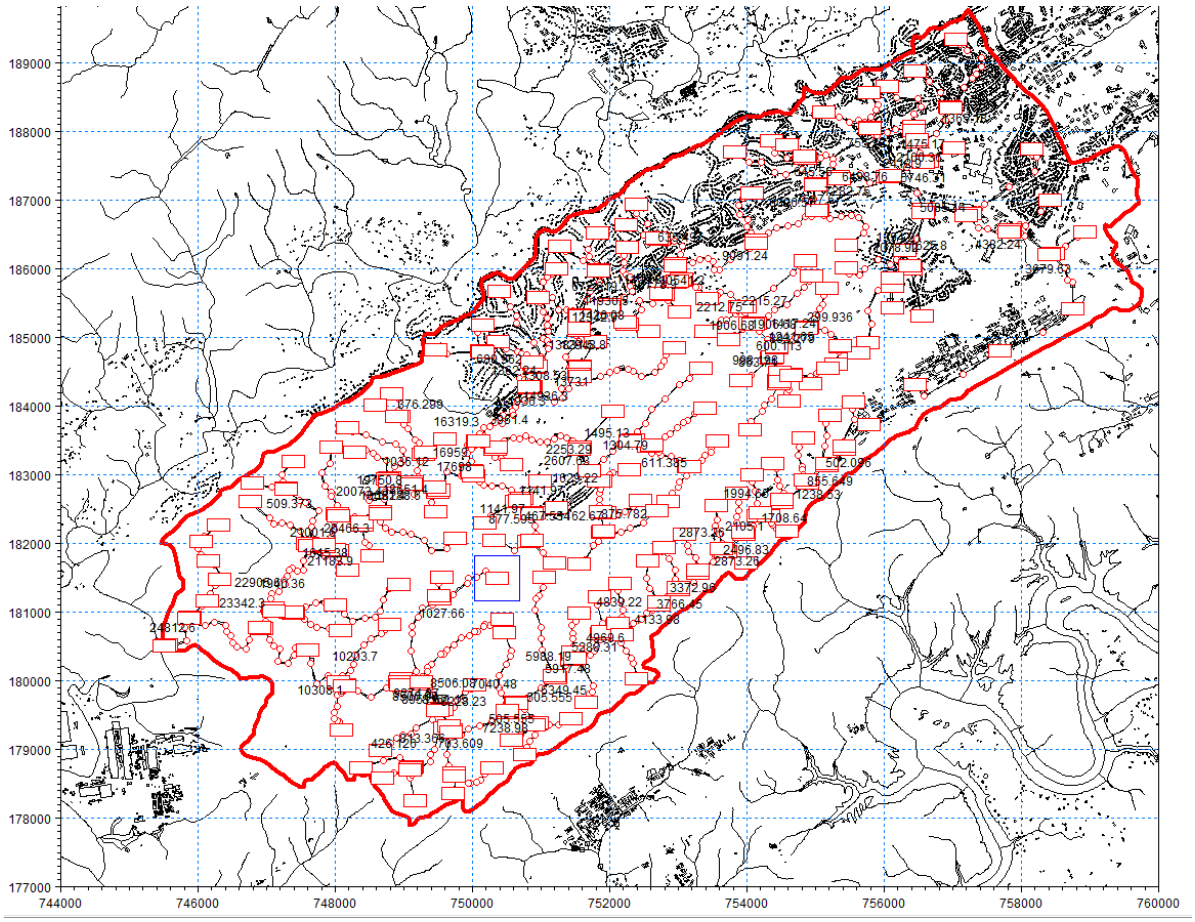

Figure 16 Overview of all river cross sections in the model.

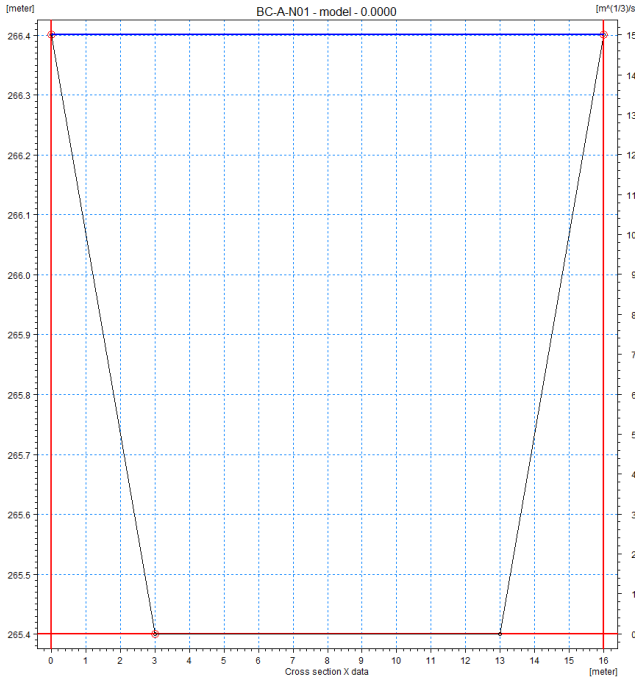

Figure 17 Sample trapezoidal cross section for Branch BC-A-N01 at Chainage 0.00.

4.6 ECO Lab

The activated ECO Lab module within the Advection Component of Rivers and Lakes currently contains 6 state variables, 11 auxiliary variables, 16 constants, 15 processes, 3 forcing, and 11 derived outputs. The description of the ecosystem state variables is formulated via a series of ordinary coupled differential equations describing the rate of change of each state variable within the ecosystem. Mercury, adsorbed mercury, dissolved mercury in sediment, adsorbed mercury in sediment, suspended solids, and mass of sediment constitute the state variables. Model constants account for the organic-carbon partitioning coefficient, desorption rate in both water and sediment, the fraction of organic carbon in suspended solids (ss) and sediment, thickness of the water film, the ratio between the thickness of diffusion layer in sediment, factor for diffusion as a byproduct of bioturbation, molecular weight of heavy metal, density and porosity of dry sediment, settling velocity of suspended solids, resuspension rate, particle production rate, and critical current velocity for sediment resuspension. The forcing used to represent external variables affecting the ecosystem under analysis includes the current speed, total water depth, and thickness of the computational layer. These components are summarized in Table 5 below.

Table 5 Summary of ECO Lab Input

STATE VARIABLES		Ratio between thickness of diffusion layer	0.2
Mercury	0.01 mg/l	Diffusion factor due to bioturbation	1
Adsorbed Mercury	0.1 mg/l	Mole weight of heavy metal	92 g/mole
Dissolved Mercury in Sediment	0.1 g/m^2	ECO Lab time step	30 Seconds
Adsorbed Mercury in Sediment	10 g/m^2	Density of dry sediment	250 g/m^3
Suspended Solids	50 mg/l	SS settling velocity	0.8 m^3 H2O/ m^3
Mass of Sediment	10000 g/m^2	SS settling velocity	0.1 m/day
CONSTANTS		Resuspension Rate	1000 gDW/ m^2/day
Organic-Carbon Partitioning Coefficient	50000 l/kg	Particle Production Rate	1 gDW/ m^2/day
Desorption rate in water	1 per day	Critical current velocity	1 m/s
Desorption rate in sediment	0.1 per day	**FORCINGS**	
Fraction of organic carbon in SS	0.1	Thickness of Computational Layer	2 m
Fraction of organic carbon in sediments	0.2	Total Water depth	8 m
Diffusion thickness layer ratio	0.1 mm	Current Speed	0.2 m/s

5 RESULTS

While keeping all other parameters constant, one parameter at a time was varied within the verified range and the computed TSS and mercury concentration timeseries at the selected key stations (EFK 18, EFK 14, and EFK 6) compared with historically recorded timeseries. Figure 18 below depicts this concept. The value for the parameter was selected based on a least mean square error analysis on the computed and recorded timeseries. This process was then repeated for the rest of the parameters and the best combination of values for the significant parameters that provide the least mean square error between the computed and observed timeseries selected.

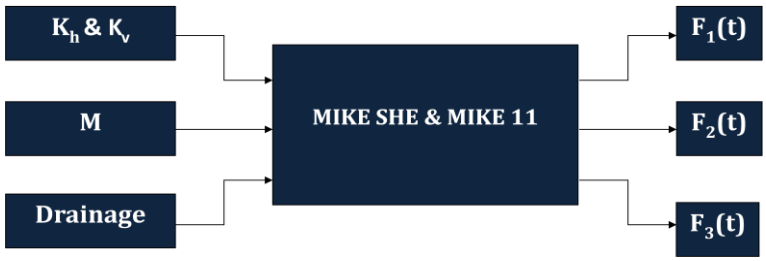

Figure 18 Simulation concept.

A variety of simulations have been executed with the purpose of calibrating the recently modified model for Manning's number. Simulations were executed for 1 year (2000 – 2001) and pertain only to the water movement within the system. Point sources from the Y-12 Model were added to the boundary file with their respective time series for flow and mercury. The hydraulic conductivity settings remain spatially uniform. Manning's number is the only variable. The graph in Figure 19 below shows the variability in time of discharge (m^3/s) for simulations EFPC001 (Manning's at 100% of original), and EFPC004 (at 25%) shown in black and blue respectively in comparison to observed data from Station 17 (shown in green). The general base flow is observed in all; the extent of the peaks appears to be slightly accentuated by a decrease in Manning's number.

In an effort to better match the simulated discharge to the observed; the threshold water depth for overland flow was reduced from 0.00254m to 0.0001 m. Simulations were executed for the new threshold water depth. This constitutes EFPC001A, and EFPC004A. Simulated and computed discharges are fairly consistent. Minor discrepancies will be addressed in future calibrations.

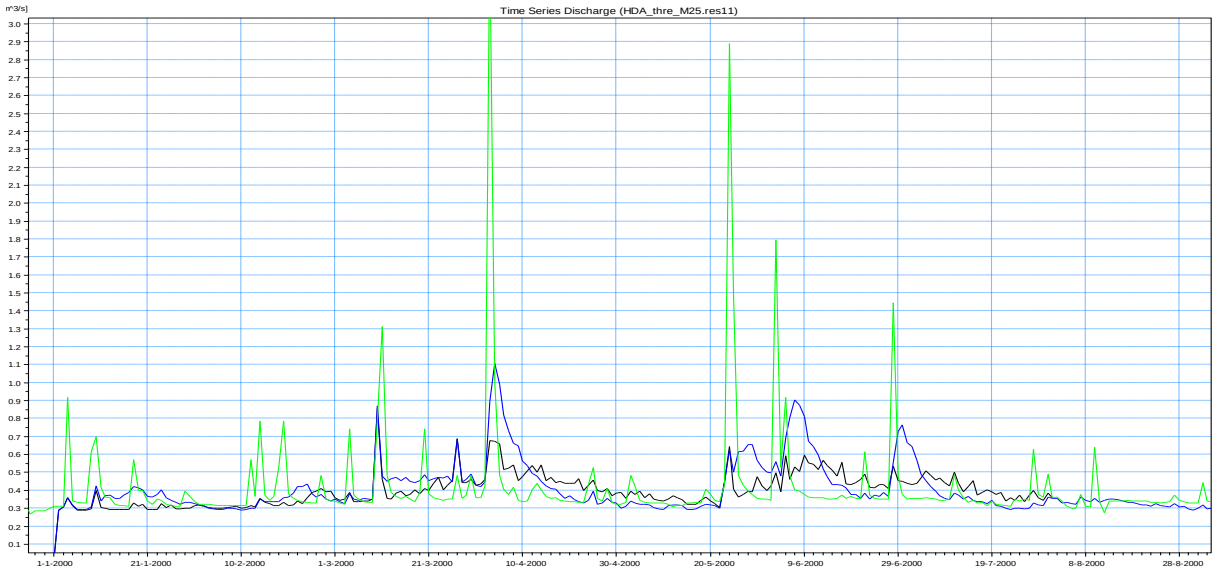

Figure 19 Simulated discharge for EFPC001 and EFPC004 compared to observed at Station 17.

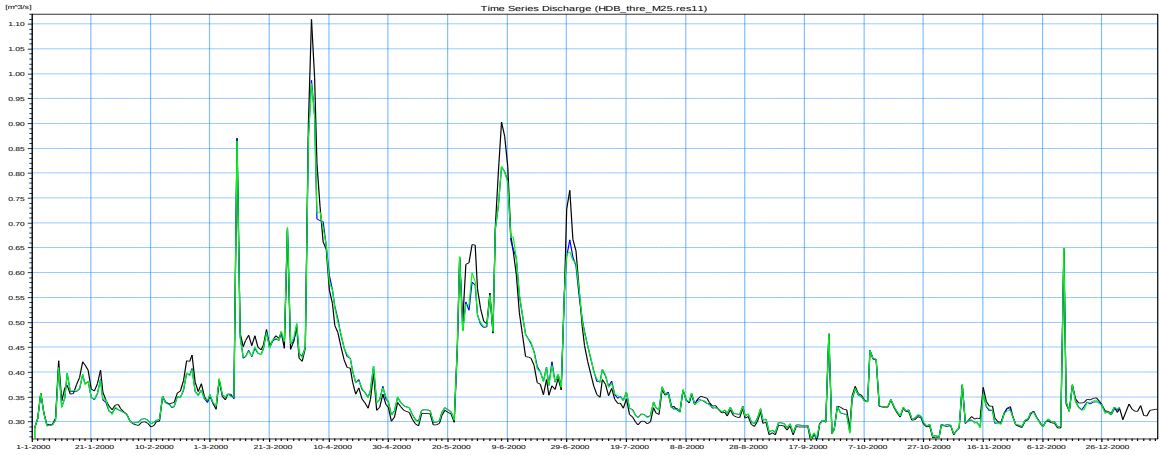

Figure 20 EFPC001A and EFPC004A compared to observed at Station 17.

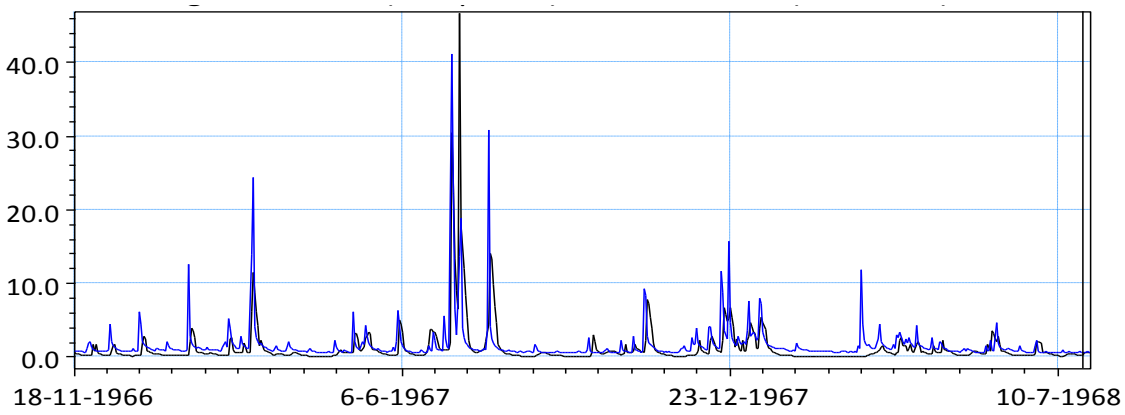

Figure 21 Discharge (m^3/s) at EFK 6.3 (simulated) and 03538250 (observed).

6 CONCLUSIONS

6.1 Subtask 1: Extension of the Water Quality and Sedimentation Module

The sedimentation module which was developed for the UEFPC (the section of EFPC upstream of Station 17) was extended to include the entire EFPC down to EFK 6 and Bear Creek. The sedimentation module provides the coupling between the flow and transport within the creek and the overland flow and was used to analyze the significance of floodplain contamination downstream EFPC. Fifty-two (52) outfalls were added to the EFPC model. Van Genuchten parameters for the unsaturated flow in the aquifer were updated. The model was reconfigured following the incorporation of the sedimentation module and outfalls. A series of numerical simulations have been performed using a range of Manning's number values, threshold run-off water depths, and drainage coefficients to calibrate the flow for the period of 2000 – 2008.

MATLAB scripts were prepared for the statistical analysis of observed and computed data. Laboratory and field data on surface water level and discharge, groundwater level, and mercury contamination in soil, groundwater and surface water were obtained from OREIS database. Data was organized and incorporated into the numerical model for calibration and verification purposes.

6.2 Subtask 2: EFPC Model Uncertainty and Sensitivity Analysis

The probabilistic distribution of critical subsurface parameters, such as hydraulic conductivity, porosity, pore size distribution, and storage coefficients were defined specifically for the karst areas. MATLAB's statistical toolbox and scripting tools were used to develop a series of functions for a random generation of distributed hydrologic parameters based on a selected probability density function and statistical parameters. Randomly generated grids were created using the MATLAB toolbox for the uncertainty analysis. Numerical simulations were then conducted for each randomly generated input grid. The output was used to generate daily timeseries for selected hydrological, fate and transport parameters, including

groundwater flow velocity at selected points, potential head at selected points, rate of mercury absorption at various locations, concentrations of total mercury at the key stations (EFK 6, EFK 14, EFK 18), total mercury load at the key stations, flux exchange between subsurface and surface. The simulations were used to determine the model uncertainty in terms of stochastic variations of input parameters. Graphical plots of the variation of the output parameters were then used to present the results of the sensitivity analysis, identifying significant parameters and a range of certainty for the model.

7 FUTURE WORK

FIU will use the numerical model of EFPC to determine the impact of remediation alternatives on the complete hydrologic cycle, the transport overland and in surface water and rivers, sediment transport and reactions, and mercury exchange with sediments. The research will be coordinated with the site and ORNL personnel. The major objective of this task is to provide analysis of the coupling between hydrology and mercury transport within the context of decreasing the risk of D&D activities. The major deliverable of this task will be numerical and stochastic analysis of observed and computed time series for flow and contaminant concentration for NPDES-regulated outfalls within the watershed. Model simulations will be used to account for a range of hydrological impacts related to planned remediation alternatives, including:

- Statistical analysis of observed data and development of timeseries, probability exceedance curves, and probability distribution models of flow, concentration and load data that integrates already downloaded data, and new data that will be obtained from contactors with the support of ORNL personnel. The data will include groundwater well monitoring, concentrations in groundwater wells, outfall flow, and concentration and load data. The task will also provide a refinement of the existing EFPC model by inclusion of historical outfall flow data for the area extending from WEMA to Station 17 to determine the effects of precipitation and stormwater drainage on the flux of mercury into EFPC. The deliverable of this subtask will include timeseries, probability exceedance curves, load exceedance curves, probability distribution models for each monitoring point and a report. The subtask will provide support for the team developing the mercury conceptual model and will provide considerably better estimates for the stochastic nature of mercury fluxes within the EFPC domain.
- Reduction of model parameter uncertainty (i.e., uncertainty analysis) for existing EFPC model via a series of probability distributions derived from running multiple simulations for selected specified parameters. In the previous scope the major variables were the hydraulic conductivities of each of the five geological layers. The current scope will focus

on analysis of the upper layer and the leakage factor between the creek and subsurface media, and on the exchange of flow and mercury between the creek and the river. Uncertainty analysis will be provided for the parameters governing the distribution of mercury species within pore water, sorbed mercury within pores, sorbed mercury on suspended particles and "free" mercury (dissolved and chelated mercury species). The major variable that will be analyzed will be total mercury considering that all regulatory documents are expressed as total mercury. The work in this subtask will help to improve the confidence in the predictive capability of the watershed-scale model. The deliverables from this task will include analysis of the uncertainties associated with the parameters governing exchange of mercury within each of the subdomains (mercury migration in the vadose zone during flooding, pore space in the sediments, sorption on sediments, sorption on particles, and aqueous species) and a report.

- Re-creation of the existing ORNL stormwater management system layout via a numerical surface water one dimensional model (SWMM or similar) to provide a better understanding of the flow patterns on-site, including flow rates as a function of rainfall intensity and the fraction of drainage volumes and rates reaching each outfall. The objective is to create a detailed surface water flow and contaminant transport model for the ORNL area using XPSWMM, incorporating flow data and other significant drainage system parameters, initially starting with a smaller model for the ORNL area. This would be a benchmark study to be extended to the Y-12 NSC (once reviewed and accepted by ORNL and the site). The deliverable of this subtask will be a calibrated and validated drainage model that will provide detailed analysis of how much water reaches each outfall and the source of the water. By providing better understanding of the drainage system, the site will be provided with a tool that can be used to investigate the best remediation scenarios for setting up remediation priorities, e.g., helping identify the greatest contributors to mercury loads.
- Simulations of surface water flow and contaminant transport utilizing collected piezometric data for EFPC. This will facilitate calibration and validation of the existing EFPC model developed by FIU and will provide data for comparison with new

measurements to be taken by ORNL in their effort to refine the existing conceptual model for EFPC. This task will be executed in collaboration with ORNL. Additionally, modifications of the flow hydrology along EFPC, including reduction of the flow augmentation, addition of a down-gradient diversion ditch, alternatives which result in reduced mercury fluxes in major outflows and simulation of flow and transport of other contaminants whose partitioning coefficients vary several orders of magnitude (including uranium and other contaminants of interest) will be investigated within this subtask.

8 REFERENCES

[1] R. R. Turner and G. R. Southworth, "Mercury contaminated industrial and mining sites in North America: an overview with selected case studies," *Springer-Verlag*, pp. 89 -112, 1999.

[2] Tennessee Department of Environment and Conservation, "2008 303 (d) List," Division of Water Pollution Control Planning and Standards Section, 2008.

[3] F. X. Han, Y. Su, D. L. Monts, C. A. Waggoner, and M. J. Plodinec, "Binding, distribution, and plant uptake of mercury in a soil from Oak Ridge, Tennessee, USA.," *Science of The Total Environment*, vol. 368, no. 2-3, pp. 753-768, September 2006.

[4] S. Malek-Mohammadi, G. Tachiev, E. Cabrejo, and A. Lawrence, "Simulation of Flow and Mercury Transport in Upper East Fork Poplar Creek, Oak Ridge, Tennesse," *Remediation*, pp. 119-131, 2012.

[5] E. Cabrejo, "Mercury Interaction with Suspended Solids at the Upper East Fork Poplar Creek, Oak Ridge, Tennessee.," Florida International University, Environmental Engineering Department, Miami, Master Thesis 2010.

[6] U.S. Department of the Interior. U.S. geological Survey (USGS), Mercury in the Environment, 2000, fact sheet 146-00.

[7] U.S. Department of Energy (US DOE), "Record of Decision for Phase I Interim Source Control Actions in Upper East Fork Popler Cereek Characterization Area, Oak Ridge, Tennessee," U.S. Department of Energy, Office of Environmental Management, DOE/OR/01-1951&D3.n Oak Ridge, TN, 2002.

[8] U.S. Department of Energy (US DOE), "Record Decision for Phase II Interim Source Control Actions in Upper East Fork Poplar Creek Characterization Area, Oak Ridge, Tennessee," U.S.

Department of Energy, Office of Environmental Management, Oak Ridge, Tennessee, DOE/OR/01-2229%D3.n Oak Ridge, 2006.

[9] H. R. Sorensen, T. V. Jacobsen, J. T. Kjelds, J. Yan, and E. Hopkins, "Application of MIKE SHE and MIKE 11 for Integrated Hydrological Modeling in South Florida," South Florida Water Management District (SFWMD) & Danish Hydraulic Institute (DHI), 2012.

[10] Danish Hydraulic Institute. (2012, May) MIKE by DHI. [Online]. http://www.mikebydhi.com/~/media/Microsite_MIKEbyDHI/Publications/SuccessStories/MIKE%20by%20DHI%20Success%20Story-MSHE-BrowardCounty.ashx

[11] North Carolina Department of Environment and Natural Resources, "Total Maximum Daily Load for Mercury in the Cashie River, North Carolina, Public Review," North Carolina Department of Environment and Natural Resources, 2004.

[12] N. Gandhi et al., "Development of mercury speciation, fate, and biotic uptake (BIOTRANSPEC)," *Environmental Toxicology and Chemisty*, vol. 26, pp. 2260-2273, 2007.

[13] Danish Hydraulic Institute (DHI), MIKE 11 Short Descriptions, 2008.

[14] Danish Hydraulic Institute (DHI), MIKE SHE Reference Manual, 2008.

[15] Danish Hydraulic Institute, ECOLAB Reference Manual, 2008.

[16] S. Long, "An Integrated Flow and Transport Model to Study the Impact of Mercury Remediation Strategies for East Fork Poplar Creek Watershed, Oak Ridge, Tennessee," Florida International University, Environmental Engineering Department, Miami, Master Thesis 2009.

[17] Oak Ridge national Laboratory (ORNL), "Conceptual Model of Primary Mercury Sources, Transport Pathways, and Flux at the Y-12 Complex and Upper East Fork Poplar Creek," Oak Ridge, Tennessee, ORNL/TM-2011/75, 2011.

[18] R. R. Truner, C. R. Olsen, and W. J. Jr. Wilcox, "Environmental Fate of Hg and 137 Cs Discharged from Oak Ridge Facilities," in *CONF-8406143-2*, 1985.

[19] U.S. Department of Energy (US DOE), "2009 Remediation Effectiveness Report for the U.S. Department of Energy Oak Ridge Reservation, Oak Ridge, Tennessee," U.S. Department of Energy Office of Environmental Management, Oak ridge, Tennessee, 2009.

[20] G. R. Southworth et al., "Controlling Mercury Release from Source Zones to Surface Water: Initital Results of Pilot Tests at the Y-12 National Security Complex," 2009.

[21] G. R. Southworth, M. Greely, M. Peterson, K. Lowe, and R. Kettelle, "Sources of Mercury to East Fork Poplar Creek Downstream from the Y-12 National Security Complex: Inventories and Export Rates.," Oak Ridge National Laboratory, Oak Ridge, 2010.

9 APPENDICES

Appendix A: Boundary Conditions

Table 6 New Boundary Conditions Added to the Model

Boundary Description	Boundary Type	Branch Name	Chainage	Boundary ID
Point Source	Inflow	EFPC	7.697023084	200
Point Source	Inflow	EFPC	15.18155778	135
Point Source	Inflow	EFPC	28.53370347	134
Point Source	Inflow	EFPC	93.20450316	126
Point Source	Inflow	EFPC	99.90745336	125
Point Source	Inflow	EFPC	144.2674186	114
Point Source	Inflow	EFPC	253.3027567	113
Point Source	Inflow	EFPC	318.6750278	110
Point Source	Inflow	EFPC	364.9030893	109
Point Source	Inflow	EFPC	370.0378034	102
Point Source	Inflow	EFPC	390.3649678	99
Point Source	Inflow	EFPC	459.8039479	87
Point Source	Inflow	EFPC	459.8039479	88
Point Source	Inflow	EFPC	484.0940429	86
Point Source	Inflow	EFPC	487.1986358	83
Point Source	Inflow	EFPC	551.8687869	71
Point Source	Inflow	EFPC	582.1503784	67
Point Source	Inflow	EFPC	622.5874959	62
Point Source	Inflow	EFPC	628.4185439	64
Point Source	Inflow	EFPC	632.5713737	63
Point Source	Inflow	EFPC	697.0702256	58
Point Source	Inflow	EFPC	701.9097042	57
Point Source	Inflow	EFPC	716.7804288	55
Point Source	Inflow	EFPC	741.4763903	51
Point Source	Inflow	EFPC	764.0229817	54
Point Source	Inflow	EFPC	785.4044498	48
Point Source	Inflow	EFPC	787.8234603	47
Point Source	Inflow	EFPC	804.5023182	46
Point Source	Inflow	EFPC	820.9522629	44
Point Source	Inflow	EFPC	845.4465328	42
Point Source	Inflow	EFPC	883.1519529	41
Point Source	Inflow	EFPC	933.004587	34
Point Source	Inflow	EFPC	943.0027275	33
Point Source	Inflow	EFPC	1020.787721	21
Point Source	Inflow	EFPC	1059.242447	20
Point Source	Inflow	EFPC	1177.782843	19

Point Source	Inflow	EFPC	1347.737005	16
Point Source	Inflow	EFPC	1399.696776	14
Point Source	Inflow	EFPC	1946.269668	6
Point Source	Inflow	EFPC	2050.329252	7
Point Source	Inflow	EFPC	2398.767234	3
Point Source	Inflow	EFPC	2456.77397	2
Open	Water Level	EFPC	25485.2	
Open	Inflow	EFPC-A-N01	0	
Open	Inflow	EFPC-A-N02	0	
Open	Inflow	EFPC-A-N03	0	
Open	Inflow	EFPC-A-N04	0	
Open	Inflow	EFPC-A-N04-N01	0	
Open	Inflow	EFPC-A-S01	0	
Open	Inflow	EFPC-A-S02	0	
Open	Inflow	EFPC-A-S03	0	
Open	Inflow	EFPC-A-S04	0	
Open	Inflow	GHB-A-S05	0	
Open	Inflow	Gum Hollow Branch	0	
Point Source	Inflow	EFPC	2740	4
Open	Inflow	Milton Branch	0	
Open	Inflow	Pinhook Branch	0	
Closed		BC-A-S01	0	
Closed		BC-A-N01	0	

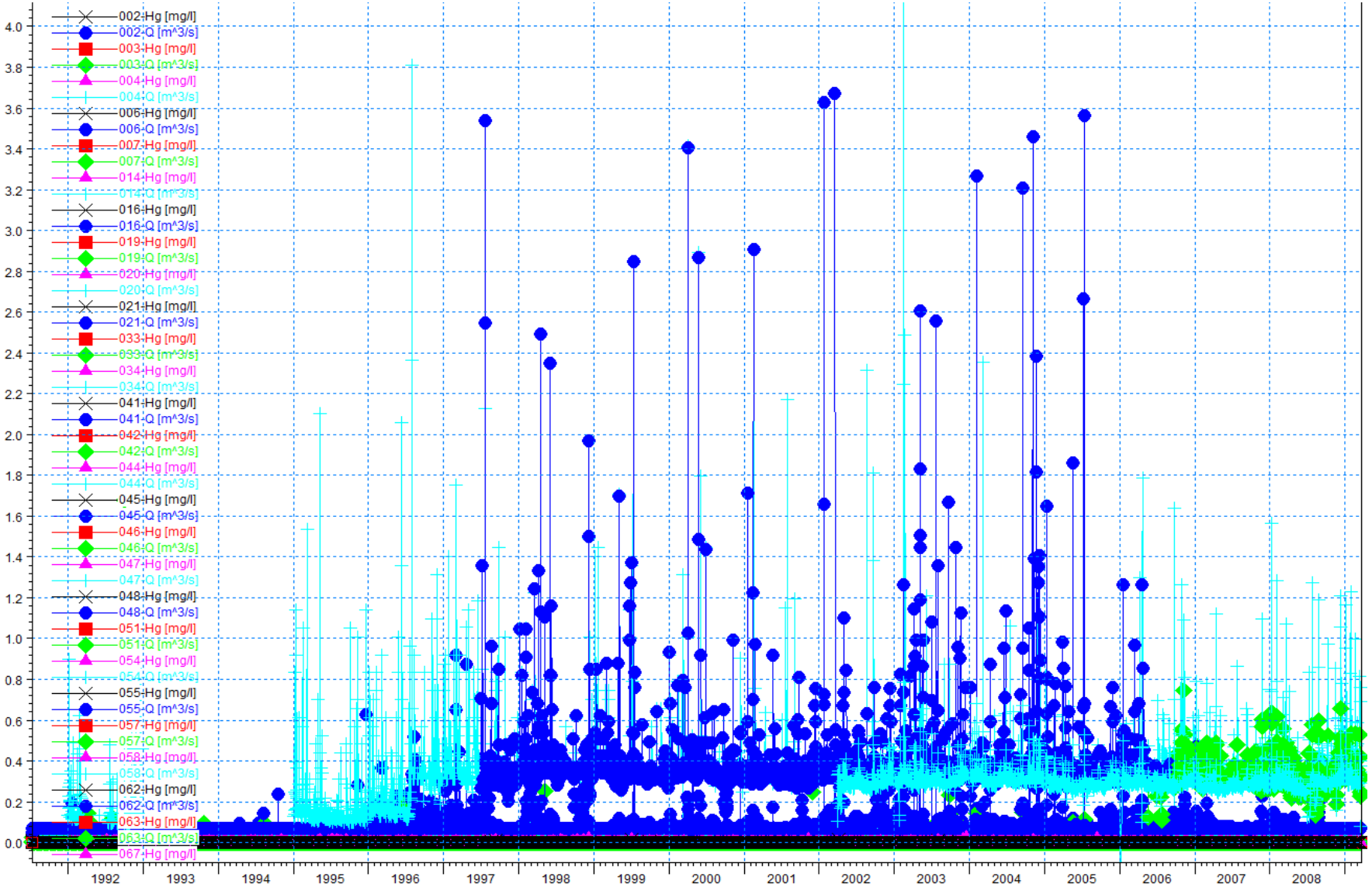

Figure 22 Flow rate timeseries linked to new point sources in boundary conditions.

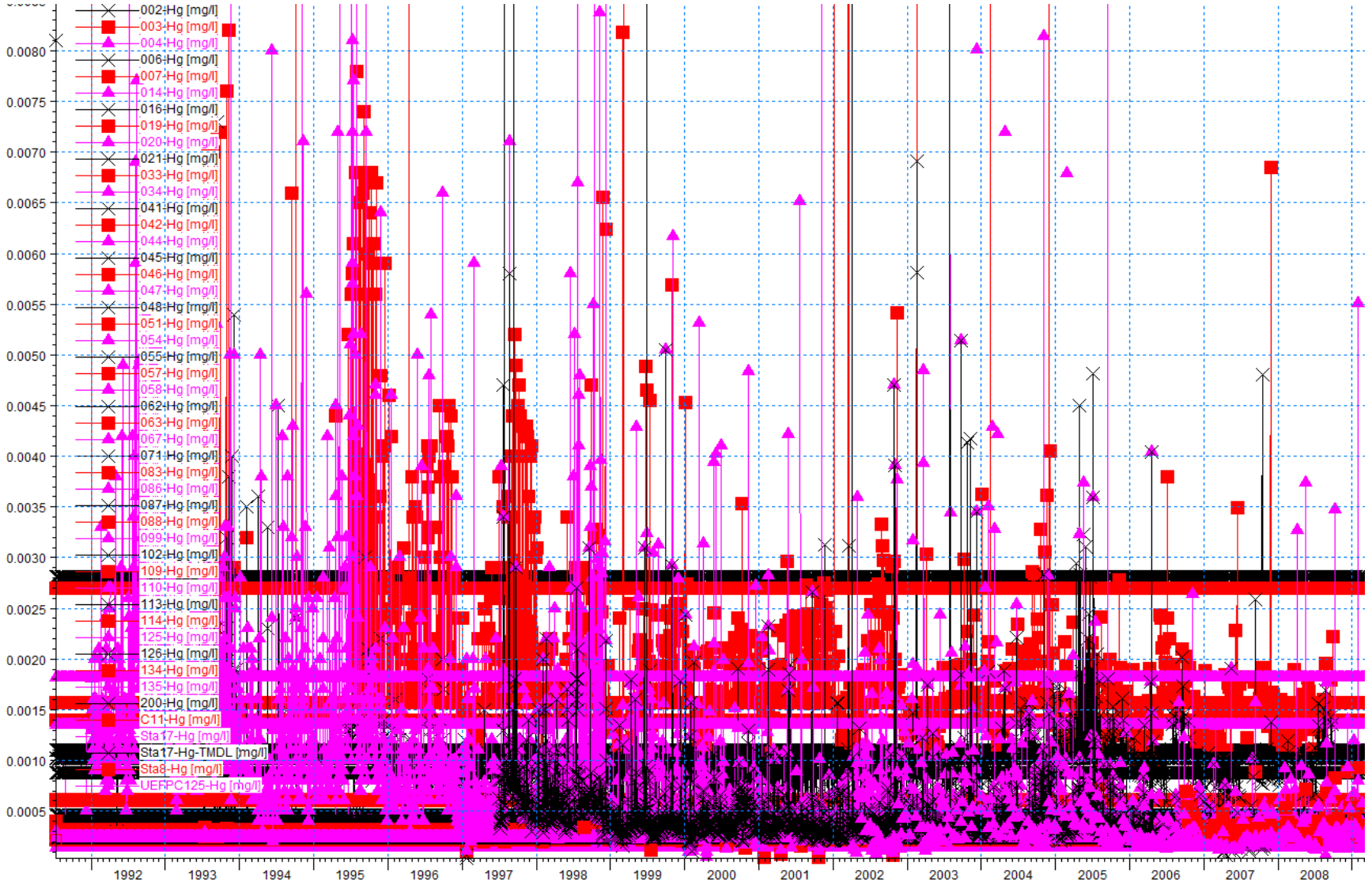

Figure 23 Mercury timeseries linked to new point sources in boundary conditions.

Appendix B: Research Poster

Improvements of an Integrated Flow and Mercury Transport Model in East Fork Poplar Creek Watershed, Oak Ridge, Tennessee

Lilian Marrero (DOE Fellow), Dr. Georgio Tachiev
Applied Research Center, Florida International University, Miami, Florida 33174

Introduction

The environment in the vicinity of Y-12 National Security Complex (Y-12 NSC), Oak Ridge, TN has been contaminated by mercury due to nuclear processing activities during the 1950s. The contamination exists within the soil, shallow groundwater beneath and adjacent to former process buildings, storm sewers, drains, stream sediment, and surface water. A significant reduction in mercury concentrations has been proposed in the area's natural waters. In order to achieve a more effective clean up effort the Environment and Water Resources Group at Florida International University's (FIU) Applied Research Center (ARC) has been tasked with developing a model for the site with the ultimate aim of assessing the impact of selected remediation scenarios.

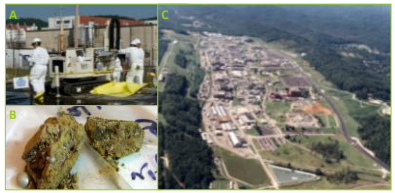

Figure 1: Soil sample collection at Y-12 (A), mercury contaminated soil (B), Y-12 NSC (C)

An integrated surface/subsurface model has been developed using the numerical model, MIKE, created by the Danish Hydraulic Institute (DHI). The purpose is to investigate the flow and transport of mercury in EFPC under the influence of a series of hydrologic events, to predict transport patterns within the watershed.

The conceptual model, summarized in Figure 2, was designed to consider the transport pathways of water-borne mercury from (i) stormwater and industrial wastewater outfalls, (ii) land surface and shallow groundwater, and (iii) streambed sediment to EFPC including outfalls, groundwater flow, and surface sheet flow.

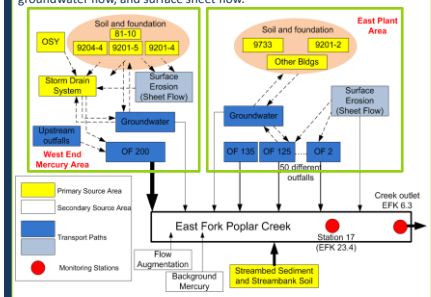

Figure 2: East Fork Poplar Creek Conceptual Model

Numerical Model

The model consists of MIKE 11, MIKESHE, and ECOLAB. These components are designed to couple the watershed hydrology with mercury transport. MIKESHE describes the hydrologic processes using physical laws (conservation of mass, energy, and momentum). It is 2-D in the overland phase, 1-D in the unsaturated, and 3-D in the saturated and vadose layers. MIKE 11 details the river flow and transport model through the hydrodynamic and advection modules. ECOLAB is an equations solver for the sedimentation and exchange of mercury within sediments, suspended particles, pore water, and dissolved mercury species.

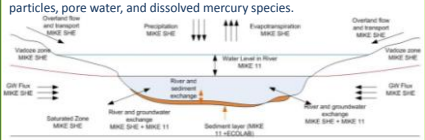

Figure 3: Numerical model diagram depicting MIKESHE, MIKE 11, ECOLAB, & their interaction phases

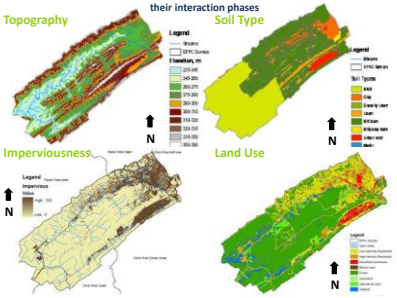

Figure 4: Typical Input Parameters

Layers	Sub-layers	Thickness, m	Lower level, m
UZ1	2	0.1	-0.2
UZ2	4	0.5	-2.2
UZ3	8	5.0	-52.2

Saturated moisture content = 0.35, Saturated hydraulic conductivity = 0.0082[1] m/d,
Soil bulk density ρ_b = 1720[2] kg/m³ and Residual moisture content θr=0.15, Dispersivity = 0.07[3] m

[1] USEPC RI Report, 1998, Table E. 9.3 (DOE/OR/01-1641V-H&D2)
[2] Tang et al., 2010

Table 1: Unsaturated zone profile definition

Layers	Lower level, m	Thickness, m
SZ1	-3	3
SZ2	-10	10
SZ3	-50	50
SZ4	-100	50
SZ5	-150	50

Primary effective porosity = 0.1[1&2], Secondary effective porosity = 0.05[2], Soil bulk density = 1700[2] Kg/m³, Specific yield = 0.2, Specific storage = 0.0001 1/m, Longitudinal Dispersivity = 0.007 m, Transverse Dispersivity = 0.001 m

[1] USEPC RI Report, 1998, Table E. 9.3 (DOE/OR/01-1641V-H&D2) [2] Martin Marietta Systems, Inc., 1995
*Groundwater Table contours are extracted from OREIS database

Table 2: Saturated zone profile definition

Modifications

The following changes were made to the model:

- ❑ Van Genuchten's hydraulic conductivity and moisture content parameters for the upper and lower portions of the aquifer

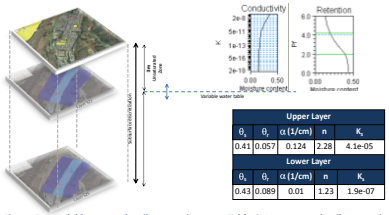

Figure 5: Model layers and soil properties

Upper Layer				
θ_s	θ_r	α (1/cm)	n	K_s
0.41	0.057	0.124	2.28	4.1e-05
Lower Layer				
θ_s	θ_r	α (1/cm)	n	K_s
0.43	0.089	0.01	1.23	1.9e-07

Table 3: Unsaturated soil properties

- ❑ Drainage system changed to routing based on gridded codes. A grid code map (level, time constant, drain code) is used to restrict the search area for the source-recipient reference system. Drain levels are used to calculate the amount and the code is used for routing.
- ❑ 25% of original Manning's number yield best fit.
- ❑ Hydraulic conductivity was changed from uniform to spatially distributed.
- ❑ Observation stations were added for water elevations, and discharge data (timeseries & shapefiles generated); existing stations were reviewed for quality assurance.
- ❑ Processed total mercury and methyl mercury data.

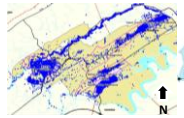

Figure 6: OREIS database used for data extraction

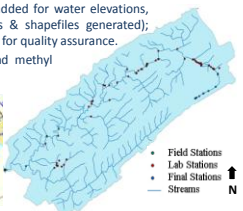

Figure 7: Final stations added

- ❑ ECOLAB incorporated as a MIKE 11 water quality module

State Variables	Value	Constants	Value
Mercury	0.01 mg/l	Organic-carbon partitioning coefficient	50000 l/kg
Adsorbed Mercury	0.1 mg/l	Desorption rate in water	1 day⁻¹
Dissolved Mercury in sediment pore water	0.1 g/m²	Desorption rate in sediment	0.1 day⁻¹
Adsorbed Mercury in sediment	10 g/m²	Fraction of organic carbon in SS	0.1
Suspended solids	50 mg/l	Fraction of organic carbon in sediment	0.2
Mass of sediment	10000 g/m²	Thickness of water film	0.1 mm
Forcing		Moleweight of heavy metal	92 g/mole
Thickness computational grid layer	2 m	Density of dry sediment	250 kg/m³ bulk
Total water depth	8 m	Porosity of sediment	0.8 m³ H₂O / m³ Bulk
Current Speed	0.2 m/s	Settling velocity of SS	0.1 m/day

Table 3: ECOLAB state variables, constants, and forcing

Simulations

Figure 8: Simulations summary diagram

Simulations were executed for a series of scenarios to assess the impact of the hydraulic parameters (i.e. horizontal and vertical hydraulic conductivity, and Manning's number were varied within accepted ranges) and determine the best fit with observed data. Drainage routing alternatives were also incorporated.

Results

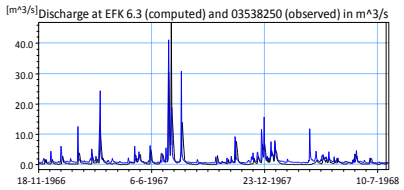

Figure 9: Simulations summary diagram

Computed results for station EFK 6.3 are within 2% of observed for station 0358250 as shown in Figure 9 above.

Conclusions

- ❑ Rainfall facilitates the exchange of mercury through hydrologic zones
- ❑ Mercury attenuates downstream of EFPC
- ❑ Sediment-mercury interactions significantly affect Hg transport
- ❑ High flow conditions re-suspend mercury particulates increasing concentration in the creek

Future Research

- ❑ Statistically determine hydraulic conductivity spatial distribution, porosity, and storage coefficients.
- ❑ Calibrate EFPC model using total suspended solids (TSS) and total mercury (TM) concentration timeseries at key stations.
- ❑ Incorporate sedimentation module
- ❑ Perform an uncertainty analysis and statistical tests

References

1. DOE, 2010. Remediation Effectiveness Report for the U.S. DOE ORR, DOE/OR/01-2437&D1.
2. Elsa Cabrejo, 2010, Mercury Interaction with Suspended Solids at the Upper East Fork Poplar Creek, Oak Ridge, TN, Florida International University, Environmental Eng. Dept., Master Thesis
3. FIU, 2010, Integrated Surface and Subsurface Mercury Transport Model of Y-12 National Security Complex, oak ridge, Tennessee
4. Stephanie Long, 2009, An Integrated Flow and Transport Model to Study the Impact of Mercury Remediation Strategies for East Fork Poplar Creek Watershed, Oak Ridge, Tennessee, Florida International University, Environmental Eng. Dept., Master Thesis

FIU Applied Research Center — Acknowledgements: Dr. Georgio Tachiev, Dr. Siamak Malek-Mohammadi, Angelique Lawrence, Dr. Leonel Lagos, DOE/FIU Science & Technology Workforce Development Initiative — FIU Applied Research Center

APPENDIX T2-001: TASK 2 FINAL REPORT

APPENDIX T2-001

TASK 2: SIMULATION OF TMDL FOR THE ENTIRE EFPC

OF

REMEDIATION AND TREATMENT TECHNOLOGY DEVELOPMENT AND SUPPORT

Prepared for:
U.S. Department of Energy
Oak Ridge Operations Office
Oak Ridge Reservation

FINAL REPORT, VERSION 1, 06/17/2012

Prepared by:
Siamak Malek-Mohammadi, PhD
Angelique Lawrence, MS, GISP
Lilian Marrero, DOE Fellow
Georgio Tachiev, PhD, PE

Principal Investigator: David Roelant, PhD
david.roelant@fiu.edu
phone: 305-348-6625
fax: 305-348-1852

Applied Research Center
Florida International University
10555 W. Flagler Street, EC 2100
Miami, Florida 33174

DISCLAIMER

TABLE OF CONTENTS

LIST OF FIGURES

LIST OF TABLES

EXECUTIVE SUMMARY

Since operation of the Y-12 Plant in Oak Ridge, TN in the 1950s, approximately 2,000,000 lbs of mercury used in weapons production was unaccounted for or lost to the surrounding environment. It is surmised that much of this mercury is present in soil, bedrock, and groundwater and constitutes a continuous source of contamination to Upper East Fork Poplar Creek (UEFPC). The initial release of elemental mercury is followed by a series of physico-chemical transformations as it is transported through the topsoil to the surface and/or shallow groundwater and sediments, and then through the reach of the stream drainage. Under natural environmental conditions (dissolved oxygen in water greater than 0 mg/L, and pH 6.0 to 9.0), elemental mercury is oxidized and converted to mercuric ion, which has greater solubility in aqueous media, and respectively greater mobility within the watershed. Mercuric ion is complexed with commonly occurring inorganic and organic ligands in the environment, such as chlorides, humic acids and colloids, which increase its mobility. Furthermore, natural organic matter can enhance the dissolution of mercuric sulfide, HgS(s), which is the predominant form of mercury in soil and sediments, and result in release of dissolved and particulate (primarily colloidal) Hg species in surface water. Discharge from stormflow outfalls has also been found to be a major source of mercury to UEFPC.

In an effort to better understand mercury transport and contamination within the watershed at East Fork Poplar Creek (EFPC), Oak Ridge, Tennessee an integrated flow and transport (water quality) model was developed by FIU-ARC using the MIKE software packages created by the Danish Hydraulic Institute (DHI). The integrated flow and water quality model (MIKE-SHE and MIKE-11) analyzes the impact of hydrological events on mercury contamination in Upper EFPC (UEFPC). A sediment transport module was incorporated into the model to provide analysis of the intearaction of mercury with sediments. The sedimentation module provides the coupling between the flow and transport within the creek and the overland flow, which will be used to analyze the significance of floodplain contamination downstream EFPC. This document details the extensions and modifications that were made to the existing sedimentation module in order to now include the entire EFPC as well as Bear Creek and provides analysis of typical

TMDL scenarios. The research emphasizes the stochastic modeling of the system and includes an analysis of the spatial and temporal patterns as a result of the stochastic variations of selected properties of the subdomain. The simulation results reveal rainfall as a facilitating and mobilizing hydrologic event that impacts the exchange of mercury and its movement through hydrologic zones. The attenuation of mercury concentrations downstream of EFPC is consistent with previous studies.

This work is based on the primary hypothesis that the concentration of total mercury in the hydrologic subdomains (surface, subsurface, streams and sediments) and the transport of mercury species are the governing factors for the levels of mercury in fish from East Fork Popular Creek (EFPC). The numerical model described in this report covers sections of the Upper East Fork Poplar Creek (UEFPC) and Upper Bear Creek (UBC) watersheds and provides a tool for analyzing the coupling between watershed hydrology and transport of total mercury. An average mercury concentration was computed from summing the total contribution of mercury mass from each outfall and dividing by the total flow volume. Comparison of the concentrations measured at Station 17 and those calculated from the average mercury concentration from all outfalls shows that measured mercury peaks are considerably higher than the averages computed from all outfalls. This indicates that sediment transport in surface water is important to consider for modeling. The exchange of mercury between sediments and stream flow was accounted for by implementing a sedimentation module. The model was calibrated using observed data of flow, stage, and mercury concentrations in soil, surface water, groundwater and sediments at Station 17. The modeling work focused on analyzing the results for the period 1/1/2000-12/31/2008 for which the flow augmentation strategy of adding an average of 2.4 million gallons per day (MGD) was already in place.

For each of the nine proposed actions simulated in this report, the computed load duration curves at Station 17 were compared with the historical load duration curves to determine the percent daily reduction of mercury discharges downstream of Station 17. The percent reduction was computed based on the ratio between the mean values of the computed load duration curves versus the mean values of observed load duration curves. Simulations were conducted

for each individual action, and for the stepwise approach developed in the Mercury Remediation Strategy that included concurrent application of remedial actions. For each alternative, multiple simulations were conducted to determine the uncertainties (defined as one standard deviation) of the computed load for selected parameters for which the model had high sensitivity (defined as rate of change of the modeling output to rate of change of parameter input).

The analysis of the individual performance of each remediation scenario showed the reduction of the daily mercury loads/removal of liquid elemental mercury and that source isolation can reduce the mercury load by 16% (3.0 ± 2.8 g/day). An upgradient diversion ditch would result in 4% reduction of mercury (0.7 ± 0.6 g/d). The load reduction resulting from the diversion ditch is significantly dependent upon the soil/water partitioning coefficient and the extent and strength of overland contamination which is on the path of diverted overland flow. The relocation of flow augmentation to Station 17 will reduce the daily mercury load by 15% (1.5 ± 0.7 g/d). Relocation and rerouting of clean water and stormflow will result in reduction by 15% (2.7 ± 1.3 g/d). By collecting and treating contaminated process and drain water, the mercury load can be reduced by 23% (4.2 ± 2.8 g/d). Construction of a groundwater collection system for UEFPC drainage eliminates mercury influx into UEFPC from groundwater baseflow and can reduce the total mercury load by 7% (1.3 ± 0.6 g/d). Removal and abandonment of existing storm drains will result in reduction of 20% (3.7 ± 2.2 g/d). Treatment of discharges from Outfall 200 will result in overall reduction of 17% (3.2 ± 1.8 g/d provided that the treatment efficiency is 50%). Finally, a downgradient diversion collection trench at Alpha 4 and 5 will result in reduction of 7% (1.4 ± 0.6 g/d).

The numerical model was applied to determine the composite effect of concurrent and stepwise execution of remediation alternatives based on the schedule proposed by Pro2Serve. The results showed the timeline for accomplishing load reduction at Station 17 (cumulative uncertainty was not computed). In the year 2011, the proposed remediation strategy will accomplish 17% (3.2 g/d) of total mercury reduction at Station 17 by reducing the mercury flux from Outfall 200 by 50%. In 2012, the proposed remediation strategy will include 50%

relocation of flow augmentation, collection and treatment of contaminated flow, groundwater collection for UEFPC from WEMA, and removal and abandonment of existing storm drains from WEMA, all of which will provide a combined effect of 47% (8.7 g/d) reduction of mercury load at Station 17. With the relocation of flow augmentation, the daily mercury load at Station 17 will be reduced by 55% (10.2 g/d) by year 2013. The addition of an upgradient diversion ditch will provide additional reduction of mercury flux to 59% (10.9 g/d).

The most significant factor which determined the efficiency of source elimination (soil excavation) is the soil/water partitioning coefficient, which describes the linear equilibrium between aqueous and soil concentration. The magnitude of the partitioning soil/water coefficient has significant impact on remedial actions related to soil excavation on surface water since it is correlated to the retardation factor and more specifically, the velocity of the plume. Due to its high affinity to forming complexes with solid species, mercury has a large retardation factor, the significance of which is that source removal in the vicinity of the stream will have greatest effect where there is exchange between the river and subsurface domain. Contaminant reduction at the small sources of highest contamination can therefore be an effective short-term remediation strategy for immediate reduction of downstream contamination. The majority of mercury in soil is present as HgS(s) which is a mineral of low solubility. HgS(s) can become mobilized by complexing with organic ligands naturally occurring in soil and migrate to surface waters. Therefore, closing off the outfalls (by plugging and abandonment) eliminates this pathway to UEFPC. Migration of HgS complexes in groundwater occurs to a lesser degree in low permeability soils with high organic content and high distribution coefficients. Therefore, removing the outfalls is effective in hydrologic isolation of mercury sources in soil and groundwater above the shale. Simulations for reducing the flow augmentation showed that concentrations of total mercury increased less than 30% as there was less dilution. Elimination of augmented surface water flow reduced infiltration of contaminated surface water and no longer recharged the groundwater system along the creek. The total flow of water needing potential treatment in the watershed is reduced by 0.48 MGD.

1 INTRODUCTION

Section 303(d) of the 1972 Clean Water Act (CWA) [1, 3] requires each state to list those waters within its boundaries for which technology-based effluent limitations are not stringent enough to protect any water quality standard applicable to such waters. Listed waters are prioritized with respect to designated use classifications and the severity of the pollution. In accordance with this prioritization, states are required to develop Total Maximum Daily Loads (TMDLs) for those waterbodies that are not attaining water quality standards. State water quality standards consist of designated uses for individual waterbodies and appropriate numeric and narrative water quality criteria protective of the designated uses. The TMDL process establishes the maximum allowable loadings of pollutants for a waterbody that will allow the waterbody to maintain water quality standards. The TMDL may then be used to develop controls for reducing pollution from both point and non-point sources in order to restore and maintain the quality of water resources [2]. Application of TMDLs has been broadened significantly in the last decade to include many watershed-scale efforts.

East Fork Poplar Creek (EFPC), bordering the Y-12 National Security Complex (Y-12 NSC) and located inside of the Oak Ridge Reservation (ORR), has recently been identified on the Final 2008 303(d) List by the Tennessee Department of Environment and Conservation (TDEC) [13] as an impaired waterbody not supporting designated uses due to contamination by mercury, PCBs, nitrates, and phosphates. EFPC lies entirely inside the state of Tennessee, shared by Roane and Anderson counties. The waterbody is in moderate priority for the development of a TMDL for mercury [13, pages 85 and 86].

To support the TMDL development for the EFPC, the need for an integrated, receiving water, hydrodynamic and water quality modeling system was identified. Models are frequently used to support development of TMDLs—to estimate source loading and evaluate loading capacities that will meet water quality standards. The modeling should demonstrate the allocation of point and non-point source loads that would result in meeting the water quality standards. This requires that point and non-point sources be evaluated as separate sources so that they can be

simulated under various loading scenarios [38].

1.1 Scope of the document

This report documents the application of a hydrology and transport model developed to support the TMDL analysis of mercury for the EFPC watershed. The integrated surface/subsurface model was built using the numerical package, MIKE (MIKE-11 coupled with MIKE-SHE and ECOLAB), developed by the Danish Hydraulic Institute (DHI). The MIKE package has been identified by EPA as an effective model to support TMDL analysis [38].

The report presents details of TMDL development for the entire East Fork Poplar Creek (EFPC). The main pollutant sources in the creek were identified as stormwater and industrial wastewater outfalls (point sources) and contaminated streambed sediments, floodplain and streambank soils (non-point sources) [13, Pages 85 and 86]. The numerical model was used to develop flow and load duration curves at several stations along the creek.

1.2 Waterbody Description

The EFPC watershed is a sub-watershed of the larger Poplar Creek watershed, which is one of four sub-watersheds of the Lower Clinch River watershed (Hydrologic Unit Code (HUC) 06010207, based on USGS) in the eastern part of Tennessee. The EFPC watershed is enclosed by the City of Oak Ridge and is divided by Anderson County to the north and east and Roane County to the south and west as shown in Figure 1. The watershed lies within the Ridge and Valley (67) Level III ecoregion and contains two Level IV ecoregions as defined by the U.S. EPA National Health and Environmental Effects Research Laboratory [14]:

- The Southern Limestone/Dolomite Valleys and Low Rolling Hills (67f) form a heterogeneous region composed predominantly of limestone and cherty dolomite. Landforms are mostly low rolling ridges and valleys, and the solids vary in their productivity. Landcover includes intensive agriculture, urban and industrial, or areas of thick forest. White oak forests, bottomland oak forests, and sycamore-ash-elm riparian

forests are the common forest types, and grassland barrens intermixed with cedar-pine glades also occur here.

- The Southern Dissected Ridges and Knobs (67i) contain more crenulated, broken, or hummocky ridges, compared to smoother, more sharply pointed sandstone ridges. Although shale is common, there is a mixture and interbedding of geologic materials. The ridges on the east side of Tennessee's Ridge and Valley tend to be associated with the Ordovician-age Sevier shale, Athens shale, and Holston and Lenoir limestones. These can include calcareous shale, limestone, siltstone, sandstone, and conglomerate. In the central and western part of the ecoregion, the shale ridges are associated with the Cambrian-age Rome Formation: shale and siltstone with beds of sandstone. Chestnut oak forests and pine forests are typical for the higher elevations of the ridges, with areas of white oak, mixed mesophytic forest, and tulip poplar on the lower slopes, knobs, and draws.

Two broad hydrologic units dominate the subsurface landscape: the Knox aquifer in which flow is controlled by solution conduits, and the Chickamauga Group, leaky confining units, in which flow is dominated by fractures, and relatively low hydraulic conductivity. Both groups are described by a stormflow zone, a vadose zone, a groundwater zone, and the confining unit [15, 16].

EFPC watershed contains two relatively small rivers (>12,500 m long); Bear Creek and East Fork Poplar Creek (EFPC), and several tributaries as shown in Figure 2. This report is focused on EFPC, which runs primarily in a NE – SW direction and is about 24.5 Km long. The creek bottom begins at a depth of about 287 m above the mean sea level and ends at about 226 m near the river's hydrologic boundary, for a general slope of about 0.23% or 0.13 degrees. Stream valley width along EFPC ranges from 60 to 300 m. EFPC receives discharge from four major streams (Bear Creek, Gum Hollow Branch, Mill Branch, and Pin Hook Branch) and about 30 unnamed tributaries. The stream network in EFPC watershed is shown in Figure 2. In total, East Fork Poplar Creek receives discharge from about 107 kilometers of streams.

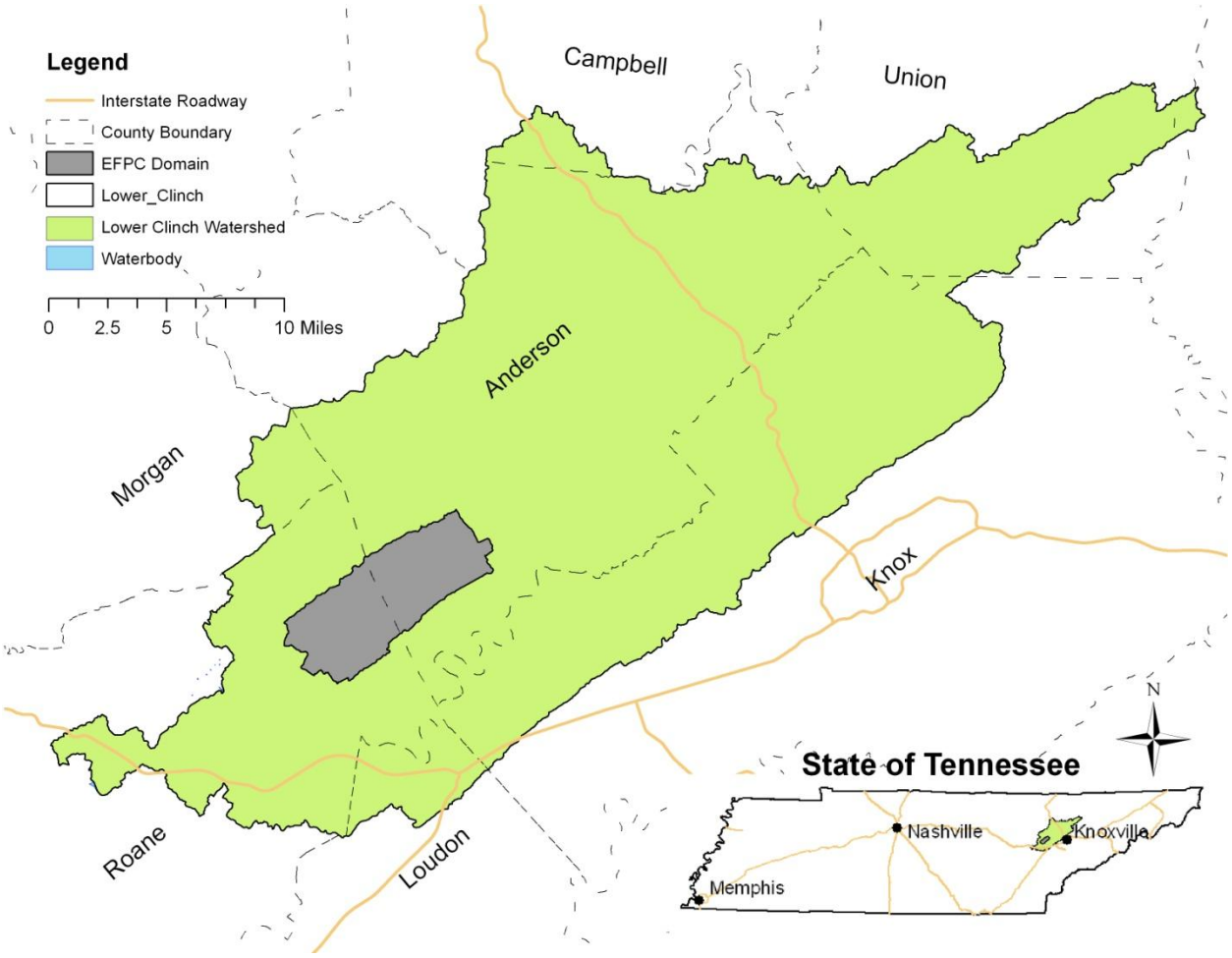

Figure 1. Regional settings of the EFPC watershed.

The EFPC watershed is 29.7 mi^2 and is laid on relatively even surface at around 270 to 280 meters above mean sea level. Based on Multi-Resolution Land Characteristic (MRLC), 2001, the watershed is over 62% forest land followed by urban (33.2%). About 87% of the forested areas considered deciduous forests (typical hardwoods such as oaks, maples, hickories, etc.). About one third of the watershed is used for agricultural purposes. About 9.3% of the total watershed area has an imperviousness of 50% or greater. Land use for the EFPC watershed is summarized in Table 6 and shown in Figure 18. The impervious percentage mainly comes from residential areas, cities, and highways. About 4.4% of the total area has an imperviousness of 75% or greater, this includes most of the Y-12 NSC and the commercial areas in the City of Oak Ridge. These areas of high imperviousness may tend to transport contaminants more rapidly due to the increased rate of overland flow and infrastructure facilitation. Upper portion of the

watershed is dominated by industrial areas of USDOE's Y-12 National Security Complex. Y-12 NSC is approximately 800 acres in size.

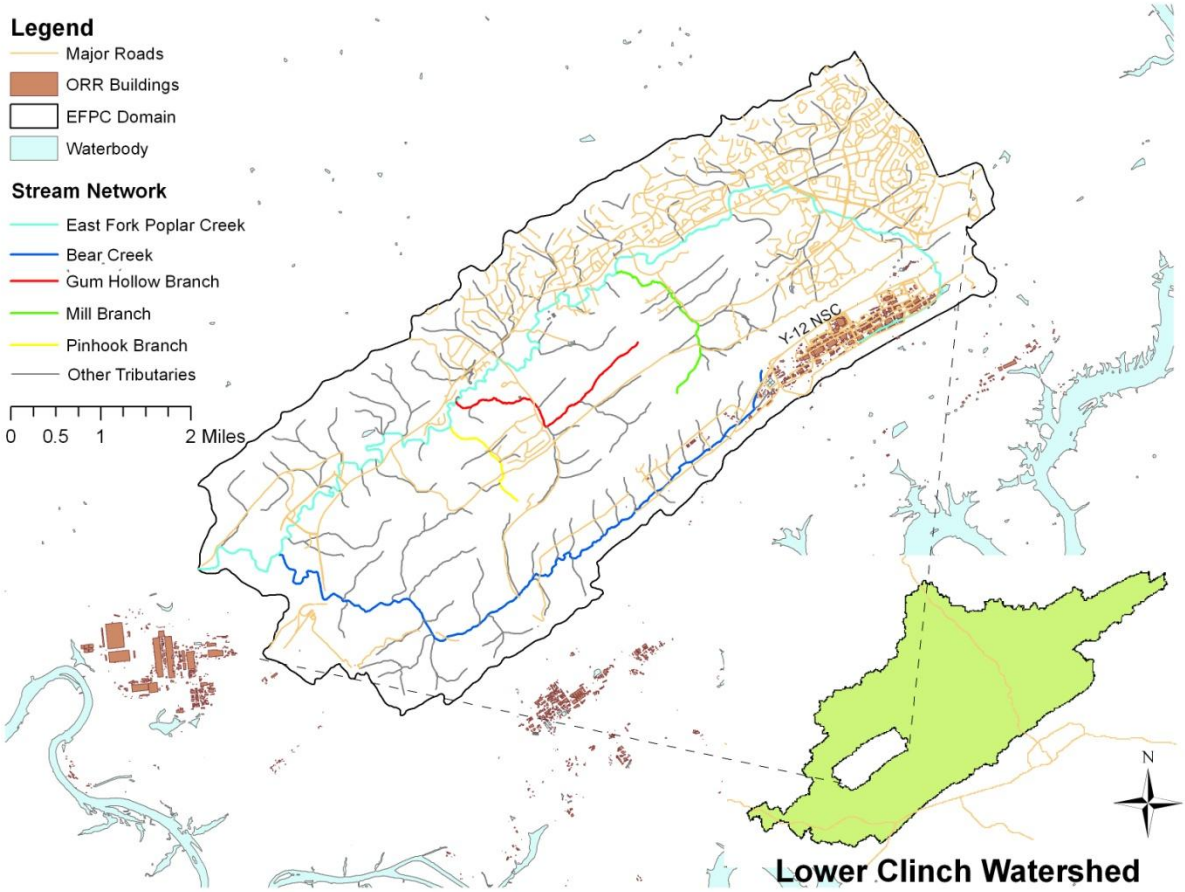

Figure 2. Primary streams within EFPC watershed.

2 ASSESSMENT OF MERCURY SOURCES

The main objective of this step was to identify the major sources of mercury contamination to EFPC and the load contributed by each of these sources resulting in impairment of the creek. The most significant information collected and reviewed included source locations, magnitude, discharge behavior, distribution density and frequency, and seasonality. For the EFPC watershed, data was retrieved from OREIS, DOE reports, USGS reports, literature and TN state databases (e.g., TDEC). The steps included:

1. Identification and characterization of point sources (e.g., wastewater treatment plants, industrial facilities, outfalls, and any other direct polluted discharge to the waterbody, such as groundwater discharges).
2. Identification and characterization of non-point sources (e.g., sediments and river bank soils).

Under the Clean Water Act, sources are classified as either point or non-point sources. A point source is defined as a discernable, confined, and discrete conveyance from which pollutants are or may be discharged to the waterbody. The NPDES program regulates point source discharges. Point sources can be described by three broad categories: 1) NPDES regulated municipal and industrial wastewater treatment facilities (WWTFs), 2) NPDES regulated industrial and municipal storm water discharges, and 3) NPDES regulated Concentrated Animal Feeding Operations (CAFOs) [9]. A TMDL must provide Waste Loading Analyses (WLAs) for all NPDES regulated point sources. Non-point sources are diffuse sources that cannot be identified as entering a waterbody through a discrete conveyance at a single location, such as pollution loading from sediments and groundwater.

EFPC originates on the DOE Y-12 NSC from groundwater in the subsurface storm drain system in the western part of the complex. These drains were installed during construction of the Y-12 NSC in the 1940's. The central drainage line (North/South Pipe) extends approximately 2,000 ft west of OF200. This is the location where the highest concentrations of mercury discharge have been measured, associated with the process building sumps feeding the North/South Pipe

before being released to the creek [24]. After emergence at OF200, EFPC flows 5,400 ft in an aboveground channel before being directed through about 900 ft of drain line in the eastern portion of the complex. Flow is then aboveground to Station 17, located near Bear Creek Road, where the stream exits federal property [24]. The aboveground portion of the EFPC was originally diverted into the New Hope Pond, a sediment- and flow-control basin. In 1989, New Hope Pond was closed and capped under the Resource Conservation and Recovery Act (RCRA) and Lake Reality, a 2.5-acre lined retention basin, was constructed along with a concrete-lined distribution channel. Flow was routed around the former New Hope Pond site via a concrete-lined distribution channel and into Lake Reality. Annual evaluation of mercury in EFPC indicated that Lake Reality, over time, had entrapped sediments, which were acting as a secondary source of contamination to the creek. To address this issue, the distribution channel was modified in July 1998 to allow unrestricted flow of water in EFPC to Station 17; however, the distribution channel still has an option to direct the water in EFPC into Lake Reality in an emergency [25].

Between 1950 and 1963, large quantities of elemental mercury were used at the Y-12 NSC in lithium isotope separation processes. Buildings in which large quantities of mercury were used are referred to as “Mercury Use” areas. Most large-scale mercury use occurred in building 9201-2 (Alpha 2) between 1953 and 1955, and in buildings. 9201-4 and 9201-5 (Alpha 4 and Alpha 5) from 1955 to 1963. An estimated 230,000 Ibs of elementary mercury were lost from the West End Mercury Area during the period of lithium isotope separation activities, primarily before 1960. At building 9201-2, one release of 95,000 Ibs of mercury and three additional process spills inside of the building have been reported. Mercury was released to EFPC via building drains and as process discharges in the form of dilute acidic wastes. Spills and leaks also account for some losses. Although estimates of mercury losses vary, it is believed to have been in excess of one million pounds [25].

Residual contamination exists within soil and shallow groundwater beneath and adjacent to the former process buildings and within former process equipment inside the buildings. Mercury contamination is widespread within the EFPC watershed and has been identified as a

contaminant in soil, storm sewer and stream sediment, surface water, buildings, and drains. Long-term deposition of mercury within EFPC and Lake Reality sediments and bank soils has resulted in a secondary source term that contributes flux to EFPC [25].

2.1 Point Sources

Oak Ridge facilities are authorized to release cooling waters, process wastewaters, contaminated ground water, and storm water runoff to EFPC under NPDES Permit TN0002968 [6].

2.1.1 Stormwater Outfalls

There are over 100 stormwater outfalls along EFPC, many of which discharge concentrations of total mercury ranging from 200 to 2,000 ppb. These stormwater outfalls drain the West End Mercury Area (WEMA) and approximately two-thirds of the 800-acre industrial site (eastern side). The three main stormwater outfalls are OF200, which drains the western half of the site (WEMA), and OF109 and OF021, which together drain approximately half of the eastern plant area. The most significant stormwater discharges from the Y12 NSC are shown in Figure 3 and are addressed in the National Pollutant Discharge Elimination System (NPDES) Permit TN0002968 [6]. For better illustration of the relative location of the outfalls (mercury point sources) regulated by the NPDES and the water quality monitoring stations, they are shown together in Figure 3.

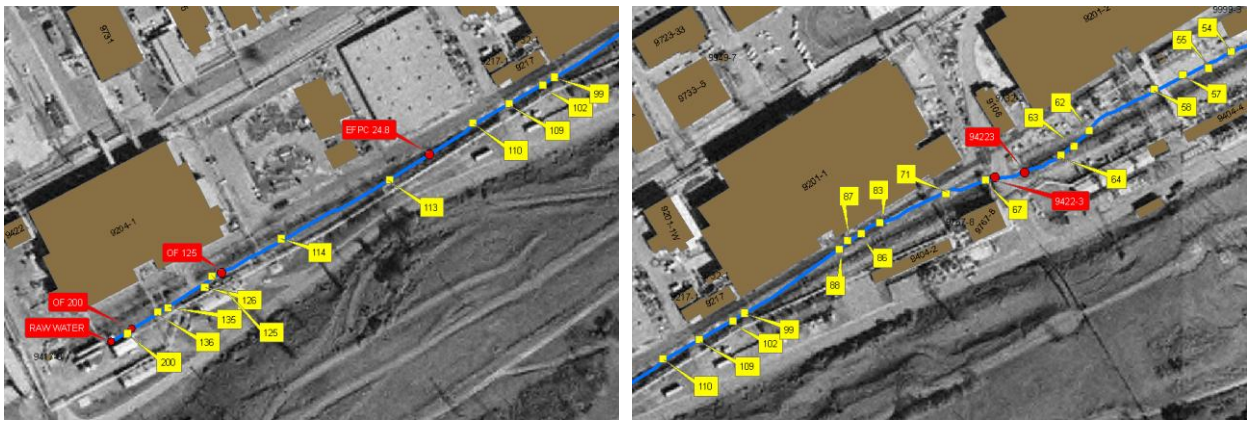

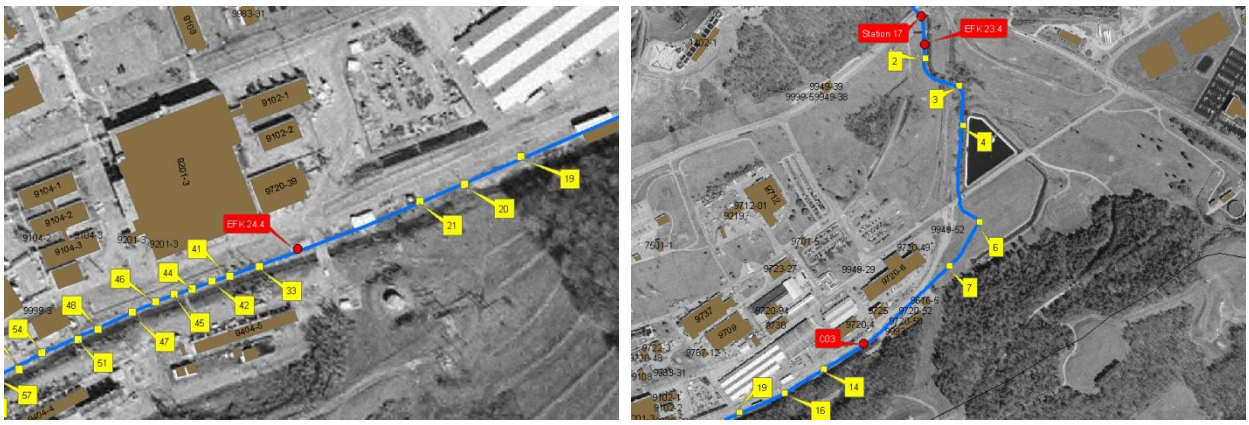

Figure 3. Water quality monitoring stations and mercury outfalls (point sources) in EFPC.

There is no outfall after Station 17, so the downstream part of the creek after Station 17 is not shown in this figure. NPDES-regulated outfalls along with their characteristics are listed in Table 1. Flow and load duration curves for selected outfalls are shown in Figure 4.

2.1.2 Wastewater Outfalls

Specific wastewater treatment facilities at the site include the Central Pollution Control Facility, the West End Treatment Facility, the Steam Plant Wastewater Treatment Facility, the Central Mercury Treatment System, and the Groundwater Treatment Facility. Locations of the facilities and corresponding outfalls are shown in Figure 5. Characteristics of the outfalls are listed in Table 2.

Table 1. Characteristics of NPDES Regulated Stormwater Outfalls Along EFPC (OREIS)

Stormwater Outfall	Category	Flow Samples	Mean Q m^3/s	Mercury Samples	Mean C_{Hg}, ppm	Hg Load g/day
C11	IV	651	25865.6	26	0.36	9.3E+00
2	II	147	3.70E-03	1	2.20E-04	7.00E-02
3	I	31	3.30E-04			
4	II	58	6.30E-04	1	3.00E-04	1.60E-02
6	I	31	5.00E-04	3	1.10E-03	4.70E-02
7	I	29	1.50E-03	1	1.40E-03	1.80E-01
14	II	60	1.10E-03	5	4.00E-04	3.80E-02
16	II	63	3.30E-04	2	2.80E-03	8.10E-02

19	II	58	2.90E-04	0		
20	II	61	3.80E-04	0		
21	IV	1417	5.00E-03	2	3.10E-04	1.40E-01
33	I	39	2.00E-04	3	6.10E-04	1.10E-02
34	III	139	5.50E-03	5	1.30E-04	6.20E-02
41	I	44	9.20E-05	3	3.00E-04	2.40E-03
42	III	127	2.00E-04	1	2.20E-04	3.80E-03
44	I	52	1.70E-04			
45	I	30	2.10E-04	2	4.60E-04	8.30E-03
46	I	38	3.10E-04			
47	II	183	1.20E-03	28	3.50E-04	3.60E-02
48	II	147	1.00E-04	10	1.10E-03	9.50E-03
54	II	151	6.70E-05	0		
55	IV	1342	8.80E-05	48	4.00E-04	3.00E-03
57	I	55	3.40E-05			
58	I	35	4.20E-04	2	1.40E-03	4.90E-02
62	I	28	1.00E-04	1	2.40E-04	2.00E-03
63	I	56	2.00E-04	2	2.70E-03	4.70E-02
67	II	65	1.00E-03	1	2.60E-04	2.20E-02
71	III	128	5.00E-04			
83	II	59	3.30E-04	0		
86	I	31	3.30E-05	2	1.80E-03	5.20E-03
87	I	40	1.70E-04			
88	II	63	1.00E-04	4	3.20E-04	2.70E-03
99	II	53	5.00E-04	1	2.40E-04	1.00E-02
102	I	37	1.00E-03			
109	IV	41	4.70E-03	2	3.30E-04	1.30E-01
110	I	35	2.50E-04			
113	III	126	6.10E-05	3	8.80E-04	4.60E-03
114	III	131	5.00E-04	3	2.90E-04	
125	IV	647	1.60E-02	3	2.50E-04	3.50E-01
126	II	58	1.00E-04	0		
134	I	32	1.00E-04	1	6.20E-04	5.30E-03
135	IV	1489	7.40E-03	1	2.20E-04	1.40E-01
200	IV	558	7.20E-02	237	1.00E-03	6.40E+00

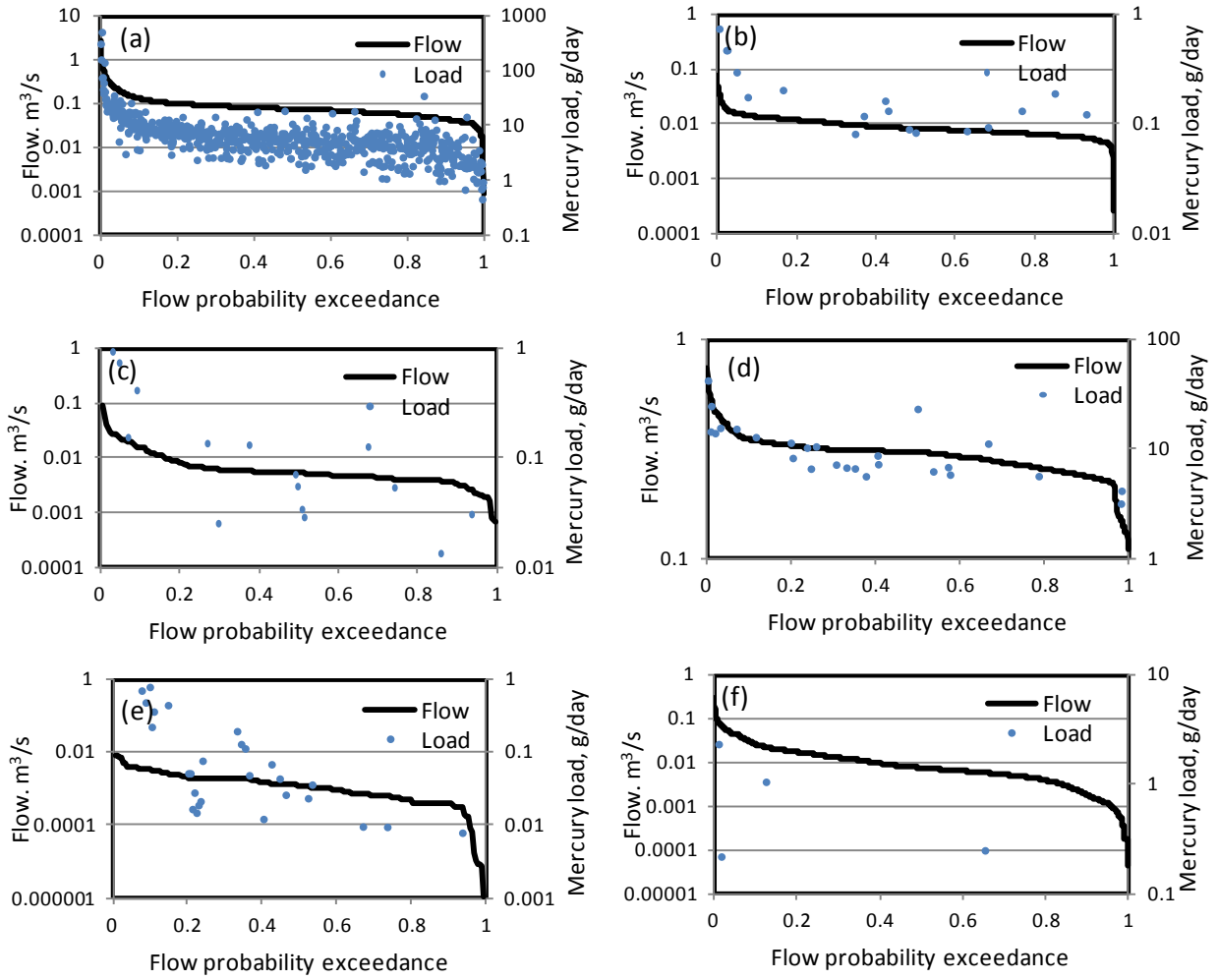

Figure 4. Flow and load duration curves for selected outfalls: (a) OF200, (b) OF135, (c) OF109, (d) C11, (e) OF047, (f) OF021.

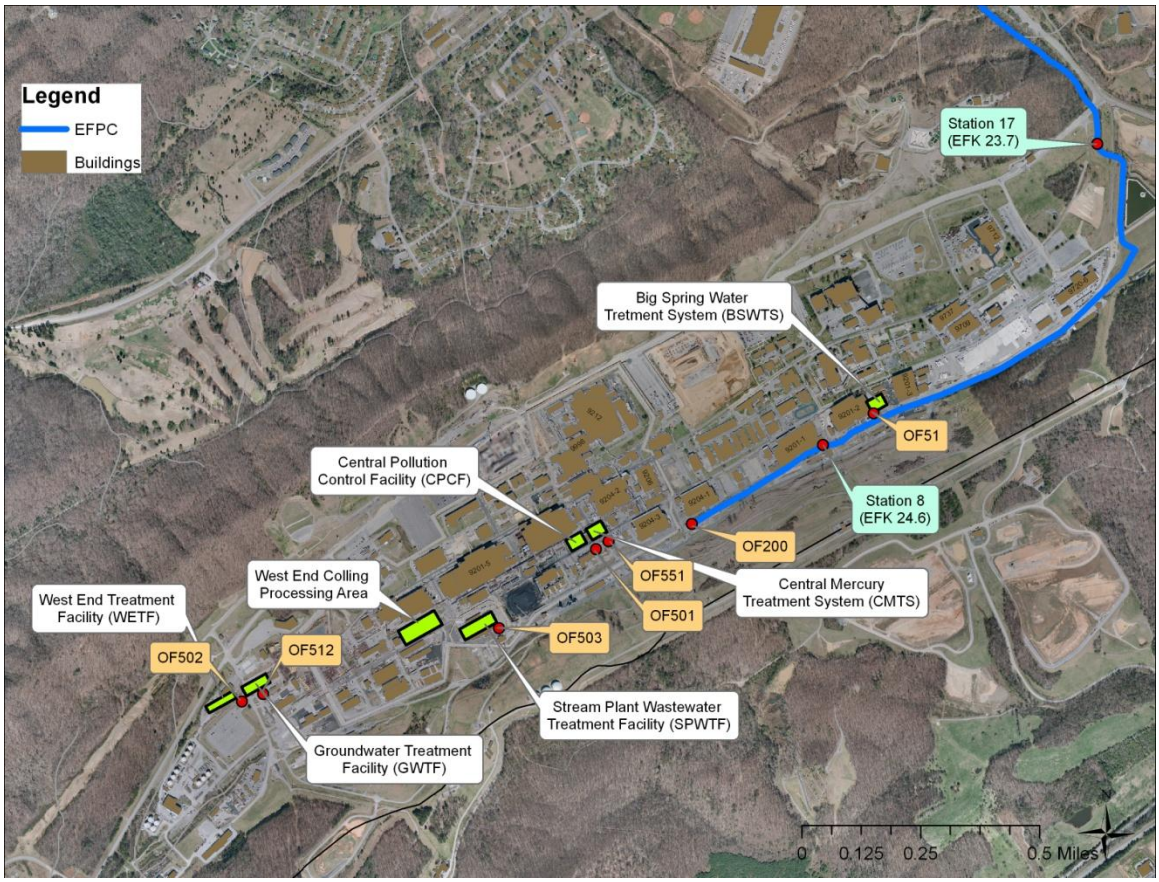

Figure 5. Cooling water, process wastewater facilities and corresponding facilities.

Table 2. Characteristics of NPDES -Regulated Wastewater Outfalls Along EFPC

Wastewater Outfall	Outfall Category	Flow samples	Mean Discharge m^3/day	Mercury samples	Hg Concentration ppm	Hg Load g/day
51	IV	1446	4.60E-03	265	1.60E-03	6.30E-01
501	IV	226	35.9	226	1.1E-03	4.3E-02
502	IV	450	62.7	450	1.0E-03	6.8E-02
503	IV	820	531.0	820	4.0E-04	2.1E-01
512	IV	2693	42.6	0	-	-
520	IV	0	-	0	-	-
550	IV	3859	52.5	118	4.1E-04	2.1E-02
551	IV	3817	38.7	225	7.5E-04	2.9E-02

Central Pollution Control Facility (CPCF)

The CPCF is designed to treat dilute wastewater, concentrated wastewater, or dilute metal-

plating-shop rinse water generated at Y-12 facilities. Dilute wastewater has higher organic content and lower metal content than concentrated wastewater. Concentrated wastewater is typically derived from chemical processes and has a high level of dissolved metal, including various compounds of soluble uranium, and high acidity or alkalinity levels. Since no component at CPCF removes nitrates, effluents from nitrate receipts are shipped to the West End Treatment Facility (WETF) for nitrate destruction. Dilute metal-plating-shop rinse water is typically clean compared to dilute and concentrated wastewater. This wastewater is characteristically contaminated with trace amounts of heavy metals that are effectively removed in the treatment process. Effluent flow from CPCF is roughly 7,500 gallons per day and is monitored at NPDES Outfall 501 before being discharged to EFPC [27]. The flow and load duration curves based on recorded data is shown in Figure 6.

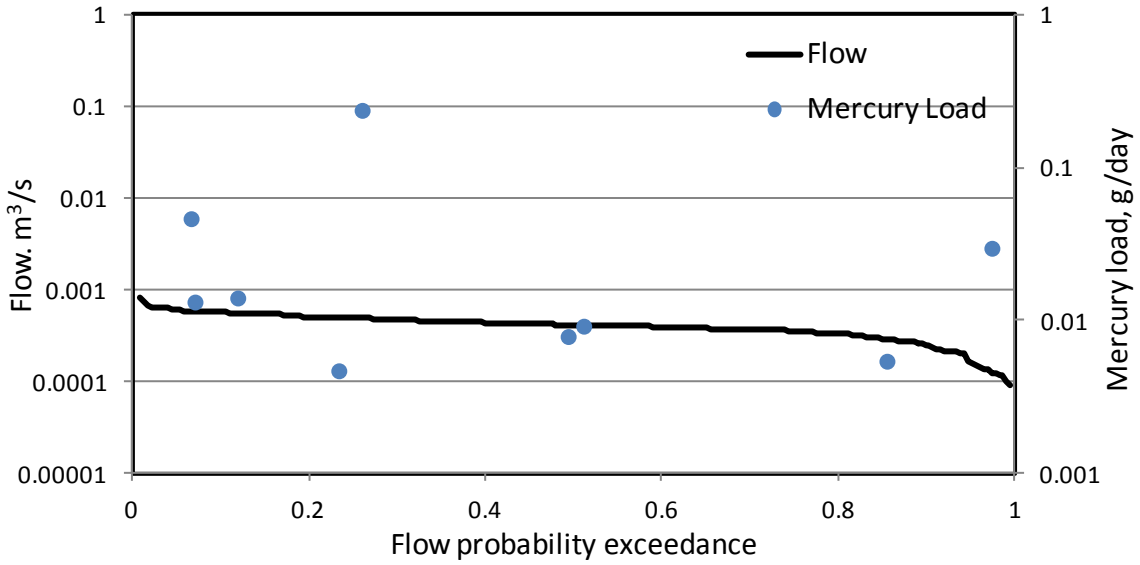

Figure 6. Flow and load duration curves for OF501.

West End Treatment Facility (WETF)

The WETF is designed to treat nitrate-bearing wastewater of the Y-12 Plant production operations. Effluent flow from the WETF ranges from 16,000 to 36,000 gallons per day and is monitored at NPDES Outfall 502 before being discharged to EFPC [27]. The flow and load duration curves for OF502 are shown in Figure 7.

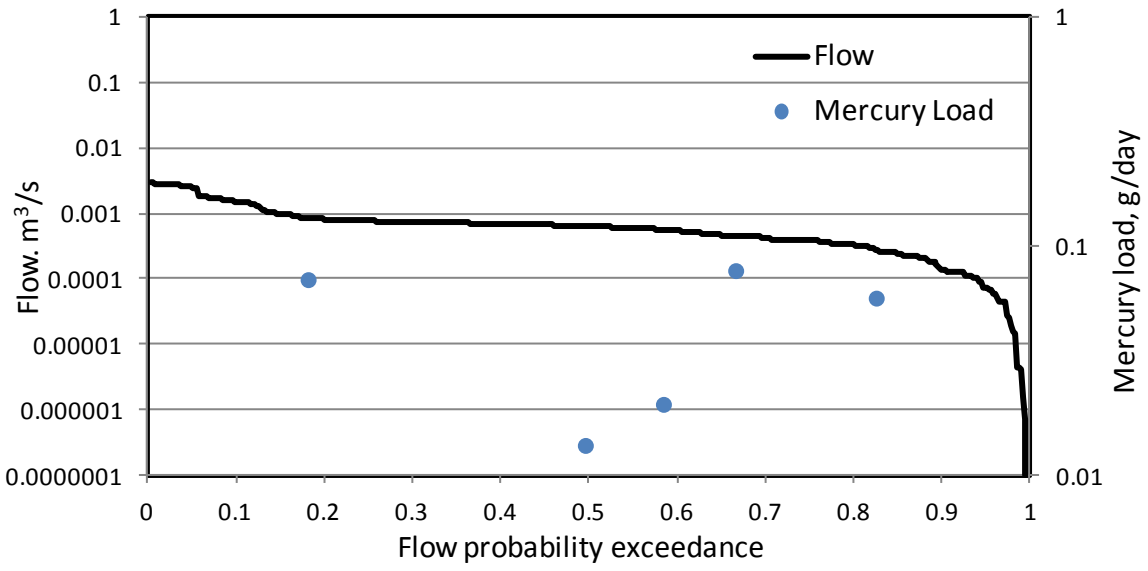

Figure 7. Flow and load duration curves for OF502.

Groundwater Treatment Facility (GWTF)

The GWTF treats contaminated groundwater seeps from the Bear Creek Burial Grounds. The water is generally contaminated with various volatile and nonvolatile organic compounds. The collected seep water is processed through an oil/water separator before entering the GWTF where it is treated to remove volatile and nonvolatile organic compounds and iron. The GWTF discharges approximately 2.5 million gallons per year from Y-12 and approximately 1.5 million gallons per year of effluents from the K-25 site. It is monitored at the NPDES Outfall 512 before being discharged to EFPC [27]. The flow duration curve for OF512 is shown in Figure 8. Mercury data was unavailable for this outfall to calculate the mercury loads.

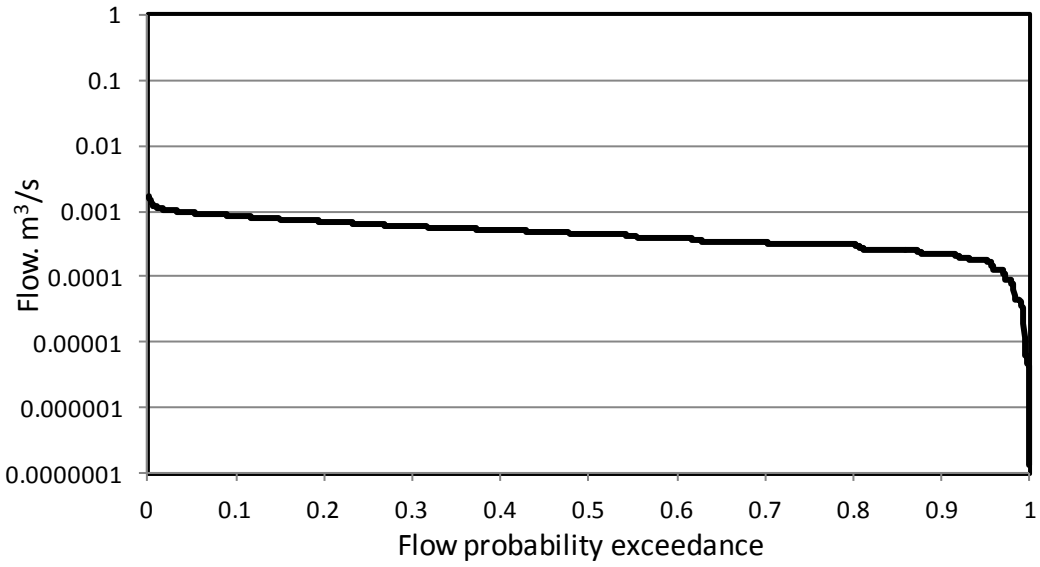

Figure 8. Flow duration curve for OF512.

Stream Plant Waste Treatment Facility (SPWTF)

The SPWTF provides treatment for an estimated 65 million gallons a year of acid discharges from the Y-12 facilities. The facility treats demineralized regeneration wastewater, sodium- and acid-softener regeneration wastewater, boiler blowdown, wet ash decant, and coal pile runoff. Coal pile runoff typically contains suspended coal fines, low pH, metals (e.g., iron, copper, aluminum, manganese), and a high sulfate concentration. Currently, effluent is not discharged to EFPC; it is discharged to the sanitary sewer. The NPDES monitoring point (Outfall 503) is inactive. The flow and load duration curves for OF503 are shown in Figure 9.

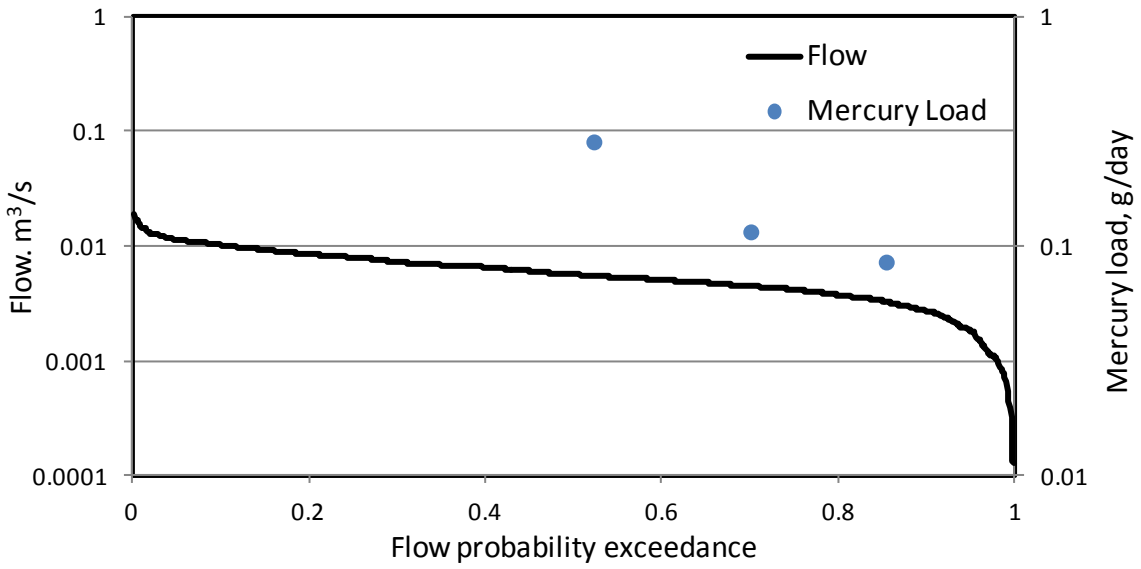

Figure 9. Flow and load duration curves for OF503.

Central Mercury Treatment Facility (CMTF)

The CMTS treats sump water from buildings 9201-4, 9201-5, and 9204-4, which were formerly used for lithium isotope separation processes involving mercury at the Y-12 facilities. Effluent from the CMTF will be monitored at the future NPDES Outfall 551 before being discharged to EFPC [28]. The flow and load duration curves for OF551 are shown in Figure 10.

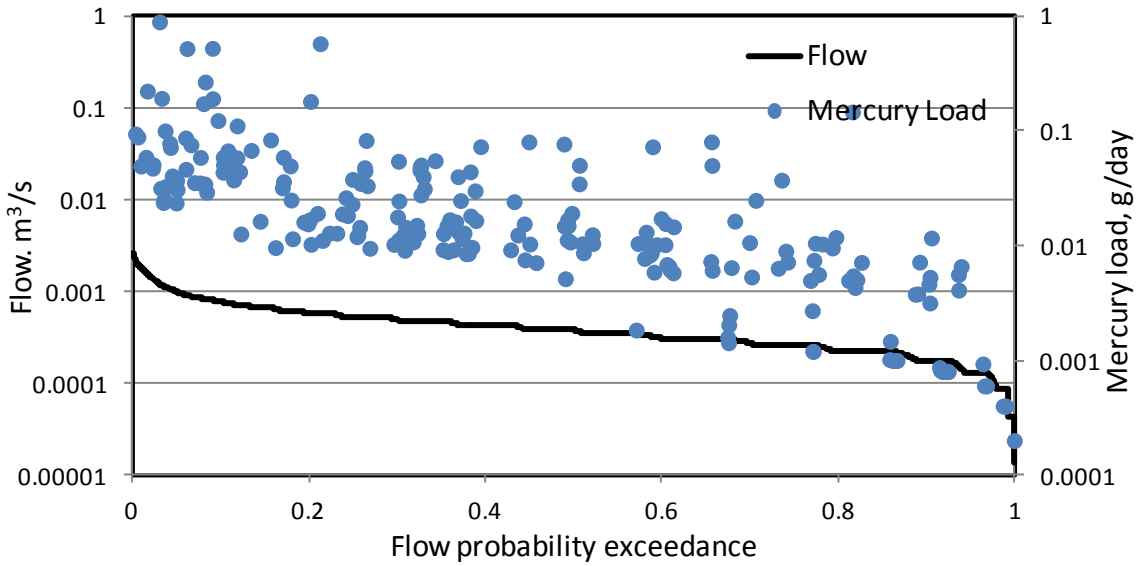

Figure 10. Flow and load duration curves for OF551.

Big Spring Water Treatment System (BSWTS)

The U.S. DOE has recently operated this mercury treatment facility for groundwater located at OF051. The mean flow of treated groundwater is approximately 0.3 MGD. The facility is designed to treat the entire flow from a large spring source of contaminated groundwater, yet, approximately 0.1 MGD of untreated groundwater bypasses the treatment system and is released to EFPC. This treatment facility is known to be responsible for the drastic decrease in mercury in EFPC as recorded at Station 17. The flow and load duration curves for OF051 are shown in Figure 11.

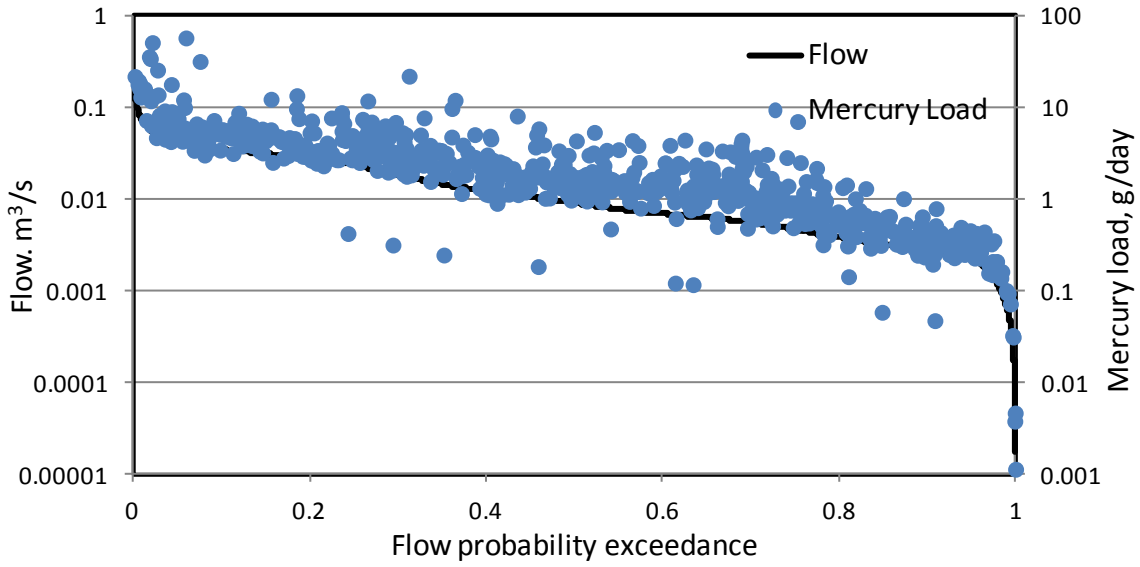

Figure 11. Flow and load duration curves for OF051.

2.1.3 Flow Augmentation from Clinch River

Decreased water usage within the Y-12 NSC in the early 1990s has resulted in a substantial reduction in flow in Upper East Fork Poplar Creek[1] (UEFPC). In 1996, to temporarily support the

[1] Upper East Fork Poplar Creek is a section of EFPC discharging south of Y-12 NSC and extends from OF200 to Station 17.

water quality in EFPC and restore its ecological life, the Y-12 facility in an agreement with TDEC pumped approximately 4.5 MGD of raw water from the Melton Hill Reservoir on the Clinch River to UEFPC at the stream head, OF200, to increase the flow in EFPC. This action was in accordance with the 1996 NPDES permit (TN0002968) which required Y-12 to maintain a daily average flow of 7 MGD at Station 17 [26].

2.1.4 Municipal Wastewater Treatment Facilities

The City of Oak Ridge sewage treatment plant (STP) discharges to EFPC at mile 8.3 (EFK 13) at a design flow rate of 30 MGD. In addition to municipal wastewaters, the STP treats all domestic sewage generated at the Y-12 NSC. The City of Oak Ridge reported influent mercury concentrations of less than 200 ng/L, which was the detection level used at the time prior to EPA's adoption of the new methodology of 1631 in 2002 with a detection level of 0.2 ng/L. The magnitude of the contribution of the Oak Ridge STP to the concentration of mercury in EFPC is not known at this time.

2.2 Non-point Sources

Non-point sources are diffuse sources that are not entering a waterbody through a distinct passage and at a single specific location. The principal origins of non-point sources of mercury contamination in the EFPC watershed are:

- Contaminated floodplain and streambank soils from legacy releases at the Y-12 NSC.
- Contaminated surface soil from stormwater runoff at Y-12 and the City of Oak Ridge, which transport adsorbed mercury compounds into the EFPC stream channel.
- Streambed sediments that are getting resuspended following the flow management actions in UEFPC started since 1997 and other fluctuations in creek flow resulting from seasonal storm events.
- Contaminated groundwater exchange.
- Atmospheric sources from coal-fired power plants and airborne mercury emissions from Y-12 activities.

2.2.1 Floodplain and streambank soils

Historical mercury deposition in the EFPC watershed left highly contaminated soil on the floodplain and streambank surface along the entire length of the stream (more than 200 ha of contaminated soil [35]). That material can re-enter the aquatic system by surface erosion of floodplain soils or by erosion and collapse of streambank soils where the contaminated soil is directly exposed to flow of the stream during storm events [34]. Mercury release to EFPC from floodplain and streambank soils has been documented since the 1980's. During 1996 and 1997, approximately 45,000 cubic yards of contaminated soils with mercury concentrations above 400 mg/kg was removed from the portion of EFPC downstream of Station 17 at EFK 22.4 and EFK 17.4 following the ROD decision in 1995 and 1996 [32, 33]. Mean mercury concentrations of floodplain and streambank soils along EFPC were reduced and currently vary from 10 to over 150 mg/kg. In late 1999, eroding stream banks were protected using sand-filled geotextile tubes. That effort reduced the storm flow transport of mercury from the streambank to the EFPC, but appeared to have the least effect on mercury inputs from the base flow [29]. Contributions from peak flow events continue to expose aquatic life to floodplain soils containing elevated levels of mercury; however, the deposition has not resulted in exceedances of the cleanup target level [25].

A field study performed by ORNL in 2010 revealed that contaminated floodplain and streambank soils along approximately two-thirds of the total length of EFPC (downstream of Station 17) undoubtedly contribute additional mercury to the system when freeze/thaw cycles, rainfall, and elevated stream stage act to erode those surfaces. Measurements of mercury and methylmercury (MeHg) in eroding streambanks were taken at four locations (EFK 23.4, EFK 18.2, EFK 13.8, and EFK 6.3) in EFPC downstream of the headwater mercury source within Y-12 [34]. Those locations were selected to coincide with locations where mercury bioaccumulation in fish has been routinely monitored by Oak Ridge National Laboratory/Environmental Science Division (ORNL/ESD) since 1985. Waterborne Hg and MeHg are also monitored twice annually at these locations by the DOE, managed by Bechtel Jacobs (BJC) [34]. Measurements are summarized in Table 3.

Table 3. Inventory of Mercury (Hg) in 1-cm Layer of Lower EFPC Streambank [34]

Reach	Length m	Bank height, m	Bank depth, m	Soil Hg mg/kg	% Erodable bank	Hg inventory, kg
EFK 23.4	5000	0.89	0.01	127 ± 48	53	10.8
EFK 18.2	5000	1.13	0.01	39 ± 13	90	7.1
EFK 13.8	5000	1.47	0.01	13 ± 6.6	51	1.8
EFK 6.3	5000	1.50	0.01	18 ± 3.8	63	2.9

Mercury concentrations in streambank soils decrease farther downstream from EFK 23.4 (Station 17) as presented in Table 3. Streambank erosion rates of 1–2 cm/y are required to contribute an amount of mercury comparable to that estimated to be exported annually from sources in EFPC. This erosion rate corresponds to a loss of soil equivalent to 29 - 55 kg/m/y in EFPC. Considering the bank erosion rates in the neighboring rivers (for example [36] the South River similar in geology and gradient to EFPC), a 1–2 cm/y rate would perhaps more likely typify conditions similar to EFPC. Inputs from surface erosion of floodplain and land surface soils were a relatively small fraction (<10%) of total mercury export to the EFPC under wet weather conditions, indicating that most of the mercury (>80%) is transported from the streambed and streambank sediments during high flows.

2.2.2 Suspended Solids from Stormwater Runoff

Highest concentrations of mercury at Station 17 are generally recorded for days of high precipitation (storm events) rather than an expected decrease in concentration due to the dilution as a consequence of the increase in flow volume. In general, species adsorbed on suspended particles had higher mean total concentrations during storm events than normal conditions, indicating that the increase in concentrations is mainly due to a higher suspended load [24]. The Y-12 stormwater program has identified total mercury concentrations as high as 4,000 ng/L during routine stormwater outfall monitoring; however, approximately 80 percent of the sample concentrations were reported at or below the detection limit of 200 ng/L [25].

After performing a series of field studies at the EFPC watershed in 2011, ORNL reported that 100 – 140 g of total mercury is exported from the floodplain and land surface into EFPC via

surface runoff during a 24-hr period of a typical storm event. However, annual export from land and floodplain surface erosion and runoff contributes only a small fraction of total mercury export from the watershed and bank erosion and streambed sediments are responsible for most of the annual mercury export from the watershed [34].

Concentration of mercury in shallow soil (0 to 1.5 m below ground surface) at sampling points is shown in Figure 12. Data was extracted from the OREIS database from 1986 to present.

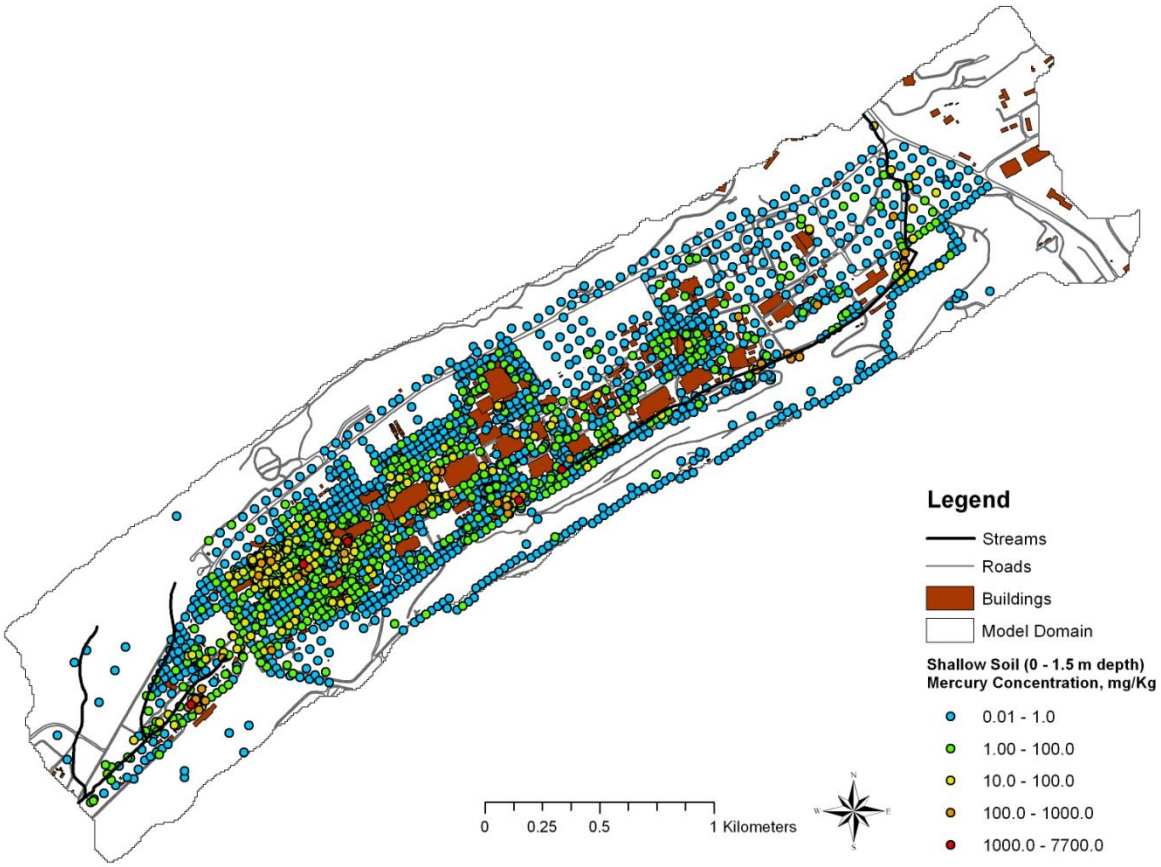

Figure 12. Mercury concentration in shallow soil (0 – 1.5 m below ground surface).

2.2.3 Streambed and Streambank Sediments

Due to the high affinity of mercury for solids ($K_d \sim 10^6$), fine particulate material retained in the

biofilm coating contains high concentration of waterborne inorganic mercury. This material is readily disturbed and returned to the water column, and thus, represents an important contribution to mercury export into EFPC. Field surveys were performed by ORNL during 2008 to 2010 on streambed biofilm and streambed gravels for 4 stations downstream of EFK 23.4 (Station 17) [34]. The estimated mercury content of the streambed biofilm is presented in Table 4. The inventory of mercury retained in this compartment (317 g in Table 4) was relatively small.

Table 4. Estimated Inventory of Mercury (Hg) in Solids in the Surface Biofilm of EFPC [34]

Reach	Biofilm mass (kg/m^2)	Hg (mg/kg)	Width (m)	Length (m)	Hg inventory (g)
EFK 23.4	0.12 ± 0.03	20 ± 3.2	5.5	5000	66
EFK 18.2	0.20 ± 0.04	18.2 ± 4.0	6.5	5000	118
EFK 13.8	0.12 ± 0.02	14.7 ± 3.1	7.5	5000	66
EFK 6.3	0.13 ± 0.05	12.0 ± 4.3	8.5	5000	66
Total					317

The field survey also analyzed the streambed sediments containing sand/silt/clay fraction (< 1 mm) at the same locations. The streambed mercury inventory estimated from this analysis is summarized in Table 5. The mass of mercury stored within the EFPC streambed sediments is in excess of 170 kg. Although a substantial amount, this is only equivalent to about three years of mercury export from the EFPC system at the estimated rate of 53 kg/y, and needs continual replenishment to sustain current rates of mercury export to EFPC [34]. The maximum mercury concentration in streambed sediments was reported at EFK 18.2. This location, as mentioned earlier in section 2.2.1, was one of the two main locations of the stream floodplain and streambank soil excavations as part of CERCLA actions in 1997. The high mercury content of streambed in this reach may reflect historic contamination that is resistant to removal by erosion. This might suggests that much of the mercury in the streambed in that reach may be relatively unsusceptible to erosion [34].

Most mercury (> 90%) exported from the EFPC watershed under wet weather flow arises from

the watershed downstream of Y-12, not within the headwater industrial complex. Inputs from surface erosion of floodplain soils were a relatively small fraction (~10%) of total mercury export from the LEFPC under wet weather conditions, indicating that mobilization of mercury from streambed and streambanks was the source of most high flow mercury export [34].

Table 5. Estimated Inventory of Mercury (Hg) in Streambed Gravel of EFPC, Assuming 50% of EFPC is Gravel Riffles [34]

Reach	Fines (kg/m^2)	Hg (mg/kg)	Width (m)	Length (m)	Hg inventory (kg)
EFK 23.4	76 ± 31	7.8 ± 1.3	5.5	5000	8.2
EFK 18.2	165 ± 31	43.5 ± 10.9	6.5	5000	117
EFK 13.8	91 ± 26	8.3 ± 2.3	7.5	5000	14
EFK 6.3	98 ± 23	15.8 ± 4.9	8.5	5000	33
Total					172

The aforementioned field study [34] did not cover the reach of the EFPC upstream of EFK 23.4 (Station 17). Decreased water usage within the Y-12 NSC in the early 1990s resulted in a substantial reduction in flow in Upper East Fork Poplar Creek[2] (UEFPC). In 1996, in order to support the water quality in EFPC and restore its ecological life, the Y-12 facility in an agreement with TDEC pumped approximately 4.5 MGD of raw water from the Melton Hill Reservoir on the Clinch River to UEFPC at the stream head, OF200, to increase the flow in EFPC. This action was in accordance with the 1996 NPDES permit (TN0002968) which required Y-12 to maintain a daily average flow of 7 MGD at Station 17 [26].

The added water mixed with the storm drain flow discharged at OF200, was expected to dilute the mercury concentration in UEFPC and produce a concomitant decrease in the concentration of mercury in fish. After flow management was implemented in August 1996, total mercury concentration and loading in UEFPC increased as a result of resuspension of mercury-laden fine

[2] Upper East Fork Poplar Creek is a section of EFPC discharging south of Y-12 NSC and extending from OF200 to Station 17.

particulates from streambed sediments; however, this situation was thought to be temporary and a new steady state was anticipated to be established between suspended load and bed sediments, which did not occur [29]. Further studies found that a gradual increase in waterborne mercury concentration occurred across a 250 m reach of stream at approximately 100 m (roughly bounded by C11 and OF109) from the headwater at OF200 [30]. The streambed pore water within that reach contains very high concentrations of dissolved mercury, often exceeding 20 ug/L (approximately 50 to 100 times the concentration in overlying surface water, which is 0.3 ppb). It is believed that augmented flow most likely increased the circulation across the water column in the creek allowing the surface water to flow in and out of the streambed pore water resuspending sediment particles bounded by mercury species [30]. In 1998, the flow management system was temporarily shut off to investigate this hypothesis. This appeared to have reduced mercury loading in the sediment source from 8 g/d to approximately 3 g/d [31].

2.2.4 Contaminated Groundwater Exchange

Within the EFPC domain, USGS has defined shallow aquifer material as being any alluvium, regolith, and (or) fill materials that occur above bedrock and are water bearing [Carmichael, 1988]. As determined by visual inspection, soil sampling, and observation-well drilling at selected sites in the study area, thickness of the naturally occurring shallow-aquifer materials generally ranges from essentially zero where bedrock is exposed at land surface (commonly occurring along the floodplain periphery) to about 3 m near the center of the flood plain.

Locally, thickness may be as much as 6 m where fill materials have been placed above the flood-plain deposits. Alluvial soils consisting primarily of silt and clay with lesser amounts of sand and gravel comprise the upper 0.3 to 1.5 m of the undisturbed floodplain sediments. These soils are classified as either Hamblen or Newark variety silt-clay-loams which have vertical permeability rates ranging from 0.3 to 1.2 m/d (3.5e-06 to 1.4e-05 m/s) and are moderately resistant to erosion. A blue-gray to brown, moderately to highly erosion-resistant, silty-clay glei horizon underlies the alluvium, the top of the glei marking the base of the more recent alluvial deposits [Carmichael, 1988]. As determined from observation well drilling, where

present, this material directly overlies bedrock and ranges from only inches to as much as 1.5 m in thickness. Because of its higher clay content relative to the overlying alluvium, the glei horizon likely impedes the rate of groundwater movement downward through the alluvium, probably causing perched water table conditions during drier periods. No samples of the glei collected in undisturbed floodplain areas and analyzed as part of the ongoing off-site sediment sampling program have shown mercury contamination. The model used an average of 1.5 m of soil in the upper layer.

Furthermore, USGS [Carmichael, 1988] reported that precipitation is the principal source of recharge to the shallow aquifer. Precipitation falling on the floodplain surface moves directly through the zone of soil contamination as it percolates to the water table. Locally, floodplain sections of the shallow aquifer may also receive minor amounts of recharge in the form of bank storage when the water table is lower than stream level. This may occur during the summer and fall as:

- The stream stage rises during and immediately after storms.
- The discharge of sufficient process water from the Y-12 plant causes the stream stage to be maintained at an artificially higher altitude than the water table adjacent to the stream.
- During years having normal precipitation, these sources of recharge probably account for only a small percentage of groundwater stored in the shallow aquifer because their influence is limited to areas adjacent to the stream channel and because water in bank storage drains back into the stream relatively rapidly as the stage recedes.
- Most discharge from the shallow aquifer during normally wet years is presumed to be through springs and seeps to East Fork Poplar Creek and its tributaries, comprising the baseflow component of these streams. During the spring, summer, and fall, evapotranspiration also accounts for the removal of water in storage in the shallow aquifer.

Generally, the depth to water in the wells in late winter ranged from about 0.3 to 1.2 m below

land surface and in the fall, from about 0.6 to 2.1 m below land surface. During the winter and early spring months, the water table rises in the shallow aquifer due in combination to a large decrease in evapotranspiration and a small increase in precipitation relative to summer and fall months. Seasonal rise of the water table was evidenced during the winter and spring both by higher water levels measured in nearly all monitoring wells and through visual observation of water standing on the land surface in many low lying floodplain areas. Because wells were installed in several of these areas, visual correlation of water occurring at the same elevation in the wells as on the land surface indicates that, at these times, the shallow aquifer in these areas was fully saturated.

During the summer and fall months, depth to the water table increases in the shallow aquifer, and water level declines during these months result from a significant increase in groundwater losses to evapotranspiration, a small decrease in precipitation relative to winter and spring months, and continued groundwater discharge to the streams. Using well data, lithologic and water table transects were developed for two sides along East Fork Poplar Creek, which demonstrated that during the winter and spring, the water table generally sloped towards East Fork Poplar Creek and/or other floodplain drainage channels, indicating local discharge to the streams. However, during the late summer and fall, abnormally dry weather in the study area caused the water table to recede below the top of bedrock in some floodplain areas. Due to the low water table, shallow groundwater gradients sloped away from East Fork Poplar Creek, suggesting that during these periods, the stream may have been losing water to the shallow aquifer along some reaches.

The main groundwater path at the site is the Maynardville Limestone at the eastern end of the watershed, a karst, fractured carbonate formation that functions as a preferential groundwater flow pathway in the valley. Other groundwater pathways are:

- Storm drains that capture the former UEFPC tributary system.
- Seeps and springs.
- An underdrain system (10 cm perforated pipe and gravel backfill) beneath the

UEFPC distribution channel to Lake Reality that functions as a highly permeable, shallow groundwater pathway.

Groundwater monitoring at the watershed scale is conducted at key exit pathway locations along the eastern boundary of the watershed. Wells GW-744, -747, and -816, located along UEFPC within the water gap (Rome Formation) through Pine Ridge north of the ORR boundary, monitor shallow groundwater flowing north off of the ORR coincident with surface water flow. These monitoring locations historically have not indicated off-site transport to the north within the bedrock units below the Maynardville Limestone. Data collected during FY 2005 continue to show a lack of signature groundwater contaminants (VOCs, radiological constituents, or nitrate) along this pathway (e.g., concentrations below or close to detection limits or background levels).

Along the eastern boundary of the watershed, semiannual sampling in conjunction with the Y-12 Environmental Compliance Division (ECD) of well GW-733 and quarterly sampling of well GW-722 is conducted to monitor groundwater in intermediate and deep intervals of the Maynardville Limestone that flows to the east from the ORR into Union Valley. These wells have been monitored continuously over the past five years under the Water Resources Restoration Program (WRRP) and/or other programs (e.g., DOE Order 450.1 and RCRA post-closure corrective action). Five-year review technical assessment data for these locations, inclusive of FY 2005, are presented as part of the East End Volatile Organic Compound (EEVOC) plume action performance.

The model used the observed groundwater table to provide initial conditions of the groundwater as shown in Figure 13. Groundwater in adjacent formations flows from west to east in the Maynardville Limestone because of the formation's relatively high hydraulic conductivity and well developed karst system. Groundwater in the UEFPC watershed typically flows along strike from west to east in the Maynardville Formation between 30 m and 120 m below ground. Groundwater direction in this area is also influenced by anthropogenic structures such as pipes, drains and other underground structures which have created

preferential flow paths for contaminated groundwater.

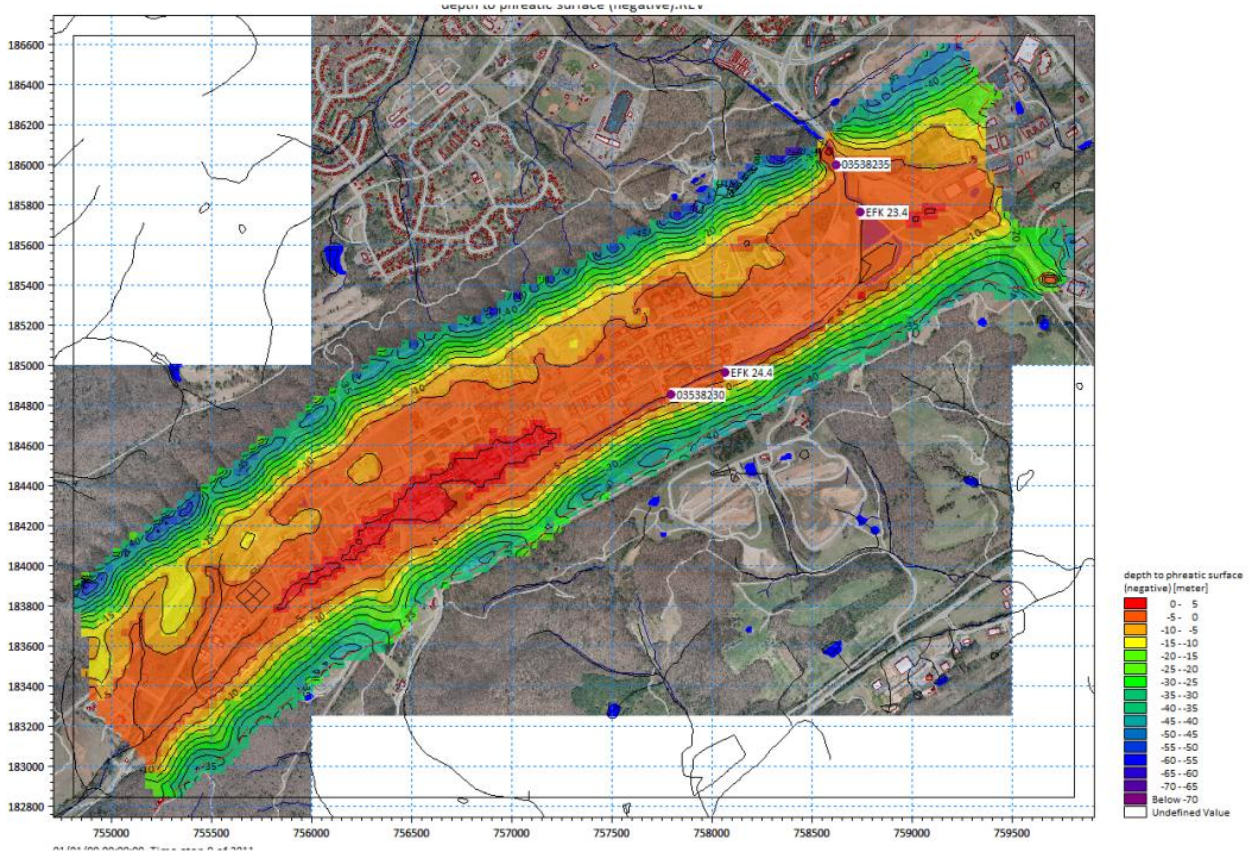

Figure 13. Initial groundwater potentiometric map (used as model initial condition)

However, the Maynardville Limestone is the primary pathway for contaminant migration off-site from Y-12. Groundwater from adjacent formations tends to flow toward the Maynardville Limestone because of its well developed karst-system. Because of the high interconnectivity with surface water, groundwater discharges at seeps and springs constitutes much of the base flow of Scarboro Creek and UEFPC. Depth to groundwater in this area is between 0.3 and 1.2 m below ground during the winter and between 0.6 and 2.1 m below ground in the summer, (USGS). Groundwater in this area responds quickly to storms and can exhibit high flow rates with rapid dilution. A silty-clay glei horizon exists beneath EFPC and impedes downward groundwater migration (Carmichael, 1988).

Concentration of mercury in deep soil (between 1.5 to 17 m below ground surface) at sampling points is shown in Figure 14. Data was extracted from OREIS database from 1986 to present.

Concentrations of mercury in shallow soil were earlier shown in Figure 12.

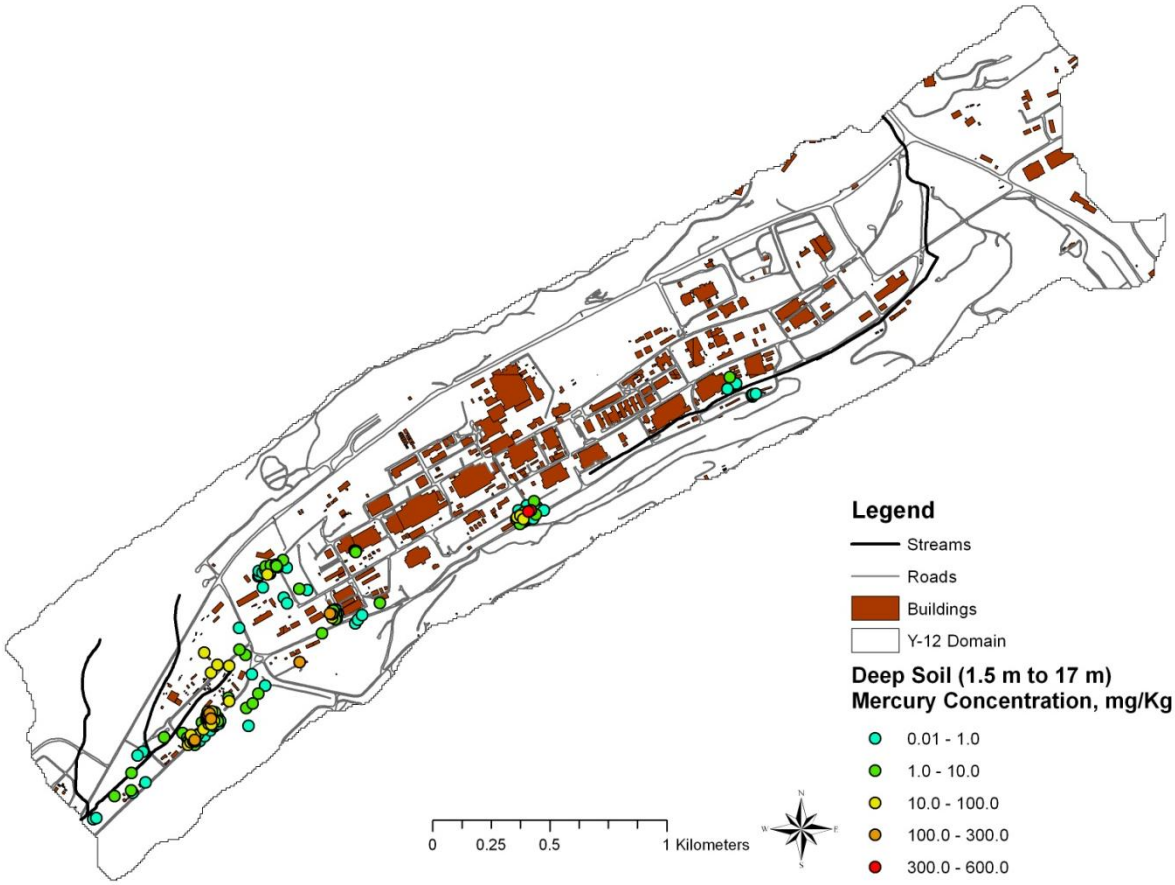

Figure 14. Mercury concentration in deep soil (1.5 – 17 m below ground surface).

2.2.5 Atmospheric Sources

EFPC is located between two TVA coal-fired power plants. The magnitude of the potential contribution of these facilities is not known at this time. ORNL and K-25 have both operated steam plants in the past. The largest contribution of mercury to atmospheric sources is from coal-fired power plants. TVA's old ash ponds may contribute to the atmospheric source as well. TDEC is not aware of any other potential atmospheric sources of mercury in or near the EFPC watershed. Airborne mercury emissions at two Y-12 monitoring stations document an upward trend since 2003. A concentration of 0.0055 µg/m^3 was measured at the western station. The

increase in ambient concentrations may be due to the recent increased demolition and excavation in the western end of the plant, resulting in possible disturbances of Hg-contaminated soil and sediment airborne emissions on-site [37]. Additional monitoring may be necessary in order to determine the impact of atmospheric deposition of mercury on the EFPC watershed.

3 NUMERICAL MODEL

To provide a better understanding of the hydrological factors which govern the flow and transport of mercury within the EFPC watershed, an integrated surface/subsurface hydrologic and transport model was developed using the MIKE numerical package (MIKE-SHE/MIKE-11/ECOLAB). The model includes the main components of the hydrological cycle and contaminant transport; groundwater flow and transport (3D saturated and unsaturated), overland flow, flow in rivers, precipitation, and evapotranspiration. The objective of the model is to analyze the mercury cycle in the environment and forecast the fate and transport of mercury within the watershed. The model is built to support the development of a TMDL for the entire EFPC watershed and to extend the development of flow and load duration curves for locations lacking sufficient recorded data to perform TMDL analysis. The regional setting of the EFPC watershed and the model domain are shown in Figure 1 and Figure 2, respectively.

MIKE-11 is a 1D river modeling system developed by DHI. Based on a recent evaluation performed by EPA, MIKE-11 was deemed the most advanced and comprehensive of its type today, and is presently used by more than 1,500 users worldwide. It is routinely used by state regulators for analysis of natural stream flow and flow in canals and rivers in complex water management scenarios, including floodplain calculations, dam breaks, and control structures. The hydrodynamic module contains an implicit, finite difference computation of unsteady flow in rivers. The complete nonlinear equations of open channel flow (Saint-Venant) can be solved numerically between all grid points at specified time intervals for given boundary conditions. In addition to this fully dynamic description, other descriptions are also available to choose from including high-order, fully dynamic, diffusive wave, kinematic wave, quasi-steady state, and kinematic routing (Muskingum, Muskingum-Cunge).

MIKE-SHE is a fully integrated model for the 3D simulation and linkage of hydrologic systems including overland, subsurface, and river flows. It has been successfully applied at multiple scales, using spatially distributed and continuous climate data to simulate a broad range of integrated hydrologic, hydraulic, and transport problems. MIKE-SHE couples partial differential

equations that describe flow in the saturated and unsaturated zones with the overland and river flow. Different numerical solution schemes are then used to solve the different partial differential equations for each process. A solution to the system of equations associated with each process is found iteratively by use of different numerical solvers.

ECOLAB is an ecological solver provided by DHI which can be coupled with MIKE-11 for the purpose of ecological modeling. An ECOLAB template can be developed by the user to model the ecological processes as required by any specific project; however, some templates have already been developed by DHI in the areas of water quality (17 templates), heavy metal transport (1 template), eutrophication (3 templates), and xenobiotics (1 template). For the modeling of mercury fate and transport in EFPC, the heavy metal transport template of ECOLAB is used coupled with both MIKE-11 and MIKE-SHE to simulate the interaction of mercury species with the sediment particles and water molecules in the creek. The heavy metal template describes the adsorption/desorption of mercury to suspended matter, the sedimentation of sorbed mercury to the streambed, as well as resuspension of the settled mercury. It also includes exchange of mercury between particulates of the bed sediment and the interstitial waters of the bed. The diffusive exchange of dissolved mercury in the water and in the interstitial waters is also described. These processes simulated in ECOLAB for this project are shown in Figure 15.

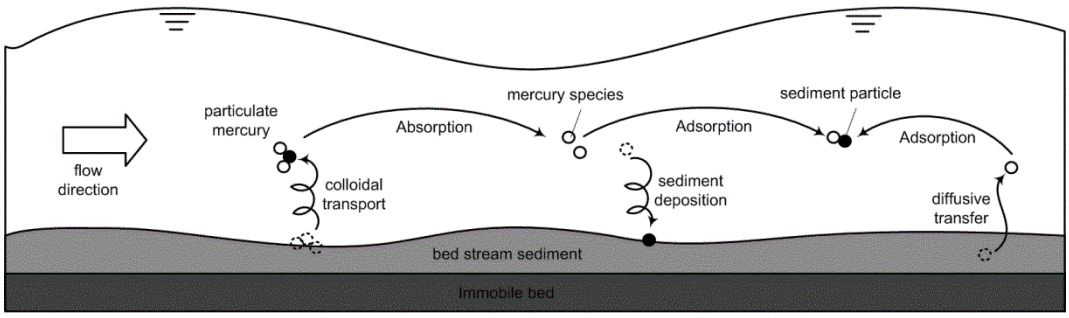

Figure 15. Processes involved in the interaction of mercury species with water and sediments.

Figure 16 shows the processes that are simulated by each of the modules (MIKE-11, MIKE-SHE, and ECOLAB) in the model developed for EFPC.

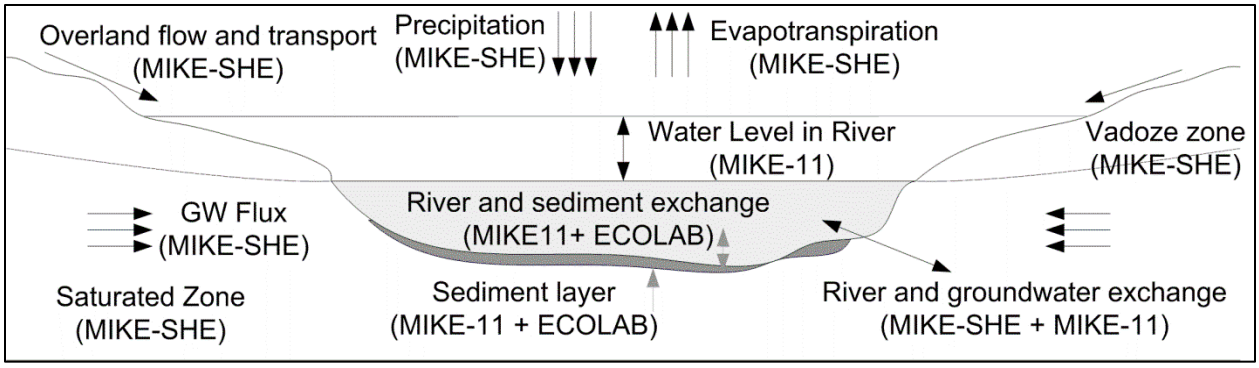

Figure 16. Flow and transport components included in the model.

The most important strengths of the models developed using the MIKE package in supporting TMDL development, are described by EPA as follows [38]:

- They interface with GIS allowing for preparation of model input data and presentation of model outputs within a GIS environment.
- The modules are easily integrated with each other (e.g., MIKE-SHE, ECOLAB, and MIKE-21).
- The modular structure offers great flexibility. Each module can be operated separately, data transfer between modules is automatic, complex physical processes can be coupled (e.g., river morphology, sediment re-suspension and water quality), updating or expansion of existing installations or models with new modules is simple.
- Ultimate facility in the model input; graphical data input/editing; simultaneous input/editing of various data types; copy and paste facility for direct import (export) from for example spreadsheet programs; fully integrated tabular and graphical windows; importing of river network and topography data from ASCII text files.

The integrated flow and transport model of UEFPC used for this study was developed in four phases. In the first phase, a MIKE-11 model of the river network was developed. In the second phase, an overland and subsurface flow model of the proposed domain was developed and coupled with the river model (MIKE-11). In the third phase, historical hydrological boundary

data (timeseries for precipitation, evapotranspiration, groundwater levels, river discharges) were applied to calibrate the model. In the fourth phase, the transport model for the river and surface/subsurface domains were incorporated in the flow model to simulate the regional hydrology and transport. Concentration measurements were used to calibrate the transport parameters of the model.

The model enables full, dynamic coupling of surface and subsurface flow processes, which allows calculations of water and contaminant exchange between the land, rivers, and the groundwater. By providing detailed spatial information and characteristics including hydrological and transport properties in the four subdomains, Saturated Zone (SZ), Unsaturated Zone (UZ), Overland Flow (OL), and Transport in Streams (OC), the model provides accurate water and contaminant mass balance for the domain.

3.1 EFPC Conceptual Model

As discussed in Chapter 2, three major sources of mercury to EFPC include (i) water-borne mercury from stormwater and industrial wastewater outfalls; (ii) land surface and shallow groundwater; and (iii) streambed sediment and streambank soil [8]. Considering the transport pathways to EFPC including outfalls, groundwater flow and surface sheet flow, a conceptual model has been developed for the mercury transport in EFPC watershed as shown in Figure 17.

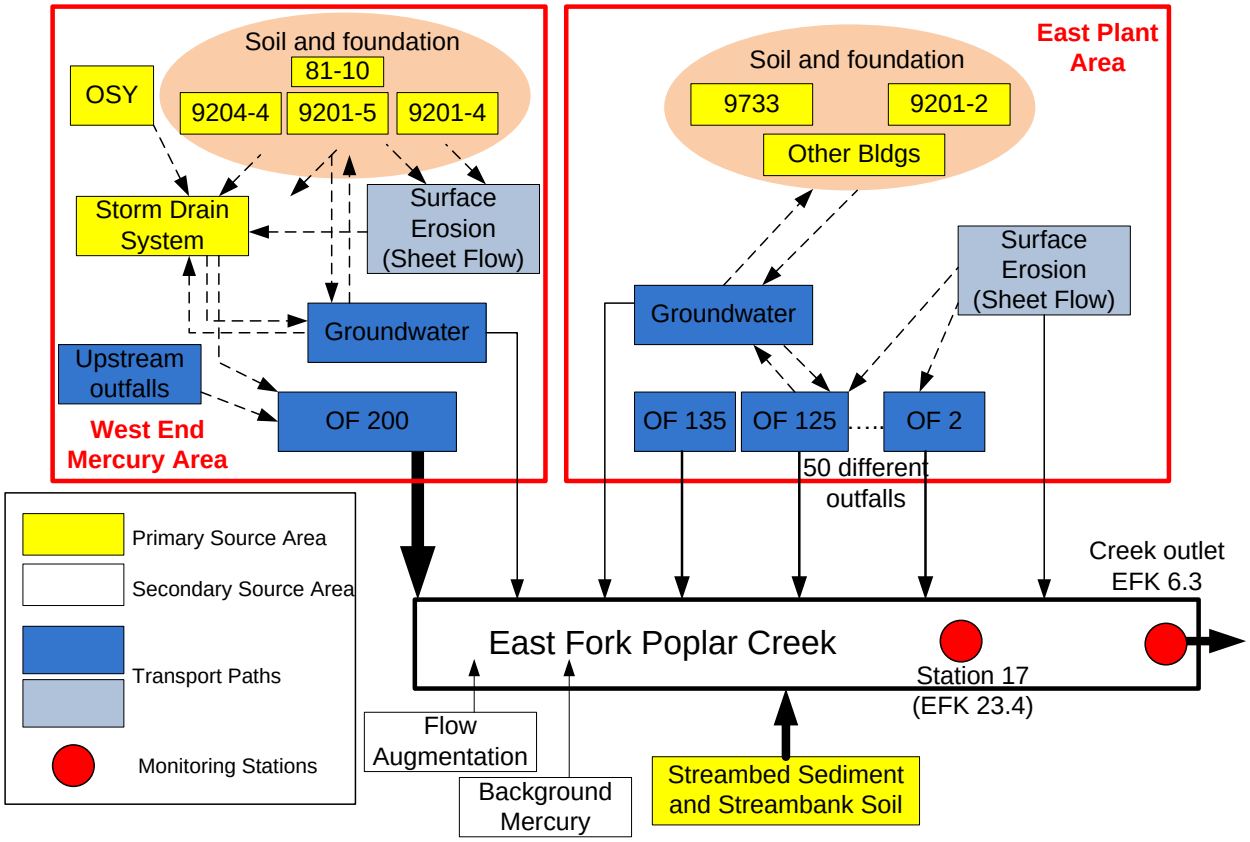

Figure 17. Conceptual model of EFPC.

3.2 Model Components

3.2.1 River

The MIKE-11 river model requires a shapefile of all streams, which in this case was obtained from the USGS. Most of the cross sections of the major streams were determined from a topography transect; for small rivers, generic cross sections were used. The river model has hydrodynamic and advection-dispersion transport modules, the input parameters for which were based on DOE field reports and other literature resources.

3.2.2 Overland (OL)

The model for flow and transport in the overland, saturated and unsaturated zones requires a number of spatial and temporal parameters which were introduced to the model in the form of

standard GIS data. Overland flow is calculated using the diffusive wave approximation of the Saint Venant equations. Overland flow requires data for the physical parameters of the system including topography, land use, and imperviousness. The ground surface topography was extracted from the Tennessee Spatial Data Server (TSDS) database. The land use data imported into the model are shown in Figure 18 and Table 6. Some of the input GIS files for the overland module of the model are shown in Figure 19. Manning's numbers for different regions were estimated from Manning's charts based on land use and vegetation information extracted from the OREIS database. The original Manning's number, n, ranges between 0.01 and 0.05 $s/m^{1/3}$ (MIKE-SHE assumes an inverse Manning's number, M=1/n in the calculations and values range from 3 to 100 $m^{1/3}/s$). The Manning values for different land uses are listed in the last column of Table 6. The model allows input of contaminants in the overland domain (e.g. ponded water).

Table 6. MRLC Land Use Distribution – EFPC Watershed

Land Use	Area		Manning's
	[acres]	[%]	M
Open Water	15	0%	5
Developed, Open Space	2,407	13%	5
Developed, Low Intensity	2,136	11%	2
Developed, Medium Intensity	1,160	6%	1
Developed, High Intensity	601	3%	0.7
Barren Land, Rock, Sand, Clay	53	0%	1.1
Deciduous Forest	9,060	48%	1.0
Evergreen Forest	855	5%	0.9
Mixed Forest	578	3%	1.0
Shrub, Scrub	1	0%	2.0
Grassland, Herbaceous	179	1%	2.9
Pasture, Hay	945	5%	3.0
Cultivated Crops	38	0%	2.7
Woody Wetlands	963	5%	1.0
Emergent Herbaceous Wetlands	1	0%	2.2
Unclassified	1	0%	-
Total	18,993	100%	

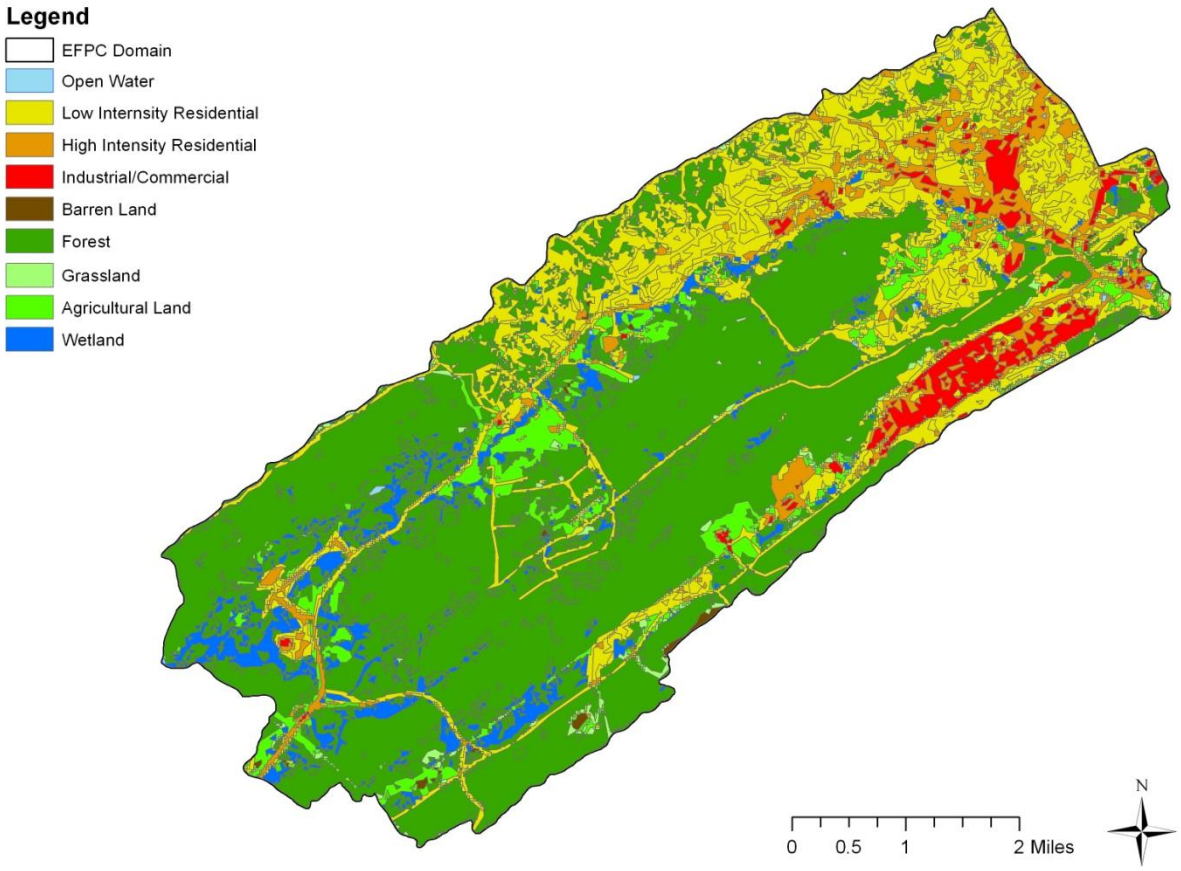

Figure 18. Land use characteristics of the EFPC watershed.

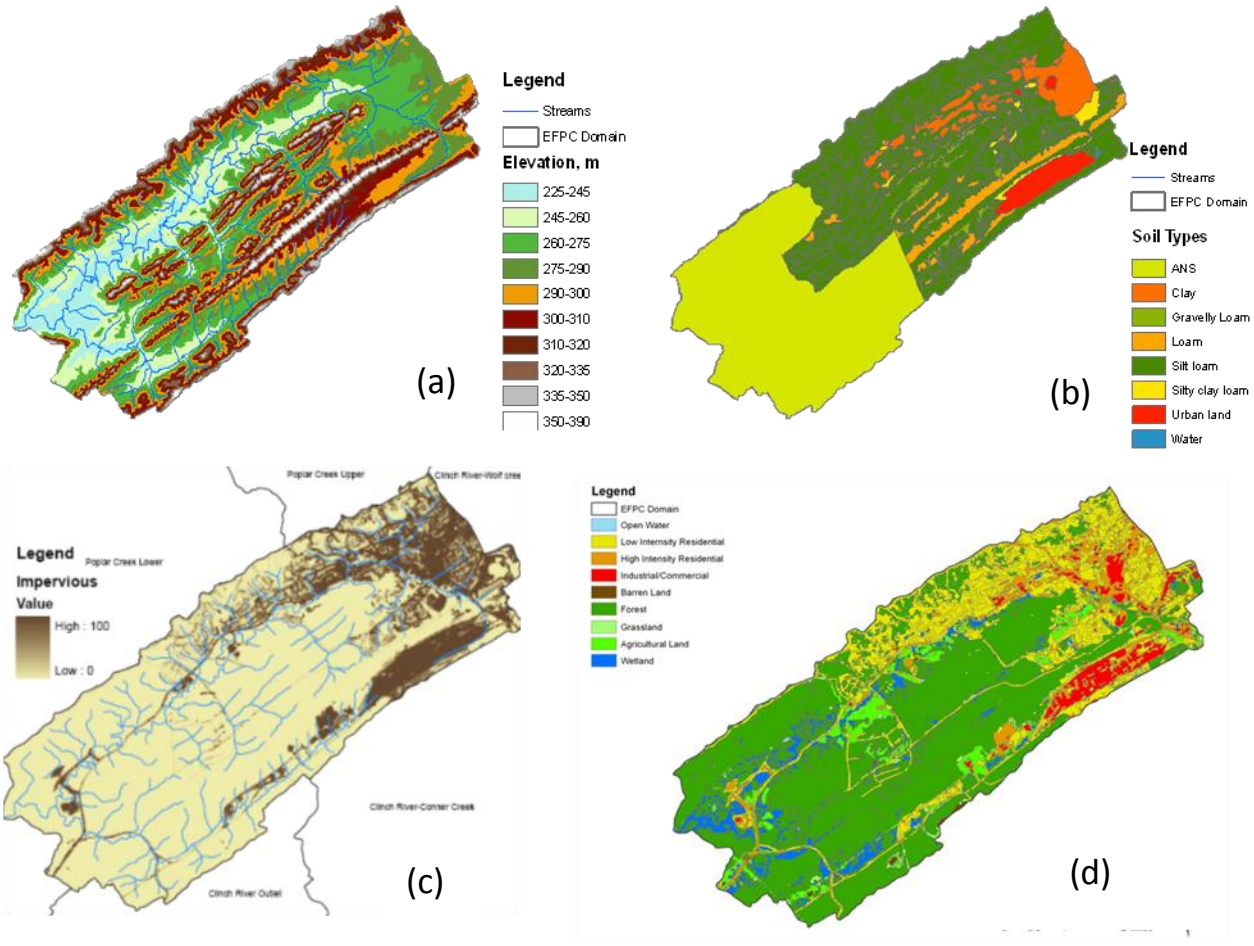

Figure 19. Input GIS files used in the numerical model: (a) Topography (b) Soil type (c) Imperviousness (d) Land use.

3.2.3 Unsaturated Zone (UZ)

Flow in the unsaturated zone is computed using Richard's equation, which requires Van Genuchten's parameters for computing the hydraulic conductivity of soil as a function of moisture content. The spatial distribution of the soil profile definitions were obtained in GIS shapefile format from SSURGO. Each of the soil codes was mapped to 12 mixed soil textures, for which the statistical characteristics of the Van Genuchten parameters have been derived. The identified soil groups were further categorized into five textural types including loam, silt loam, clay loam, silty clay loam, and clay.

For the unsaturated zone, the aquifer incorporates an approximated 1 m root zone and a 5 m underlying soil matrix, and the upper shallow saturated zone with a groundwater depth which in general varies between 1 to 25 m. For more accurate representation of the processes in the unsaturated zone, vertical discretization was used (14 layers with thicknesses varying between 0.1 and 5.0 m). The unsaturated zone is represented by 14 layers in the MIKE-SHE model with the characteristics listed in Table 7.

Table 7. Unsaturated Zone Soil Profile Definition

Layers	Number of sub-layers	Thickness, m	Lower level, m	Dispersivity, m
Layer UZ1	2	0.1	-0.2	0.07[2]
Layer UZ2	4	0.5	-2.2	0.07[2]
Layer UZ3	8	5.0	-52.2	0.07[2]
Saturated moisture content = 0.35, Saturated hydraulic conductivity = 0.0086[1] m/d, Soil bulk density (ρ_{bs}) = 1700[1] kg/m^3 and Residual moisture content (θ_r) = 0.15				

[1] UEFPC RI Report, 1998, Table E. 9.3 (DOE/OR/0l-16411V 4&D2)
[2] Tang et al., 2010

3.2.4 Saturated Zone (SZ)

Flow and transport in the saturated zone is three dimensional, using Darcy's law. For each layer, flow and transport parameters including lower level, vertical and horizontal hydraulic conductivity, specific yield, specific storage, and initial potential head were defined. Five different layers have been defined for the EFPC model for the saturated zone. Characteristics of each layer are listed in Table 8.

The model assumes that flow in the unsaturated zone is only in the vertical direction (Figure 20a) and occurs when there is significant infiltration or evapotranspiration, which drives water to move in a vertical direction. The conductivity in the unsaturated zone is a function of the moisture content and ranges from 8.6E-06 m/d, when the residual water content is 0.10 of the saturated conductivity, to 8.6E-03 m/d, when the pores are filled with water. Once the unsaturated zone becomes saturated, the flow is three dimensional and the predominant direction of flow is in the horizontal direction (Figure 20b). At the interface of the saturated and

unsaturated zones, however, the water table fluctuates over time and dissolved and sorbed contaminants are transferred between the zones. The contaminant which moved downward to the saturated zone may therefore return to the unsaturated zone at another point due to these water table fluctuations (Figure 20c).

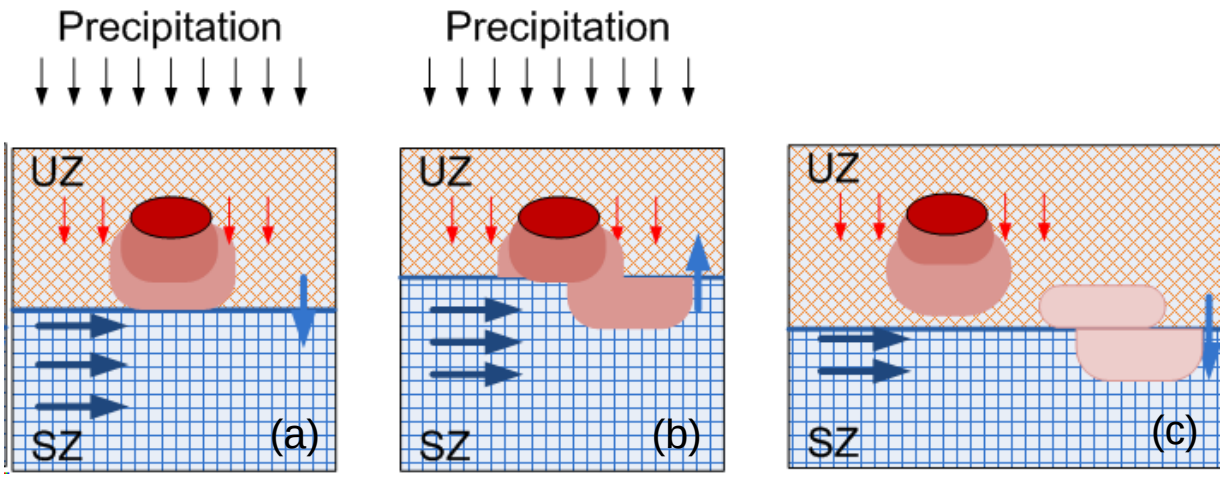

Figure 20. Conceptual diagram of contaminant transport in the unsaturated zone for a variable water table.

Table 8. Saturated Zone Soil Profile Definition

	Lower level, m	Thickness, m	Longitudinal Dispersivity, m	Transverse Dispersivity, m
Layer SZ1	-3	3	0.07[2]	0.001
Layer SZ2	-10	10	0.07	0.001
Layer SZ3	-50	50	0.07	0.001
Layer SZ4	-100	50	0.07	0.001
Layer SZ5	-150	50	0.07	0.001
Primary effective porosity = 0.1[3&2], Secondary effective porosity = 0.05[3], Soil bulk density = 1700[1] Kg/m^3, Specific yield = 0.2, Specific storage = 0.0001 1/m				
[1] UEFPC RI Report, 1998, Table E. 9.3 (DOE/OR/0l-16411V 4&D2) [2] Tang et al., 2010 [3] Martin Marietta Systems, Inc., 1995 [4] Groundwater table contours are extracted from OREIS database				

To improve the prediction of transport processes in fractured rock, a dual porosity model, was

incorporated. This required additional information about an empirical transfer coefficient between primary and secondary porosity. At higher values of the mass transfer coefficient, the solute diffusion occurs at a faster rate which causes a slower attenuation of the peak in a concentration break through curve. The SZ includes adsorption/desorption and decay processes. The model allows input of distributed and time dependent parameters for dispersion in each of the four domains (OL, SZ, UZ, OC) using GIS file formats.

The sorption in the unsaturated and saturated zones was represented as an equilibrium or kinetic equilibrium process using linear or nonlinear (Freundlich, Langmuir) sorption isotherms. Experimental work conducted at FIU with the predominant oxidation form, Hg^{2+}, has determined the soil/water partitioning coefficient of mercury to be 0.5±0.1 m^3/kg [40]. The initial contaminant concentrations were entered in the mobile and/or immobile phases and can be either fully distributed or spatially varied for discrete levels. This provides a flexible approach for entering initial concentrations.

The flow in the saturated zone requires information about the geological layers within the domain. Each layer was entered using GIS data files (grid, shapefile, ASCII) providing its lowest elevation and information such as the spatial variability of horizontal hydraulic conductivity, vertical hydraulic conductivity, specific yield, specific storage, primary and secondary porosity, and bulk density. For more accurate description of the subsurface, geological lenses, which have a limited horizontal extent, were incorporated into the model domain. GIS grid files were created for the hydraulic conductivity values of 5 geological layers based on the data provided in Appendix A of the "Decision Document for Performing a Long-Term Pumping Test at the S-3 Site, Oak Ridge Y-12 Plant, Oak Ridge, Tennessee", a report submitted by Martin Marietta Energy Systems, Inc. to US DOE in 1995 [41]. The hydraulic conductivity maps used for the SZ layers (Table 8) are shown in Figure 21.

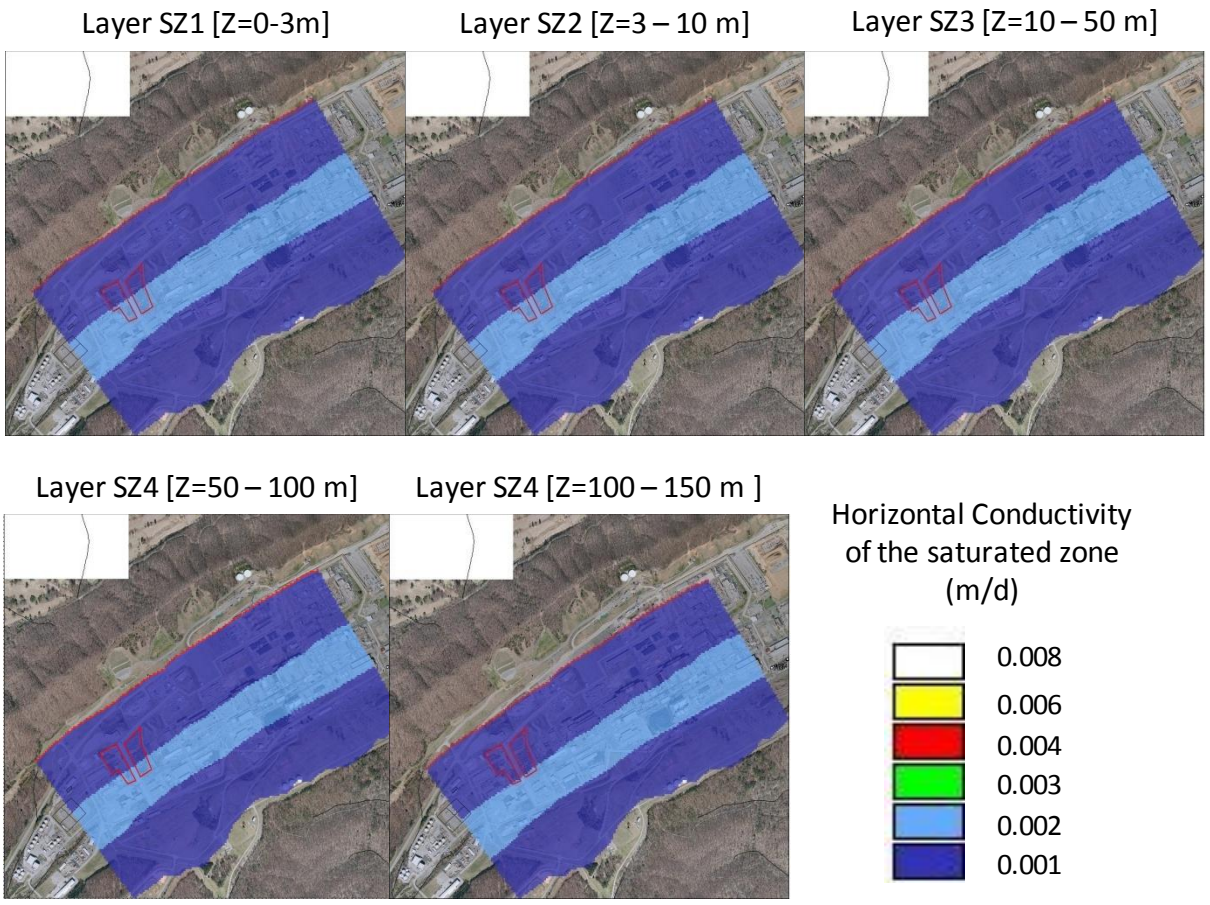

Figure 21. Discretized hydraulic conductivities (layer SZ1 through SZ5) used in the numerical model.

3.3 Flow Calibration

The flow was calibrated using USGS records for discharges in EFPC streams. The model was first calibrated for the entire EFPC watershed and the hydraulic parameters were obtained from this calibration. Figure 22 shows the locations of the USGS stations which provided observed timeseries of daily discharges.

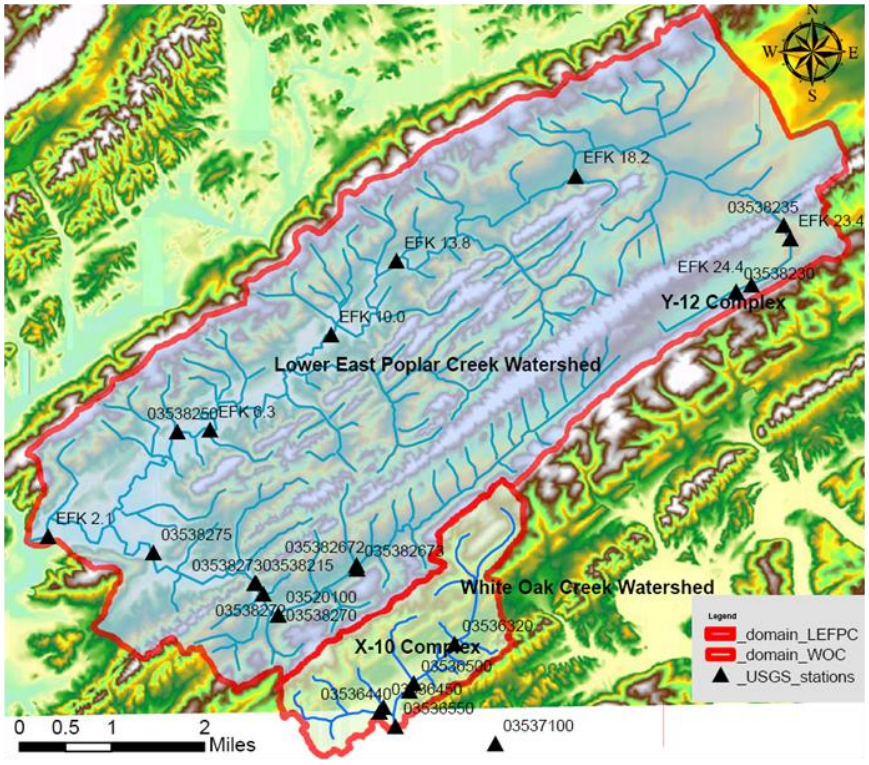

Figure 22. USGS stations used for calibration of discharges in EFPC streams.

This calibration included Manning's number for overland and river flow, hydraulic conductivities (vertical and horizontal) and a range of other parameters required by the MIKE-SHE and MIKE-11 modules. The hydrologic parameters were varied until the best match was obtained between computed and observed data. Figure 23 compares the computed data (black lines at Station EFK 6.3) with the recorded data (blue lines at Station 03538250).

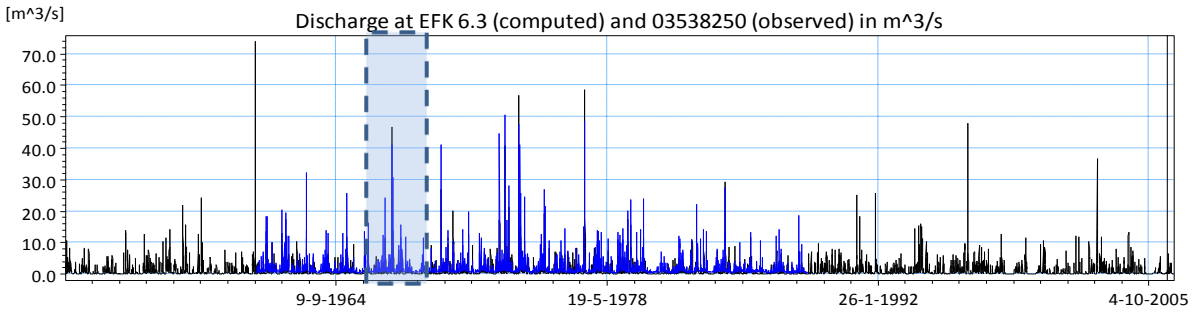

Figure 23. Timeseries of computed discharges (units in m^3/s).

A section of Figure 23 is shown in greater detail in Figure 24. The figure shows a close match

between observed and computed discharges at Station 03538250.

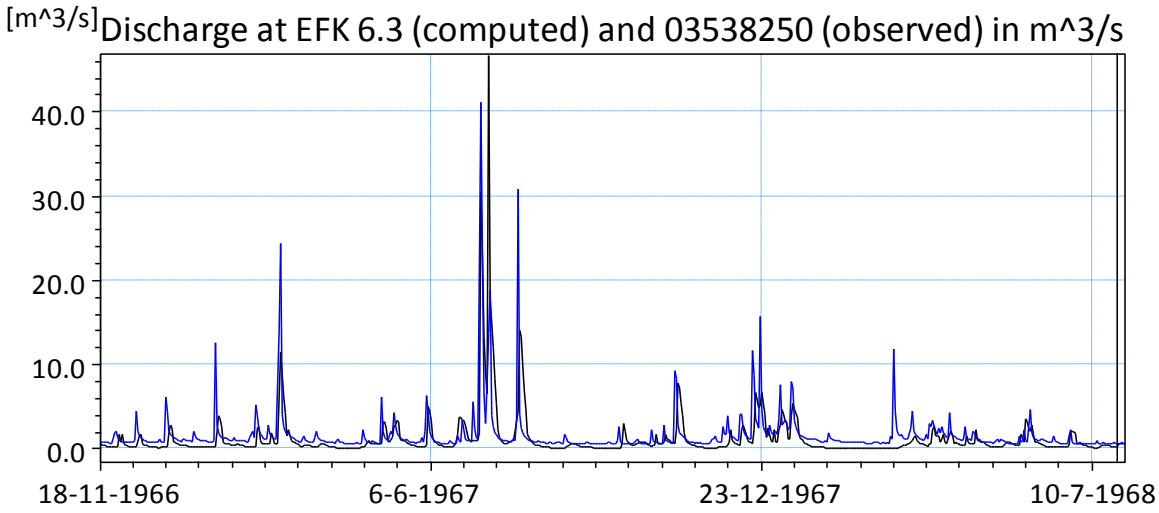

Figure 24. Time series of computed discharges (section A of Figure 23).

The model was calibrated in more detail for the upper section of EFPC. The computed flow is compared with the recorded flow at Station 17 (EFK 23.4) in Figure 25.

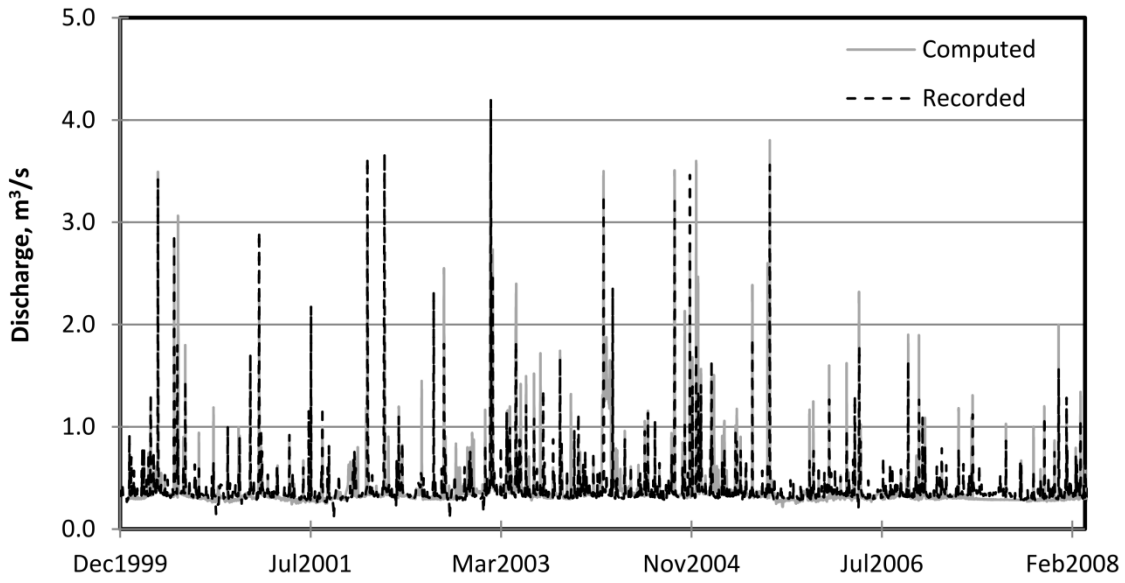

Figure 25. Comparison of computed and observed discharge at Station 17 (EFK 23.4).

3.4 Sediment Transport Calibration

The numerical model was calibrated for the sediment transport using an extensive collection of historical records of total suspended solids (TSS) in the creek water recorded at key stations along EFPC. For calibration purposes, four parameters were considered in the ECOLAB module that directly affect the concentration of TSS in the water column; critical current velocity (Vc), settling velocity (Vs), resuspension rate (RR), and particle production rate (PPR). Simulations were performed for a range of these parameters and sensitivity and uncertainty analyses conducted for each parameter from which the best values were selected. The sensitivity analysis on these parameters is shown in Figure 26.

In Figure 27, the recorded TSS load is compared with the numerical simulation results at Station 17 (EFK 23.4). The TSS load is calculated by multiplying the concentration of TSS by the discharge at a particular time.

3.5 Mercury Transport Calibration

The most important parameters in calibration of mercury transport were the carbon partitioning and diffusive transport coefficients, as well as the effective parameters on sediment transport which were mentioned earlier in Section 3.4. The computed mercury concentration at Station 17 (EFK 23.4) is compared with the recorded timeseries in Figure 28.

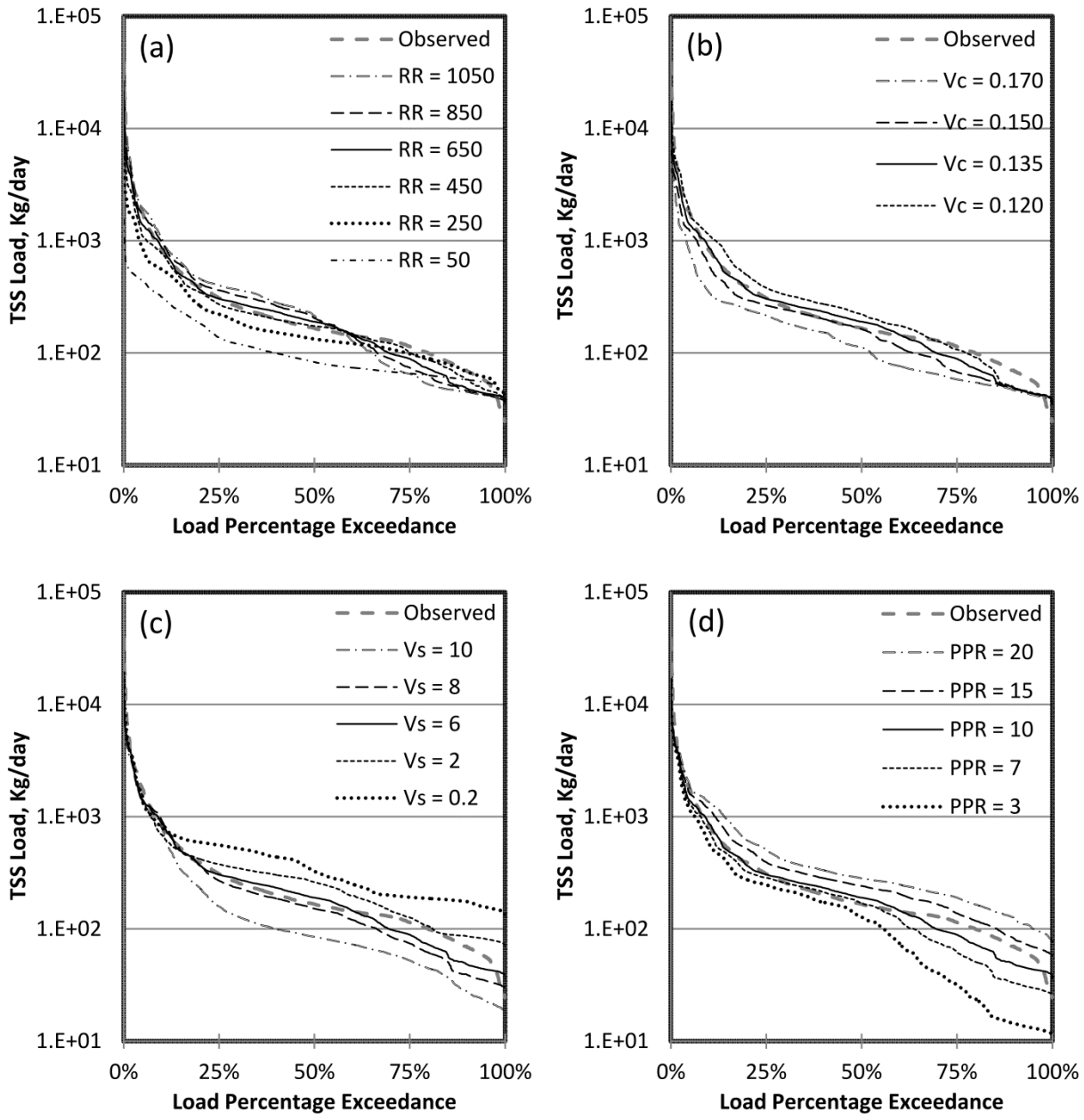

Figure 26. Sensitivity analysis on TSS load for effective parameters: (a) resuspension rate, g/m^2/day, (b) critical current velocity, m/s, (c) settling velocity, m/day, (d) particle production rate, g/m^2/day.

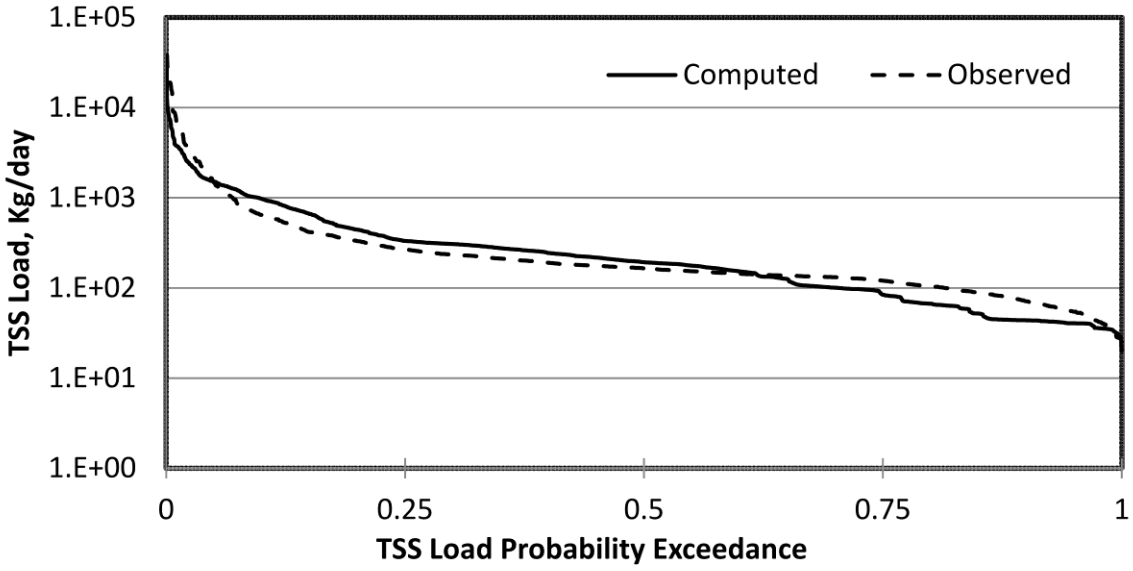

Figure 27 computed and recorded TSS load at Station 17 (EFk 23.4)

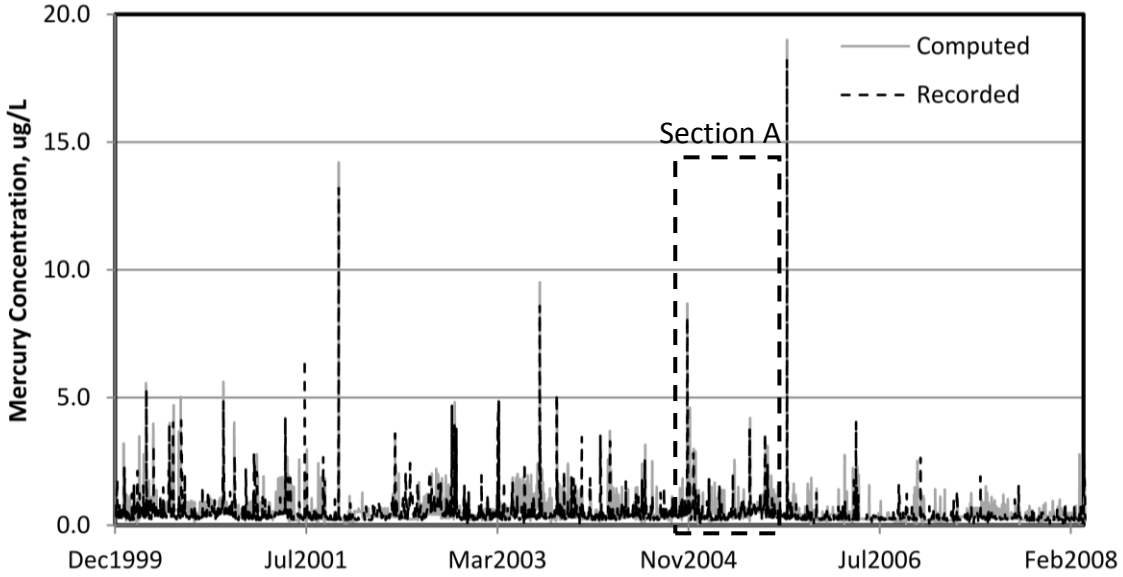

Figure 28. Comparison of computed and observed mercury concentration at Station 17 (EFK 23.4).

A section of Figure 28 is shown in greater detail in Figure 29. The figure shows a close match between observed and computed mercury concentration at Station 17 (EFK 23.4).

Based on the numerical results, it is clear that most of the mercury in the creek is in a form that

is sorbed to the suspended particles. As shown in Figure 30, more than 75% of the total mercury is adsorbed and only 25% is in the form of dissolved mercury. This was confirmed by field investigations performed by ORNL in the latter 2000's [7, 8]. This highlights the significance of suspended particles in affecting the total mercury concentration in the creek.

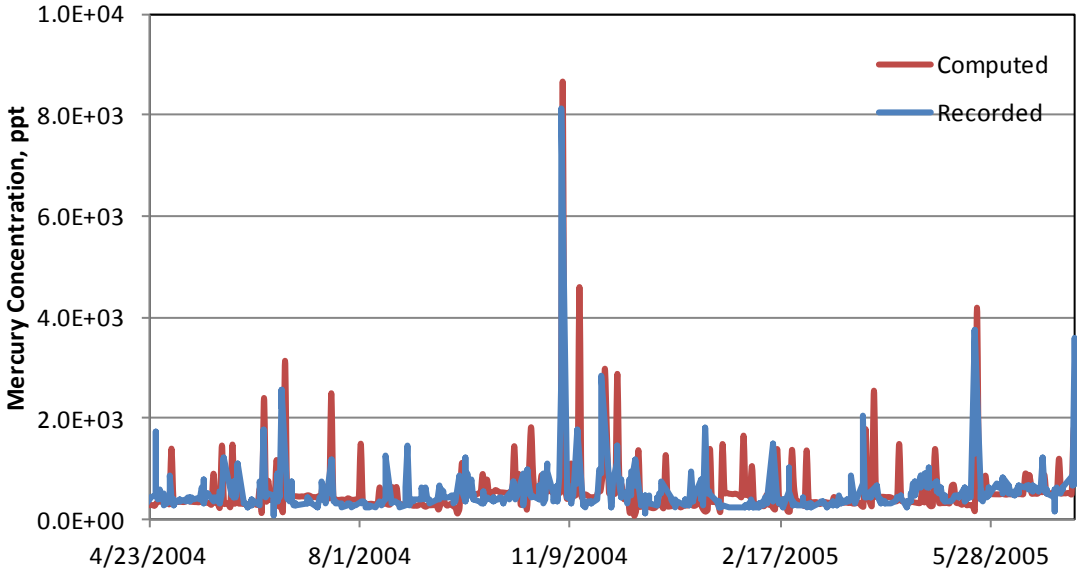

Figure 29. Timeseries of computed and observed mercury concentration (section A shown in Figure 28).

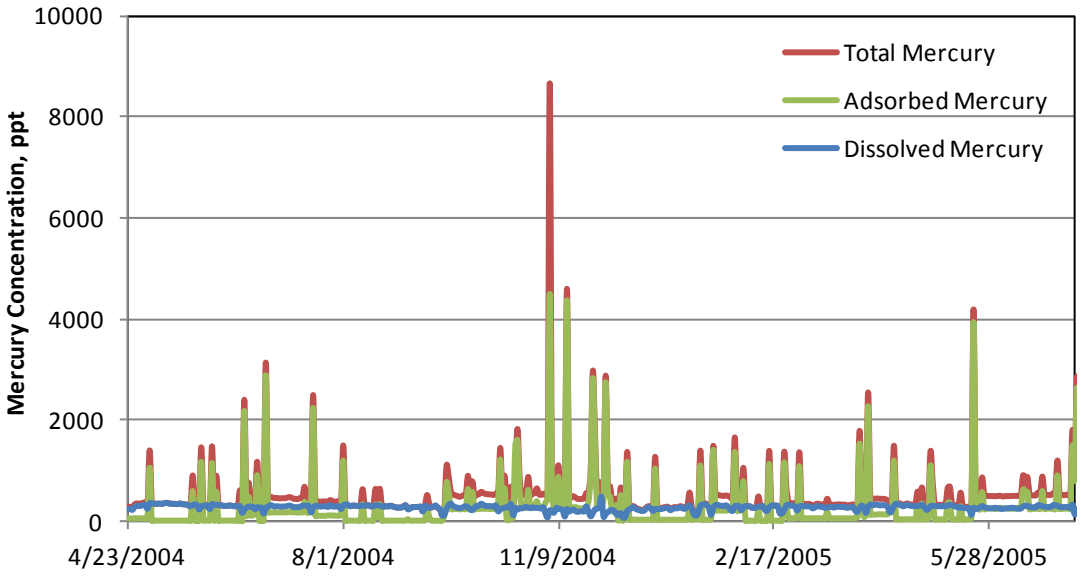

Figure 30. Comparison between numerical results for the adsorbed and dissolved mercury timeseries in the creek at Station 17 (EFK 23.4).

There is limited water quality data available at Station EFK 6.3 in EFPC. The computed timeseries is compared with the few data points available for mercury concentration at EFK 6.3 in Figure 31.

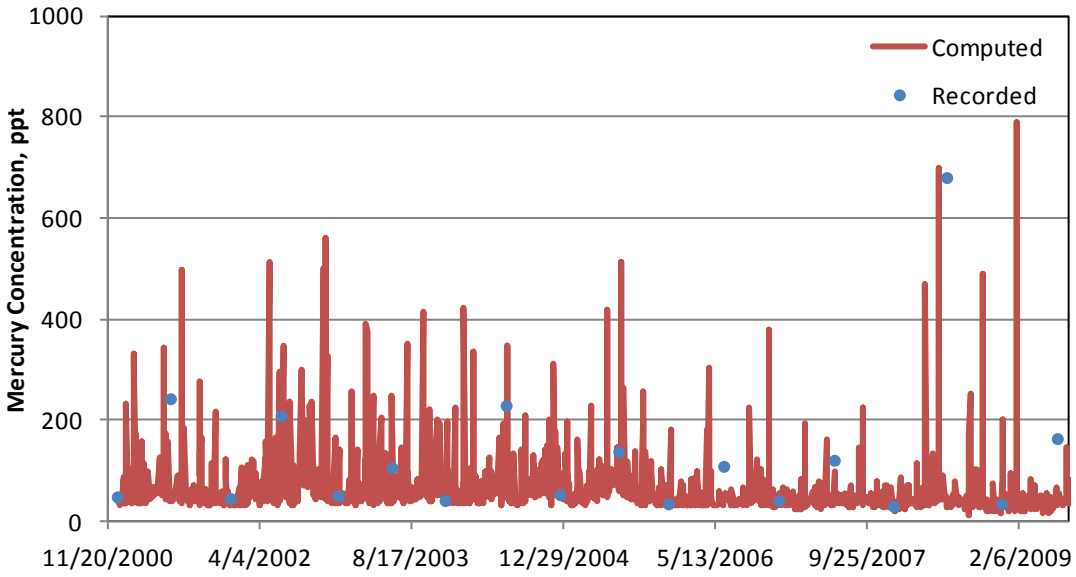

Figure 31. Timeseries of computed and observed mercury concentration at EFK 6.3.

In order to assess the significance of sediment transport on the fate and transport of mercury within UEFPC, numerical simulations were performed for two different cases; with and without consideration of sediment-mercury interactions. Computed mercury load duration curves at Sta. 17 for the period 2000-2009 were compared with corresponding historical records for both scenarios (Figure 32).

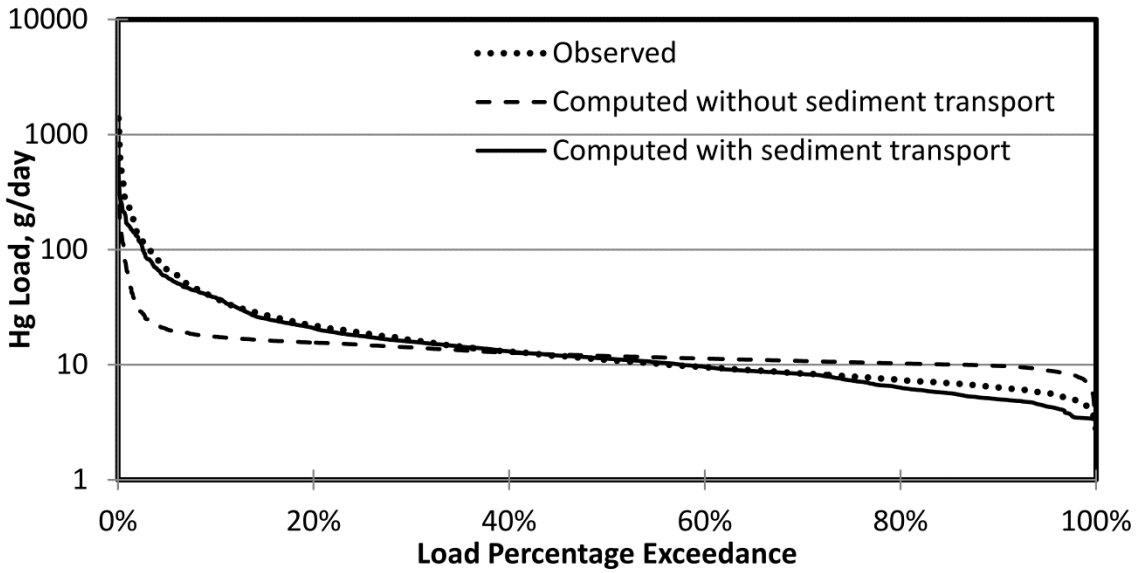

Figure 32. Mercury load duration curves at Station 17 (EFK 23.4).

As shown in Figure 32, sediment-mercury interactions significantly affect the concentration of mercury recorded at Station 17 (EFK 23.4). Higher velocity during the wet seasons increases the shear stress on highly contaminated streambed sediments, and therefore, through a process often called “colloidal transport”, resuspends more mercury-laden fine particulates.

4 WATER QUALITY ASSESSMENT AND TMDL TARGET

The State of Tennessee's final 2008 303(d) list [9] was approved by the U.S. Environmental Protection Agency (EPA), Region IV in June of 2008. This list identified portions of East Fork Poplar Creek in the Lower Clinch River Watershed as not supporting designated use classifications due, in past, to mercury. Table 9 depicts the impairment regions and sources as documented by TDEC and approved by EPA.

Table 9. Final 2008 303(d) List for Mercury Impaired Waterbodies - East Fork Poplar Creek Subwatershed [9, 13]

Waterbody ID	Impacted Waterbody	Miles Impaired	Cause/ TMDL Priority	Pollutant Source	Comments
TN0601020 7026 – 1000	EFPC (from Clinch River embayment to Gum Hollow Rd.)	9.7	PCBs / L Mercury / L Escherichia coli / NA Loss of biological integrity due to siltation / M Nitrates / M Phosphates / M	Industrial Point Source Municipal Point Source Contaminated Sediments Collection System Failure High Density Municipal Area	Impacted by releases at DOE's Oak Ridge facilities (K-25, Y-12, and ORNL). Fishing advisory due to mercury and PCBs. Bacteria levels are also elevated due to sources in the Oak Ridge area. Category 5. Impaired, but EPA has approved a pathogen TMDL that addresses some of the known pollutants. EPA should develop the TMDL for pollutants originating from DOE facilities.
TN0601020 7026 – 2000	EFPC (from Gum Hollow Rd. to headwaters)	11.3	PCBs / L Mercury / L Escherichia coli / NA Loss of biological integrity due to siltation / M Nutrients / M Other Anthropogenic Habitat Alterations / M	Industrial Point Source Contaminated Sediments High Density Municipal Area	Same as above. Stream is Category 5. Impaired, but EPA has approved a pathogen TMDL that addresses some of the known pollutants. EPA should develop the TMDL for pollutants originating from DOE facilities.

4.1 Use Classifications of EFPC

The designated use classifications for the EFPC includes fish and aquatic life, irrigation, livestock watering and wildlife, and recreation [17].

4.1.1 Recreational Use

In the case of recreational use, the total mercury concentration of 50 ppt in surface water has been suggested by TDEC, EPA, and DOE. The mercury water quality criteria for protection of recreational use surface waters, is established by the State of Tennessee Water Quality Standards, Chapter 1200-4-3, General Water Quality Criteria, June 2008 [19], Section 1200-4-3-.03 (4) (j). The TDEC water quality document [19] has suggested water quality criteria associated with inorganic compounds for recreational-use surface waters .

Table 10. Water Quality Criteria for Toxic Inorganic Substances in Recreational-use Surface Waters suggested by TDEC[19]

Inorganic Compound	Water & Organisms Criteria (ppb)	Organisms Only Criteria (ppb)
Antimony	5.6	640
Arsenic	10	10
Mercury	0.051	0.051
Nickel	610	4600
Thallium	0.24	0.47
Cyanide	140	140

4.1.2 Fish and Aquatic Life

The State of Tennessee Water Quality Standards, Chapter 1200-4-3, General Water Quality Criteria, June 2008, Section 1200-4-3-.03 (3) (g) [19] has suggested water quality criteria for the protection of fish and aquatic life from toxic inorganic substances. As shown in Table 11, TDEC suggested the total concentration of 0.77 ppm for the mercury to protect the Fish and aquatic life.

4.1.3 Irrigation, Livestock Watering and Wildlife

When compared to the other usage classifications, the irrigation, livestock watering and wildlife water quality criteria designated by TDEC has been unclear. . The State of Tennessee Water Quality Standards, Chapter 1200-4-3, General Water Quality Criteria, June 2008 [19], Section 1200-4-3-.03 (5) (f) and Section 1200-4-3-.03 (6) (f) states that, "The waters shall not contain toxic substances whether alone or in combination with other substances which will produce toxic conditions that adversely affect the quality of the waters for irrigation."

Table 11. Water Quality Criteria Suggested by TDEC for the Protection of Fish and Aquatic Life from Toxic Inorganic Substances [19]

Compound	Criterion Maximum Concentration (ppm)	Criterion Continuous Concentration (ppm)
Chromium, III	570	74
Chromium, VI	16	11
Copper	13	9.0
Compound	Criterion Maximum	Criterion Continuous
Lead	65	2.5
Mercury	1.4	0.77
Nickel	470	52
Selenium	20	5
Silver	3.2	---
Zinc	120	120
Cyanide	22	5.2
Chlorine (TRC)	19	11

4.1.4 Fish Tissue

Mercury concentrations of approximately 2 mg/kg in fish tissue were first reported by ORNL in 1982 [23]. EPA's current recommended 304(a) water quality criterion for methylmercury [22] is expressed as a fish tissue concentration value (0.3 milligrams methylmercury per kilogram of wet-weight fish tissue, or 0.3 mg/kg). The EPA believes that a fish tissue residue water quality criterion for methylmercury is more appropriate than a water column-based water quality criterion. EFPC was placed on the State's 303(d) 2008 List based on fish tissue concentrations.

4.2 Water Quality Criteria and TMDL Target

In Table 12, the target concentration values for mercury suggested by TDEC [19] for each surface water usage classification are compared.

Table 12. Water Quality Criteria for Mercury Suggested by TDEC for Different Usage Classifications of Surface Waters

Usage Classification	Mercury Concentration (ppt)
Recreation	51
Fish and aquatic life	770
Irrigation	Not any specific numeric target
Livestock watering and wildlife	Not any specific numeric target

In this TMDL analysis, of the use classifications with numeric criteria for mercury, the recreational use classification is the most stringent and will be used to establish target levels for TMDL development [18].

In EFPC, early remedial actions on source isolations near the Y-12 NSC in the latter 1980's and early 1990's reduced mercury release to the creek, and therefore, reduced the mercury contamination in both the water and fish tissue. The total mercury concentration in water decreased from approximately 1 ppm to 0.5 ppm and concentration in the fish tissue decreased from approximately 2 ppb to 0.6 ppb in the upper reach between the mid 1980's and 2005. This trend demonstrated clear progress toward reducing mercury concentrations in fish tissue that would be protective of humans consuming the fish. At sampling locations further from facility discharges, however, a more complex pattern has been documented – total mercury concentrations in the water decreased as a result of remedial actions (from 1 ppm to approximately 0.4 ppm), but concentrations in the fish remained relatively stable (approximately 0.8 ppb). Follow-up research has documented the importance of mercury speciation to the observed concentrations in fish tissue. Fish tissue concentration is related to methylmercury (rather than total mercury) and differences in the trends in time and space are ultimately explained in terms of complex, interrelated and interacting transport and transformation processes [18]. Following these observations, fish tissue concentration has also

been taken into consideration by Comprehensive Environmental Resources Compensation and Liability Act (CERCLA) and DOE. This TMDL analysis however, has not been performed based on this criterion as it has not yet been completely defined for this target..

4.3 Water Quality Assessment of EFPC

Mercury concentration data for the stations along EFPC were extracted from the OREIS database. After an initial study of the data, stations with less than 3 data points and stations with data for a very short period of time (less than a few months) were removed from the database, resulting in14 stations along EFPC being selected for use in verification of the numerical simulations and performing TMDL analysis. The 14 stations are shown in Figure 33.

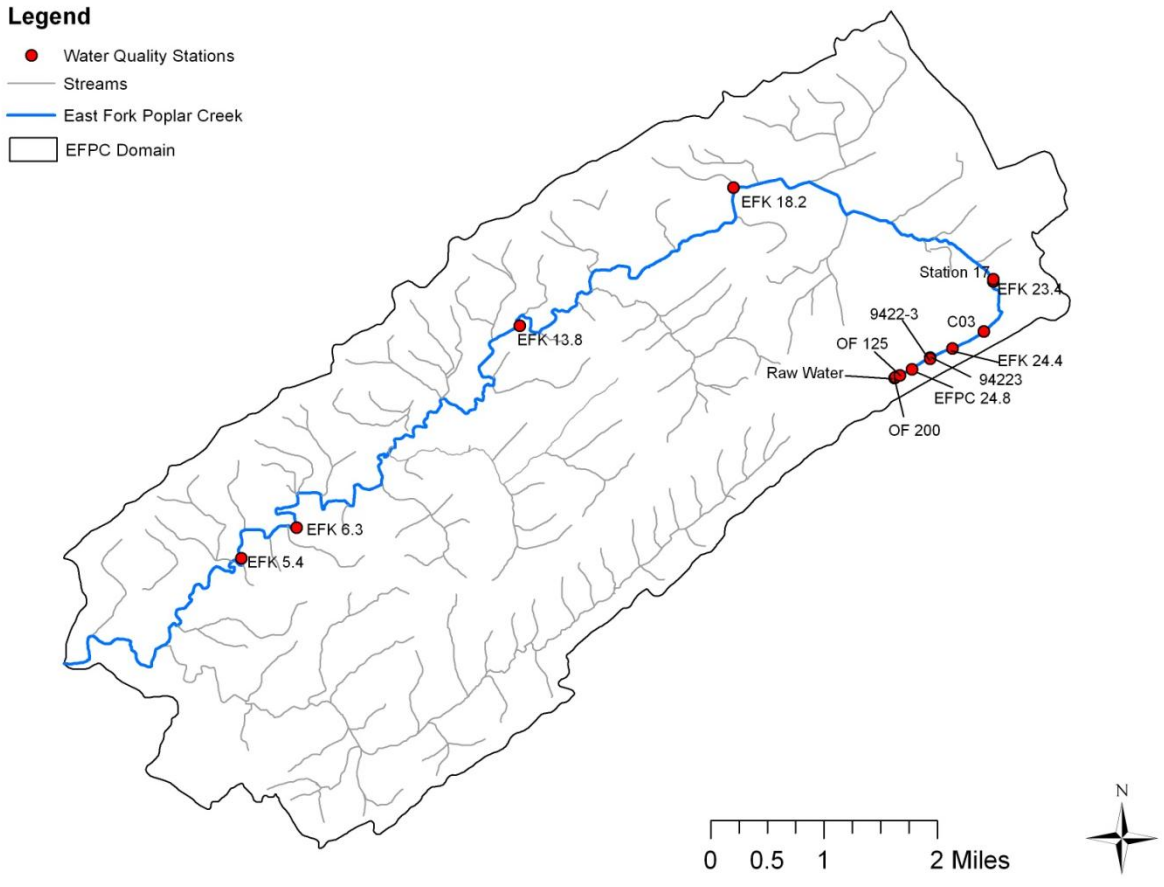

Figure 33. Water quality monitoring stations along EFPC.

The Raw Water station shown in Figure 33 at the outset of the creek is uncontaminated

management water which was purchased by the Y-12 NSC facility from the city of Oak Ridge in 1997 to maintain a daily average flow of 7 MGD at Station 17 in accordance with the 1996 NPDES permit (TN0002968). The augmented water is pumped from the Melton Hill Lake on the Clinch River and discharged to the creek adjacent to Outfall 200 (OF200) at a constant rate of 4.5 MGD [26].

Examination of the water quality data shows exceedances of the 50 ppt maximum mercury concentration standard at all of the monitoring stations along EFPC. Characteristics of water quality data following the data analysis are summarized in Table 13.

Table 13. Summary of Water Quality Monitoring Data

Station	Data Pts.	Date Range	Min., ppt	Mean, ppt	Max., ppt	Exceed WQ Max. Target Pts. (50 ppt)
OF125	347	12/00 – 12/10	200.6	704.8	27,777	347
94223	1353	01/92 – 08/10	200.5	1009.6	15,000	4308
EFK 24.4	20	05/96 – 12/10	235.6	456.5	1927.2	12
EFK 23.4	4308	01/92 – 12/10	200.7	741.6	11,000	347
EFK 18.2	12	11/96 – 12/10	206.0	294.1	430.4	1353
EFK 13.8	10	11/96 – 12/10	213.8	323.3	458.4	20
EFK 6.3	9	12/00 – 12/10	201.4	442.6	1346.2	4308

Annual average concentrations of total mercury at different stations are summarized in Table 14. Values show a continuous decrease in concentration following the remedial actions that started since the mid 1990's; however, there is an increase after 2002 in OF125, EFK 24.4, EFK 23.4, and 92334. This might be the consequence of augmenting the flow at OF200 which resulted in resuspension of highly contaminated bed sediment to the creek water as reported in field investigations. The average total concentration of mercury at all stations downstream of OF200 however, is still above the State of Tennessee water quality standard of 51 ppt. Variations of total mercury concentration at different stations along the creek from 1992 to

2010 are compared in Figure 34.

Table 14. Concentrations of Total Mercury at Different Stations along EFPC in ppt

YEAR	OF 125	94223	EFK 24.4	EFK 23.4	EFK 18.2	EFK 13.8	EFK 6.3
1992		1159.87		1498.59			
1993		1075.86		1205.39			
1994		1166.38		1231.82			
1995		1134.52		1292.94			
1996		977.46		768.31	206.00		
1997		648.46		740.56			
1998		637.78		1072.99			
1999		525.00		647.54			
2000		500.00	316.00	543.13			
2001		339.64	341.90	474.75	370.95	392.09	465.67
2002	508.20	574.77	423.40	615.55	282.90	346.20	400.30
2003	1787.15	974.15	1168.35	521.73	209.90		
2004	886.78	572.43	382.40	529.73	430.40	450.40	443.00
2005	688.10	591.10	461.95	526.38	415.00	389.95	251.50
2006	313.16	1165.50	348.93	347.30	280.70	225.25	201.40
2007	285.43	1165.50	312.90	324.98	279.00	230.30	223.50
2008	343.92	1070.00	259.05	383.47	339.05	458.40	1346.20
2009	618.59	552.50	484.93	374.47	236.73	280.00	315.05
2010	395.18	1010.00	365.00	541.03	230.70	234.80	336.70

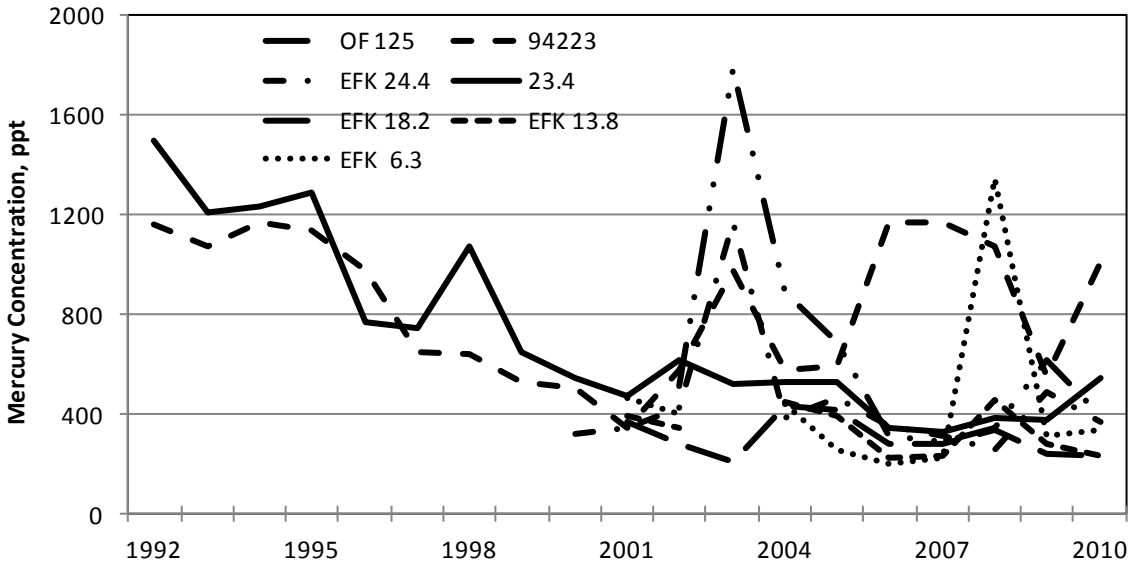

Figure 34. Variation of average mercury concentration at the stations along EFPC.

5 DEVELOPMENT OF TOTAL MAXIMUM DAILY LOADS

Total Maximum Daily Load (TMDL) is a regulatory term defined in section 303 (d) of the 1972 U.S. Clean Water Act (CWA) as the maximum amount of a pollutant that a body of water can receive while still meeting water quality standards [1]. Alternatively, a TMDL is defined as the allocation of a particular pollutant as acceptable to receiving waters [2]. This includes both point and non-point pollutant sources within a watershed. The TMDL concept has long been used by the United States Environmental Protection Agency (EPA) and state environmental agencies (such as the Tennessee Department of Environment and Conservation [TDEC] in the case of Oak Ridge watersheds) in implementing the CWA by establishing maximum pollution limits for industrial wastewater dischargers. EPA published regulations in 1992 establishing TMDL procedures [3].

A TMDL is the sum of all point source loads (Waste Load Allocations, WLAs), non-point source loads and natural background (Load Allocations, LAs) [3], with a margin of safety (MOS) that takes into account any uncertainty about the relationship between pollutant loads and receiving water quality [1], and can be generically described as [5]:

$$TMDL = \Sigma WLA + \Sigma LA + MOS \quad (1)$$

The objective of a TMDL analysis for EFPC is to allocate loads among pollutant sources that are contributing to the watershed impairment, and thereby, to implement appropriate control measures to achieve water quality standards. This document describes TMDL, Waste Load Allocation (WLA), and Load Allocation (LA) development for EFPC which has been identified as impaired due to mercury on the Final 2006 303(d) List. In this document, TMDLs are expressed as the percentage reduction required to maintain the desired mercury concentration target levels in fish tissue. WLAs and LAs are also expressed as required percentage reductions in mercury loading.

The TMDL for EFPC was developed based on the analysis of water quality data. Concentration of mercury in the water of EFPC from 1992 was examined, but load reductions were estimated

based on more recent data (1992 to the present). The percentage load reduction required to decrease the mercury concentration in water from the "mean + 95% confidence interval" to the desired target level was calculated at each sampling location. Load reductions ranged from 84.6% to 95.1%. The highest percentage load reduction (at location 92334) was selected as the TMDL for the entire waterbody. A summary of monitoring data of mercury concentration in water from 1992 to 2010 is presented in Table 15.

Table 15. Analysis of Mercury Concentration in Creek Water (2000 - Present)

	OF125 ppt	C11 ppt	92334 ppt	EFK 23.4 ppt	EFK 24.4 ppt	EFK 18.2 ppt	EFK 13.8 ppt	EFK 6.3 ppt
Number of samples	347	108	1353	4308	20	12	10	9
Minimum	200.6	210.0	200.5	200.7	235.6	206	213.8	201.4
Mean	704.85	389.02	1009.58	741.64	456.52	294.15	323.26	442.59
Standard Deviation	1861.16	413.86	693.53	780.56	356.82	77.72	95.42	351.60
95% CI	195.82	78.05	36.95	23.31	156.38	43.98	59.14	229.71
Mean + 95% CI	900.68	467.07	1046.53	764.95	612.89	338.13	382.41	672.30
90% CI	164.34	65.50	31.01	19.56	131.24	36.90	49.63	192.78
Mean + 90% CI	869.20	454.52	1040.59	761.20	587.75	331.06	372.90	635.37
Target	51	51	51	51	51	51	51	51
%Reduction from 90%	94.1%	88.8%	95.1%	93.3%	91.3%	84.6%	86.3%	92.0%
%Reduction from 95%	94.3%	89.1%	95.1%	93.3%	91.7%	84.9%	86.7%	92.4%
Note: The % Reduction from 95% is calculated as follows: % Reduction = [(Mean + 95% CI) - Target] / (Mean + 95% CI). **The % Reduction from 90% is calculated in a similar manner.**								

5.1 Margin of Safety

There are two methods for incorporating MOS in TMDL analysis: a) implicitly incorporate the MOS using conservative model assumptions; or b) explicitly specify a portion of the TMDL as the MOS and use the remainder for allocations [5]. For development of the mercury TMDL in EFPC, an implicit MOS was utilized for determination of WLAs and LAs. The conservative assumption is that the TMDL was selected based on the percentage load reduction from the worst-case stretch of EFPC (Station 92334). This approach assumes that the mercury concentration is the same along EFPC and equals the highest concentration recorded at OF125.

5.2 Determination of TMDL, WLAs and LAs

Mercury load reductions were calculated for impaired segments of EFPC based on an analysis of mercury concentration in water. WLAs and LAs were determined based on currently available information. WLAs for existing STPs are equal to their existing NPDES permit limits. No additional load reduction is required at this time. Based on currently available data, treated wastewater and groundwater from the Y-12 facility are the only known point sources for mercury in the EFPC watershed. Therefore, a WLA equal to the TMDL should be assigned to the Y-12 facility. Due to lack of adequate data regarding non-point sources, a LA equal to the TMDL has also been assigned. TMDL, WLAs, and LAs are summarized in Table 16.

Table 16. TMDL, WLAs, and LAs for EFPC in the Lower Clinch River Watershed

Waterbody ID	Impacted Waterbody	Miles Impaired	TMDL % Reduction	WLAs % Reduction	Las % Reduction
TN06010207026 – 1000	EFPC (from Clinch River embayment to Gum Hollow Rd.)	9.7	95.10%	95.10%	95.10%
TN06010207026 – 2000	EFPC (from Gum Hollow Rd. to headwaters)	11.3	95.10%	95.10%	95.10%

5.3 Flow Duration Curves

As a first step in developing load duration curves, flow duration curves need to be generated. Flow duration analysis looks at the cumulative frequency of historic flow data over a specified period for a particular location. A flow duration curve relates flow values to the percent of time those values have been equaled or exceeded. This includes the following steps [4, 11].

5.3.1 Extracting the Historical Flow Data

Flow data for riverine systems in the United States is available from a number of sources including the United States Geological Survey (USGS), Water Management Districts (WMDs), and county, city or privately operated gauges. EFPC flow data was mainly obtained from the OREIS database (USGS gauges) provided by Bechtel Jacobs for key stations. The key stations along the creek include Station 17 (EFK 23.4), EFK 18.2, EFK 13.8, and EFK 6.3.

Flow data will be estimated for the other key stations for which there is no flow data availabl. There are two different ways of performing this estimation, (i) using flow data of a similar representative creek, or (ii) using rainfall/runoff models to estimate the flow.

5.3.2 Flow Data Analysis

Before using flow data obtained from the OREIS database for the load duration analysis, a preliminary data analysis was conducted. . This started with simple graphical plots of flow data to evaluate the completeness and consistency of the data visually. Statistical characteristics of flow data at OF125, EFK 24.4, EFK 23.4, EFK 18.2, EFK 13.8, and EFK 6.3 are summarized in Table 17 for the period of 1995 to 2010. Figure 35 shows a comparison of the flow data at Station 17 (EFK 23.4) with the flow data recorded at the other outfalls being studied along with the flow augmentation. This was to ensure that the data follows the normal hydrological pattern (for a specific period of time, adding the upstream flow from upstream sources should result in the total flow in the downstream station). Rainfall does not significantly contribute to the total flow in EFPC, so there was no need to compare the flow at Station 17 with the rainfall patterns. Recorded flow data summarized in Figure 35 shows a consistent trend between the flow

sources and the total discharge in EFPC from 1995 to 2010. There was enough flow data at Station 17 (EFK 23.4) for statistical comparison with computed timeseries data; however, there was insufficient recorded data available for the other stations downstream of Station 17 (i.e. EFK 18.2, EFK 13.8, and EFK 6.3), so other techniques were used to fill the data gaps and create timeseries for these stations. Since there is no outfall beyond Station 17 towards the end of the creek at EFK 6.3, the daily contribution to total flow in the creek was assumed to be from overland flow, groundwater exchange and municipal water outlets to the creek. Therefore, typical statistical or linear interpolation/extrapolation techniques can be used to estimate the flow timeseries at the downstream stations, such as (i) precipitation-runoff relationships; (ii) ratio of drainage area method; (iii) correlation of records from similar gauging stations; (iv) comparison with similar flow duration curves; or (v) some other hydrological synthesis method such as the Markov process or autoregressive models, or moving average models [12].

Table 17. Statistical Characteristics of Flow Data from 1995 to 2010, in m^3/s

	EFK 24.4	EFK 23.4	EFK 18.2	EFK 13.8	EFK 6.3
Number of Data	17	3961	17	18	17
Min	0.14	0.03	0.37	0.41	0.60
Max	0.44	3.81	0.81	1.15	2.07
Mean	0.34	0.34	0.53	0.61	1.08
Median	0.34	0.32	0.49	0.51	0.82
Range	0.30	3.78	0.44	0.74	1.47
Interquartile Range	0.07	0.07	0.13	0.28	0.67
Variance	0.00	0.04	0.02	0.04	0.23
Standard Deviation	0.07	0.21	0.13	0.21	0.48
Coefficient of Variation	0.20	0.60	0.25	0.35	0.44

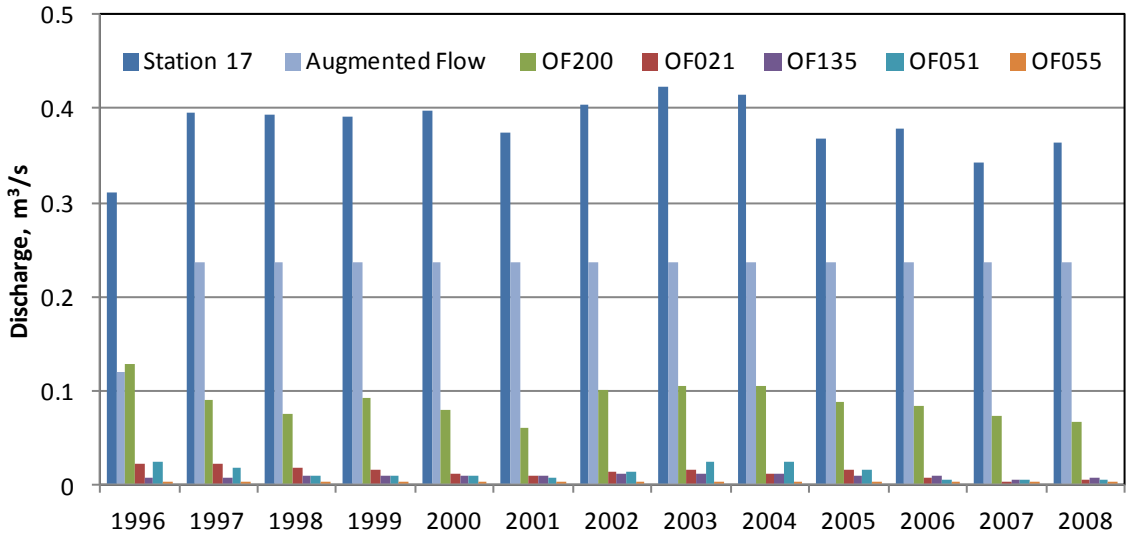

Figure 35. Flow contribution chart for EFPC.

As shown in Figure 35, a major portion of the flow in EFPC originates from the outfall discharges. Figure 35 compares the contribution of major outfalls and augmented flow to the total discharge recorded at Station 17 (EFK 23.4).

The result of the numerical simulation for the total flow at Station 17 solely as a result of flow from the outfalls and flow augmentation is shown in Figure 36a; and the total flow at Station 17 considering the contribution from precipitation (overland runoff) and groundwater exchange is shown in Figure 36b. The contribution of overland flow and groundwater is calculated as the difference between the results shown on Figure 36. The numerical results show that the contribution from the groundwater and overland flow to the total flow recorded at Station 17 (EFK 23.4) is only 11%. Stormwater and wastewater outfalls and flow augmentation produce the largest contributions at 37% and 57%, respectively.

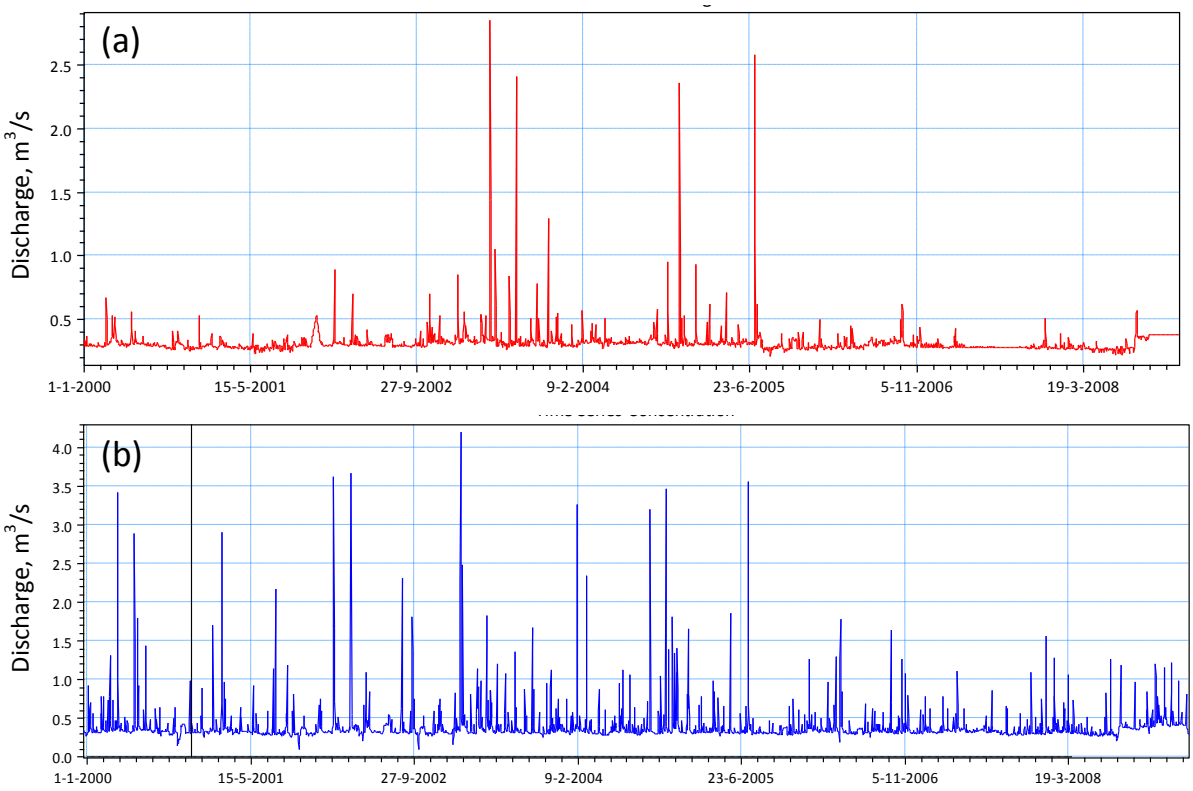

Figure 36. (a) Recorded discharge timeseries from all outfalls with flow augmentation excluding groundwater exchange; (b) Recorded discharge timeseries at Station 17.

5.3.3 Generating the Flow Duration Curves

A flow duration curve for EFPC was constructed from daily flow measurements taken at Station 17 (EFK 23.4) from 1/1/1995 through 12/26/2010. This 15-year period contained a range of hydrologic conditions that included both low and high stream flows. The flow duration curve is shown in Figure 37 and represents the cumulative distribution of daily discharges arranged to show the percentage of time specific flows were exceeded during the period of record (the highest daily mean flow during this period was exceeded 0% of the time and the lowest daily mean flow was equaled or exceeded 100% of the time).

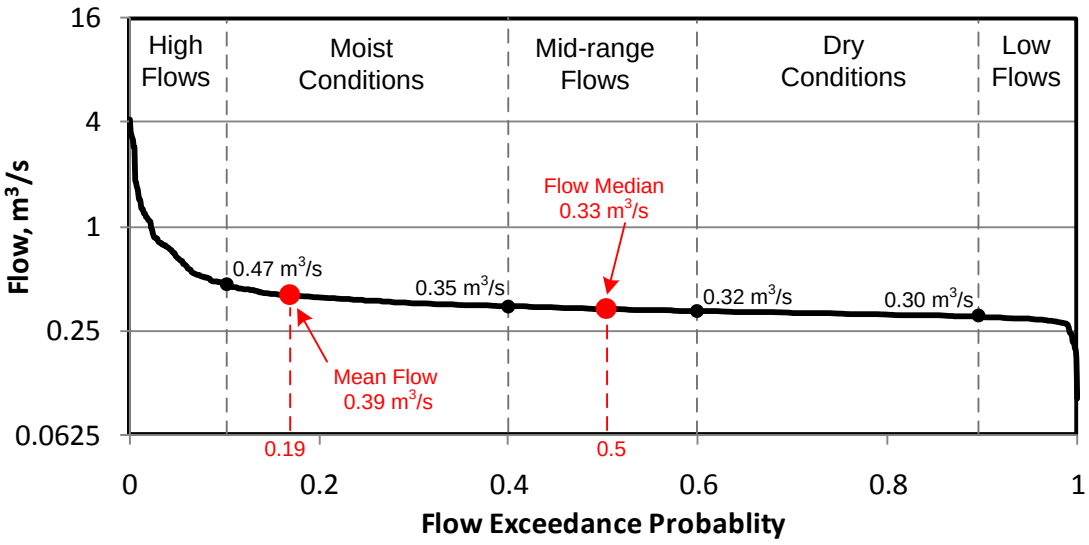

Figure 37. Flow duration curve for Station 17.

In order to provide insight regarding the conditions and patterns associated with creek impairment, flow duration curves are divided into five zones: high flows (0-10%), moist conditions (10-40%), mid-range flows (40-60%), dry conditions (60-90%), and low flows (90-100%), as shown in Figure 37 for the flow duration curve of Station 17. This approach places the midpoints of the moist, mid-range, and dry zones at the 25th, 50th, and 75th percentiles respectively (i.e., the quartiles).

The computed flow duration curve is compared with the observed flow duration curve at Station 17 (EFK 23.4) in Figure 38. The computed and observed mean values are exactly the same up to the second decimal place as shown in Figure 38. The flow duration curves and the mean flow values for groundwater/overland flow, outfalls/augmentation, and total flow at Station 17 (EFK 23.4), are compared in Figure 39.

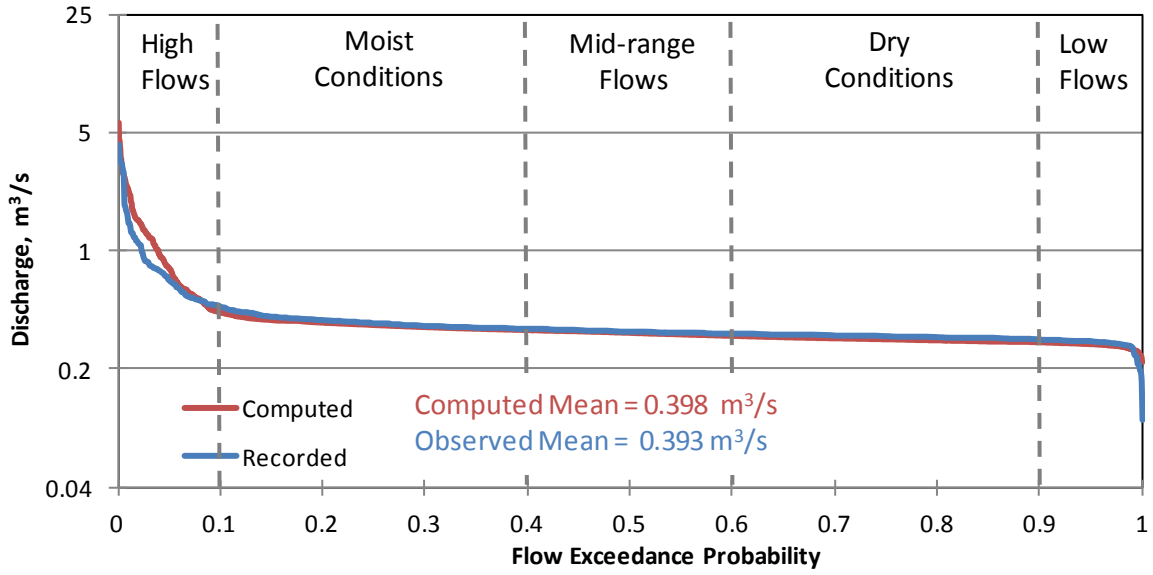

Figure 38. Computed and observed flow duration curves at Station 17 (EFK 23.4).

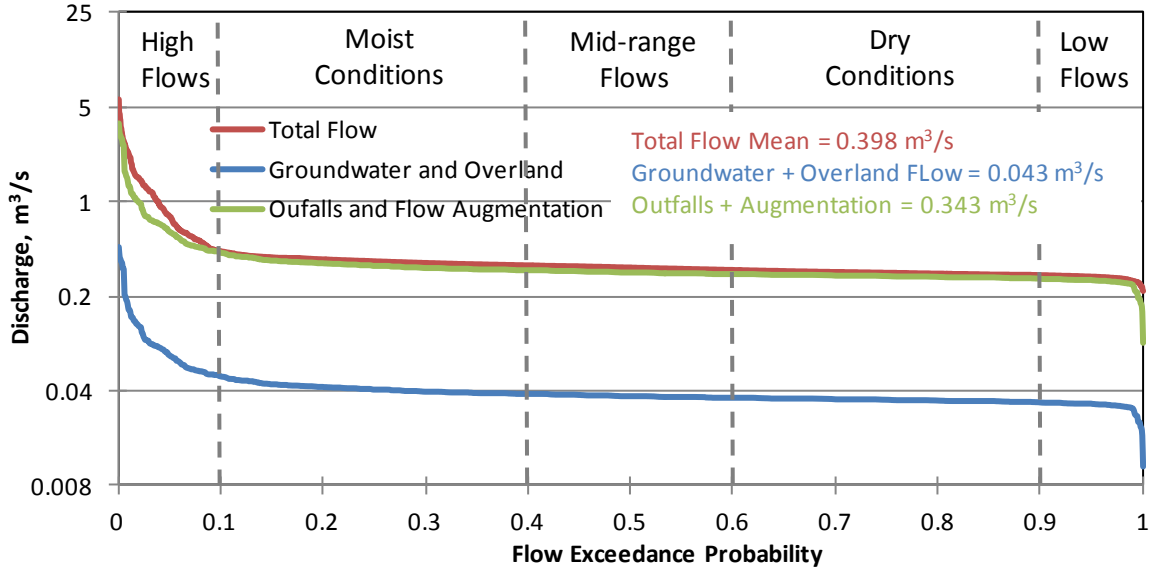

Figure 39. Computed load duration curves for overland flow/groundwater, outfalls/flow augmentation, and total flow at Station 17 (EFK 23.4).

5.4 Load Duration Curves

Instantaneous load values are calculated by multiplying the computed concentration of the contaminant of concern (e.g. mercury) at that particular station (e.g. Station 17) with the corresponding value of the computed flow on the flow duration curve. In other words, concentration of the contaminant of concern, taken with some measure or estimate of flow at the time of sampling, can be used to compute an instantaneous load. Using the relative percentage exceedance from the flow duration curve that corresponds to the stream discharge at the time the water quality sample was taken, the computed load can be plotted in what is called a load duration curve. The x-axis still represents flow duration intervals while the y-axis represents the load values.

The mercury load duration curve for the EFPC was developed from the flow duration curve generated in Section 5.3 (Figure 37) and available water quality monitoring data.

A load duration curve is a cumulative frequency graph that illustrates existing water quality conditions (as represented by loads calculated from monitoring data), how these conditions compare to desired targets, and the portion of the waterbody flow regime represented by these existing loads. The load duration curve was developed using the following procedure:

Step1 – Target Load Duration Curve

This is done in order to specify criteria for the TMDL analyses to evaluate attainment of water quality standards in the waterbody of interest. In general, the target for the TMDL analyses is the numeric water quality criterion for the pollutant of concern for a specified waterbody. In the case of EFPC, the target concentration is defined in Section 4.2 of this report and is based on the detailed description of water uses and regulations established by EPA and TDEC. The numeric water quality targets are translated into TMDLs through the loading capacity. EPA's current regulation defines loading capacity as "the greatest amount of loading that a waterbody can receive without violating water quality standards". The loading capacity provides a reference, which helps guide pollutant reduction efforts needed to bring a waterbody into

compliance with standards [4]. The maximum allowable concentration of mercury in EFPC at Station 17 (EFK 23.4) is defined by EPA and TDEC as 51 ppt. There is also the ROD target of 200 ppt for Station 17 (EFK 23.4) proposed by DOE. A target load duration curve was generated for EFPC by applying the mercury target concentration of 51 ppt to each of the ranked flows used to generate the flow duration curve and plotting the results.

The maximum mercury load target corresponding to each ranked daily mean flow is [(51 ppb) x (Q) x (UCF)], where Q is daily mean flow and UCF is the required unit conversion factor. The same calculation was performed for the ROD target concentration of 200 ppt. The target TMDL for mercury at Station 17 based on these numerical target values was calculated and depicted in Figure 40.

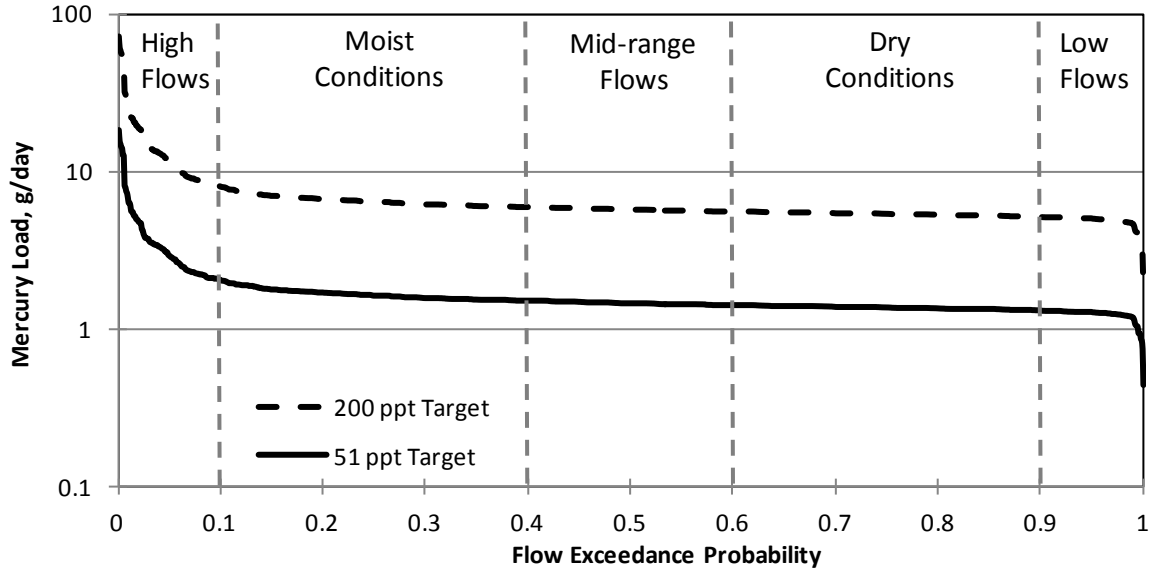

Figure 40. Target TMDL for Station 17.

Step 2 – Calculating Daily Loads

Daily loads were calculated for each of the water quality samples collected at Station 17 (EFK 23.4) by multiplying the sample concentration by the daily flow for the sampling date and the required unit conversion factor.

Step 3 – Calculating Percent of Days the Flow was Exceeded (PDFE)

Using the flow duration curve developed in Section 5.3, the PDFE was determined for each sampling event. Each sample load was then plotted on the load duration curve developed in Step 1 according to the PDFE. The resulting mercury load duration curve is shown in Figure 41 for the observed data at Station 17. In this figure the continuous black line is the 51 ppt water quality target established by EPA and TDEC; the dashed black line is the 200 ppt limit from the measurement technique EPA-245.1 used before 2001 and the ROD water quality target defined for Station 17 (EFK 23.4); and the dashed red line is the 90th percentile for the mercury load under each flow regime. The 90th percentile by definition is the Hg load value for which 90 percent of the values are lower or equal to that value for that particular flow regime.

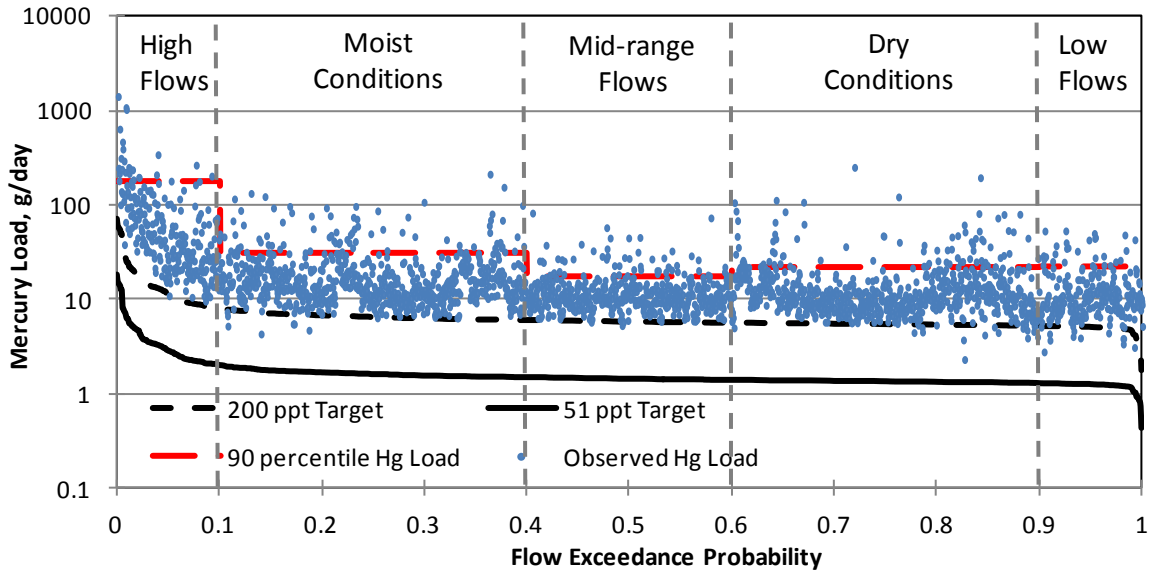

Figure 41. Mercury load duration curve for EFPC at Station 17 (EFK 23.4).

The 90th percentile was determined for flow conditions duringtwo different time periods, 1992 – 2000 and 2001 – 2010, which are compared with the 200 ppt and 51 ppt target load duration curves in Figure 42.

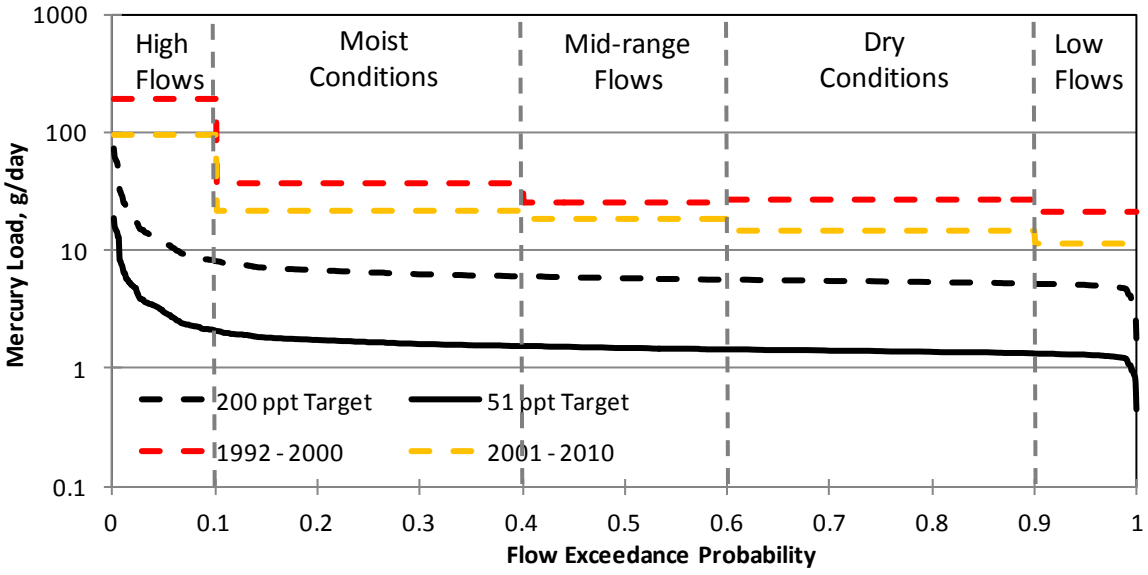

Figure 42. Comparison of mercury loading levels for EFPC at Station 17 (EFK 23.4) - (1992 – 2000) vs (2001 – 2010).

The mercury loads were calculated at Station 17 (EFK 23.4) utilizing the recorded timeseries for flow and mercury concentrations at the outfalls.. Figure 43 shows the flow and load duration curves at Station 17 (EFK 23.4) solely derived from the outfalls and flow augmentation.

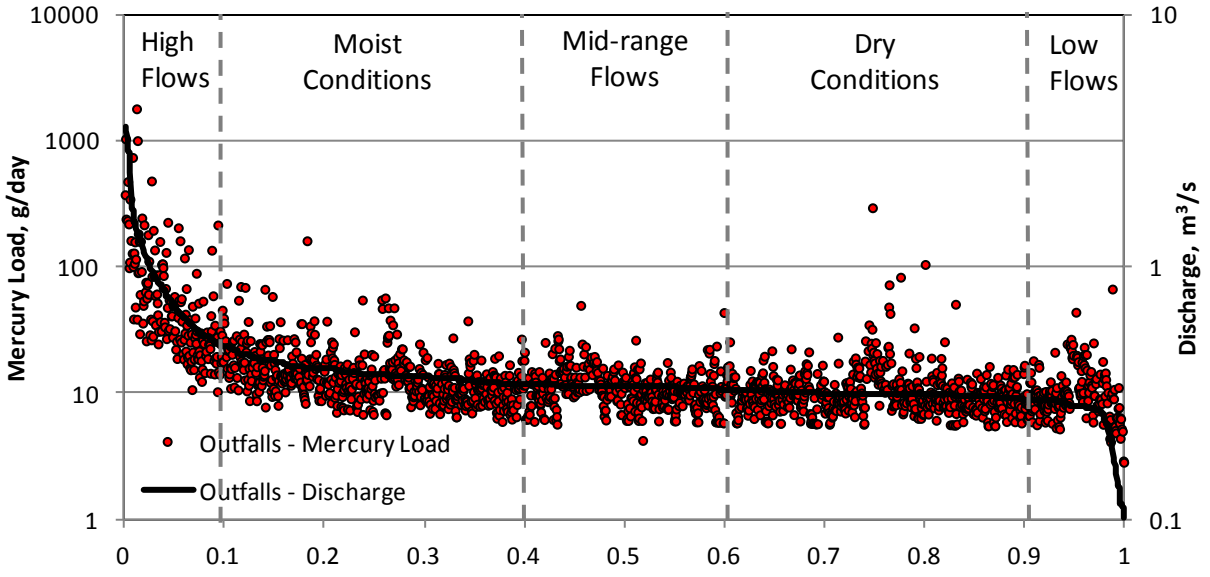

Figure 43. Flow and load duration curves resulting from the sum of all outfalls (excluding groundwater, sediment and overland contribution).

In order to identify the contribution from sediments, groundwater, and overland flow to the total mercury at Station 17 (EFK 23.4), the mercury loads calculated in the previous step were subtracted from the total mercury load recorded at Station 17 (EFK 23.4). The results are compared in Figure 44 in terms of percentiles for each of the flow regimes. Statistical characteristics of this contribution to the total mercury load at Station 17 are summarized in Table 18.

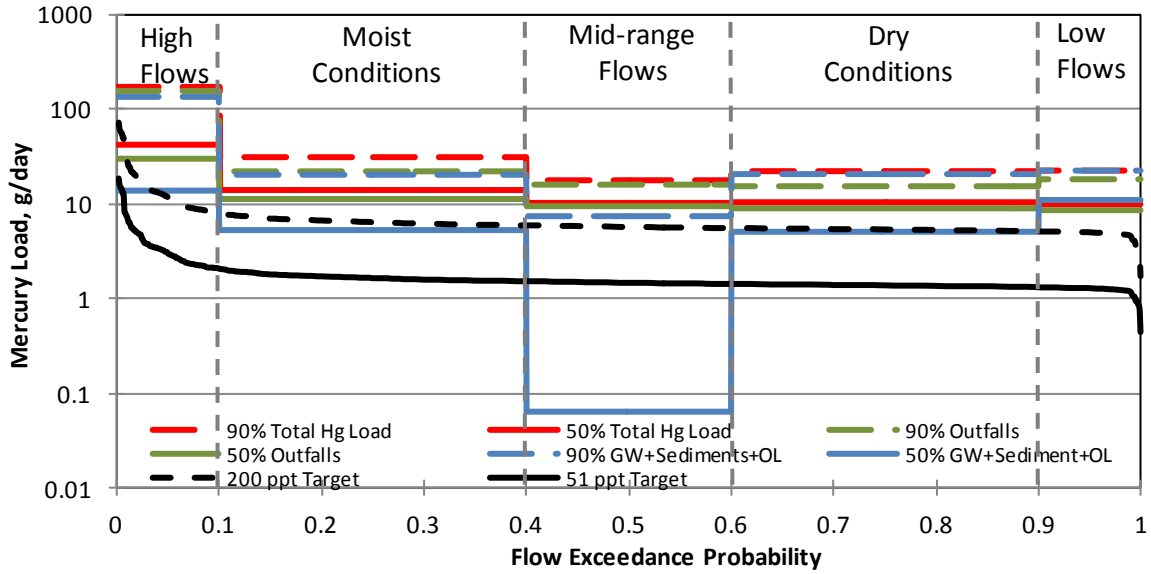

Figure 44. Contribution of outfalls, groundwater, sediments and overland flow to the total mercury load at Station 17 (EFK 23.4).

Table 18. Contribution of Mercury Sources to the Total Mercury Load Recorded at Station 17 (EFK 23.4), g/day

Flow Condition	GW + OL + Sediments			Outfalls			Total mercury		
	Mean	Median	90%	Mean	Median	90%	Mean	Median	90%
High Flows	51.1	13.6	136.2	73.8	29.8	160.1	81.7	41.7	174.3
Moist Conditions	9.8	5.2	20.7	12.5	11.3	21.8	18.9	14.1	31.2
Mid-range Flows	2.2	0.06	7.6	9.1	9.5	15.7	12.1	10.3	17.7
Dry Conditions	8.6	5.0	21.0	10.0	9.0	15.0	14.4	10.5	22.1
Low Flows	14.6	10.8	22.8	9.7	8.7	17.9	12.6	10.0	22.5

Step 4 – Mercury Water Quality Duration Curve

Based on the PDFE determined in Step 3, recorded mercury concentration values were plotted and compared to the water quality criterion of 51 ppt. The resulting mercury water quality duration curve is shown in Figure 45 for the period 1992 – 2010. Figure 46 compares the 90th percentile of Hg concentration with the target values for the two separate periods, 1992 – 2000 and 2001 – 2010.

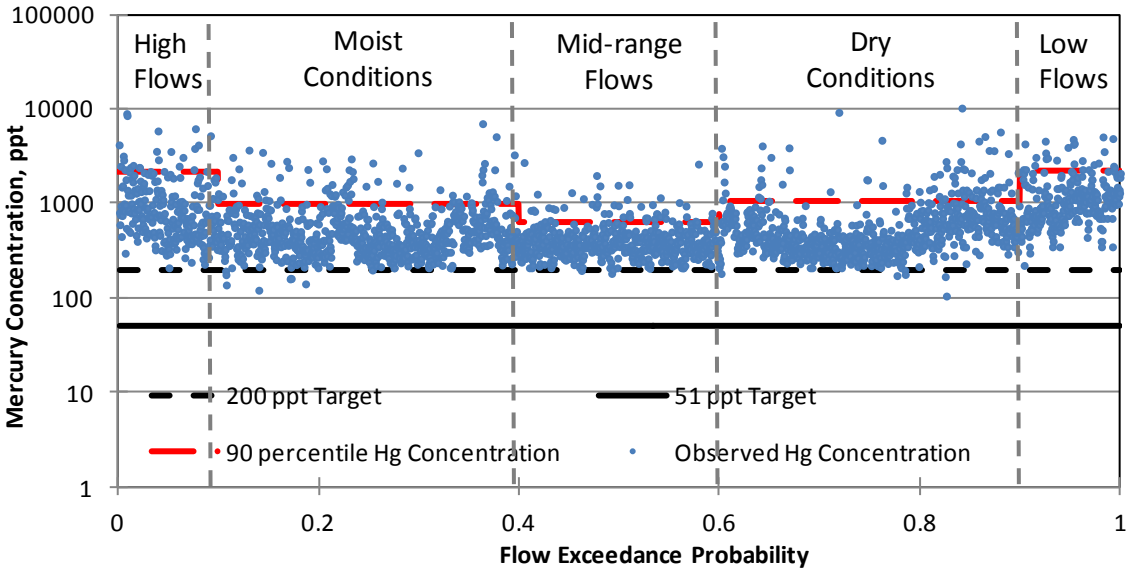

Figure 45. Mercury water quality duration curve for EFPC at Station 17 (EFK 23.4).

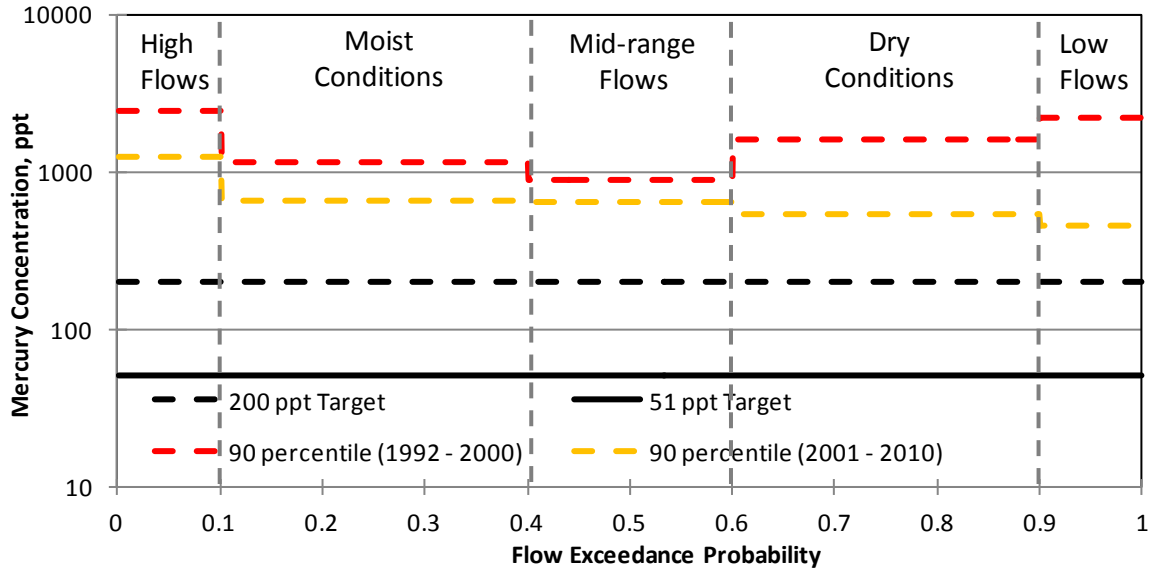

Figure 46. Comparison of mercury concentration recordings for EFPC at Station 17 (EFK 23.4) - (1992 – 2000) vs (2001 – 2010).

Step 6 – Water Quality Statistical Characteristics

Statistical analysis of recorded mercury values at Station 17 was conducted for two different periods, 1992 – 2000 and 2001 – 2010, and listed in Table 19. The reduction required to decrease the water column concentration from the "mean + 95% confidence interval" to the desired target level was calculated to be 89.5%.

Table 19. Analysis of Water Column Monitoring Data at Station 17 (EFK 23.4)

	1992 - 2000		2001 - 2010	
	Mercury Concentration, ppt	Mercury load, g/day	Mercury concentration, ppt	Mercury load, g/day
Number of samples	1511	1511	1143	1143
Minimum	210	3.3	105.5	2.3
Mean	868.3	26.1	460.9	16.2
Standard Deviation	816.1	58.0	499.4	36.2
95% CI	41.1	2.9	28.9	2.1
Mean + 95% CI	909.4	29.0	489.9	18.3

90% CI	34.5	2.5	24.3	1.8
Mean + 90% CI	902.8	28.6	485.2	18.0
WQ Target	51		51	
%Reduction from 90%	94.4%		89.5%	
%Reduction from 95%	94.4%		89.5%	
ROD Target	200		200	
%Reduction from 90%	77.8%		58.8%	
%Reduction from 95%	78.0%		59.2%	

Recorded and computed TSS and mercury load duration curves are compared for different flow conditions in Figure 47. Resuspension of mercury-laden fine particulates during high flow conditions (i.e., the wet seasons) plays a significant role in the enhancement of local concentration of mercury along the creek. Furthermore, the streambed pore water within the reach contains very high concentrations of dissolved mercury, often exceeding 20 µg/L (approximately 30 to 50 times the concentration in overlying surface water); thus, a higher flow in the river not only resuspends the mercury-laden particulates, but also recirculates the highly contaminated water trapped in sediment pores back into the water column of the creek. Therefore, dissolved mercury in sediment pore water contributes to the high mercury concentration in the creek water column through diffusive transport and porewater recirculation or advection. Close conformity between computed and recorded mercury and TSS loads at Station 17 (EFK 23.4) is clearly depicted in Figure 47. For the purpose of better visualization, a comparison has been made between percentiles of the computed and observed mercury loads in Figure 44.

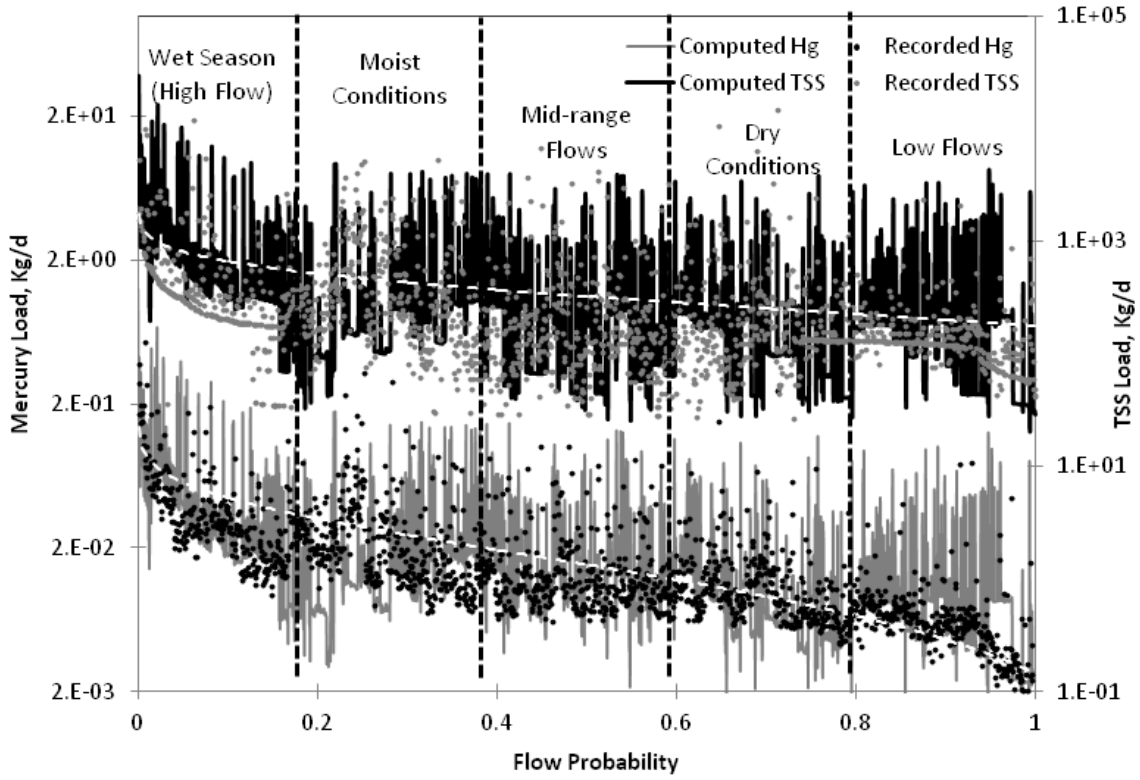

Figure 47. Load duration curves at Station 17 based on flow probability. White dashed lines are linear-moving average trendlines.

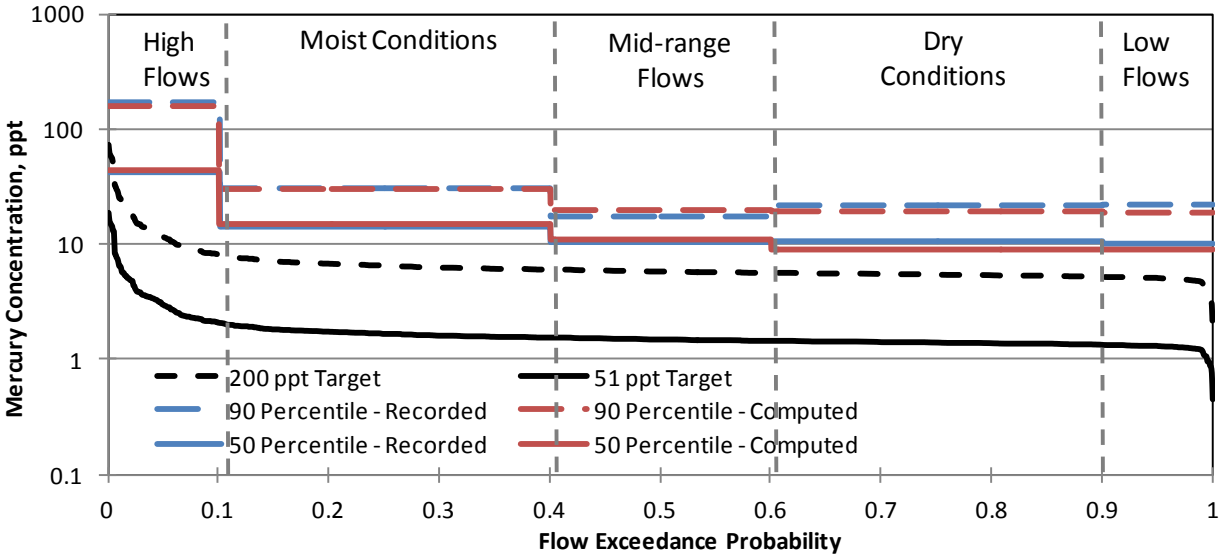

Figure 48. Comparison of computed and observed mercury loads at Station 17 (EFK 23.4) in terms of percentiles for different flow conditions.

6 CONCLUSIONS

In order to analyze the mercury cycle in the environment and provide forecasting capabilities for the flow and transport of mercury within the EFPC, an integrated surface and subsurface flow and transport model was developed using the hydrodynamic and transport numerical package MIKE, developed by the DHI. The model was calibrated for the flow and transport using historical field records obtained from the OREIS database.

Computed model outputs show close correlation with the water discharge, mercury concentration, and TSS field data recorded at different stations along the creek, which implies a high level of accuracy and reliability of the model. TSS and mercury concentration time-series data were compared at the integration point of the creek, Sta. 17. Due to the high dependency of suspended solids and mercury concentration on the level of discharge in the creek, results and discussions are mostly presented based on load duration curves for both suspended solids and total mercury.

The significance of sediment-mercury interactions on the fate and transport of mercury along the creek was investigated, performing simulations for two different cases: with and without consideration of sediment-mercury interactions. As reported in recent field surveys, stream sediments highly affect the concentration of mercury in the creek. Diffusive transfer through sediment pore water and colloidal transport were identified as two main mechanisms responsible for at least 90 percent of the mercury in the creek water. However, resuspension of mercury-laden fine particulates plays the most important role in the unexpectedly high concentration of mercury (peaks in mercury concentration time series) reported at different locations along the UEFPC. Simulations show that at least 65 percent of the total mercury concentration in the water is in a form that is adsorbed to suspended particles, which is consistent with the field surveys at the site. High flow conditions in the river following heavy rainfalls increase the velocity in the river and intensify the resuspension of mercury particulates, thereby increasing the concentration of mercury in the creek, as clearly indicated by numerical simulation results. Sensitivity analysis performed on parameters affecting TSS in

the water column revealed the high dependence of TSS to critical current velocity. Four parameters have been considered in the model that directly affects the concentration of TSS in the water column: critical current velocity (Vc), settling velocity (Vs), resuspension rate (RR), and particle production rate (PPR). The sensitivity of the TSS load at Sta. 17 to each of these parameters was examined by performing simulations for a range of values.

The results from this work show that a well calibrated computer model can provide a information that is critical for a TMDL study and particularly for determining remediation objectives and how to accomplish TMDL targets.

The results presented in this study can be considerably improved by incorporating additional boundary and calibrating data: timeseries of flow and mercury concentration measurement across the entire domain, including creeks, soil and subsurface data.

7 REFERENCES

1. U.S. Clean Water Act 1972 Section 303 (d), 33 U.S. Code Section 1313 (d).
2. U.S. EPA, 1991. “Guidance for Water Quality-Based Decisions: The TMDL Process.” Doc. No. EPA 440/4-91-001. April 1991.
3. U.S. EPA, 1992. “Water Quality Planning and Management.” *Code of Federal Regulations,* 40 CFR 130.7.
4. U.S. EPA, 2007. “An Approach for Using Load Duration Curves in the Development of TMDLs.”, EPA 841-B-07-006.
5. U.S. EPA, 2009. “Handbook for Developing Watershed TMDLs”.
6. TDEC 2006. State of Tennessee NPDES Permit No. TN0002968, “Authorization to discharge under the National Pollutant Discharge Elimination System (NPDES),” Issued March 13, 2006; effective May 1, 2006.
7. Southworth, G.R., et al. Controlling Mercury Release from Source Zones to Surface Water: Initial Results of Pilot Tests at the Y-12 National Security Complex. Oak Ridge, TN: ORNL, 2009.
8. Southworth, George, Max Greeley, Mark Peterson, Kenneth Lowe, and Richard Kettelle. Sources of Mercury to East Fork Poplar Creek Downstream from the Y-12 National Security Complex: Inventories and Export Rates. Oak Ridge: Oak Ridge National Laboratory, 2010.
9. TDEC, Tennessee Department of Environment and Conservation, Division of Water Pollution Control. "Proposed Total Maximum Daily Load (TMDL) for Mercury in East Fork Poplar Creek, Lower Clinch River Watershed, Preliminary Second Draft. Anderson and Roane Counties." Oak Ridge, TN, 2008.
10. Moran, Barry. "Modeling of the Hydrologic Transport of mercury in the Upper East Fork Poplar Creek." Knoxville (Ternnessee), December 1996.
11. TMDL Protocol, Florida Department of Environmental Protection, June 2006, Version 6.0.
12. D.R. Maidment, Handbook of Hydrology, McGraw-Hill, 1993.

13. TDEC. 2006. Final 2006 303(d) List. State of Tennessee, Department of Environment and Conservation, Division of Water Pollution Control, October 2006.
14. U.S. EPA. 1997. Ecoregions of Tennessee. U.S. Environmental Protection Agency, National Health and Environmental Effects Research Laboratory, Corvallis, Oregon. EPA/600/R-97/022.
15. ATSDR (Agency for Toxic Substances and Disease Registry), Federal Facilities Assessment Branch and Division of Health Assessment and Consultation. 2006. Public Health Assessment: Evaluation of Potential Exposures to Contaminated Off-Site Groundwater from the Oak Ridge Reservation (USDOE) Oak Ridge, Tennessee.
16. Hatcher, R. D., Lemiszki, P. J., Dreier, R. B., Ketelle, R. H., Lee, R. R., Leitzke, D. A., McMaster, W. M., Foreman, J. L., and S. Y. Lee. 1992. Status Report on the Geology of the Oak Ridge Reservation, ORNL/TM-12074. Prepared for the Office of Environmental Restoration and Waste Management.
17. TDEC, 2007, Rules of Tennessee Department of Environment and Conservation, Division of Water Pollution Control, Chapter 1200-4-4, Use Classification for Surface Waters.
18. U.S. DOE, 2008, Recommendations to Address Technical Uncertainties in the Mitigation and Remediation of Mercury Contamination at the Y-12 Plant, Oak Ridge, Tennessee, WSRC-STI-2008-00212.
19. TDEC, 2008, Rules of Tennessee Department of Environment and Conservation, Division of Water Pollution Control, Chapter 1200-4-3, General Water Quality Criteria.
20. U.S. EPA, 2006, Data Quality Assessment: Statistical Methods for Practitioners, EPA QA/G-9S.
21. U.S. EPA, 2006. Data Quality Assessment: A Reviewer's Guide, EPA QA/G-9R.
22. U.S. EPA, 2006. Draft Guidance for Implementing the January 2007 Methylmercury Water Quality Criterion. U.S. Environmental Protection Agency, Office of Science and Technology, Washington, DC. EPA-823504-001, August 2006.
23. Van Winkle, W., et al. 1982, Mercury Contamination in East Fork Poplar Creek and Bear Creek, Publication 2051, October 7. 1982.
24. U.S. DOE. 1998. Report on the Remedial Investigation of the Upper East Fork Poplar

Creek Characterization Area at the Oak Ridge Y-12 Plant, Oak Ridge, Tennessee. DOE/OR/01-1641V1&D2, August 1998.

25. U.S. DOE. 2006, 2006 Remedial Effectiveness Report/CERCLA Five-Year Review for the US Department of Energy, Oak Ridge Reservation, Oak Ridge, TN. DOE/OR/01-2290&D1. U.S. Department of Energy. March 2006.
26. U.S. DOE. 2002. Phase I Interim Source Control Actions in the Upper East Fork Poplar Creek Characterization Area, Oak Ridge, TN - Record of Decision (ROD) dated May 2002.
27. U.S. DOE. 1996. Wastewater Control Report for the Oak Ridge Y-12 Plant. Y/TS-1466/R1.
28. U.S. DOE. 1997. Final Report for the Central-Mercury Treatment System in Building 9623 at the Oak Ridge Y-12 Plant, Oak Ridge, Tennessee, Y/ER-282.
29. ORNL. 2009. Controlling Mercury Release from Source Zones to Surface Water: Initial Results of Pilot Tests at the Y -12 National Security Complex, ORNL/TM-2009/035.
30. BJC (Bechtel Jacobs Co. LLC). 1998. Mercury Abatement Report for the U.S. DOE Oak Ridge Y-12 Plant for Fiscal Year 1998. BJC/OR-183.
31. BJC. 1999. Mercury Abatement Report for the U.S. Department of Energy Oak Ridge Y-12 Plant for Fiscal Year 1999, Oak Ridge, Tennessee. BJC/OR-422.
32. U.S. DOE. 1995. Record of Decision for Lower East Fork Poplar Creek, Oak Ridge, Tennessee. DOE/OR/02-1370&D2.
33. U.S. DOE. 1996. Explanation of Significant Differences for the Lower East Fork Poplar Creek Record of Decision, Oak Ridge, Tennessee. DOE/OR/02-1443&D2.
34. Southworth, G., Greeley, M., Peterson, M., Lowe, K., & Kettelle, R. 2010. Sources of Mercury to East Fork Poplar Creek Downstream from the Y-12 National Security Complex: Inventories and Export Rates. Oak Ridge: Oak Ridge National Laboratory.
35. Turner, R. R. and G. R. Southworth. 1999. Mercury-Contaminated Industrial and Mining Sites in North America: an Overview with Selected Case Studies. In Mercury Contaminated Sites, R. Ebinghaus, R. R. Turner, L. D. de Lacerda, O. Vasiliev, and W. Salomons (Eds.) Springer-Verlag, Berlin, FRG.
36. Rhoades, E. L., M. A. O'Neal, and J. E. Pizzuto. 2009. Quantifying bank erosion on the South River from 1937 to 2005, and its importance in assessing mercury contamination.

Applied Geology 29:125 – 134.

37. U.S. DOE. 2005. The Oak Ridge Annual Site Environmental Report. U.S. DOE. March 2005.
38. U.S. EPA 2005. TMDL Model Evaluation and Research Needs, November 2005. EPA/600/R-05/149.
39. U.S. DOE 1998. Report on the Remedial Investigation of the Upper East Fork Poplar Creek Characterization Area at the Oak Ridge Y-12 Plant, Oak Ridge, Tennessee, DOE/OR/01-1641/V1-V4&D2.
40. Tachiev, G., Garcia R. Modeling of the White Oak Creek and East Fork Poplar Creek Watersheds. Applied Research Center Florida International University, 2009.
41. Martin Marietta Inc. 1995. Decision Document for Performing a Long-Term Pumping Test at the S-3 Site, Oak Ridge Y-12 Plant, Oak Ridge, Tennessee, submitted to DOE.

APPENDIX T3-001: TASK 3 FINAL REPORT

APPENDIX T3-001

TASK 3: PARAMETERIZATION OF MAJOR TRANSPORT PROCESSES OF MERCURY SPECIES

OF

REMEDIATION AND TREATMENT TECHNOLOGY DEVELOPMENT AND SUPPORT

Prepared for:
U.S. Department of Energy
Oak Ridge Operations Office
Oak Ridge Reservation

FINAL REPORT, VERSION 1, 06/17/2012

Prepared by:
Yong Cai, PhD
Yanbin Li, PhD
Guangliang Liu, PhD
Georgio Tachiev, PhD, PE

Principal Investigator: David Roelant, PhD
david.roelant@fiu.edu
phone: 305-348-6625
fax: 305-348-1852

Applied Research Center
Florida International University
10555 W. Flagler Street, EC 2100
Miami, Florida 33174

DISCLAIMER

This report was prepared as an account of work sponsored by an agency of the United States government. Neither the United States government nor any agency thereof, nor any of their employees, contractors, or subcontractors makes any warranty, express or implied, or assumes any legal liability or responsibility for the accuracy, completeness, or usefulness of any information, apparatus, product, or process disclosed, or represents that its use would not infringe upon private copyrights. Reference herein to any specific commercial product, process, or service by trade name, trademark, manufacturer, or otherwise does not necessarily constitute nor imply its endorsement, recommendation, or favor by the United States government or any other agency thereof. The views and opinions of authors expressed herein do not necessarily state or reflect those of the United States government or any agency thereof.

TABLE OF CONTENTS

LIST OF FIGURES

1 INTRODUCTION

The overall objective of this task is to provide laboratory measurements for critical mercury (Hg) transport, transformation, and exchange processes (i.e., methylation/demethylation, and dissolution) to be used in the numerical model. The laboratory experimental work will provide insight on parameters relevant to the Oak Ridge Reservation (ORR) and which are required in the numerical model, such as dissolution rate of mercury and the proportion of mercury species available for methylation/demethylation in sediments. In addition, experimental work will be conducted to analyze the effect of significant environmental factors (pH, Eh, sunlight) on the major transport and transformation processes of Hg.

Under this task the stability, bioavailability, and mobility of the aged mercury species in soils and sediments will be systematically investigated. The proportion of Hg species available for methylation and demethylation in sediments will be estimated by using isotope addition techniques. In addition, the dissolution of cinnabar and Hg beads, which have often been observed at this site and are thought to be recalcitrant mercury species, will be investigated by using both experimental and theoretical calculation methods. Three factors, oxidation-reduction, pH, and complexation with organic ligands (e.g., low molecular weight thiols such as cysteine and glutathione and large molecular NOM), will be particularly investigated for their role in mobilizing the aged mercury species. These studies will provide a better understanding of the bioavailability and dissolution of aged Hg species in soils and sediments. In FY11, we studied 1) photomethylation of Hg^{2+} in natural water, 2) bioavailability of Hg^{2+} and methylmercury for methylation and demethylation in sediment, and 3) enhancement of cinnabar dissolution by thiol-containing compounds.

1.1 Background

Mercury occurs in a variety of species, such as elemental mercury (Hg^0), mercury sulfide (HgS), mercury hydroxides (e.g., HgO and $Hg(OH)_2$), ionic mercury salts (e.g., $HgCl_2$), and methylmercury (MeHg), in the environment. Mercury species sequestered in soils and

sediments (e.g., HgS) are generally considered low in solubility and reactivity, which prevents this mercury from being released into solution and from being transported into the aquatic environment. Despite the limited solubility, mobility, and reactivity, the aged mercury species in soils and sediments may undergo a series of physicochemical processes under certain environmental conditions, releasing dissolved (and maybe including colloidal and particulate) mercury species into the solution. This process is particularly important for areas where soils and sediments are heavily contaminated with mercury, (e.g., some DOE sites), because even the release of a small fraction of the sequestered mercury would remarkably increase the amount of the mercury in the aquatic cycling[1]. Cinnabar has often been suggested to act as an important sink for mercury in soils and sediments due to its extremely low solubility[2-3]. However, some ligands, such as polysulfides, thiol, and chloride, may promote the dissolution of cinnabar in soils and sediments[4-8]. Oxidation of S (-II) could be another important factor for the dissolution of cinnabar[8-10]. Previous studies have suggested that the coordination of thiol-containing substances with Hg (II) was the most important factor to enhance its dissolution[6-7, 11-16]. However, contrary results were observed by other researchers who found that there was no significant correlation between cinnabar dissolution and reduced sulfur contents in thiol-containing substances[6].

Methylation and demethylation are a crucial part of cycling of mercury in aquatic systems. Methylation of Hg in sediment by anaerobic bacteria (sulfate reducing bacteria[17] or iron reducing bacteria[18]) was deemed to be the major pathway for MeHg production[18-23] in most aquatic systems, while photodemethylation in water was widely proposed to be the major process of MeHg elimination.[24-25] Methylation of inorganic mercury in the water column could be a significant pathway of MeHg formation in some ocean (e.g., the Arctic[26]) and freshwater[27] systems. A recent study showed that methylation in the water column can be an important source of MeHg in the Arctic, accounting for around 47% of MeHg present in Arctic waters[26]. The double stable isotope addition technique is a useful tool for measuring Hg methylation/demethylation rates owing to its high accuracy, precision, and simultaneous determination of the methylation and demethylation rates. In recent years, this technique has been widely applied in estimating the net production of MeHg. However, two significant

defects exist in previous models using this technique. One is the omission of the difference between the ambient and newly input Hg species in methylation/demethylation efficiency[28]. Their difference was often neglected in previous studies conducted to estimate the net MeHg production rate[29-30]. A significant error could occur with this omission since they have been reported to have a significant difference in methylation efficiency[31]. The other defect is related to the calculation of the Hg methylation rate constant of the spiked mercury tracer (k_m) in water. This constant was usually calculated by the measured per day increase in the amount of Me^nHg (assuming $^nHg^{2+}$ was spiked)[32-33]. This calculation assumes that the degradation of ambient and the newly produced Me^nHg is negligible. However, this assumption may often not be valid for natural waters, where the MeHg demethylation rate constant (k_d) can be 2-3 orders larger than k_m[26]. These two defects should be corrected for an accurate estimation of the production or degradation of MeHg utilizing stable isotope tracer techniques.

1.2 Technical Approach

1.2.1 Subtask 1: Photomethylation of Hg^{2+} in Natural Water

Water samples (200 mL) were transferred to 0.5-L FEP (fluorinated ethylene-propylene) Teflon bottles, and then spiked with $^{199}HgCl_2$ and $Me^{201}Hg$ to form final concentrations of approximately 50 and 0.6 ng L^{-1} as Hg, respectively. Spiked samples were divided into two groups and were incubated for 6 days to examine the effect of sunlight on Hg^{2+}methylation. One group was incubated under ambient temperature and light conditions, while the other was incubated under dark conditions by wrapping the bottles with aluminum foil. Concentrations of $Me^{199}Hg$, $Me^{201}Hg$, and $Me^{202}Hg$ in the incubated samples were determined after 0, 2, 4, and 6 days of incubation. A new model with the consideration of $Me^{199}Hg$ demethylation was developed to calculate the methylation rate constant of the spiked $^{199}Hg^{2+}$ (k_m) in water.

1.2.2 Subtask 2: Bioavailability of Hg^{2+} and Methylmercury for Methylation and Demethylation in Sediment

The double stable isotope addition method ($^{199}HgCl_2$ and $Me^{201}Hg$) was employed to

simultaneously measure the methylation and demethylation rate constants. Predetermined quantities of isotope-enriched $^{199}HgCl_2$ and $Me^{201}Hg$ were added to approximately 30 g of sediment samples under a N_2-saturated atmosphere. Spiked samples were divided into two portions, of which one was immediately frozen to -20 °C, representing t=0 days (t_0). The other portion was incubated in darkness under a N_2-saturated atmosphere for two days, representing t=2 days (t_2). Samples were collected and preserved at -20 °C, and then analyzed for $Me^{199}Hg$, $Me^{201}Hg$, and $Me^{202}Hg$ using aqueous phenylation followed by gas chromatography hyphenated with inductively coupled plasma mass spectrometry (GC-ICP-MS). The specific methylation and demethylation rate constants of newly spiked $^{199}Hg^{2+}$ and $Me^{201}Hg$ (k_m and k_d) and measured net ambient MeHg production (or degradation) rate (R) were then calculated and used to estimate the differences of newly spiked and ambient Hg species in methylation/demethylation efficiencies.

1.2.3 Subtask 3: Enhancement of Cinnabar Dissolution by Thiol-Containing Compounds

Experiments were conducted to measure the influence of thiol-containing compounds on the dissolution of cinnabar (HgS). Two types of thiol-containing compounds (Cysteine and Glutathione) were employed in this study. Dissolution of cinnabar was examined in the presence or absence of these two compounds. In order to study the effect of oxygen on the cysteine-promoted dissolution of cinnabar, experiments were conducted under various redox conditions: 1) anaerobic condition by purging with N_2, 2) aerobic condition by opening to the air, and 3) aerobic condition by purging with O_2. A model based on chemical thermodynamics and Hg^{2+} adsorption/desorption equilibrium on cinnabar particles was then developed to calculate the dissolution of cinnabar under different pH and redox conditions and cysteine concentrations. The model was validated by comparing the modeled results with the experimental data.

2 RESULTS

2.1 Photomethylation of Hg^{2+} in Natural Water

The double isotope addition technique ($Me^{201}Hg$ and $^{199}Hg^{2+}$) was adopted to study the methylation of Hg^{2+} in water. A new model was developed to calculate the methylation rate constant of the spiked $^{199}Hg^{2+}$ (k_m) in water (Eq. (2)). In this model, contributions of both $^{199}Hg^{2+}$ methylation and $Me^{199}Hg$ demethylation are taken into account in the function. The $[Me^{199}Hg]_t$ /$[Me^{202}Hg]_t$ ratio ($R_{202}^{199}(t)$), was employed to calculate the k_m in water. The rate constant of MeHg degradation, k_d, was included in this equation to represent the photodegradation of $Me^{199}Hg$. k_d was obtained by linear regression of $\ln([Me^{201}Hg])_t$ against t (Eq. (1)) [24, 34].

$$\ln([Me^{201}Hg]_t) = \ln([Me^{201}Hg]_0) - k_d t \quad (1)$$

$$R_{202}^{199}(t) = \frac{[Me^{199}Hg]_t}{[Me^{202}Hg]_t} = \frac{k_m[^{199}Hg^{2+}]_0 - (k_m[^{199}Hg^{2+}]_0 - k_d[Me^{199}Hg]_0)e^{-k_d t}}{k_m[^{202}Hg^{2+}]_0 - (k_m[^{202}Hg^{2+}]_0 - k_d[Me^{202}Hg]_0)e^{-k_d t}} \quad (2)$$

$(k_d > 0)$

$$R_{202}^{199}(t) = \frac{[Me^{199}Hg]_t}{[Me^{202}Hg]_t} = \frac{k_m[^{199}Hg^{2+}]_0 t + [Me^{199}Hg]_0}{k_m[^{202}Hg^{2+}]_0 t + [Me^{202}Hg]_0}$$

$(k_d = 0)$

where $[Me^m Hg]_0$ (m=199, 201 or 202) is the concentration of m isotope MeHg at 0 day (ng L^{-1}); $[Me^m Hg]_t$ is the concentration of m isotope MeHg at t time (ng L^{-1}); $[^{199}Hg^{2+}]_0$ and $[^{202}Hg^{2+}]_0$ are the concentrations of $^{199}Hg^{2+}$ and $^{202}Hg^{2+}$ at 0 day (ng L^{-1}).

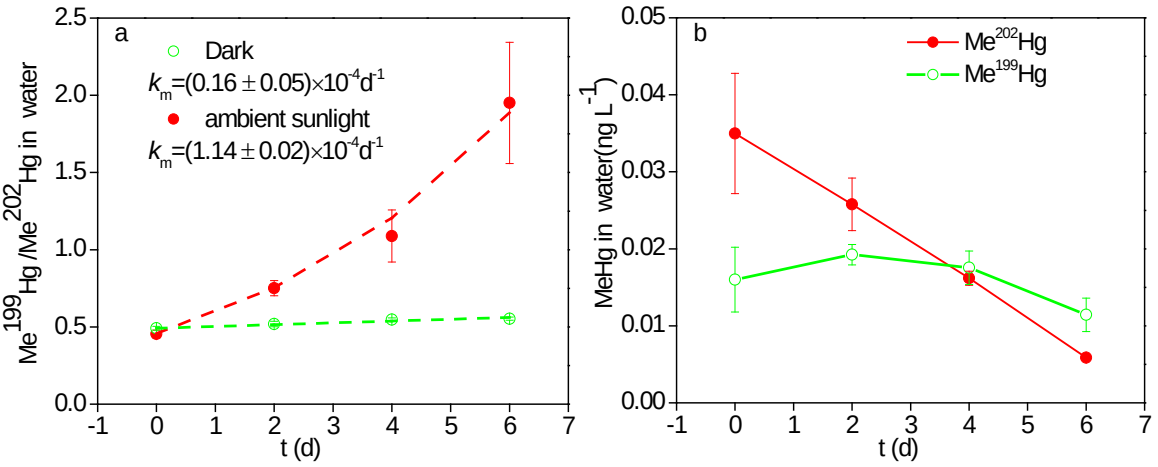

Figure 1. Variation of $Me^{199}Hg/Me^{202}Hg$ ratio (a) and concentrations of $Me^{199}Hg$ and $Me^{202}Hg$ (b) during the incubation of natural water. $Me^{199}Hg/Me^{202}Hg$ ratio was used to calculate the methylation rate constant of spiked $^{199}Hg^{2+}$ (Eq. (2)). Points in plot 2a represent the measured values, while the dashed line shows the simulated results.

Fig. 1a shows the methylation of spiked $^{199}Hg^{2+}$ in surface water. The 199/202 ratio of MeHg increased gradually from 0.5 to approximately 2 after 6 days of exposure to sunlight, while negligible change occurred in the dark. To further validate the effect of sunlight on methylation, k_m values at trials with and without sunlight were calculated according to Eq. (2). The $^{199}Hg^{2+}$ in water had a k_m of 1.14±0.02 ($\times10^{-4}$ d^{-1}) under ambient sunlight, while it was 0.16±0.05 ($\times10^{-4}$ d^{-1}) in the dark. These results suggest that methylation, which is dependent upon sunlight, occurs in natural water. However, its rate was much slower than that of MeHg photodemethylation (k_d = 0.26±0.04 d^{-1}), indicating that methylation in water plays a minor role in the cycling of MeHg. The changes in $Me^{202}Hg$ concentration were taken into account in order to correct for the effect of MeHg demethylation during the incubation. No significant increase in $Me^{199}Hg$ concentration was observed, but a substantial decrease in $Me^{202}Hg$ did occur (Fig. 1b), due to the faster rate of photodemethylation compared to methylation. This indicates that contributions of the photodemethylation of ambient and newly produced $Me^{199}Hg$ were not negligible for the variation of $Me^{199}Hg$. These results suggest that photodegradation of ambient and newly produced $Me^{199}Hg$ should be considered when determining k_m in water, especially for systems with $k_m << k_d$.

2.2 Estimation of the Bioavailability of Hg^{2+} and Methylmercury for Methylation and Demethylation in Natural Sediment

The difference between the ambient and newly input Hg species in methylation/demethylation efficiency was often neglected in the previous models[28] which may cause a significant error. Here, a model was developed to calculate the bioavailability of Hg^{2+} and methylmercury for methylation and demethylation in natural sediment using double stable isotope ($^{199}Hg^{2+}$ and $Me^{201}Hg$) addition experiments. The specific methylation and demethylation rate constants of newly spiked $^{199}Hg^{2+}$ and $Me^{201}Hg$ (k_m and k_d) and measured net ambient MeHg production (or degradation) rate (R) were calculated from the increased amount of $Me^{199}Hg$ derived from the spiked $^{199}Hg^{2+}$ ($\Delta[Me^{199}Hg]_{SP}$), the decreased amount of spiked $Me^{201}Hg$ ($\Delta[Me^{201}Hg]_{SP}$), and the net change in the amount of ambient $Me^{202}Hg$ ($\Delta[Me^{202}Hg]_{N}$), respectively (Eq. (3-5)). In many previous studies[32], the changes in concentrations of measured $Me^{199}Hg$ and $Me^{201}Hg$ were used to substitute for $\Delta[Me^{199}Hg]_{SP}$ and $\Delta[Me^{201}Hg]_{SP}$ to simplify the calculation. However, this simplification could cause a significant error if the methylation or demethylation of ambient mercury is not negligible.

In this study, this defect was overcome by directly calculating the values of $\Delta[Me^{199}Hg]_{SP}$, $\Delta[Me^{201}Hg]_{SP}$, and $\Delta[Me^{202}Hg]_{N}$ to determine the k_m, k_d and R. They were calculated using equations similar to previously proposed functions for detecting transformations of Hg species.[35] Then, α (ratio of methylation rate constant of ambient to newly spiked Hg) and β (ratio of demethylation rate constant of ambient to newly spiked MeHg) were calculated by fitting the data of measured net MeHg production (or degradation) rate against the potential methylation rate ($k_m[Hg^{2+}]$) and potential demethylation rate ($k_d[MeHg]$) (Eq. (6)). This method was applied to estimate the values of α and β in two types of sediment (Figure 2). α and β in these two sediments were estimated to be 0.06 and 0.93, and 0.02 and 0.71, respectively, indicating that there is a significant difference between the ambient and newly input Hg species in methylation/demethylation efficiency. If α and β were

not considered, the estimated net production (or degradation) rate of MeHg in sediment 1 could be overestimated by a factor of 20. The average of the estimated net production (or degradation) rate of MeHg in sediment 2 would increase from -70 to 600 ng m^{-2} d^{-1}. In that case, the net per day increase in MeHg concentration in soil would account for 400% of ambient MeHg concentration. This fails to account for the mass balance of ambient MeHg. This ratio is decreased to 20% if the estimated α and β are included in the calculation. These results indicate that the difference in methylation/demethylation efficiency of the ambient and newly input Hg species must be taken into account when net MeHg production (or degradation) rates are estimated.

$$k_{\mathrm{m}} = \frac{\Delta[\mathrm{Me}^{199}\mathrm{Hg}]_{\mathrm{SP}}}{[^{199}\mathrm{Hg}^{2+}]_{\mathrm{SP}} \times \mathrm{t}} \tag{3}$$

$$k_{\mathrm{d}} = \frac{\ln \dfrac{[\mathrm{Me}^{201}\mathrm{Hg}]_{\mathrm{SP}}}{[\mathrm{Me}^{201}\mathrm{Hg}]_{\mathrm{SP}} - \Delta[\mathrm{Me}^{201}\mathrm{Hg}]_{\mathrm{SP}}}}{\mathrm{t}} \tag{4}$$

$$R = \frac{\Delta[\mathrm{Me}^{202}\mathrm{Hg}]_{\mathrm{N}}}{P_{202} \times \mathrm{t}} \tag{5}$$

$$R_{\mathrm{x}} = k_{\mathrm{m}}(\mathrm{X}) \times \alpha_{\mathrm{x}} \times [\mathrm{Hg}^{2+}]_{\mathrm{x}} - k_{\mathrm{d}}(\mathrm{X}) \times \beta_{\mathrm{x}} \times [\mathrm{MeHg}]_{\mathrm{X}} \tag{6}$$

where k_{m} is the specific methylation rate constant of spiked $^{199}Hg^{2+}$ (d^{-1}); k_{d} is the specific demethylation rate constant of spiked $Me^{201}Hg$ (d^{-1}); R is the measured production (R > 0) or degradation (R < 0) rate of ambient MeHg (ng g^{-1} d^{-1}); t is the incubation time (d); $[^{199}Hg^{2+}]_{sp}$ and $[Me^{201}Hg]_{sp}$ are the concentrations of spiked $^{199}Hg^{2+}$ and $Me^{201}Hg$ (ng g^{-1}), respectively; P_{202} is the natural abundance of ^{202}Hg in ambient mercury (29.86%); X represents a specific compartment (soil (X = S), floc (X = F), periphyton (X = P), or water (X = W)); $\overline{R}_{\mathrm{x}}$ is the average net production or degradation rate of ambient MeHg (ng g^{-1} d^{-1}); α_{x} is the ratio of methylation rate constant of ambient to newly spiked Hg for X compartment and β_{x} is the ratio of demethylation rate constant of ambient to newly spiked MeHg; $[\mathrm{Hg}^{2+}]_{\mathrm{x}}$ and $[\mathrm{MeHg}]_{\mathrm{x}}$ are the concentrations of Hg^{2+} and MeHg in X compartment (ng g^{-1} or ng L^{-1}).

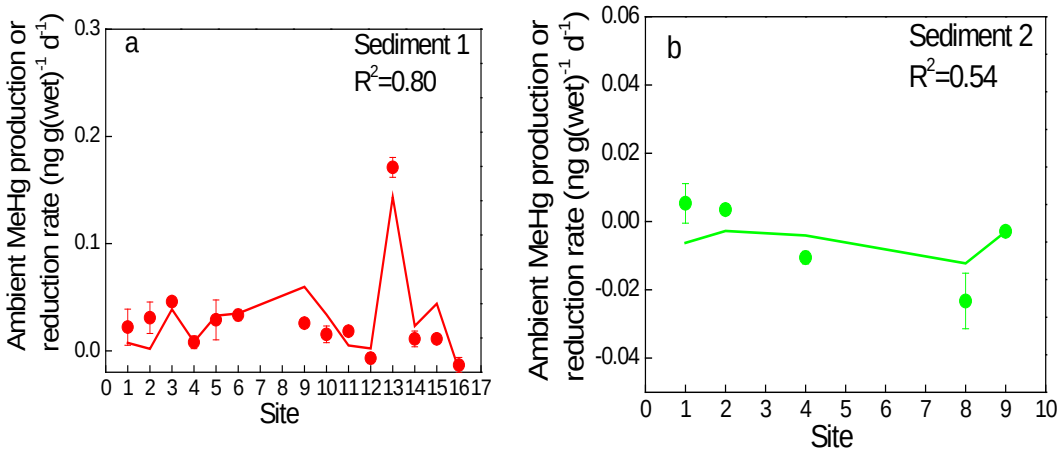

Figure 2. Simulation (line) and measured results (scatter) of net MeHg change rate in sediment 1 (with a relatively lower water content) and sediment 2 (flocculent, with a relatively higher water content).

2.3 Enhancement of Cinnabar Dissolution by Thiol-Containing Compounds

2.3.1 Effect of Thiol-Containing Compounds on Cinnabar Dissolution

Effects of thiol-containing compounds on cinnabar dissolution were shown in Figure 3. In the absence of thiol-containing compounds, Hg^{2+} concentration in water was at the level of ~1-2 μg/L (see Fig.3). The addition of 10μmol/L L-cysteine increased it to more than 100 μg/L, indicating the dramatic increase of cinnabar dissolution by cysteine. Glutathione could also increase the dissolution of cinnabar. However, its effect was much smaller compared to cysteine, suggesting that the effect of thiol varies in different species.

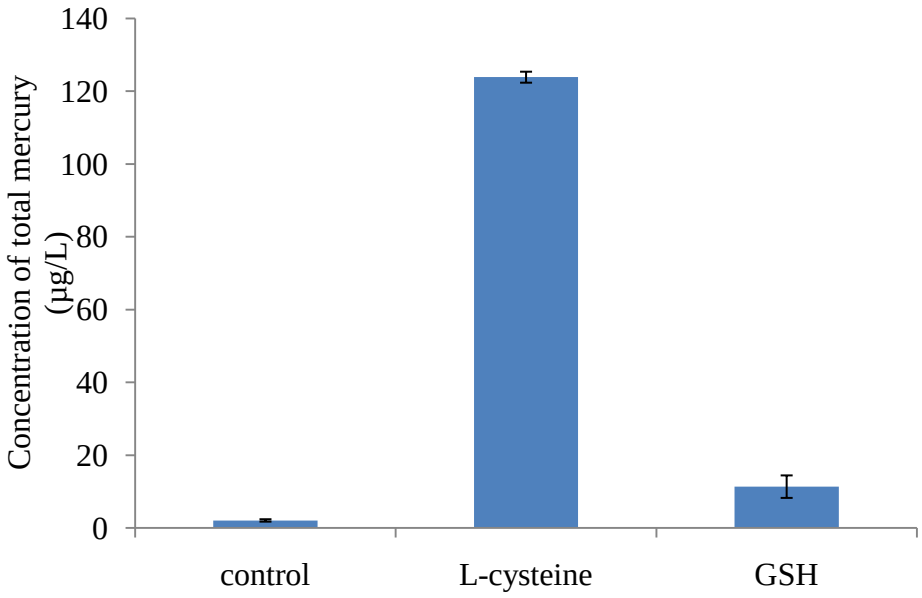

Figure 3. Effects of thiol-containing group on the dissolution of cinnabar under oxic conditions.

2.3.2 Effect of Dissolved Oxygen on Cysteine-Promoted Dissolution of Cinnabar

Figure 4 shows the effect of dissolved oxygen on the cysteine-promoted dissolution of cinnabar. The concentration of Hg^{2+} in aqueous phase was in the order of saturated oxygen> air> anaerobic. Under oxic conditions, Hg^{2+} in water could be as high as 120 μg Hg/L, while this value decreased to about 30 μg Hg/L under anaerobic conditions. These results indicate that oxygen plays a significant role in the dissolution of cinnabar.

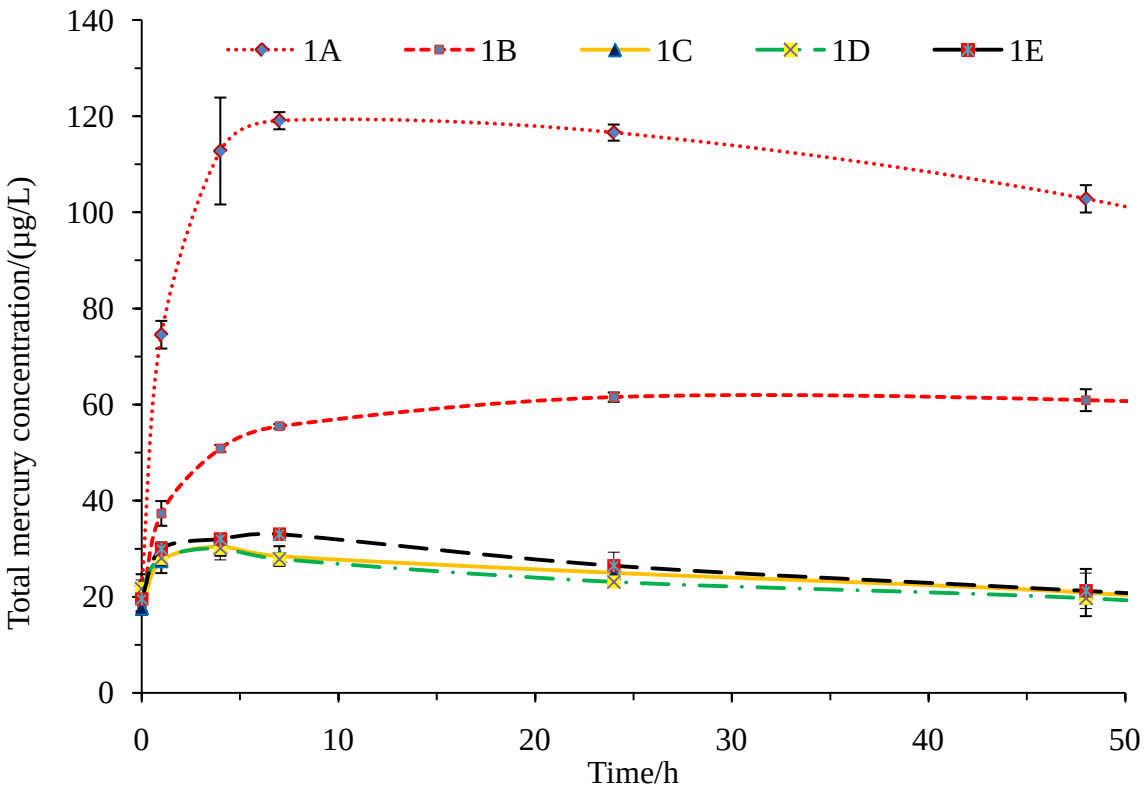

Figure 4. Effects of dissolved oxygen on thiol-promoted dissolution of cinnabar. 1A, in the presence of saturated oxygen; 1B, in the presence of air; 1C, 1D, 1E, under anaerobic conditions.

2.3.3 Modeling Dissolution of Cinnabar in an Aquatic Environment

A model based on chemical thermodynamics was developed to calculate the dissolution of cinnabar under different conditions and elucidate the relative importance of pH, O_2 and cysteine in cinnabar dissolution. Results of the model indicate that dissolved oxygen has the largest enhancing effect on cinnabar dissolution, while pH and cysteine concentrations have no significant promotion on this process. According to the prediction from chemical thermodynamics principles, the solubility of cinnabar in anaerobic environment of pH 8.0 are $8.0\times10^{-14\ \sim\ -2}$ μg/L, this value increased to ~100 μg/L in the presence of dissolved saturated oxygen. In addition, there is no significant difference in the solubility of cinnabar with or without cysteine under oxic conditions. The experimental results suggested that the concentration of Hg^{2+} in water was close to the predicted value in the presence of cysteine.

However, it was much lower than the predicted value in the absence of cysteine. Further adsorption experiments showed that a large proportion of added Hg^{2+} could be adsorbed on the surface of cinnabar. By taking consideration of the adsorption of released Hg^{2+} on cinnabar, the proposed model could well predict the dissolution of cinnabar with or without cysteine. These results indicate that oxidization of S (-II) may be the driving force for cinnabar dissolution in aquatic environments. Complexation of cysteine compounds with Hg^{2+} also plays an important role in this process by inhibiting the absorption of released Hg^{2+} on the cinnabar surface.

3 CONCLUSIONS

3.1 Photomethylation of Hg^{2+} in Natural Water

The double isotope addition technique ($^{199}Hg^{2+}$ and $Me^{201}Hg$) was applied to measure the photomethylation of Hg^{2+} in water. A new model was developed to calculate the methylation rate constant of the spiked Hg^{2+} in water. This model corrected for the defect of previous models, in which the degradation of ambient MeHg and the newly produced MeHg was not taken into account. Methylation of Hg^{2+} was observed in natural water, with a rate of 1.14±0.02 ($\times 10^{-4}$ d^{-1}). This process is mediated by sunlight. However, its rate was much slower than that of MeHg photodemethylation (k_d=0.26±0.04 d^{-1}), indicating that methylation in water plays a minor role in the cycling of MeHg. In addition, the contributions of the photodemethylation of ambient and newly produced $Me^{199}Hg$ were proven not to be negligible for the variation of $Me^{199}Hg$.

3.2 Estimation of the Bioavailability of Hg^{2+} and Methylmercury for Methylation and Demethylation in Natural Sediment

The difference between the ambient and newly input Hg species in methylation/demethylation efficiency was often neglected in the previous models which may cause a significant error. Here, we developed a method to calculate the bioavailability of Hg^{2+} and methylmercury for methylation and demethylation in natural sediment using double stable isotope ($^{199}Hg^{2+}$ and $Me^{201}Hg$) addition experiments. The percentage of bioavailable Hg^{2+} and MeHg for methylation/demethylation (α_x and β_x) was estimated to be 0.02-0.06 and 0.71-0.93, separately in studied sediments, indicating that there is a significant difference between the ambient and newly input Hg species in methylation/demethylation efficiency. The difference in methylation/demethylation efficiency of the ambient and newly input Hg species must be taken into account when net MeHg production (or degradation) rates are estimated. If α and β were not considered, the estimated net production (or degradation) rate of MeHg in sediment could be overestimated by a factor of 20.

3.3 Effect of Thiol-Containing Compounds on Cinnabar Dissolution

Thiol-containing compounds could significantly promote the dissolution of cinnabar. In the absence of thiol-containing compounds, Hg^{2+} concentration in water was at the level of ~1-2 μg/L. The addition of 10μmol/L L-cysteine increased it to more than 100 μg/L. Glutathione could also increase the dissolution of cinnabar. However, its effect was much smaller compared to cysteine, suggesting that the effect of thiol varies in different thiol species. In addition, oxygen plays a significant role in the dissolution of cinnabar. The concentration of Hg^{2+} in the aqueous phase was in the order of saturated oxygen > air > anaerobic. A model based on chemical thermodynamics was developed to calculate the dissolution of cinnabar under different conditions and elucidate the relative importance of pH, O_2 and thiol-containing compounds in cinnabar dissolution. By taking into consideration the adsorption of released Hg^{2+} on cinnabar, the proposed model could well predict the dissolution of cinnabar with or without cysteine. Both model and experimental results suggest that oxidization of S (-II) may be the driving force for cinnabar dissolution in aquatic environments. Complexation of cysteine with Hg^{2+} also plays an important role in this process by inhibiting the absorption of released Hg^{2+} on the cinnabar surface.

4 FUTURE WORK

1. It was found from our previous year's work that dissolution of cinnabar can significantly increase Hg concentrations in water and cysteine and glutathione (model substances for thiol compounds) can significantly promote this process. These findings indicate that natural organic matter (NOM) may play an important role in the dissolution of cinnabar, and thiol compounds could be the functional group that dominates this process. However, the effects of other common functional groups in NOM on cinnabar dissolution are still unknown and needed to be investigated.
2. Complexation of thiol-containing compounds with Hg^{2+} was found to play an important role in the dissolution of cinnabar via inhibiting the absorption of released Hg^{2+} on cinnabar surface, rather than increasing the solubility of HgS. This conclusion could be refined by applying stable isotope technique to simultaneously determine the dissolution of cinnabar and adsorption of Hg^{2+} on cinnabar.
3. As model substances for NOM, thiol-containing compounds showed an enhancement effect on cinnabar dissolution. Investigation of NOM and other complexing reagents (e.g., Cl^-) on the dissolution of cinnabar could further improve our understanding of the dissolution of cinnabar in natural environments.

5 REFERENCES

(1) Liu, G. L.; Cabrera, J.; Allen, M.; Cai, Y. Mercury characterization in a soil sample collected nearby the DOE Oak Ridge Reservation utilizing sequential extraction and thermal desorption method. *Science of the Total Environment* **2006,** *369* (1-3), 384-392.

(2) Mikac, N.; Foucher, D.; Niessen, S.; Fischer, J. C. Extractability of HgS (cinnabar and metacinnabar) by hydrochloric acid. *Analytical and Bioanalytical Chemistry* **2002,** *374* (6), 1028-1033.

(3) Mikac, N.; Foucher, D.; Niessen, S.; Lojen, S.; Fischer, J. C. Influence of chloride and sediment matrix on the extractability of HgS (cinnabar and metacinnabar) by nitric acid. *Analytical and Bioanalytical Chemistry* **2003,** *377* (7-8), 1196-1201.

(4) Paquette, K.; Helz, G. SOLUBILITY OF CINNABAR (RED HGS) AND IMPLICATIONS FOR MERCURY SPECIATION IN SULFIDIC WATERS. *Water Air and Soil Pollution* **1995,** *80* (1-4), 1053-1056.

(5) Paquette, K. E.; Helz, G. R. Inorganic speciation of mercury in sulfidic waters: The importance of zero-valent sulfur. *Environmental Science & Technology* **1997,** *31* (7), 2148-2153.

(6) Ravichandran, M.; Aiken, G. R.; Reddy, M. M.; Ryan, J. N. Enhanced dissolution of cinnabar (mercuric sulfide) by dissolved organic matter isolated from the Florida Everglades. *Environmental Science & Technology* **1998,** *32* (21), 3305-3311.

(7) Waples, J. S.; Nagy, K. L.; Aiken, G. R.; Ryan, J. N. Dissolution of cinnabar (HgS) in the presence of natural organic matter. *Geochimica Et Cosmochimica Acta* **2005,** *69* (6), 1575-1588.

(8) Burkstaller, J. E.; McCarty, P. L.; Parks, G. A. Oxidation of cinnabar by iron(III) in acid mine waters. *Environmental Science & Technology* **1975,** *9* (7), 676-678.

(9) Holley, E. A.; McQuillan, A. J.; Craw, D.; Kim, J. P.; Sander, S. G. Mercury mobilization by oxidative dissolution of cinnabar (alpha-HgS) and metacinnabar (beta-HgS). *Chemical Geology* **2007,** *240* (3-4), 313-325.

(10) Barnett, M. O.; Turner, R. R.; Singer, P. C. Oxidative dissolution of metacinnabar (beta-

HgS) by dissolved oxygen. *Applied Geochemistry* **2001,** *16* (13), 1499-1512.

(11) Ngu-Schwemlein, M.; Merle, J. K.; Healy, P.; Schwemlein, S.; Rhodes, S. Thermodynamics of the complexation of Hg(II) by cysteinyl peptide ligands using isothermal titration calorimetry. *Thermochimica Acta* **2009,** *496* (1-2), 129-135.

(12) Ravichandran, M. Interactions between mercury and dissolved organic matter - a review. *Chemosphere* **2004,** *55* (3), 319-331.

(13) Mah, V.; Jalilehvand, F. Mercury(II) complex formation with glutathione in alkaline aqueous solution. *Journal of Biological Inorganic Chemistry* **2008,** *13* (4), 541-553.

(14) Aiken, G.; Waples, J.; Nagy, K. L.; Ryan, J.; Ravichandran, M. Dissolution of cinnabar by dissolved organic matter. *Abstracts of Papers of the American Chemical Society* **2001,** *222*, U425-U425.

(15) Ravichandran, M.; Aiken, G. R.; Reddy, M. M.; Ryan, J. N. Enhanced dissolution of cinnabar (mercuric sulfide) by aquatic humic substances. *Abstracts of Papers of the American Chemical Society* **1998,** *216*, U785-U785.

(16) Nagy, K. L.; Kerr, M. Enhanced dissolution of cinnabar by dissolved organic matter in anoxic solutions. *Geochimica Et Cosmochimica Acta* **2010,** *74* (12), A744-A744.

(17) Compeau, G. C.; Bartha, R. Sulfate-reducing bacteria: principal methylators of mercury in anoxic estuarine sediment. *Appl. Environ. Microbiol.* **1985,** *50* (2), 498-502.

(18) Kerin, E. J.; Gilmour, C. C.; Roden, E.; Suzuki, M. T.; Coates, J. D.; Mason, R. P. Mercury methylation by dissimilatory iron-reducing bacteria. *Appl. Environ. Microbiol.* **2006,** *72* (12), 7919-7921.

(19) Gilmour, C. C.; Henry, E. A. Mercury Methylation by Sulfate-Reducing Bacteria - Biogeochemical and Pure Culture Studies, In *American Chemical Society*; San Francisco, USA, 1992.

(20) Gray, J. E.; Hines, M. E. Biogeochemical mercury methylation influenced by reservoir eutrophication, Salmon Falls Creek Reservoir, Idaho, USA. *Chem. Geol.* **2009,** *258* (3-4), 157-167.

(21) Mitchell, C. P. J.; Gilmour, C. C. Methylmercury production in a Chesapeake Bay salt marsh. *J. Geophys. Res. (G Biogeosci.)* **2008,** *113*, G00C04.

(22) Tsui, M. T. K.; Finlay, J. C.; Nater, E. A. Effects of Stream Water Chemistry and Tree Species on Release and Methylation of Mercury during Litter Decomposition. *Environ. Sci. Technol.* **2008,** *42* (23), 8692-8697.

(23) Zizek, S.; Guevara, S. R.; Horvat, M. Validation of methodology for determination of the mercury methylation potential in sediments using radiotracers. *Anal. Bioanal. Chem.* **2008,** *390* (8), 2115-2122.

(24) Hammerschmidt, C. R.; Fitzgerald, W. F. Photodecomposition of methylmercury in an arctic Alaskan lake. *Environ. Sci. Technol.* **2006,** *40* (4), 1212-1216.

(25) Li, Y. B.; Mao, Y. X.; Liu, G. L.; Tachiev, G.; Roelant, D.; Feng, X. B.; Cai, Y. Degradation of Methylmercury and Its Effects on Mercury Distribution and Cycling in the Florida Everglades. *Environ. Sci. Technol.* **2010,** *44* (17), 6661-6666.

(26) Lehnherr, I.; St Louis, V. L.; Hintelmann, H.; Kirk, J. L. Methylation of inorganic mercury in polar marine waters. *Nat. Geosci.* **2011,** *4* (5), 298-302.

(27) Siciliano, S. D.; O'Driscoll, N. J.; Tordon, R.; Hill, J.; Beauchamp, S.; Lean, D. R. S. Abiotic Production of Methylmercury by Solar Radiation. *Environ. Sci. Technol.* **2005,** *39* (4), 1071-1077.

(28) Gilmour, C. C.; Riedel, G. S.; Ederington, M. C.; Bell, J. T.; Benoit, J. M.; Gill, G. A.; Stordal, M. C. Methylmercury concentrations and production rates across a trophic gradient in the northern Everglades. *Biogeochemistry* **1998,** *40*, 327-345.

(29) Gray, J. E.; Hines, M. E.; Biester, H. Mercury methylation influenced by areas of past mercury mining in the Terlingua district, Southwest Texas, USA. *Appl. Geochem.* **2006,** *21* (11), 1940-1954.

(30) Gray, J. E.; Hines, M. E.; Higueras, P. L.; Adatto, I.; Lasorsa, B. K. Mercury speciation and microbial transformations in mine wastes, stream sediments, and surface waters at the Almaden Mining District, Spain. *Environ. Sci. Technol.* **2004,** *38* (16), 4285-4292.

(31) Hintelmann, H.; Keppel-Jones, K.; Evans, R. D. Constants of mercury methylation and demethylation rates in sediments and comparison of tracer and ambient mercury availability. *Environ. Toxicol. Chem.* **2000,** *19* (9), 2204-2211.

(32) Drott, A.; Lambertsson, L.; Bjorn, E.; Skyllberg, U. Do potential methylation rates reflect

accumulated methyl mercury in contaminated sediments? *Environ. Sci. Technol.* **2008,** *42* (1), 153-158.

(33) Eckley, C. S.; Hintelmann, H. Determination of mercury methylation potentials in the water column of lakes across Canada. *Sci. Total Environ.* **2006,** *368* (1), 111-125.

(34) Lehnherr, I.; St. Louis, V. L. Importance of Ultraviolet Radiation in the Photodemethylation of Methylmercury in Freshwater Ecosystems. *Environ. Sci. Technol.* **2009,** *43* (15), 5692-5698.

(35) Hintelmann, H.; Evans, R. D. Application of stable isotopes in environmental tracer studies - Measurement of monomethylmercury (CH_3Hg^+) by isotope dilution ICP-MS and detection of species transformation. *Fresenius J. Anal. Chem.* **1997,** *358* (3), 378-385.

APPENDIX T4-001: TASK 4 FINAL REPORT

APPENDIX T4-001

TASK 4: GEODATABASE DEVELOPMENT IN SUPPORT OF CONTAMINANT FATE & TRANSPORT MODELING AT OAK RIDGE RESERVATION, TENNESSEE

OF

REMEDIATION AND TREATMENT TECHNOLOGY DEVELOPMENT AND SUPPORT

Prepared for:
U.S. Department of Energy
Oak Ridge Operations Office
Oak Ridge Reservation

FINAL REPORT, VERSION 1, 06/17/2012

Prepared by:
Georgio Tachiev, PhD, PE,
Angelique Lawrence, MS
Elias Patsalos, MS

Principal Investigator
David Roelant, PhD
david.roelant@fiu.edu
phone: 305-348-6625
fax: 305-348-1852

Applied Research Center
Florida International University
10555 W. Flagler Street, EC 2100
Miami, Florida 33174

DISCLAIMER

TABLE OF CONTENTS

LIST OF TABLES

LIST OF FIGURES

LIST OF ACRONYMS

ARC	Applied Research Center
CR	Clinch River
DCE	Dichloroethene
DOE	Department of Energy
EFPC	East Fork Poplar Creek
EPA	Environmental Protection Agency
FIU	Florida International University
FP	Floodplain
LEFPC	Lower East Fork Poplar Creek
LC	Land Cover
LU	Land Use
MRLC	Multi-Resolution Land Characteristics (MRLC) Consortium
NLCD	National Land Cover Database
NRCS	Natural Resources Conservation Service
NSC	National Security Complex
OREIS	Oak Ridge Environmental Information System
ORNL	Oak Ridge National Laboratory
ORR	Oak Ridge Reservation
OSY	Old Salvage Yard
PCE	Tetrachloroethene
QA	Quality Assurance
SSURGO	Soil Survey Geographic Database
STATSGO	State Soil Geographic (STATSGO) Database
TDEC	Tennessee Department of Environment and Conservation
TMDL	Total Maximum Daily Load
TN	Tennessee
UBC	Upper Bear Creek
UEFPC	Upper East Fork Poplar Creek
USGS	United States Geological Survey
VC	Vinyl Chloride
VOC	Volatile Organic Compound
WEMA	West End Mercury Area
WOC	White Oak Creek
WS	Watershed
Y-12 NSC	Y-12 National Security Complex

EXECUTIVE SUMMARY

During 2007-2011, researchers at the Applied Research Center (ARC) at Florida International University (FIU) developed three integrated watershed models for the Y-12 National Security Complex (Y-12 NSC), White Oak Creek (WOC), and East Fork Poplar Creek (EFPC), and have used them to model hydrology and the fate and transport of contaminants. These models include overland, stream and groundwater flows in the variable and fully saturated zones, and implement the complex biological and chemical dynamics of mercury species to simulate the broader range of mercury distribution throughout the delineated WOC and EFPC watersheds. They provide information about the fluxes of water and concentration of mercury, and provide a better understanding of the fate and transport of mercury within the watersheds in the temporal and spatial domains. More than a hundred simulations were completed to calibrate the models, to derive model uncertainties and to provide analysis of remediation scenarios, resulting in hundreds of gigabytes of simulation data. There was need therefore for an advanced spatial data structure to address the management, processing, and analysis of spatial and temporal numerical modeling data derived from multiple sources, and to produce hydrogeological maps for visualization.

In order to store and retrieve model configuration input and output files and to facilitate file processing and management, an ArcSDE-based hydrogeological geographic information system (GIS) database (or geodatabase) was developed using the ArcGIS 10 suite of software. The geodatabase provides a centralized data storage and management system for model files (in many cases exceeding 20 GB per simulation), with versioning tools which provide a framework for security management and quality assurance in data editing. The geodatabase provides a foundation for building GIS-based water resources applications and facilitates concurrent use by multiple users. The configuration files that are stored in the database include high-resolution spatial and temporal data such as shapefiles which represent the spatial properties of the model domain, and timeseries data for the boundary conditions (e.g. rainfall and evapotranspiration), land use, and other spatially distributed surface parameters required by the MIKE SHE/MIKE 11

model. The output files include computed simulation data parameters (e.g. discharge and contaminant concentrations) which were used for model calibration and sensitivity analyses during model development, and which will be used for comparative contaminant flow and transport analyses and calculation of TMDLs for EFPC based on various simulated D&D scenarios within the Y12-NSC.

1 INTRODUCTION

1.1 Background and Technology Need

Three integrated hydrological models were developed during 2007-2011 by researchers from the Applied Research Center (ARC) at Florida International University (FIU) to model the hydrology and the fate and transport of contaminants in the watersheds encompassing the Y-12 National Security Complex (NSC), White Oak Creek (WOC), and East Fork Poplar Creek (EFPC) [Figure 1].

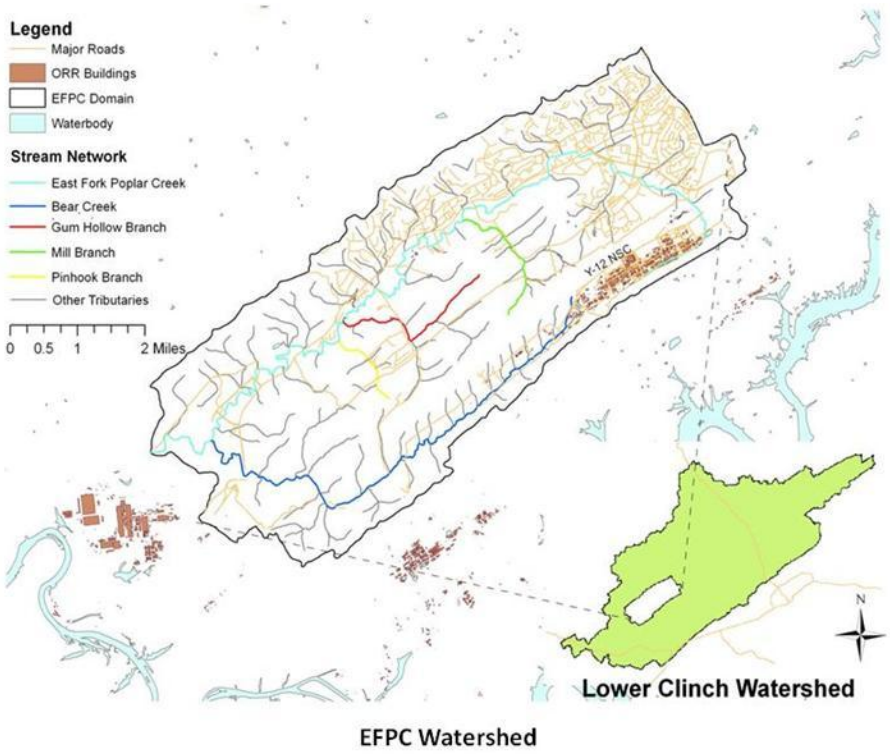

Figure 1. EFPC watershed (one of the study domains).

These models include overland, stream and groundwater flows in the variable and fully saturated zones, and implement the complex biological and chemical dynamics of mercury species to simulate the broader range of mercury distribution throughout the delineated WOC and EFPC watersheds. They provide information about the fluxes of water and concentration of mercury, and provide a better understanding of the fate and transport of mercury within the

watersheds in the temporal and spatial domains. More than a hundred simulations were completed to calibrate the models, to derive model uncertainties and to provide analysis of remediation scenarios, resulting in hundreds of gigabytes of simulation data. There was need therefore for an advanced spatial data structure to address the management, processing, and analysis of spatial and temporal numerical modeling data derived from multiple sources, and to produce hydrogeological maps for visualization.

Advances in ArcGIS software through the development of geodatabase technology, coupled with the development of data models such as ArcHydro which possesses a spatial relational database management (RDMS) schema and relationship structure specific to hydrologic systems, provides modelers with tools and applications to assist in the processing, analysis and visualization of flow and contaminant transport data. In addition, the coupling of this type of geodatabase structure with a numerical model such as MIKE SHE/11 can serve as an efficient tool that significantly reduces the time needed for data preparation [1]. ARC-FIU has therefore developed a geodatabase to support the research activities of the “Remediation and Treatment Technology” project, which can be integrated with the MIKE SHE/11 model making the data more accessible to project team members for editing and data management purposes as well as for external requests.

Development of an ArcSDE-based hydrogeological geographic information system (GIS) database (or geodatabase) facilitates centralized storage, backup, accessibility, organization and management of observed model data inputs as well as computed simulation data. Gogu et al., 2001 [5] stress the benefits of putting large volumes of data into a structured, coherent and logical computer-supported system to ensure validity and availability for concurrent use by multiple users and provide a foundation for building GIS-based water resources applications. The ORR Geodatabase is a multiuser relational database management system (RDBMS) built upon a Microsoft SQL Server platform developed using Environmental Systems Research Institute (ESRI) ArcSDE technology. The system was deployed on an advanced Windows server with the latest technology and hardware and provides a user interface which facilitates data

access, database connectivity, cryptography, web application development, numeric algorithms, and network communications. The ORR Geodatabase is based on the ArcHydro and ArcGIS Base Map data models. The Arc Hydro data model is designed to support water resources applications within the ArcGIS environment and possesses a structure that enables linkage with scalable hydrologic modeling tools and applications to model hydrologic systems [7] and, in this case, test the potential impacts of various D&D scenarios on the ORR watersheds. These data models were used as templates as there were many input data types in common with the ORR Geodatabase. Modifications were then made for MIKE SHE/11 model-specific input parameters.

The ArcSDE geodatabase can be used to automate and simplify the process of calling stored GIS and timeseries data required to populate the hydrologic modeling tools with required parameters. This can serve as a powerful tool for contaminant flow and transport analyses which require large amounts of high-quality spatial and temporal data in order to ensure reliability and validity of modeling results.

1.2 Objectives

The overall objective of this task was to create a geodatabase to support hydrological model development and simulation of contaminant fate and transport at Oak Ridge Reservation (ORR), TN. The ORR Geodatabase serves as a centralized data management system which facilitates storage, retrieval, and optional versioning of model configuration parameters and output files, and provides a framework for security management and quality assurance in data editing.

As FIU-ARC continues to conduct model simulations to support the D & D remediation activity at ORR, there will be an ongoing need for update of the geodatabase and utilization of the integrated GIS-hydrological modeling system developed. The objectives outlined herein therefore describe the work accomplished during FY 2011 and involve:

1. Compilation of MIKE-SHE/MIKE-11 model configuration files and conversion when necessary to GIS format to facilitate easy integration into the system being developed.

2. Import of simulation input and output files for the Y-12 NSC, WOC and EFPC models into the geodatabase, utilizing the in-built ArcGIS versioning utility when necessary during simultaneous multi-user editing of data files and geoprocessing tasks.

2 ORR GEODATABASE DEVELOPMENT METHODOLOGY

Development of the geodatabase structure involved the following steps:

1. System architecture and database configuration.
2. Identification and compilation of model configuration parameters.
3. Organization of data into geographic datasets based on model requirements.
4. Geodatabase design.
5. Building a working prototype.
6. Documentation of the geodatabase design.
7. Assignment of geodatabase user roles and responsibilities.
8. Import and versioning of model configuration and simulation files.

2.1 System Architecture and Database Configuration

The ORR Geodatabase [Figure 2] is a multiuser relational database management system (RDBMS) built upon a Microsoft SQL Server platform developed using Environmental Systems Research Institute (ESRI) ArcSDE technology. The system was deployed on an advanced Windows server with the latest technology and hardware. ARC-FIU put together a custom server that far exceeds ESRI's ArcGIS Server 10 minimum requirements with respect to memory, CPU speed, security and backup capabilities [**Error! Reference source not found.**]. The Microsoft indows 2008 R2 Server Standard, Enterprise (64-bit) operating system was paired with MS Advanced SQL Server 2008, and the Microsoft .NET framework was installed with ArcGIS Server, which provides a user interface that facilitates data access, database connectivity, cryptography, web application development, numeric algorithms, and network communications [**Error! eference source not found.**]. Once the Server Object Manager (SOM), Service Object Container (SOC), and the GIS Services were installed, the ESRI authorization keys were entered to complete the post installation process. This included the set-up and addition of user accounts to facilitate direct SQL connection from our ArcGIS Desktop 10 clients to the ArcGIS Server and the ORR Geodatabase according to the guidelines specified in the online ESRI Support Center [**Error!**

Reference source not found.].

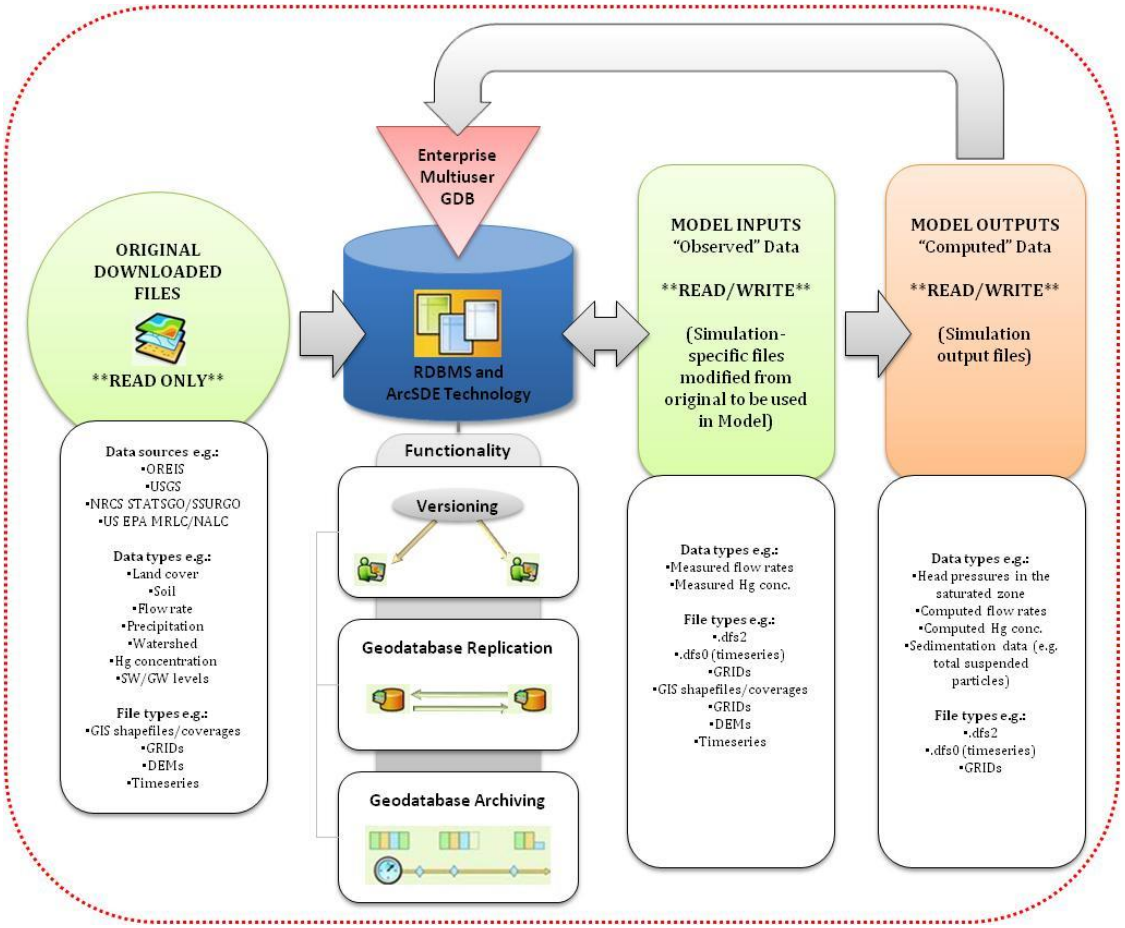

Figure 2. The Oak Ridge Reservation Geodatabase system architecture.

The geodatabase structure facilitates concurrent multi-user editing and management of spatial data within the ArcGIS framework and is comprised of a series of tables which contain feature, raster and attribute data, as well as metadata. Since the ORR database, as previously mentioned, is primarily based on the ArcHydro data model, it possesses a spatial relational database management (RDMS) schema and relationship structure specific to hydrologic systems where spatial relationships between hydrological parameters and geographical features can be defined. Key characteristics of the Oak Ridge Reservation geodatabase are provided in Table 1.

Table 1. Significant Characteristics of the Oak Ridge Reservation Geodatabase

Data Storage	RDBMS Platform, Microsoft SQL Server
Management Interface	ArcCatalog, RDBMS, ArcSDE command line
Supported OS Platform	Any platform
Number of Concurrent Users	Unlimited editors and readers
Network Application	Intranet and Internet
Database Administration Tools	Full DBMS functions for backup, recovery, replication, SQL support, security, etc.
Security and Permissions	Provided by DBMS
Multiuser Functionality	Supports versioning, multiuser editing, geodatabase replication and archiving, various spatial data types & enterprise IT integration.

A variety of interfaces exist for accessing the ORR Geodatabase, including ESRI ArcMap/ArcCatalog, SQL Server or the ArcSDE command line, which allows for better management of data and easier extraction of parameters, with visualization of both input and output from the hydrologic model. The ArcSDE geodatabase structure also supports features such as geodatabase replication and archiving which facilitates efficient data storage, backup and management. A variety of data files and formats are supported by the geodatabase including shapefiles, computer-aided drafting (CAD) files, triangulated irregular networks (TINs), grids, imagery, Geography Markup Language (GML) files, and numerous other GIS data sources.

Tools to support the import, export or conversion of various file formats [Table 2] also exist, which is especially important for interoperability between the ArcGIS and MIKE modeling software. MIKE 11 GIS [8] for example, which is a pre- and post-processing module for MIKE 11 that is included as an extension to the ESRI ArcMap 10.0 version, was used to assist in the import, processing and export of network, cross-section and boundary files used within the MIKE 11 models. MIKE 11 GIS can also be used for comprehensive timeseries data management to present timeseries results and maps from MIKE 11 simulations, and includes non-point and point pollutant load estimation tools for MIKE 11 water quality simulations. These types of tools are useful in this case as the GIS and MIKE SHE/11 model are, as Gogu et al., 2001 [5] describe,

"loosely coupled" at this stage of development, where the software packages remain independent systems and data is transferred as predefined input/output model files, the advantage of this being that it facilitates potential future changes in the software in an independent manner.

Table 2. MIKE SHE/MIKE 11 Model Configuration File Types

Model Input/Output File Types	Description
.dfs0	Timeseries
.dfs2/.dfs3	DHI Grid file
.nwk11	River Network file
.shp	GIS Shapefile
.uzs	Unsaturated Zone Soil Profile
.ecolab	Surface Water Quality data file
.xns11	Cross-section Database
.bnd11	Boundary Condition file
.hd11	Hydrodynamic Setup file
.dem	Digital Elevation Model
.ascii	ASCII text file
.txt	Text file

Two types of tables exist in the geodatabase. These include the user-defined dataset tables (e.g. as seen in Figure 3) which store feature and raster attribute data, and system tables (e.g. Figure 4) that store metadata which supports data management by providing information such as dataset definitions and relationships as well as geodatabase properties. The feature classes (i.e., vector data such as shapefiles and coverages) are represented in the dataset tables with each row in the table representing a feature (i.e. point, line or polygon), while a "Shape" column in each row stores the spatial geometry of that feature. Raster and imagery data are managed and stored in relational tables within the geodatabase as well. Raster data, however, is typically

much larger in size and is therefore accompanied by a side/"block" table for storage. Each raster is cut into smaller pieces, or blocks, and stored in individual rows in the separate block table. ArcGIS provides a comprehensive suite of data conversion tools which facilitate easy migration of existing data into the geodatabase. ArcSDE and/or ArcGIS Server provide a gateway between GIS clients and the RDBMS, which in this case, is SQL Server.

OBJECTID *	Shape *	AREA	PERIMETER	SOILS_ID	RASOIL6_	SOIL5_	S_CODE	GEOL_C	GEOM_C	SOIL_C	SLOPE_C	EROSION_C	SOILSERIES
293	Polygon	15329.82513	1135.977770	293	277	1	01043	0	1	0	4	3	10
294	Polygon	3370.834102	272.1132085	294	275	1	00523	0	0	5	2	3	5
295	Polygon	8114.430214	628.1726104	295	281	1	00161	0	0	1	6	1	1
296	Polygon	3670.908997	269.5777955	296	291	1	00841	0	0	8	4	1	8
297	Polygon	21597.64674	835.4351894	297	289	1	00651	0	0	6	5	1	6
298	Polygon	3071.110511	341.5546058	298	282	1	00161	0	0	1	6	1	1
299	Polygon	56069.37910	1550.099033	299	269	1	80011	8	0	0	1	1	800
300	Polygon	22219.74957	924.4146134	300	285	1	00843	0	0	8	4	3	8
301	Polygon	7231.454275	777.7984870	301	273	1	00543	0	0	5	4	3	5
302	Polygon	12136.17818	799.0664867	302	288	1	00161	0	0	1	6	1	1
303	Polygon	2868.087582	282.6764269	303	284	1	00151	0	0	1	5	1	1
304	Polygon	5520.334858	415.4340139	304	292	1	00161	0	0	1	6	1	1
305	Polygon	5806.989627	521.0081400	305	302	1	01041	0	1	0	4	1	10
306	Polygon	10206.42588	524.0834803	306	327	1	96021	9	6	0	2	1	960
307	Polygon	4572.815743	354.6568304	307	294	1	00151	0	0	1	5	1	1
308	Polygon	4637.293139	359.9022834	308	295	1	00741	0	0	7	4	1	7
309	Polygon	7753.583513	441.1641078	309	280	1	99532	9	9	5	3	2	995
310	Polygon	11604.56649	641.0893176	310	299	1	00841	0	0	8	4	1	8
311	Polygon	28787.36438	1705.628763	311	305	1	00841	0	0	8	4	1	8
312	Polygon	5971.444522	333.4203140	312	303	1	00951	0	0	9	5	1	9
313	Polygon	4234.384814	309.9673227	313	311	1	00651	0	0	6	5	1	6
314	Polygon	3509.302305	292.7305613	314	312	1	00161	0	0	1	6	1	1
315	Polygon	18407.26500	943.1902418	315	314	1	00851	0	0	8	5	1	8
316	Polygon	41690.60048	984.8046132	316	337	1	00841	0	0	8	4	1	8
317	Polygon	15532.80161	670.7689412	317	301	1	00852	0	0	8	5	2	8
318	Polygon	10541.01818	548.7281163	318	300	1	00851	0	0	8	5	1	8
319	Polygon	17881.98271	756.7144718	319	310	1	00451	0	0	4	5	1	4
320	Polygon	12013.61074	570.5020435	320	309	1	00852	0	0	8	5	2	8
321	Polygon	8024.155664	572.1020032	321	298	1	01043	0	1	0	4	3	10
322	Polygon	38751.36672	1702.523713	322	283	1	00543	0	0	5	4	3	5
323	Polygon	7979.122844	549.0069457	323	308	1	00161	0	0	1	6	1	1
324	Polygon	41458.37687	1575.095151	324	293	1	01243	0	1	2	4	3	12
325	Polygon	10280.01743	657.8060632	325	322	1	00633	0	0	6	3	3	6
326	Polygon	6383.654175	451.3172705	326	326	1	00161	0	0	1	6	1	1
327	Polygon	17849.92965	879.6823303	327	321	1	00842	0	0	8	4	2	8
328	Polygon	55328.52736	2959.932104	328	325	1	96121	9	6	1	2	1	961
329	Polygon	7837.350710	527.9826617	329	316	1	01041	0	1	0	4	1	10
330	Polygon	4579.218606	413.6110480	330	319	1	00161	0	0	1	6	1	1
331	Polygon	5745.835547	503.1966797	331	290	1	00543	0	0	5	4	3	5
332	Polygon	6883.401660	355.7646614	332	313	1	00343	0	0	3	4	3	3
333	Polygon	14215.92574	808.2794441	333	351	1	01141	0	1	1	4	1	11
334	Polygon	8881.380926	725.8474087	334	287	1	96211	9	6	2	1	1	962
335	Polygon	3512.644901	312.6107915	335	331	1	00161	0	0	1	6	1	1
336	Polygon	29699.27123	858.8123330	336	297	1	01233	0	1	2	3	3	12
337	Polygon	8879.870520	671.2736673	337	307	1	96021	9	6	0	2	1	960
338	Polygon	16048.28037	689.9268396	338	334	1	00753	0	0	7	5	3	7
339	Polygon	42418.62433	1998.380528	339	324	1	01233	0	1	2	3	3	12
340	Polygon	14015.03703	740.4220542	340	330	1	01033	0	1	0	3	3	10

Figure 3. ORR Geodatabase “Soils” dataset table storing the soil feature attributes.

OBJECTID *	KeyName	KeyValue
1	DHI Basic Data Model Version	2008
2	Version	501
3	EUM_VERSION	09/27/2011 22:06:40
4	DefaultUnitSystem	SI
5	Network Features Data Model Version	2007
6	Mike 11 Features Data Model Version	2007
7	Mike 11 Max XSec Points	100
8	Mike 11 XSec Point Spacing	10
9	Mike 11 XSec Outside DEM	FALSE
10	TemporalAnalystVersion	501
11	Network DEM Z Unit	1000
12	DEM Raster Cell Size	10
13	Surface Layer.Type	Raster
14	Surface Layer.Path	
15	Surface Layer.Name	
16	Network DEM	G:\DOE_Project3\DOE_ORR_GeodB\DOE_ORR_GeodB\DOE_ORR_GeodB.mdb\DEMs\Raster.
17	Nwk11 File Path	E:\EWR\MODELS\EFPC_Model\Simulations\EFPC001\RN.nwk11

Figure 4. ORR Geodatabase system table storing metadata of certain network features.

The multiuser functionality of this system is its most significant feature as it facilitates simultaneous editing of the geographic data utilized and generated during hydrological model development and model simulation. A mechanism referred to as "versioning" records all the database changes as rows in tables, so that GIS transactions can be stored in the database and the metadata for each “version” can be used to isolate multiple edit sessions, share replicas, synchronize contents across multiple databases, perform automatic archiving, and support historical queries.

2.2 Identification and Compilation of Model Configuration Parameters

Modeling of hydrologic systems requires large amounts of historical data and involved the download and assimilation of vector and raster map products as well as timeseries data from multiple sources including the Oak Ridge Environmental Information System (OREIS), USGS, NRCS STATSGO or SSURGO soil database, and the U.S. EPA MRLC or NALC land cover database. Associated metadata was also collected to be stored in the geodatabase. The information collected directly supports hydrological model development and calibration [Table 3] and includes, for example, GIS coverages/shapefiles of the delineated watersheds, surrounding buildings and man-made structures which may serve as sources of contamination, roads, stream gauge locations, monitoring wells, bore holes, land cover and soils; raster imagery; and

observed/measured timeseries data such as flow rates, precipitation, evapotranspiration, mercury concentration and surface and groundwater levels.

The MIKE SHE/11 model uses GIS data inputs for many of its configuration parameters which contain spatial features within the model domain such as points representing monitoring stations, lines representing rivers/stream networks, or polygons which outline areas such as watershed and catchments. The significance of using GIS data is not just the spatial representation of hydrologic features, but their association with timeseries data attributes such as flow rates and directions, contaminant concentrations, water levels, precipitation, etc. Availability of data in this format shortens the time for data preparation and ultimately model development. Figure 5 and Figure 6 show some of the spatial data inputs used for model development.

Table 3. Model Configuration Files Stored in the ORR Geodatabase

Spatial Data	**Characteristics Represented**
Admin_Features	EFPC, WOC, Y-12 & OSY Model domains (polygons)
	ORR Boundary
Admin_GRIDs	Model domains (GRIDs)
Conductivity_GRIDs	Hydraulic conductivity GRIDs
Contaminant_Conc_Features	Monitoring points (has associated timeseries attribute data)
	Plume Contours
Contaminant_Conc_GRIDs	Interpolated contaminant plumes (GRIDs)
DEMs	Clinch River, EFPC & WOC Watershed DEMs
Digital_Orthophotos	ORR DOQs (.bmp)
Drainage_GRIDs	Drainage Time Constant, Drainage Codes, Detention Storage (GRIDs)
GW_Features	Groundwater level contours
GW_GRIDs	Groundwater level GRIDs
Hydro Features	Watersheds, subwatersheds, catchments, hydroareas (lakes/ponds) (polygons)
	Floodplain polygons
	Hydrography, Hydrodrainage, hydrostructures (polylines)
Impervious_GRIDs	Paved runoff coefficient (GRID)
Landcover_Landuse_Features	Landuse/Landcover polygons
Landcover_Landuse_GRIDs	Vegetation grid codes
Manning	Manning's coefficients (GRIDs)
Monitoring_Stations	USGS SW monitoring stations, outfalls, GW monitoring wells
Network_Features	Rivers, streams, reaches, cross sections, diversion ditch, utilities (polylines)
	Nodes (points)
Physical_Features	Buildings, obscured areas, natural outlines, man-made outlines (polygons)
	Margins, man-made structures (polylines)
Soils	Geology, soils (polygons)
Topo_Features	Elevation contours
Transport_Features	Roads, railroads, transportation structures (polylines)
Temporal Data	**Characteristics Represented**
Monthly_RF_TS	Monthly rainfall timeseries
Flow_Aug_TS	Flow augmentation timeseries
DHI_Timeseries	Flow rate/discharge timeseries

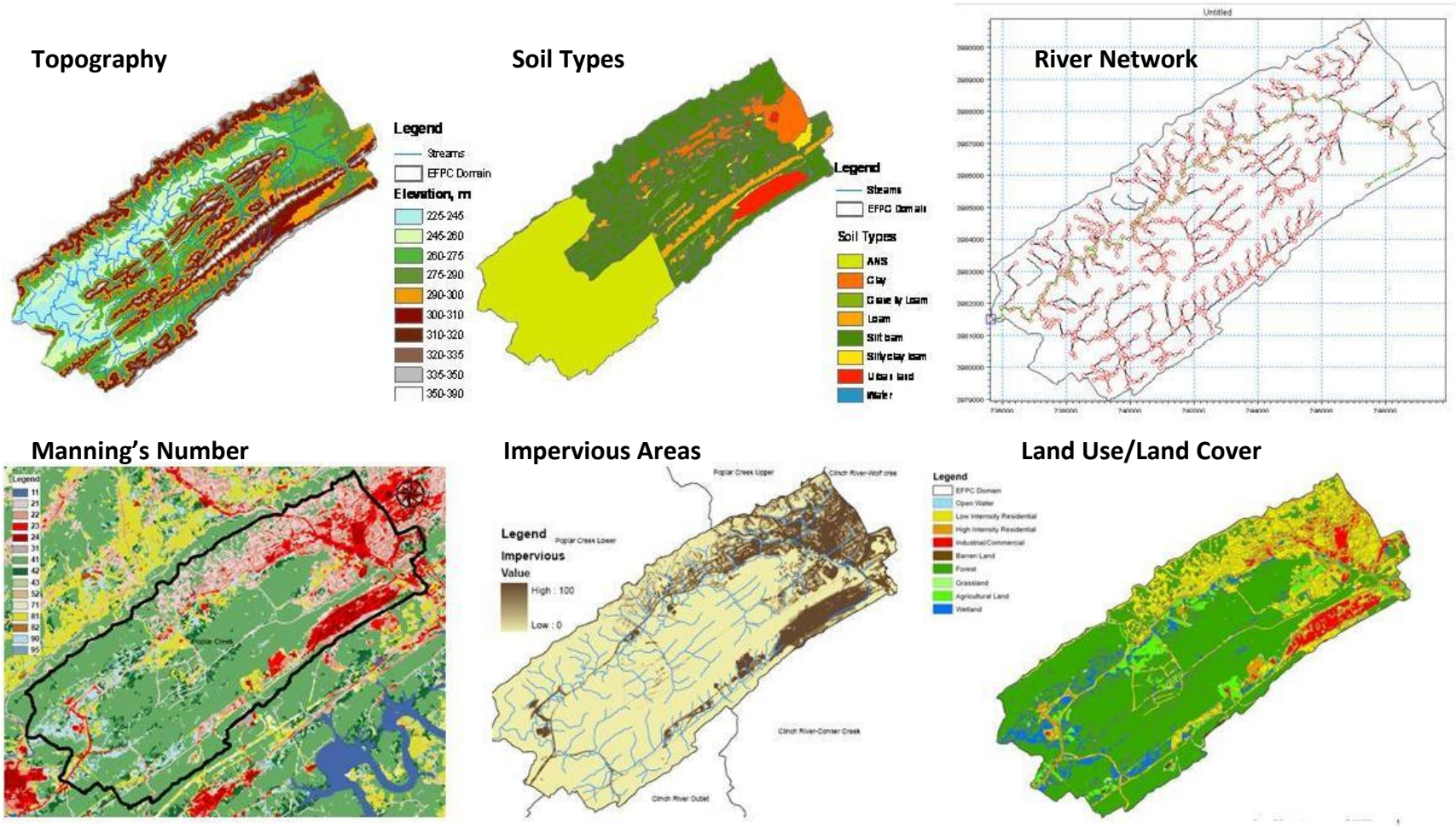

Figure 5. Gridded and network overland flow input data files used for model development.

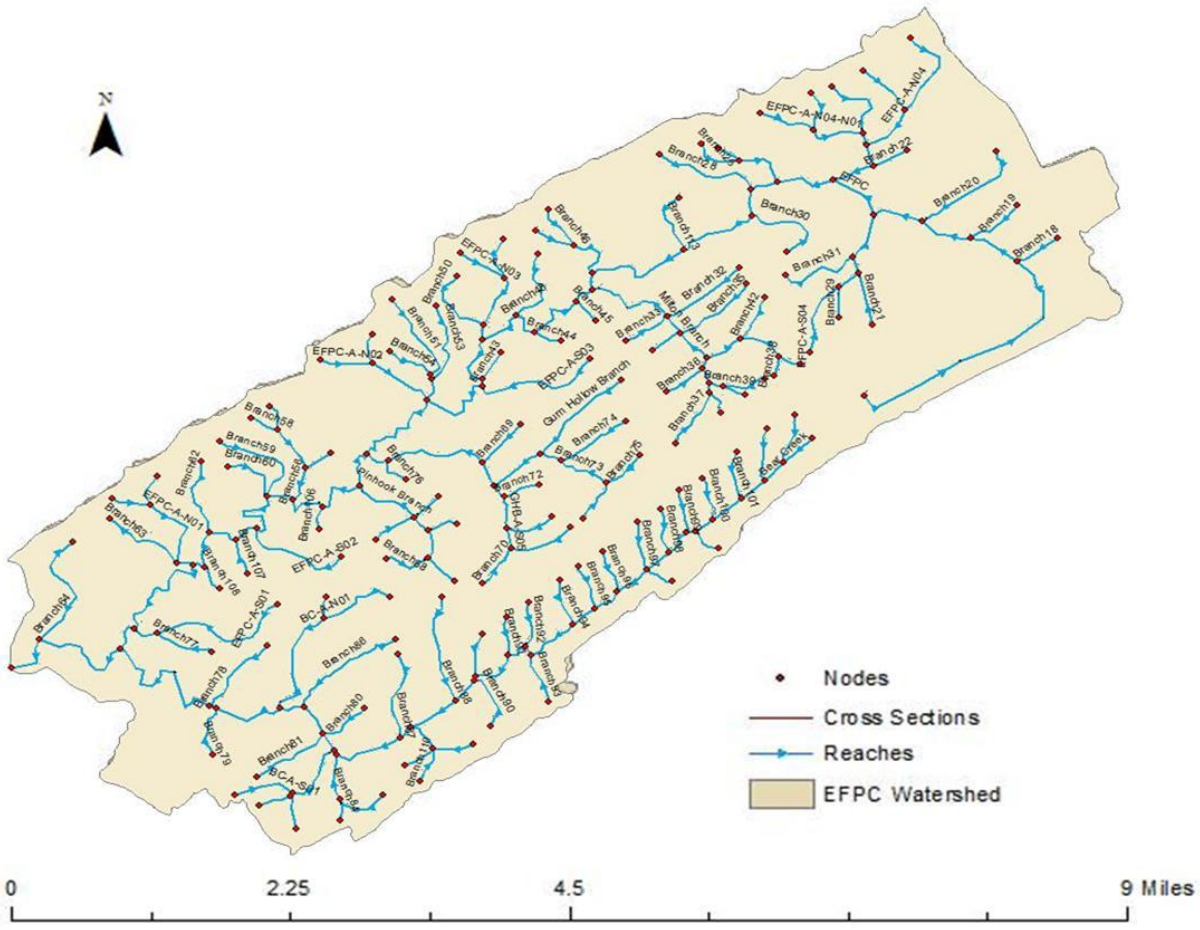

Figure 6. GIS map showing EPFC network features used for model development.

2.3 Organization of Data into Geographic Datasets Based on Model Requirements

All spatial and temporal data files that were downloaded were initially archived within system folders organized according to their intended use such as GIS mapping and 3D display and/or hydrological modeling and analysis. Metadata was also collected to ensure records were kept of data sources (e.g. OREIS data dictionary). It was important to store metadata at all times, as during model development file modification is often necessary, for example in modeling an entire watershed vs. modeling a small subdomain of the watershed. This involves the use of

built-in geoprocessing tasks facilitated by the ArcGIS system which aid in generalization of feature representations for use at larger scales. In these instances, specifications such as whether the data was an original downloaded file, a file modified for model development or a file generated from running model simulations should be defined in the associated metadata.

All data files were then reorganized according to the data categorization specified in the MIKE SHE/11 model prior to import into the geodatabase (e.g. hydrological features, network features, landcover/landuse, topography, etc.). Feature datasets and raster catalogs were then defined within the geodatabase based on this categorization. Discrete features were generally represented as feature classes of points, lines, and polygons, however, advanced data types such as networks representing the surface water system and timeseries data were also represented.

2.4 Geodatabase Design

At the beginning of the project, the data themes required for hydrological model development were defined and the geodatabase then designed based on existing ArcGIS data models which were studied for ideas, patterns and best practices. The ORR Geodatabase is based on the ArcHydro and ArcGIS Base Map data models. These models were used as templates as there were many input data types in common with the ORR Geodatabase. Modifications were then made for project specific input parameters. The Arc Hydro data model [Figure 7] is designed to support hydrologic simulation models within the ArcGIS environment, such as MIKE SHE/11 which requires and generates spatial and temporal data, most significantly data such as channel cross sections, stream geometric networks and nodes, monitoring points, watersheds and subwatersheds, and other hydrographic and drainage files.

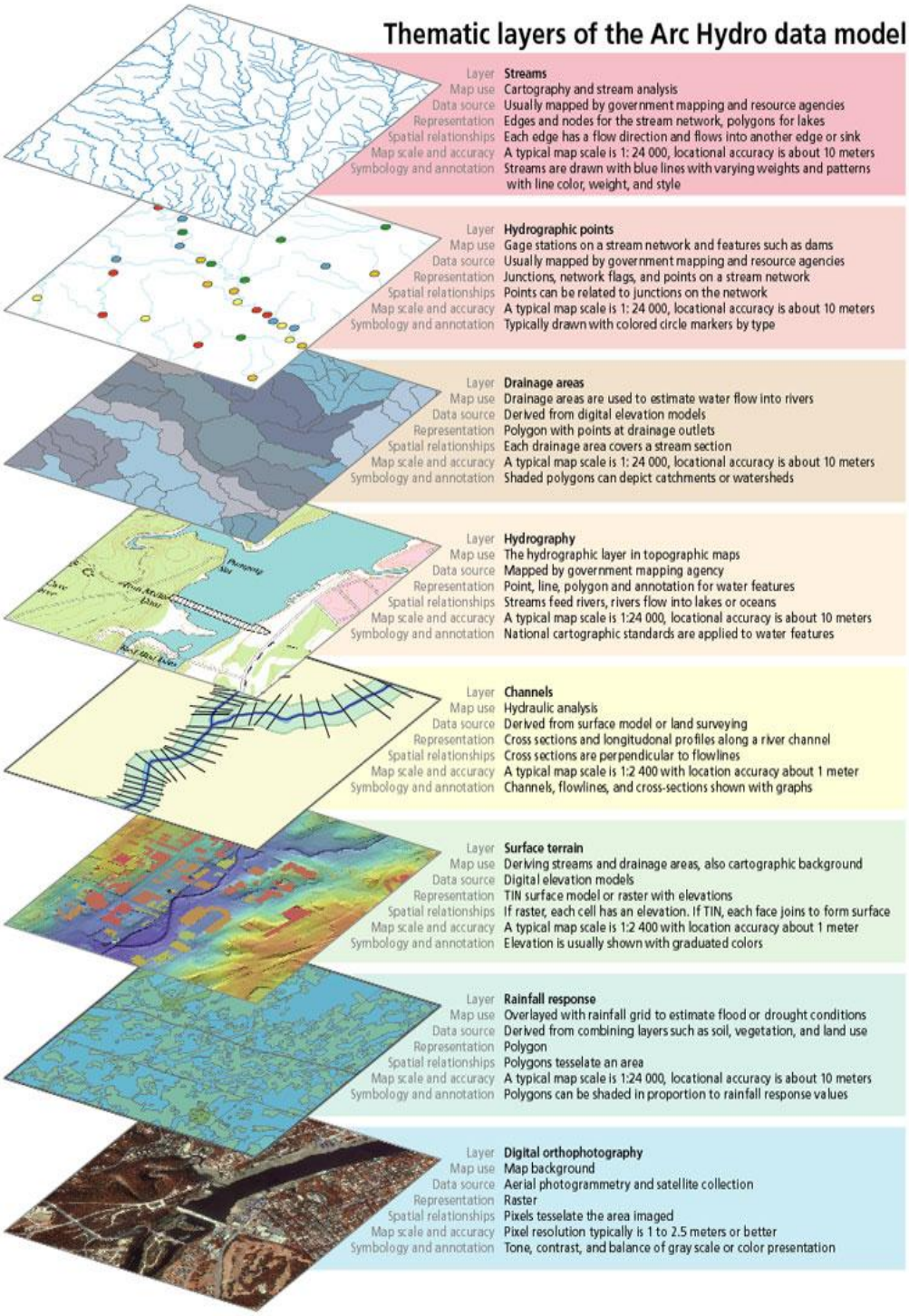

Figure 7. The ArcHydro data model [7].

The geodatabase structure of this model uses tables which each have a field in common with a unique identification number that is used to establish relationships between the various hydrologic files [Figure 8]. This structure enables linkage with scalable hydrologic modeling tools and applications to model hydrologic systems and, in this case, test the potential impacts of various D&D scenarios on the ORR watersheds [7].

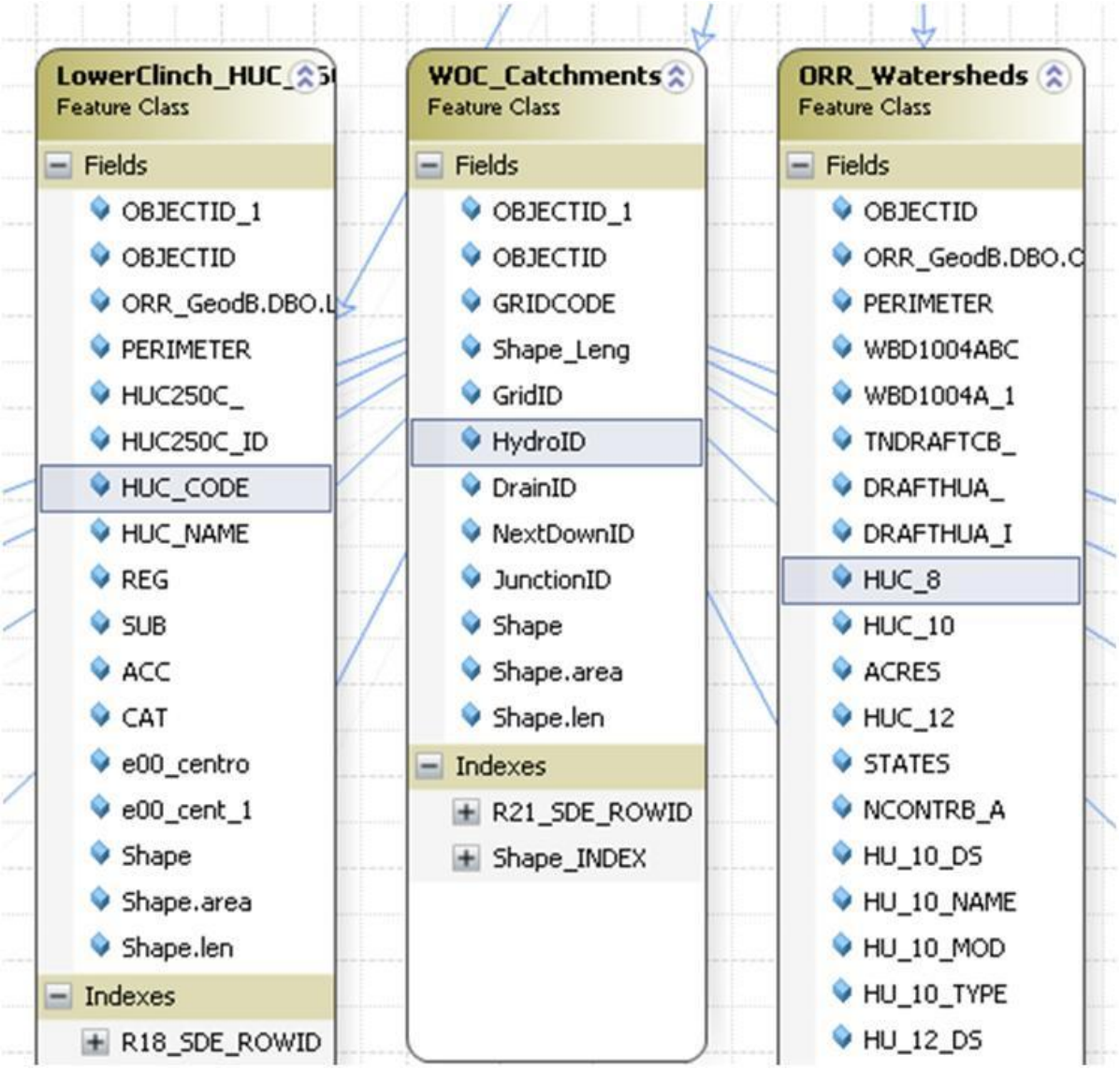

Figure 8. ORR geodatabase schema showing feature classes with common fields (HydroID/HUC codes) used to establish relationships between hydrologic features.

Arc Hydro has a standardized data structure which helps in the organization of hydrologic features (e.g. river/stream networks, drainage lines, catchments, monitoring stations, etc.) and their relationships to each other, providing a common framework that can be utilized by various hydrologic models. The Arc Hydro data model also facilitates the import of timeseries data into ArcGIS object classes which are tables within the geodatabase that store temporal data that is often related to the hydrologic spatial features [Figure 9]. These object classes are comprised of four basic fields (FEATURE, TYPE, TIME and VALUE) and provide information on the hydrologic feature the data is referring to, the type of parameter recorded, the date and time the data was collected and the data value.

OBJECTID *	DHI_ID	Name	Origin	StartTime	EndTime	TimeStep	TimeStepUnit	TimeType	ValueType	EUMType	EUMUnit
4359	183	55-2B		4/9/1997	3/4/2009	-1	1400	4	0	100059	1000
4360	184	55-2C		4/9/1997	3/4/2009	-1	1400	4	0	100059	1000
4361	185	AB8110-1		4/9/1997	3/4/2009	-1	1400	4	0	100059	1000
4362	186	AB8110-2		4/9/1997	3/4/2009	-1	1400	4	0	100059	1000
4363	187	AB8110-3		4/9/1997	3/4/2009	-1	1400	4	0	100059	1000
4364	188	AB8110-4		4/9/1997	3/4/2009	-1	1400	4	0	100059	1000
4365	189	AB8110-5		4/9/1997	3/4/2009	-1	1400	4	0	100059	1000
4366	190	AB8110-6		4/9/1997	3/4/2009	-1	1400	4	0	100059	1000
4367	191	ED4		4/9/1997	3/4/2009	-1	1400	4	0	100059	1000
4368	192	EU4		4/9/1997	3/4/2009	-1	1400	4	0	100059	1000
4369	193	EW-01		4/9/1997	3/4/2009	-1	1400	4	0	100059	1000
4370	194	GW-064		4/9/1997	3/4/2009	-1	1400	4	0	100059	1000
4371	195	GW-087		4/9/1997	3/4/2009	-1	1400	4	0	100059	1000
4372	196	GW-108		4/9/1997	3/4/2009	-1	1400	4	0	100059	1000
4373	197	GW-115		4/9/1997	3/4/2009	-1	1400	4	0	100059	1000
4374	198	GW-141		4/9/1997	3/4/2009	-1	1400	4	0	100059	1000
4375	199	GW-149		4/9/1997	3/4/2009	-1	1400	4	0	100059	1000
4376	200	GW-151		4/9/1997	3/4/2009	-1	1400	4	0	100059	1000
4377	201	GW-152		4/9/1997	3/4/2009	-1	1400	4	0	100059	1000
4378	202	GW-153		4/9/1997	3/4/2009	-1	1400	4	0	100059	1000
4379	203	GW-154		4/9/1997	3/4/2009	-1	1400	4	0	100059	1000
4380	204	GW-156		4/9/1997	3/4/2009	-1	1400	4	0	100059	1000
4381	205	GW-159		4/9/1997	3/4/2009	-1	1400	4	0	100059	1000
4382	206	GW-161		4/9/1997	3/4/2009	-1	1400	4	0	100059	1000
4383	207	GW-168		4/9/1997	3/4/2009	-1	1400	4	0	100059	1000

Figure 9. Timeseries data stored as an ArcGIS object class.

2.5 Building a Working Prototype

This involved testing, review and refinement of the geodatabase design. A sample geodatabase was first generated using a personal geodatabase, and samples of each data type required for model development or generated from the numerical simulations were uploaded to ensure that there were no data incompatibility issues before populating the final geodatabase. Once a working schema was established, data was loaded into the ArcSDE geodatabase.

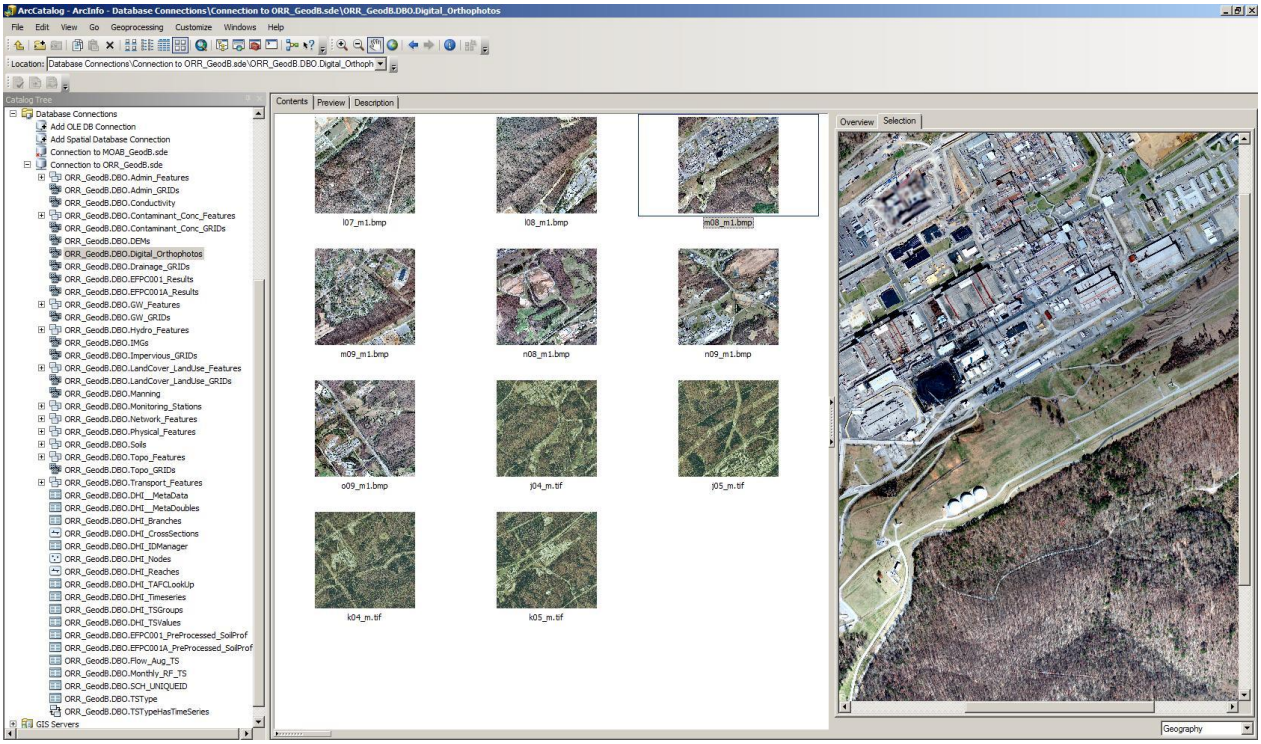

Figure 10. The Oak Ridge Reservation Geodatabase viewed through ArcCatalog.

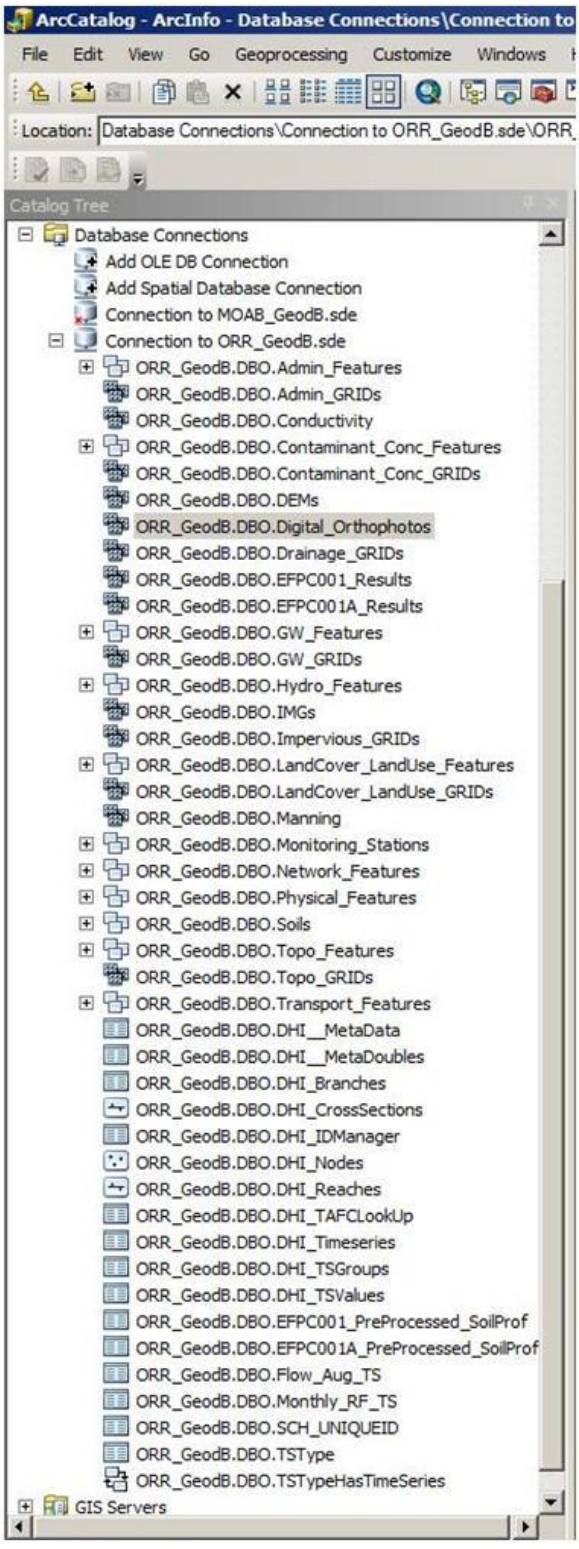

Figure 11. The ORR geodatabase ArcCatalog tree showing feature datasets, raster catalogs and object classes (tables).

2.6 Documentation of the Geodatabase Design

Documenting the geodatabase design can assist in representation of the map layers, metadata and other elements specific to the data model used to create the geodatabase. ESRI provides a downloadable diagramming utility for generation of MS Visio graphics of these geodatabase datasets and elements (http://arcscripts.esri.com), which can be easily cut and pasted into MS Word or PowerPoint, or any application that accepts .wmf files. The "Geodatabase Diagrammer" for ArcGIS 10 is a productivity tool which uses the MS Visio GUI for creation, editing or analysis of geodatabase schema. The schema consists of editable graphics created within the MS Visio application. The ArcGIS "Geodatabase Diagrammer" is essentially a visual editor for ESRI's XML Workspace Document created by ArcCatalog which is the management application in the ArcGIS Desktop product suite. The "Geodatabase Diagrammer" tool for ArcGIS 10 was used to generate a schema diagram in MS Visio of the ORR geodatabase as seen in Figure 12, Figure 13, Figure 14 and Figure 15 below.

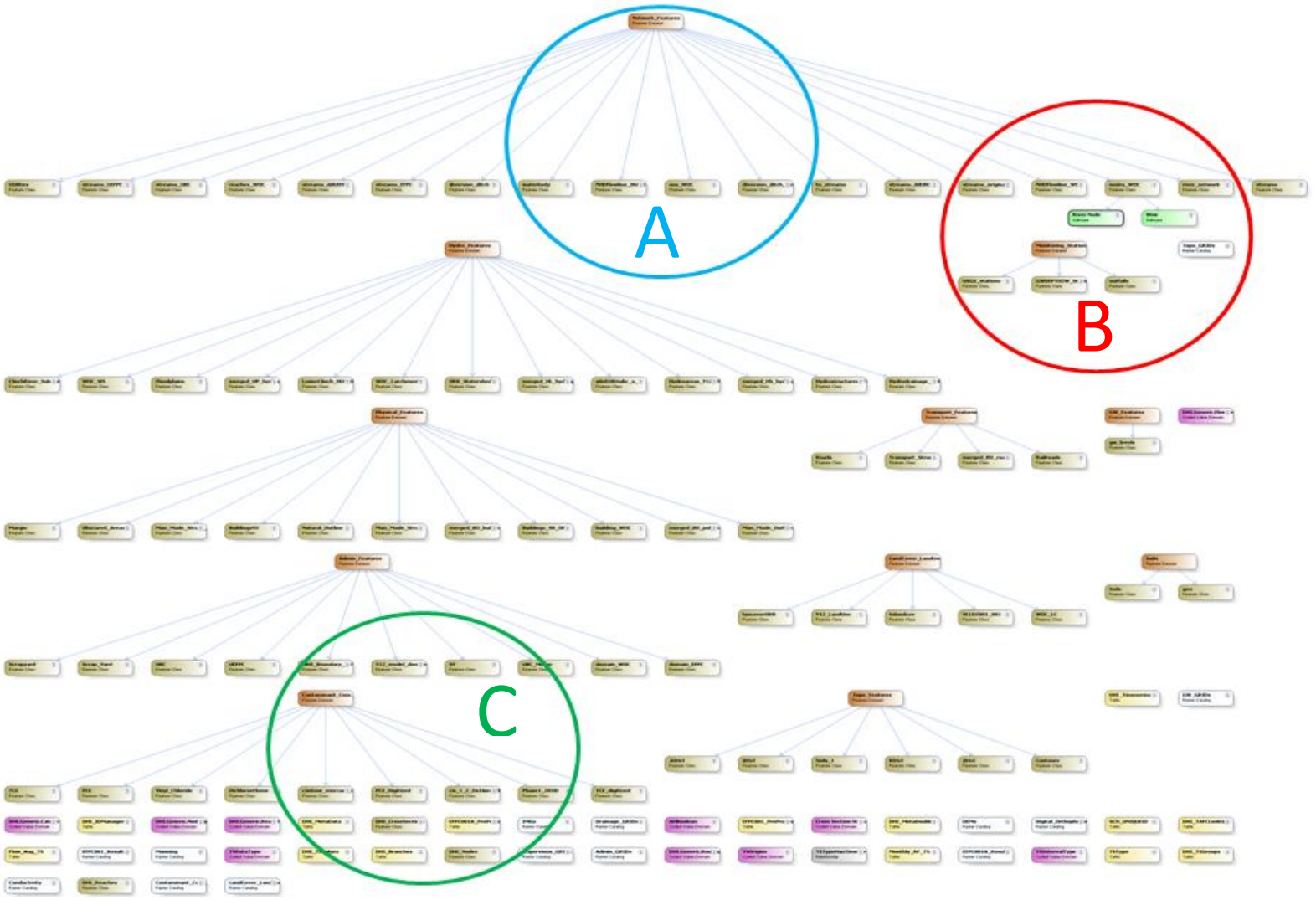

Figure 12. The ORR Geodatabase schema generated using the ArcGIS “Geodatabase Diagrammer” utility for ArcGIS 10.

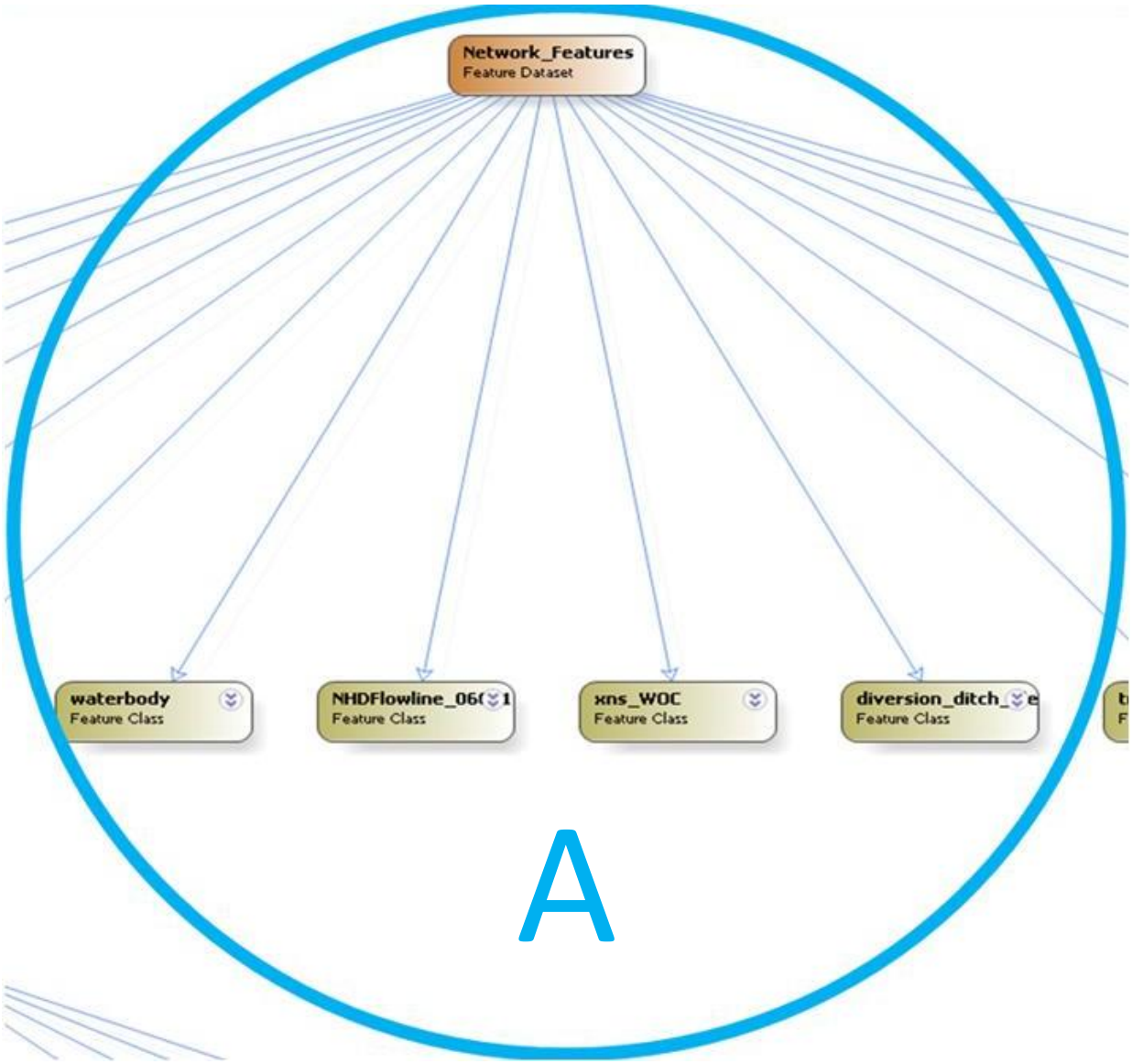

Figure 13. Closer view of circle A in the schema diagram shown in Figure 12 above.

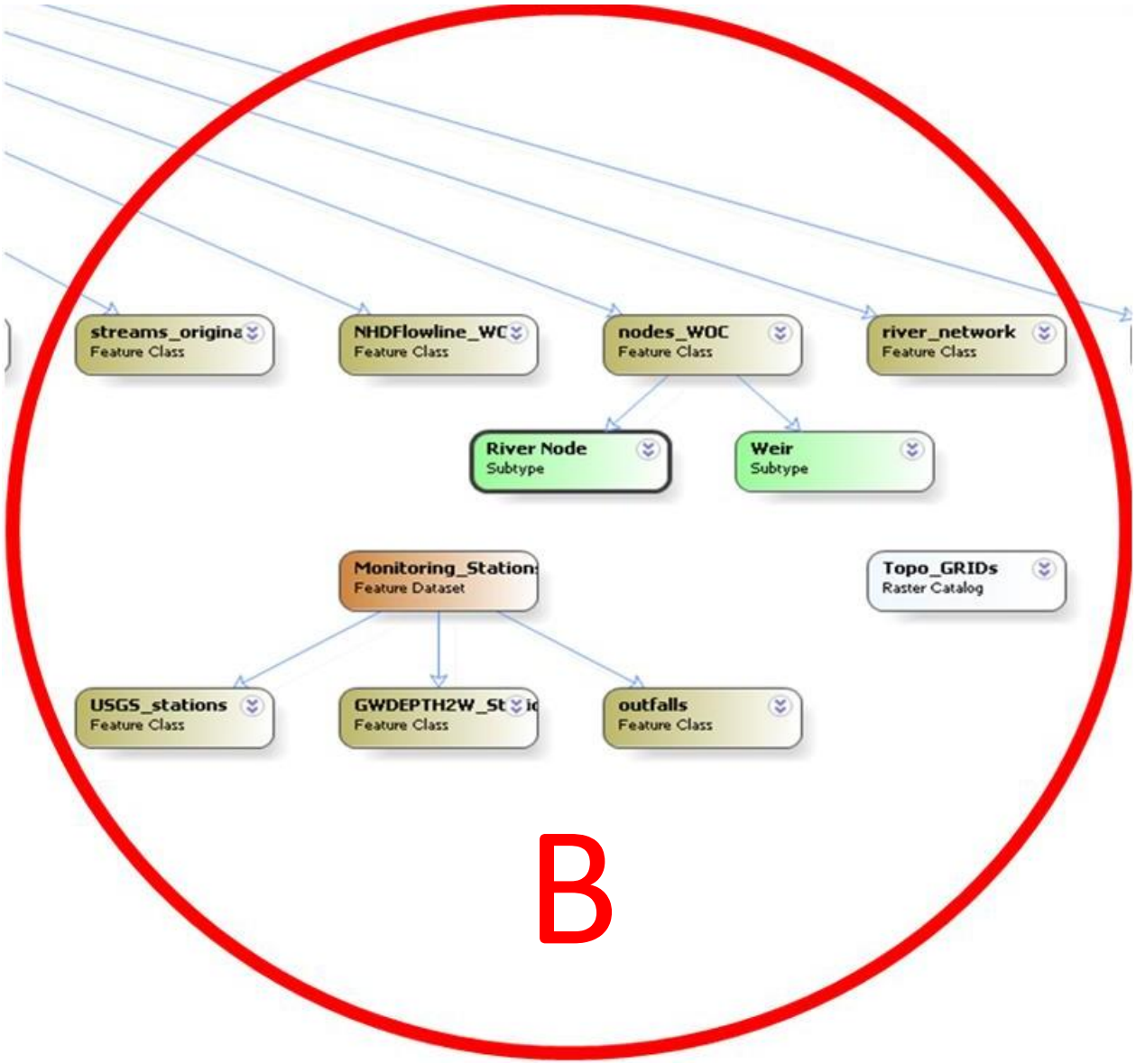

Figure 14. Closer view of circle B in the schema diagram shown in Figure 12 above.

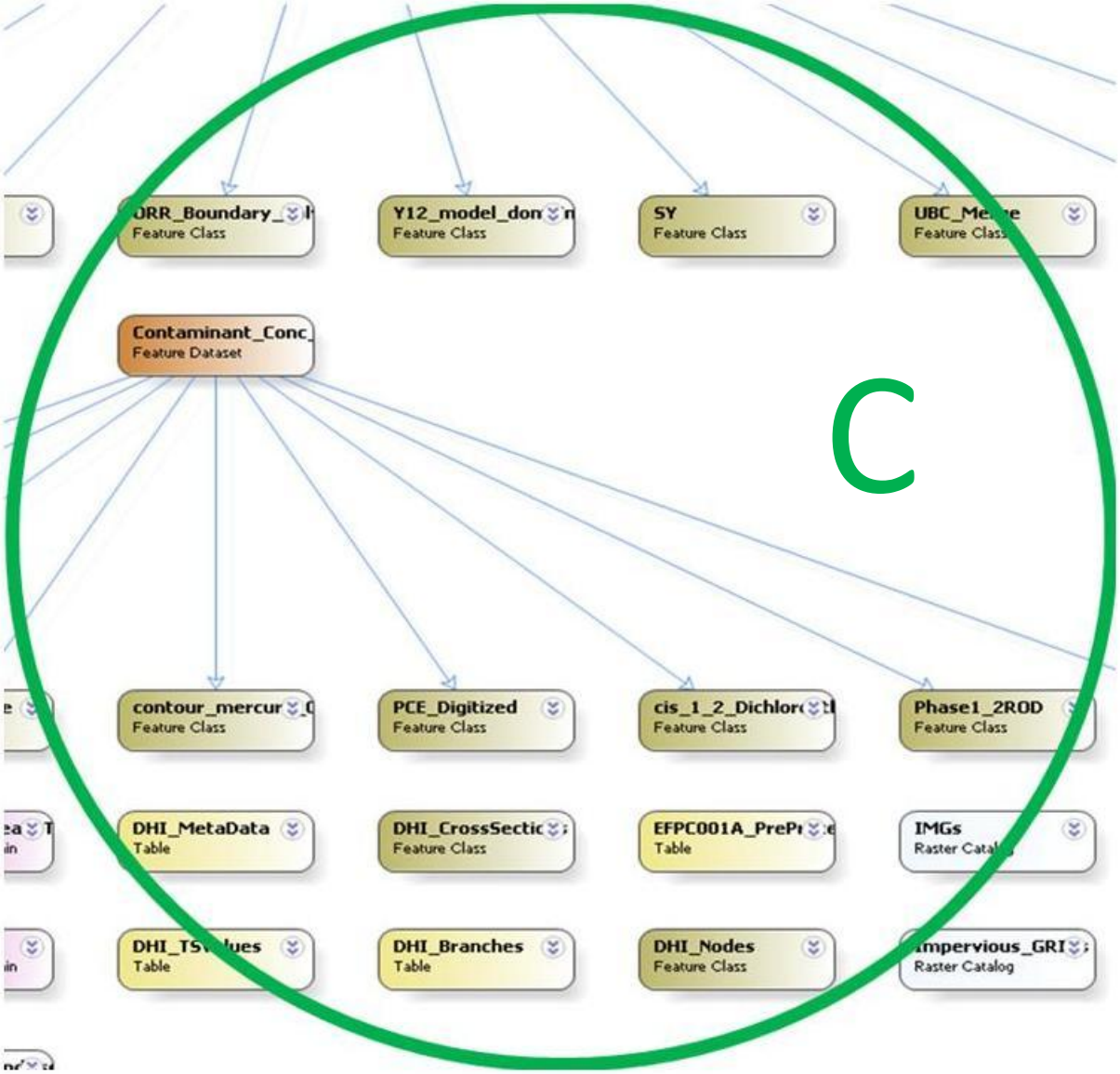

Figure 15. Closer view of circle C in the schema diagram shown in Figure 12 above.

The ArcGIS geodatabase is an XML-based GIS data exchange system which facilitates the export and import of preconfigured data as XML files which contains both the data definition and the data itself. The data definition is what provides the basic information for creating the schema diagram described above as well as information related to the feature classes. Subtypes, domains, and relationship classes can also be specified. The data part provides the data values to be inserted into each feature class or table. Some of these key elements are described below:

- **Datasets** – The "Geodatabase Diagrammer" utility displays the dataset properties to the right of the schema diagram, as seen in Figure 16. Specifications such as feature type (i.e., feature class, raster, relationship class, etc.); shape (i.e., point, line or polygon); spatial coordinate properties (i.e., map projection, horizontal and vertical coordinate systems, spheroid, datum, XY units, and z and m properties); and field names and field types among others can be observed. If subtypes exist, their properties can be viewed here as well.

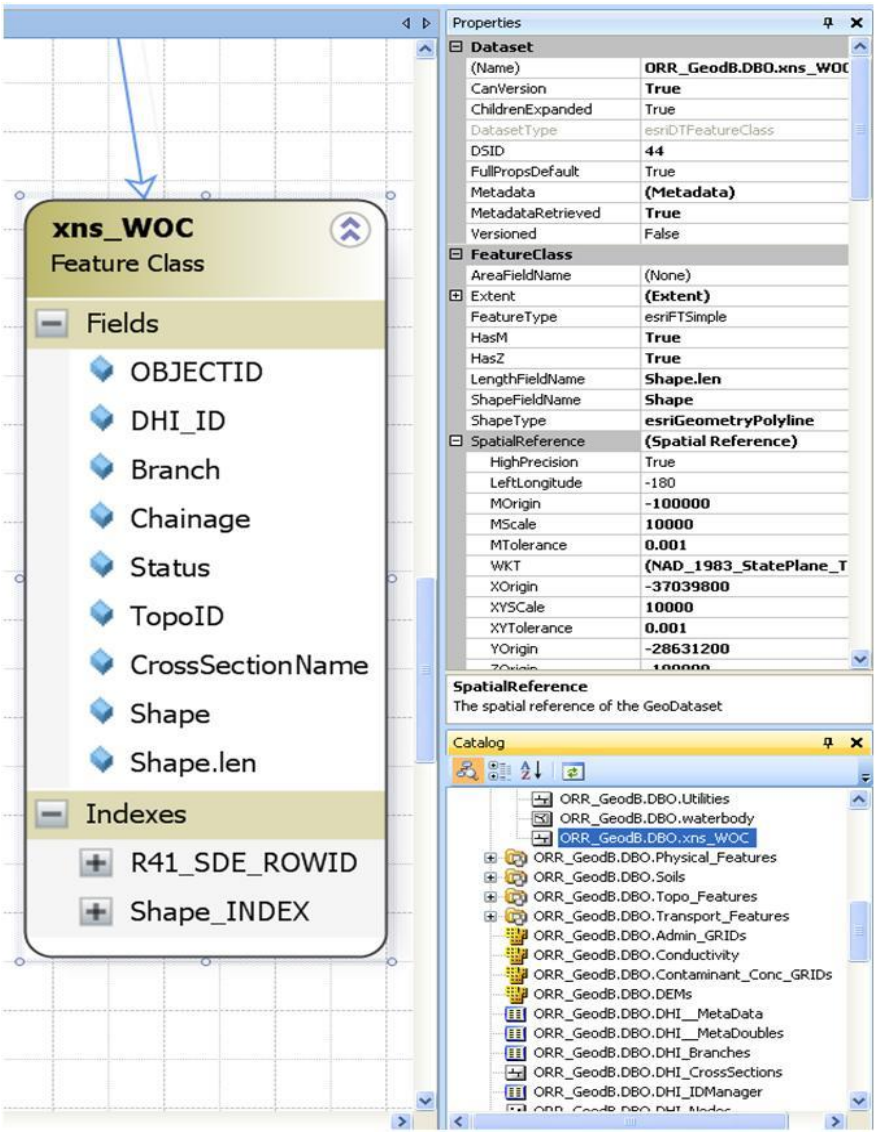

Figure 16. Properties of the river cross section dataset viewed using the "Geodatabase

Diagrammer" utility for ArcGIS 10.

- **Relationship Classes** – Relationships between various features are defined here in the same manner as in all RDBMS applications. Common attributes in each table are linked to each other through a common field and the rows in one table can be associated with rows in another table as a one-to-one, one-to-many, or many-to-many relationship.
- **Domains** – Domains can be represented in the database schema for each feature to specify valid value lists or ranges for each attribute column, which serves as a means by which data integrity can be enforced.

Spatial relationships and rules such as topologies and networks can also be documented in the geodatabase XML schema diagram in addition to map layer specifications (i.e., how the map features and labels are symbolized and rendered). Other general properties that were documented included tables containing metadata derived from data sources such as the OREIS database dictionary.

2.7 Assignment of Geodatabase User Roles and Responsibilities

Roles and responsibilities of the ArcSDE geodatabase users were defined at this stage into common categories or groups, which included those who simply view data, data editors, and those who create new data. Permissions were then assigned which determined what users were authorized to do within the geodatabase and with the actual data based on their roles (see Table 4). User permissions can be set at the database or dataset levels. Permissions at the database level authorize users to create new datasets or administer the geodatabase, whereas at the dataset level, users are granted either read-only or read/write access. Read-only users can only view the data, while those granted read/write privileges (i.e., data editors) can update, insert and delete data. Specific permissions can also be designated to control user access to a geodatabase version. This however is not set through the SQL DBMS, but is determined by the creator of a versioned file within the geodatabase who decides what type of access other users have to the versioned geodatabase. "Public" access grants all users access and the ability to

make modifications. A “Private” version can only be accessed by the creator, and a “Protected” version permits viewing by other users but modification by the creator only.

Table 4. ORR Geodatabase User Privileges Based on User Type

Type of user	Database/Dataset permissions
Data viewer	• SELECT (read-only users)
Data editor	• SELECT, INSERT, UPDATE, and DELETE other users' data objects if necessary • EXECUTE stored procedures associated with the data to be edited
Data creator	• CREATE TABLE • CREATE PROCEDURE
ArcSDE administrator	Automatically granted permissions to work with the geodatabase when it is created and datasets are registered as versioned.

The SQL database management system (DBMS) has built-in roles and responsibilities which were used to group users and assign privileges based on data access needs, and which in this case, simplified the administration of privileges for multiple users with common functions. ARC-FIU researchers working on the various hydrological models of the ORR watersheds were granted access to the ORR geodatabase and in most cases assigned the role of “Data editor” to facilitate required tasks such as data import, conversion, transformation and export. At this stage, data maintenance and any data creation will be carried out by the ArcSDE administrator, and project stakeholders not directly involved in model development will only be given data viewing privileges.

2.8 Database Configuration for Remote Access

The ORR geodatabase was configured for concurrent multi-user access and editing capability, adhering to the appropriate security and quality assurance protocols necessary to maintain data integrity. This process exerts control on the type of access all users have to the geodatabase and

its datasets, and enables specification of user data management privileges. Connection to the geodatabase requires Windows-authenticated credentials, and permissions are assigned to users according to the existing roles contained in SQL Server which already have predefined sets of permissions; however, the option to create new roles and set associated permissions is also possible if necessary. Windows authentication for access to the geodatabase was selected for simple configuration utilizing a certificate-based security mechanism, which is more secure than an operating system (OS)-based authentication. A "GIS & Hydrological Modeling Data Server Management" document was created as an internal reference document which provides system configuration details and credentials to be used for accessing the database.

2.9 Import and Processing of Model Configuration and Simulation Files

Once the ORR geodatabase was created, observed hydrogeological data was imported into existing feature and raster datasets which were defined according to their use (e.g. for hydrological modeling and analysis, mapping or 3D display) and the model compartment where the file was to be utilized (e.g. land cover/land use, transportation, topologies, networks, contaminant concentrations, etc.). Metadata which specifies whether the data is an original downloaded file, a file modified for model development or a file generated from running model simulations was also defined at this point.

2.9.1 Processing of Model Input/Output Files

MIKE SHE/11 requires several model-specific input parameters as described in Table 3. Many of these file types, described in Table 2, can be imported into a geodatabase through the ArcGIS GUI via MIKE 11 GIS and are stored as both feature and object classes, or as raster grid files. Object classes represent some of the timeseries (dfs0) data used for model simulations.

MIKE 11 GIS is a pre- and post-processing ArcGIS extension tool for MIKE 11 files, which essentially serves as a geodata model that generates a geodatabase within the ArcMap interface to store MIKE 11 spatial and timeseries (i.e., geographic, numeric and text) input data and

simulation results. This dynamic geodatabase serves as a temporary repository of MIKE 11 files in this case, and GIS and hydrologic model integration is achieved via the import and export of data between the ArcGIS system and the MIKE SHE/11 hydrological model. Data is ultimately stored in the static ORR Geodatabase which serves as what is described by Olivera et al., 2006 [10] as a "hub data model", which is a non-model-specific repository of information from various sources that the models developed for the different areas of Oak Ridge Reservation may have in common.

Several model-specific output files including computed flow data at each node (head pressures in the saturated zone for each timestep), computed flow data in the rivers for each time step, computed concentrations in the overland, unsaturated, saturated zones and river (daily timeseries) and sedimentation information (total suspended particles, mercury concentrations, sediments) are created after model simulation, many of which are raster (dfs2) grid files. These files can be loaded into the database in several ways including: (1) the ArcGIS/geoprocessing graphical user interface (GUI), (2) the SDERASTER command line loader, (3) the ArcObjects COM API customized application, or (4) using geoprocessing functions such as scripting [**Error! eference source not found.**]. Raster files generated by model simulations can also be kept in the default system folders created by the MIKE SHE/11 model, and instead system tables within the ORR Geodatabase used to store the metadata related to these files with hyperlinks that serve as pointers to the locations of the actual data files.

In many instances, file modification is necessary either for use at smaller scales or to modify appended timeseries or attribute data to run comparative simulations. This was done using ArcGIS geoprocessing tools to generate compatible MIKE SHE/11 model input data. Versioning facilitates concurrent editing by authorized users and tracks the edits made to a specific dataset. A user can then specify the level of user access (i.e. public, protected or private) to a particular version. In order to prevent accidental corruption or loss of data in the geodatabase, particularly of the parent versions, a quality assurance (QA) version was generated from the parent file (see Figure 17) for editing purposes. In addition, user access levels were set to “private” for the

parent file so only the owner was able view and edit it, and "protected" for the QA versions so that all users were able to view a file version, but only the owner of that version could edit it.

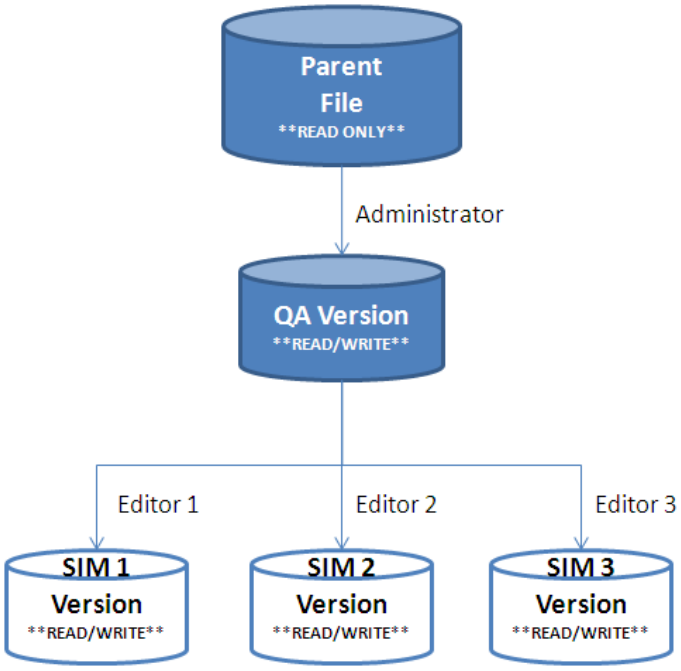

Figure 17. Versioning workflow within the ORR geodatabase.

Versioning is especially beneficial for management of the hydrological modeling workflow within a geodatabase environment, where different stages of the modeling process can be represented by different file versions. This facilitates simulation of what-if scenarios without affecting original datasets and provides a framework for security management and quality assurance in data editing.

Once a user has completed editing, changes made in a new version may be merged into a previous version. This process of version reconciliation facilitates effective conflict resolution between the version being edited and any of its ancestor versions, which is especially important when edits are being made to the data by various editors. Version reconciliation in the ORR geodatabase however, was restricted up to the QA version. The parent file remained as a "Read Only" file.

2.9.2 Hydrologic Model Integration

It is significant to note that ArcObjects which is a part of the ArcGIS system is based on Microsoft's Component Object Model (COM) which is an interface-based programming model that can be used to extend the functionalities of existing ArcGIS applications. COM defines a protocol that enables functionality of Windows-based applications within ArcGIS, so that modules or components of various software products can be dynamically interchanged [12]. MIKE 11 GIS takes advantage of the ArcGIS GUI and uses ArcObjects for programming that conforms to the COM design standard.

Since the MIKE 11 GIS geodatabase is model-specific, the ORR Geodatabase was designed as a non-model-specific repository for data from various sources used for model development and also for transfer of simulation data from the MIKE 11 GIS geodatabase. Future plans which are not within the work scope for FY 2011, include the development of a protocol to automate the process of data transfer between the dynamic MIKE 11 GIS geodatabase and the static hub ORR Geodatabase. According to Olivera et al., 2006 [10], this concept was derived from Olivera et al., 2003 which describes the use of an ArcHydro geodatabase as a data “hub”, which is the same manner in which the ORR Geodatabase is used.

The ArcHydro geodatabase structure incorporates hydrologic elements and their topographic relationships used in hydrologic simulations, and is therefore suitable for integration with the MIKE SHE/11 models developed by ARC-FIU for the ORR which share the same watershed structure and stream network, for example the models developed for the Old Salvage Yard (OSY) at Y-12 NSC and Upper East Fork Poplar Creek (UEFPC) which share data common data files related to the entire EFPC watershed (see Figure 18). Once the ORR data "hub" is populated with data copied from the dynamic MIKE 11 GIS geodatabase, its contents are available for use in any of the other models.

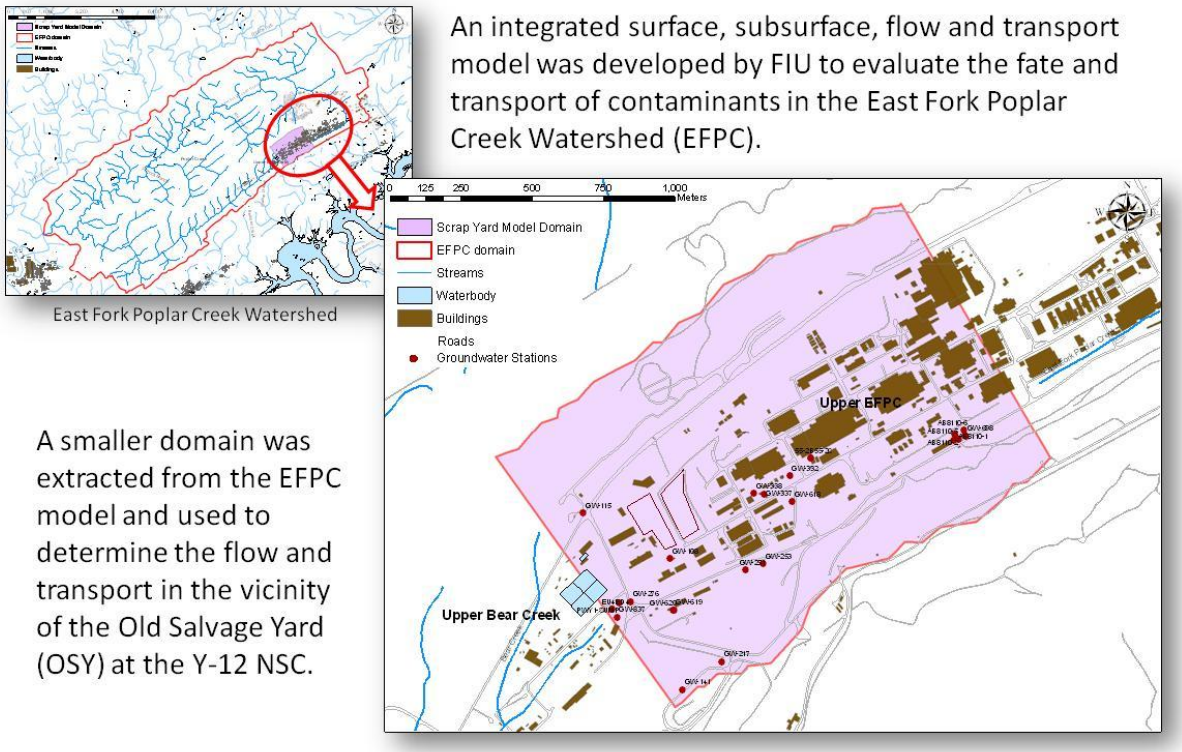

Figure 18. Model domain of the Old Salvage Yard clipped from EFPC watershed domain.

3 SUMMARY AND FUTURE WORK

The ORR geodatabase was developed by FIU-ARC researchers during FY 2010 for storage and management of spatial and temporal data used in the development of hydrological models of the EFPC and WOC watersheds. It is based primarily on the ArcHydro data model which has a structure that can support hydrologic model simulations through incorporation of traditional spatial and temporal hydrogeologic parameters within the ArcGIS system. This geodatabase serves as a central data "hub" or repository of information from various sources required for model configuration and simulation of surface and subsurface flow and contaminant transport. The ArcGIS interface also enables storage, processing and visualization of model results. Some of the data outputs generated can be viewed in Figure 19, Figure 20 and Figure 21 below. MIKE 11 GIS was used as an extension tool embedded within the ArcMap interface to assist in the interchange of files between the MIKE SHE/11 model and the ArcGIS system. A dynamic geodatabase is generated upon the use of MIKE 11 GIS which is used to temporarily import and process model-specific data files. Processed data is then either exported for use in model simulations or transferred to the ORR Geodatabase for storage, backup and retrieval when necessary.

A "GIS & Hydrological Modeling Data Server Management" document was created as an internal reference document which provides system configuration details and credentials to be used for accessing the database. As FIU-ARC continues to conduct model simulations to support the D&D remediation activity at ORR, there will be an ongoing need for update of the geodatabase and the utilization of the integrated GIS-hydrological modeling system developed. As such, there is a continuous import/export of spatial data into the geodatabase and execution of geoprocessing tasks as necessary for model simulations. The update of metadata is also a continuous work in progress as a data quality assurance measure.

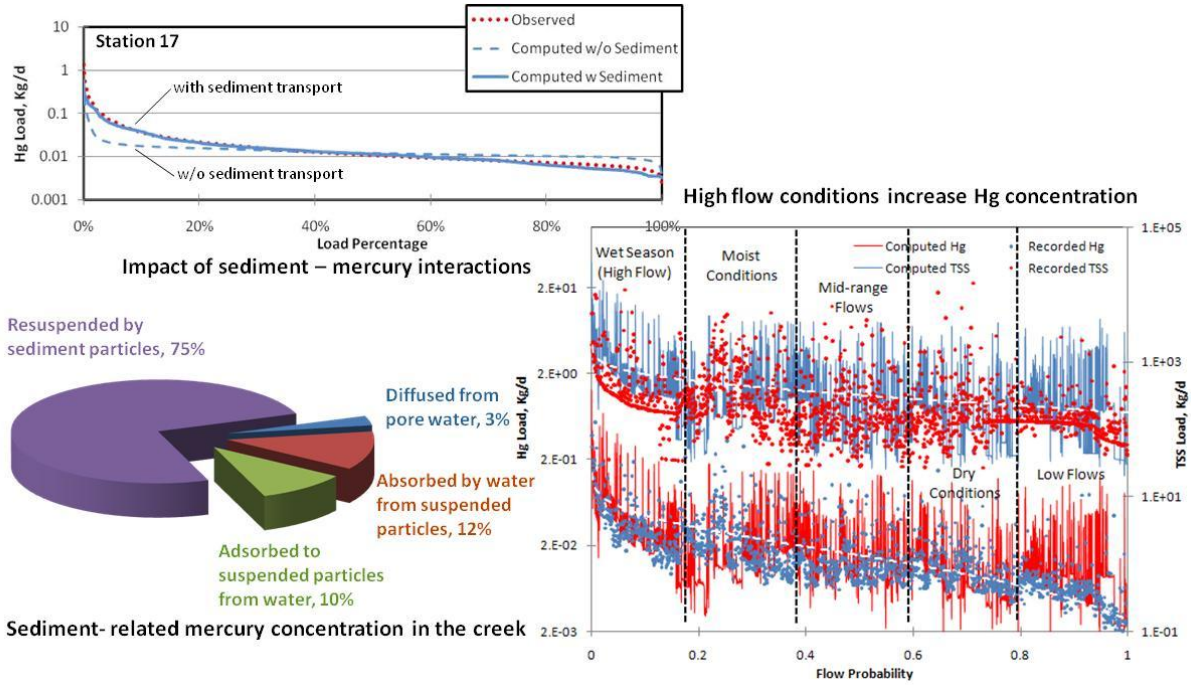

Figure 19. Graphical representations of total Hg transport at Sta. 17.

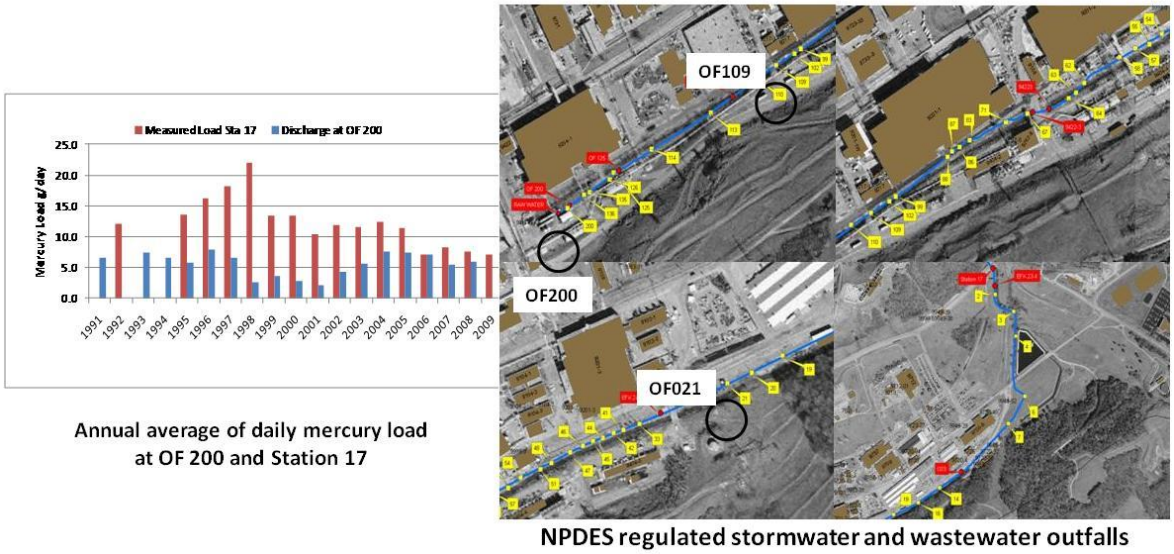

Figure 20. GIS maps and graph of Hg point source loads from various outfalls.

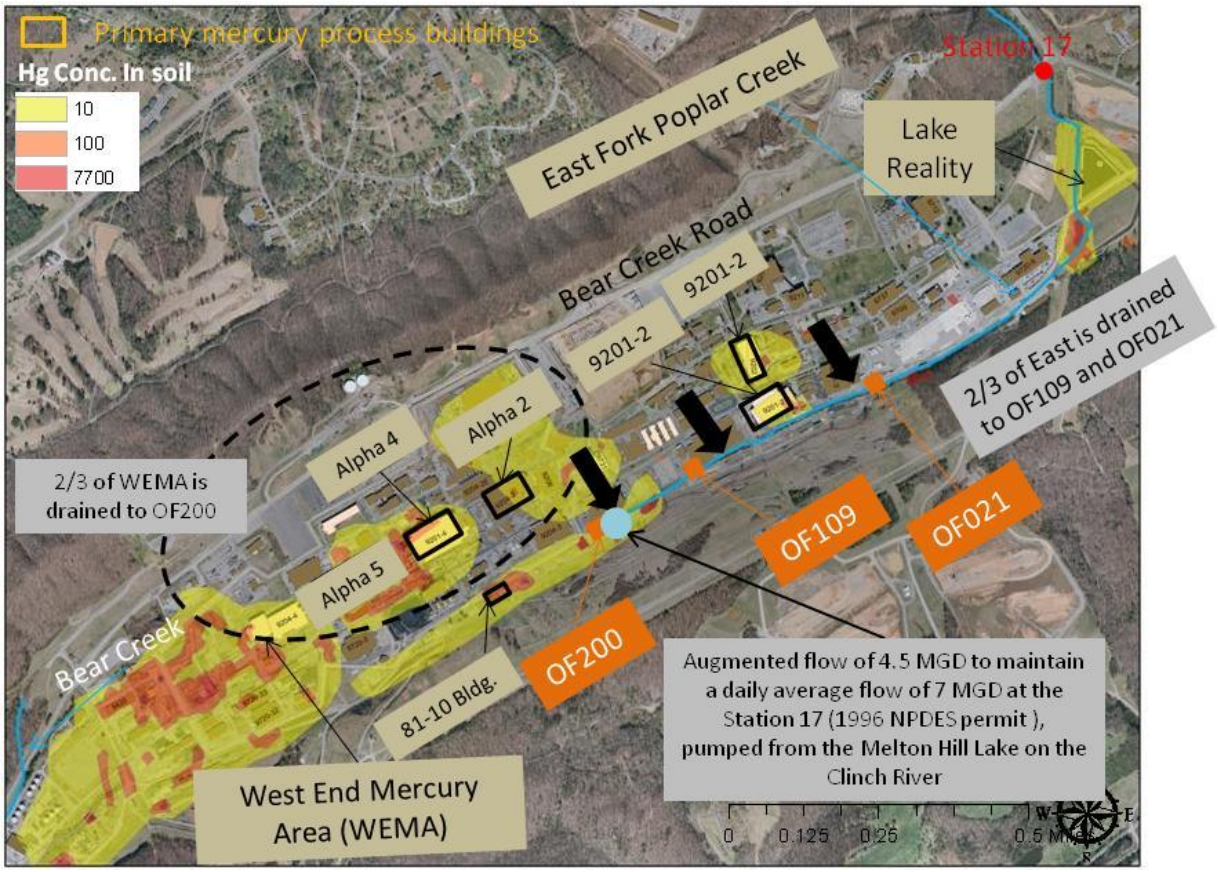

Figure 21. Mercury sources included in the model.

The work proposed for FY12 will serve to extend the geodatabase capabilities by creating a GIS-based model using ArcGIS Model Builder as well as Python scripting that will automate the process of data transfer between the dynamic MIKE 11 GIS geodatabase and the static hub ORR Geodatabase, querying the existing ORR Geodatabase based on specific environmental parameters, performing analyses based on specified algorithms and generating maps with the spatial distribution of computed and observed data. This can then be further extended to facilitate online querying of the database using downloadable freeware and generation of maps, graphs and reports, to more easily share the data with other project stakeholders such as DOE personnel and ORR site contractors.

It is envisioned that the model created to extend the capabilities of the ORR Geodatabase will be similar in concept to the Map to Map model [Figure 22] created by Maidment et al., 2004 at the University of Texas' Center for Research in Water Resources (CRWR) described by Castle, E., 2003 in his thesis [1]. This model combines geographical information systems (GIS), a hydrologic geodatabase utilizing the Hydro schema, TR-55, HEC-RAS and HEC-HMS hydrologic models.

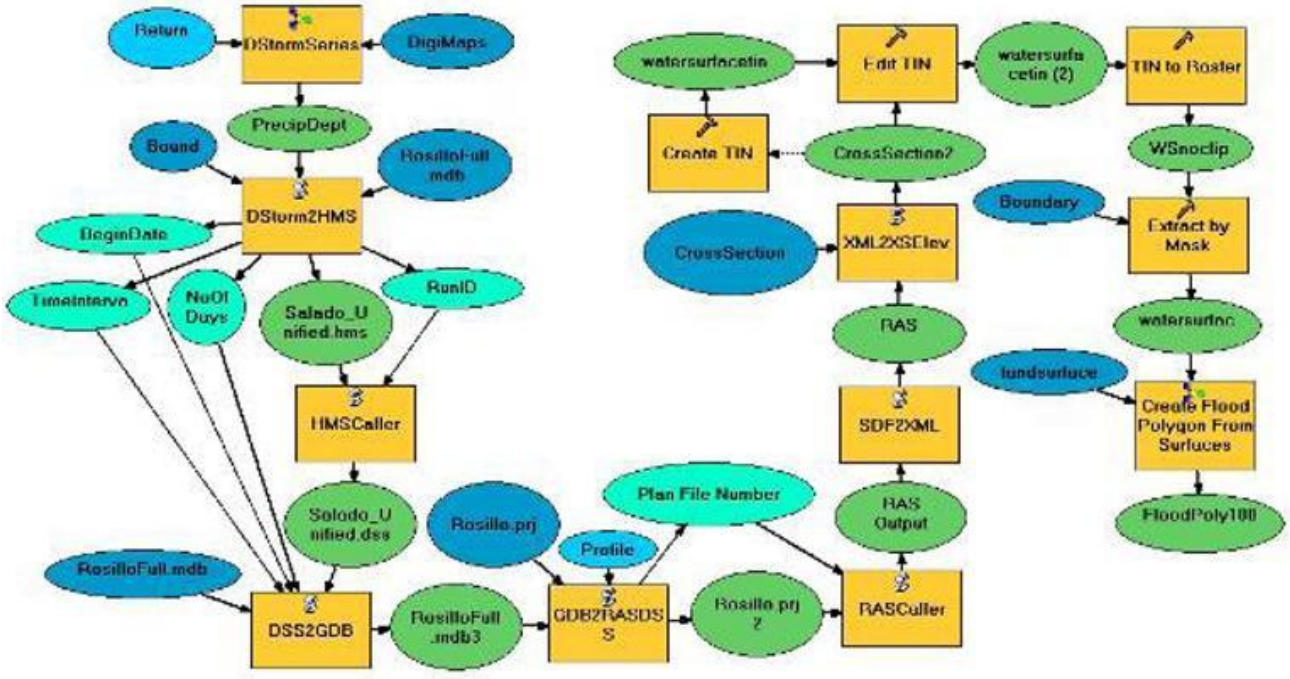

Figure 22. Snapshot of the Map to Map model created by Maidment at CRWR. Blue circles represent inputs, yellow squares are processes, and green circles are outputs [1].

In our case, the ArcGIS Model Builder program will be used to automate the process of calling output data retrieved from the external hydrologic model MIKE SHE/11, importing it into the temporary MIKE 11 GIS geodatabase and then either exporting the processed file for additional model simulations or incorporating it into the ORR Geodatabase which already uses the ArcHydro data model infrastructure that serves as the central "Remediation and Treatment Technology" project data hub.

4 REFERENCES

1 Castle, E. (2003). Geodatabases in Design: A Floodpain Analysis of Little Kitten Creek. Thesis. Brigham Young University.

2 ESRI. (n.d.). ArcGIS Server .NET Help - Setting up a direct connection to SQL Server. Retrieved 2010, from ArcGIS Resource Center: http://goo.gl/N4jpq.

3 ESRI. (n.d.). ArcGIS Server 10 Server Requirements. Retrieved 2010, from ArcGIS Resource Center: http://goo.gl/hNMP5.

4 ESRI. (n.d.). Server 10 .NET Install Guide - Installing ArcGIS Server for the Microsoft .NET Framework overview. Retrieved 2010, from ArcGIS Resource Center: http://goo.gl/4Xy7W.

5 Gogu, R. (2001). GIS-based hydrogeological databases and groundwater modelling. Hydrogeology Journal, 9:555–569. DOI 10.1007/s10040-001-0167-3.

6 Law, D. (2010). Versioning 101: Essential information about ArcSDE geodatabases. ArcUser Online (Winter), 42-48.

7 Maidment, D. R. (2002). Arc Hydro: GIS for Water Resources. ESRI Press.

8 Miessau, R. R. (2007). Using ArcGIS to Support a Regional Hydrologic Model - Paper 2191. ESRI User Conference Proceedings. San Diego, CA: ESRI.

9 MIKE by DHI. (2011). MIKE 11 GIS User's Guide.

10 Olivera, F. V. (2006). ArcGIS-SWAT: A Geodata Model and GIS Interface for SWAT. Journal of the American Water Resources Association.

11 ESRI. (2005). Raster Data in ArcSDE 9.1. An ESRI White Paper. Retrieved 2010, from ArcGIS Resource Center: http://goo.gl/sRvOy.

12 ESRI. (n.d.). Programming against ArcObjects. Introduction to COM. Retrieved 2010, from ArcGIS Resource Center: http://goo.gl/qZjQR.

APPENDIX T5-001: TASK 5 DOE FELLOW SUMMER INTERNSHIP REPORT

DOE-FIU SCIENCE & TECHNOLOGY WORKFORCE DEVELOPMENT PROGRAM

STUDENT SUMMER INTERNSHIP TECHNICAL REPORT

June 6, 2011 to August 12, 2011

PRELIMINARY STUDIES OF NITROGEN CONCENTRATION IN WELLS 0437, 0438, AND 0439

Principal Investigators:

Alexander Henao (DOE Fellow)
Florida International University

Ken Pill, Mentor
Moab Site

Acknowledgements:
Ryan Barker

Florida International University Collaborator and Program Director:

Leonel Lagos Ph.D., PMP®

Prepared for:

U.S. Department of Energy
Office of Environmental Management
Under Grant No. DE-EM0000598

ABSTRACT

Uranium ore was mined in significant quantities in the United States for more than 40 years. Initially, the ore was mined and milled by private companies for federal government use in national defense programs. After the 1950s, uranium was also needed as fuel for nuclear power plants to produce electricity. These milling operations created process-related wastes and tailings, a radioactive sandlike material. The tailings were slurried to unlined impoundments that accumulated over time, forming piles. Excess water in the piles drained into underlying soils, contaminating the groundwater. Scientists, community leaders, and public officials became more aware of the potential health risks associated with long-term exposure to uranium mill tailings during the 1970s. Public concern about potential human health and environmental effects of uranium mill tailings led the U.S. Congress to pass the Uranium Mill Tailings Radiation Control Act (UMTRCA) in 1978 (Public Law 95–604), which required the cleanup of inactive uranium-ore processing sites. In 1983, the U.S. Environmental Protection Agency (EPA) developed regulations [Title 40 Code of Federal Regulations (CFR) Part 192] to protect the public and the environment from potential radiological and nonradiological hazards at inactive uranium-ore processing sites. The U.S. Department of Energy (DOE) is responsible for cleaning up the millsites and for bringing groundwater contamination at the former processing sites into compliance with EPA standards (Subpart B of 40 CFR 192). The radioactive materials are encapsulated in U.S. Nuclear Regulatory Commission (NRC)-accepted disposal cells. The NRC general license for post-closure requirements of UMTRCA sites is established in 10 CFR 40.27.

TABLE OF CONTENTS

LIST OF FIGURES

1. INTRODUCTION

In 2003, DOE implemented the first phase of an interim action system at the Moab site to address concerns regarding elevated ammonia levels in groundwater discharging to the Colorado River. This first phase consisted of 10 extraction wells (called Configuration 1). Four additional configurations of wells have been added since then, for a current total of 42 wells that are designed to prevent ammonia from discharging to the river. To date, a total of more than 168 million gallons of groundwater has been extracted through the interim action system, preventing more than 687,000 pounds of ammonia and about 3,150 pounds of uranium from reaching the river.

With installation of the Configuration 5 wells, extraction is now from wells located closer to the tailings pile. Extraction was restarted for 2011 on March 31. Extraction was suspended in May due to the level of the river and was restarted on August 24. Extracted groundwater is pumped via pipeline to a lined evaporation pond or to forced air evaporators. The evaporation pond covers approximately 4 acres and is located on top of the tailings pile. Two forced air evaporators operate when weather conditions are conducive to help evaporate the extracted groundwater.

Wells in Configurations 1 through 4 along the river are used to inject freshwater (diverted river water) as an additional way to minimize the discharge of ammonia to the Colorado River. Freshwater injection through wells in Configuration 4 was suspended in May due to the level of the river and restarted on August 3. About 5,505,000 million gallons of freshwater has been injected during 2011. DOE continues to evaluate the effectiveness of the interim action system, which will likely become part of the final groundwater remedy. The well configurations are shown in Figure 1.

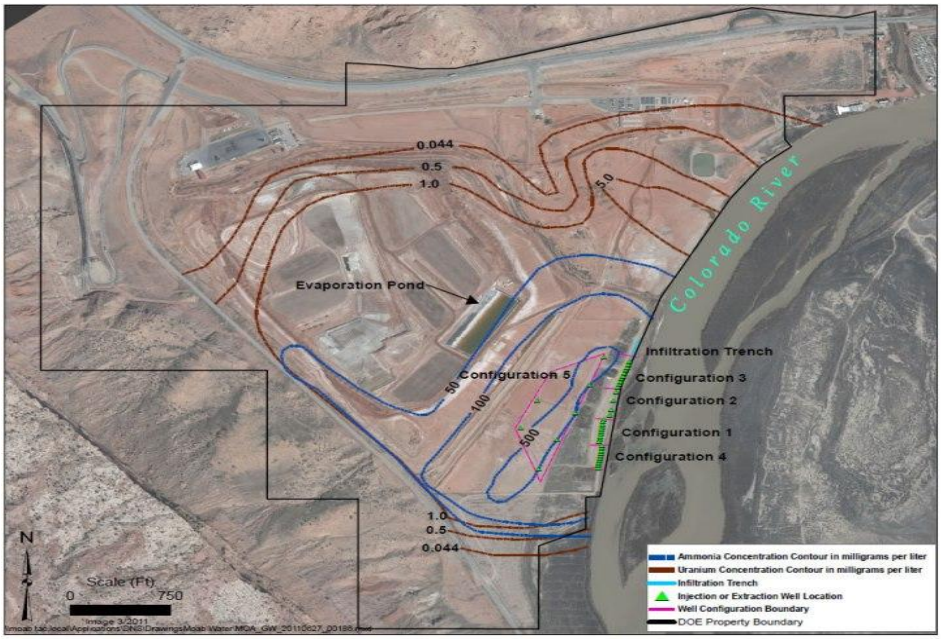

Figure 1. Well configurations.

2. EXECUTIVE SUMMARY

This research work has been supported by the DOE-FIU Science & Technology Workforce Initiative, an innovative program developed by the US Department of Energy's Environmental Management (DOE-EM) and Florida International University's Applied Research Center (FIU-ARC). During the summer of 2011, a DOE Fellow intern (Alexander Henao) spent 10 weeks doing a summer internship at the Moab site under the supervision and guidance of Ken Pill. The intern's project was initiated on June 7, 2011, and continued through August 12, 2011.

The DOE Moab Uranium Mill Tailings Remedial Action (UMTRA) Project site is located approximately 3 miles northwest of the city of Moab in Grand County, Utah, and includes the former Atlas Minerals Corporation (Atlas) uranium-ore processing facility. The site is situated on the west bank of the Colorado River at the confluence with Moab Wash. The site encompasses 439 acres, of which approximately 130 acres is covered by a uranium mill tailings pile. The Moab mill was constructed in 1956 by the Uranium Reduction Company, which operated the mill until 1962 when the assets were sold to Atlas. Uranium concentrate, the milling product, was sold to the U.S. Atomic Energy Commission through December 1970. During its years of operation, the mill processed an average of approximately 1,400 tons per day. Atlas operated the site until 1984 under a license and regulatory authority provided by NRC. When the processing operations ceased in 1984, an estimated 12 million cubic yards (16 million tons) of mill tailings and tailings-contaminated soil were present in a pile located in the western portion of the property. Atlas placed an interim cover over the tailings pile in 1995 as part of decommissioning activities conducted between 1988 and 1995. Atlas proposed to reclaim the tailings pile for permanent disposal in its current location but declared bankruptcy in 1998 and, in doing so, relinquished its license and forfeited its reclamation bond. Because NRC could not legally possess a site it regulated, NRC appointed Pricewaterhouse Coopers as the Trustee of the Moab Mill Reclamation Trust and the licensee for the site. The Trustee used the forfeited reclamation bond funds to initiate site reclamation, conduct groundwater studies, and perform site maintenance. The Floyd D. Spence National Defense Authorization Act for Fiscal Year 2001, Public Law 106–398, stipulated that the license issued by NRC for the materials at the Moab site be terminated and that the title and responsibility for cleanup be transferred to DOE. Title to the site was transferred to DOE on October 25, 2001. Specifically, the DOE Office of Environmental Management in Grand Junction, Colorado, now has primary responsibility for the Moab site. The act further designated that the Moab site undergo remediation in accordance with Title I of UMTRCA.

3. RESEARCH AND RESULTS

The main purpose of the research in this report is to observe if there are any trends or patterns in the concentration of nitrogen from water sampled at 3 different wells. The three wells that are going to be analyzed include Well 0437 (6665399.33/2183802.67), 0438 (6665241.03/2185009.53) and 0439 (6664189.32/2184731.49), all located near the Colorado River. Nitrogen in its different forms will be the main element investigated. The different forms that will be studied include: ammonia as nitrogen, ammonia as NH_4^+, nitrate and nitrite, and nitrogen as NO_3. When comparing the three wells in the same categories, the distance to the Colorado River, the depth of the wells and the depth of the sampling will be taken into consideration. Well 0437 is located farthest from the Colorado River then Well 0438 and, finally, closest to the river is Well 0439.

On the graphs below, the activity in concentration of ammonia as nitrogen is shown over a particular period time (Figures 2, 3, and 4). As the distance of the wells from the river increases, the concentration of ammonia tends to decrease. The highest concentration of ammonia was recorded for Well 0438 at a level of about 21 parts per million on July 2005. One particular trend that is persistent with the data is that there seems to be peak periods, especially during the summer season. This might occur due to the fact that, in the winter time, the volume of the river decreases and more sediment settles to the bottom of the river. When the snow pack starts to melt in the spring and the flow of the river increases, the sediment mixes with the water and increases the concentration of ammonia. As a whole, the concentration is decreasing as time passes for Wells 0438 and 0439; yet it can be seen that in Well 0437, where the concentration is relatively low, the concentration is increasing as times passes. This particular form of nitrogen is very harmful to marine wildlife and is dependent on water temperature as well as pH level.

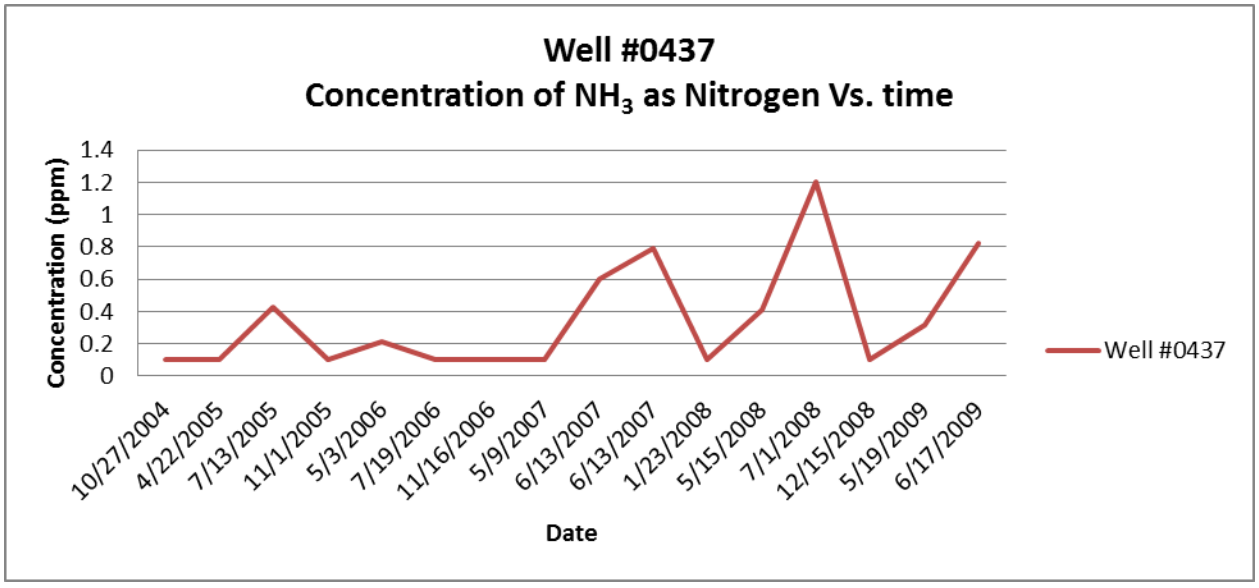

Figure 2. Concentration of nitrogen vs time for Well 0437.

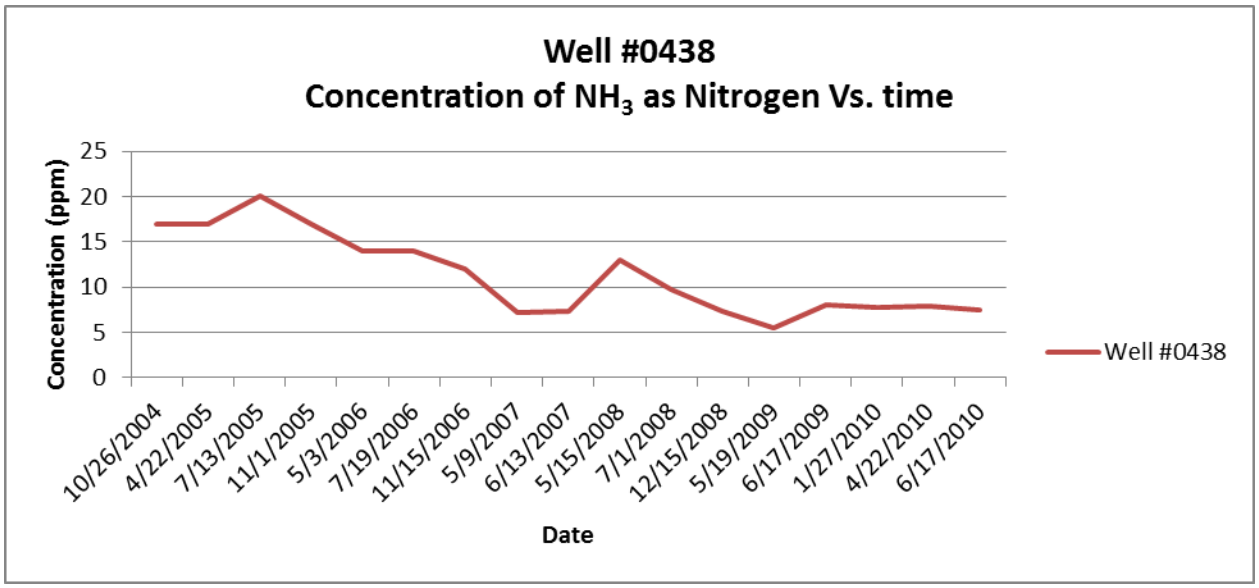

Figure 3. Concentration of nitrogen vs time for Well 0438.

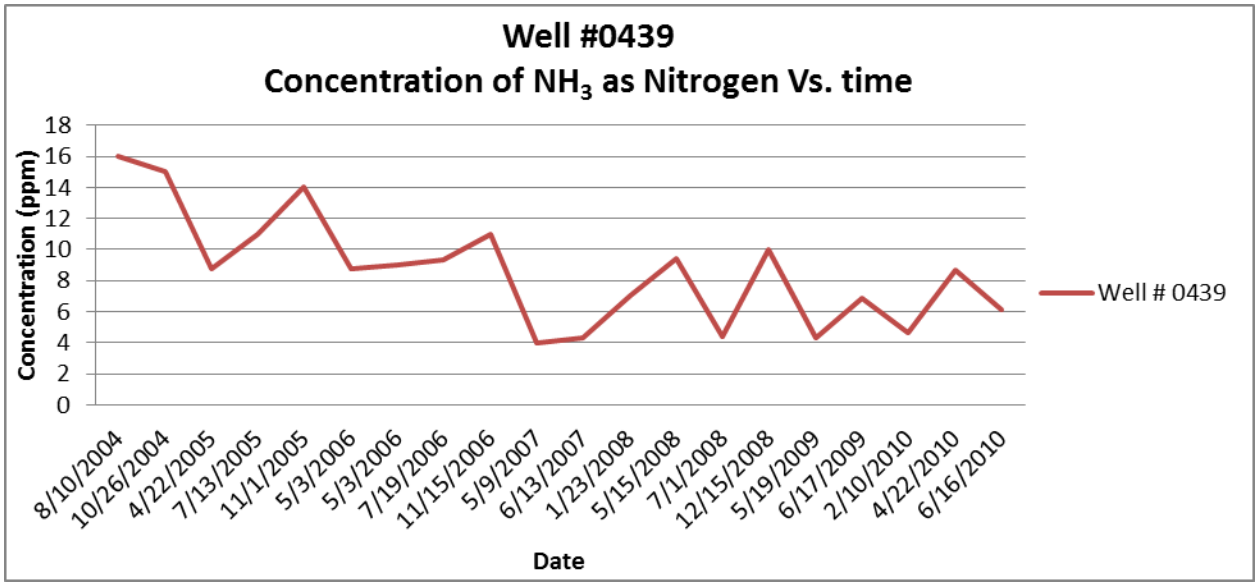

Figure 4. Concentration of nitrogen vs time for Well 0439.

Ammonia in the form of NH_3 is harmful to marine wildlife, while ammonium (NH_4^+) is not; however, it is very important to determine the concentration of NH_4^+ because the composition of nitrogen can rapidly change from one form to another.

The chemical equation that drives the relationship between ammonia and ammonium is:

$$NH_3 + H_2O \leftrightarrow NH_4^+ + OH^- \quad \textbf{(Equation 1)}$$

As the pH increases, the reaction will shift to the right side, making more of the ammonia cation, while if the pH decreases, the reaction will go into the left, producing the ammonia as nitrogen. It can be observe that in all three wells, at the low depth sampling points, the concentration of ammonia as nitrogen is the highest, sometimes as high as 100 times the deeper sampling points. Additionally, the same trend is observed when it comes to distance to the river; the closer the well is to the river, the higher the concentration. Overall, the concentration of ammonia as nitrogen at the other depths seems to be very stable in all three wells. One particular sampling point at 252 ft of Well 0437 showed a significant concentration of ammonia.

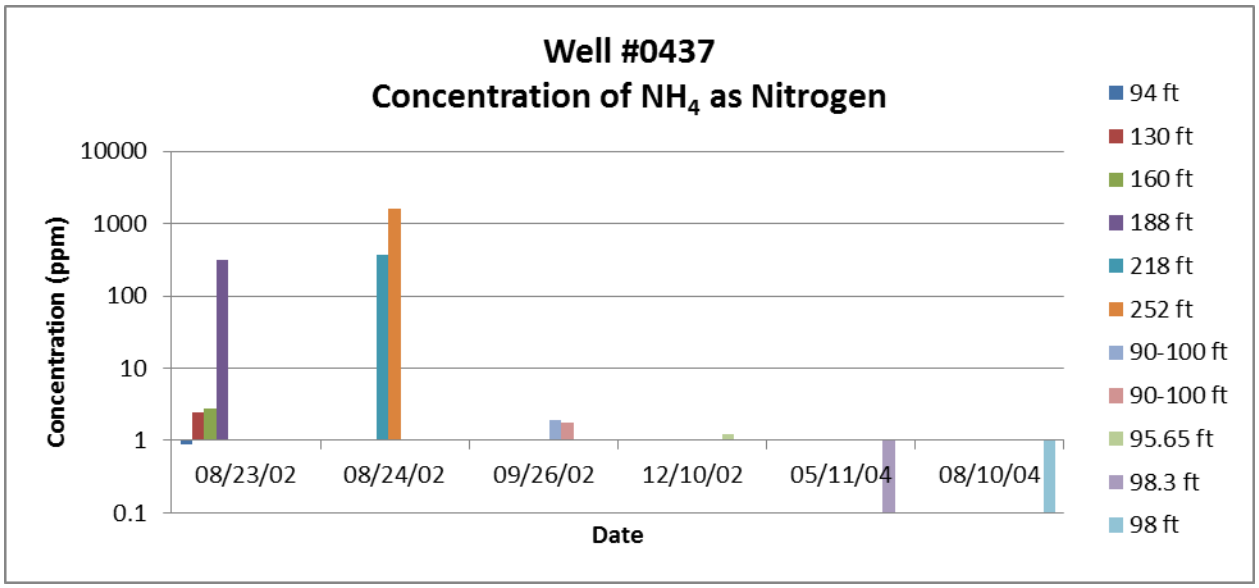

Figure 5. Concentration of NH_4 as nitrogen for Well 0437.

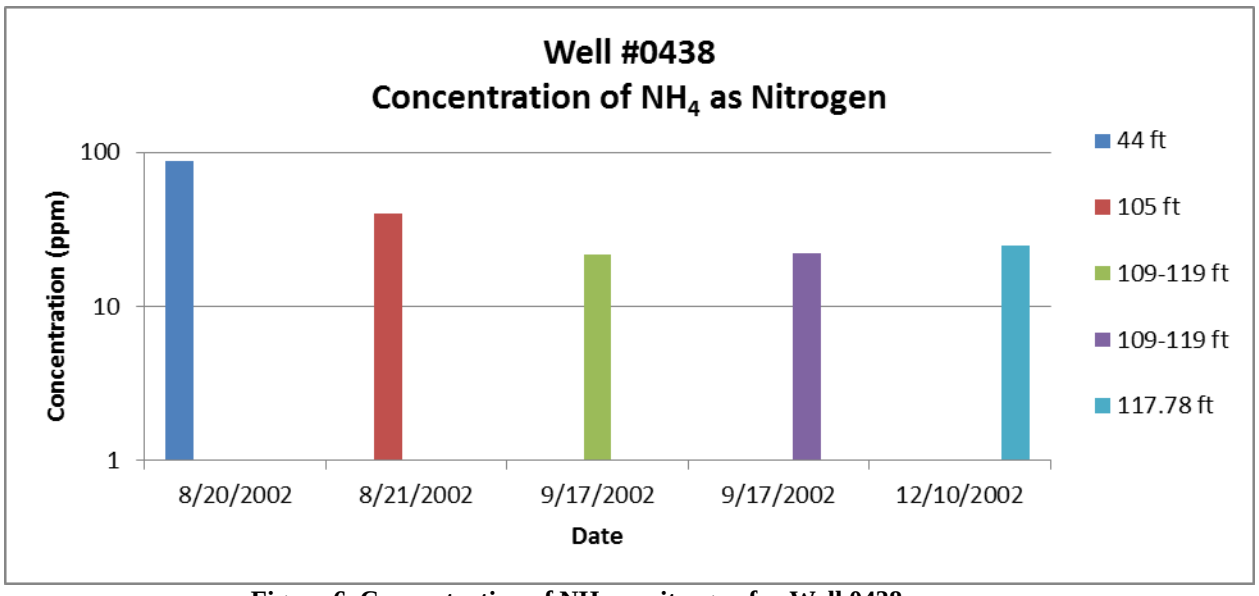

Figure 6. Concentration of NH_4 as nitrogen for Well 0438.

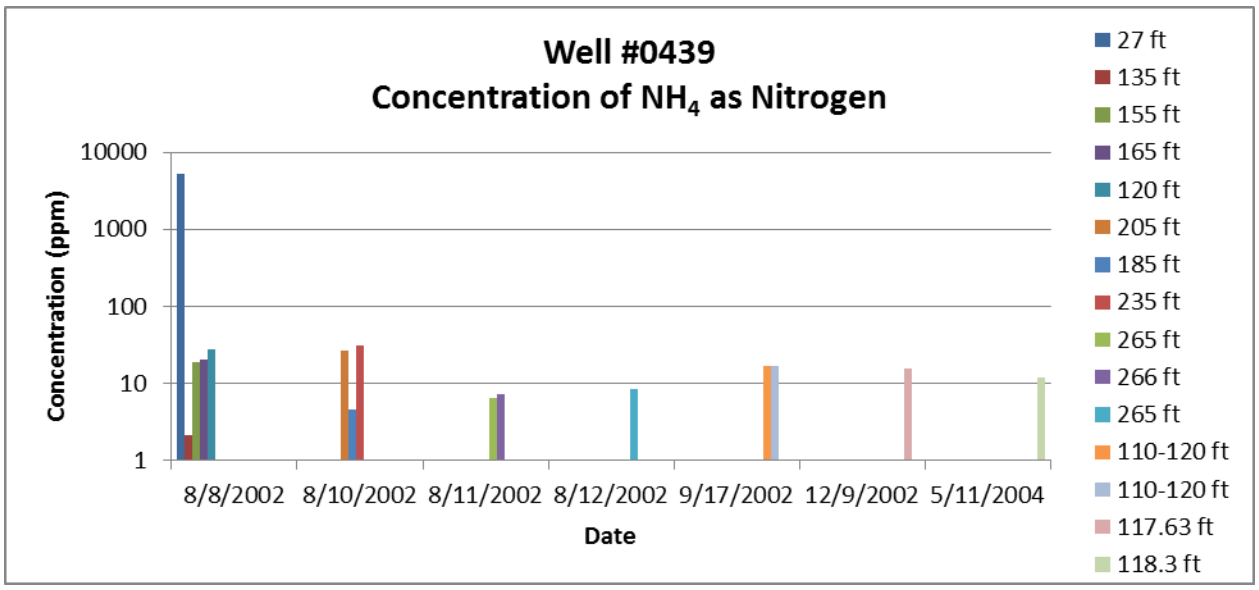

Figure 7. Concentration of NH_4 as nitrogen for Well 0439.

As previously stated, the relationship between NH_4^+ and NH_3 is influenced by temperature and pH levels. As shown in the figures below, it can be observed that for Well 0437, the concentration of ammonia as NH_4^+ is higher for mid-range depths compared to low-level depths on the other 2 wells (Figures 8, 9 and 10). Nonetheless, the highest concentration is in Well 439 (closest to the river) at a about 8000 ppm. This result could indicate a low pH in that particular area.

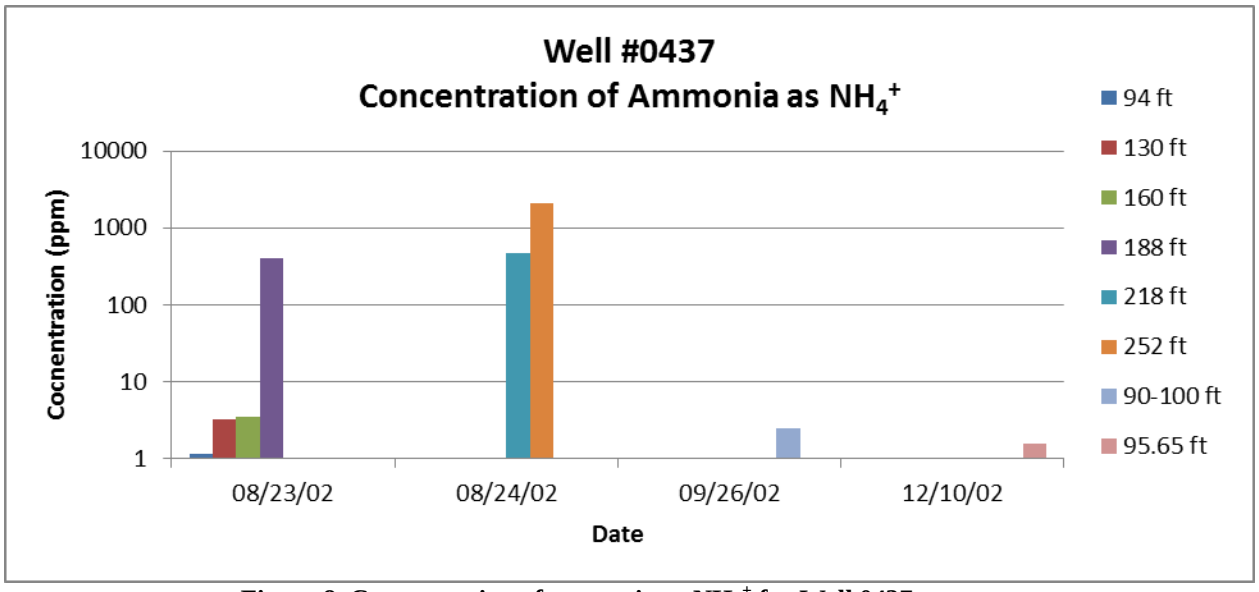

Figure 8. Concentration of ammonia as NH_4^+ for Well 0437.

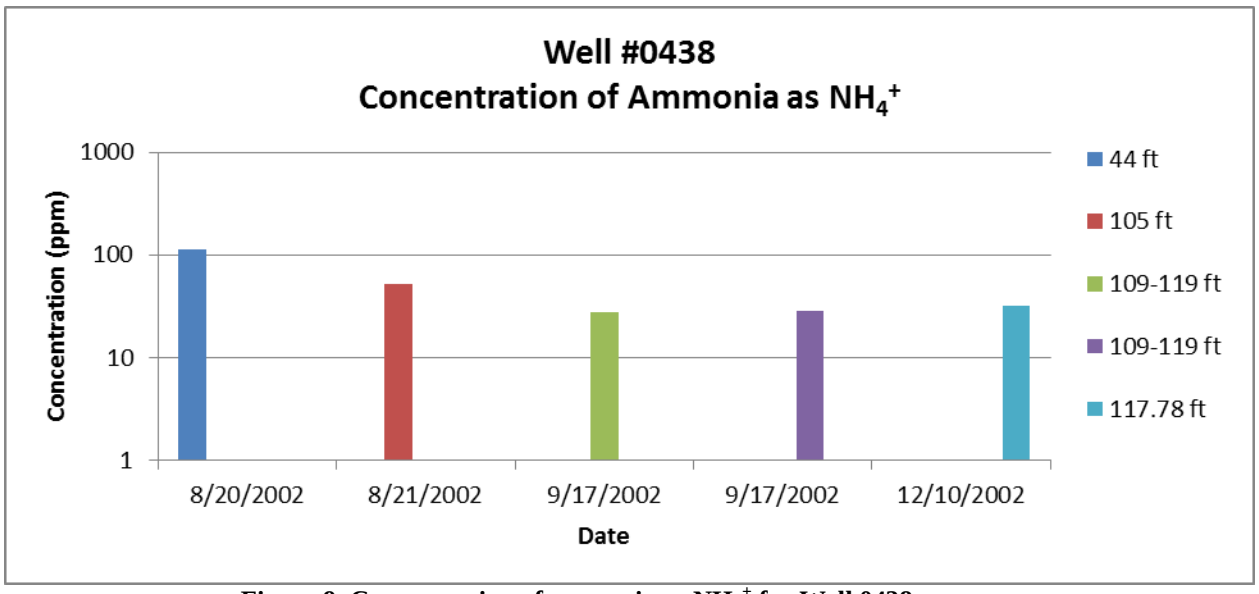

Figure 9. Concentration of ammonia as NH_4^+ for Well 0438.

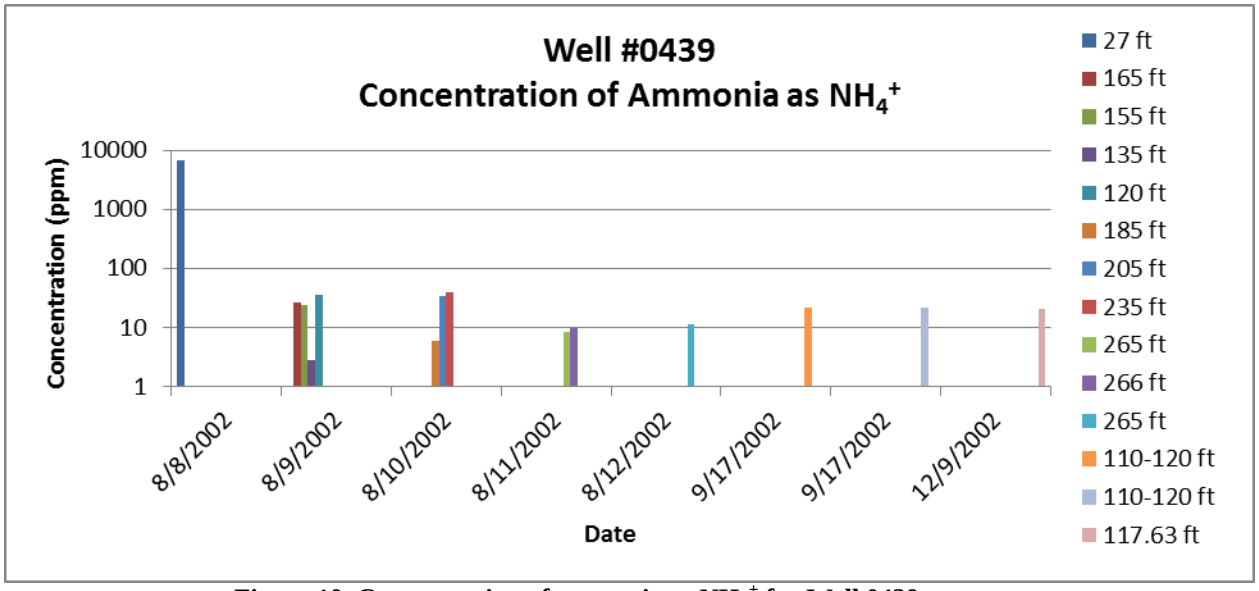

Figure 10. Concentration of ammonia as NH_4^+ for Well 0439.

Nitrate concentration (NO_3^-) in fresh water can cause oxygen depletion. Thus, aquatic organisms depending on the supply of oxygen in the stream will perish or find it very difficult to survive. On the other hand, nitrites (NO_2^-) can produce a serious condition in fish called "brown blood disease." For these reasons, it is very important to know the concentration of these chemicals. For the most parts, when nitrogen concentrations are observed in this particular form, the results are low. Once again, the same pattern is observed. As the distance between the well and the river decreases, the concentration of nitrogen increases. Yet, it is also noted that regardless of the depth of the sampling point, the concentration remains low, but only a little higher in the range of 185 to 252 ft at two different wells, one being the closest to the river and the other farthest from it.

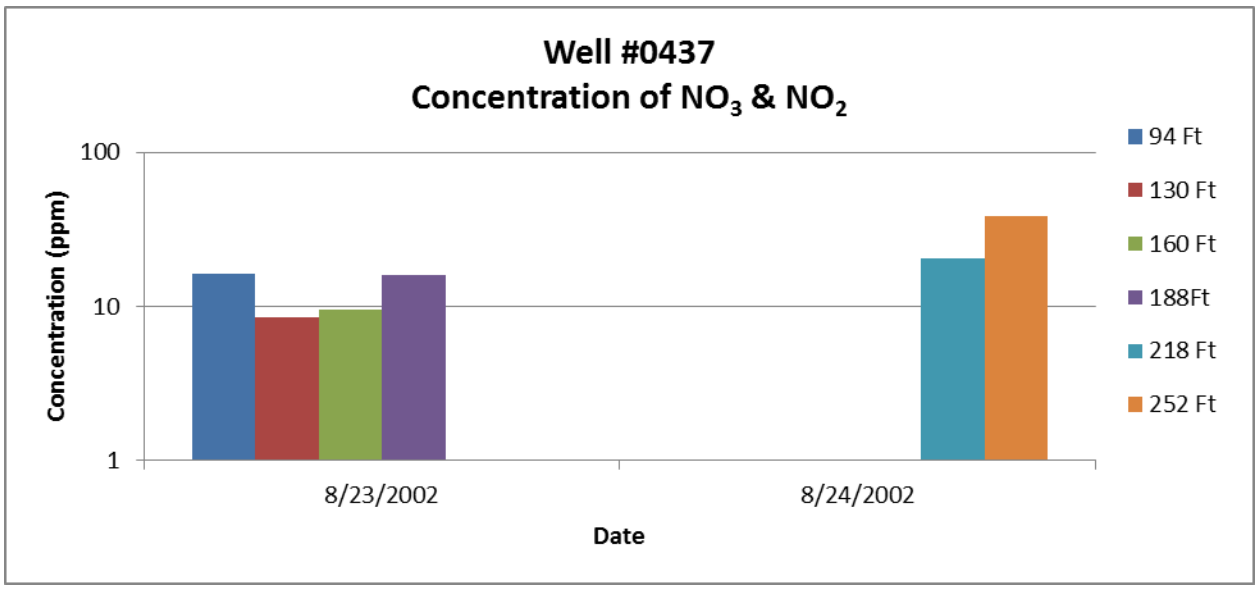

Figure 11. Concentration of NO_3^- and NO_2^- for Well 0437.

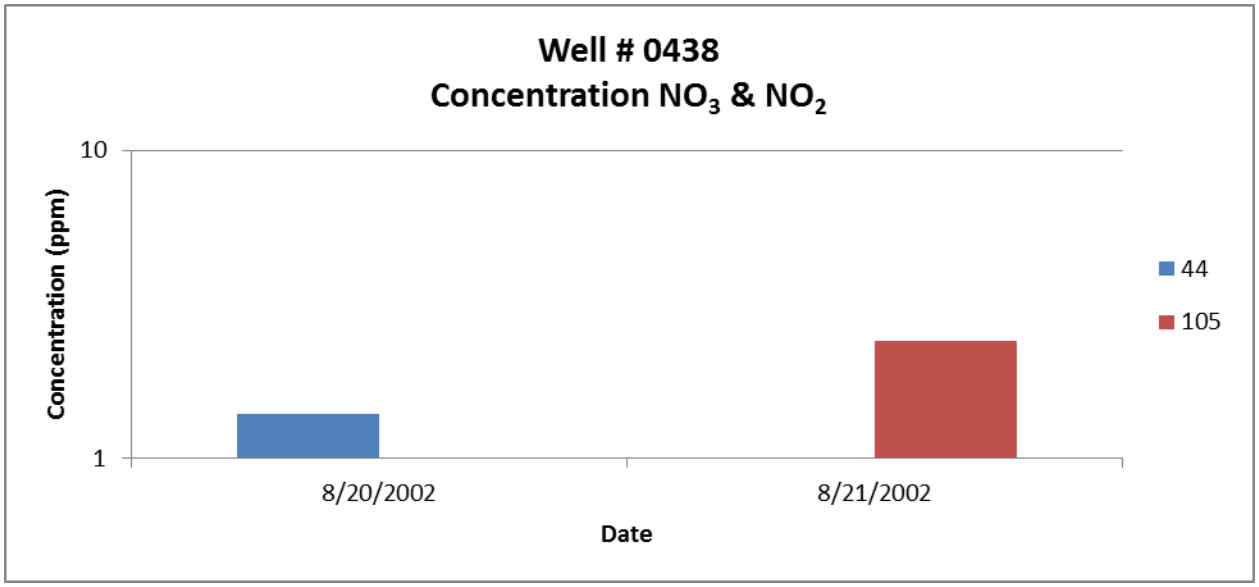

Figure 12. Concentration of NO_3^- and NO_2^- for Well 0438.

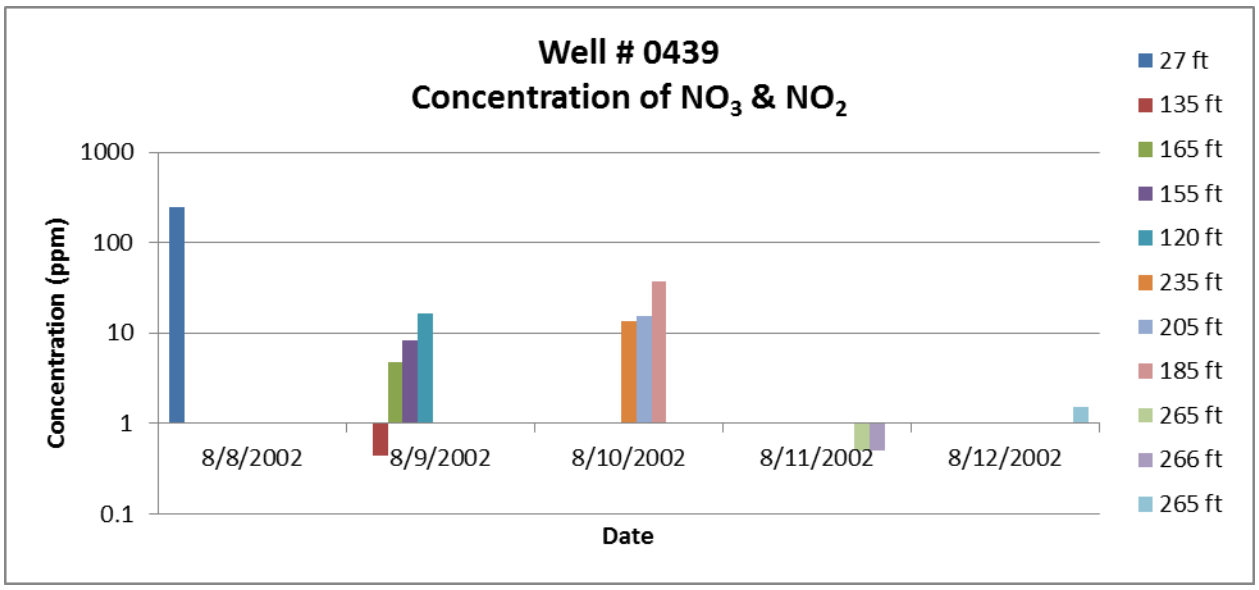

Figure 13. Concentration of NO_3^- and NO_2^- for Well 0439.

In order to have a better understanding of the complexity of nitrogen, different analyses are necessary. In the following figures, the concentration of NO_3^- can be studied (Figures 14, 15, and 16). Once again, it can be seen that the concentration of nitrogen is higher at the well located close to the river (Well 0439). For this particular analysis, Well 0438 showed the lowest concentration of the three wells studied. One particular result appeared on 12/09/2002 – 12/10/2002, where the highest concentration was found over an eight year period on Well 0439 at a depth of 117.63 ft.

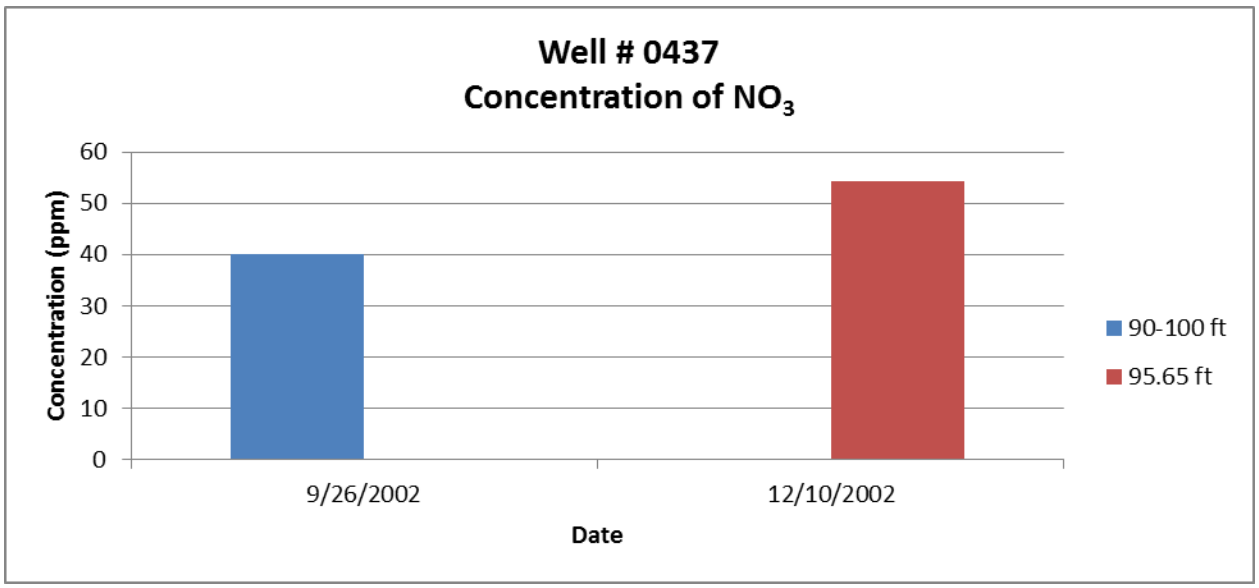

Figure 14. Concentration of NO_3 for Well 0437.

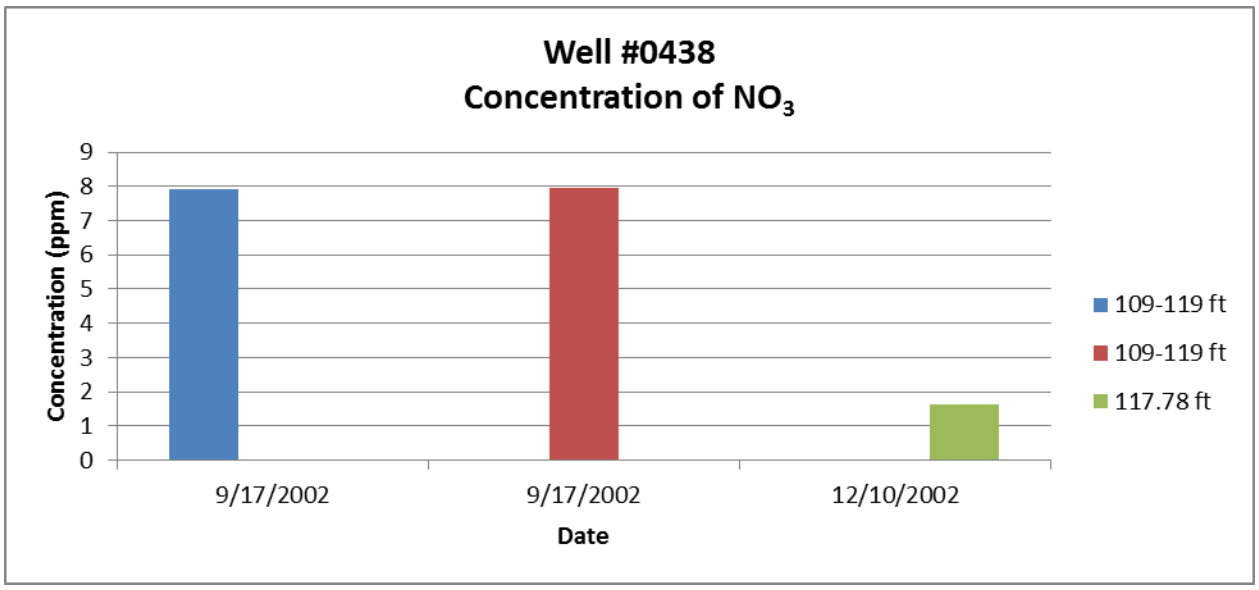

Figure 15. Concentration of NO_3 for Well 0438.

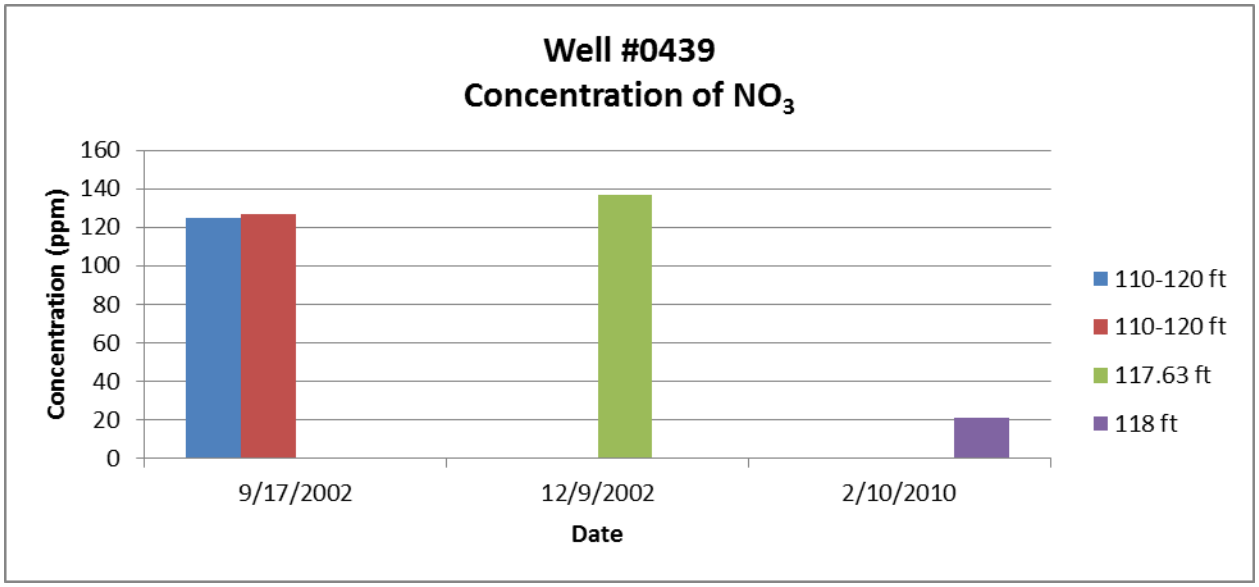

Figure 16. Concentration of NO_3 for Well 0439.

4. CONCLUSION

As the data has shown for the three wells studied for this report, wells located closer to the river contain more nitrogen related species. The depth of the sampling point was not an overall factor, apart from some particular sampling results. In future reports, we will examine a larger number of wells to obtain a better understanding of the movement of nitrogen in this particular zone of the Colorado River.

APPENDIX T5-002: TASK 5 FINAL REPORT

APPENDIX T5-002

TASK5: MODELING OF GROUNDWATER FLOW AND TRANSPORT AT THE URANIUM MILL TAILINGS SITE IN MOAB, UTAH

OF

REMEDIATION AND TREATMENT TECHNOLOGY DEVELOPMENT AND SUPPORT

Prepared for:
U. S. Department of Energy

FINAL REPORT, VERSION 1, 06/17/2012

Prepared by:
Georgio Tachiev, PhD, PE
Mandar Zope, MS
Angelique Lawrence, MS, GISP

Acknowledgements:
Kent Bostick and Anamary Daniel (Pro2Serve, Oak Ridge)
Ken Pill, Liz Glowiak, and Joe Ritchey (Pro2Serve, Grand Junction)

Principal Investigator:
David Roelant, PhD
david.roelant@fiu.edu
phone: 305-348-6625 fax: 305-348-1852

Applied Research Center
Florida International University
10555 W. Flagler Street, EC 2100
Miami, Florida 33174

DISCLAIMER

This report was prepared as an account of work sponsored by an agency of the United States government. Neither the United States government nor any agency thereof, nor any of their employees, contractors, or subcontractors makes any warranty, express or implied, or assumes any legal liability or responsibility for the accuracy, completeness, or usefulness of any information, apparatus, product, or process disclosed, or represents that its use would not infringe upon private copyrights. Reference herein to any specific commercial product, process, or service by trade name, trademark, manufacturer, or otherwise does not necessarily constitute nor imply its endorsement, recommendation, or favor by the United States government or any other agency thereof. The views and opinions of authors expressed herein do not necessarily state or reflect those of the United States government or any agency thereof.

EXECUTIVE SUMMARY

An estimated 16 million tons of uranium mill tailings have been left behind following the cessation of processing operations at the Moab Uranium Mill Tailings Remedial Action (UMTRA) Project site in 1984. These tailings were accumulated in an unlined impoundment, a portion of which is in the 100-year floodplain of the Colorado River. In 2001, ownership of the Moab site was transferred to DOE along with the responsibility for its remediation in accordance with Title I of the Uranium Mill Tailings Radiation Control Act (UMTRCA). Results of investigations indicate that site-related contaminants have leached from the tailings pile into the shallow groundwater and some of the more mobile constituents have migrated downgradient and are discharging to the Colorado River adjacent to the site. The most pervasive and highest concentration constituents are ammonia and uranium. In order to address concerns regarding elevated ammonia levels in groundwater discharging to the Colorado River from the Moab site, DOE implemented an interim action system consisting of a series of extraction wells which have removed more than 168 million gallons of groundwater and prevented more than 687,000 lbs of ammonia and about 3,150 lbs of uranium from reaching the river. In support of this effort and to better understand the subsurface hydrology, a finite difference transient groundwater flow and transport model was developed by one of DOE's contractors. FIU is applying this groundwater numerical model to evaluate the tailings pore-water seepage in order to assist in effective dewatering of the tailings pile and to optimize the groundwater extraction well field as part of the DOE UMTRA for the Moab site. In order to reduce contaminant mass in the groundwater system and to be protective of potential endangered fish habitat in backwater areas of the river, the model will be used to simulate remedial actions proposed by DOE including pumping contaminated groundwater from the shallow plume to an evaporation pond on top of the tailings pile, and injecting the diverted Colorado River water into the alluvial aquifer. Numerical simulation of the proposed remedial actions will aid in prediction of the time to reach cleanup levels and assist DOE in optimization of the operation of groundwater extraction well fields, infiltration of treated water, and injection of clean fresh water for the DOE UMTRA site in Moab, Utah.

TABLE OF CONTENTS

LIST OF TABLES

LIST OF FIGURES

LIST OF ACRONYMS

ASCEM	Advanced Simulation Capability for Environmental Management
CFR	Code of Federal Regulations
DNAPL	Dense Non-aqueous Phase Liquid
DOE	Department of Energy
DOM	Dissolved Organic Matter
EPA	Environmental Protection Agency
FIU	Florida International University
NLCD	National Land Cover Data
NPDES	National Pollutant Discharge Elimination System
NRC	Nuclear Regulatory Commission
QA	Quality Assurance
QAPP	Quality Assurance Project Plan
QC	Quality Control
RCRA	Resource Conservation and Recovery Act
ROD	Record of Decision
SOW	Statement of Work
SSURGO	Soil Survey Geographic Database
TDS	Total Dissolved Solids
TMDL	Total Maximum Daily Load
UMTRCA	Uranium Mill Tailings Radiation Control Act
USGS	United States Geological Survey

1 INTRODUCTION

1.1 Background

Uranium ore was mined in significant quantities in the United States for more than 40 years. Initially, the ore was mined and milled by private companies for federal government use in national defense programs. After the 1950s, uranium was also needed as fuel for nuclear power plants to produce electricity. These milling operations created process-related wastes and tailings, a radioactive sand-like material. The tailings were slurried to unlined impoundments that accumulated over time, forming piles. Excess water in the piles drained into underlying soils, contaminating the groundwater. Scientists, community leaders, and public officials became more aware of the potential health risks associated with long-term exposure to uranium mill tailings during the 1970s. Public concern about potential human health and environmental effects of uranium mill tailings led the U.S. Congress to pass the Uranium Mill Tailings Radiation Control Act (UMTRCA) in 1978 (Public Law 95–604), which required the cleanup of inactive uranium-ore processing sites. In 1983, the U.S. Environmental Protection Agency (EPA) developed regulations [Title 40 Code of Federal Regulations (CFR) Part 192] to protect the public and the environment from potential radiological and non-radiological hazards at inactive uranium-ore processing sites. The U.S. Department of Energy (DOE) is responsible for cleaning up the mill sites and for bringing groundwater contamination at the former processing sites into compliance with EPA standards (Subpart B of 40 CFR 192). The radioactive materials are encapsulated in U.S. Nuclear Regulatory Commission (NRC)-accepted disposal cells. The NRC general license for post-closure requirements of UMTRCA sites is established in 10 CFR 40.27.

The DOE Moab Uranium Mill Tailings Remedial Action (UMTRA) Project site (Figure 1 and Figure 2) is located approximately 3 miles northwest of the city of Moab in Grand County, Utah, and includes the former Atlas Minerals Corporation (Atlas) uranium-ore processing facility. The site is situated on the west bank of the Colorado River at the confluence with Moab Wash. The Moab site is irregularly shaped and encompasses approximately 400 acres; a 130-acre uranium mill tailings pile occupies much of the western portion of the site. The Moab site is bordered on the north and southwest by steep sandstone cliffs. The Colorado River forms the southeastern

boundary of the site. The entrance to Arches National Park is located less than 1 mile northwest of the site across US-191; Canyonlands National Park is about 12 miles to the southwest. The Union Pacific Railroad traverses a small section of the site just west of SR-279, then enters a tunnel and emerges several miles to the southwest. Moab Wash runs northwest to southeast through the center of the site and joins with the Colorado River. The wash is an ephemeral stream that flows only after precipitation or during snowmelt. Courthouse Wash, another ephemeral stream, but with a larger drainage than Moab Wash, discharges to the Colorado River about 300 ft east of the easternmost boundary of the site [1].

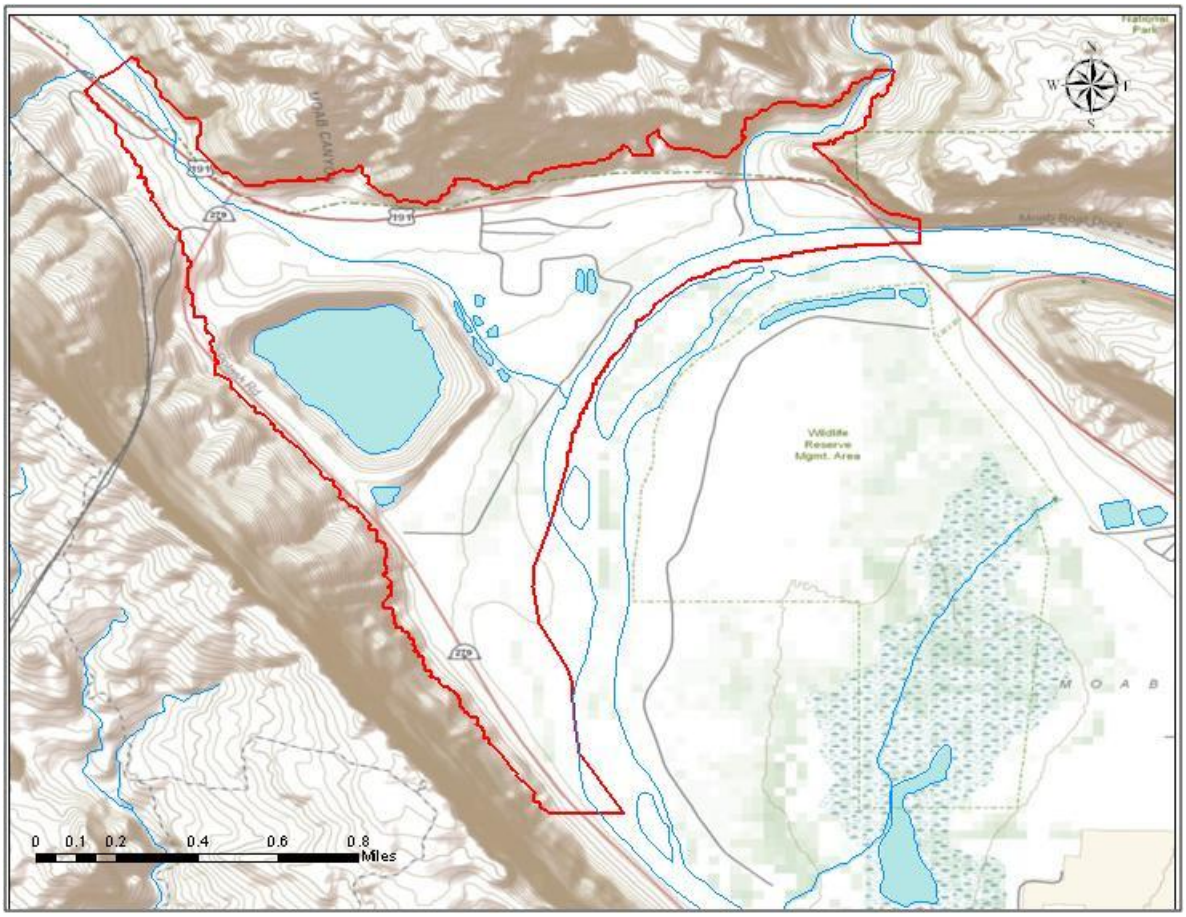

Figure 1 Location of Moab site.

Figure 2 Moab site [nap.edu].

The Moab mill was constructed in 1956. Processing operations ceased in 1984, leaving behind an estimated 16 million tons of uranium mill tailings, material that ranges from dry sand to wet "slime" clay that remains after the ore is processed. These tailings were accumulated in an unlined impoundment, a portion of which is in the 100-year floodplain of the Colorado River. In 2001, ownership of the Moab site was transferred to DOE along with the responsibility for its remediation in accordance with Title I of UMTRCA. Relocation of the tailings, by rail, began in April 2009 to a disposal cell constructed 30 miles north near Crescent Junction, also in Utah. Results of investigations indicate that site-related contaminants have leached from the tailings pile into the shallow groundwater and some of the more mobile constituents have migrated downgradient and are discharging to the Colorado River adjacent to the site. The most pervasive and highest concentration constituents are ammonia and uranium.

In 2003, DOE implemented the first phase of an interim action system (Figure 3) at the Moab site to address concerns regarding elevated ammonia levels in groundwater discharging to the Colorado River. This first phase consisted of 10 extraction wells (called Configuration 1). Four additional configurations of wells have been added since then, for a current total of 42 wells that are designed to prevent ammonia from discharging to the river. The well configurations are shown in Figure 3. To date, a total of more than 168 million gallons of groundwater have been extracted through the interim action system, preventing more than 687,000 pounds of ammonia and about 3,150 pounds of uranium from reaching the river. DOE continues to evaluate the effectiveness of the interim action system, which will likely become part of the final groundwater remedy.

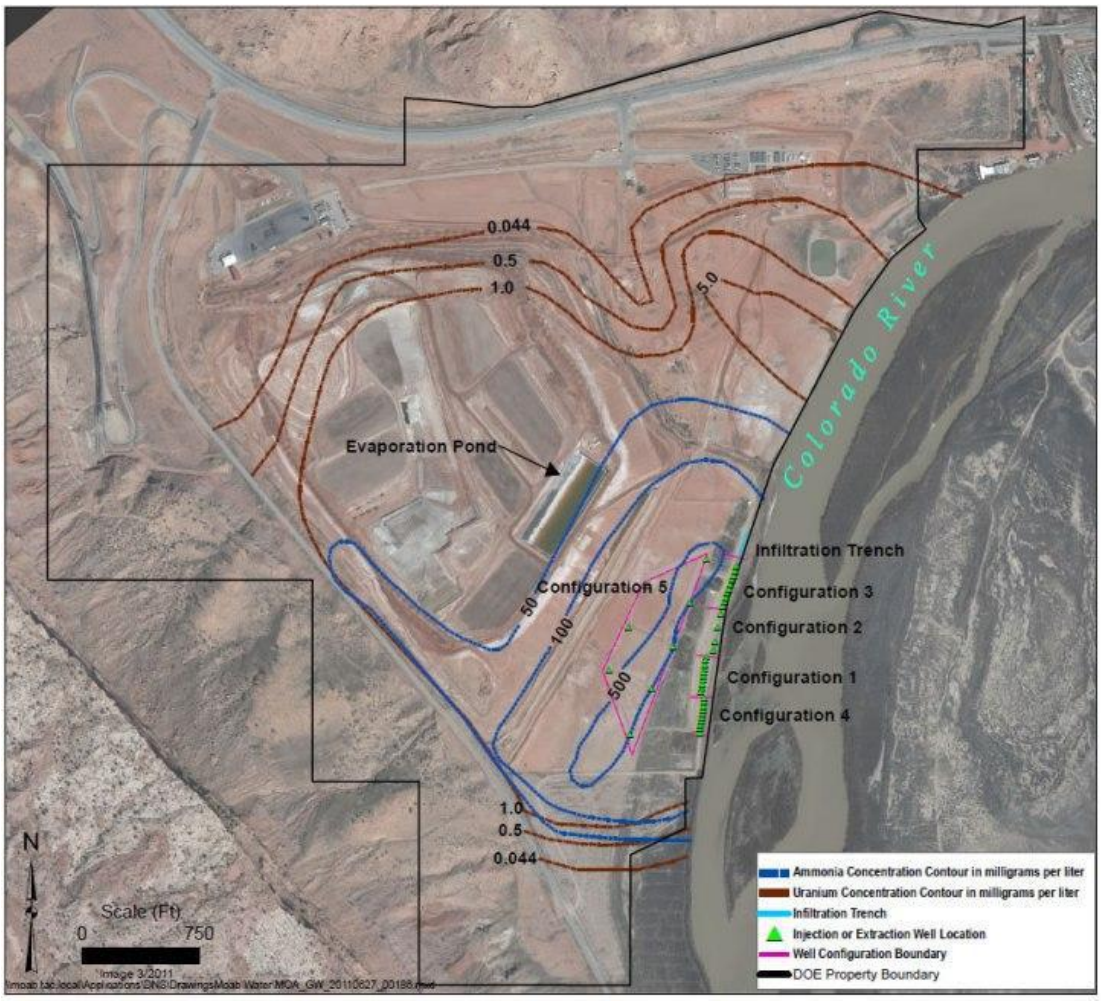

Figure 3 Interim action well field [5].

1.2 Objectives

In accordance with Title I of UMTRCA, DOE has implemented an interim action system at the Moab site to address concerns regarding elevated ammonia levels in groundwater discharging to the Colorado River. In support of this effort and to better understand the subsurface hydrology, a finite difference transient groundwater flow and transport model was developed by one of DOE's contractors. FIU, in collaboration with DOE's Moab site project director, will use this existing groundwater numerical model to evaluate the tailings pore-water seepage in order to assist in effective dewatering of the tailings pile and to optimize the groundwater extraction well field as part of the DOE Uranium Mill Tailings Remedial Action (UMTRA) for the Moab site.

The main objectives of this project are to:

1. Use an existing groundwater numerical model to simulate the fate and transport of contaminants, including uranium and ammonia, in the subsurface domain at the Moab site in Utah. Where deemed necessary, FIU will collaborate with the ASCEM Program and other site-specific experts to optimize the existing model in order to produce the best possible site model which will have the capability to simulate nitrogen and uranium transformations along the flow path and density dependent flow related to brines in the groundwater system beneath the site.
2. Perform numerical simulations of remedial scenarios proposed by DOE including pumping of contaminated groundwater from the shallow plume to an evaporation pond on top of the tailings pile, and injecting the diverted Colorado River water into the alluvial aquifer in order to predict the outcome of each remedial action and to investigate the effectiveness of each scenario in reducing contaminant mass in the groundwater system and protecting potentially endangered fish habitat in the backwater areas of the river. Numerical simulation of the proposed remedial actions will aid in prediction of the time to reach cleanup levels and assist DOE in optimization of the operation of groundwater extraction well fields, infiltration of treated water, and injection of clean fresh water for the DOE UMTRA site in Moab, Utah.

1.3 Technical Approach

The following outlines the series of proposed subtasks to be executed in order to achieve the aforementioned project objectives.

- Subtask 1: Model Update and Improvement

    1. Hydrologic budget calculations will be evaluated using historical meteorological data, surface water flow rate data, seep flow rate data and human induced stresses. The locations where these inputs and outputs manifest will be detailed, along with known or expected changes with time due to climatic variations, pumping, seepage and surface-groundwater interaction. Results of the water budget analysis will be used for developing constraints for the surface water model and the groundwater model.
    2. New geostatistically interpolated plumes will be created for model input and the model will be used to predict concentration in habitat areas for various river stages. The lateral extent of groundwater contamination emanating from the tailings pile will be delineated.
    3. Analysis of groundwater quality data adjacent to the Colorado River for calculating the flux of contamination into the river will be conducted. Water quality contour maps will be generated by using analyzed results from all of the monitoring wells and will be used to assess the pattern of contaminant transport.
    4. Flow boundary conditions to represent the inflow from the Glen Canyon Group and Entrada Sandstone aquifers will be implemented along with inflow from bedrock along the Moab Fault zone, evapotranspiration, inflow due to seepage from the tailings pile, and with hydraulic heads for simulating the inflow from the Moab Wash.

- Subtask 2: Model Calibration and Validation

    1. The model will be calibrated with water level measurements collected from 44 different wells. In addition to water level elevations, the model will be calibrated to estimated fluxes for Moab Wash, the surrounding bedrock, the Colorado River during the base flow

conditions and evapotranspiration. In the existing model, rather than using zones corresponding to like hydraulic conductivity values, hydraulic conductivity distribution was determined using pilot points. Variable hydraulic conductivity values will be used for the top 3 layers and uniform conductivity values for the rest.

2. Pumping test data and several years of regular monitoring data which shows the natural seasonal variations and responses to other stresses will be used for transient calibration of the model.
3. Calibration effort would involve systematically adjusting the values of effective porosity (ne), dispersivities (αL, αT), and distribution coefficients (K_d) in successive simulations, and comparing the results against the observed concentration at the monitoring wells.

- Subtask 3: Prediction and Sensitivity Analysis

1. Predictive simulations will be carried out with maximum and minimum values of flow parameters such as the hydraulic conductivity fluxes from Glen Canyon and Moab Fault, evapotranspiration and recharge. Predictive simulations will be carried out with maximum and minimum values of transport parameters such as dispersivities, ammonia distribution coefficients, effective porosities and ammonia tailings seepage.
2. Simulations to analyze the effects of pumping at well field Configuration 5 on ammonia and uranium concentrations in the upper saline zone and infiltration of freshwater in Configuration 1 to 4 will be conducted. Upgradient infiltration locations will be optimized relative to the tailings and extraction wells to maximize the number of pore volumes for flushing and reduce remediation time. The rate at which ammonia in the brine zone will migrate into the overlying brackish and freshwater will be calculated. The model will also be used for well field optimization to predict capture zones and mass removal.
3. Simulations to identify the discharge zone for the legacy plume in the brine zone and to identify areas of uncertainty will be conducted. The effect of discharge of a legacy plume in the brine zone after the extraction wells have been shut off will be modeled.

2 SITE CHARACTERISTICS

2.1 Hydrology

2.1.1 Surface Water

The Colorado River which is located along the eastern boundary of the site is bounded by the coalesced alluvial fans of Moab and Courthouse Washes in the north and by a large topographic depression known as the Matheson Wetlands Preserve to the south. The USGS Cisco, Utah, gaging station (Station No. 09180500) located approximately 31 river miles upstream of Moab is the closest gaging station to the Moab site along the Colorado River. Post 1950 flow data show an average peak flow of approximately 28,000 cfs. Daily mean discharges measured at the Cisco gaging station from 1950 through 2010 are shown in Figure 4.

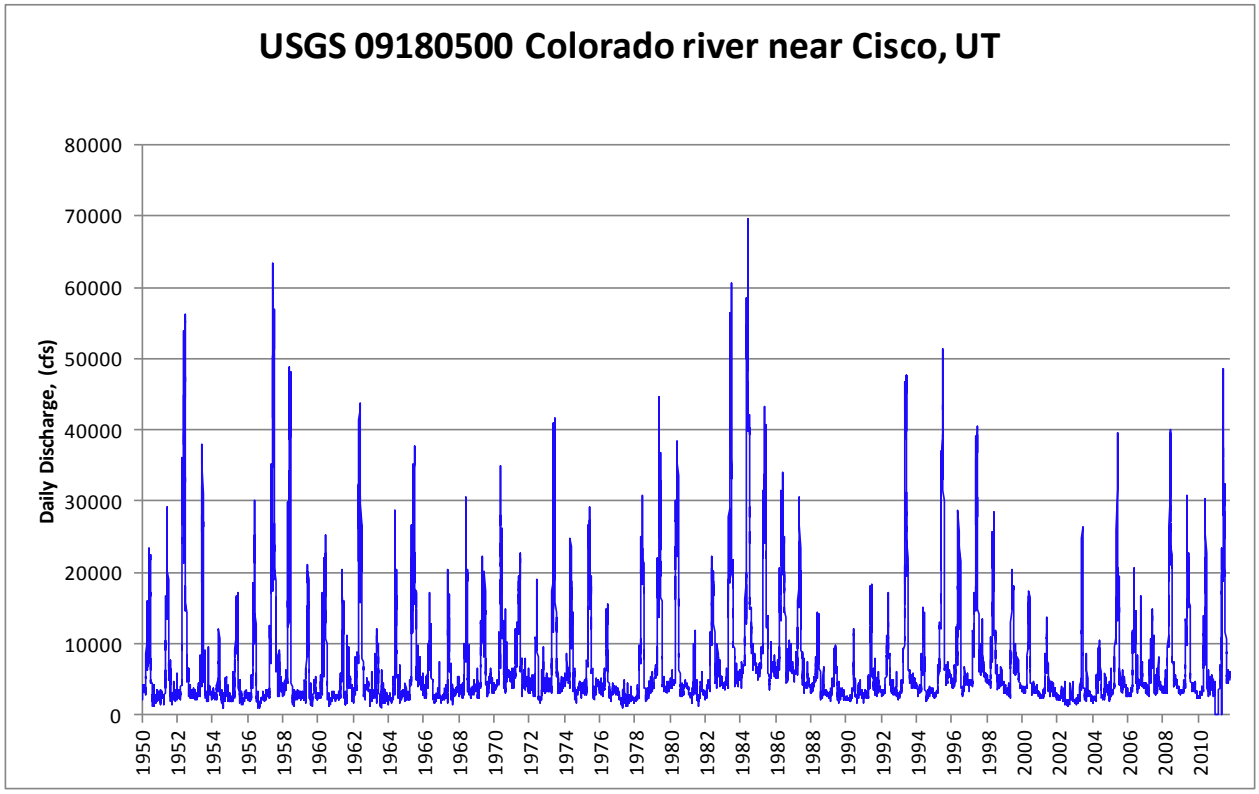

Figure 4 Average peak flows for the Colorado River measured at the Cisco gaging station, through 1950 to 2010.

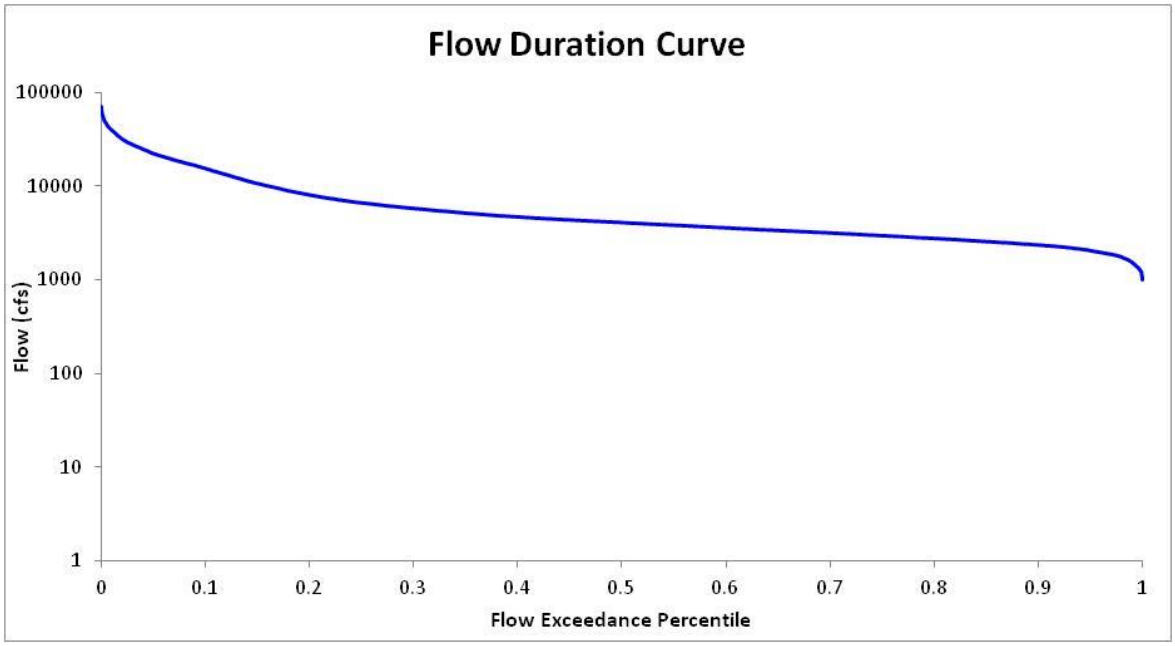

Figure 5 Flow duration curve for Cisco Station No. 09180500.

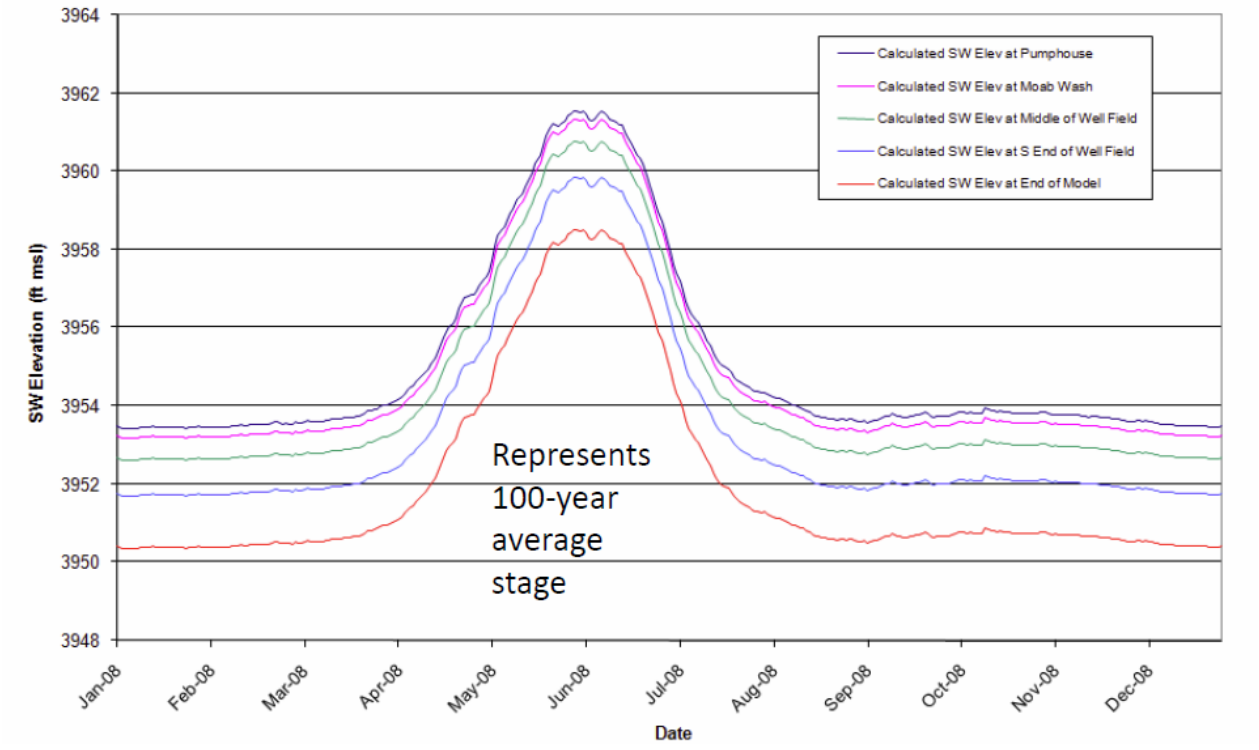

Figure 6 Colorado River stage.

As the Colorado River crosses the valley it generally curves to the south-southeast toward the downstream portal where it is once again confined and flows toward the southwest. Because of the snowmelt runoff, annual peakflow events in the Colorado River are of long duration and occur during late spring. The base flow is about 3,000-4,000 cfs and the maximum recorded discharge at the Cisco, Utah, gage of 76,800 ft^3/s occurred on June 19, 1917 [1].

The probable maximum flood (PMF) value of the USGS for the Moab Valley is 300,000 cfs [1], and the 500-year flood for the Cisco gauging station is 120,000 cfs whereas the 100-year flood is 97,600 cfs. During the highest recorded flood (1984) of 66,500 cfs, the water level was 4 feet above the toe of the tailings pile, and for the PMF, the water level would be 29 feet above the toe of the tailings pile.

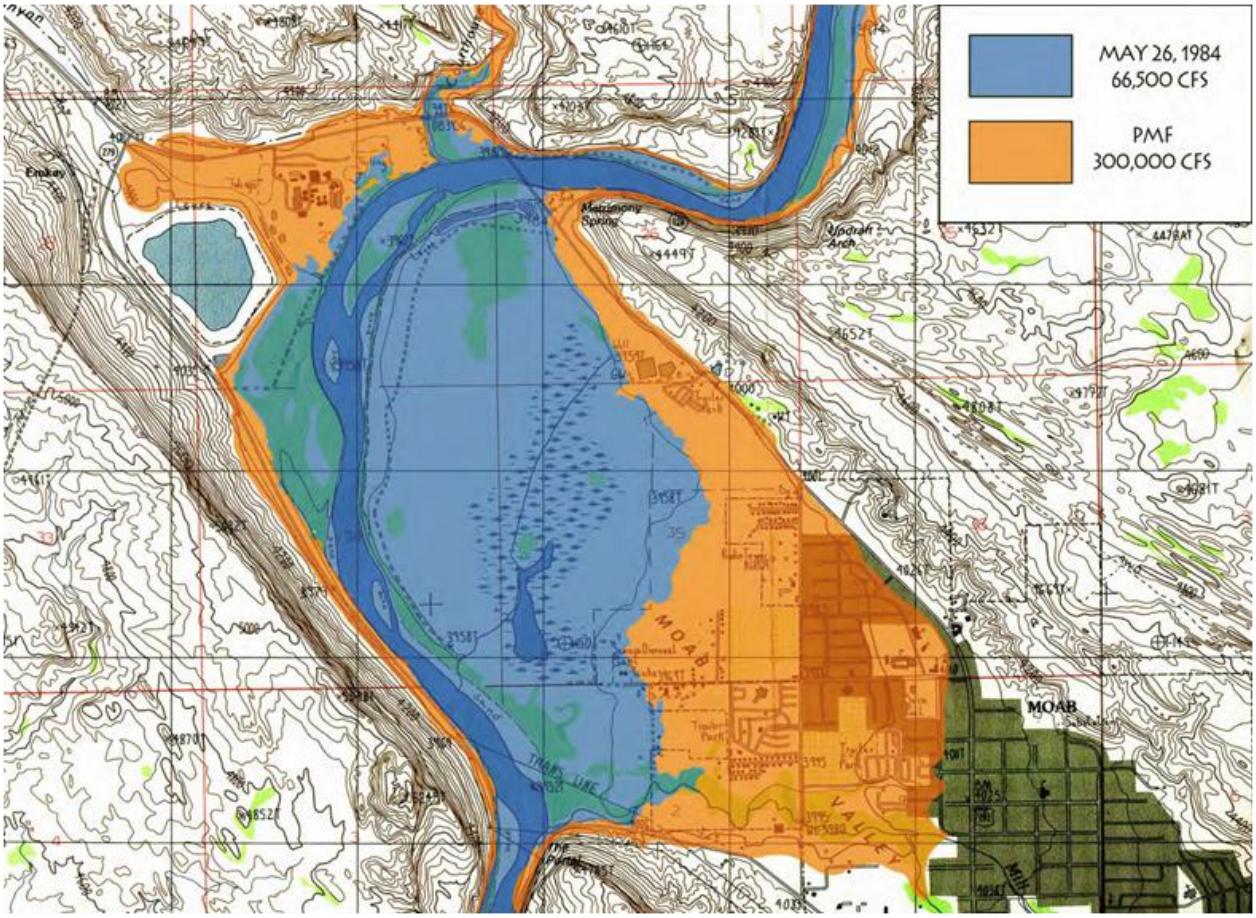

Figure 7 Extent of a 66,500 and 300,000 cfs flood in the Moab Valley [7].

2.1.2 Groundwater

Groundwater aquifers in the Moab region occur in the unconsolidated Quaternary material deposited on the floor of Moab and Spanish Valleys and in consolidated bedrock formations. The upper groundwater system consists of the unconsolidated and bedrock formations above the very low permeability salt beds of the Paradox Formation. The lower groundwater system includes all stratigraphic units below the Paradox Formation. The salt beds of the Paradox Formation confine units in the regional lower system and occur over most of Moab and Spanish valleys. The Paradox Formation also underlies the Moab site.

2.1.3 Water Budget

Groundwater flows from the entrance of Moab Canyon towards the Colorado River; however during high river stages, surface water inflow may penetrate as much as 200 ft inland from the river bank. Inflows and outflows for an estimated water budget for the Moab Site are presented in Table 1, Table 2 and Table 3. These tables indicate that most of the fresh water in the alluvial aquifer enters the site upgradient along geologic contacts between the alluvium and the Glen Canyon Group and Entrada Sandstone bedrock aquifers, which are present beneath the northwestern and northern portions of the site. None of the bedrock aquifer inflow is attributed to flows through the Paradox Formation, since this formation is of very low permeability. Short-term transient effects such as the small contribution to bank storage via losses from the Colorado River during periods of high flow are not reflected in Table 3. Not accounting for this in the water balance partially explains why estimated minimum and maximum total inflows to the site are less than comparable estimated total outflows. Though this disparity tends to reflect the considerable uncertainty in estimated water budget components, total flows listed in Table 3 suggest that the rate of water moving through the ground water system during an average year could lie somewhere between the maximum total inflow of 400 gpm and the minimum estimated total outflow of 500 gpm. It appears reasonable to assume that an average of 450 gpm passes through the Moab site groundwater system (DOE 2003).

Table 1 Minimum Water Inflows and Outflows for Moab Site

COMPONENT	In [gpm]	Out [gpm]
Areal Recharge	16	
Moab Wash	0.5	
Bedrock Aquifers	28	
Tailings Pile	20	
Evapotranspiration		208
Colorado River		300
TOTAL	64.5	508

Table 2 Maximum Water Inflows and Outflows for Moab Site

COMPONENT	In [gpm]	Out [gpm]
Areal Recharge	65	
Moab Wash	33	
Bedrock Aquifers	280	
Tailings Pile	20	
Evapotranspiration		504
Colorado River		460
TOTAL	398	964

Table 3 Average Water Inflows and Outflows for Moab Site

COMPONENT	In [gpm]	Out [gpm]
Areal Recharge	40.5	
Moab Wash	16.75	
Bedrock Aquifers	154	
Tailings Pile	20	
Evapotranspiration		356
Colorado River		380
TOTAL	231.25	736

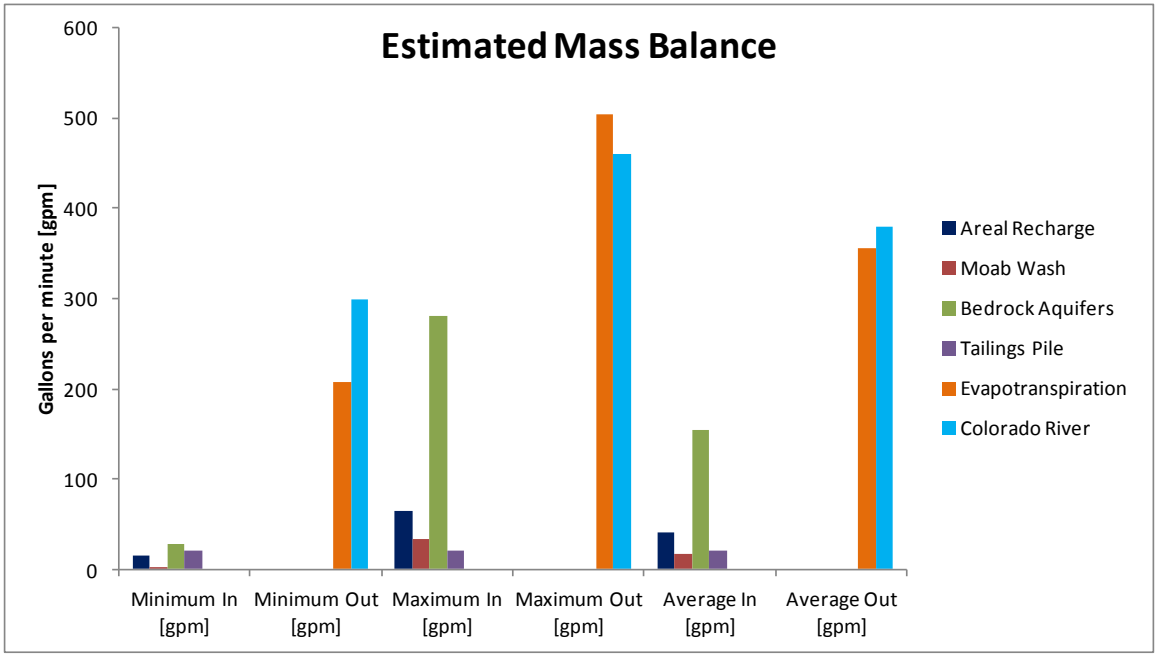

Figure 8 Estimated mass balance.

2.2 Hydrogeologic Characterization

The Moab site is in the fold and fault belt in the northern part of the ancestral Paradox Basin. The fold and fault belt is characterized by northwest-striking salt-cored anticlines and synclines that are cut in places by normal faults and joints that also mainly strike northwest.

The Moab site is located at the northwest end of Moab Valley, which formed during late Tertiary and Quaternary time by salt-dissolution-induced subsidence along the axis of the Moab-Spanish Valley salt-cored anticline [6]. The site is situated at the mouth of Moab Canyon where Moab Wash, an ephemeral drainage passing through the site, follows Moab Canyon northwestward and also is approximately along the trace of the Moab fault. At the northeast and southwest edges of Moab Valley, the Colorado River flows in deeply incised bedrock canyons cut by the superimposed river during the past several million years. The Colorado River flows southward out of Moab Valley through the Portal, the 1,000-ft sandstone cliffs flanking the river canyon mouth. The steep slope southwest of the site flanking Moab Valley rises 1,200 to 1,400 ft to the top of Poison Spider Mesa, capped by sandstones of the Wingate and Kayenta Formations. Just north of the site, north of US-191 and at the north end of Moab Valley, is a

steep slope that rises approximately 600 ft and consists of highly fractured and faulted sandstones of the Wingate, Kayenta, and Navajo Formations (composing the Glen Canyon Group of Jurassic age). Dips of bedrock on this slope express the form of the Moab anticline, which is the northwest extension of the Moab Valley salt-cored anticline.

Groundwater at the site occurs mostly in alluvial sediments that may be as deep as 120 m or more. Total dissolved solids (TDS) concentrations in the alluvial groundwater vary naturally from those for slightly saline water (TDS = 1 to 3 kg/m^3 [1000 to 3000 mg/l]), to those categorized as moderately saline (TDS = 3 to 10 kg/m^3), very saline (TDS = 10 to 35 kg/m^3), and briny (TDS > 35 kg/m^3) (McCutcheon et al. 1993).

The primary source of the slightly saline water, which is found only in the shallowest parts of the saturated zone, appears to be groundwater discharge from bedrock aquifers that subcrop both near the site's northwest border and north of the tailings pile.

Brine waters dominate the deepest parts of the alluvium and are attributed to chemical dissolution of the underlying Paradox Formation, a large and relatively deep evaporite unit that has been deformed to create a salt-cored anticline aligned with and underlying the Moab Valley (Doelling et al. 2002).

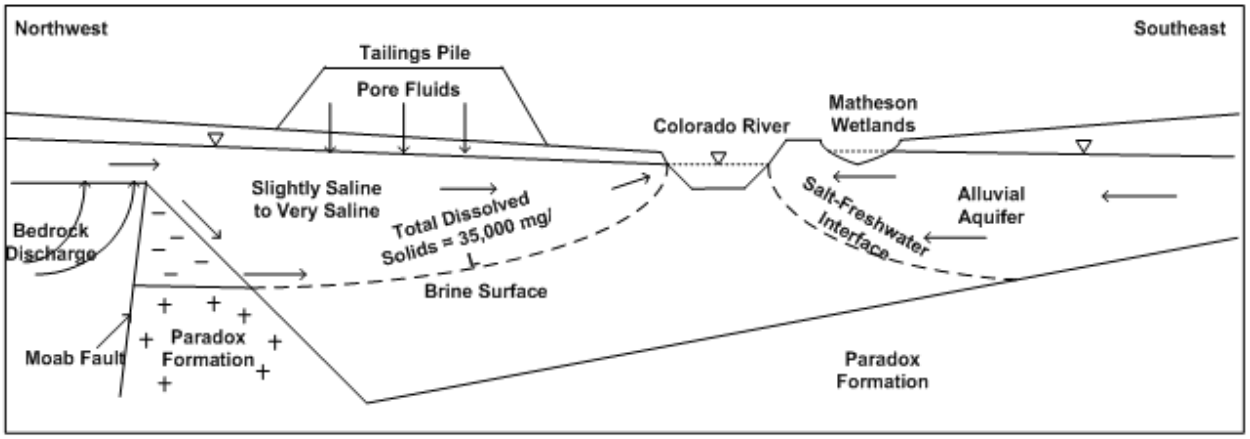

Figure 9 Conceptual model, Saltwater/Freshwater Interface [1].

Over the geologic history of the alluvial basin, mixing of the brine with overlying slightly saline water appears to have created an interlying and relatively diffuse high salinity zone. However, some of the highly saline groundwater can likely be attributed to downward seepage of high-TDS fluids (TDS > 35 kg/m^3) from the base of the tailings pile, a process that occurred during and immediately after the years of facility operation.

Depth to the top of the brine (brine surface) is greatest in the western portion of the site (~45 m) and shallowest at the Colorado River, where TDS concentrations directly below the riverbed appear to exceed 35 kg/m^3.

Hydrologic data indicate that the river and much of the alluvium immediately adjacent to it collectively act as a site of groundwater discharge, both on a regional scale (Blanchard 1990) and locally (Sumsion 1971). These observations suggest that brine is discharging to the Colorado River naturally. However, because some of the saline groundwater west of the Colorado River was probably derived from tailings seepage, a portion of the saline discharge to the river is likely anthropogenic (DOE 2003b).

Flow directions and the observed distribution of TDS in the local alluvial aquifer are analogous to those in a groundwater system overlying a salt dome (e.g. Oldenburg and Preuss 1995, Konikow et al. 1997). Such a system maintains distinct zones of recharge and discharge, and groundwater dissolves formation salts as it moves slowly between the two zones and across the dome.

Depth to brine is greatest under the zone of recharge and gradually decreases with distance toward the discharge zone. At the Moab site, the Paradox Formation is analogous to a salt dome; the greatest depth to the brine surface is observed a short distance downgradient from bedrock units that contribute system recharge; and the brine surface approaches ground level in the vicinity of the Colorado River, where regional discharge of groundwater appears to concentrate.

2.2.1 Hydraulic Conductivity

Rather than use zones corresponding to like hydraulic conductivity values, hydraulic conductivity distribution in the model was determined using pilot points (Figure 10). To implement, the pilot points are located within the model domain and assigned initial, minimum, and maximum hydraulic conductivity values. Automated model calibration adjusts the hydraulic conductivity value at the pilot points between the minimum and maximum allowable values using nonlinear regression techniques. Kriging was used to interpolate hydraulic conductivities in areas between the pilot points. The "calibrated" hydraulic conductivity configuration is the continuous hydraulic conductivity field that produces the best match with the calibration targets.

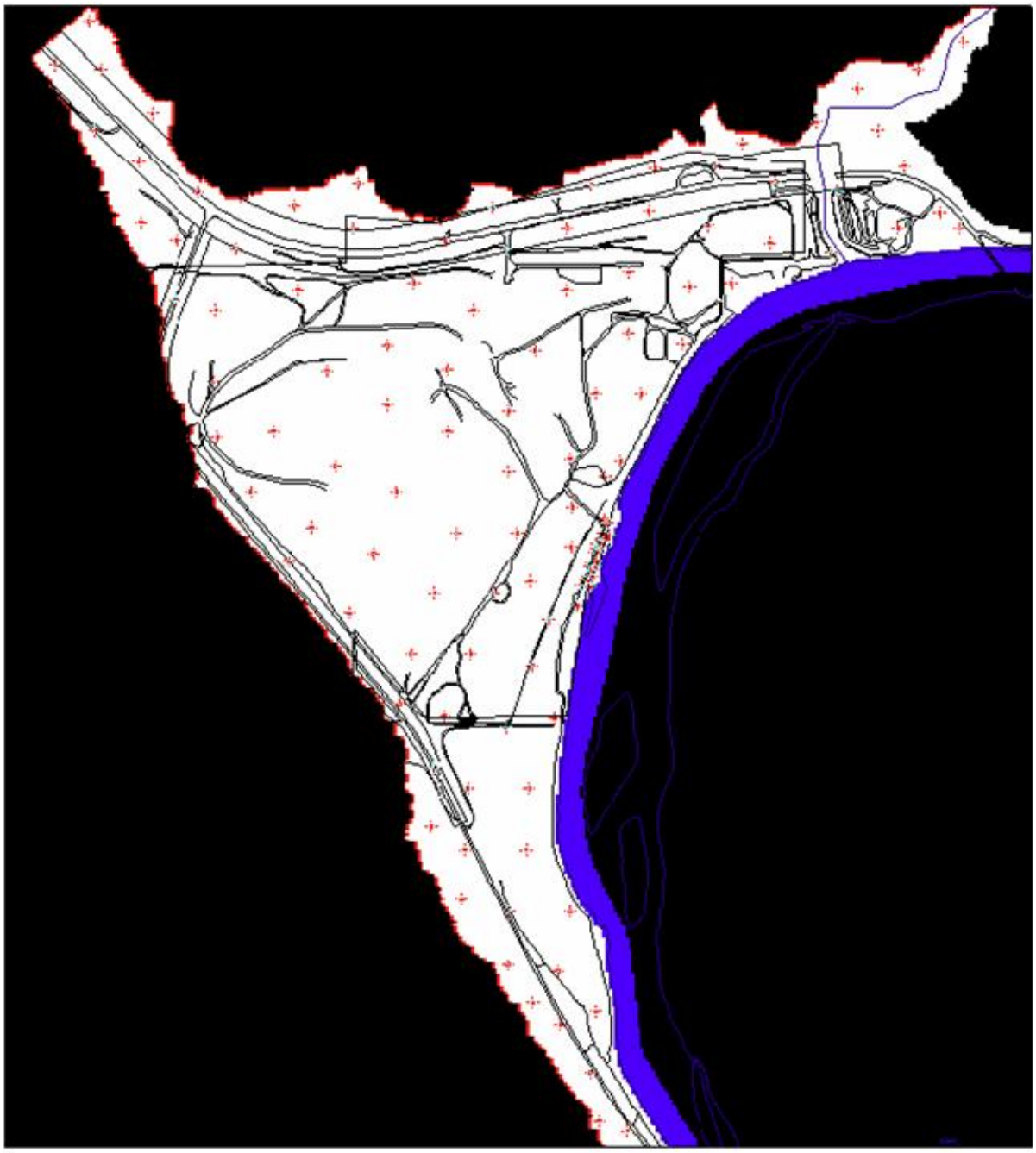

Figure 10 Pilot points used to determine hydraulic conductivity distribution.

Variable hydraulic conductivity fields were determined for model layers 1 through 3 using pilot points (see Figure 11, Figure 12 and Figure 13). Due to a lack of targets in model layers 4 through 15, these layers were assigned uniform hydraulic conductivity zones for calibration (Figure 14).

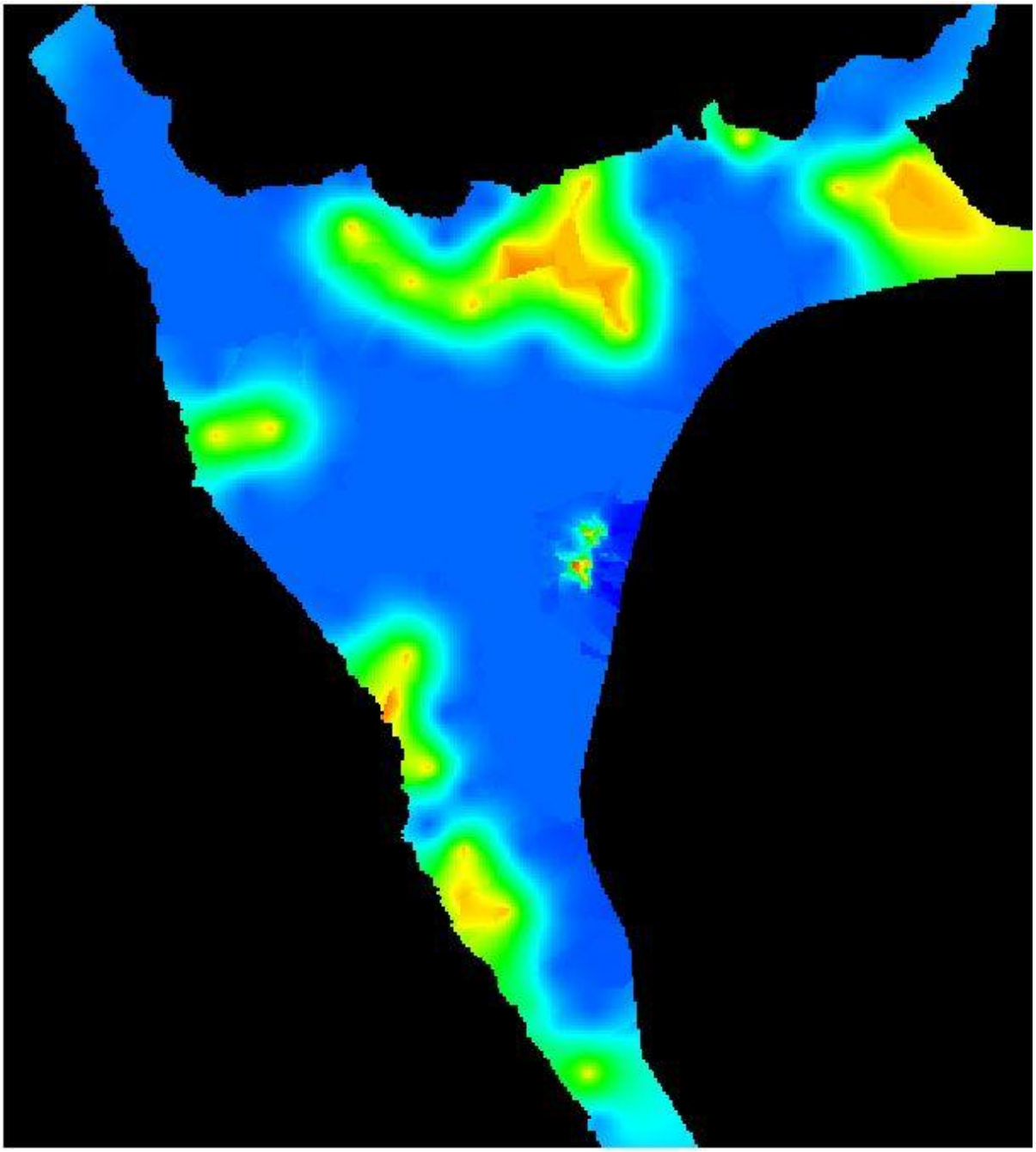

Figure 11 Hydraulic conductivity for Layer 1.

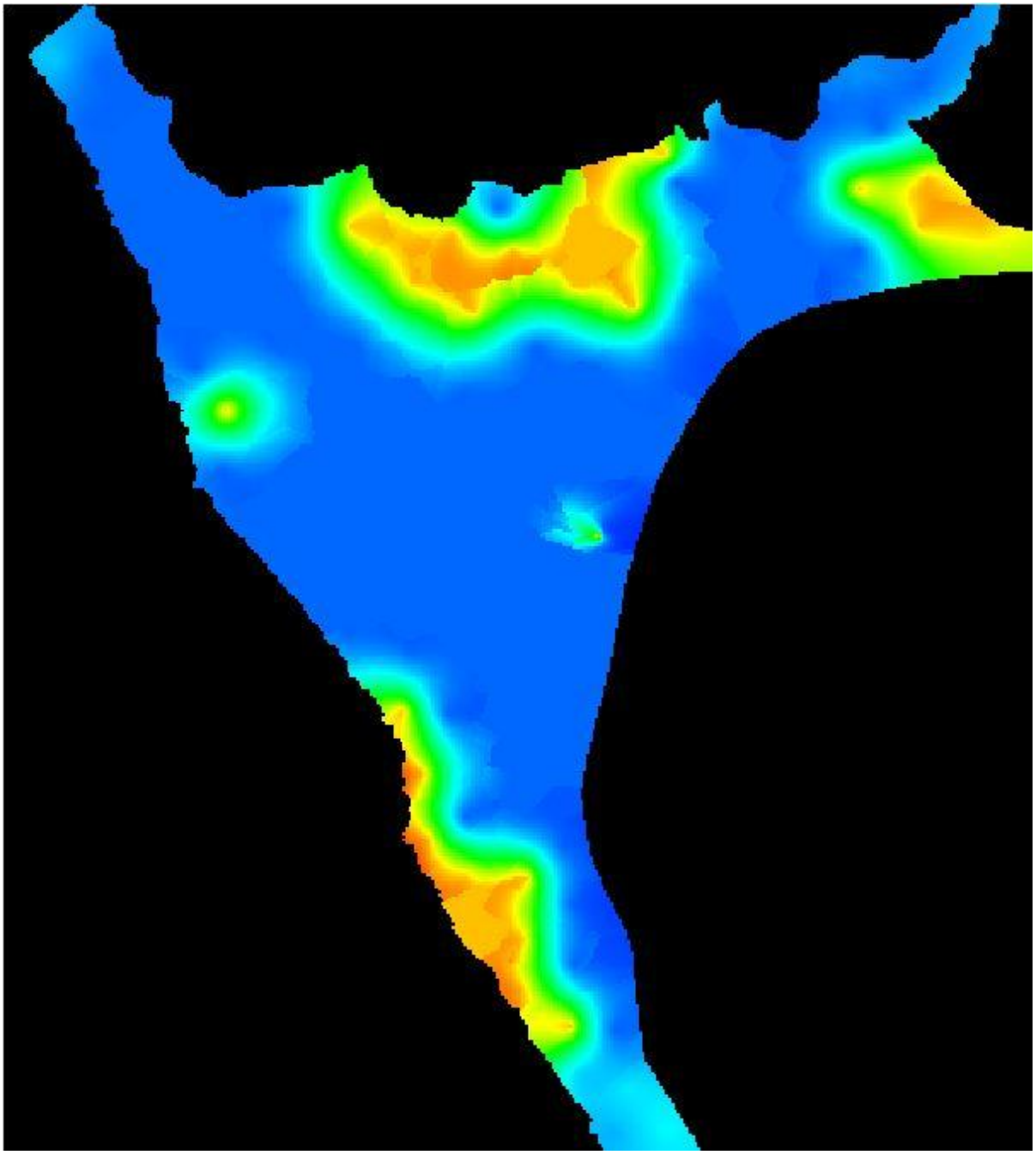

Figure 12 Hydraulic conductivity for Layer 2.

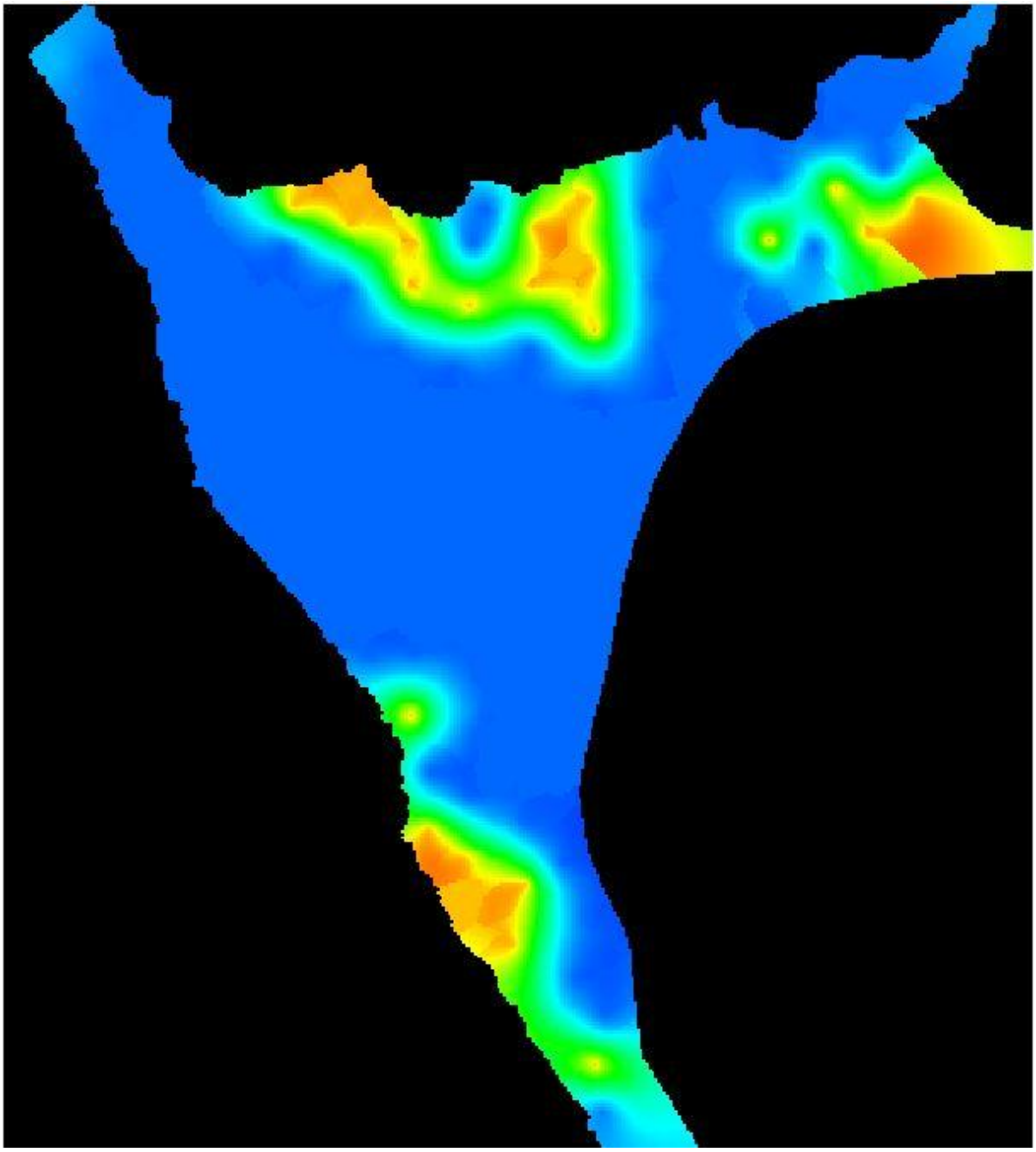

Figure 13 Hydraulic conductivity for Layer 3.

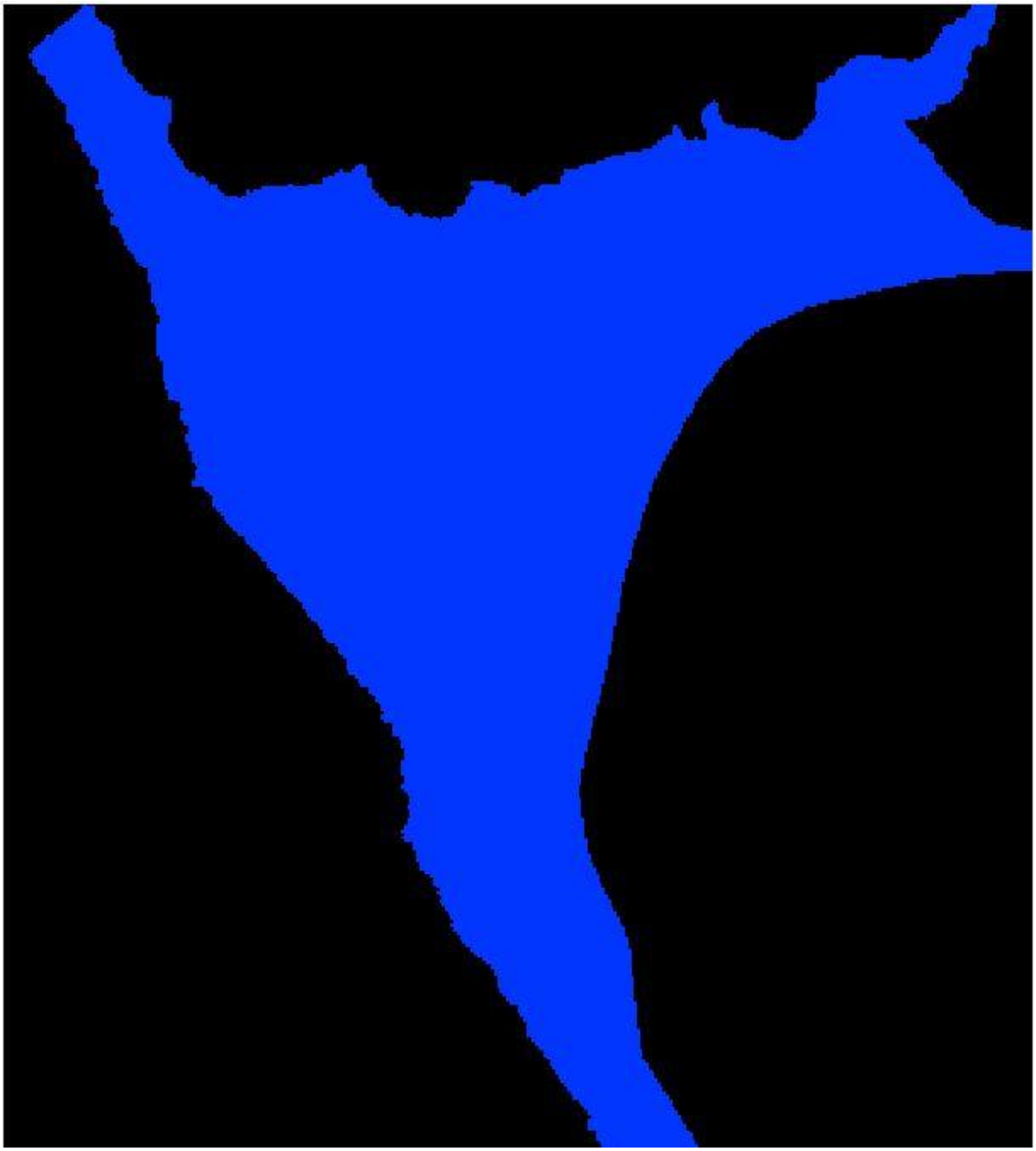

Figure 14 Hydraulic conductivity for Layers 4 to 10 – 20 ft/d & Layers 11 to 15 – 30 ft/d.

2.2.2 Porosity

Porosity is a required parameter in modeling simulations because it enters into transport calculations not only in the seepage velocity term, but also in expressions for the solute mass in a given volume of aquifer and the rate at which that mass changes with time (Zheng and Bennet 1995). Porosity was not determined specifically for the Moab site. Rather, literature values compiled by Morris and Johnson (1967) were used because their values are regarded as reputable averages that span a wide variety of lithologic materials and are widely used in the field of hydrology. On the basis of these published values, bedrock materials were assigned a porosity of 20 percent, and alluvial materials were assigned a porosity of 30 percent.

2.2.3 Storativity

The storativity was defined by creating 10 different zones of the model domain [Figure 15]. Estimates of aquifer storativity were derived from aquifer tests performed at groundwater wells.

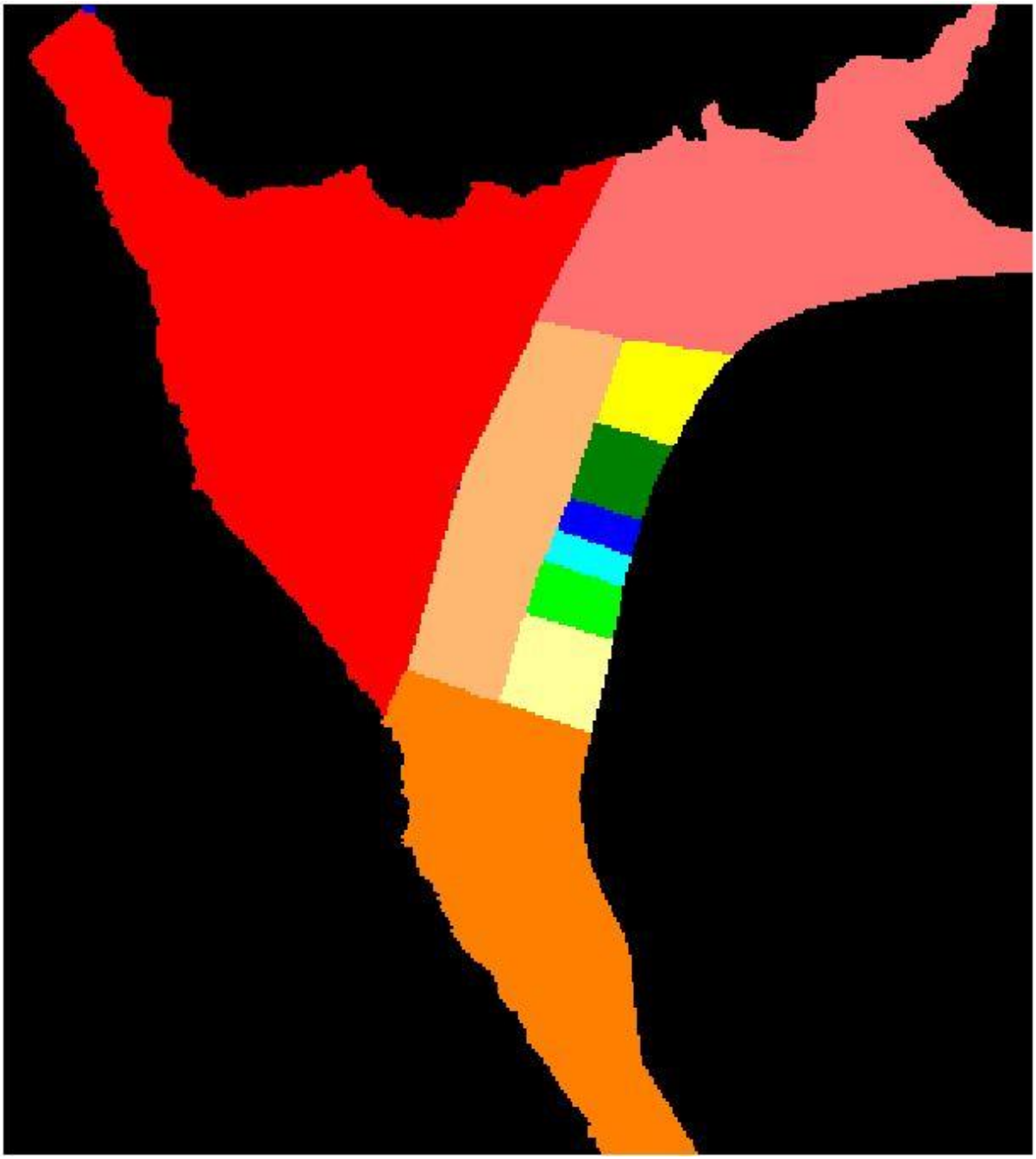

Figure 15 Storativity.

2.3 Nature and Extent of Groundwater Contamination (lab results only)

2.3.1 Ammonia Plumes

During milling, the tailings pile may have contained fluids with TDS ranging from 50,000 to 150,000 mg/L. Because these salinities exceed the 35,000 mg/L concentrations at the saltwater interface, they are believed to have had sufficient density to migrate vertically downward into the brine. This vertical migration of the tailings pore fluids into the saltwater system is believed to have created a reservoir of ammonia that now resides below the saltwater interface. This ammonia plume below the interface probably came to rest at an elevation where it was buoyed by brine having a similar density. Under present conditions, the ammonia plume beneath the saltwater interface represents a long-term source of ammonia to the upper alluvial groundwater system. The ammonia source at the saltwater interface (basal or ammonia flux), the legacy plume, and seepage of ammonia concentrations from the tailings pore fluids are illustrated in the conceptual model presented in

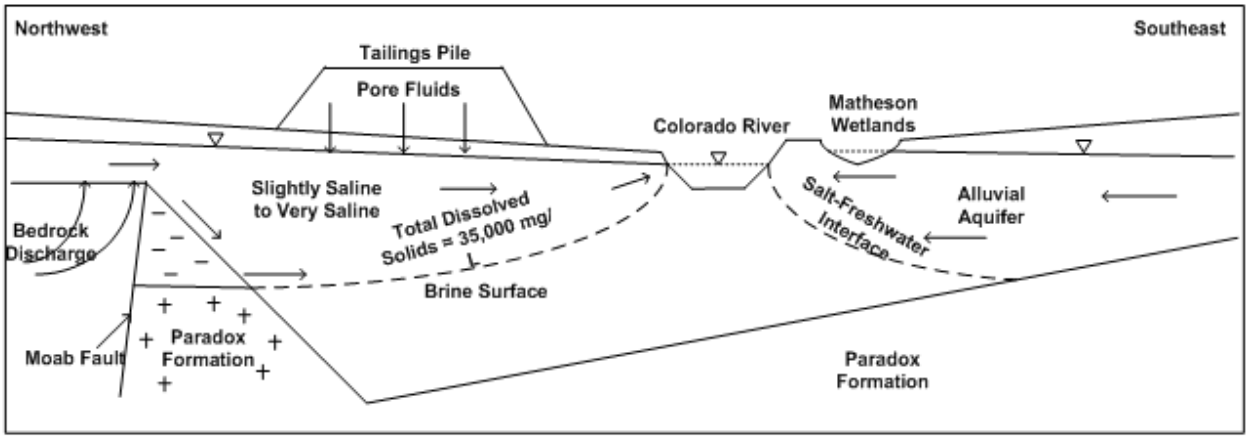

Figure 9.

Since the release of tailings pond fluids containing high TDS concentrations infiltrated the groundwater during milling operations, the volume of relatively fresh water entering the site upgradient of the tailings pile may have diluted the ammonia levels in the shallow groundwater. Advective flow of fresh water through the higher-density fluids is insignificant, and thus the ammonia concentrations persist at depth. Oxidation of ammonia to nitrate or nitrogen may also

contribute to lower ammonia concentrations observed in the upgradient shallow groundwater beneath the tailings pile where aerobic conditions are more likely.

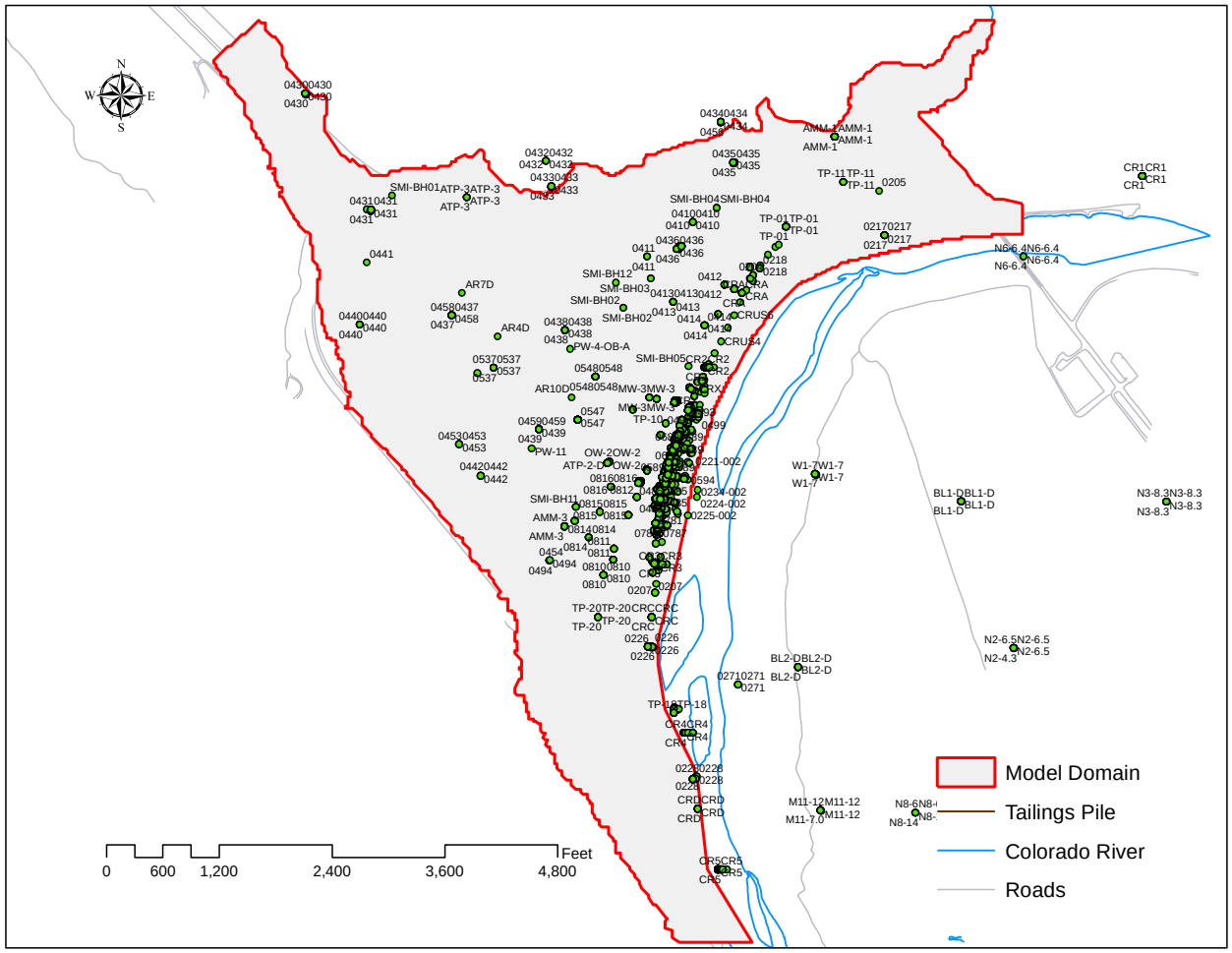

Figure 16 Ammonia monitoring wells.

2.3.2 Total Dissolved Solids (TDS)

Total dissolved solids (TDS) concentrations in the alluvial groundwater vary naturally from those for slightly saline water (TDS = 1 to 3kg/m^3 [1000 to 3000mg/l]), to those categorized as moderately saline (TDS = 3 to 10 kg/m^3), very saline (TDS = 10 to 35 kg/m^3), and briny (TDS > 35kg/m^3) (McCutcheon et al. 1993).

Data was collected from 27 different locations at depths ranging from 9 ft to 212 ft below ground surface. In general, TDS increases with depth and TDS increases north to south across the site.

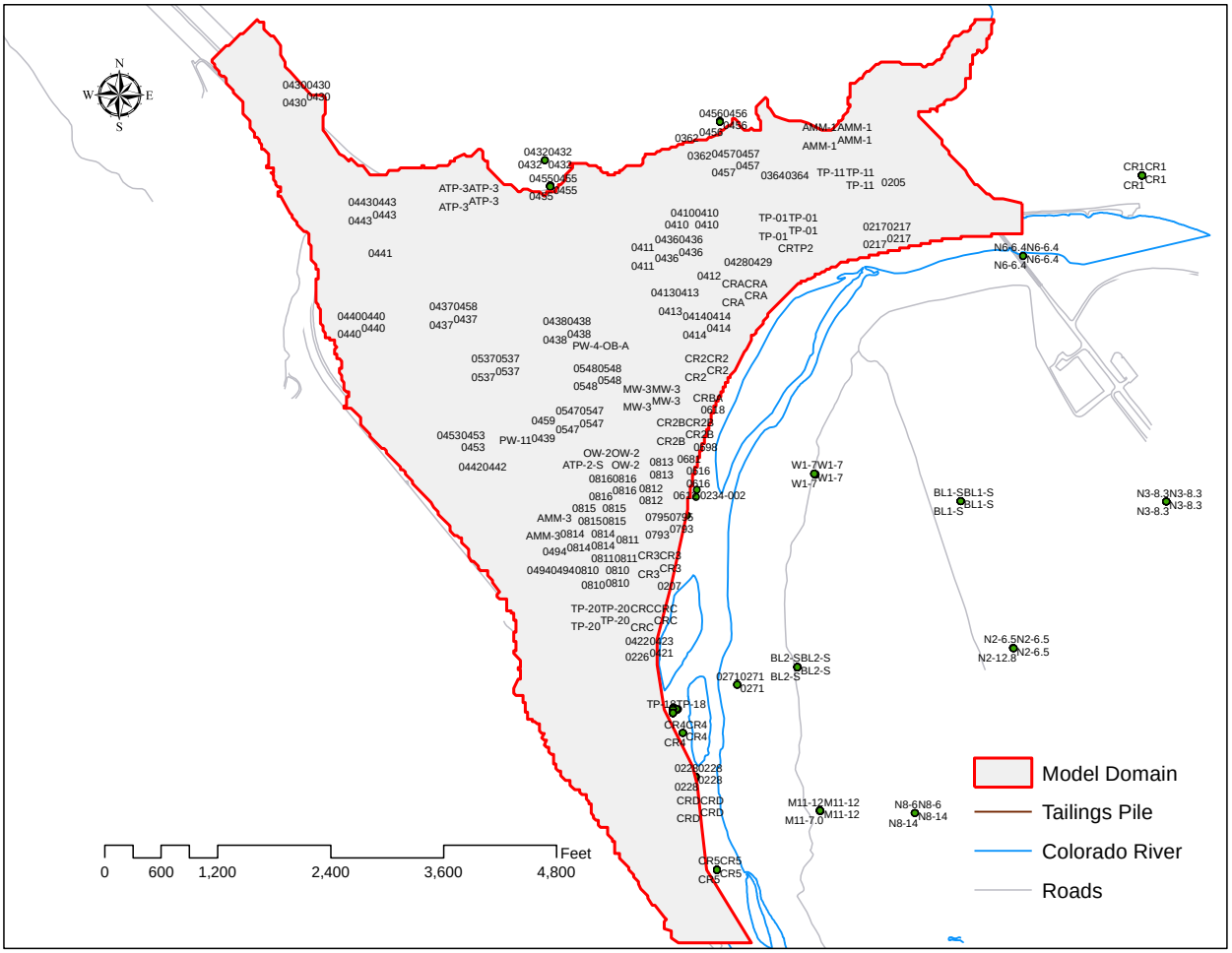

Figure 17 TDS monitoring wells.

3 MODEL DEVELOPMENT

The groundwater system includes a relatively shallow groundwater in alluvium that mostly contains slightly saline to very saline and flows southeastward toward the Colorado River over an extensive deeper zone containing brine [1]. Levels of salinity in groundwater on both sides of and below the river can be described with respect to TDS concentrations as in Table 4. The TDS concentrations are larger than the TDS levels commonly reported for river water (100 to 1,000 mg/L).

Table 4 Classifications of Salinity Levels

Salinity levels	Concentration
Midly Saline	1,000 – 3,000 mg/L
Moderately Saline	3,000 – 10,000 mg/L
Very Saline	10,000 – 35,000 mg/L
Briny	> 35,000 mg/L

Salinity data collected from groundwater in alluvium on both sides of the river show that TDS concentrations in both areas span a large range, typically from as low as 700 mg/L to as high as 110,00 mg/L or more. Thus much of the groundwater in these areas consists of very saline and brine. In accordance with the DOE site conceptual model, the TDS concentrations generally increased with increasing depth.

The data collected at the Matheson Wetlands indicate a mirror image of brine distribution below the Moab site, as depth to brine is greatest in wells located some distance southeast of the river and much smaller near the river's east bank. Such observation when combined with previous studies showing the river acting as a site of regional groundwater discharge, suggest that the larger TDS concentrations in shallow groundwater at the river are due to saltwater upcoming, with the river acting much like a well that induces the upward migration of underlying brine when shallow groundwater is pumped.

Also for data collected at wells located both on and downgradient of the tailings pile, the brine source appears to be dissolution of the Paradox Formation sediments located part of the way down a steep bedrock face situated just to the northwest of the pile. Extrapolation of TDS concentration data close to the river indicates that the brine surface intersects the river near its west bank. With such a large range of TDS concentrations on either side of the river, groundwater flow toward the river from both the project site and the wetlands preserve is a density-dependent process, since water density increases with increasing salinity.

As a consequence, the vertical interval containing most groundwater flow between the brine surface and the top of the saturated zone decreases with proximity to the river, causing progressively larger groundwater velocities as the river approaches.

3.1 Domain

The model domain [Figure 18] was selected on the basis of local hydrogeological features which control flow and transport at the site and the site conceptual model. The SEAWAT model consists of 15 layers [Figure 19]. The top of model layer 1 corresponds to ground surface and the bottom of the layer has a uniform elevation of 3,945 feet mean sea level (msl). The remaining model layers (2-15) have uniform thicknesses of 10 feet. Horizontally the SEAWAT model has uniform 25 foot by 25 foot grid cells, in all the model consists of 671,055 active cells.

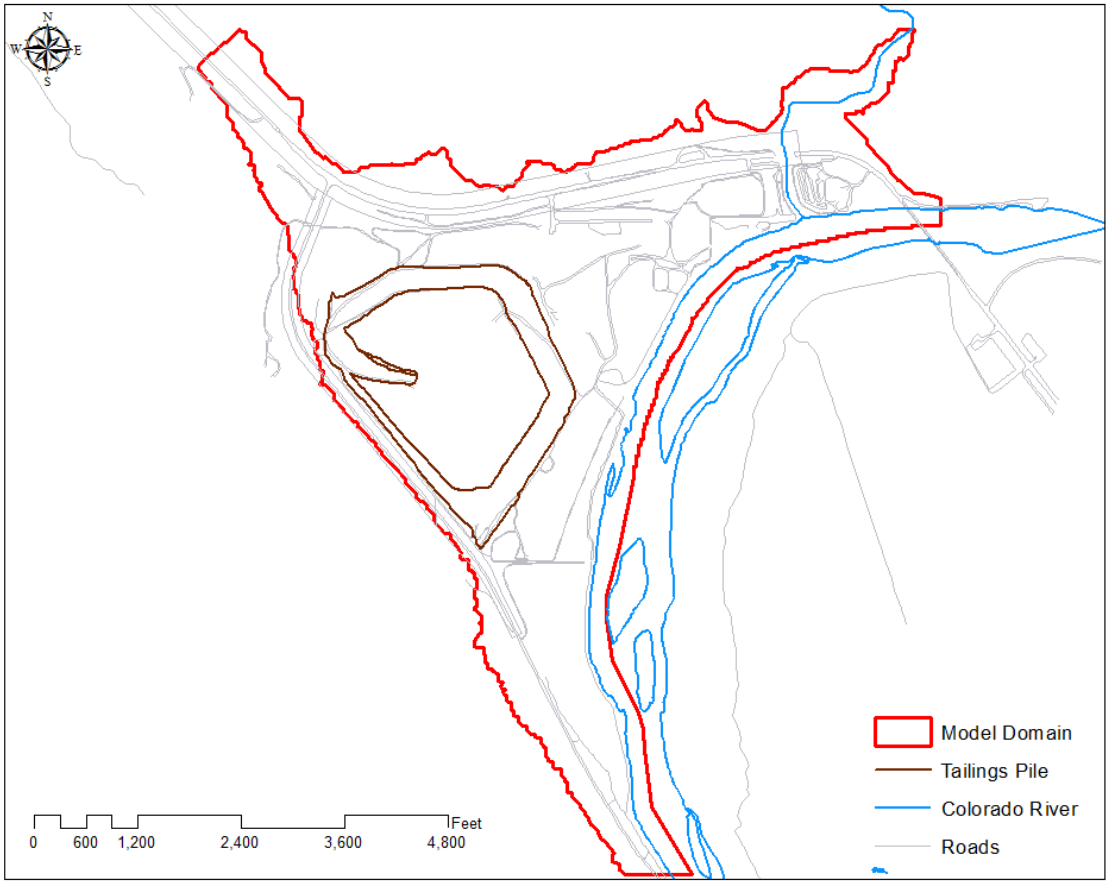

Figure 18 Model domain.

Table 5 Numerical Model Discretization

Number of Layers	15
Number of Rows (y-direction)	393
Number of Columns (x-direction)	354
Total Number of Cells (Active and Inactive)	2086830
Total Number of Active Cells	671055

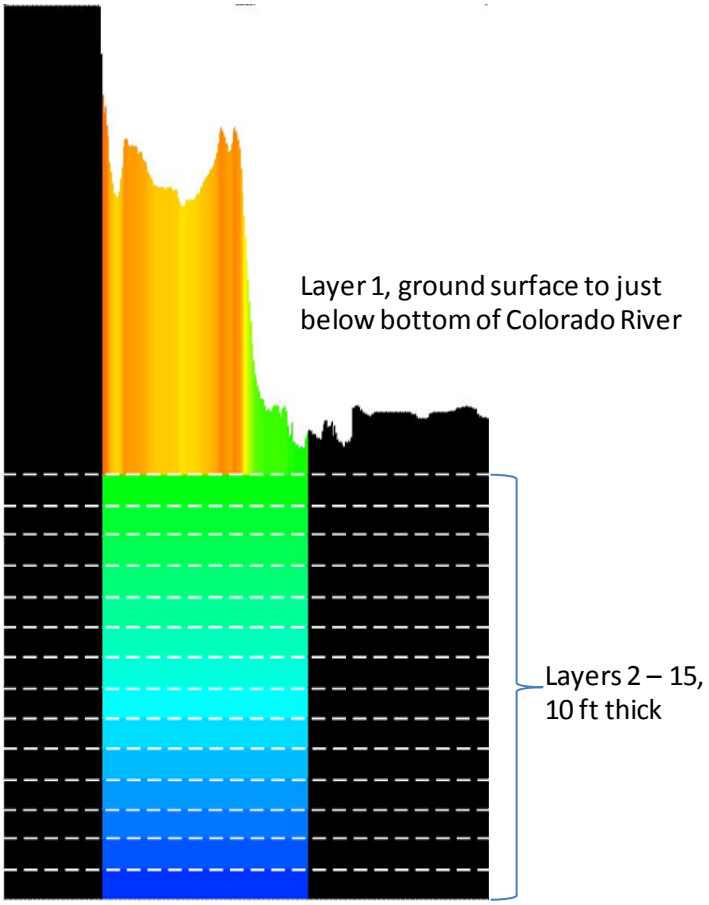

Figure 19 Model layers.

The currently observed spatial variations in groundwater salinity at the Moab site reflect both historical density-dependent flow processes (during mill operations), and relatively steady density-affected processes in recent years. However, none of the collected data by DOE indicate that high TDS concentrations observed in groundwater southeast of the river were partly caused by milling operations, thus inferring that water chemistry in the Matheson Wetlands is the result of natural phenomenon and possibly some anthropogenic influences between the City of Moab and the wetlands preserve.

The density-dependent flow modeling was performed to help quantify the processes shown in

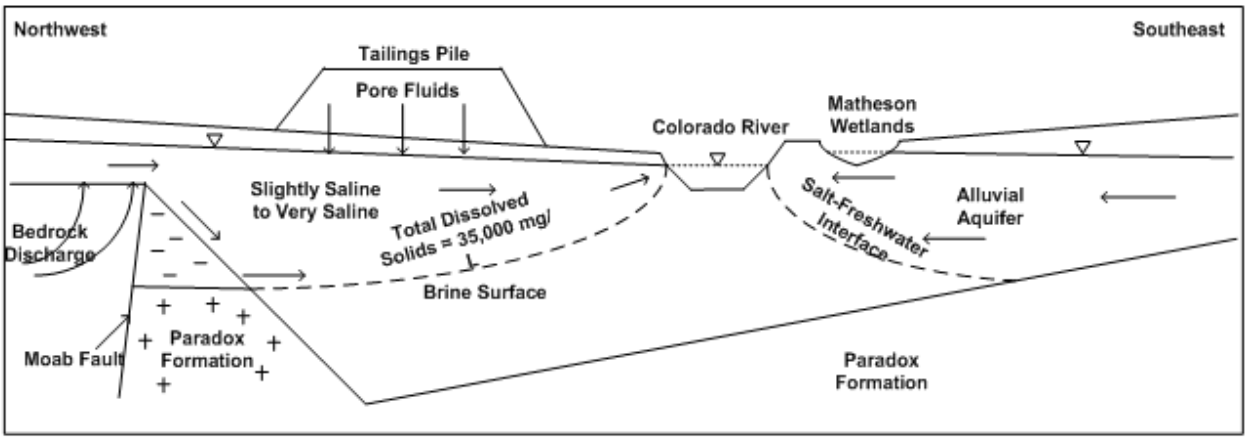

Figure 9. The model concept was simulated two-dimensional groundwater flow and transport in a vertical cross-section, the trace for which followed a streamline that originated in the northwest corner of the site on the northeast side of Moab Fault, then trended southeastward across the tailings pile, and terminated in the center line of the Colorado River. A no-flow condition was applied at the vertical model boundary aligned with the river centerline to represent a line of convergence for surmised flow coming from both the southeast and northwest.

The numerical model used in this study is SEAWAT 2000. SEAWAT 2000 (Langevin et al. 2003) is a widely used program that was developed to simulate three-dimensional, variable density, transient groundwater flow in porous media. SEAWAT is formulated using finite-difference principles and combines the code MODFLOW (Harbaugh and McDonald 1996) for porous media flow with advective-dispersive transport algorithms found in MT3DMS (Zheng and Wang 1999). The MT3DMS code allows model users to simulate the transport of multiple dissolved constituents. When applying it with SEAWAT, TDS is treated as the primary constituent, and a formula built into the code facilitates the conversion of TDS into values of water density. Individual chemical components are treated as secondary constituents.

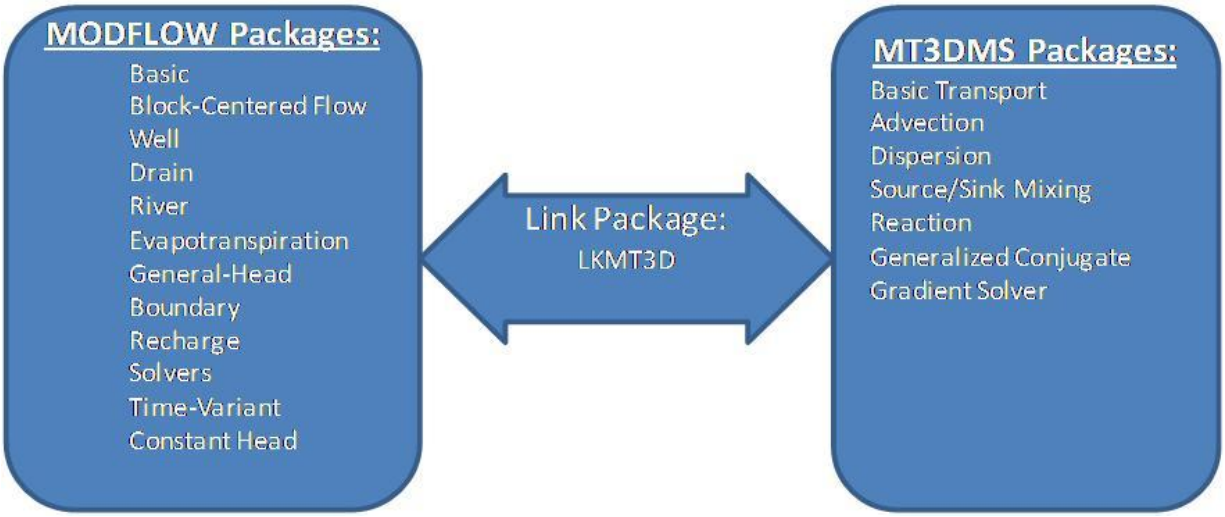

Figure 20 MODFLOW and MT3DMS packages.

3.2 Methodology

Modeling of the groundwater flow and transport at Moab site is composed of five major tasks:

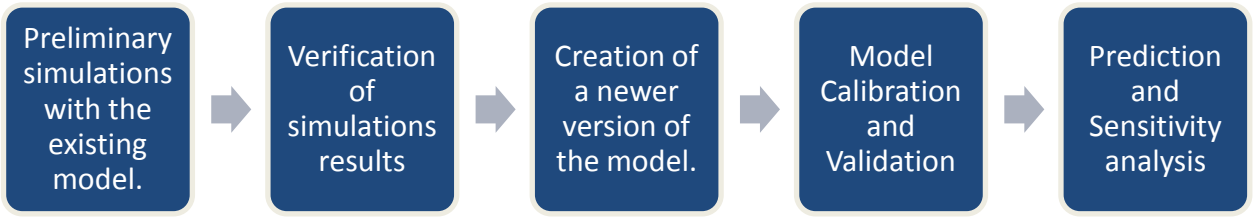

SEAWAT was used to model variable density groundwater flow and transport at Moab site. Groundwater Vistas was selected as the modeling platform because of its superior modeling capabilities, such as advanced solvers and the ability to change model parameters easily and quickly. The SEAWAT model of Moab site consists of 15 layers. The top of model layer 1 corresponds to ground surface and the bottom of the layer has a uniform elevation of 3,945 feet mean sea level (msl). The remaining model layers (2-15) have uniform thicknesses of 10 feet. Horizontally, the SEAWAT model has uniform 25 foot by 25 foot grid cells and consists of 671,055 active cells. Temporally, the model was divided into 13 stress periods, an initial steady-state period followed by 12 transient stress periods corresponding to the months of January through December. The SEAWAT model used a fixed total dissolved solids (TDS) concentration.

The model was calibrated to 2006 water level measurements collected from 44 different wells. Typically multiple water-level measurements were available for the wells. In addition to water-level elevations, the model was calibrated to estimated fluxes for Moab Wash and the surrounding bedrock, the Colorado River during base flow conditions, and evapotranspiration. A calibration target is a point in space and time where one of the model dependent variables has been measured. Calibration targets provide a means of assessing calibration quality because an error term, called a residual, is computed for each target location. A residual is computed as the field measurement minus the model-computed value. The range of errors helps you determine whether the quality of the calibration is adequate for your purposes.

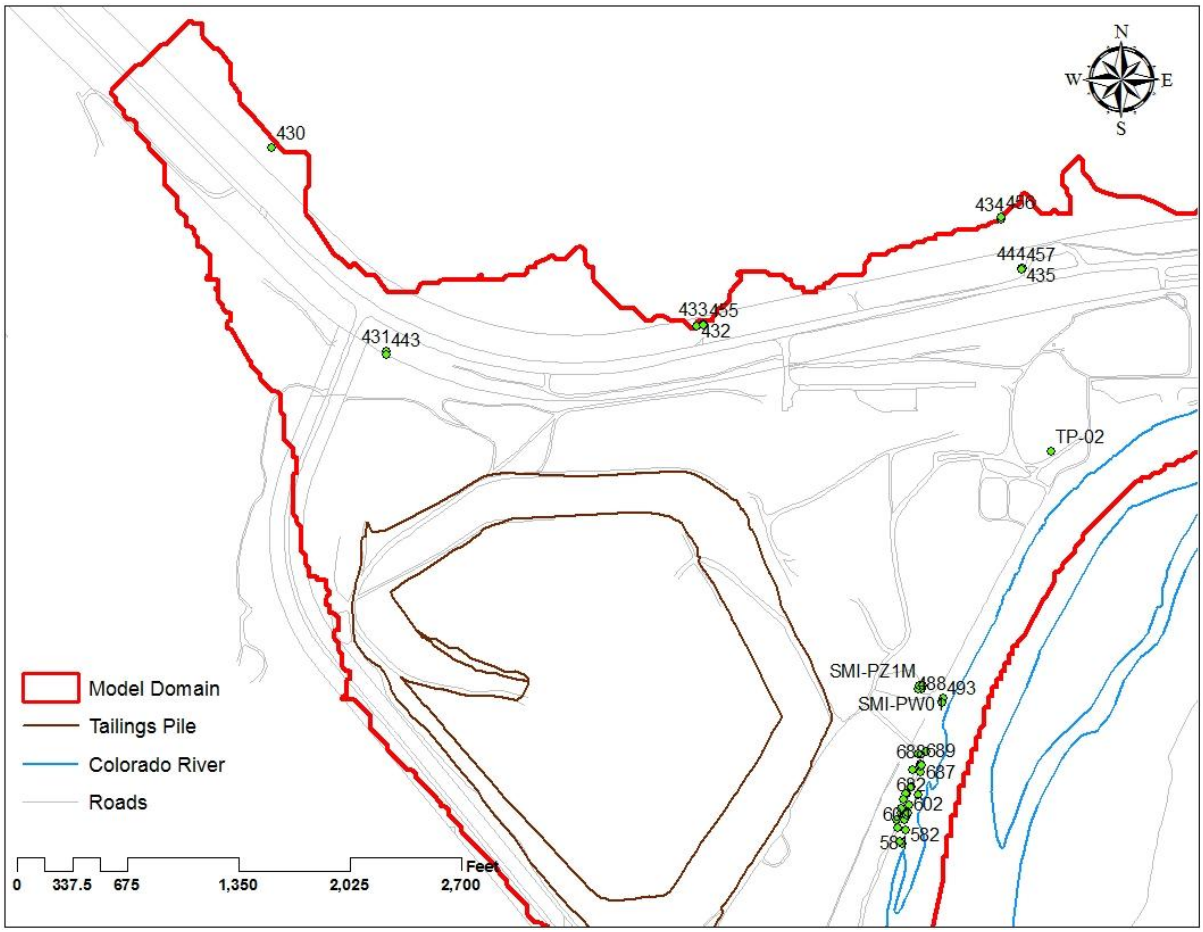

Figure 21 Target points used for model calibration.

The model was configured with two different recharge zones, ambient precipitation and the tailings pile. While it is assumed recharge from the tailings pile was constant throughout the

year, recharge from precipitation was assumed to vary monthly. Evapotranspiration was assigned to areas of the site having significant plant density and was assumed to vary monthly. The Colorado River was simulated using river cells which can contribute or receive water from the aquifer depending on the river stage and the adjacent groundwater relationship. For the simulation the Colorado River was assigned monthly stage values corresponding to the average monthly river stage.

3.3 Boundary Conditions

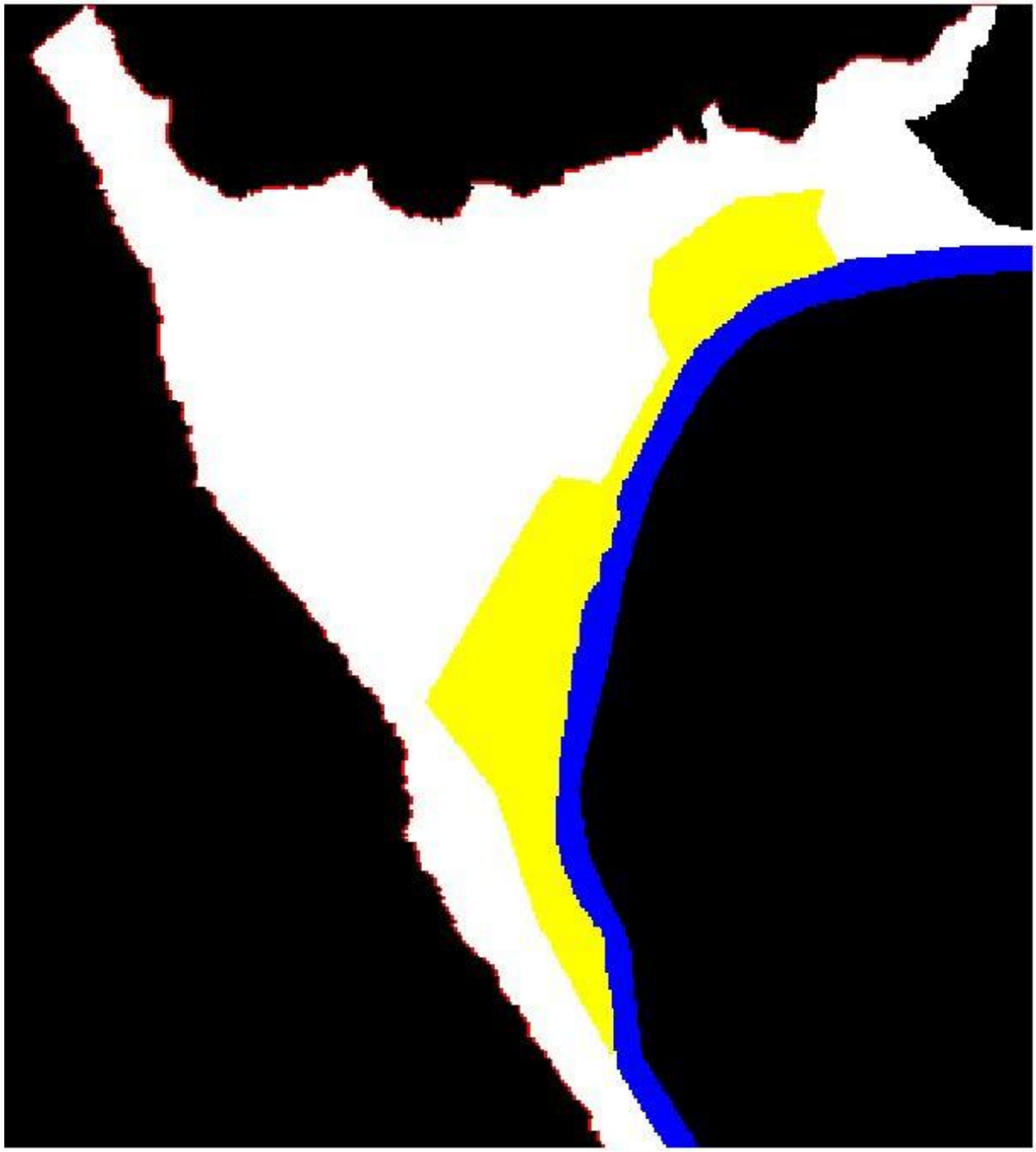

Figure 22 Prescribed head boundary conditions along the Colorado River.

3.3.1 Well Operations

DOE has been operating an interim action to evaluate two scenarios for treating contaminated groundwater and protecting the endangered fish habitat in backwater areas of the river adjacent to the site. One method is to extract contaminated groundwater from a series of wells installed in the shallow plume and pump it to an evaporation pond on top of the tailings pile. The other method is to pump diverted Colorado River water into a storage pond, allow time for settlement of fines, and then, after sediment filtration, inject this water into a series of wells installed into the alluvial aquifer and/or an infiltration trench.

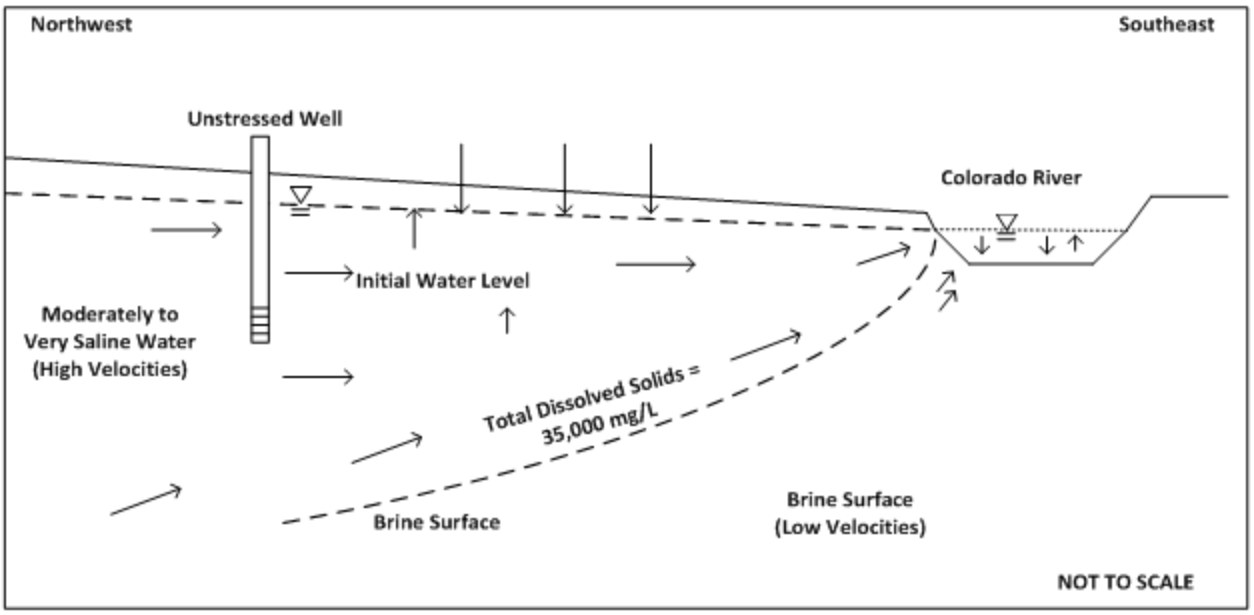

Figure 23 Observed subsurface flow patterns.

In efforts to reduce the potential environmental from contaminated groundwater in the alluvium discharging to the nearby Colorado River, a well field was installed at the Moab UMTRA site in 2003.

The various types of data were collected from 2003 through January 2009 and were analyzed to determine which wells have been efficient at groundwater extraction and under what river stage they remove the most contaminant mass.

The primary purpose of operating any of the well-field configurations in extraction mode is to intercept ammonia in high-concentration areas, thereby reducing mass loading to the river. Results of system operation and monitoring indicate that extraction can pull river water into the aquifer and reverse the groundwater flow gradient, at least locally. Figure 24 shows this reversal conceptually. This reversal should result in reduced discharge of ammonia to near-shore areas. However, it is not clear how groundwater extraction affects the brine surface below the river and locations of ammonia discharge to the river.

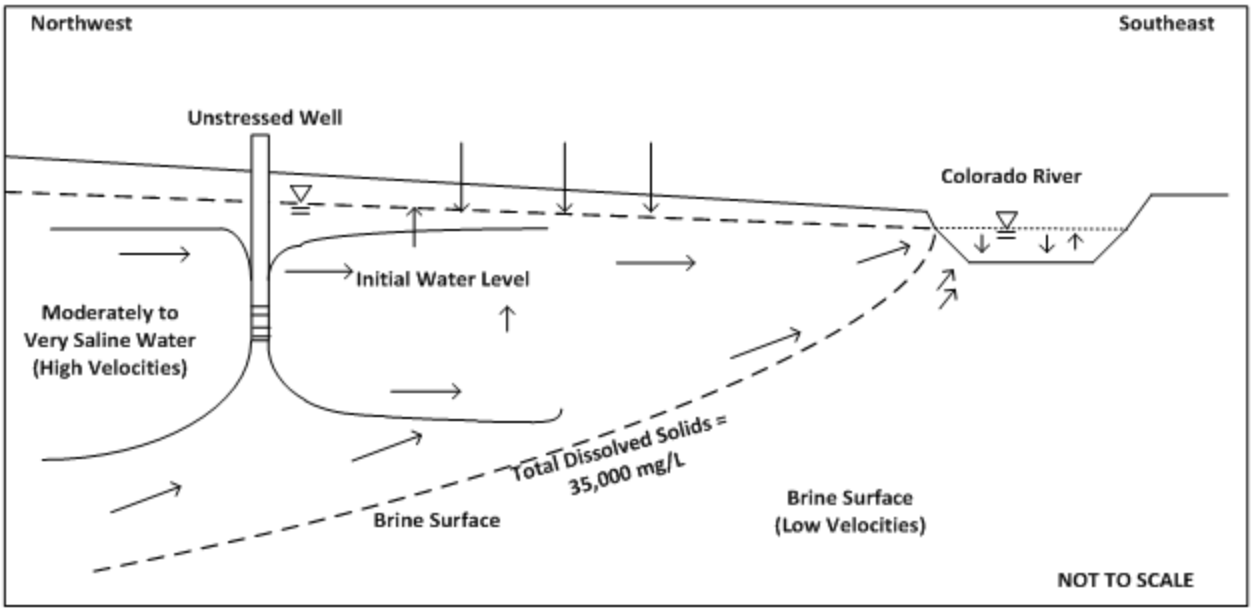

Figure 24 General effects of operating remediation wells for the purpose of contaminant mass removal.

The purpose of operating Configurations 2, 3, or 4 in injection mode is to determine the feasibility of and capacity for diluting ammonia concentrations in the backwater habitat via injection of fresh water into the aquifer close to the Colorado River. A conceptual depiction of the effects of operating remediation wells for fresh-water injection is shown in Figure 25. Mounding of fresh water at the injection well(s) helps provide a hydraulic barrier between the ammonia plume and the river near its western shore. At this time, the purpose of the infiltration trench is to obtain operational performance data regarding flow rates and associated

groundwater mounding.

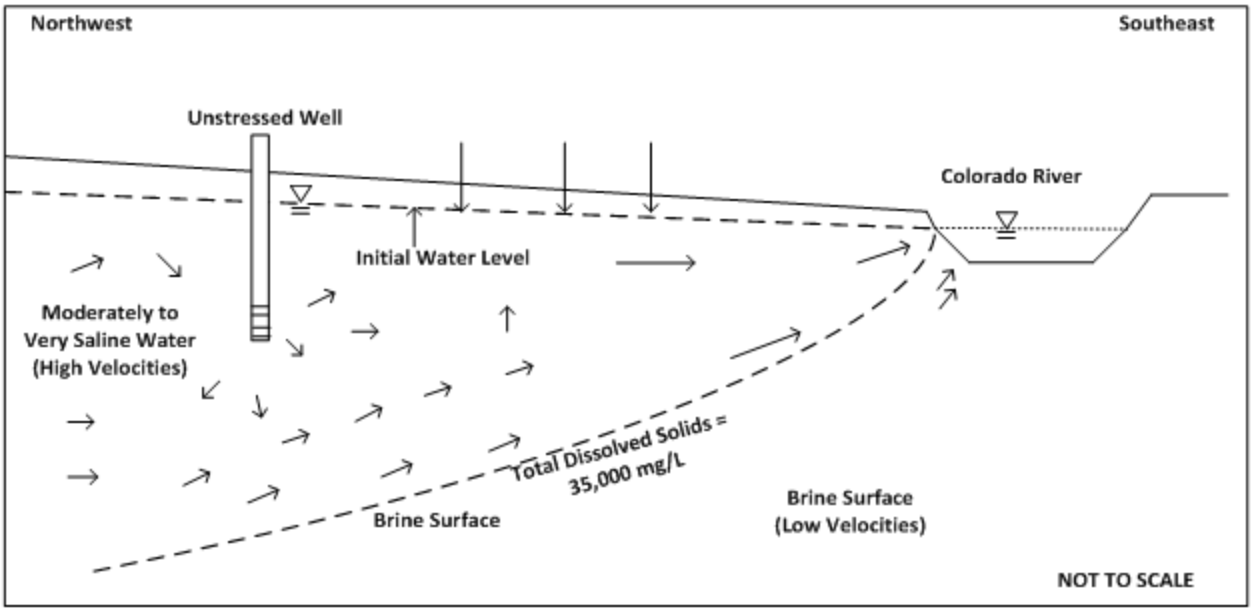

Figure 25 General effects of fresh water injection via remediation wells.

Freshwater injection through wells in Configuration 4 was restarted for 2011 in early March. As the river level rises associated with spring snowmelt, the benefit of injecting additional water is reduced. Therefore, injection was suspended on May 9 due to the level of the river and remains shut down. About 4,420,000 million gallons of freshwater has been injected during 2011.

3.3.2 Recharge

The model was configured with two different recharge zones, ambient precipitation and the tailings pile. While it is assumed recharge from the tailings pile was constant throughout the year, recharge from precipitation was assumed to vary monthly. Evapotranspiration was assigned to areas of the site having significant plant density and was assumed to vary monthly. The Colorado River was simulated using river cells which can contribute or receive water from the aquifer depending on the river stage and the adjacent groundwater relationship. For the simulation the Colorado River was assigned monthly stage values corresponding to the average monthly river stage.

Table 6 Rainfall Recharge

Area of model domain available for rainfall recharge	451 acres
Mass balance volumetric estimate: 16 gpm to 65 gpm	3,080 ft^3 to 12,513 ft^3
Mass balance estimate rainfall recharge rate	1.55 x 10^{-4} ft/d to 6.37 x 10^{-4} ft/d; 0.69 in/yr to 2.79 in/yr
Thornthwaite method recharge rate estimate	1.87 in/yr to 1.97 in/yr

Table 7 Tailings Pile Recharge

Area of model domain available for tailings pile recharge	5,831,250 ft^2
Mass balance volumetric estimate	20 gpm; 3,850 ft^3
Mass balance estimate tailings pile recharge rate	6.60 x 10^{-4} ft/d; 2.89 in/yr

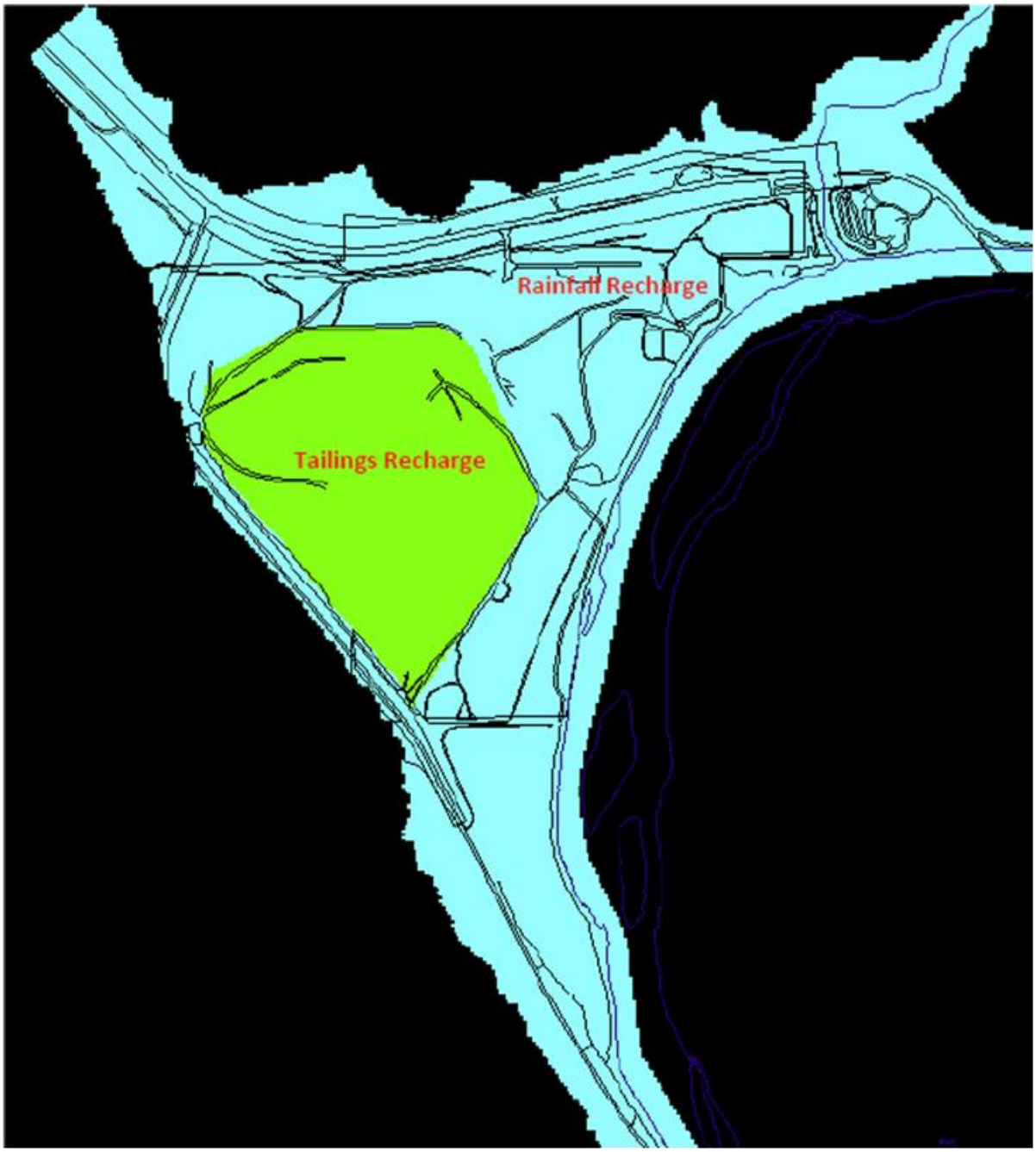

Figure 26 Recharge distribution.

4 SIMULATIONS AND RESULTS

FIU has applied the groundwater numerical model to evaluate the tailings pore-water seepage in order to assist in effective dewatering of the tailings pile and to optimize the groundwater extraction well field as part of the DOE UMTRA for the Moab site. Preliminary simulation results show a good match of observed and computed monthly data [Figure 27].

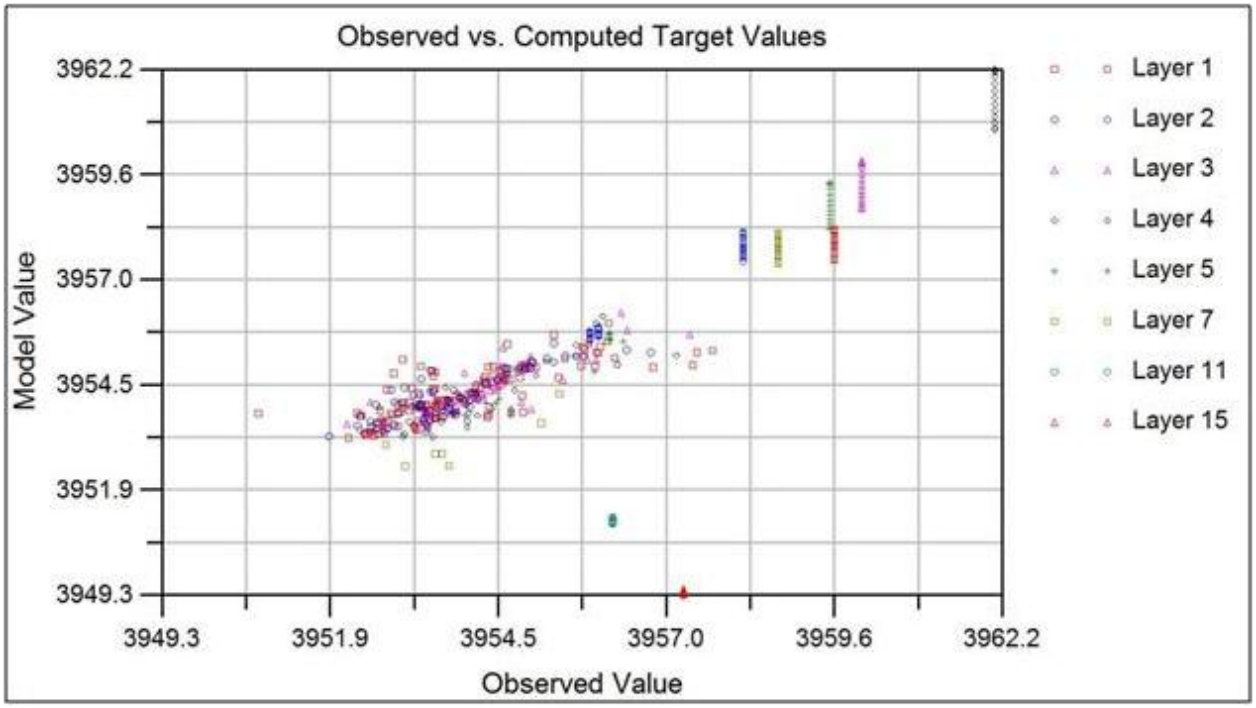

Figure 27 Calibration plot of observed vs. computed heads.

The calibrated model predicts a median monthly groundwater mass balance of 275 gallons per minute. With the exception of April through June, groundwater discharges to the Colorado River from the Moab Site. For April through June, the river recharges the aquifer at between 340 to 1,449 gallons per minute. Simulations results show that ambient recharge (precipitation) occurs in January, February, November and December at rates ranging from 46 to 195 gallons per minute. Tailings pile recharge is constant monthly at 9 gallons per minute. Recharge associated with Moab Wash and the surrounding bedrock is also constant monthly at 39 gallons per minute.

Discharge to the Colorado River is predicted to range between 159 to 495 gallons per minute. Evapotranspiration (ET), which is active May through September and again in November ranges from 22 to 840 gallons per minute.

The model predicts that approximately 60% of the water entering the groundwater flow system from Moab Wash and bedrock occurs in the upper three model layers. This result is in agreement with the conceptual model that hypothesizes that recharge and salinity are correlated, the fresher the groundwater the higher the recharge rate.

Examination of the simulated water table shows that January through March groundwater discharges to the Colorado River. The model-predicted April through June water tables shows Colorado River water recharging the aquifer. In July and August simulation results show the effects of ET. September through December the simulated water table once again shows groundwater discharge to the Colorado River.

The model reasonably reproduces the general trends present in site well hydrographs [Figure 29, Figure 30 and Figure 31]. Differences in measured and modeled hydrographs are likely a function of assigned Colorado River stage. In summary, the model reasonably matches conceptual mass balance information and replicates expected temporal groundwater flow patterns.

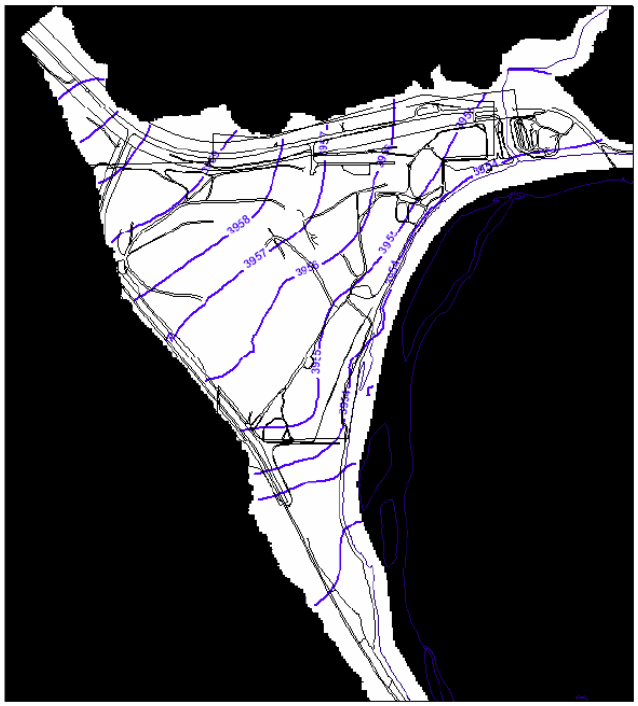

January Water table

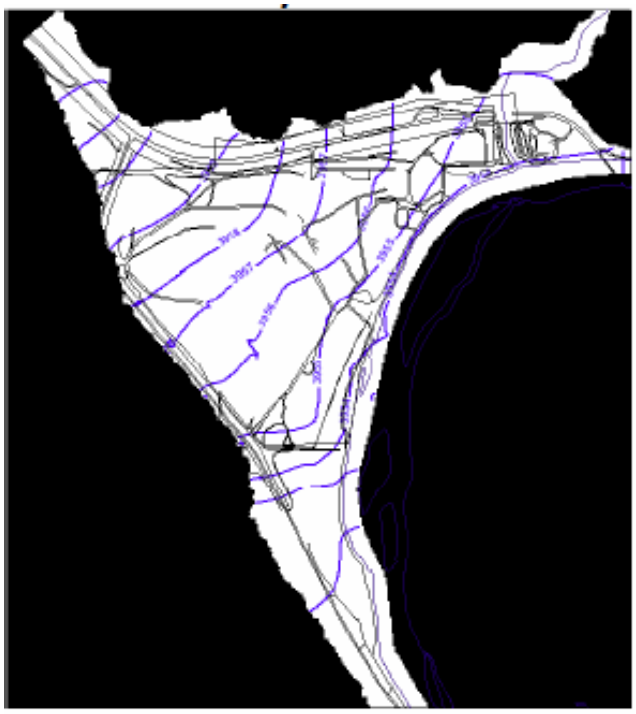

February Water table

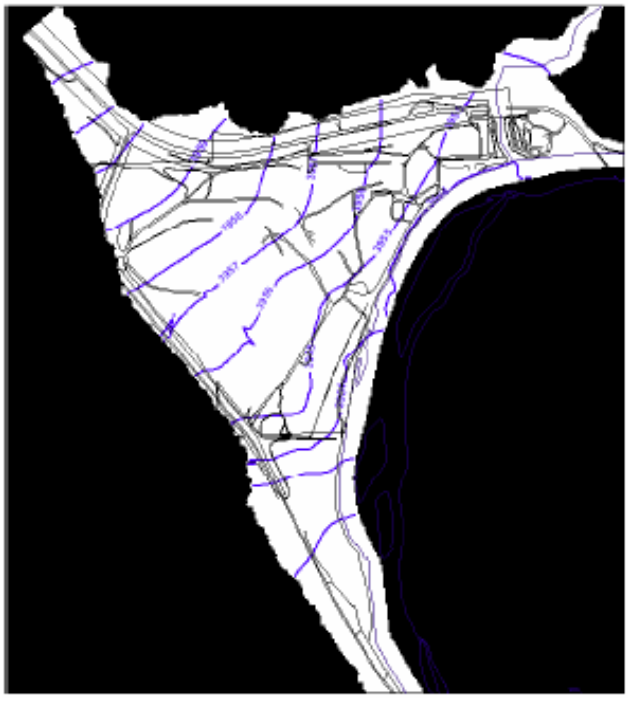

March Water table

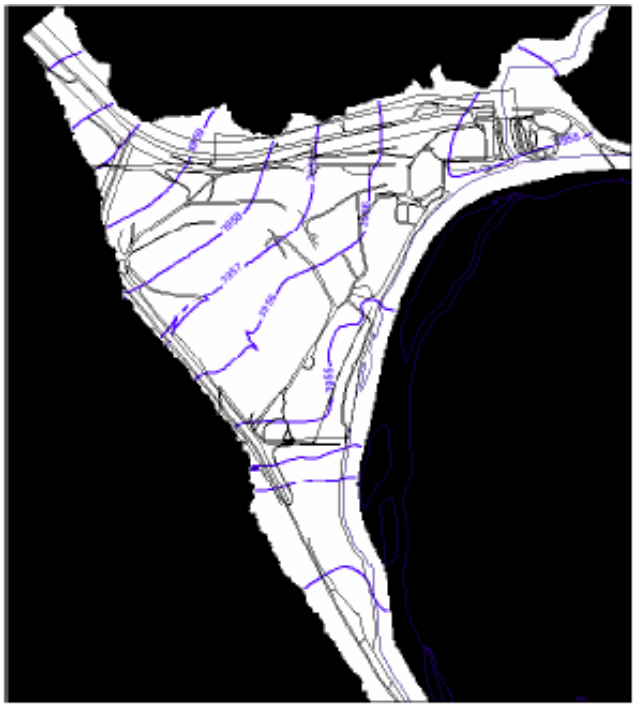

April Water table

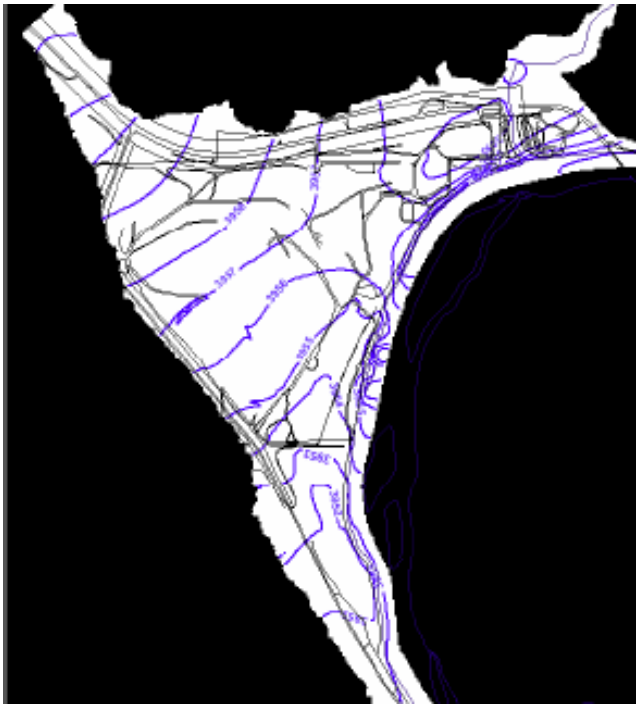

May Water table

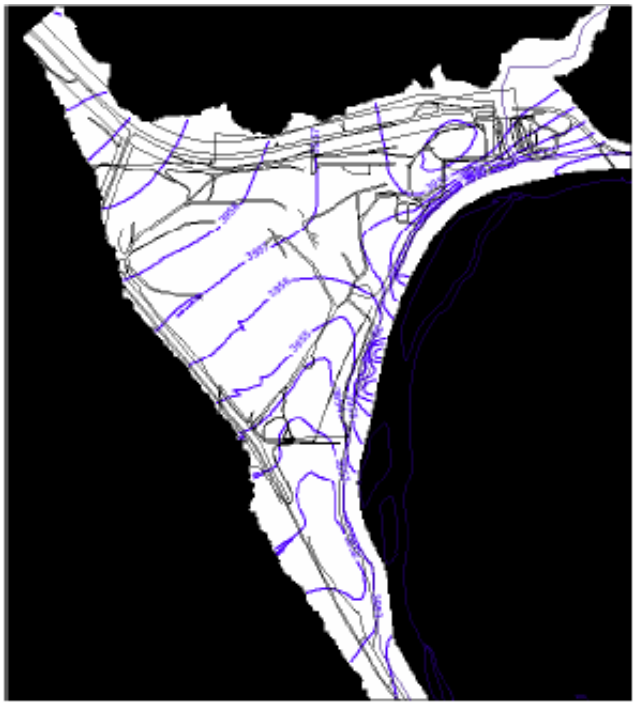

June Water table

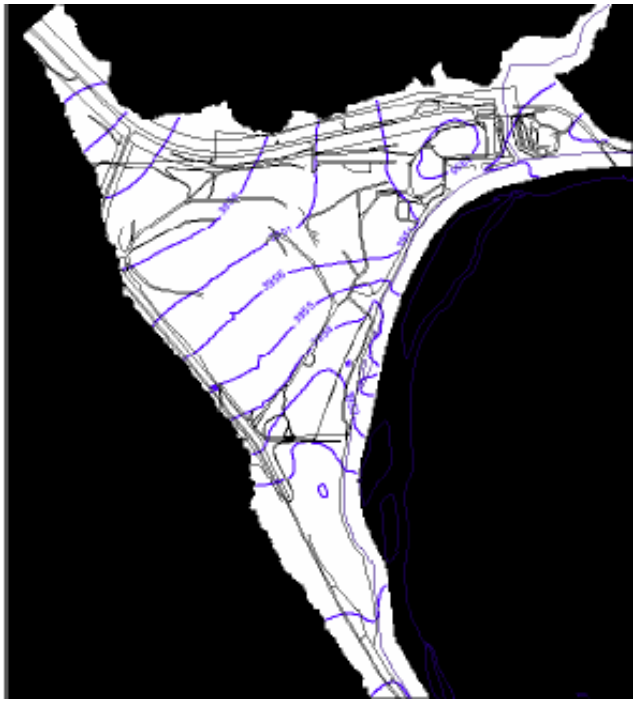

July Water table

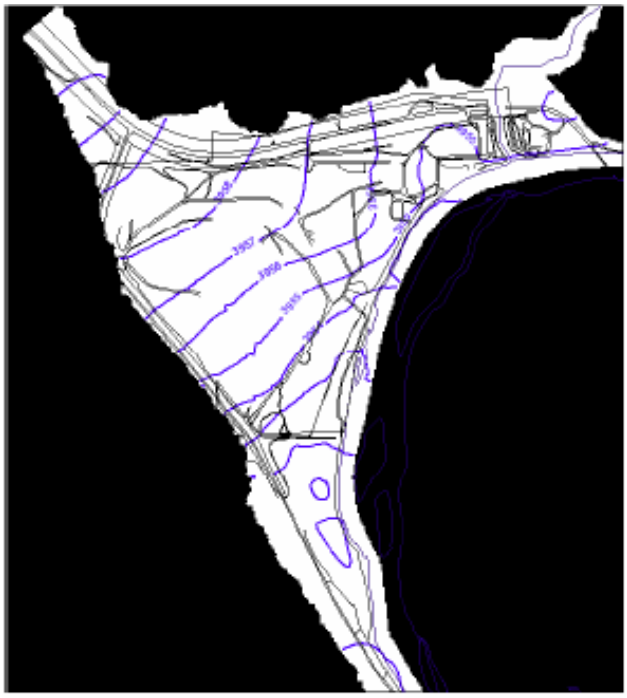

August Water table

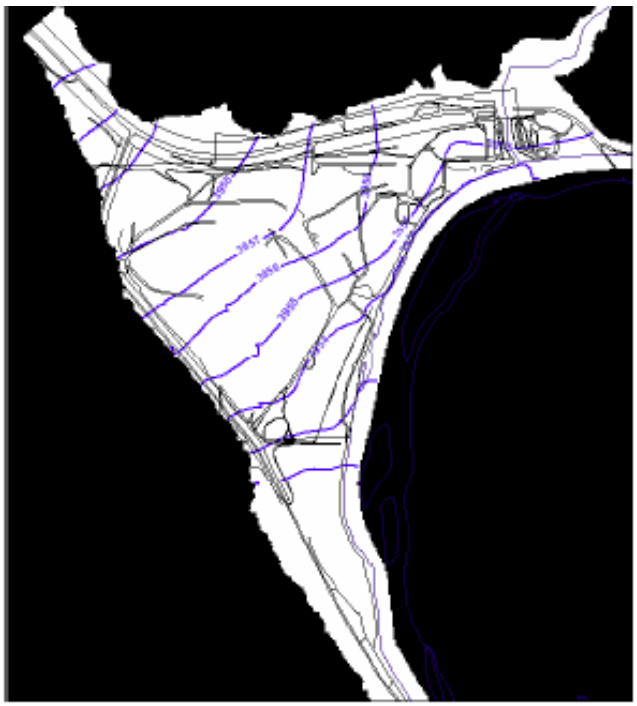

September Water table

October Water table

November Water table

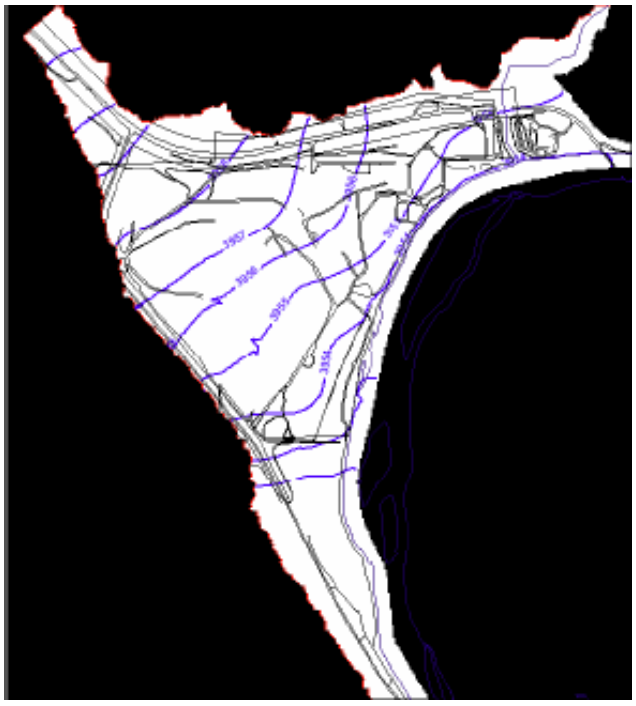

December Water table

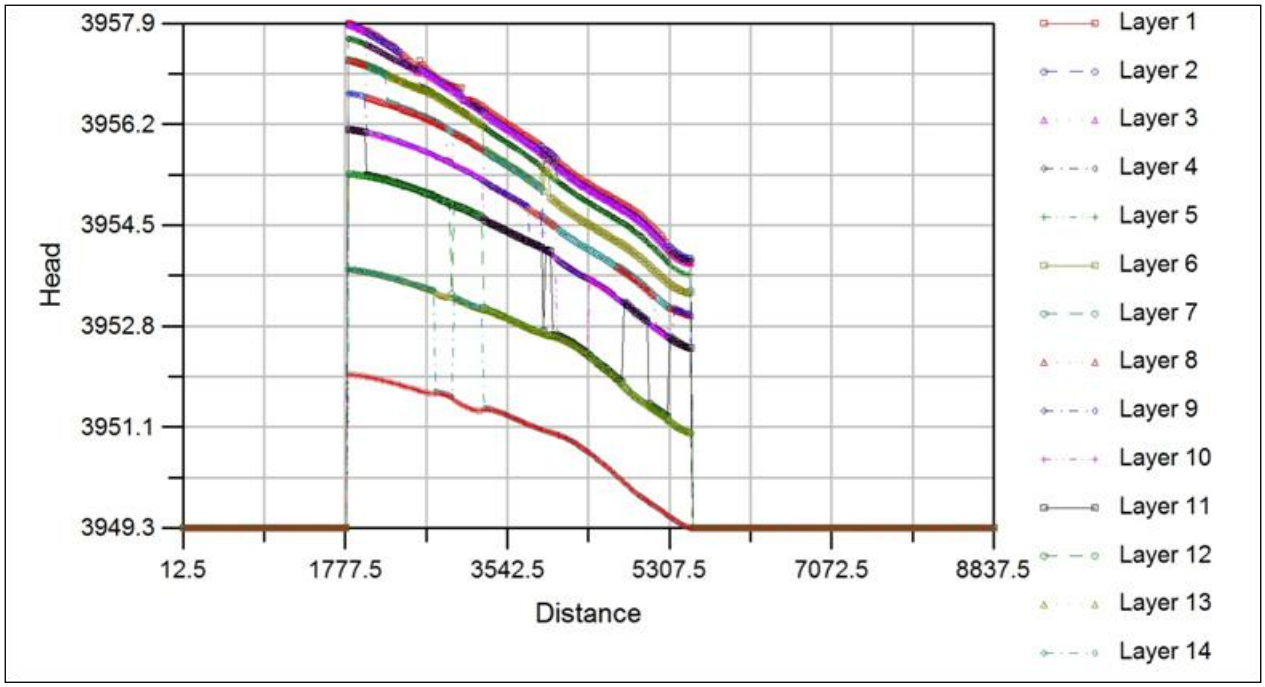

Figure 28 Sectional profile of heads for all layers

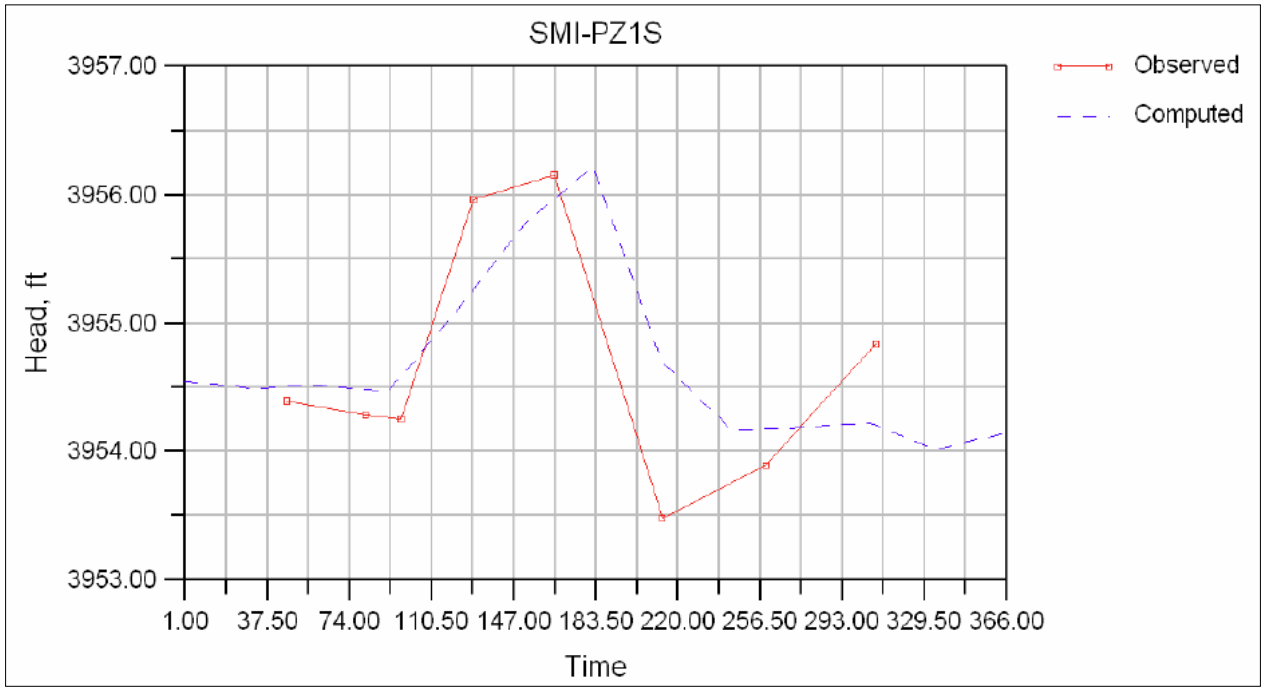

Figure 29 Layer 1 hydrograph at SMI-PZ1S.

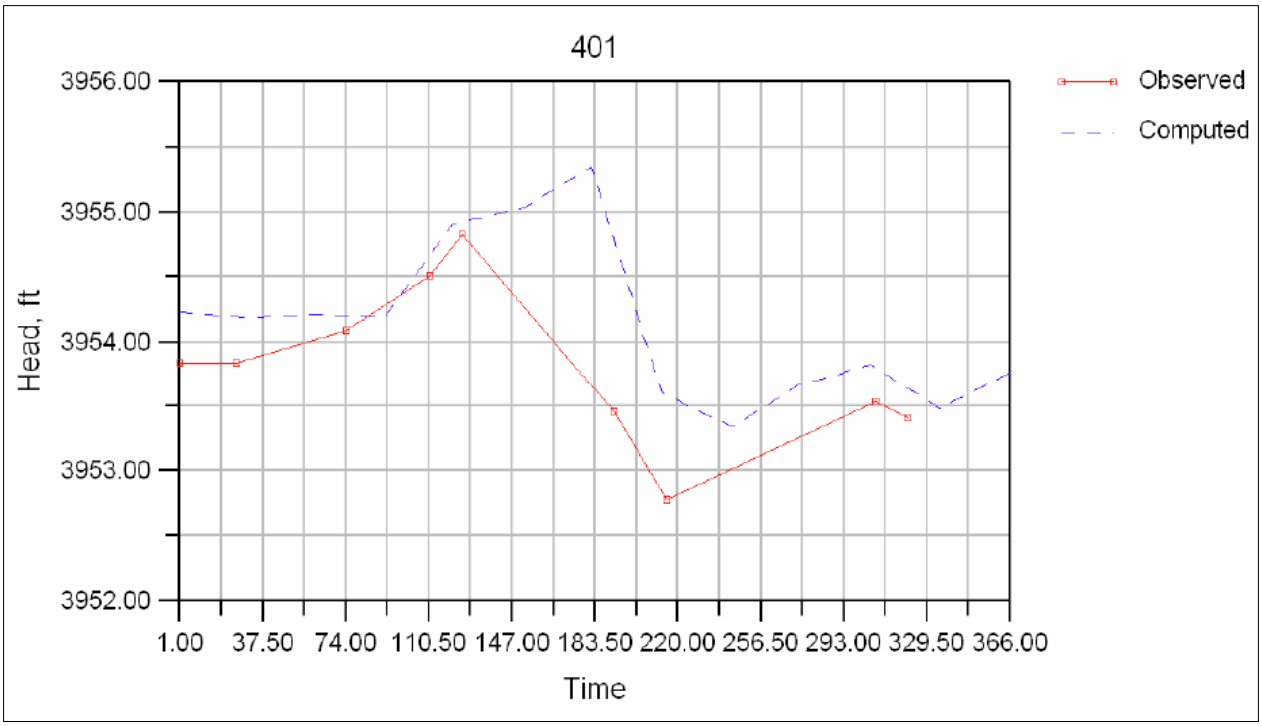

Figure 30 Layer 1 hydrograph at well no. 401.

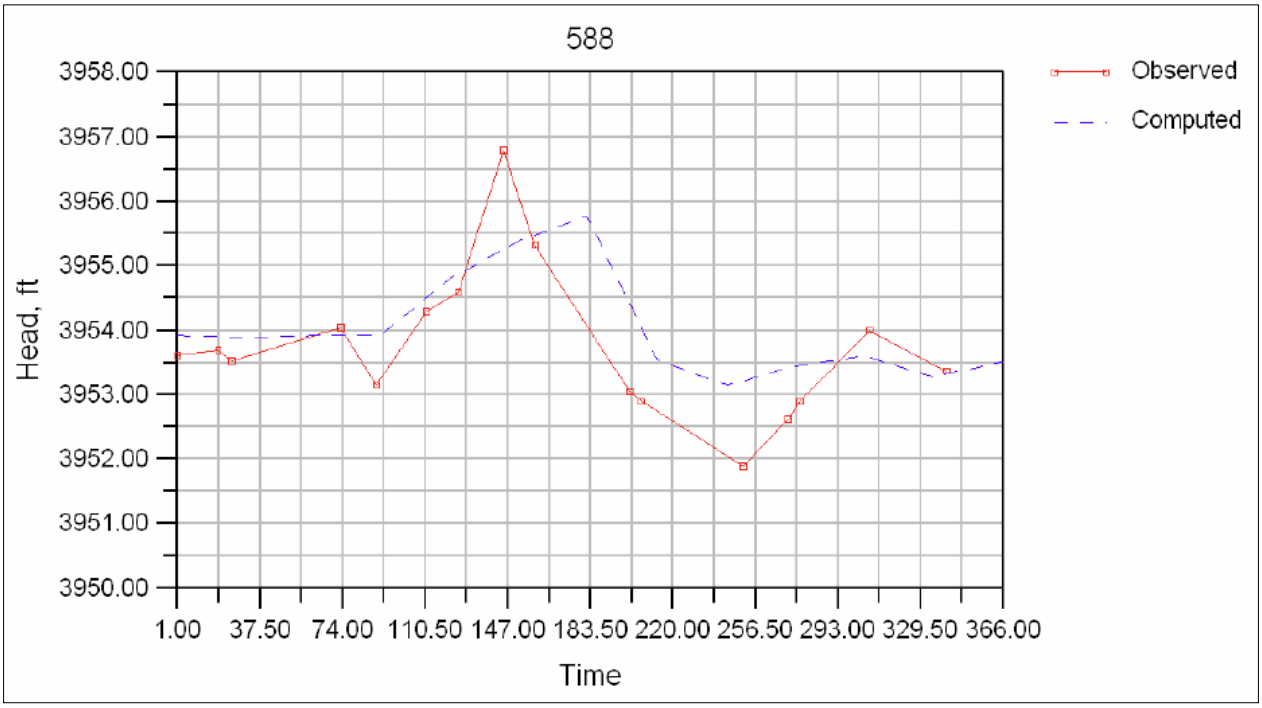

Figure 31 Layer 2 hydrograph at well no. 588.

4.1 Simulation for comparing heads at 10 different locations

The Following graphs show relationship of stage data obtained from the simulation results for ten points close to the Colorado river [Figure 32].

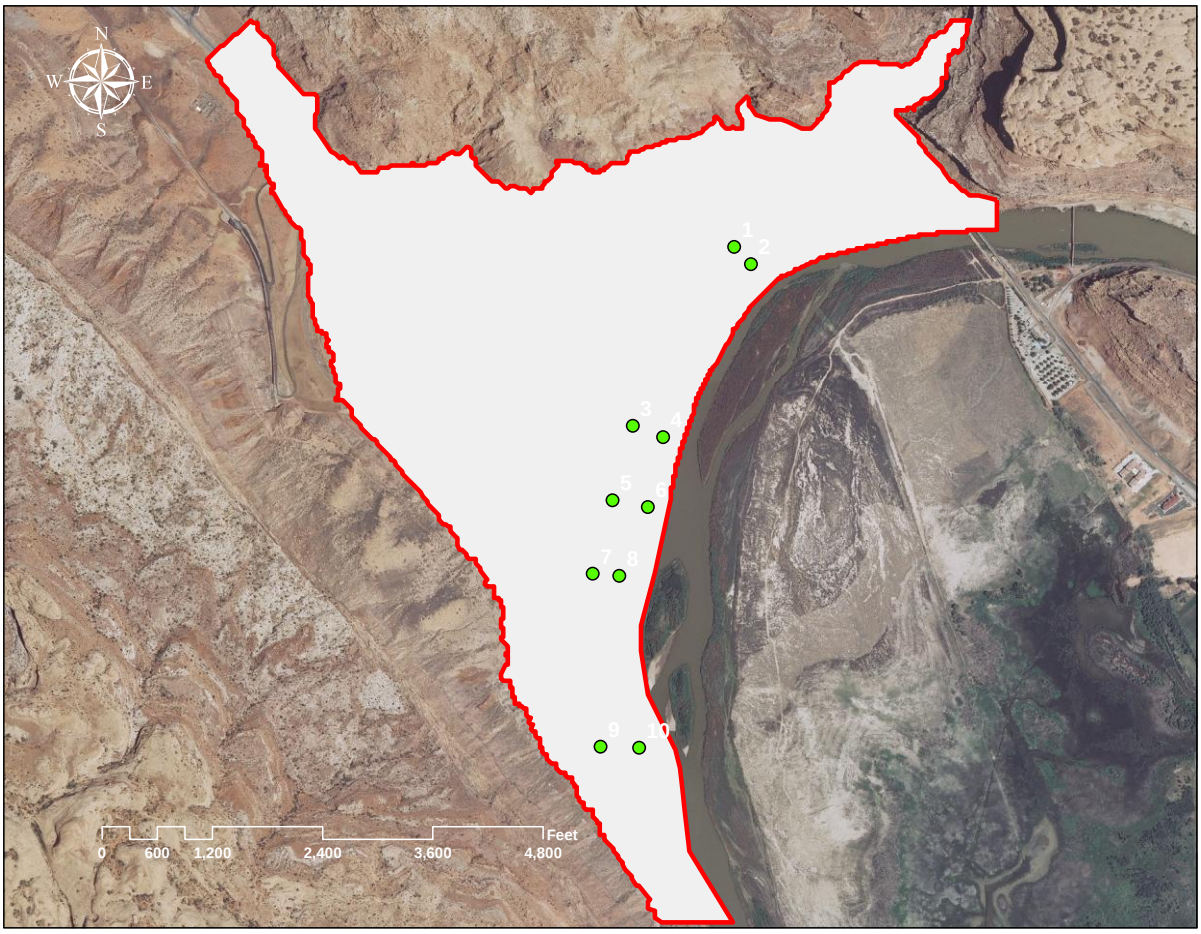

Figure 32 Points selected for showing relationship of stage data.

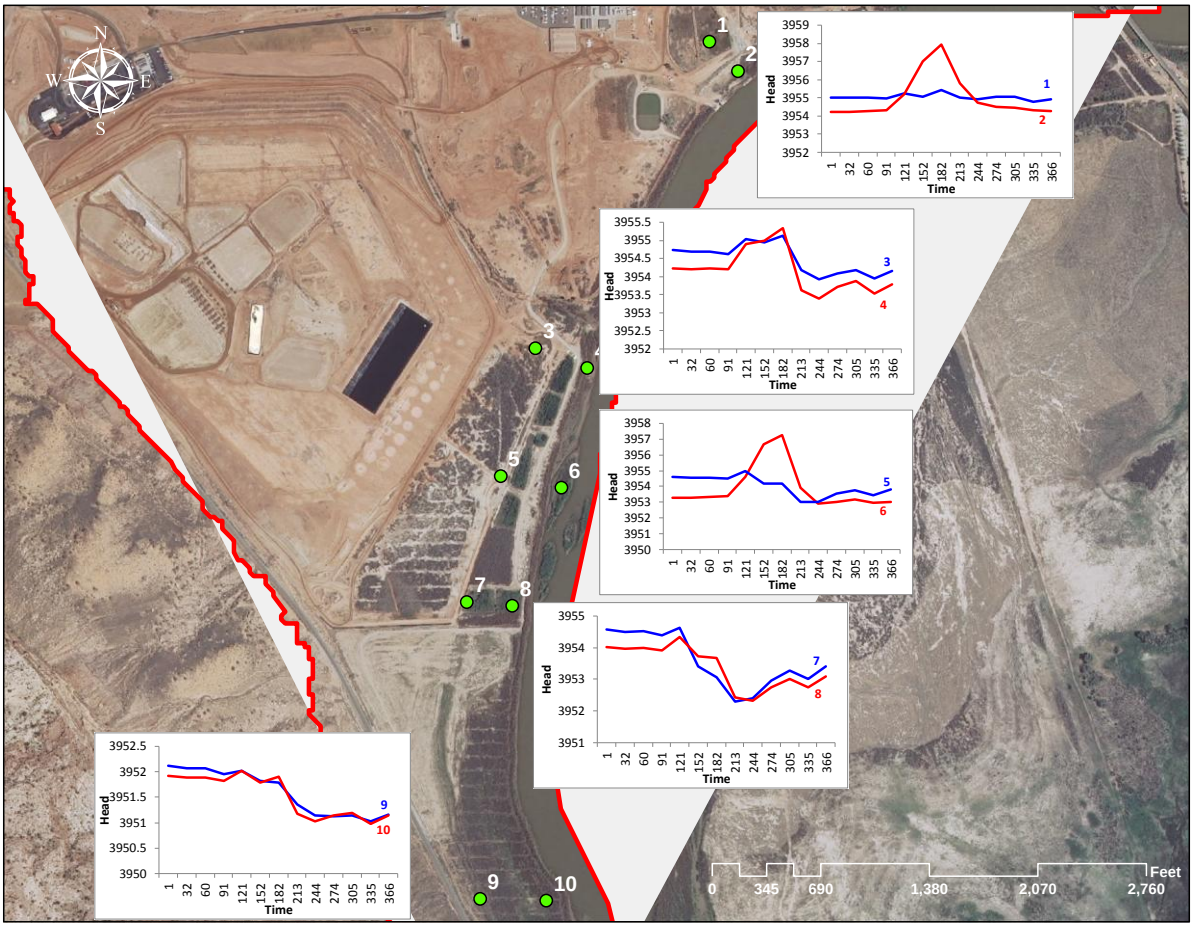

Figure 33 Comparison of stage data at different locations close to Colorado river.

4.2 Simulation for Pumping and Injection systems

Simulations were carried out for scenarios involving various increases in groundwater-pumping/injection rates and were analyzed with the calibrated groundwater-flow model to assess possible changes in the flow system. Pumping rates were increased by 25%, 50%, 100% and 200%. For comparison, simulation results were extracted for a small area close to the Colorado river, tailings and the well fields [Figure 34]. Following simulation were carried out:

- No Pumping and Injection
- Actual scenario for pumping and injection
- 0.25 x pumping and injection
- 0.5 x pumping and injection

- 2 x pumping and injection
- 3 x pumping and injection

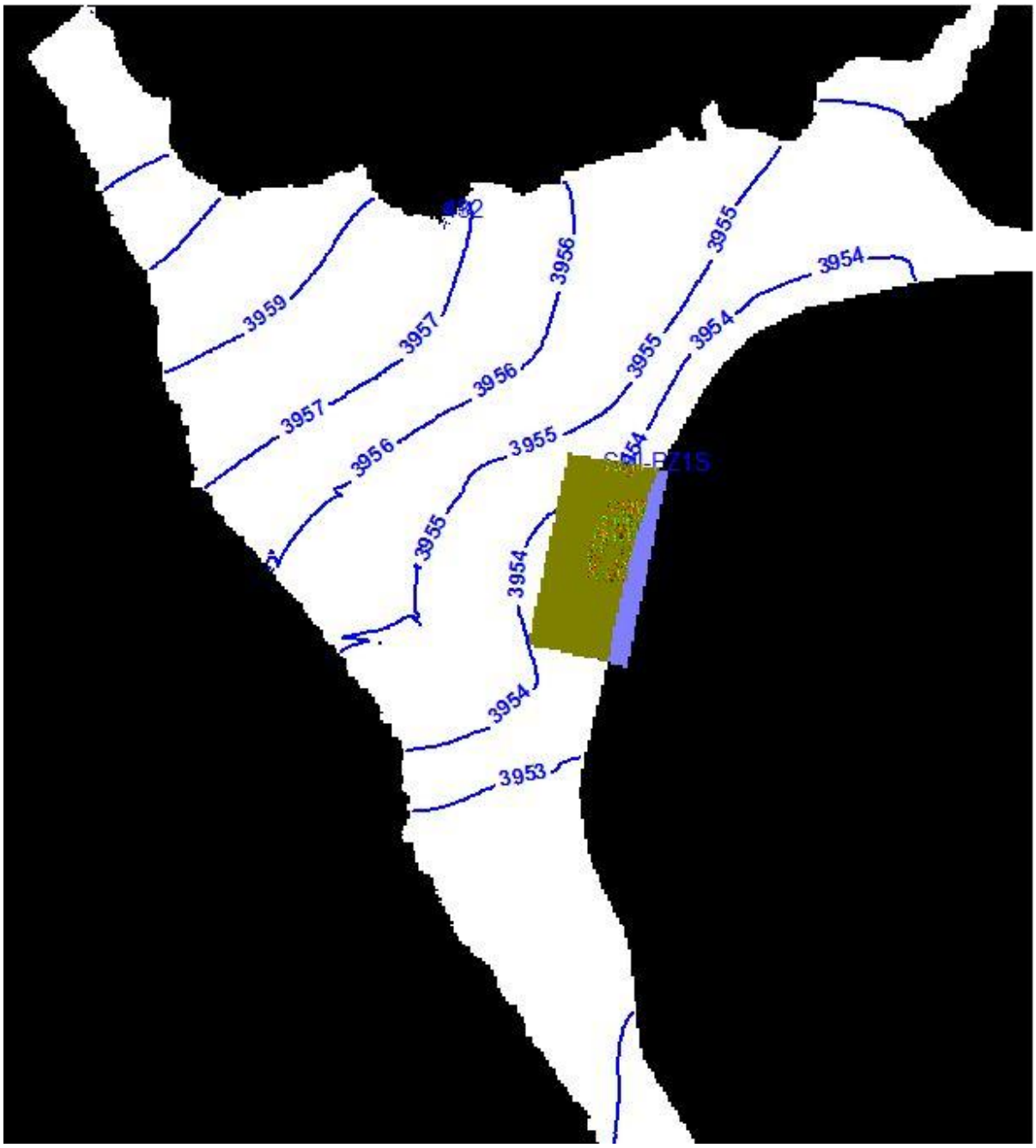

Figure 34 Polygon which was used for extracting results for mass balances.

Figure 34 shows the polygon which was used for extracting results for carrying out the mass balances.

4.2.1 Comparison of inflows and outflows from wells

Mass balances analysis was done for the hypothetical scenarios to assess the groundwater flow in and out of the selected polygon area shown in Figure 34. Results in Figure 35show an increase in flux by approximately 25% after each simulation where the pumping and injection rates were increased [Table 8].

Table 8 Inflows and Outflows from wells.

Scenario	Inflows (gpm)	Outflows(gpm)
No Pumping	0	0.00
Actual scenario	21.4	118.11
0.25 X actual	26.75	147.64
0.5 X actual	32.1	177.16
2 X actual	42.8	224.28
3 X actual	64.2	270.70

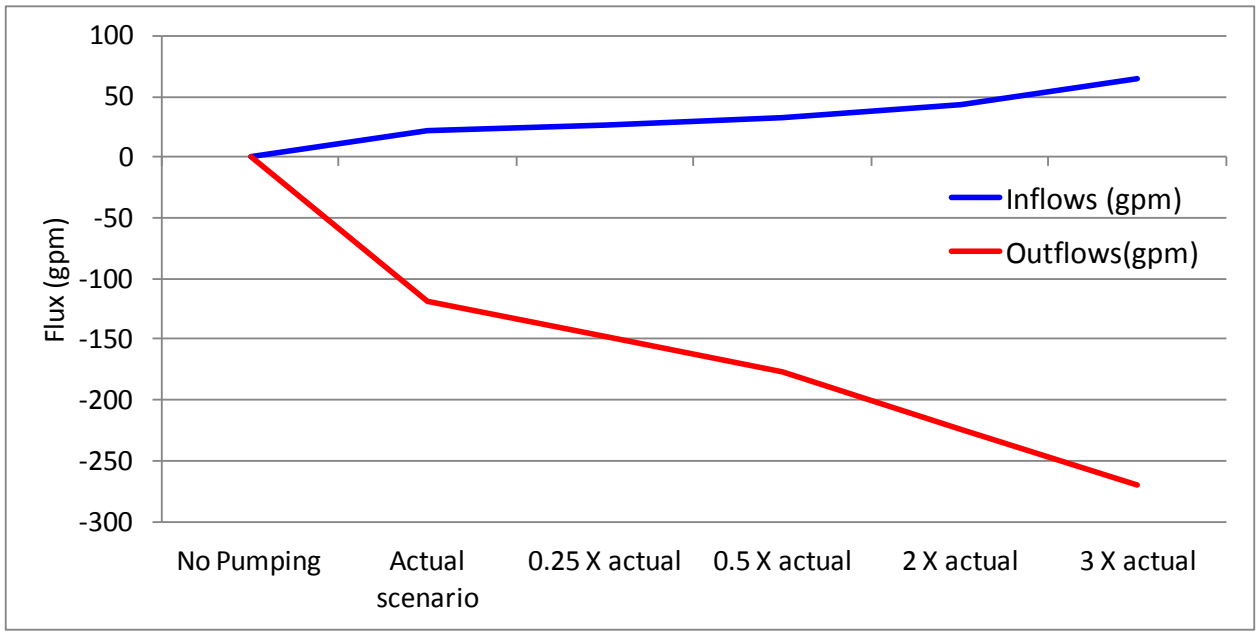

Figure 35 Inflows and Outflows from the wells [for selected polygon].

4.2.2 Comparison of inflows and outflows to river

Mass balances analysis was done for the hypothetical scenarios to assess the inflows and outflows to the Colorado river for the selected polygon area shown in Figure 34. Results in Figure 36 show an increase in flux by approximately 30% after each simulation where the pumping and injection rates were increased [Table 9].

Table 9 Inflows and outflows from river

Scenario	Inflows (gpm)	Outflows(gpm)
No Pumping	0.00	50.69
Actual scenario	15.12	5.41
0.25 X actual	28.02	3.56
0.5 X actual	41.31	2.50
2 X actual	60.51	1.18
3 X actual	71.31	0.71

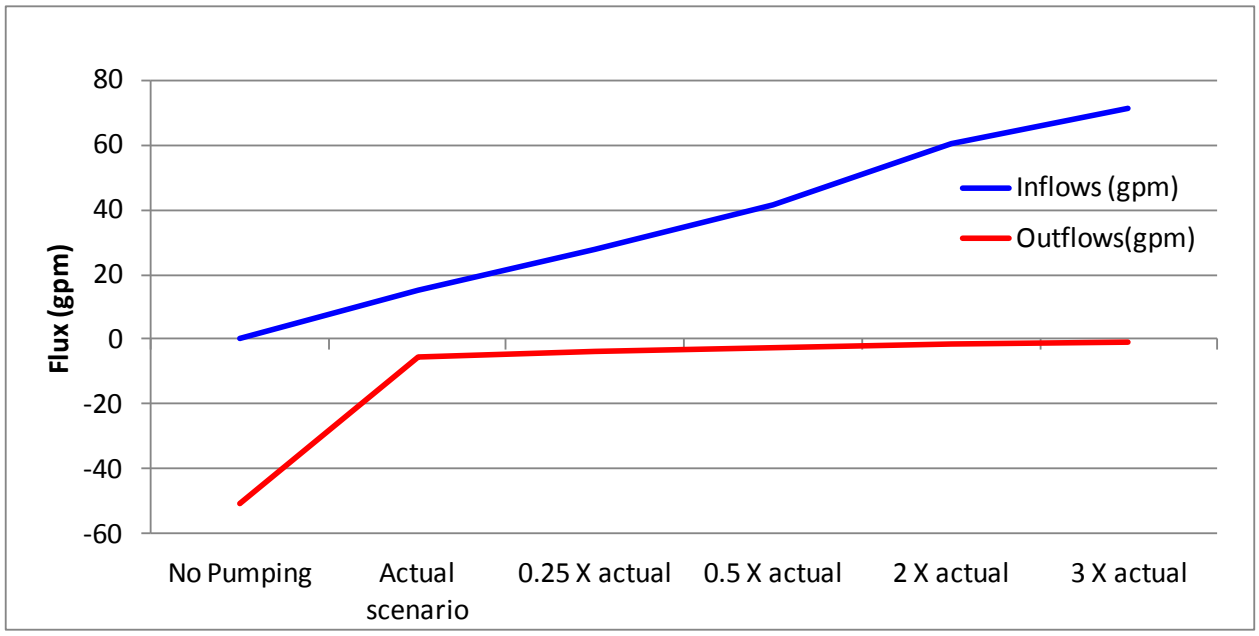

Figure 36 Inflows and Outflows from river [for selected polygon].

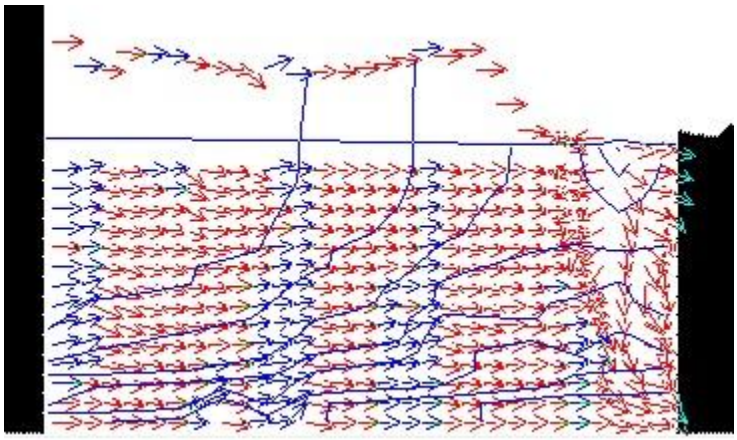

Figure 37 Cross Sectional view showing the groundwater flow pattern.

Figure 37 shows the groundwater flow pattern at the Moab site and it follows the conceptual model shown in Figure 25 for the general effects of freshwater injection.

5 CONCLUSION

Preliminary simulation results show a good match of observed and computed monthly data. The calibrated model predicts a median monthly groundwater mass balance of 275 gallons per minute. Tailings pile recharge is constant monthly at 9 gallons per minute. Recharge associated with Moab Wash and the surrounding bedrock is also constant monthly at 39 gallons per minute. Discharge to the Colorado River is predicted to range between 159 to 495 gallons per minute. Evapotranspiration (ET), which is active May through September and again in November ranges from 22 to 840 gallons per minute.

The model predicts that approximately 60% of the water entering the groundwater flow system from Moab Wash and bedrock occurs in the upper three model layers. This result is in agreement with the conceptual model that hypothesizes that recharge and salinity are correlated, the fresher the groundwater the higher the recharge rate.

The model reasonably reproduces the general trends present in site well hydrographs [Figure 29, Figure 30 and Figure 31]. Differences in measured and modeled hydrographs are likely a function of assigned Colorado River stage. Simulations with increased pumping and injection rates show an increase in inflows and outflows by approximately 25%. In summary, the model reasonably matches conceptual mass balance information and replicates expected temporal groundwater flow patterns.

6 FUTURE WORK

During FY12, students will be involved in the DOE-FIU Science and Technology Workforce Development Program, and will work with the transport model to perform numerical simulations of remedial scenarios proposed by DOE including pumping of contaminated groundwater from the shallow plume to an evaporation pond on top of the tailings pile, and injecting the diverted Colorado River water into the alluvial aquifer in order to predict the outcome of each remedial action and to investigate the effectiveness of each scenario. Numerical simulation of remedial actions assists DOE in deciding their effectiveness. Modeling is to be performed with MODFLOW, SEAWAT and FEFLOW as a benchmark. The following is a list of the proposed tasks to support this initiative:

1. Predictive simulations will be carried out with maximum and minimum values of flow parameters such as the hydraulic conductivity fluxes from Glen Canyon and Moab Fault, evapotranspiration and recharge.
2. Simulations to analyze the effects of pumping at well field Configuration 5 on ammonia and uranium concentrations in the upper saline zone and infiltration of freshwater in Configuration 1 to 4 will be conducted. Upgradient infiltration locations will be optimized relative to the tailings and extraction wells to maximize the number of pore volumes for flushing and reduce remediation time.
3. Simulations to identify the discharge zone for the legacy plume in the brine zone and to identify areas of uncertainty will be conducted. The effect of discharge of a legacy plume in the brine zone after the extraction wells have been shut off will be modeled.

7 REFERENCES

1. DOE (U.S. Department of Energy), 2003b. Site Observational Work Plan for the Moab, Utah, Site, GJO-2003-424-TAC, prepared by the U.S. Department of Energy, Grand Junction, Colorado.
2. Kenney, T., 2005, Initial-phase investigation of multi-dimensional streamflow simulations in the Colorado River, Moab Valley, Grand County, Utah, 2004: U.S. Geological Survey Scientific Investigations Report 2005-5022, 69 p.
3. Morris, D.A., and A.I. Johnson, 1967. Summary of hydrologic and physical properties or rock and soil materials as analyzed by the Hydrologic Laboratory of the U.S. Geological Survey 1948-1960, U.S. Geological Survey Water Supply Paper 1839-D, 42 pp.
4. Zheng, C., and G.D. Bennett, 1995. Applied Contaminant Transport Modeling Theory and Practice, Van Nostrand Reinhold, New York.
5. DOE (U.S. Department of Energy), 2009. Moab UMTRA Project Well Field Optimization Plan, DOE–EM/GJTAC1791, prepared by the U.S. Department of Energy, Grand Junction, Colorado.
6. Peterson D, Kautsky M, Karp K, Wright T, Metzler D (2004) Modeling of density-dependent groundwater flow and transport at the uranium mill tailings site near Moab, Utah. Tailings and Mine Waste ‘04, A.A. Balkema.
7. Kenney, T.A., 2005, Initial-Phase Investigation of Multi-Dimensional Streamflow Simulations in the Colorado River, Moab Valley, Grand County, Utah, 2004: U.S. Geological Survey Scientific Investigations Report 2005-5022, 69 p.

Appendices: Appendix_I_FY11_p3_TTP

Appendix_II_Overview_Presentation_i.pdf

Appendix_III_Overview_Presentation_II.pdf

Appendix_IV_Projects_Factsheets.pdf

Appendix_V_Publications.pdf